

A Thesis Submitted for the Degree of PhD at the University of Warwick

Permanent WRAP URL:

<http://wrap.warwick.ac.uk/82115>

Copyright and reuse:

This thesis is made available online and is protected by original copyright.

Please scroll down to view the document itself.

Please refer to the repository record for this item for information to help you to cite it.

Our policy information is available from the repository home page.

For more information, please contact the WRAP Team at: wrap@warwick.ac.uk

A Mutagenic Approach to Elucidating
Aquaporin Function

by

Philip Kitchen

A thesis submitted in fulfilment of the requirements for the
degree of
Doctor of Philosophy in Mathematical Biology and
Biophysical Chemistry

Molecular Organisation and Assembly in Cells Doctoral
Training Centre, University of Warwick

January 2016

Table of Contents

Acknowledgments	6
Declarations	8
Summary	11
List of Abbreviations.....	13
List of Tables	15
List of Figures.....	16
1 Introduction.....	20
1.1 Structural biology of the AQP family	24
1.2 The principles of AQP solute selectivity remain to be established.....	28
1.3 Physiological water transport by AQPs.....	31
1.3.1 Central nervous system (CNS)	31
1.3.2 Kidneys	36
1.4 Solute transport by AQPs	36
1.4.1 Glycerol transport	36
1.4.2 Urea transport	41
1.4.3 Ammonia transport	43
1.4.4 Carbon dioxide transport	46
1.4.5 Hydrogen peroxide transport	47
1.4.6 Ion permeability of AQPs: An unresolved controversy	49
1.5 AQPs and cell volume regulation	51
1.6 Regulation of AQPs	55
1.6.1 Transcriptional regulation of AQPs.....	55

1.6.2	Subcellular relocalization of AQPs	55
1.6.3	AQP gating	58
1.7	Outline of the thesis	61
2	Materials and Methods.....	63
2.1	DNA constructs	63
2.1.1	pDEST47 expression constructs	63
2.1.2	QuikChange site-directed mutagenesis.....	63
2.1.3	Agarose gel electrophoresis.....	68
2.1.4	Mutagenic oligonucleotide primers	68
2.1.5	Preparation of competent cells.....	68
2.1.6	Transformations	70
2.1.7	Growth and isolation of plasmids	70
2.1.8	Sequencing.....	71
2.2	Mammalian cell culture	71
2.2.1	HEK293	71
2.2.2	MDCK	72
2.2.3	U-251 MG.....	72
2.2.4	Rat primary cortical astrocytes	72
2.2.5	Cell culture.....	72
2.2.6	Frozen cell stocks	73
2.3	Transfections.....	74
2.3.1	Transient	74
2.3.2	Stable	74
2.4	Confocal Microscopy	75
2.4.1	Tonicity-mediated translocation	76
2.4.2	Fluorescence recovery after photobleaching (FRAP).....	77
2.4.3	Forster resonant energy transfer (FRET).....	77

2.6	Lance cAMP assay	79
2.7	PKA activity assay	80
2.8	Calcein fluorescence quenching	81
2.8.1	Water permeability	82
2.8.2	Solute permeability	82
2.9	Cell-surface biotinylation	87
2.10	SDS-PAGE	89
2.11	Blue native (BN)-PAGE	92
2.12	Western blotting	92
2.13	Antibodies	92
2.13.1	Primary antibodies	92
2.13.2	Secondary antibodies	94
2.14	Inhibitors and agonists	94
2.15	Molecular dynamics simulations	95
3	Results – Hypotonicity-induced relocalization of AQP4	96
3.1	Aims	96
3.2	Background	96
3.3	Results	99
3.3.1	AQP4-GFP undergoes a rapid and reversible sub-cellular relocalization in HEK293 cells in response to changes in the tonicity of the extracellular environment	99
3.3.2	Both AQP4 isoforms relocalized equally in HEK293 cells	104
3.3.3	CaM, calcium and PKA regulate AQP4 relocalization	106
3.3.4	Endogenous AQP4 in cultured primary rat astrocytes undergoes sub-cellular relocalization in response to hypotonicity	106
3.3.5	PKA activity is required for endogenous AQP4 relocalization in primary astrocytes	109

3.3.6	Hypotonicity induces intracellular cAMP production and PKA activity in primary rat astrocytes	110
3.3.7	S276 phosphorylation is required for relocalization.....	112
3.3.8	AQP5 surface localization is controlled by phosphorylation, PKA and hypotonicity.....	115
3.4	Discussion	120
3.4.1	AQP4	120
3.4.2	AQP5	125
4	Results – A comparative analysis of AQP solute exclusion and selectivity	
	132	
4.1	Aims	132
4.2	Background	132
4.3	Results.....	137
4.3.1	AQP4 has a novel molecular mechanism for excluding glycerol and urea. 137	
4.3.3	Water permeability of AQP4 mutants	140
4.3.4	GLP-mimetic mutants of AQP4 are not solute permeable	143
4.3.5	AQP3 urea and glycerol permeability can be altered independently of each other	145
4.3.6	AQPs 3, 9 and 10 have different relative permeability for glycerol and urea 147	
4.3.7	Molecular dynamics and <i>in silico</i> mutagenesis	149
4.4	Discussion	158
5	Results – Molecular determinants and functional consequences of AQP4 tetramerization	164
5.1	Aims	164
5.2	Background	164

5.3	Results	166
5.3.1	Compound mutations of loop D of AQP4 reduce tetrameric assembly ...	166
5.3.2	Surface expression of non-tetrameric mutants	169
5.3.3	Mutants in the plasma membrane have reduced oligomeric state	172
5.3.4	Loop D mutants have wild-type water permeability	175
5.3.5	Loop D mutants do not relocalize in response to hypotonicity	177
5.3.6	Molecular dynamics simulations suggest a dynamic network of loop D interactions	177
5.3.7	Loop D may represent a common motif for oligomeric assembly across the AQP family	183
5.4	Discussion	184
6	Conclusions	191
6.1	General discussion and future directions	191
6.1.1	Hypotonicity-induced translocation of AQP4	191
6.1.2	Regulation of AQP5 localization.....	192
6.1.3	AQP solute permeability.....	193
6.1.4	AQP4 tetramerization	193
	Appendix: Publications arising from the data presented in this thesis.....	218

Acknowledgments

I would like to thank my supervisor Alex for consistently doing far more than he needed to, and for all the coffee and computer games!

I would like to thank my second supervisors Mark and Alison for lots of helpful thoughts and suggestions and always remembering what I was doing despite our infrequent meetings.

I would like to thank Luke for convincing me to do the MOAC miniproject that led on to this PhD project, and Mike for all his help and time and for not complaining about my lab mess and annoying pipette tip habits!

Thanks to team aquaporin: Ros, Matt, Rebecca and Mootaz for all their collaborative efforts and for making the Cluj 2015 conference so much fun!

I thank the MOAC doctoral training centre for funding my research, the MOAC admin staff (particularly Sarah, Naomi and Anne) for making everything associated with the MOAC experience run smoothly and the 2011 cohort for their support (scientific and otherwise).

I would like to thank the Rainger and Nash groups, and especially Hafsa, Bonita, Jas and Claire at the University of Birmingham for making me feel welcome.

Finally, I thank my family and friends, Mum and Mark, Dad and Lidia, Grandad Kitchen and Maribel, Laura, George and Becky (and Katie and Olivia too!), Jason and Phill for 4 years of sustained support and fun and helping to make sure that I didn't spend all of my time holed up in the lab!

Declarations

This thesis is submitted to the University of Warwick in support of my application for the degree of Doctor of Philosophy. It has been composed by myself and has not been submitted in any previous application for any degree.

The terms *we*, *our*, etc. are used throughout this thesis to indicate that the experimental approaches and interpretation of data resulted from discussion between my supervisors and me. All experiments, computations and analysis leading to the results reported in this thesis represent entirely my own work, except in the specific cases outlined below:

1. Figure 1-1 was drawn by Ashton Moran for the publication **Human aquaporins: Regulators of transcellular water flow**.
2. The PKA inhibition experiments in primary astrocytes reported in chapter 3 were done by Rebecca Day (Sheffield Hallam University) and analyzed by me as part of an ongoing collaboration.
3. Some data reported in Table 3-1 were collated with data collected by Luke Taylor and analyzed by me. 3 experimental repeats are reported per condition; I collected data for at least 2 experimental repeats in each condition.
4. Site-directed mutagenesis for AQP5-GFP translocation studies was done by Dr Matthew Conner.

Parts of this thesis have been published:

Parts of the introduction (specifically those concerning solute transport by aquaporins, regulatory cell volume changes and the role of water transport by aquaporins in human physiology and disease) have been published in two review articles:

Kitchen P, Day RE, Salman MM, Conner MT, Bill RM and Conner AC.

Beyond water homeostasis: Diverse functional roles of mammalian aquaporins *Biochimica et Biophysica Acta* 2015

Day RE, **Kitchen P**, Owen DS, Bland C, Marshall L, Conner AC, Bill RM and Conner MT. **Human aquaporins: Regulators of transcellular water flow** *Biochimica et Biophysica Acta* 2014

A large part of the data contained in the first part of chapter 3 has been published as:

P. Kitchen, R.E. Day, M.M. Salman, R.M. Bill, M.T. Conner and A.C. Conner.

Identification and molecular mechanisms of the rapid tonicity-induced relocalization of the aquaporin 4 channel *Journal of Biological Chemistry* 2015

The data contained in the latter part of chapter 3 concerning AQP5 translocation along with a supporting X-ray crystal structure have been published as:

Philip Kitchen, Fredrik Öberg, Jennie Sjöhamn, Kristina Hedfalk, Roslyn M Bill, Alex C Conner, Matthew T Conner and Susanna Horsefield.

Plasma membrane abundance of human aquaporin 5 is dynamically regulated by multiple pathways *PloS One* 2015

The data on water permeability of AQP4 mutants contained within chapter 4 has been published as:

P. Kitchen and A.C. Conner

Control of the aquaporin-4 channel water permeability by structural dynamics of aromatic/arginine selectivity filter residues *Biochemistry* 2015

The majority of the data contained within chapter 5 has been published as:

P. Kitchen, M.T. Conner, R.M. Bill and A.C. Conner. **Structural determinants of the oligomerization of the aquaporin-4 channel** *Journal of Biological Chemistry* 2016

Full texts of all publications are included in an appendix at the end of the thesis.

Summary

Aquaporins (AQPs) are transmembrane proteins that facilitate the movement of water molecules across biological membrane by osmosis.

Green fluorescent protein-tagged aquaporin 4 relocalized to the plasma membrane of HEK293 cells in response to reduced tonicity and this phenomenon was reproduced for endogenous AQP4 in primary astrocyte cultures. The mechanism was dependent on phosphorylation at serine-276 by PKA and required activation of CaM. AQP4 knockout animals are protected from brain edema so pharmacologically modulating the subcellular localization of AQP4 may provide a platform for an alternative or complementary approach to hyperosmotic solution based edema therapies. Using the same methodology, we also describe some of the factors controlling AQP5 plasma membrane abundance.

AQPs have a signature aromatic/arginine (ar/R) motif that is thought to aid in solute selectivity. Mutants of AQP4 in this region permitted the passage of small solutes differently to AQP1, questioning the validity of a generalized model of AQP solute exclusion. Furthermore, the relative selectivity for glycerol and urea of AQPs could be modulated independently of the physical size of the Ar/R region, suggesting that lack of solute exclusion and solute selectivity are not the same thing.

AQPs retain homotetrameric quaternary structures, but the structural basis and functional relevance of this assembly is not known. Mutants of an intracellular loop of AQP4 had reduced ability to form tetramers and, despite no change in constitutive levels of membrane localization or water permeability, had reduced capacity to relocalize in response to hypotonicity.

List of Abbreviations

ADH	anti-diuretic hormone
AQP	aquaporin
AVP	arginine vasopressin
BN-PAGE	blue native polyacrylamide gel electrophoresis
CaM	calmodulin
cAMP	cyclic adenosine monophosphate
CFP	cyan fluorescent protein
DMSO	dimethyl sulfoxide
FRAP	fluorescence recovery after photobleaching
FRET	Forster resonant energy transfer
GFP	green fluorescent protein
HEK293	human embryonic kidney cells, clone 293
IBMX	3-isobutyl-1-methylxanthine
LB	lysogeny broth
MDCK	Madin-Darby canine kidney cells
PAGE	polyacrylamide gel electrophoresis
PBS	phosphate-buffered saline
PCR	polymerase chain reaction
ar/R	aromatic/arginine
RPCA	rat primary cortical astrocytes
SDM	site-directed mutagenesis
SDS	sodium dodecyl sulphate
SDS-PAGE	sodium dodecyl sulphate polyacrylamide gel electrophoresis

TBE	tris-borate-EDTA
TBS	tris-buffered saline
YFP	yellow fluorescent protein

List of Tables

Table 1-1 – Permeability of mammalian AQPs	23
Table 2-1 Inhibitors and agonists used for elucidation of cell signalling pathways	94
Table 3-1 Translocation of AQP4-GFP in HEK293 cells in the presence of various inhibitors.....	107
Table 3-2 Translocation of phosphomimetic and phospho-blocking mutants of AQP4-GFP in HEK293 cells.	114
Table 5-1 Oligomerization state and surface expression of AQP4 mutants.....	168

List of Figures

Figure 1-1 Distribution of AQP expression throughout the human body	21
Figure 1-2 Sequence alignment of human AQPs	24
Figure 1-3 Structural biology of the AQP family	26
Figure 1-4 Localization of AQP4 in the central nervous system	32
Figure 1-5 Glycerol permeable AQPs contribute to mammalian glycerol physiology and homeostasis	37
Figure 1-6 Comparison of human and mouse AQP8 selectivity filters	44
Figure 1-7 The central pore of AQP1	52
Figure 1-8 Regulation of AQPs	59
Figure 2-1 Vector map of the DEST47 vector	64
Figure 2-2 DNA and amino acid sequences of the human AQP4 construct	65
Figure 2-3 DNA and amino acid sequences of the human AQP3 construct	66
Figure 2-4 DNA and amino acid sequences of the human AQP1 construct	67
Figure 2-5 Representative agarose gel of site-directed mutagenesis product, with and without digestion of methylated template by <i>dpnI</i>	69
Figure 2-6 Calculation of the relative membrane expression of GFP fusion proteins from confocal fluorescence micrographs.	78
Figure 2-7 Plate reader setup for calcein fluorescence quenching	91
Figure 2-8 Calibration curve for conversion of relative calcein fluorescence to relative volume	85
Figure 2-9 inhibition of AQP9 glycerol permeability by phloretin	86
Figure 2-10 Schematic representation of cell surface biotinylation protocol	96
Figure 2-11 Validation of cell surface biotinylation	90

Figure 2-12 Western blotting of AQP constructs.....	93
Figure 3-1 Hypotonicity-induced relocalization of AQP4-GFP in HEK293 cells	100
Figure 3-2 Representative cross-sectional areas of HEK293 cells.	102
Figure 3-3 Threshold tonicity for the relocalization response	103
Figure 3-4 Comparison between M1 and M23 isoforms of AQP4.....	105
Figure 3-5 Hypotonicity-induced relocalization of endogenous AQP4 in primary rat astrocytes.....	108
Figure 3-6 cAMP and PKA signalling in response to hypotonicity.....	111
Figure 3-7 Locations within the AQP4 structure of identified putative PKA sites	113
Figure 3-8 Localization of AQP5-GFP mutants in HEK293 cells.....	117
Figure 3-9 Effect of PKA inhibition on AQP5-GFP localization	118
Figure 3-10 Hypotonicity-induced relocalization of AQP5-GFP	119
Figure 3-11 Lack of AQP4 translocation in U373 glioblastoma cells	124
Figure 3-12 Schematic of the proposed signalling mechanisms involved in hypotonicity-induced relocalization of AQP4	126
Figure 3-13 – A proposed model of the equilibrium between vesicular and surface-localized AQP5	129
Figure 4-1 Structure of the AQP ar/R region	135
Figure 4-2 Solute permeability of AQP4 and AQP1 ar/R region mutants.....	138
Figure 4-3 Representative calcein fluorescence timeseries for urea and glycerol permeability of AQP4 mutants.....	139
Figure 4-4 Water permeability of AQP4 ar/R region mutants.	141

Figure 4-5 Representative calcein fluorescence timeseries for water permeability of the AQP4 mutants	142
Figure 4-6 Solute permeability of AQP4 GLP-mimetic mutants.....	144
Figure 4-7 Solute permeability of AQP3 ar/R region mutants.....	146
Figure 4-8 Relative solute permeabilities of AQPs 3, 9 and 10.....	148
Figure 4-9 Molecular dynamics simulations of AQP4.....	150
Figure 4-10 Channel radius profiles of AQP4 and AQP3 mutants	152
Figure 4-11 Pore-lining residues of AQP4 mutants at the selectivity filter and cross-sectional areas.....	153
Figure 4-12 Correlation between selectivity filter size and solute permeability	154
Figure 4-13 Correlation between selectivity filter geometric properties and glycerol permeability of AQP4 mutants	155
Figure 4-14 V187-water hydrogen bonds	157
Figure 5-1 Residues at the AQP4 tetrameric interface.....	167
Figure 5-2 BN-PAGE and Western blotting of AQP4 mutants.	170
Figure 5-3 Plasma membrane localization of non-tetrameric mutants..	171
Figure 5-4 A FRET biosensor for AQP4 oligomerization	174
Figure 5-5 Reduced FRET from AQP4 mutants.....	176
Figure 5-6 Water permeability of non-tetrameric mutants.....	178
Figure 5-7 Tonicity-induced translocation of non-tetrameric mutants	179
Figure 5-8 A dynamic network of loop D hydrogen bonds in simulations of AQP4.....	181
Figure 5-9 A dynamic network of loop D hydrogen bonds in simulations of AQP4 II.....	182

Figure 5-10 Comparison of loop D between different human AQPs.....**185**

1 Introduction

The aquaporin (AQP) protein family is comprised of integral membrane proteins, found in all phylogenetic kingdoms, which facilitate the bidirectional movement of water across biological membranes by osmosis. There are up to 13 mammalian AQPs (depending on the mammal in question), which are found in most tissues (see Figure 1-1), with physiological functions ranging from the regulation of renal water balance and reabsorption [1], brain fluid homeostasis [2], triglyceride cycling between adipocytes and the liver [3] and structural integrity of the eye lens [4]. Because of this, understanding AQP function is crucial for the study of healthy ageing as well as the onset of many disease states such as brain swelling following stroke or head injury [5], nephrogenic diabetes insipidus [6, 7], cataracts [8], obesity [9], cancer cell proliferation and migration [10] and tumour angiogenesis [11].

For many years it was assumed that biological membranes are freely permeable to the osmotic movement of water. However, biophysical measurements of the water permeabilities of erythrocyte (red blood cell) and kidney tubule membranes demonstrated that different cell types can have very different membrane permeabilities [12]. Since the unequivocal determination of the structure of biological membranes in the 1970s by Engelman's X-ray diffraction experiments [13], culminating in the fluid-mosaic model of Singer and Nicholson [14], it was clear that osmotic movement of water across lipid bilayers could not explain the differences in membrane permeabilities between different cell types.

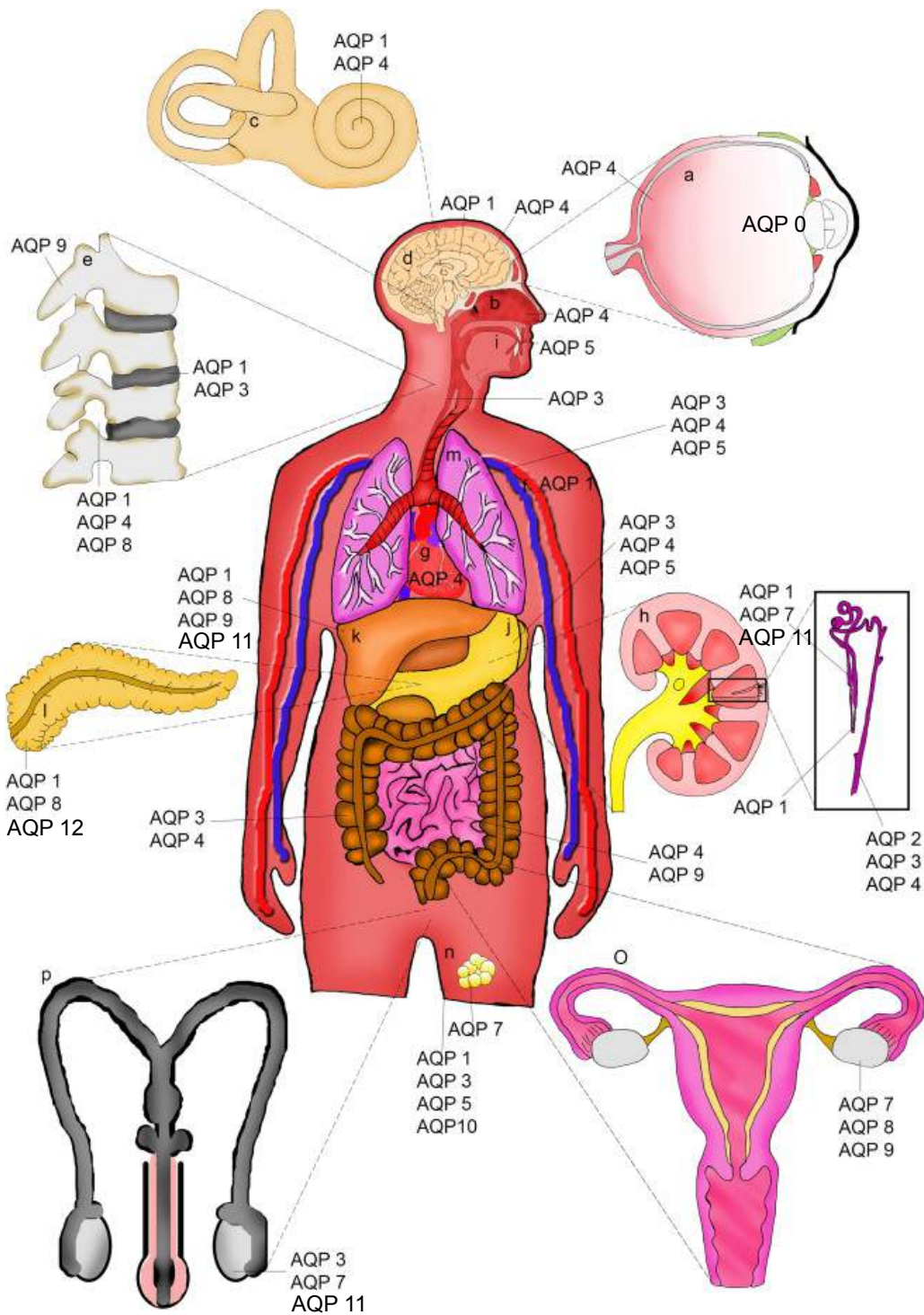


Figure 1-1 Distribution of AQP expression throughout the human body. Letters denote: a) Retina; b) Olfactory epithelium; c) Inner ear; d) Brain; e) Spinal cord; f) Blood vessels; g) Heart; h) Kidney; i) Salivary glands; j) Gastrointestinal tract; k) Liver; l) Pancreas; m) Lungs; n) Fat, Skin; o) Female reproductive tract; p) Male reproductive system [15].

The concept of a membrane water pore was developed to explain these permeability differences: if some cells contained molecules that spanned the membrane and allowed water to pass through unimpeded by interactions with membrane lipids, this might explain the different rates of water passage across different cellular membranes [16]. Additionally, if the level of expression of these molecules could vary, the permeabilities of different membranes could form a continuous spectrum, depending on the density of pores in the membrane. The existence of a water channel protein was first demonstrated conclusively by Gheorghe Benga's work using NMR to measure the water permeability of red blood cell membranes [17] and the molecular identity of this water channel protein was elucidated in 1992 by Preston and Agre [18], for which Peter Agre was jointly awarded the 2003 Nobel Prize in Chemistry. This protein was subsequently named aquaporin 1 (AQP1).

Thirteen mammalian AQPs have been discovered to date (AQPs 0-12); they range in size (before post-translational modification) from 27 kDa (AQP8) to 37 kDa (AQP7) and, for those proteins for which single channel water permeability has been quantified, have a 100-fold range in water permeability. A sub-set of the AQPs also function as channels for glycerol (and other small neutral solutes) and are referred to as (aqua)glyceroporins (GLPs). In humans, these are AQPs 3, 7, 9 and 10. The permeability properties of the mammalian AQPs are summarized in Table 1-1, and a sequence alignment is presented in Figure 1-2.

Table 1-1 – Water, glycerol, urea and ammonia (NH₃) permeabilities of known mammalian AQPs. *Quantitative water permeability is per AQP channel i.e. after subtraction of the basal permeability of the expression membrane and normalized to the number of AQP molecules. Expression systems: X – Xenopus oocytes, PL – proteoliposomes, M – mammalian cells, V – vesicles derived from membrane fragmentation of AQP-expressing mammalian cells, Y – ammonia transport deficient yeast. . *estimated from membrane fragment vesicle water permeability relative to AQP1-containing vesicles and relative expression level. **These data have not been independently replicated.*

AQP	Single channel water permeability ($\times 10^{-14} \text{ cm}^3 \text{ s}^{-1}$)	Glycerol permeability	Urea permeability	Ammonia permeability
AQP0	0.25 [19]; gated by CaM [20]; X, PL	No [19]; X	No [21]; X	No [22]; X
AQP1	6.0 [19]; X	No [19]; X	No [23]; X	No [23]; X
AQP2	3.3 [19]; X	No [19]; X	No [21]; X	No [22]; X
AQP3	2.1 [19]; X	Yes [19]; X	Controversial [21, 23-25]; X	Yes [22, 23]; X
AQP4	24 [19]; X	No [19]; X	No [26]; X	No [22]; X
AQP5	5.0 [19]; X	No [19]; X	No [27]; X	No [22]; X
AQP6	Low pH and Hg ²⁺ induce water permeability [28, 29]. Basal permeability either is very low [29, 30] or zero [31, 32]; X	Yes** [32]; X	Yes** [32]; X	Yes [22]; X
AQP7	Permeable [33]; no quantitative data; X	Yes [33]; X	Yes [33]; X	Yes [22]; X
AQP8	Permeable [34, 35]; no quantitative data; X, PL	No [34, 35]; X, PL	Controversial [34-36]; X, PL	Yes [23, 37]; X, Y
AQP9	Permeable [38]; no quantitative data; PL	Yes [23, 38]; X, PL	Yes [23, 38]; X, PL	Yes [23]; X
AQP10	Permeable [39]; no quantitative data; X	Yes [39]; X	Yes [39]; X	Unknown
AQP11	Permeable [40], ~2 [41]*; M, V	Yes** [42]; M	Unknown	Unknown
AQP12	Unknown	Unknown	Unknown	Unknown

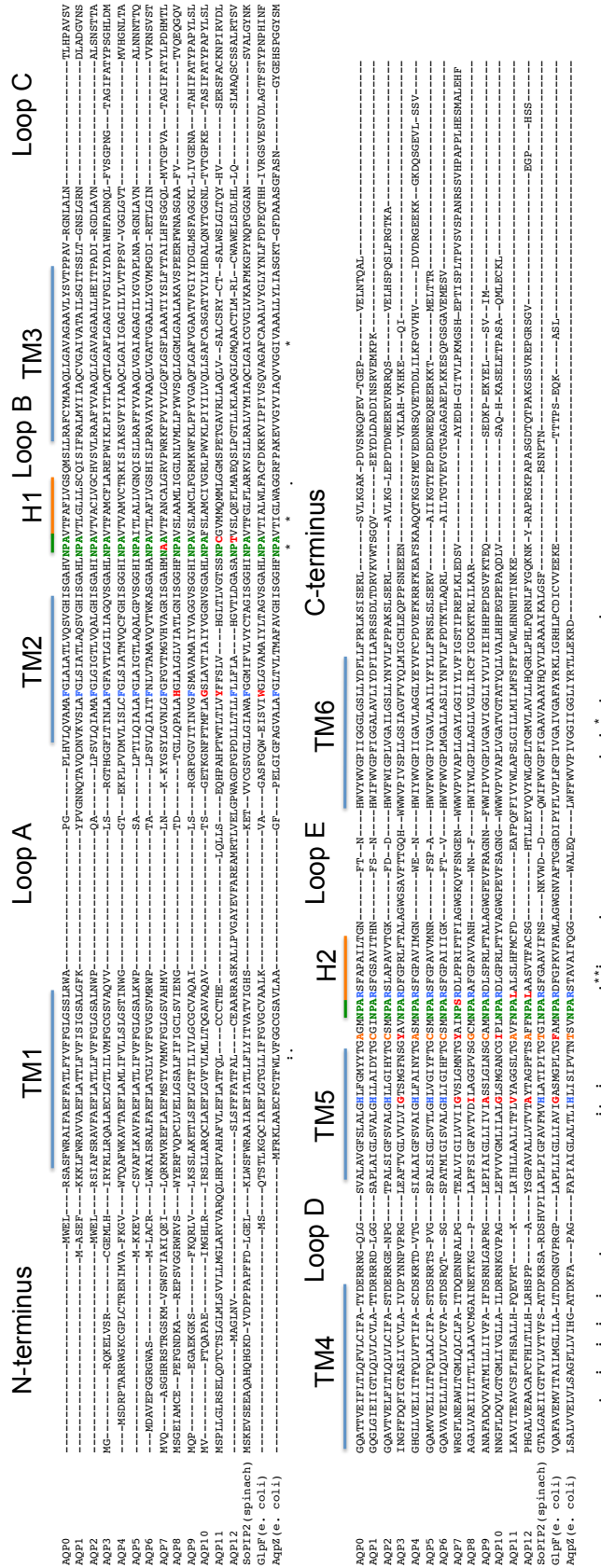


Figure 1-2 Sequence alignment of human AQPs, and bacterial and plant AQPs for comparison. NPA motifs are green, selectivity filter residues blue, and deviations from conservation red.

1.1 Structural biology of the AQP family

There is a large amount of medium-to-high-resolution structural data available for the AQP family (43 structures deposited in the Protein Data Bank for 11 different AQPs). These structures suggest that the AQPs share many common structural features. The AQP monomer is composed of six tilted transmembrane (TM) helices that surround a central cavity containing two helix-forming loops that enter and exit from the same side of the membrane (labelled as HH1 and HH2 in Figure 1-3 A). This central cavity is the pathway for water and solute transport. The two helical loops contain highly conserved asparagine-proline-alanine (NPA) motifs. Crystallography and molecular dynamics (MD) simulations suggest that the asparagine residues act, in concert with surrounding backbone carbonyl groups, to enable water transport by providing hydrogen bonds to water molecules [43], thereby lowering the free energy penalty (caused by breaking of water-water hydrogen bonds) of removing a water molecule from bulk solution. Recent biophysical experiments comparing AQPs with gramicidin and the potassium channel KcsA [44] suggest that the number of pore-lining hydrogen-bonding sites for water determines the channel water permeability. In addition to providing hydrogen-bonding sites, the asparagine residues help to orient the water molecules such that the hydrogen atoms point ‘outwards’ from the pore, creating a barrier to proton transport [45]. A recent sub-angstrom crystal structure of the *Pichia pastoris* AQY1 found overlapping water densities in the pore that, supported by MD simulations, suggested a correlated pairwise movement of water molecules through the extracellular end of the pore. This correlated motion may help to minimise water-water hydrogen bonds in this

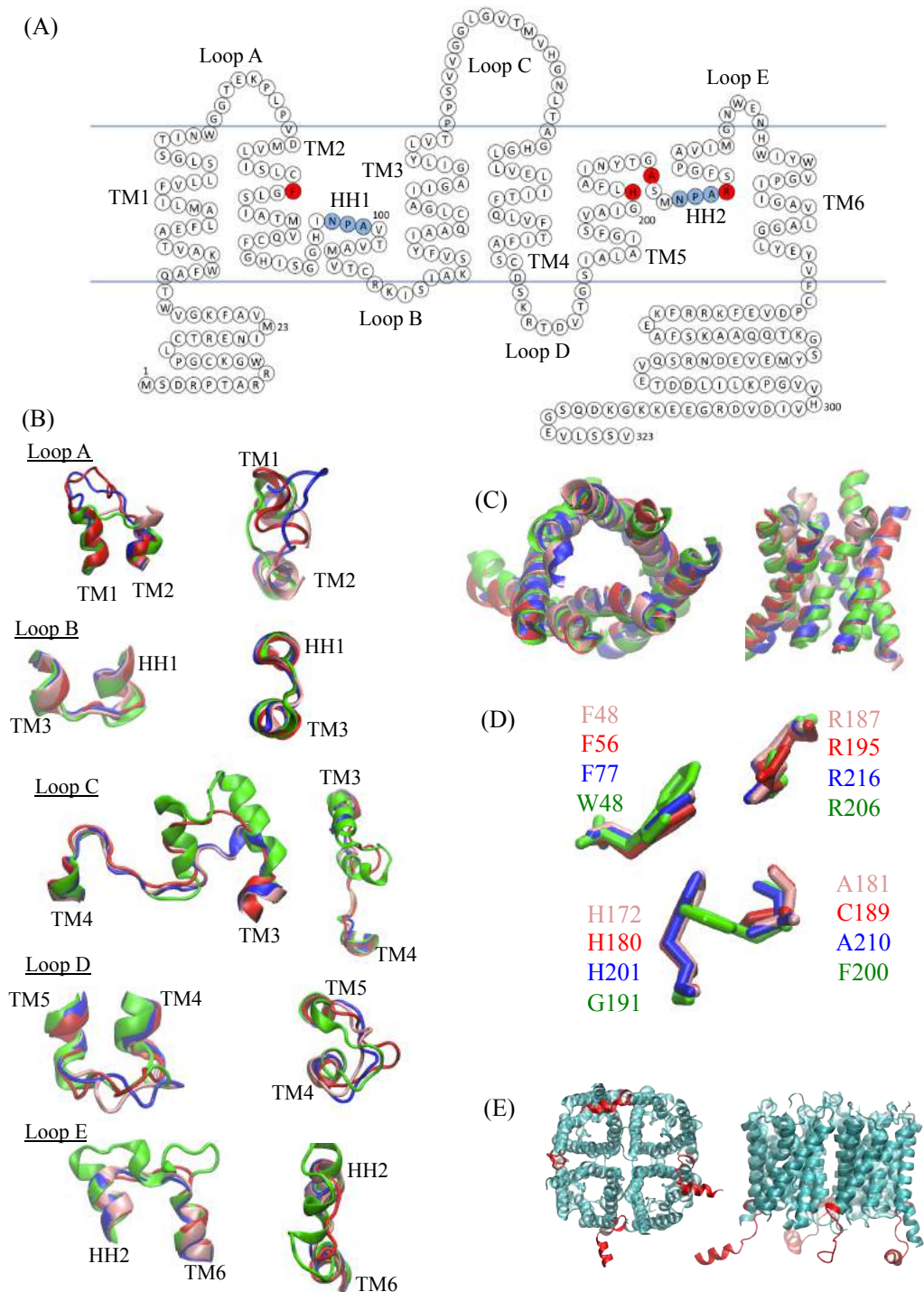


Figure 1-3 Structural biology of the AQP family. (A) Primary sequence and secondary structural motifs of the AQP family, exemplified by human AQP4 with NPA motifs (blue) and selectivity filter residues (red) highlighted; (B) Structural alignment of the soluble loops of human AQP1 (dark blue), human AQP4 (red), bovine AQP0 (pink) and *E. coli* GlpF (green) from x-ray crystal structures; (C) Structural alignment of the TM regions of human AQPs 1 and 4, bovine AQP0 and *E. coli* GlpF. Colours as in (B); (D) Structural alignment of amino acid residues of the Ar/R selectivity filter; (E) Crystal structure of human AQP2 with the C-terminal helix (red) in four different conformations.

region, providing a further barrier to proton permeation, without compromising water transport [43]. Crystallographic analysis of the *E. coli* GlpF (a GLP), suggested that the same asparagine residues also form hydrogen bonds with glycerol [46]. This is likely to be also true of other polar solutes that permeate GLPs.

AQPs have intracellular amino (N-) and carboxyl (C-) termini of varying lengths; AQP8 has a short C-terminus of 10-15 residues, whereas AQP4 has a large C-terminus consisting of ~70 residues. AQP11 has a large N-terminal tail of ~40 residues, whereas AQPs 1,2 and 5 have short N-termini of <10 residues. In contrast to the structural conservation of the TM domains of AQPs (see Figure 1-3 C), much less is known about the structure of the termini. This is because the majority of AQP crystal structures are obtained using constructs in which the N- and C-terminal tails of the protein have been truncated due to the difficulty of obtaining well-diffracting crystals using full-length AQP molecules [47]. This suggests an inherent structural flexibility in these regions of AQP molecules and indeed a recent X-ray structure of AQP2, which included ~20 residues of the (truncated) C-terminal tail, found this fragment of the C-terminus in four strikingly different conformations in each of the four AQP2 monomers within the tetrameric unit cell [48] (see Figure 1-3 E).

AQPs retain a homotetrameric quaternary structure despite wide variety in the permeability properties, subcellular localization and trafficking responses between different members of the AQP family. Early biochemical work, using carboxyl-amine fusion dimers consisting of one wild-type unit and one unit

missing the cysteine residue required for mercurial inhibition, showed that the functional units of AQPs are the monomers [49] and numerous molecular dynamics simulation studies support this [50]. Recent work on GlpF reconstituted into liposomes at low density has suggested that isolated AQP monomers may be equally capable of facilitating water transport as those incorporated into a tetramer [44]. Therefore it is not clear why AQPs retain this oligomeric structure. Data presented in chapter 5 shows a correlation between AQP4 tetramerization and a regulatory subcellular relocalization response. Regulation of AQP permeability and subcellular localization by the formation of heterotetramers has been demonstrated for some plant AQPs [51]. A fifth, central pore is formed at the fourfold axis of the tetramer. Several functional roles have been suggested for this pore, including carbon dioxide [52] and cation permeation [53]. Some biochemical studies have suggested that tetramers formed by GLPs have reduced stability compared to tetramers formed by AQPs with strict water selectivity [54, 55], although it is not clear whether there is any functional relevance to this correlation. Furthermore, data presented in chapter 5 suggests that the human GLPs AQP9 and AQP10 are fully tetrameric, so this correlation may not hold for the entire GLP subfamily.

1.2 The principles of AQP solute selectivity remain to be established

All AQPs (with the possible exception of AQP12, which has yet to be characterized) transport water (Table 1), whilst some also transport glycerol. The glycerol permeable GLPs (e.g. human AQPs 3, 7, 9 and 10) are also permeable to urea. The urea permeability of AQP3 is controversial, with some studies

reporting urea transport and others no transport [21, 23-25]. This may be due to methodological differences, and is discussed in detail in section 3.2.1.

Of the mammalian GLPs AQP3, AQP7, and AQP9 are also permeable to ammonia. AQP8 is the only glycerol impermeable mammalian AQP that is permeable to ammonia. The ammonia permeability of the most recently discovered member of the GLP group, AQP10, is still unknown.

AQP11 and AQP12 are the most recently discovered members of the AQP family [56, 57]; due to this and their localisation to intracellular membranes, there have been minimal functional studies reported for AQP11 and AQP12. There is one report that AQP11 increased the glycerol permeability of an adipocyte cell line [42], but this permeability of AQP11 has yet to be replicated.

The size exclusion model of AQP selectivity posits a correlation between these different permeabilities and the channel cross-sectional area at its narrowest point, known as the selectivity filter. This model is based primarily on *in silico* experiments using MD simulations and analysis of X-ray crystal structures, but only one *in vitro* set of experiments, using site-directed mutagenesis (SDM) to alter the selectivity of AQP1 [58]; it is therefore unclear whether this model is broadly applicable to the AQP family as a whole. A conserved arginine residue (in the second helical loop directly after the NPA motif) forms part of the channel constriction known as the aromatic/arginine (ar/R) selectivity filter (see Figure 1-3). *In silico* and crystallographic analyses of AQP1 [59], AQP4 [60] and AQPZ [61] have suggested that fluctuations of this arginine residue could

modulate channel water permeability, and *in vitro* evidence of this for human AQP4 is presented in chapter 4. In water-selective AQPs, the other components of this filter are a phenylalanine in the top half of the pore-facing side of TM helix 2 (TM2) and a histidine in a similar position in TM5 (see Figure 1-3D). In glycerol and urea permeable AQPs, this histidine is replaced by a small amino acid residue such as glycine (AQP3, -7, -10) or alanine (AQP9), although if the histidine is mutated to alanine in AQP1 it does not become a glycerol channel. In chapter 4, data is presented which suggests that the same mutation to AQP4 renders it glycerol permeable, suggesting that the details of solute exclusion may differ between family members.

If both aromatic members of the filter (histidine and phenylalanine) are mutated to alanine, AQP1 functions as a urea channel and to a lesser extent as a glycerol channel [58]. Based on this observation and molecular simulations of AQP1 and the *E. coli* GLP, GlpF [58, 62], it has been suggested that the cross-sectional area of the pore at the ar/R region determines AQP selectivity for neutral polar solutes. Additionally, based on crystallographic analysis of GlpF and the bacterial water-selective AQP, AQPZ, it has been suggested that the positioning of the ar/R residues by the surrounding unstructured loops has a role in determining the channel size [63]. In AQP8, the only glycerol-impermeable, ammonia-permeable mammalian AQP, the third member of the filter is likely an isoleucine residue (based on sequence alignment), which is considerably larger than alanine or glycine. Overall, current thinking on solute selectivity suggests that the aromatic residues of the ar/R filter are important for solute exclusion in the water selective AQPs, but further molecular factors may be involved in mediating solute selectivity.

1.3 Physiological water transport by AQPs

AQP-mediated water transport around the body is important for a variety of physiological processes in several different organs.

1.3.1 Central nervous system (CNS)

The predominant AQPs found in the central nervous system are AQP4 in glial cells, particularly those in direct contact with capillaries and the pia mater [64], AQP1 in the choroid plexus epithelium (which is thought to be responsible for the secretion of cerebrospinal fluid, CSF) [65], and AQP9 in glial cells and catecholaminergic (adrenergic, noradrenergic and dopaminergic) neurons [66]. Localization of AQP4 in astrocytes is polarized to the foot processes that make contact with endothelial cells, forming the blood-brain barrier, and areas of astrocyte membranes that encapsulate neuronal synapses [2] (see Figure 1-4). The localization to foot processes is mediated by a physical interaction with the dystrophin complex via the protein α -syntrophin, which binds to the three C-terminal residues (SSV) of AQP4 [67]. The density of AQP4 in these regions is very high, with AQP4 molecules occupying up to 50% of the total surface area of these membranes [64].

AQP4 knockout animals have provided some indication of the physiological roles and pathophysiological complications of AQP4 in the CNS.

AQP4 $-/-$ mice had a 28% increase in brain extracellular volume [68] and increased brain water content by ~1% [69], and glial-conditional deletion of AQP4 in mice caused a 31% reduction in brain water uptake after hypo-osmotic stress [70], suggesting that the astrocytic layer ensheathing the brain vasculature is rate-limiting for water movement and that AQP4 is important either directly or indirectly for the control of brain water content and extracellular volume.

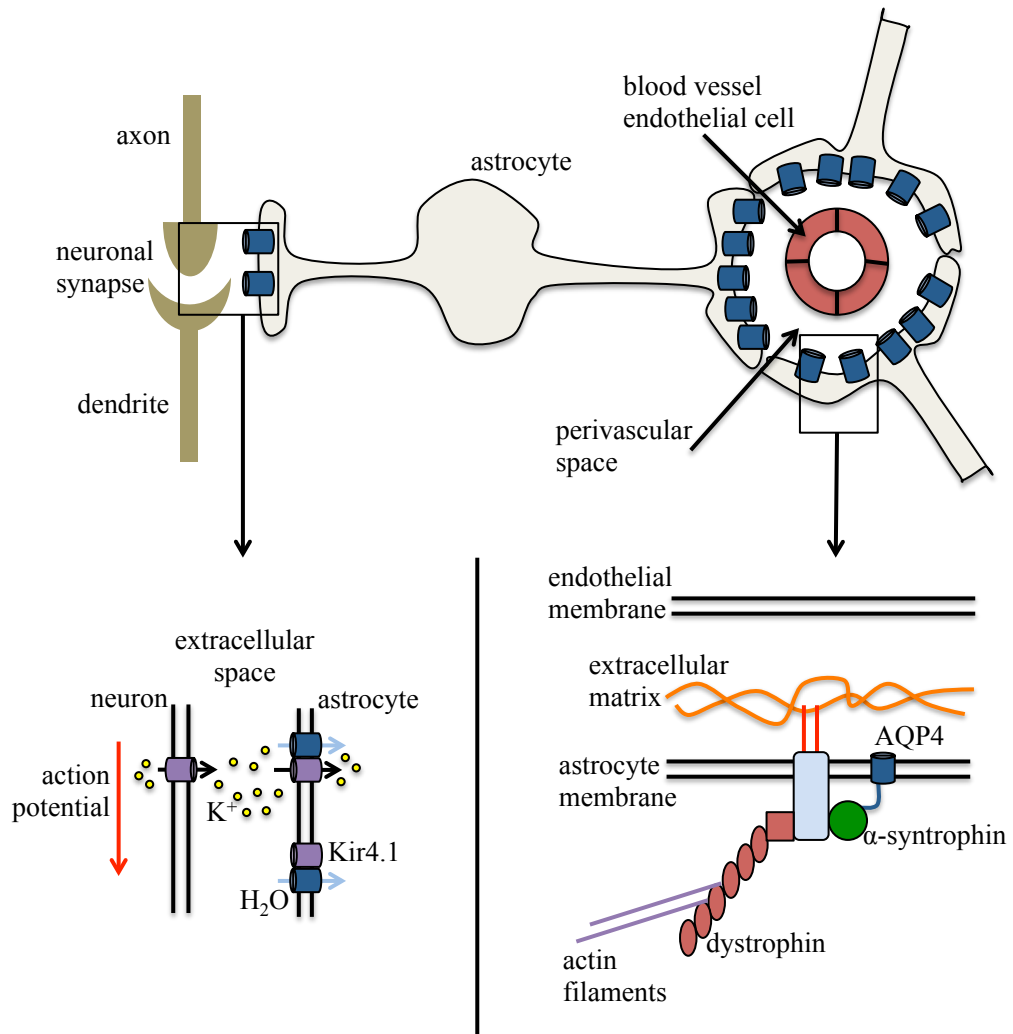


Figure 1-4 Localization of AQP4 in the central nervous system in support of brain water homeostasis, waste clearance and potassium handling. Blue cylinders represent AQP4. Purple cylinders represent potassium channels and yellow circles potassium ions. Dystrophin-associated protein complex schematic adapted from Fairclough et al [71]

Recent work has suggested that there is a paravascular network of spaces that allow the recycling of CSF along spaces around arteries, into the brain parenchyma and to spaces surrounding veins and that this bulk flow impacts on water and waste clearance from the brain. AQP4 $-/-$ mice had reduced fluorescent tracer flow along these routes and increased build-up of injected amyloid- β (build-up and plaques of which are thought to responsible for the development of Alzheimer's disease) [72], suggesting that AQP4-mediated transcellular water flow across astrocyte membranes is crucial for brain homeostasis.

AQP4 appears to have an indirect role in potassium homeostasis of the brain extracellular fluid during and following synaptic activity. Neuronal depolarization involves the movement of K^+ ions from the inside to the outside of neurons, and any increase of extracellular K^+ concentration ($[K^+]_o$) can cause hyperexcitability and reduce the efficacy of synaptic transmission. To prevent this, astrocytes perform a regulatory function whereby excess K^+ is taken up, correlated with a reduction of the extracellular volume by up to 30% and swelling of the astrocyte [73], which is impaired in AQP4 $-/-$ mice [74]. This swelling suggests coupled movement of K^+ and water. AQP4 $-/-$ mouse brain slices had smaller stimulus-induced $[K^+]_o$ increases but slower $[K^+]_o$ clearance kinetics compared to wild-type mice [75]. Mathematical modelling explicitly accounting for intracellular K^+ diffusion suggested that water permeability of the perisynaptic astrocyte membrane can control the rate of K^+ uptake by allowing volume changes that modulate $[K^+]_o$ on either side of the astrocyte membrane [76]. A link between K^+ uptake and AQP4 is further suggested by the observation that the AQP4-mediated water permeability of primary rat astrocytes

was increased by 46% upon increase of $[K^+]_o$ from 2.5 mM to 10 mM for 1 minute and by 55% after 5 minutes [77]. Data presented in chapter 3 suggests that this response may be mediated by relocalization of AQP4 to the plasma membrane rather than the gating response suggested in this study. Furthermore, the inward rectifying potassium channel, Kir4.1, forms part of the same dystrophin-associated protein complex as AQP4 in glial cells [78]. Elevated $[K^+]_o$ is associated with the pathophysiology of epilepsy [79]. In excised sclerotic hippocampal tissue from temporal lobe epilepsy (TLE) patients, AQP4 expression was elevated at the transcript and protein levels, but decreased dystrophin expression suggested that AQP4 could have lost its polarized expression [80]. In a rat model of epilepsy, loss of AQP4 polarization, and a mild increase in AQP4 expression, preceded the onset of seizures [81]. Furthermore, three single nucleotide polymorphisms (SNPs) in non-coding regions of the AQP4 gene were found to be associated with temporal lobe epilepsy in humans [82]. The localization of AQP4 in the CNS is shown schematically in Figure 1-4.

Although the data discussed here demonstrate a key requirement for AQP4 in brain homeostatic mechanisms, there also appears to be a disadvantage to AQP4 expression in the brain: reduction of AQP4 expression was protective against cytotoxic edema formation in various models of pathology including water intoxication and middle cerebral artery occlusion (a stroke model) in AQP4 $-/-$ mice [83], carotid artery ligation and hypoxia in AQP4 siRNA-treated piglets [84], transient retinal ischemia in AQP4 $-/-$ mice [85] and traumatic brain injury (TBI) in rats treated with intravenous anti-AQP4 antibodies [86, 87].

Furthermore, glial specific overexpression of AQP4 in transgenic mice

accelerated cytotoxic swelling and intracranial pressure (ICP) elevation after water intoxication compared to wild-type and AQP4 $-/-$ controls [88]. Disruption of AQP4 localization to perivascular endfeet by deletion of the dystrophin [89] or α -syntrophin [90, 91] genes in mice had the same protective effect. Taken together these data identify AQP4 as a clear molecular target for intervention into the various devastating pathologies, including stroke and traumatic brain injury, which involve cytotoxic cerebral edema. AQP4 could be modulated in several ways: direct inhibition of the water channel, protein expression levels or subcellular relocalization. In chapter 3, data is presented suggesting AQP4 subcellular localization is dynamically regulated in response to changes in extracellular tonicity, which is a key driver of cytotoxic edema via misregulation of Na^+ , K^+ and Cl^- homeostasis [92].

The role of AQP1 in the choroid plexus appears to be to provide the high water permeability required for secretion of CSF, and water permeability may be rate limiting in this process as AQP1 knockout mice had a 25% reduction in CSF secretion and 56% reduction in intracranial pressure [65]. There is some controversial evidence that AQP1 may act as a cGMP-gated cation channel (see section 1.4.6). The secretion of CSF primarily involves active transport of Na^+ , K^+ , Cl^- and HCO_3^- across the choroid plexus epithelium driving the osmotic movement of water [93], so it is possible that AQP1 could be performing a dual role in CSF secretion. Recent evidence using magnetic resonance imaging to measure influx of spin-labelled H_2O into the CSF of live AQP1 $-/-$ and AQP4 $-/-$ mice suggests that AQP4 is more important for CSF secretion than AQP1 [94].

1.3.2 Kidneys

AQPs 1, 2, 3, 4, 6, 7, 8 and 11 are expressed in the mammalian kidney [1]. AQPs 1 and 7 are thought to contribute to the renal water absorption mechanism by providing high water permeability to the descending limb of the loop of Henlé in order to return water to the blood and set up the osmotic gradient that forms the counter current multiplier mechanism [95]. AQP2-mediated water permeability is rate limiting for water reabsorption in the collecting duct, and dynamic regulation of the subcellular localization of AQP2 is used to modulate water reabsorption via arg8-vasopressin (AVP) signalling stimulated by hypovolaemia (low blood volume) and hypernatraemia (high blood sodium) [96]. AQPs 3 and 4 are thought to provide a route back to the blood for water reabsorbed in the collecting duct via AQP2.

1.4 Solute transport by AQPs

1.4.1 Glycerol transport

The movement of glycerol around the body is predominantly thought to include glycerol release from fat tissue through AQPs 7 and 10, entry into the liver through AQP9, reabsorption in the kidney through AQP7 and movement in the skin through AQP3. The contributions of AQPs to mammalian glycerol homeostasis are summarized in Figure 1-5.

1.4.1.1 AQP7 glycerol transport

AQP7 is expressed in adipose tissue in adipocytes [97] and capillary endothelia [98]. Upon hypoglycaemia, triglycerides are broken down within adipocytes to glycerol and free fatty acids [99]. Adrenaline [97] and noradrenaline [100],

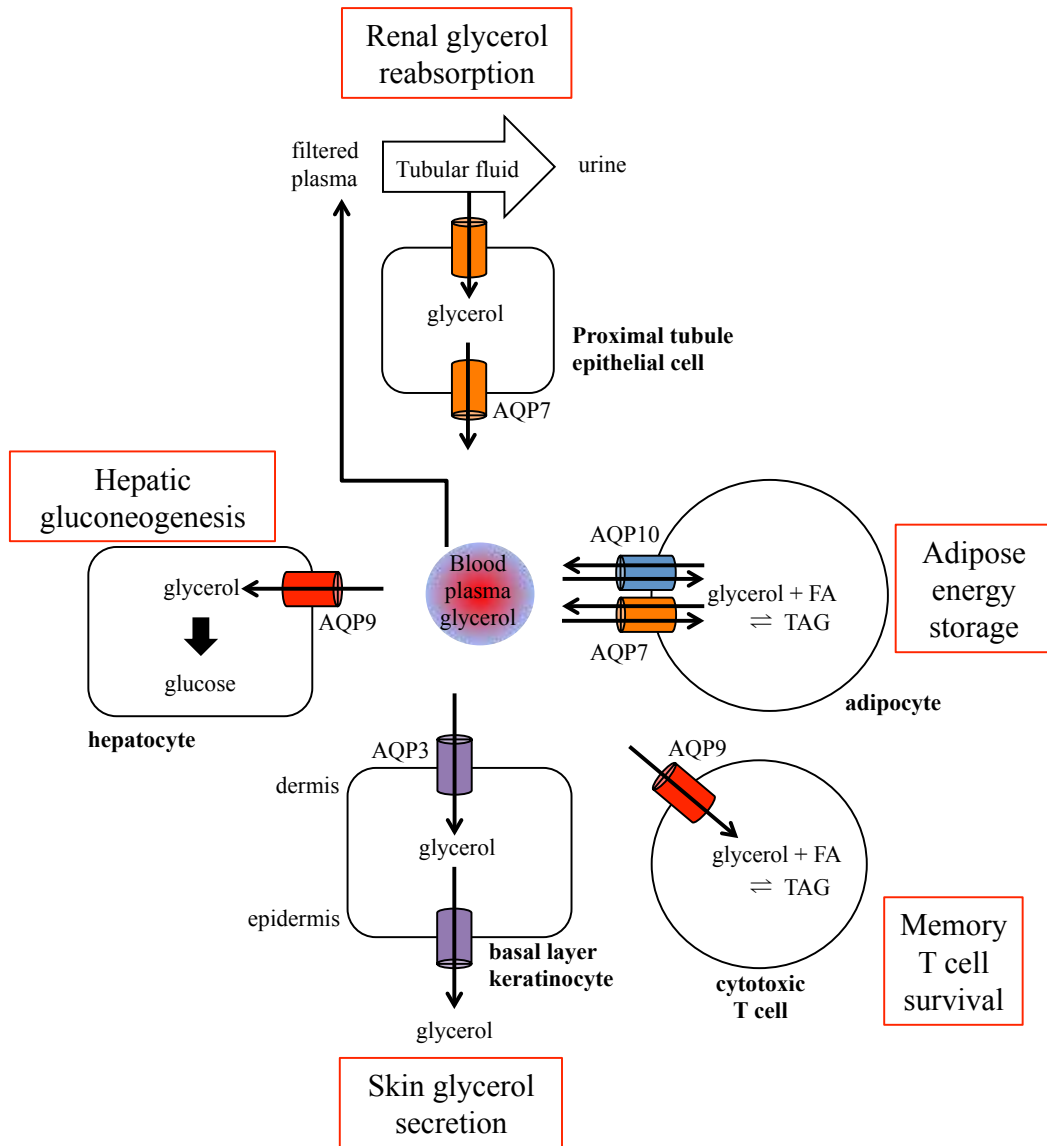


Figure 1-5 Glycerol permeable AQPs contribute to mammalian glycerol physiology and homeostasis.

which are involved in activation of lipolysis, were reported to cause subcellular relocalization of AQP7 to the plasma membrane and lipid droplets of adipocytes. Glycerol liberated from triglyceride storage is released from adipocytes [101] into the blood and this was reduced threefold in AQP7 $-/-$ mice [102]. Plasma glycerol levels in AQP7 $-/-$ mice before and after adrenergic agonist stimulation were reduced and adrenaline-induced glycerol secretion by cultured mouse adipocytes was reduced approximately two-fold [103]. These results suggest that the major pathway for glycerol efflux from adipocytes after lipolysis is via AQP7.

AQP7 $-/-$ mice have enlarged adipocytes and obesity in adulthood [102]. A loss of function mutation in the human AQP7 gene has been discovered (G264V) but was not correlated with obesity [104]. This may be due to the presence of AQP10 in human adipocyte membranes, which was found to contribute ~50% of the water and glycerol permeability of human adipocyte plasma membrane vesicles [105]. Mouse AQP10 is a pseudogene [106] which probably explains the differential effects of loss of AQP7 function between mice and humans.

Glycerol is almost completely reabsorbed by the kidneys [107] (unless it is raised above ~0.3 mM[108]), suggesting the existence of a glycerol reabsorption pathway. AQP7 is expressed in the proximal tubule of the kidney. AQP7 $-/-$ mice showed marked glyceroluria in comparison to wild type (~400-fold increase in urine glycerol) [109]. Human children homozygous for the AQP7 G264V mutant were found to have hyperglyceroluria, with a ~1000-fold increase in urine glycerol compared to heterozygous familial controls [110]. The G264V mutant

has been shown to have no activity as a glycerol or water channel in *Xenopus* oocytes [104], although plasma membrane expression was not verified in this study so that it could not differentiate between a non-functional channel and an incorrectly localised channel. The mutation disrupts a conserved GxxxG motif in TM6. These motifs are important for TM helix-helix packing interactions, allowing close contact between backbone atoms of two helices of an interacting pair [111]. Regardless of the loss of function mechanism of G264V, these data strongly suggest that AQP7 is the TM glycerol reabsorption pathway in the renal proximal tubule.

1.4.1.2 AQP9 glycerol transport

AQP9 is expressed in the liver [112], primarily in hepatocytes [113]. Upon fasting, glycerol released into the plasma from adipocytes is taken up by hepatocytes and used as a substrate for gluconeogenesis [114].

In rats, AQP9 protein expression was increased up to 20-fold after 24-96 hours fasting [38]. In mice, AQP9 expression measured in purified hepatocyte plasma membrane vesicles increased 10-fold after 18 hours fasting. This increase was accompanied by a two-fold increase in hepatocyte plasma membrane glycerol permeability, which was reversed by addition of phloretin (an apple polyphenol that inhibits AQP9). The increase was abolished in AQP9 *-/-* mice [115]. Fasted AQP9 *-/-* mice had elevated plasma glycerol compared to wild-type [115, 116]. In addition, plasma glucose concentration was decreased [116], indicating a gluconeogenic deficiency. This data suggests a role for AQP9-mediated glycerol uptake by hepatocytes during fasting-induced hypoglycaemia.

CD8⁺ (cytotoxic) T cells are white blood cells that facilitate the destruction of infected or otherwise damaged cells. In mouse T-cells, AQP9 expression was upregulated post-infection, allowing cells to import glycerol for triglyceride synthesis. AQP9 ^{-/-} cells had reduced long-term survival compared to ^{+/+} cells and the long-term survival of the ^{+/+} cells could be inhibited by phloretin [117]. This suggests that AQP9 expression can act as a metabolic switch, enabling long-term survival of T cells by enabling glycerol import for triglyceride synthesis to build up an energetic reserve, allowing cell survival in nutrient poor conditions.

1.4.1.3 AQP3 glycerol transport

AQP3 is expressed in the skin in keratinocytes below the stratum corneum (SC) [118]. The ability of the epidermis to maintain hydration is impaired in AQP3 ^{-/-} mice. In dry conditions, AQP3 ^{-/-} mice showed comparable (reduced) levels of SC hydration to wild-type mice, whereas at normal humidity, SC hydration was lower in the AQP3 ^{-/-} mice [119]. Elevated humidity (which prevents water loss via evaporation) did not correct the deficiency, which suggests that the primary role of AQP3 in skin hydration is not to provide water to replace that lost by evaporation.

SC glycerol concentration in AQP3 ^{-/-} mice was reduced to ~40% of that of wild-type, with no significant difference in the levels of other osmolytes (ions, glucose, urea, lactate and free amino acids) [120]. Glycerol acts as a humectant (a ‘water-retaining’ osmolyte), which may be the mechanism by which it maintains skin hydration. It has also been suggested that glycerol may prevent SC water loss by inhibiting the phase transition of intercellular lipids from the liquid crystalline to the solid phase [121]. The rate of transport of glycerol from blood to the SC was reduced in AQP3 ^{-/-} mice resulting in reduced lipid

biosynthesis [122]. This suggests a further role for glycerol in maintaining skin hydration by allowing the maintenance of the SC lipid barrier. Furthermore, topical or systemic administration of glycerol was found to correct the skin deficiencies in AQP3 $-/-$ mice [122].

1.4.2 Urea transport

Urea is produced in the liver (as a non-toxic carrier of waste nitrogen) from ammonia, which is a neurotoxic product of protein degradation. Ammonia causes cell death of astrocytes by stimulating the mitochondrial permeability transition [123]. An adult human excretes about 25 g/day of urea in the urine, and urea transport in the kidney is vital for the urinary concentrating mechanism [124]. The physiological roles of urea transport by AQPs are less clear than those of water and glycerol transport.

1.4.2.1 Which mammalian AQPs are urea channels?

AQPs 7 [33], 9 [125] and 10 [39] have been shown to be urea permeable and there is a consensus in the literature on the urea permeability of these AQPs. There is conflicting evidence in the literature on whether AQPs 3 and 8 are urea channels.

Early work on AQP3 suggested that rat AQP3 was urea permeable, with expression of AQP3 in *Xenopus* oocytes increasing urea uptake twofold after 30 minute incubations of oocytes with radiolabelled urea [126] or threefold in oocyte swelling assays [24]. Further studies on rat AQP3 found no urea transport using similar oocyte volumetric techniques [21, 23]. These studies differed in that the former used 165 mM urea whereas the latter two used 20 mM urea. It

may be that AQP3 urea transport is so slow that at 20 mM it does not induce large enough volume changes to be measured on the timescale of an oocyte swelling experiment (~1 min), or that the transport is non-linear, although this seems unlikely given the linear nature of water and glycerol transport by AQP3 [127]. In one study, human AQP3 was used as a positive control for AQP urea permeability. 1 mM of urea was added to AQP3-expressing oocytes and after a 10 minute incubation, the oocytes had an intracellular urea concentration of ~75 μ M (assuming an oocyte volume of 1 μ L) [25]. This is ~10% of the expected equilibrium value, and the fact that it is still so far from equilibrium even after 10 minutes suggests that urea transport through AQP3, whilst non-zero, is very slow. This may explain the different results between short (typically ~1 min) volumetric experiments and the longer timescale radiolabelled solute uptake experiments.

Early work on mouse AQP8 suggested that it was urea permeable [36], whereas rat AQP8 was not [35], both using radiolabelled solute uptake measurements in *Xenopus* oocytes. Work on purified rat, mouse and human AQP8 in proteoliposomes suggested that neither rat nor human AQP8 were urea permeable [34]. This study did not report mouse urea permeability due to liposome swelling discrepancies, probably caused by the ionic detergent required to solubilize mouse AQP8. There is considerable interspecies amino acid sequence variability for AQP8 (e.g. 74% identity between human and mouse AQP8, c.f. 94% for AQP1 and 93% for AQP4). Interestingly, one difference between human and mouse AQP8 is a residue that is predicted to be pore-lining (based on a homology model to bovine AQP0 [34]) and situated at the ar/R filter,

G207 (in human; A205 in mouse). The idea of species-specific differences in permeability of AQP8 is intriguing, but studies performed in parallel in the same experimental system are required to validate this.

1.4.2.2 Urea transport by AQP9

AQP9 is a urea channel in the liver expressed in hepatocytes at the sinusoidal surface. Urea permeability measurements (using stopped-flow light scattering to measure vesicle volume) performed on mouse hepatocyte plasma membrane vesicles of AQP9 *-/-* and urea transporter type A1/3 (UT-A1/3) *-/-* mice showed that AQP9 contributes ~30% to mouse hepatocyte membrane permeability and a member(s) of the UT-A family contributes ~40% [128]. However, AQP9 *-/-* mice did not demonstrate any deficiency in urea clearance from hepatocytes in a state that promotes elevated hepatic urea production (high protein diet), suggesting that AQP9 and the UT proteins in concert form a urea transport system with built-in redundancy.

1.4.3 Ammonia transport

Ammonia is produced as a by-product of protein breakdown and quickly converted to urea via the hepatic urea cycle to prevent ammonia neurotoxicity. It is important for control of acid-base balance in the kidney, where ammonia synthesis and excretion are tightly regulated and change in response to acidosis or alkalosis [129]. Members of the GLP subfamily, AQPs 3 [23], 7 [22] and 9 [23], have been reported to be permeable to ammonia, as has AQP8 [23, 130]. There is also evidence of ammonia permeability of AQPs 1, 6 and 7 using microelectrode measurements of oocyte surface pH[22]. The physiological relevance of ammonia permeability of AQPs is unclear.

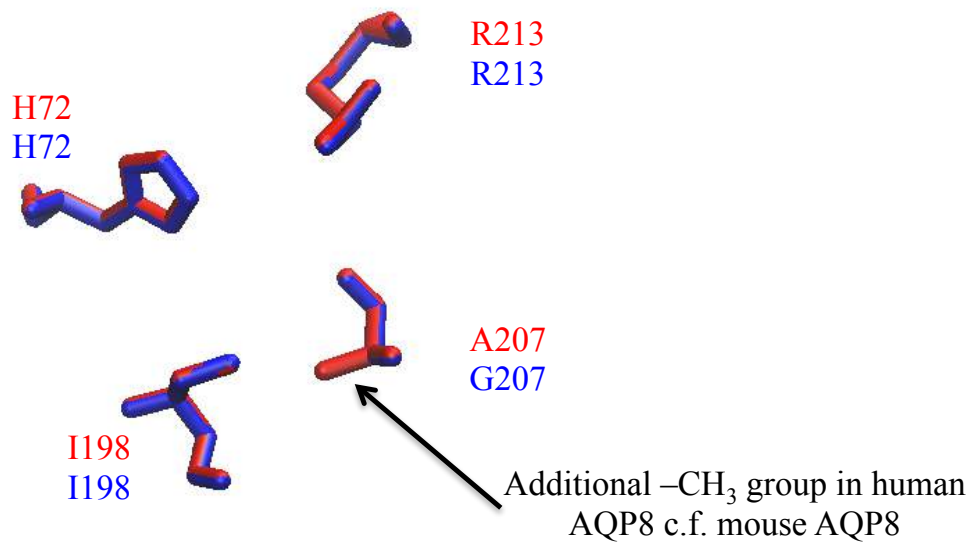


Figure 1-6 Predicted selectivity filter residues of AQP8 from *homo sapiens* (red) and *mus musculus* (blue) based on sequence alignment and homology modelling to bovine AQP0.

AQP8 *-/-* mice have only the very mild phenotypic abnormality of slight hypertriglyceridaemia after three weeks on a high (50%) fat diet [131]. AQP8 is expressed in the inner mitochondrial membrane of hepatocytes [132] and increased the transport of an ammonia analogue into AQP8-expressing *S. cerevisiae* and rat hepatocyte mitochondria by three-fold. However, AQP8 *-/-* mice do not show any impairment in ammonia clearance under physiological conditions or when chronically or acutely loaded with ammonia [133]. This suggests a secondary (non-AQP) pathway for ammonia, which either provides the majority of ammonia permeability in these tissues, or is upregulated in ammonia-permeable AQP knockouts. The proteins associated with the Rhesus (Rh) blood group system have been shown to function as ammonia channels [134]. Several of these are expressed in the liver [135] (RhB and RhC) and the kidneys (again RhB and RhC), where ammonia has an important role in acid-base balance [136]. Rh *-/-* mice have been generated, however these studies have focused on the erythrocytic Rh proteins [137, 138]. Comprehensive phenotype analyses of RhB and RhC *-/-* organisms and double AQP/Rh knockouts could provide an answer. Knockdown of AQP8 in primary rat hepatocytes by ~80% reduced ammonium chloride-induced ureagenesis by 30% and abolished glucagon-stimulated increases in ureagenesis [139]. AQP8 knockdown in a human proximal tubule cell line decreased the rate of ammonia excretion by 31% at pH 7.4 and by 90% at pH 6.9 [140], suggesting that AQP8 ammonia permeability might be required for renal ammonia excretion and be involved in the renal adaptive response to acidosis. Furthermore, acid-induced downregulation of AQP8 by 30% in primary rat hepatocytes was correlated with a 31% reduction in hepatocyte ureagenesis, and AQP8 downregulation was

correlated with reduced liver urea content in rats subjected to seven days of acidosis [141]. These data support the idea of a physiological role for AQP8 in either plasma membrane diffusion of ammonia, mitochondrial ammonia transport, or both in support of renal and hepatic ammonia handling.

AQPs 7 and 10 are present in adipocytes. It has been shown in humans that during intense exercise, adipose tissue removes ammonia from the plasma and develops an increased glutamine/glutamate ratio [142]. This suggests incorporation of ammonia into glutamine through glutamine synthase (which catalyses the reaction: $\text{glutamate} + \text{ATP} + \text{NH}_3 \rightarrow \text{glutamine} + \text{ADP} + \text{phosphate}$) in adipocytes as a secondary detoxification pathway in support of the hepatic urea cycle at times of elevated plasma ammonia. Whether AQPs 7 or 10 contribute to this ammonia uptake is yet to be investigated.

1.4.4 Carbon dioxide transport

The majority of carbon dioxide (CO_2) produced by cellular metabolism (~70%) is transported to the lungs for expulsion from the body via the bicarbonate (HCO_3^-) system. Briefly, carbon dioxide diffuses out of the cells in which it is produced and into the plasma. It moves down its concentration gradient into erythrocytes, where carbonic anhydrase catalyses conversion into carbonic acid. Upon dissociation ($\text{H}_2\text{CO}_3 \rightarrow \text{H}^+ + \text{HCO}_3^-$), the HCO_3^- is exchanged across the erythrocyte membrane for Cl^- and the proton binds to haemoglobin [124]. There has been speculation that CO_2 transport into erythrocytes might be aided by channel proteins, and that an AQP could contribute to this [143, 144]. AQP1 is expressed at the plasma membrane of erythrocytes [18]. Human AQP1 has been reported to increase the CO_2 permeability of *Xenopus* oocytes four-fold in the

presence of carbonic anhydrase suggesting that AQP1 functions as a CO₂ channel [145, 146]. AQP1 -/- human erythrocytes had a 60% reduction in CO₂ permeability when compared to human erythrocytes expressing AQP1 [147]. However, the CO₂ permeability of AQP1 -/- mouse erythrocytes from AQP1 knockout mice was not different to wild-type [148]. Stopped flow experiments with AQP1 reconstituted into liposomes have also given conflicting results. AQP1 from human blood increased the CO₂ permeability of liposomes four-fold [149], whereas mouse AQP1 showed no increase [148]. This agrees qualitatively with the results from measurements on intact erythrocytes in that human AQP1 appears to increase CO₂ permeability of the membrane, whereas mouse AQP1 does not. This may be due to methodological differences, but it also raises the intriguing possibility that human AQP1 is CO₂ permeable whereas mouse AQP1 is not. A recent review dedicated to AQPs and CO₂ permeability of biological membranes [52] concluded that “the debate about the mechanism of membrane CO₂ diffusion continues and it is difficult to draw general conclusions”. This is still very much an open question.

1.4.5 Hydrogen peroxide transport

Superoxide (O₂⁻) molecules are produced in the mitochondria as a by-product of ATP synthesis and by the NADPH oxidase (NOX) family of enzyme complexes, which couple intracellular oxidation of NADPH to extracellular production of superoxide molecules. Superoxide undergoes disproportionation to molecular oxygen and hydrogen peroxide (H₂O₂), which can be catalysed by the enzyme superoxide dismutase [150], and the highly reactive H₂O₂ can then go on to form a variety of further reactive oxygen species (ROS). High levels of ROS derived from these pathways are well known to cause cellular damage and even death

and mitochondrial ROS were long considered to be purely harmful by-products of an imperfect metabolic system. However, work in the last decade has shown that they are crucial for a variety of physiological processes including adaptation to hypoxia, immune function and regulation of autophagy [151], so clearly there is a need for tight regulation of ROS levels. H_2O_2 and H_2O are very similar molecules with similar molecular sizes, dipole moments and hydrogen bonding capacities [152], therefore it would not be surprising to find that some AQPs could transport H_2O_2 . The half-life for H_2O_2 in cells is very short (e.g. ~ 1 ms in lymphocytes [153]), making biophysical experiments of the kind used for e.g. glycerol or urea permeation very difficult. Growth assays using H_2O_2 transport-deficient yeast are typically used, and reduced growth after expression of an AQP is interpreted as an AQP-mediated increase in membrane H_2O_2 permeability causing cellular damage and/or metabolic disruption. Using this technique, human AQP8, rat (but not human) AQP1 and several mutants thereof were shown to be H_2O_2 permeable [154]. Based on this data, the authors suggested that all AQPs function as H_2O_2 channels. It is not clear whether this is a valid generalization, but clearly some mammalian AQPs are H_2O_2 channels.

Imaging studies demonstrated H_2O_2 permeability for human AQP8 and AQP3 (but not AQP1). Furthermore, AQP3 overexpression in HeLa cells allowed the cells to respond to serum starvation via ROS mediated activation of the AKT (protein kinase B) signalling pathway, whereas cells not expressing AQP3 could not. Knockdown of AQP3 in a colon cancer cell line inhibited the AKT response to epidermal growth factor (EGF) [155], which can initiate ROS signalling via activation of NOX complexes. This suggests that AQP3 is required for uptake of

NOX-generated H₂O₂ in EGF signalling. There is also evidence of involvement of AQP3 in ROS-mediated signalling in T cell migration [156], AQP8 in leukaemia cell proliferation and metabolism [157], and in minimizing oxidative stress in hepatic mitochondria [158] and AQP11 in minimizing oxidative stress to the endoplasmic reticulum in kidney proximal tubule cells [159, 160]. Taken together, these examples provide clear evidence for AQP-mediated H₂O₂ membrane permeability and suggest physiological roles in redox signalling via uptake of NOX-derived H₂O₂ and in cellular mechanisms for minimizing oxidative stress.

1.4.6 Ion permeability of AQPs: An unresolved controversy

AQPs support bulk movements of fluid by giving high water permeability to membranes that secrete osmolytes. These osmolytes are often ions (e.g. Na⁺, K⁺ and Cl⁻) and this is reflected in the fact that several AQPs form macromolecular complexes with ion channels and transporters, e.g. AQP4 and the Kir4.1 inwardly rectifying potassium channel [47]. Perhaps a more efficient way for nature to achieve this dual permeability would be to have both ions and water pass through the same channel. Indeed it has been observed that several ion channels can transport water [44], but it has also been suggested that some AQPs may function as ion channels [161].

The pH-sensitive anion permeability of AQP6 is well established, and it is likely that the monomeric pore is the ion pathway given that a point mutation to a pore-lining residue of AQP6 (T63I) abolished ion permeability [162] and AQP6-mimicking mutations of a pore-lining amino acid residue of AQP5 (L51R) conferred anion permeability [163]. There is also some evidence that the plant

AQP nodulin-26 from soybean can act as a voltage-gated, anion-biased ion channel [164, 165].

More controversial is the idea that the fifth pore formed at the fourfold axis of the tetramer of AQP1 may function as a cation channel. In *Xenopus* oocytes, heterologous expression of human AQP1 led to a PKA-activated cation permeability probably mediated by phosphorylation of AQP1 [166] and a cGMP-activated cation permeability via direct binding of cGMP to the C-terminus of AQP1 [167]. PKC activity was shown to increase the cation permeability of AQP1 in *Xenopus* oocytes via direct phosphorylation of AQP1 at residues T157 and T239 [168]. Phosphorylation at these sites by PKC is required for trigger-induced translocation of AQP1 to the plasma membrane [169], so this may represent more AQP1 molecules in the membrane rather than an increase in the cation permeability or open probability of a single channel. Phosphorylation of a tyrosine residue (Y253) in the C-terminal tail of AQP1 was recently shown to be required for activation by cGMP [170]. The cGMP-activated cation current was verified for purified AQP1 in planar artificial membranes and the AQP1 water permeability inhibitor pCMBS did not inhibit ion permeation, suggesting that the water and ion pathways through AQP1 are not the same [171]. Furthermore, point mutations to residues lining the tetrameric pore altered conductance properties [170]. The open probability was found to be very small ($<10^{-6}$) in the planar bilayer system [171], which raises doubts over the physiological relevance of this cation conductance. Furthermore, human AQP1 expressed in HEK293 cells did not induce an above-background cation conductance when cells were loaded with either cGMP or analogues thereof [172]. Additionally, several laboratories reported being unable to replicate this result in the same

experimental system (and in some cases, with exactly the same AQP1 construct) [173].

However, rat choroid plexus cells, which strongly express AQP1, were found to have a cGMP-activated cation conductance that was abolished by treatment with AQP1 siRNA. Activation of the current by atrial natriuretic peptide (ANP), which signals through guanylate cyclase, inhibited basal-to-apical fluid transport. The contribution of AQP1 to this inhibition was not confirmed directly, although Cd^{2+} , which was shown to inhibit cGMP-induced cation conduction of AQP1, reversed the inhibition of fluid transport [174]. ANP and a cGMP analogue were also shown to upregulate apical-to-basal fluid transport in cultured retinal pigment epithelial cells, but this was reversed by an inhibitor of AQP1 water permeability [175]. It seems that under the right set of circumstances, AQP1 can act as a cation channel, with the ion pathway probably residing in the central pore formed by tetrameric assembly (see Figure 1-7). Whether or not this ion conductance has physiological relevance remains an open question. However, coupled water and ion movement are vital for several pathophysiological processes including tumour angiogenesis and cell migration [176] and epilepsy [177], so it remains an intriguing possibility that AQPs can perform a dual function.

1.5 AQPs and cell volume regulation

Many cells have the ability to modulate their physical size. This is achieved by the import or export of osmolytes in order to move water into or out of the cell by osmosis. Regulatory cell volume decrease (RVD) is mediated by potassium chloride and taurine efflux and regulatory cell volume increase (RVI) by sodium

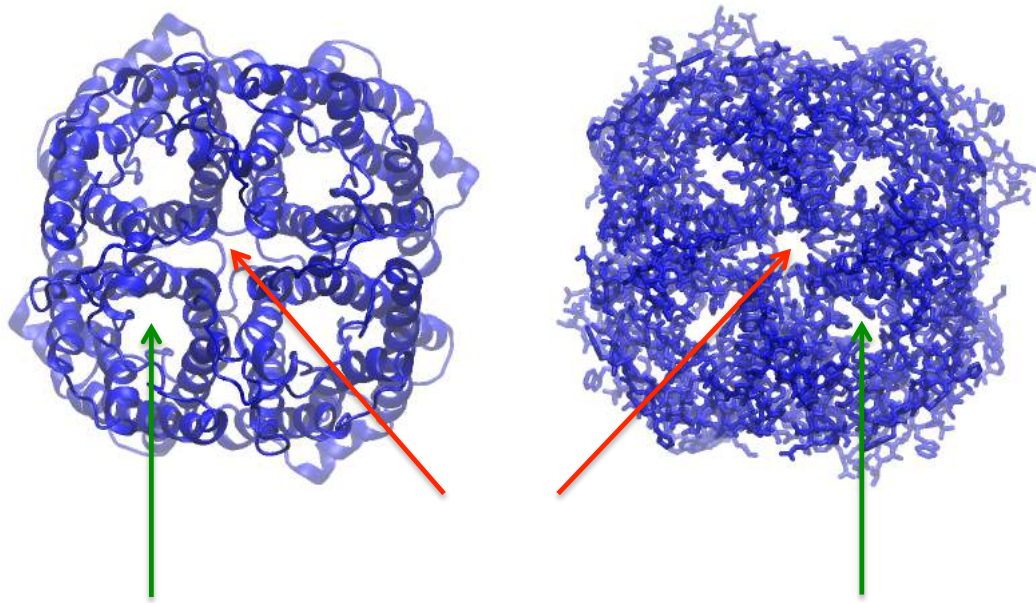


Figure 1-7 The central pore (red arrow) formed at the fourfold axis of the AQP1 tetramer, rendered in two different representations to aid visualization. This pore has been proposed as a possible pathway for CO₂ and cations through AQP1. Green arrows show the monomer water pore. Rendered using VMD from PDB entry 1J4N.

influx [178]. AQPs play a role in mediating the osmotic water movement in cell volume regulation [15], but there is evidence that their role may go beyond facilitation of osmosis.

The stretch-activated transient receptor potential vanilloid type 4 (TRPV4) channel is a Ca^{2+} -biased non-selective cation channel (NSCC) that is activated by cell swelling [179] and has been implicated in cellular responses to osmotic stimuli [180]. In some cell types TRPV4 has been shown to provide a Ca^{2+} signal that is correlated with activation of the K^+ and Cl^- channels responsible for the decrease in cellular osmolality associated with RVD [180, 181]. In human and murine salivary gland cells, TRPV4 has a functional interaction with AQP5; in AQP5 knockout cells, the hypotonicity-induced calcium influx through TRPV4 was attenuated and subsequent RVD was abolished. Hypotonicity also increased cell surface expression of both TRPV4 and AQP5 and increased their co-localisation [182]. This suggests a role for AQP5 in the regulation of TRPV4 surface expression or hypotonicity-induced activity.

In another example, the RVD of sperm of AQP3 $-/-$ mice was inhibited compared to wild-type mice and the mice displayed reduced fertility [183, 184]. Upon entry into the female reproductive tract, sperm normally encounter a decrease in extracellular osmolality, which is thought to be the signal that activates sperm motility [183]. However, this hypotonic stress also causes cell swelling which, if left uncorrected by RVD, leads to impaired fertilisation, likely due to excessive bending of the sperm tail inside the uterus [184]. If AQP3 was simply acting passively as a water channel, RVD would not be abolished in AQP3 $-/-$ sperm but rather the timescale on which the cell reaches osmotic

equilibrium would be increased. A possible explanation for reduced fertility and altered RVD in AQP3 $-/-$ mice is therefore that AQP3, either alone or as part of a macromolecular complex which is disrupted by AQP3 knockout, is involved in the signalling pathway that activates RVD in sperm.

In a further example, when exposed to a hypotonic extracellular solution, cultured renal cortical collecting duct (CCD) cells, which do not endogenously express AQP2, swelled in proportion to the change in extracellular osmolality but did not exhibit RVD. When transfected with AQP2, these cells showed an RVD of approximately 40%. Shrinkage was mediated by Ca^{2+} influx through TRPV4, which activated Ca^{2+} -dependent K^+ and Cl^- channels and Ca^{2+} -dependent Ca^{2+} release from intracellular stores. In renal CCD cells expressing AQP2, hypotonic stress caused translocation of TRPV4 to the plasma membrane. This response did not occur in AQP2-negative cells. When TRPV4 was pre-translocated to the cell surface prior to hypotonic exposure, RVD was recovered in AQP2-null cells, showing that it is not simply the high water permeability of AQP2 that allows RVD. However, there did not appear to be any co-localisation between endogenous TRPV4 and overexpressed AQP2 in this system, either before or after hypotonic shock, indicating a functional rather than physical interaction [185]. These observations suggest that AQP2 forms part of a sensory and signalling pathway that results in TRPV4 translocation, possibly via sensing of extracellular osmolality.

It has been suggested that AQPs could act as direct sensors of osmotic gradients by coupling conformational changes of the protein to a pressure gradient within the pore [186]. This argument relies on the idea of the hydrostatic pressure

within the pore and it is not clear that the application of classical fluid mechanics is applicable to a system typically consisting of <10 water molecules.

Nonetheless it is an intriguing idea, and taken together, these examples clearly support the idea of a signalling or sensory role for AQPs in cell volume regulation beyond a passive water conduction mechanism.

1.6 Regulation of AQPs

Cells may often need to modulate their membrane water or solute permeability in response to external stimuli. There are three possible ways in which this could be achieved: by up- or downregulating AQPs at the transcript level via activation or inhibition of transcription factors or RNA interference, by changing the number of AQP molecules in the membrane via exo- or endocytosis, or by directly blocking the AQP molecule via a conformational change that opens or closes the pore or by binding of a molecule that blocks the pore. There are examples of each of these approaches to AQP regulation being taken in nature.

1.6.1 Transcriptional regulation of AQPs

There is evidence of regulation of AQP copy number by activation or repression of transcription; this includes upregulation of AQP2 in response to AVP [187], downregulation of AQP3 in response to insulin [188] and upregulation of AQP1 in response to hypoxia [189].

1.6.2 Kinase-dependent subcellular relocalization of AQPs

Protein kinases are a large and diverse family of proteins that modify the structure and function of proteins by addition of a phosphate group to specific amino acid sidechains. Two kinases in particular, the cAMP-dependent PKA and the calcium and diacylglycerol-dependent PKC, have been shown to be able to

control the subcellular localization of several AQPs by direct phosphorylation of serine and threonine residues in the intracellular loop D and the C-terminal tails of AQPs.

1.6.2.1 AQP2 and arginine vasopressin

The best-studied example of kinase-mediated subcellular relocalization of an AQP to modulate cellular water permeability is that of AQP2 in the mammalian kidney collecting duct in response to AVP. AVP is released by the pituitary gland in response to elevated plasma osmolality or hypernatraemia [124] and activates the cAMP-dependent protein kinase A (PKA) in collecting duct cells by signalling through the V2 vasopressin receptor and adenylyl cyclase. PKA directly phosphorylates AQP2 at a serine residue (S256) in the C-terminal tail, which causes translocation of AQP2-containing intracellular vesicles to the apical membrane of the cells [96]. This phosphorylation event is necessary and sufficient for the translocation response as an S256A mutant of AQP2 was unable to relocalize in response to cAMP and an S256D phosphomimetic mutant was constitutively localized to the apical membrane independently of cAMP signalling [190].

Endocytosis of AQP2 may also be regulated. Protein kinase C activation led to an increased rate of internalization of AQP2 independently of AQP2 phosphorylation and independently of the phosphorylation state of S256.

Inhibition of endocytosis caused a build-up of AQP2 in the plasma membrane and this was independent of the phosphorylation state of S256 [191]. This highlights the fact that there is a constant antagonism between membrane trafficking and internalization of AQP2 (i.e. recycling) and that the membrane

abundance is controlled by modulation of the relative rates of these two processes.

1.6.2.2 AQP1 and hypotonicity

Relocalization of AQP1 in response to reduced extracellular osmolality was mediated by PKC activation by calcium released from intracellular stores after extracellular calcium influx through the mechanosensitive cation channel TRPC1. PKC directly phosphorylated AQP1 at two threonine residues in loop D (T157) and the C-terminal tail (T239), which led to relocalization of AQP1 to the plasma membrane in a calmodulin (CaM) and microtubule dependent manner [169], although the role of CaM in this response was not clear. This signalling pathway and trafficking response is represented as a cartoon in Figure 1-8. In chapter 3, results are presented which suggest that AQP4 can also relocalize in response to hypotonicity, although mediated by a different signalling pathway.

1.6.2.3 AQP5

AQP5 is expressed in the lacrimal and salivary glands and lungs, where it is thought to be important for generation of tears, saliva and pulmonary secretions [182, 192, 193]. AQP5 regulation has been shown to be mediated biphasically by cAMP in a PKA-dependent manner, with exposure to elevated intracellular cAMP levels causing a short-term (minutes) decrease in AQP5 membrane abundance, probably via regulated endocytosis, whereas long-term (8 hours) exposure increased total AQP5 protein [192]. There are two consensus PKA sites in AQP5: S156 in cytoplasmic loop D [27, 194] and T259 [195] in the C-terminus; the latter corresponds to S256 in AQP2. AQP5 can be directly phosphorylated by PKA at S156 and T259 [196]. Notably, S156 was

phosphorylated preferentially in certain tumours suggesting that cell proliferation can be modulated by phosphorylation of this site although the constitutive membrane abundance of an S156A mutant was not distinguishable from wild-type AQP5 [197]. Based on the crystal structure of human AQP5 it was hypothesized that phosphorylation of S156 could cause structural changes in loop D that would break its interaction with the C-terminus, thereby flagging the protein for translocation to the plasma membrane [198]. An investigation of this suggestion is presented in chapter 3.

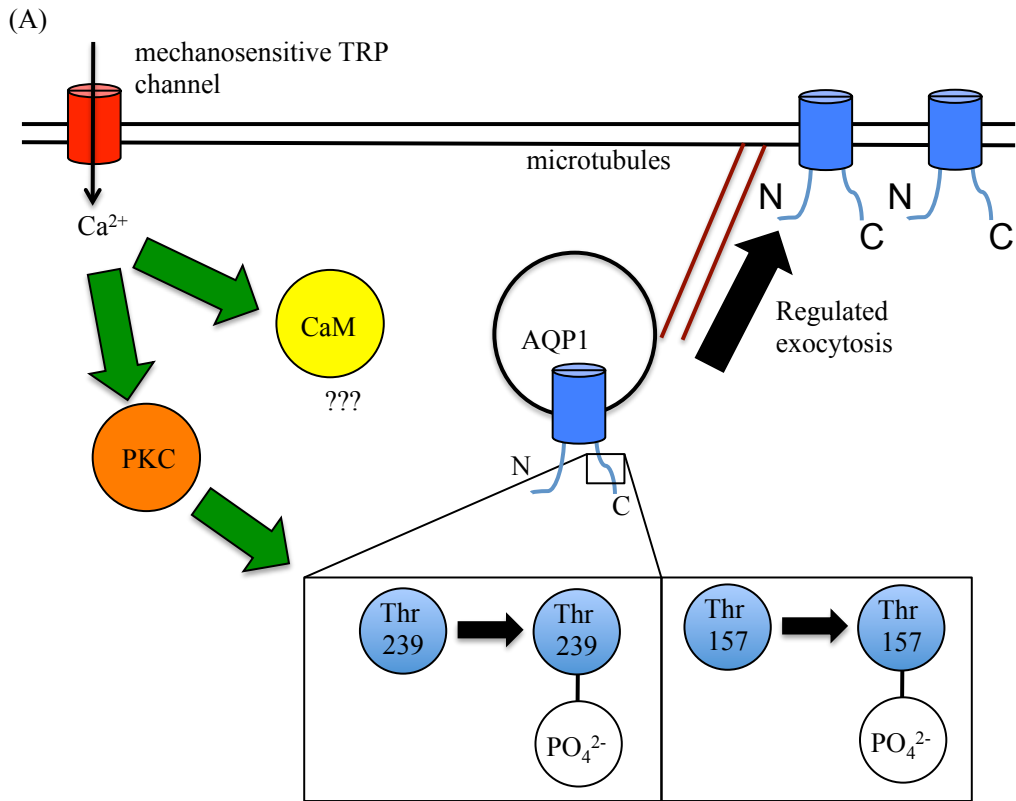
1.6.3 AQP gating

1.6.3.1 Structural gating

Although there is no evidence of gating in the mammalian AQPs, it is a well-established regulatory mechanism for some plant AQPs. The best-studied example of this is the spinach SoPIP2;1, which has been crystallized in both open and closed conformations (see Figure 1-8). In the closed conformation the sidechain of a leucine (L197) residue from the C-terminal end of the intracellular loop D protruded into the pore, physically occluding the channel and forming a hydrophobic ‘gate’ reducing the channel diameter to 0.8 Å. A large-scale motion of loop D was proposed to occur upon dephosphorylation of two serine residues in loop D and the C-terminal tail, thereby unblocking the cytoplasmic channel entrance [199] in a regulated manner and coupling cell signalling (phosphorylation) to membrane water permeability.

1.6.3.2 Gating by AQP-binding proteins

Calmodulin (CaM) is a calcium-binding protein that mediates many of the downstream signalling elements that begin with the release or influx of calcium



(B)

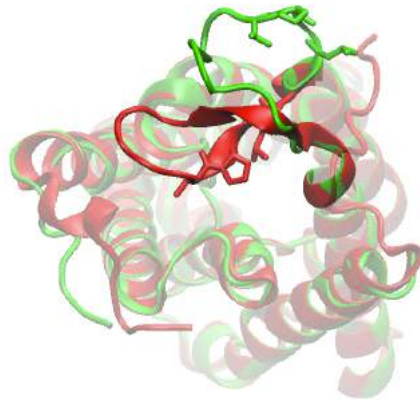


Figure 1-8 Regulation of AQPs exemplified by: (A) hypotonicity-induced translocation of human AQP1 from intracellular vesicles to the plasma membrane and (B) structural gating of spinach SoPIP2;1, crystallized in open (green) and closed (red) states, with a large scale motion of the intracellular loop D between the two states.

as a second messenger [200]. Activated (i.e. calcium-bound) CaM has been shown to be able to bind directly to a motif in the C-terminal tail of AQP0 [201], with a binding stoichiometry of two CaM molecules per AQP homotetramer. The CaM binding affinity was reduced by phosphomimetic mutation of consensus PKA and PKC sites within the CaM binding site of the AQP0 C-terminus [202]. The binding of CaM reduced AQP0 water permeability by twofold, and MD simulations suggested that CaM binding favoured a closed state of the cytoplasmic end of the AQP0 channel [201]. In this way, phosphorylation of the AQP is indirectly coupled to changes in the channel permeability (c.f. the direct coupling of SoPIP2).

1.6.3.3 Gating by small molecule inhibitors

Due to their involvement in a variety of pathophysiological processes and availability at the cell surface, AQPs are appealing drug targets. Since the discovery of the AQP family, it has been known that mercurial compounds and Hg^{2+} ions can act as inhibitors of most APQs by interacting with cysteine residues within the aqueous pore [203]. Mercurial compounds are not ideal as drugs due to the toxicity of mercury, but several organometallic compounds of gold, silver and copper have been shown to be inhibitory against AQPs 1 and 3 [204]. Several drugs already licensed for other uses such as loop diuretics, antiepileptics and carbonic anhydrase inhibitors have been suggested to have inhibitory action against AQPs, but there are conflicting data in the literature where different expression systems have been used to study the action of the same drug on the same AQP, e.g. acetazolamide was reported to inhibit AQP4 in *Xenopus* oocytes [205], but not in AQP4-expressing glial cells [206]. Drug development for AQPs is still in its infancy, but is hampered by the challenges

associated with scaling up biophysical measurements of water permeability to high-throughput systems [207].

1.7 Open questions and outline of the thesis

1. *in vivo* and *ex vivo* experiments with AQP4 $-/-$ animals clearly show a role for AQP4 in brain volume homeostasis, but the molecular mechanisms underlying this are poorly understood. Given that astrocytes can rapidly modulate their membrane water permeability and that AQP1 has been shown to rapidly relocate to the plasma membrane in response to hypotonicity and/or cell volume changes, is there a similar mechanism underlying AQP4-mediated brain volume homeostasis, and is the hypotonicity-induced relocalization of AQP1 a mechanism employed more generally to regulate other AQPs?

To address this question, chapter 3 describes the subcellular relocalization of GFP-tagged AQP4 and AQP5 constructs in HEK293 cells and endogenous AQP4 in rat primary cortical astrocytes as well as an investigation of the cell signalling pathways controlling these responses.

2. Is the generalized model of size-based exclusion of neutral solutes in the water-selective AQPs really valid, given that it is based on detailed analysis of only one member of the AQP family (AQP1)?

In chapter 4, mutants of the ar/R region of AQP4 and AQP3 are used to investigate the role of this region in solute exclusion, selectivity and water permeability and this is compared and contrasted with published data on similar mutants of AQP1.

3. Structural data and *in vitro* analysis consistently demonstrates that AQPs are assembled into homotetramers, but it is not clear how or why this happens.

Which regions of the proteins are important for homotetramerization and are there structural/functional consequences to the tetramerization?

Chapter 5 describes the use of various biophysical techniques to study AQP4 oligomerization, identifies the intracellular loop D as a key region for monomer-monomer interactions in AQP4, and suggests that loop D interactions may be important for oligomerization across the AQP family.

Finally, chapter 6 concludes the thesis with a summary of the key results and their implications, as well as suggestions for possible future extensions of this work.

2 Materials and Methods

2.1 DNA constructs

2.1.1 pDEST47 expression constructs

Human AQPs 1, 3, 4, 5, 9 and 10 cDNA cloned into the mammalian expression vector pDEST47 (Invitrogen) were kind gifts of Dr. Matthew Conner (Sheffield Hallam University). This vector contains the following elements (Figure 2-1): 1. CMV promoter for high protein expression in mammalian cells. 2. T7 promoter/priming site for insert sequencing and *in vitro* transcription. 3. attR1 and attR2 sites for gene insertion using the Gateway system. 4. BGH polyadenylation sequence for transcription termination and reverse sequencing through the insert. 5. Neomycin resistance gene for selection of stable mammalian transfectants. 6. pUC origin of replication for high copy number replication in *E. coli*. 7. Ampicillin resistance gene for selection of transformed *E. coli*. 8. Green fluorescent protein (GFP) gene for transcription of GFP fusion proteins. Sequences of the wild-type inserts used and their translations are shown in Figure 2-2, Figure 2-3 and Figure 2-4.

2.1.2 QuikChange site-directed mutagenesis

100 ng of plasmid DNA was used as template with sense and antisense mutagenic oligonucleotides at a final concentration of 300 nM in a reaction volume of 50 μ L. Final concentrations of 800 μ M dNTPs (200 μ M of each), 3 units of *Pfu* polymerase (Promega) and 1X polymerase buffer were added. The

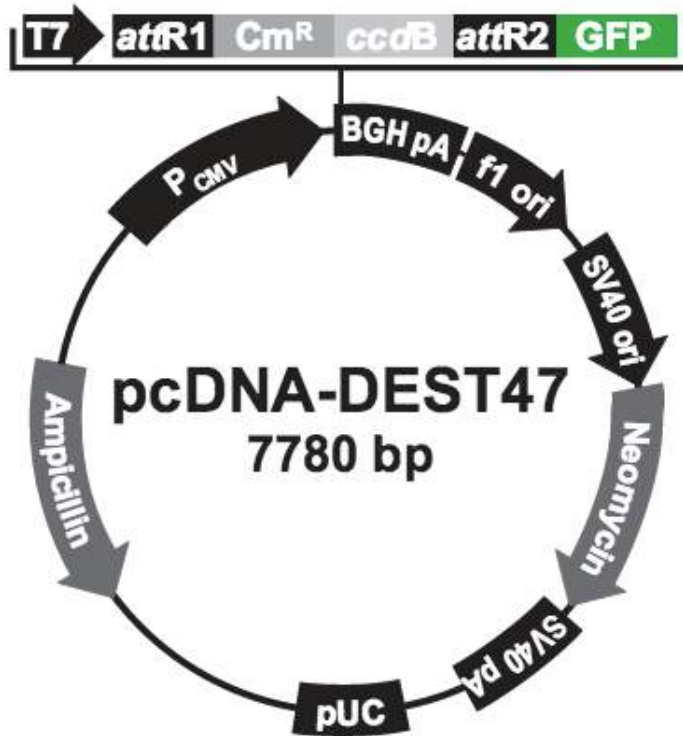


Figure 2-1 Vector map of the DEST47 vector used to transfect mammalian cells with AQP constructs. GFP – green fluorescent protein; P_{CMV} – cytomegalovirus promoter; BGH pA – bovine growth hormone polyadenylation site; SV40 ori – simian virus 40 origin of replication; pUC – origin of replication (UC = University of California).

- AQP4 N-terminus
- AQP4 C-terminus
- Linker peptide:
DPAFLYKVVRSR
- GFP N-terminus
- GFP C-terminus

```

gcaggctccaccatgtctgacagaccacagcaagcggtgggtaagtgtggacctttgtgtaccagagagaacatcatggtggctttcaaagggctggactcaagctttctggaaa
M S D R P T A R R W G K C G P L C T R E N I M V A F K G V W T Q A F W K
gcagtcacagcggaaattctggccatgcttattttgttctcctcagcctgggaccaccatcaactggggtggaacagaaaagcctttaccggtcgacatggttctcatctccctttgc
A V T A E F L A M L I F V L L S L G S T I N W G G T E K P L P V D M V L I S L C
tttggaactcagcattgcaaccatggtgcagtgctttggccatcagcgggtggccacatcaacctgcagtgactgtgcccattggtgcaccaggaagatcagcatcgccaagtctgtc
F G L S I A T M V Q C F G H I S G G H I N P A V T V A M V C T R K I S I A K S V
ttctacatcgagcccagtcgctggggccatcattggagcaggaatcctctatctgtcgcacacctcccagtggtggaggcctgggagtcaccatggttcagtaaatcttaccgct
F Y I A A Q C L G A I I G A G I L Y L V T P P S V V G G L G V T M V H G N L T A
ggtcagtgctcctggttgagtgataatcacattcaattggtgttactatctttgccagctgtgattccaaacggactgatgtcactggctcaatagcttttagcaattggatcttct
G H G L L V E L I I T F Q L V F T I F A S C D S K R T D V T G S I A L A I G F S
ggtgcaattggacatttatttgcattcaattactggtgccagcatgaatcccggcctcctttggacctgcagttatcatgggaaattgggaaaccattggatattgggttggg
V A I G H L F A I N Y T G A S M N P A R S F G P A V I M G N W E N H W I Y W V G
cccatcataggagctgctcgcgtggtggcctttatgagtatgctctctgtccagatggtgaattcaacgtcgttttaagaagccttcagcaaaagctgccagcaaaaaggaaagc
P I I G A V L A G G L Y E Y V F C P D V E F K R R F K E A F S K A A Q Q T K G S
tacatggaggtgggagacaacaggagtcaggtagagacggatgatcttatttctaaacctggaggtgcatgtgattgacgttgaccggggagaggagaagaaggggaaagaccaactc
Y M E V E D N R S Q V E T D D L I S K P G V V H V I D V D R G E E K K G K D Q S
ggagaggtattgtctcagtagaccagccttctgtacaaaagtggtcgatctagaatggctagcaaaaggagaagaacttttcaactggaggttgcocaaatctgttgaattagatggt
G E V L S S V D P A F L Y K V V R S R M A S K G E E L F T G V V P I L V E L D G
gatgttaatgggcacaaatctctgctcagtgagaggggtgaaggtgatgctacatacggaaagccttacccttaaatattttgactactggaaaactacctgttccatggccaacactt
D V N G H K F S V S G E G E G D A T Y G K L T L K F I C T T G K L P V P W P T L
gtcactactttctcttattggtgtcaatgcttttccggttatccggatcatatgaaacggcatgacttttcaagagtgccatgccogaaggttatgtacaggaacgcactatattcttcc
V T T F S Y G V Q C F S R Y P D H M K R H D F F K S A M P E G Y V Q E R T I S F
aaagatgacgggaactacaagacgctgctgaagtcgaagttggaaggtgatacccttgttaatcgtatcgagttaaaaggtattgatttaagaagatggaacattctcggacacaaa
K D D G N Y K T R A E V K F E G D T L V N R I E L K G I D F K E D G N I L G H K
ctcgagtacaactataactcacacaatgtatacatcacggcagacacacaaaagaatggaatcaaaagtaacttcaaaatcgccacacattgaagatggatccgttcaactagcagac
L E Y N Y N S H N V Y I T A D K Q K N G I K A N F K I R H N I E D G S V Q L A D
cattatcaaaaactccaattggcgatggcctgtccttttaccagacacaccattacctgtcgacacaaatcgcccttccgaaagatccaacgaaaagcgtgaccacatggtcctt
H Y Q Q N T P I G D G P V L L P D N H Y L S T Q S A L S K D P N E K R D H M V L
cttgagtttgtaactgctgctgggattacacatggcatggatgagctctacaataa
L E F V T A A G I T H G M D E L Y K STOP

```

Figure 2-2 DNA and amino acid sequences of the human AQP4 construct used in this work.

-  AQP3 N-term
-  AQP3 C-term
-  GFP N-term
-  GFP C-term
-  Linker peptide
DPAFLYKVVRSR

cttgatcaacaagttgtacaaaaagcaggctccacc

atgggtcgacagaaggagctgggtgccgctgccccgagatgctccacatccgctaccggctgctccgacagcggctggccagtgctggggaccctcatcctgggtgatgttggctgt
M G R Q K E L V S R C G E M L H I R Y R L L R Q A L A E C L G T L I L V M F G C
 ggctccgtggcccaggtgtgctcagccggggcaccacgggtgttccctcaccatcaacctggccttggcttggctgtcactctggcaccctcctcctggccaggtctctggggcc
 G S V A Q V V L S R G T H G G F L T I N L A F G F A V T L G I L I A G Q V S G A
 caectgaacctggcctgaccttggcctgtgcttccctggctcgtgagccctggatcaagctgccatctacacctggcagacagcctgggagccttctgggtgctggaatagtttt
 H L N P A V T F A M C F L A R E P W I K L P I Y T L A Q T L G A F L G A G I V F
 gggctgtattatgatgcaactcggcactcgcgacaaccagcttttggctcggcccaatggcacagccggcatctttgctacctaccctctggcacttggatgatgacaaatggc
 G L Y Y D A I W H F A D N Q L F V S G P N G T A G I F A T Y P S G H L D M I N G
 ttctttgaccagttcatagcagcctcccttctcgtgtgctgctggccattgtgaccctacaacaacctcctcccccagcctggagccttccagctggcctgggtgctgctg
 F F D Q F I G T A S L I V C V L A I V D P Y N N P V P R G L E A F T V G L V V L
 gtcattggcaccctccatggctcactccggctatgccctcaacctgccgggactttggccccgcctttttacagccttgcggctgggctctgcagctctcagccggccag
 V I G T S M G F N S G Y A V N P A R D F G P R L F T A L A G W G S A V F T A G Q
 cattgggtgggtggccctcgtgctcactcctggcctccattgggggtgctcctggtaccagctgatgatcggtgccacctggagcagccccaccctcccaacgaggaagagaat
 H W W W V P I V S S L L G S I A G V F V Y Q L M I G C H L E Q P P P S N E E E N
 gtgaagctggcccatgtgaagcacaaggagcagatcgaccagcttcttgtacaaaagtggttcgatctagaatggctagcaaggagaagaacttttactggagttgcccacttct
 V K L A H V K H K **E Q I D P A F L Y K V V R S R M A S K G E E L F T G V V P I L**
 gttgaattagatgggtgatgttaatgggcacaaaatttctgctcagtgagaggggtgaaggtgatgctacatcgggaaagccttaccctaaatttattgcaactactggaaaactacctgtt
 V E L D G D V N G H K F S V S G E G E G D A T Y G K L T L K F I C T T G K L P V
 ccatggccaacacttggcactacttctcttattggtgttcaatgcttttcccggtatccggatcatatgaaacggcatgacttttcaagagtgccatgcccgaaggttatgtacaggaa
 P W P T L V T T F S Y G V Q C F S R Y P D H M K R H D F F K S A M P E G Y V Q E
 cgcactatactttcaagatgacgggaactacaagacgctgctgaagtcaagtttgaagtgatacccttgttaactcgtatcgagttaaaaggtattgattttaagaaatggaaac
 R T I S F K D D G N Y K T R A E V K F E G D T L V N R I E L K G I D F K E D G N
 attctcggacacaaaactcgagtacaactataactcacacaatgtatacatcacggcagacacaaaagaatggaatcaagctaaactcaaaatcgccacaacattgaagatggatcc
 I L G H K L E Y N Y N S H N V Y I T A D K Q K N G I K A N F K I R H N I E D G S
 gttcaactagcagaccattacaacaaaactccaattggcgtggcctgtccttttaccagacaaccattacctgtcgacacaactcgcctttcgaaagatcccaacgaaaagcgt
 V Q L A D H Y Q Q N T P I G D G P V L L P D N H Y L S T Q S A L S K D P N E K R
 gaccacatggctccttctgagtttgaactgctgctgggttaccatggcatggatgagctcacaataa
 D H M V L L E F V T A A G I T H G M D E **L Y K STOP**

Figure 2-3 DNA and amino acid sequences of the human AQP3 construct used in this work.

- AQP1 N-term
- AQP1 C-term
- GFP N-term
- GFP C-term
- Linker peptide
DPAFLYKVVRSR

agtttgtacaaaaaacaggtccacca

atggctagcaggtcaagaagaagtattctggaggcagtggtggccagctcttctgtcttcacagcatcgggtctgcctgggttcaaataccgggtgggg
M A S E F K K K L F W R A V V A E F L A T T L F V F I S I G S A L G F K Y P V G
 aacaaccagcggcggtccaggacaacgtgaaggtgtcgtggccttcgggctgagcatgccacgctggcgcagagtggtggccacatcagcggcgcccaactcaaccggctgtca
 N N Q T A V Q D N V K V S L A F G L S I A T L A Q S V G H I S G A H L N P A V T
 ctggggtgctgctcagatgccagatcagcatctccgtgcctcatgtacatcagccagtgctggggccatcgtgccaccgccatcctcagcagtcacctcctcctgact
 L G L L L S C Q I S I F R A L M Y I I A Q C V G A I V A T A I L S G I T S S L T
 ggaactcgttggcccaatgactggctgatggtggaactcggccagggctgggcatcgagatcatcgggaccctccagctggtgctatgctgctggtactaccgaccggag
 G N S L G R N D L A D G V N S G Q G L G I E I I G T L Q L V L C V L A T T **D R R**
 cgccgtgaccttgggtgcagcccccttggccatggcctctctgtagccctggacacctcctggctattgactacactggctggtgggattaaccctgctgcttcttggctcgcg
R R D L G G S A P L A I G L S V A L G H L L A I D Y T G C G I N P A R S F G S A
 gtgatcacacaaactcagcaaccactggatttctgggtgggcccattcatcggggagccctggctgtactcactcagacttcatcctggccccagcagcagtgactcacagac
 V I T H N F S N H W I F W V G P F I G G A L A V L I Y D F I L A P R S S D L T D
 cgcgtgaaggtgtgaccagcggcaggtggaggatgacctggatgccagcacatcaactccagggtggagatgaagcccaagaccagcttcttgtacaaagtgggtcagatc
 R V K V W T S G Q V E E Y D L D A D D I N S R V E M **K P K D P A F L Y K V V R S**
 agaatggccagcaaggagaagaacttttcaactggagttgtcccaattcttggtaattagatggtgatgtaattggccacaaatttctgtcagtgagaggggtgaaggtgatctaca
R M A S K G E E L F T G V V P I L V E L D G D V N G H K F S V S G E G E G D A T
 tacgaaacttacccttaatttatttgcactactggaactacactgtccatggccaacactgtcactacttctcttatggtgttcaatgcttttcccggtatccggatcatatg
 Y G K L T L K F I C T T G K L P V P W P T L V T T F S Y G V Q C F S R Y P D H M
 aaacggcatgacttttcaagagtgccatggcgaaggttattgtacaggaacgcaactatcttcaaaagatgacgggaactacaagacgctgctgaagtcgaagtttgaaggtgatacc
 K R H D F F K S A M P E G Y V Q E R T I S F K D D G N Y K T R A E V K F E G D T
 cttgttaactgtagatgaaagtattgattttaaagaagatggaacatctcggacacaaactcgagtagcaactataactcaacaatgtatacatcagcgaagacaacaaag
 L V N R I E L K G I D F K E D G N I L G H K L E Y N Y N S H N V Y I T A D K Q K
 aatggaatcaagtaacttcaaatcggccacaacattgaagatggatccgttcaactagcagaccattatcaacaaaactccaattggcgatggcctgtcctttaccagacaac
 N G I K A N F K I R H N I E D G S V Q L A D H Y Q Q N T P I G D G P V L L P D N
 cattacctgtcgcacaactcgccttccgaagatcccaacgaaaamtgcgaccataggtcctcttgagtttgaactgctgctgggattacacatggcatggatgagctctacaaa
 H Y L S X Q S A L S K D P N E X C D H M V L L E F V T A A G I T H G M D E **L Y K**
 taa
STOP

Figure 2-4 DNA and amino acid sequences of the human AQP1 construct used in this work.

reaction mix was thermocycled between 95 °C (denaturation) for 1 min, 55 °C (primer annealing) for 1 min and 72 °C (extension) for 16 min (2 min/kbase + 2 min) for a total of 16 cycles. 5 µL was removed from the mix and 20 units of *dpnI* were added to the remaining 45 µL and incubated at 37 °C for at least 2 hours. 5 µL was taken from the resulting mix and pre- and post-*dpnI* samples were compared by agarose gel electrophoresis. A representative gel is shown in Figure 2-5.

2.1.3 Agarose gel electrophoresis

DNA was separated on 1% w/v agarose gels loaded with the GelRed (Biotium) nucleic acid dye. Gels were visualized on a UV transilluminator and imaged using a GelDoc system (BioRad).

2.1.4 Mutagenic oligonucleotide primers

Complementary sense and antisense primers were designed to introduce the desired codon change with flanking sequences of 12-18 bp either side. Where possible primers included a guanine or cytosine at both the 3' and 5' ends to enable stronger binding to the template DNA. Primers were custom synthesized by Sigma (Dorset, UK). Lyophilized primers were resuspended in an appropriate amount of sterile molecular grade water to give a 100 µM stock and these were diluted to a 1 µM working stock.

2.1.5 Preparation of competent cells

LB agar plates (without antibiotic) were streaked with Top 10 *E. coli* cells and incubated overnight at 37°C. Single colonies were picked, inoculated into 5 ml LB medium and incubated overnight at 37°C with shaking. The 5ml cultures were inoculated into 400 ml LB medium in a 2 L flask and grown at 37°C with

shaking until an OD₅₉₀ of 0.35-0.4 was reached (rapid growth phase, ~ 3-5 hrs). 50 mL cultures were incubated on ice in pre-chilled sterile plastic tubes. Cells were centrifuged at 4000 rcf at 4°C for 15 minutes, gently resuspended in 10 ml ice cold CaCl₂ solution (60 mM CaCl₂, 15% (v/v) glycerol, 10 mM PIPES, pH 7.0), centrifuged again at 4000 rcf at 4°C for 15 minutes, gently resuspended in 10 ml ice cold CaCl₂ solution and incubated on ice for 30 minutes. Cells were centrifuged at 4000 rcf at 4°C for 15 minutes, resuspended in 2 mL ice cold CaCl₂ solution, aliquoted 32 x 250 µl into pre-chilled sterile microcentrifuge tubes and frozen immediately at -80°C.

2.1.6 Transformations

Competent cells were thawed on ice. Cells were transferred into pre-chilled 1.5 mL microcentrifuge tubes. For nicked, linear SDM products, 20 µL of the SDM reaction was added to 200 µL of competent cells. For supercoiled plasmids, 200 ng was added to 20 µL of competent cells. Cells were subjected to heat shock at 42 °C for 30 seconds in a water bath and incubated on ice for 5 minutes. Cells were recovered by addition of 1 mL lysogeny broth (LB) without antibiotic and shaking incubation at 37 °C for 1 hour. Cells were pelleted by centrifugation at 4,000 rcf for 5 mins. Pellets were resuspended in 100 µL LB, plated onto 10 cm LB agar plates containing either 100 µg/mL ampicillin or 50 µg/mL kanamycin and incubated for 16 hours at 37 °C.

2.1.7 Growth and isolation of plasmids

Single colonies of transformed competent cells were picked using sterile 200 µL pipette tips. Colonies were grown for 16 hours in either 5 (for minipreps) or 200 (for maxipreps) mL LB containing either 100 µg/mL ampicillin or 50 µg/mL

kanamycin according to the plasmid being grown. DNA isolation was performed using Wizard plasmid miniprep kits (Promega) or PureLink HiPure plasmid maxiprep kits (Invitrogen) following the manufacturer's instructions.

2.1.8 Sequencing

Plasmid inserts were sequenced in both forward and reverse direction using T7 and BGH sequencing primers. Reads were typically 800 – 1000 bp and most forward and reverse sequence pairs overlapped. Where there was not an overlap, a second reverse primer targeted to bp 200-219 of the GFP gene was used to complete the sequence. Sequencing was done by GATC Biotech (Nottingham) or Functional Genomics (University of Birmingham). Putative mutant sequences were aligned to their respective wild-type sequences using Clustal Omega (European Bioinformatics Institute). Where mutations were successful, chromatograms were inspected at the mutated codon to exclude the possibility of mixed mutant/wild-type DNA (from e.g. accidentally picking two colonies).

2.2 Mammalian cell culture

2.2.1 HEK293

Human embryonic kidney cells clone 293 (HEK293), grown for four passages (P4) after purchase from the supplier were a gift of Jasmeet Reyat and Dr. Michael Tomlinson (both School of Biosciences, University of Birmingham). These cells were grown to P5 and frozen in liquid nitrogen. These P5 cells were used as stocks for this work. Cells used in experiments were between P7 and P20.

2.2.2 MDCK

Madin-Darby canine kidney cells at P6 after purchase from the supplier were a gift from Dr. Matthew Conner. These cells were grown to P7 and frozen in liquid nitrogen and these P7 cells were used as stock for this work. Cells used in experiments were between P8 and P20.

2.2.3 U-251 MG

U-373 MG (U373) human glioblastoma cells at P8 were a gift from Dr. Eric Hill (Aston University). These cells were grown to P9 and frozen in liquid nitrogen and these P9 cells were used as stock for this work. Cells used in experiments were between P10 and P12.

2.2.4 Rat primary cortical astrocytes

Rat primary cortical astrocytes (RPCAs) were purchased from Invitrogen. The supplied vial of cells was defined as P0. These cells were grown to confluence in a T75 flask, subcultured 1:5, and when confluent these P1 cells were frozen in liquid nitrogen. All experiments were performed with cells at P2 or P3.

2.2.5 Cell culture

Unless otherwise stated, all work with live cells was done in a class II biological safety cabinet. All cell culture reagents were purchased from Sigma-Aldrich (UK). Cells were cultured in a humidified 37 °C incubator with 5% CO₂. All cells were routinely cultured in Dulbecco's modified Eagle's medium (DMEM), supplemented with either 10% (HEK, MDCK, U251) or 15% (RPCA) fetal bovine serum (FBS). RPCA media was supplemented with penicillin (100 units/mL) and streptomycin (100 µg/mL). All media was pre-warmed to 37 °C before use. Cells were grown in a total volume of 1 mL/5 cm³ growth area. Cells

were subcultured at ~90% confluence by washing twice with pre-warmed calcium-free phosphate buffered saline (PBS) followed by incubation with 1 mL/cm³ of either 0.25% trypsin – 0.53 mM EDTA (HEK, MDCK, U251) or accutase (RPCA) at 37 °C until cells became visibly rounded under a phase contrast microscope and were detachable by gentle rocking.

HEK293 cells are very weakly adherent; as a result of this it is common practice to detach them by banging the culture vessel or using a pipette gun to squirt culture media onto the cells. Both of these methods increased the propensity of the cells to form dense clumps after seeding when compared to trypsin, especially when seeding into circular plates. Therefore HEK293 cells were routinely trypsinized.

2.2.6 Frozen cell stocks

Cells were grown to ~90% confluence in T75 flasks, detached and centrifuged for 5 mins at 1,000 ref. Cell pellets were resuspended in 2 mL culture media containing 5% v/v dimethylsulfoxide (DMSO) and transferred to sterile freezer vials (1 mL / vial). Vials were frozen at -80 °C in a Mr Frosty (Nalgene) container filled with isopropanol to reduce freezing speed. After 48 hours at -80 °C, vials were transferred to the liquid phase of a liquid nitrogen dewar. Cells were recovered by defrosting vials in a 37 °C water bath and adding the cell suspension to 14 mL of pre-warmed culture media in a T75 flask. Culture media was changed as early as possible on the following day to remove dead cells and cellular debris.

2.3 Transfections

2.3.1 Transient

Transient transfections were performed using polyethylenimine (PEI). For 35 mm dishes, the optimal amount of DNA for the cell type (HEK293, U251 - 2 µg, MDCK - 4 µg, RPCA - 1 µg) was added to 100 µL of serum-free DMEM, followed by the optimal amount of 1 mg/mL PEI in dH₂O, pH 7.4 (HEK293 - 12 µL, U251 - 12 µL, RPCA - 4 µL, MDCK - 18 µL). The mixture was vortexed for 10 seconds, incubated at room temperature for 10 mins, then added to 600 µL DMEM with serum. Cell culture medium was aspirated from cells and the transfection mix was added, squirting down the side of the plate to avoid agitation of the cells. Cells were incubated at 37 °C for 2 hours then 2 mL of culture media was added (leaving on the transfection mix). After a further 22 hours, cells were either used in experiments or the transfection media was removed and replaced with 2 mL culture media. This mix was scaled up or down, keeping all concentrations the same for different sized culture vessels.

2.3.2 Stable

Stable transfections of MDCK cells were performed using the neomycin resistance gene on pDEST47. Cells were transiently transfected as described above. After 24 hours, cells were trypsinized, resuspended in culture media containing 700 µg/mL G418 and reseeded at varying dilutions, 1:2, 1:5, 1:10 and 1:20 in 4 wells of a 6 well plate. Transient transfection and reseeded was done in triplicate. G418-supplemented media was refreshed every 3 days. After 14 days, resistant colonies were inspected on a widefield fluorescence microscope for GFP expression. GFP-positive colonies were picked using 150 µL cloning

cylinders (Corning). Colonies from the lowest dilution were preferentially isolated (e.g. colonies from a 1:10 plate were preferred to those from a 1:5 plate). Marker pen was used to label the plates at the positions of the desired colonies. For each stable transfection, a total of 3 clones were isolated. Plates were washed with calcium-free PBS. Cloning cylinders were placed over the pen-marked positions on the plate(s) and pressed down firmly to seal. 50 μ L trypsin-EDTA was added to cylinders and incubated until cells were removable by gentle pipetting. Cells were removed, serially diluted by a factor of 2 (to give 1:2, 1:4, etc.) up to 1:32, and seeded into wells of a 96 well plate. Culture media was added to a total volume of 100 μ L/well. The lowest dilution that grew to confluence was trypsinized and transferred to a well of a 24 well plate, grown to confluence and transferred to a T25 flask. Upon reaching confluence, 2/3 of these cells were transferred to a T75 flask to grow for frozen stocks, and the remaining cells were seeded in 3 wells of a 24 well plate to be harvested for western blotting for AQP expression. All steps were performed with 700 μ g/mL G418 in culture media. For routine culture after establishment of the stable transfection, 200 μ g/mL was used to maintain light selection pressure.

2.4 Confocal Microscopy

Live cells in 35 mm Fluorodishes (World Precision Instruments) transfected with fluorescent constructs or with added fluorophores were imaged on either a Leica SP5 with a 63 \times 1.4 NA oil-immersion objective lens or a Zeiss 780 with a 63 \times 1.2 NA water-immersion objective. Both microscopes were in temperature-controlled environmental chambers that were warmed to 37 $^{\circ}$ C. Before imaging, culture media was replaced with 1 mL pre-warmed HEPES-buffered DMEM (Sigma) to maintain pH outside of a CO₂-controlled environment. Fluorophore

excitation was achieved using either 405, 458, 488 514, or 564 nm laser lines. Cellular compartments were visualised using the following fluorophores: plasma membrane – FM4-64 (Life Technologies); nucleus – Hoechst (Sigma Aldrich); endoplasmic reticulum – CellLight ER tracker (Life Technologies); F-actin – CellLight LifeAct-RFP plasmid DNA transfected at 1 µg/35 mm plate (Ibidi).

2.4.1 Tonicity-mediated translocation

Live cells were exposed to tonicity changes whilst on the stage of the microscope to allow imaging of the same cells before and after tonicity changes. This was done by adding treatment solutions designed to give the desired final ion concentrations and osmolality to 1 mL of culture media already on the cells. Images were analysed by extraction of fluorescence line profiles covering the membrane and avoiding the nucleus using ImageJ. The profiles were processed using homemade software in Matlab. Background was subtracted using the extracellular regions of the profile. Average membrane expression was calculated as the mean of the maximal intensity at the two membrane peaks and cytosol expression was calculated as the mean intensity in the region between the membrane peaks starting 10 pixels in. Relative membrane expression (RME) was then calculated as $(I_m - I_c)/I_m$, where I_m and I_c are the average membrane and cytosol intensities respectively as described by Conner et al [169]. This gives an RME of 1 if the entire signal is at the membrane and an RME of 0 if there are equal average intensities in membrane and cytosol pixels. Five profiles from different regions were used for each cell and the resulting RME values were averaged to give an estimate of the RME for that cell. One experimental repeat consisted of analysis of 5 profiles each from at least three different cells in the same image. Results from this software were validated by comparison to results

using the non-automated procedure previously described [169]. Figure 2-6 shows a schematic of this analysis method.

2.4.2 Fluorescence recovery after photobleaching (FRAP)

FRAP was performed using a circular bleaching area of radius 1 μm . Bleaching was performed at 100% laser power, which was maintained until the fluorescence in the bleach region was reduced to <10% of the pre-bleach fluorescence. After bleaching, fluorescence from the bleached area was measured every 5 seconds and recovery curves were fitted to a single phase exponential recovery function. Diffusion coefficients were calculated using the approach and equation of Kang et. al. [208]:

$$D = \frac{r_e + r_n}{8\tau_{1/2}}$$

Where D is the diffusion constant, r_n is the bleaching radius (set by the experimenter, 1 μm in our experiments), $\tau_{1/2}$ is the half-time of recovery from the exponential fit and r_e is an effective bleaching radius, measured from a post-bleach image. This effective radius corrects for the fact that bleaching is not instantaneous and therefore during bleaching some bleached fluorophores will diffuse out of the bleaching region and some unbleached fluorophores will diffuse into the bleaching region, tending to make the actual bleached area larger than that set by the experimenter. Recovery curves were collected from 5 different cells on the same plate per experiment in 6 experimental repeats.

2.4.3 Forster resonant energy transfer (FRET)

AQP4-Turquoise2 and AQP4-Venus constructs were generated by site-directed mutagenesis of the AQP4-GFP construct described in section 2.1.1. Turquoise2

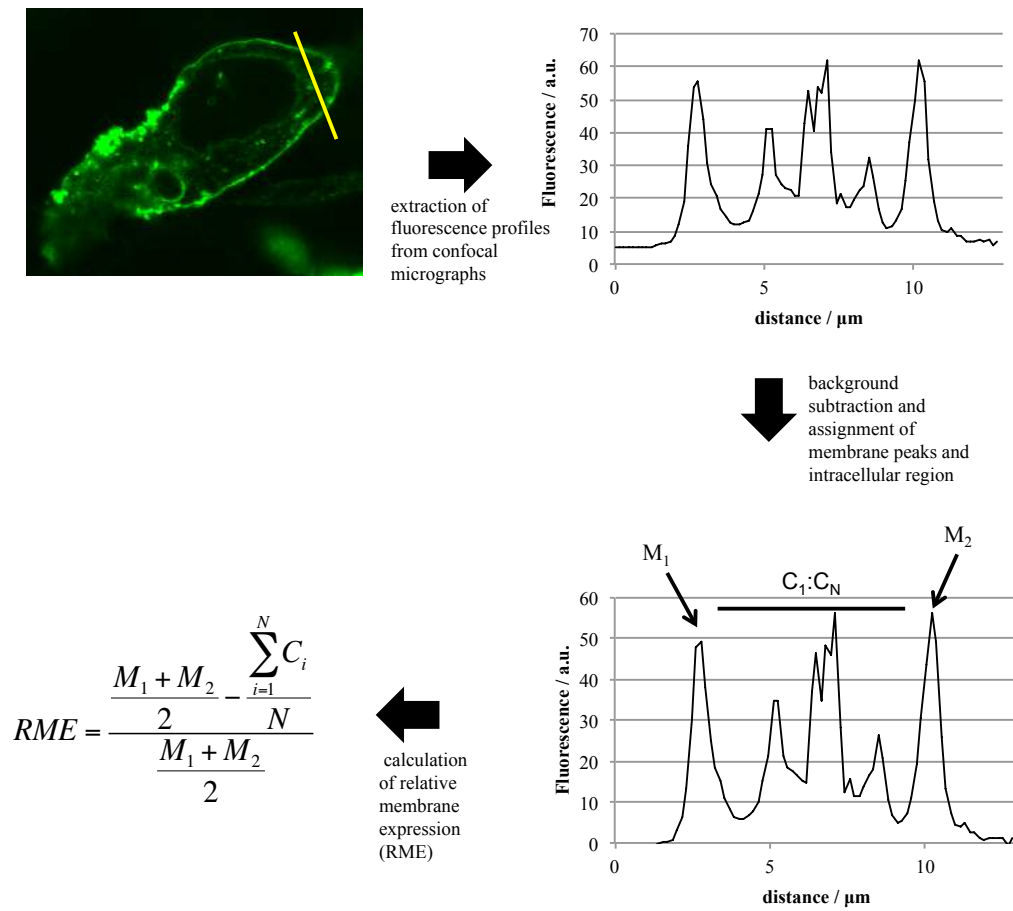


Figure 2-6 Calculation of the relative membrane expression of GFP fusion proteins from confocal fluorescence micrographs.

is a cyan fluorescent protein (CFP) derivative [209] and Venus is a yellow fluorescent protein (YFP) derivative [210].

CFP has an excitation maximum at ~425 nm and an emission maximum at 474. Venus has an excitation maximum at 515 nm and emission maximum at 528 nm. The microscope system used for this work had a 405 nm diode laser and 458 nm Argon laser line which could both be used to excite CFP. Both lasers gave similar fluorescence intensity for CFP at the same laser power, however the 405 nm laser excited Venus much less efficiently, so was chosen to minimize direct excitation of Venus in the FRET experiments.

FRET experiments were performed using the sensitized emission methodology with the FRET signal corrected for donor emission in the acceptor channel and direct excitation of the acceptor, following van Rheenen et al [211] and normalised to the acceptor emission to give a normalized apparent FRET efficiency:

$$e = \frac{F_{IA} - \beta F_D - (\gamma - \alpha\beta)F_A}{(1 - \beta\delta)F_A}$$

where F_{IA} is the measured indirect (i.e. with donor excitation) acceptor fluorescence (the FRET signal), F_D is the direct donor emission, F_A is the direct acceptor emission and the greek letters are correction factors for acceptor fluorescence excited by the donor laser and detected at through the donor filters (α), donor fluorescence detected through the acceptor filters (β), excitation of the acceptor excited by the donor laser and measured through the acceptor filters (γ), and FRET signal measured through the donor filters (δ). The correction factors were obtained by imaging samples containing donor only or acceptor only before performing full FRET experiments.

2.6 Lance cAMP assay

The Lance cAMP kit (Perkin Elmer) was used to measure intracellular cAMP according to the manufacturer's instructions. Because relatively small increases in cAMP were measured (~10-fold), the number of cells used in the assay was optimized to give a basal signal between 25% and 50% of the maximal assay response according to the produced cAMP standard curves. This was 10,000 cells/well for HEK293 cells and 20,000 cells/well for rat primary astrocytes. 10 μ M forskolin (Sigma-Aldrich) was used as a positive control for adenylyl cyclase activity. Forskolin was prepared as a 10 mM stock in DMSO and stored at -20 $^{\circ}$ C. 0.5 mM 3-isobutyl-1-methylxanthine (IBMX, Sigma-Aldrich) was used as a phosphodiesterase inhibitor. IBMX was prepared as a 1 M stock in DMSO and stored at -20 $^{\circ}$ C. All treatments were performed on cells adhered to tissue culture plates in DMEM. After treatments, cells were trypsinized and resuspended in stimulation buffer. The stimulation buffer used in the assay was $\text{Ca}^{2+}/\text{Mg}^{2+}$ -free PBS, 0.1% w/v BSA, 0.5 mM IBMX. Stimulation buffer was heated to 37 $^{\circ}$ C and vortexed to thoroughly dissolve IBMX and BSA and filtered through a 0.22 μ m filter to remove any undissolved material. The FRET signal was read on a Pherastar FS plate reader (BMG Labtech).

2.7 PKA activity assay

An ELISA-based assay kit (Abcam) was used to measure PKA activity in cell lysates according to the manufacturer's instructions. Cells were lysed in a non-denaturing, phosphatase inhibiting lysis buffer for 45 mins, centrifuged at 21,000 rcf for 10 minutes to remove insoluble material and protein was quantified using detergent-insensitive Bradford assay (Expedeon). Lysates were diluted in lysis

buffer as required to load 200 ng of total cellular protein in 30 μL (i.e. 6.66 ng/ μL) per well of the assay plate.

2.8 Calcein fluorescence quenching

Calcein is a fluorescent molecule that is quenched by protein in a concentration-dependent manner. If the volume of a cell changes, so too does the intracellular protein concentration. Therefore, on short timescales where the number of protein molecules in a cell can be taken as constant, calcein fluorescence can be used as probe of cell volume. By applying an osmotic gradient to AQP-expressing cells and measuring the rate of change of fluorescence (and thereby volume), the membrane water permeability can be quantified. This methodology was originally developed using fluorescence microscopy [212], and has since been adapted for fluorescence plate readers [213, 214]. We followed the protocol designed by Fenton et al [213] to measure membrane water permeability, and adapted it to measure membrane solute permeability.

Cells were plated in cell culture-treated black-walled clear-bottomed 96 well plates (Corning) either the day before an experiment or two days before if transient transfections were required. 90 mins before the start of experiments, cells were loaded with calcein using 5 μM calcein-AM (Life Technologies) and 1 mM probenecid (Sigma-Aldrich) in culture media (probenecid is an organic anion transporter antagonist used to prevent calcein leakage). Calcein-AM was prepared as a 5 mM stock in DMSO and stored at $-20\text{ }^{\circ}\text{C}$ in foil. Probenecid was prepared as a 175 mM stock in 200 mM NaOH and stored at $-20\text{ }^{\circ}\text{C}$. After 90 minutes at $37\text{ }^{\circ}\text{C}$, cells were washed twice in HEPES buffered DMEM with 1 mM probenecid. HEPES buffering was to allow the cells to remain buffered in

the CO₂-free environment of the plate reader. Cells were incubated for 10 mins at 37 °C to equilibrate with the new media (in a 75 µL volume). A BioTek Synergy HT plate reader was used for all experiments. The plate reader temperature control was set to 37 °C 1 hour before the experiment. The plate reader injection system was not temperature-controlled, so all solutions that were used in the injection system were pre-warmed to 37 °C in a water bath. During the experiment, injected solutions were stored in 15 mL tubes (Greiner) and kept at 37 °C using a heating block. Tubes were covered in parafilm to minimize evaporation. **Error! Reference source not found.** is a photograph of this set-up. Background was corrected for by including three wells of calcein-free cells on each plate and subtracting the average fluorescence of these wells from all readings with calcein. Fluorescence data was then normalized to the average of the first 5 readings for each well and single phase exponential decay functions were fitted by a least squares algorithm using the Solver tool in Microsoft Excel.

2.8.1 Water permeability

For water permeability measurements, 75 µL of 600 mM mannitol in HEPES-buffered DMEM (media osmolality 300 mOsm; total osmolality 900 mOsm) was injected to give a final osmolality of 600 mOsm and an osmotic gradient of 300 mOsm to induce cell shrinkage following Fenton et al. [213]. Fluorescence was measured every 50 ms. After 5 s of baseline readings, 75 µL of the mannitol-containing DMEM was injected. Relative fluorescence was converted to relative volume using a standard curve generated by measuring the relative change in fluorescence for cells subjected to varying extracellular osmolality and measuring the volume of cells from the same passage subjected to the same osmolality using a Coulter counter.

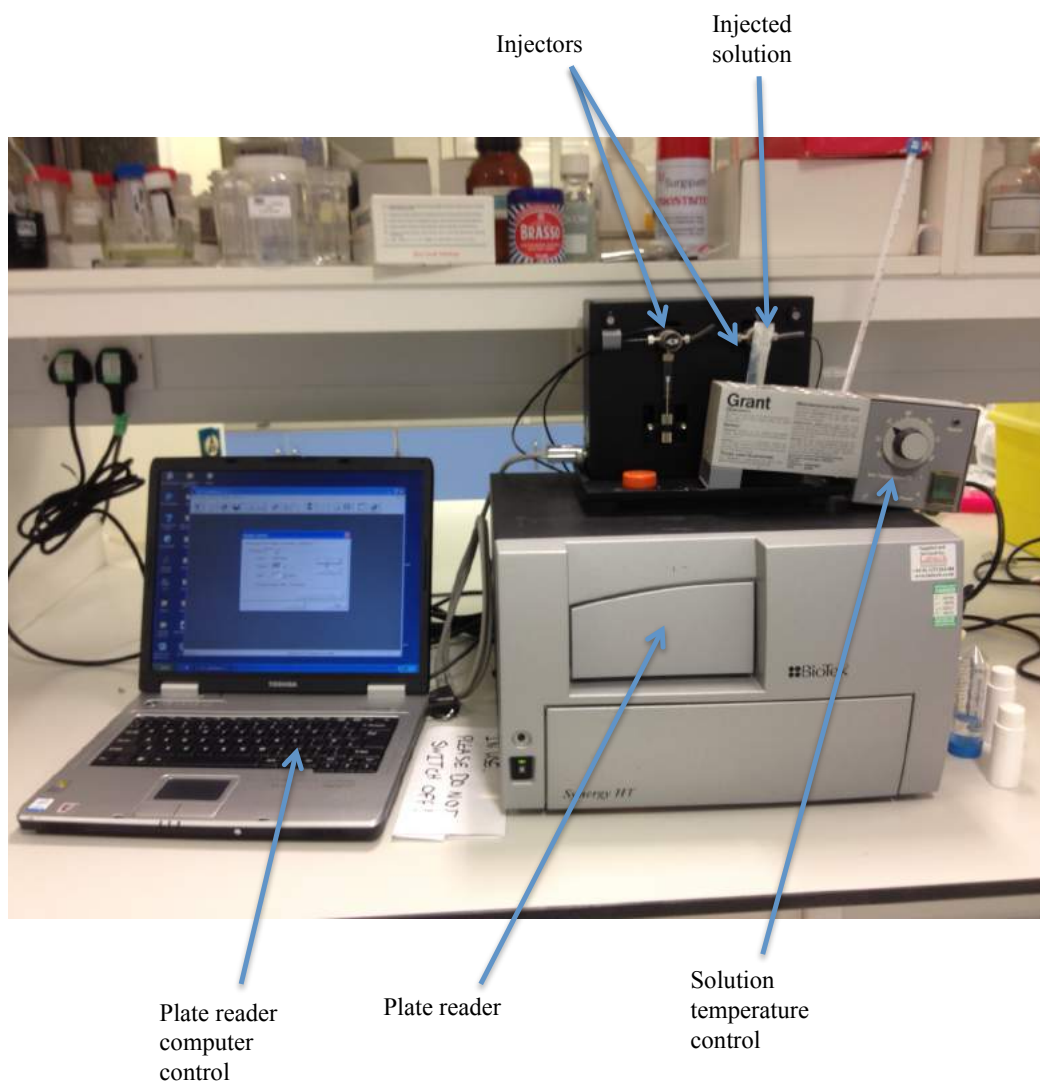


Figure 2-7 Plate reader setup for calcein fluorescence quenching.

2.8.2 Solute permeability

To measure solute permeability, isotonic solutions of the desired solute are added to AQP-expressing cells. If the cell membrane is permeable to the solute, it will enter the cell down the solute concentration gradient. This will make the inside of the cell hypertonic compared to the outside, and therefore water will follow the solute by osmosis to maintain osmotic equilibrium, causing cell swelling. This methodology has been used to quantify the permeability of AQPs expressed in *Xenopus* oocytes using video microscopy [204], but to our knowledge, the calcein fluorescence quenching methodology has never been used to quantify AQP solute permeability.

For neutral solute permeability measurements, fluorescence was measured every 50 ms. After 5 s of baseline readings, 75 μL of an isotonic (300 mM) solution of the relevant solute, in dH_2O , was injected to give a final concentration of 150 mM. Relative fluorescence was converted to relative volume using a standard curve generated by measuring the relative change in fluorescence for cells subjected to varying (0-150 mM) concentrations of isotonic glycerol and measuring the volume of cells from the same passage subjected to the same glycerol concentrations, using a Coulter counter (Figure 2-8). This method has not previously been used to quantify solute permeability; therefore to check that it gives comparable results to other methods, we quantified the inhibitory effect (IC_{50}) of a known AQP9 inhibitor, phloretin, on AQP9 glycerol permeability when transiently expressed in HEK293 cells. Phloretin has a published IC_{50} of 10 μM [215]. We found an IC_{50} of 12 μM , in good agreement with this (Figure 2-9). Interestingly, we found a better fit to the data using a dose-response curve in which the Hill coefficient was allowed to vary. The Hill coefficient controls the

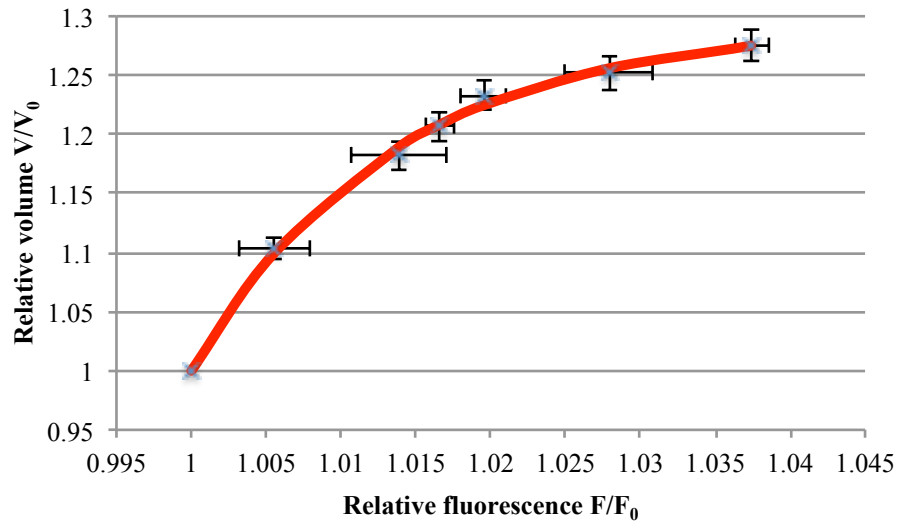


Figure 2-8 Calibration curve for conversion of relative calcein fluorescence to relative volume, measured using a Coulter counter, for intracellular glycerol concentrations of 0, 25, 50, 75, 100, 125 and 150 mM.

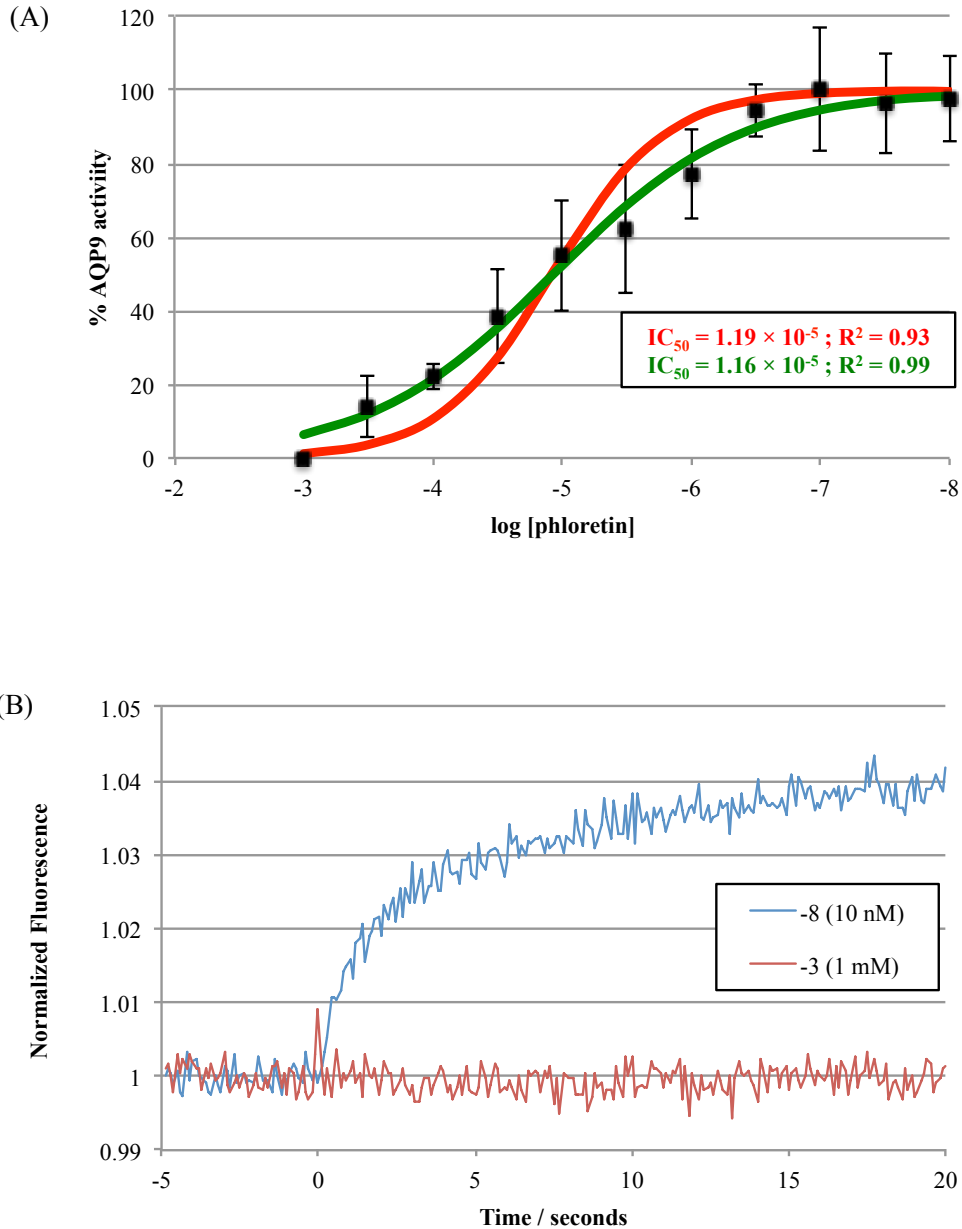


Figure 2-9 (A) Dose-response curves fitted to inhibition of AQP9 glycerol permeability by phloretin, with the Hill coefficient fixed to 1 (red), or allowed to vary (green). AQP9 activity was calculated by fitting the raw data to curves of the form $C - Ae^{-kt}$, and normalizing the rate constant to that for a vehicle-only (0.1% MeOH) control. (B) Representative single fluorescence traces for phloretin concentrations at the extreme ends of the dose-response curve (10 nM, blue; 1 mM, red).

steepness of the slope at the midpoint (IC_{50}), and a Hill coefficient different to 1 is indicative of cooperative binding or multiple binding sites with different affinities [216], which might suggest that phloretin binding to AQP9 is not a simple 1:1 reaction.

Cell-surface biotinylation

Cells were plated in 24-well plates 2 days before experiments for transient transfections and 1 day before otherwise. Transient transfections were done as described in section 2.3.1. Cell surface amines were biotinylated using a cell impermeable amine-reactive biotinylation reagent (EZ-Link Sulfo-NHS-SS-Biotin, Thermo Scientific). Cells were exposed to reductions in extracellular tonicity by diluting culture medium with dH_2O . After treatment, cell culture media was washed out with ice cold PBS (with Ca^{2+}/Mg^{2+}) adjusted to the appropriate tonicity with dH_2O , to remove amino acids and serum proteins that can compete for the NHS reaction whilst avoiding completely drying the cells. This was done by removing 375 μL of the 500 μL on the cells, keeping the plate flat, replacing it with an equal volume of PBS and repeating 5 times (corresponding to a dilution of culture media components by a factor of $4^5 = 1024$). Cells were incubated in 600 μL of 0.5 mg/mL biotinylation reagent in PBS diluted with dH_2O to the tonicity matching the cell treatment, on ice for 30 mins. For constitutive surface expression measurements, cells were washed twice in ice cold PBS instead of hypotonic treatment. Unreacted reagent was quenched 3 times in 25 mM glycine in PBS for 5 mins. Cells were lysed in 350 μL tris-triton lysis buffer (1% v/v triton X-100, 100 mM NaCl, 2 mM $MgCl_2$, 25 mM tris pH 7.4) for 45 minutes on ice. The lysate was centrifuged at 21,000 g at 4 °C for 10 minutes to remove insoluble material. Biotinylated proteins in the

supernatants were precipitated by incubation in Neutravidin-coated 96-well plates (Pierce) for 2 hours at 4 °C. 100 µL of each lysate was loaded in triplicate with the same amount of total cellular protein (measured by BCA assay) per lysate. Plates were washed three times with 0.05% PBS-tween and blocked with 3% w/v BSA in PBS for 1 hour at RT on an orbital shaker. After washing once with PBS-tween plates were incubated overnight on an orbital shaker at 4 °C with an AQP4 antibody (Abcam, ab128906) diluted 1:2,000 in 0.05% PBS-tween. Plates were washed with 3 times with 0.05% PBS-tween and incubated with HRP-conjugated secondary antibody (Santa Cruz, sc-2313) diluted 1:5,000 on an orbital shaker at RT for 1 hour. Plates were washed three times with 0.05% PBS-tween and incubated with *o*-phenylenediamine dihydrochloride (Sigma-Aldrich) HRP substrate for 30 minutes on an orbital shaker, wrapped in foil. A volume of 100 µL of each solution (block, antibodies, washes and substrate) was used. Absorbance was measured at 450 nm using a BioTek Synergy HT plate reader. Figure 2-10 is a schematic of the workflow of these experiments.

Linearity of the assay was confirmed by measuring the surface expression signal of HEK293 cells transfected with varying amounts (0-1 µg) of AQP4 DNA / 15 mm cell culture well (Figure 2-11). 0.5 µg (equivalent to 2 µg / 35 mm plate) was used for routine experiments with transfected HEK293 cells. Specificity for surface localized protein was confirmed by measuring the surface expression signal from HEK293 cells transfected with either AQP4-GFP or GFP alone, using an anti-GFP primary antibody. GFP alone should reside in the cytoplasm and give no surface signal, whereas GFP should be detected in the AQP4-GFP sample due to being covalently bound to the surface AQP4 (Figure 2-11).

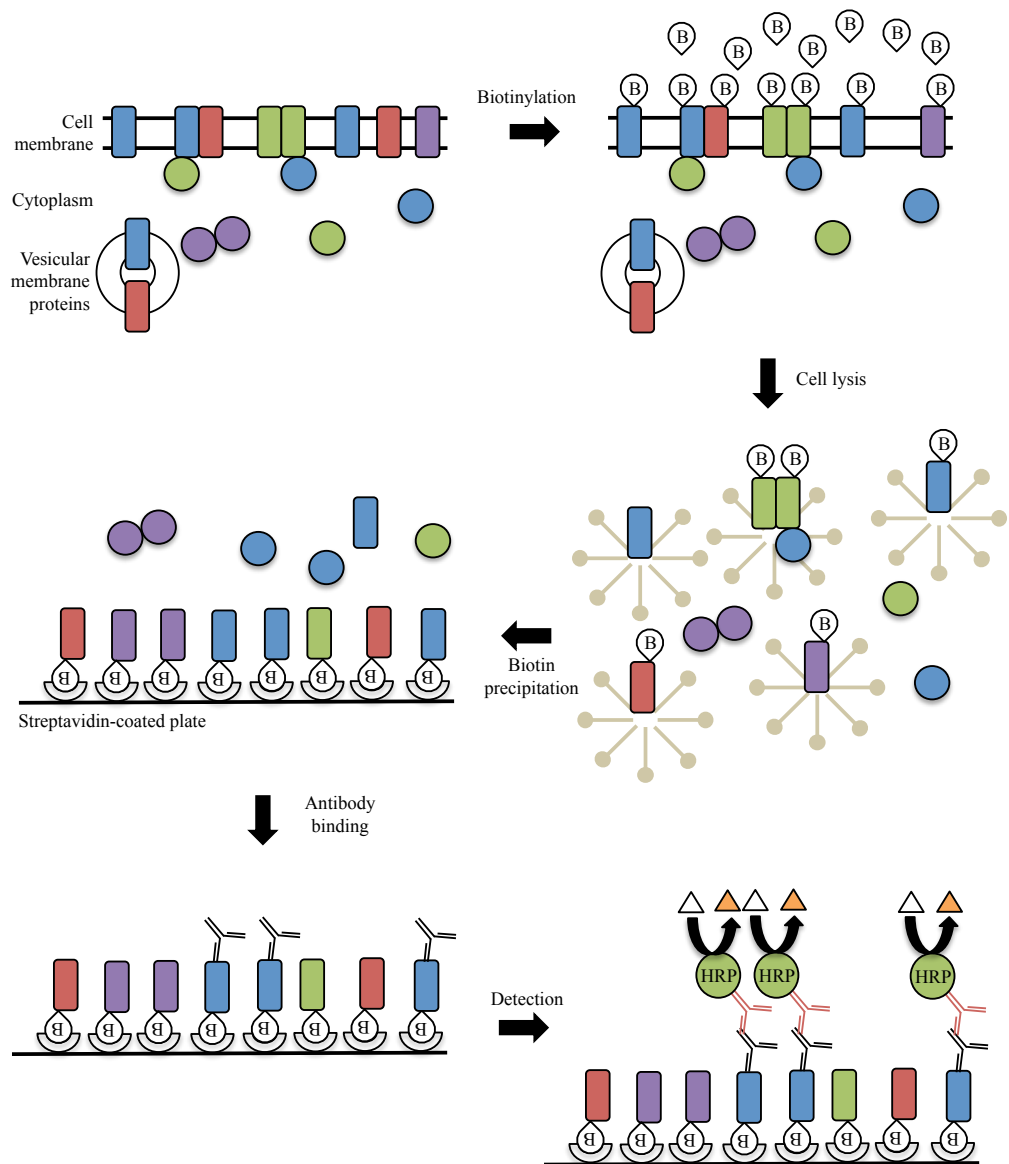


Figure 2-10 Schematic representation of cell surface biotinylation protocol. B – biotinylation reagent. HRP – horseradish peroxidase. Rectangles represent transmembrane proteins and circles represent cytoplasmic proteins.

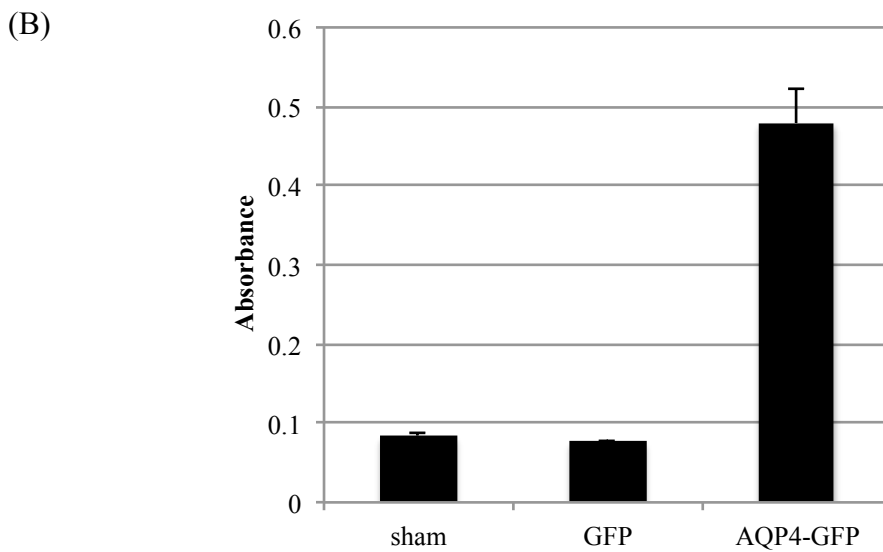
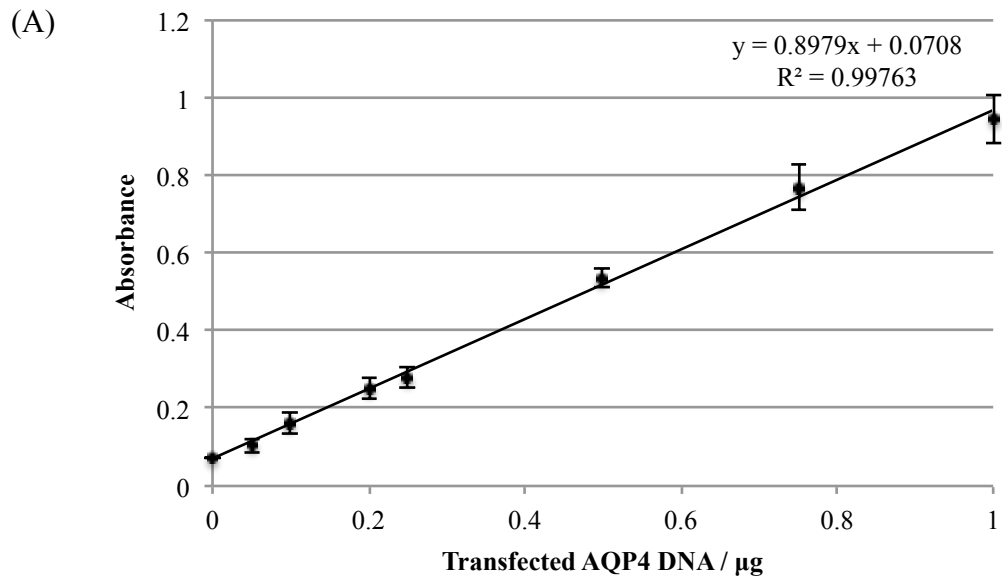


Figure 2-11 (A) Linearity of surface expression signal of AQP4-GFP transfected into HEK293 cells as a function of the amount transfected DNA. (B) Surface expression signal, detected using an anti-GFP antibody, from HEK293 cells transfected with either AQP4-GFP or GFP alone, demonstrating specificity for surface-localized protein. Data is represented as mean \pm SEM, $n=3$.

2.9 SDS-PAGE

SDS-PAGE was performed following a standard protocol. 0.75 mm thick 8% acrylamide gels were handcast using standard handcasting equipment (Bio-Rad). Stacking gels were 4% acrylamide. Samples were prepared by lysing a confluent 35 mm dish of cells in 250 μ L of ice cold RIPA buffer (1% v/v triton X-100, 0.5% w/v sodium deoxycholate, 0.1% SDS, 150 mM NaCl, 50 mM tris, pH 8) supplemented with a protease inhibitor cocktail (2 mM AEBSF, 0.3 μ M aprotinin, 16 μ M bestatin, 14 μ M E-64, 1 μ M leupeptin, 1 mM EDTA, Sigma). Lysates were centrifuged at 21,000 g for 10 mins at 4 $^{\circ}$ C to remove insoluble material. Protein concentration was determined using a detergent-insensitive Bradford assay (Bradford MX, Expedeon) according to the manufacturer's instructions. 8 concentrations (0.1-2 mg/mL) of bovine serum albumin dissolved in RIPA buffer were used to make a standard curve. For transiently transfected HEK293 cells, 200 ng of total protein per well was loaded on the polyacrylamide gel. For stably transfected MDCK cells 1 μ g was loaded. Lysates were mixed with an equal volume of 2x Laemlli buffer (4% w/v SDS, 20% v/v glycerol, 0.02% w/v bromophenol blue, 4% v/v β -mercaptoethanol, 120 mM tris, pH 6.8) and incubated for 10 mins at room temperature before loading onto the gel. High temperature (commonly 70 or 95 $^{\circ}$ C) incubation steps are commonly used at this point to facilitate protein denaturation. This was not done because high temperature was found to cause AQPs to aggregate (Figure 2-12). Electrophoresis was done at 200 V for 45 mins. Molecular weights were estimated using a commercial pre-stained protein marker (New England Biolabs).

2.10 Blue native (BN)-PAGE

Blue native PAGE was performed following the protocol of Fiala et al. [217] with the following modifications. 8% acrylamide gels were used instead of gradient gels. 1% triton X-100 was used in the lysis buffer. BSA was used as a molecular weight marker to give bands at 66 and 132 kDa (corresponding to monomeric and dimeric BSA). Lysates were not dialyzed as this was found to have no effect on protein migration (Figure 2-12). Gels were destained using 10% v/v acetic acid, 40% v/v methanol. Proteins were denatured before Western blotting by soaking in 1% w/v SDS in tris-buffered saline (150 mM NaCl, 50 mM tris, pH 7.5).

2.11 Western blotting

Proteins separated on polyacrylamide gels were transferred to methanol-activated PVDF membranes using a wet electroblotting system (Bio-Rad). Electrophoresis was done at 100 V for 1 hour. Membranes were blocked using 25 mL 20% w/v powdered skimmed milk (Marvel) in 0.1% PBS-tween for 1 hour on an orbital shaker. This was done in upside-down micropipette tip box lids. After blocking, membranes were washed 3 times for 5 mins in PBS-tween. Membranes were incubated in 5 mL of primary antibody diluted in PBS-tween at the appropriate optimized dilution (see section 2.12) overnight on a roller mixer in a 4 °C refrigerated room. This procedure was identical for SDS- and BN-PAGE.

2.12 Antibodies

2.12.1 Primary antibodies

Boster PA1220 rabbit polyclonal antibody to AQP4 and Abcam ab11026 mouse polyclonal antibody to AQP4 were tested and did not detect AQP4 transfected

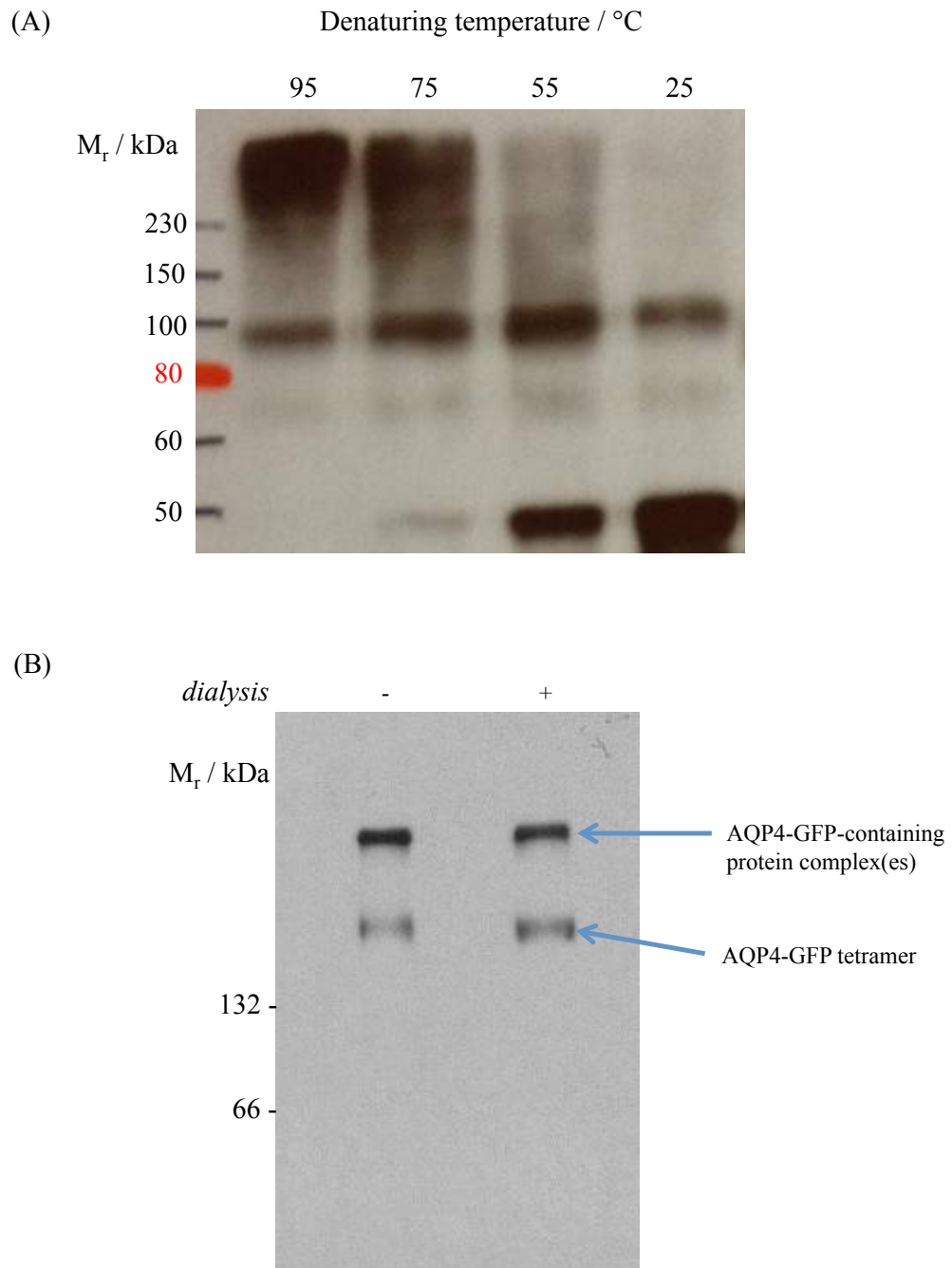


Figure 2-12 (A) Aggregation of AQP4 construct in SDS-PAGE when subjected to denaturation above room temperature. (B) Dialysis of lysates for BN-PAGE had no effect on protein migration.

into HEK293 cells or produced interfering non-specific bands. Abcam ab128906 rabbit monoclonal antibody to AQP4 and Abcam ab6556 rabbit monoclonal antibody to GFP both detected AQP4-GFP fusion proteins and gave no background for untransfected control lysates, so these were used routinely for cell surface biotinylation and SDS/BN-PAGE. Abcam ab46182 rabbit polyclonal antibody to AQP4 was raised against an extracellular loop of AQP4 so was tested in cell surface expression ELISA. Although this antibody clearly detected AQP4 in Western blots, there was no difference in cell surface ELISA signal between AQP4-transfected cells and control cells. This may represent partial occlusion of the epitope by the cell membrane in the native environment.

2.12.2 Secondary antibodies

Donkey anti-rabbit and donkey anti-mouse antibodies conjugated to horseradish peroxidase (Santa Cruz Biotechnology, sc-2313 & sc-2318) were used at the manufacturer recommended dilution (1:5,000).

2.13 Inhibitors and agonists

Compound	Target	Concentration
W-7	CaM inhibitor	500 μ M
Trifluoperazine	CaM inhibitor	127 μ M
CALP-3	CaM agonist	114 μ M
Hypericin	Broad spectrum protein kinase inhibitor	100 μ M
H-89	Non-specific kinase inhibitor (including PKA)	5 μ M
Myristoylated PKI amide	Protein kinase A inhibitor	3.6 μ M
Myristoylated PKC peptide inhibitor	Protein kinase C inhibitor	200 μ M
Demecolchine	Microtubule depolymerizing agent	24 μ M
Cytochalasin D	Actin polymerization inhibitor	100 μ M
IBMX	Phosphodiesterase inhibitor	500 μ M
Forskolin	Adenylyl cyclase agonist	10 μ M
Probenecid	Organic anion transporter inhibitor	1,000 μ M

Table 2-1 Inhibitors and agonists used for elucidation of cell signalling pathways

Where possible, inhibitors or agonists were used at 100× the IC₅₀ or EC₅₀ stated on the manufacturer's datasheet. CALP-3 was used at 3× EC₅₀ due to cost and limited solubility.

2.14 Molecular dynamics simulations

Simulations were done using Gromacs software, version 4.5.5 [218]. The GROMOS53A6 [219, 220] forcefield was used and modified to include lipid parameters [221]. An AQP4 tetramer was generated according to the biological assembly entry in the AQP4 PDB file 3GD8 [222]. N- and C-termini of the protein were truncated in the structure so proteins were simulated with neutral termini. The AQP4 tetramer was embedded into pre-equilibrated POPC bilayers using inflateGRO [223] and hydrated using Gromacs. Na⁺ and Cl⁻ were added to a final concentration of 100 mM. Equilibration was achieved by steepest gradient energy minimization, 100 ps NVT simulation with 1000 kJmol⁻¹nm⁻¹ restraints on protein heavy atoms followed by three 1 ns NPT simulations with 1000, 100 and 10 kJmol⁻¹nm⁻¹ restraints on protein heavy atoms followed by 30 ns unrestrained simulation. A Nosé-Hoover thermostat [224] (0.5 ps, 310 K) was used to maintain constant temperature and 2 Parinello-Rahmann barostats [225] (2 ps, 1 atm) were used to maintain constant pressure with zero surface tension. 1.4 nm cut-offs were applied for dispersion and short-range electrostatic interactions. Long-range electrostatics were treated using the particle mesh Ewald method [226]. Hydrogen bonds were identified using the Hbonds plugin of VMD [227] using 3Å and 20° cut-offs. Hydrogen bond occupancy was calculated according to these cut-offs at 100 ps intervals along the trajectories and averaged over the 4 monomers. All analysis was done either with tools built into Gromacs or using VMD software [227].

3 Results – Hypotonicity-induced relocalization of AQP4

3.1 Aims

The aims of the work presented in this chapter were:

1. To determine whether AQP4-GFP fusion proteins can relocalize to the plasma membrane of HEK293 cells in response to hypotonicity in a similar manner that reported for AQP1-GFP.
2. To investigate the cell signalling pathway(s) underlying this relocalization.
3. To develop a complementary method of measuring AQP surface expression that does not require the protein to be tagged.
4. To apply this complementary method to cells that are more physiologically relevant for AQP4 than HEK293 cells.
5. To apply the methods used at the beginning of the chapter to study relocalization of human AQP5 to support X-ray crystallography experiments.

3.2 Background

AQP4 is highly expressed in the glial cells of the CNS and facilitates the osmotically driven pathological brain swelling associated with stroke and traumatic brain injury. Human AQP4 is a relatively-recently discovered member of the 13-strong family of mammalian AQPs [26]. AQP4 is found in a number of tissues including the kidney and GI tract but is notable for its high levels in astrocytes and its role in water homeostasis in the brain [228].

AQP4 has been shown to be important for brain oedema formation following traumatic brain injury (TBI), stroke and meningitis [229]. AQP4 knock-out mice were protected from the formation of cytotoxic oedema in a stroke model [83], providing an explicit molecular target for managing this condition. Despite extensive research that has built on the well-understood structural biology of the AQP family, there are no drugs available to block water movement through AQP4 and in general, known AQP inhibitors are either cytotoxic (mercurial compounds) or are non-specific, leading to undesirable off-target effects [230-232]. Understanding the regulation of AQP4 subcellular localization could provide a novel therapeutic platform for the treatment and/or prevention of cytotoxic oedema.

The most well studied system in which cellular water flow is regulated is the translocation of AQP2 in response to AVP in the cells of the collecting duct of the mammalian kidney [233]. AQP2 is shuttled between the apical cell surface and intracellular vesicles in order to regulate water reabsorption. The mechanism involves AVP-mediated production of cAMP resulting in the activation of PKA and direct phosphorylation of the AQP2 C-terminal tail at serine 256 [234]. Specific SNARE proteins that facilitate the exocytosis of AQP2-containing vesicles have been identified [235]. Other AQPs have been shown to be translocated in response to environmental stimuli; a recent review suggested an emerging consensus on sub-cellular relocalization as a regulatory mechanism for the AQP family [236] following the discovery of the PKC-mediated translocation of threonine-phosphorylated AQP1 in response to changes of tonicity [169, 237].

There is a requirement for rapid, physiological regulation of AQP4, which could be achieved at the transcriptional level or by short-term sub-cellular relocalization. There is contradictory evidence of transcriptional regulation of AQP4 in animal stroke models, with some studies reporting increased expression and others decreased expression [238], but whether AQP4 relocalization could be involved in the short or long term has yet to be investigated. AQP4 localization may be regulated by numerous intracellular mechanisms including PKA [239], PKC [240] and actin reorganization [241]. It is not clear if there are common mechanisms either within the AQP family or even for AQP4 in different cell types; this indicates a general lack of mechanistic awareness of AQP regulation. In this chapter, evidence is presented which suggests that AQP4 cell surface expression can be rapidly and reversibly regulated in response to changes of tonicity in primary cortical rat astrocytes and in transfected HEK293 cells. The translocation mechanism involves influx of extracellular calcium, activation of CaM and PKA activation, probably via activation of a Ca^{2+} /CaM dependent adenylyl cyclase. Five putative PKA phosphorylation sites were identified and site-directed mutagenesis used to show that only phosphorylation at one of these sites, S276, was necessary for the translocation response in HEK293 cells. This site was phosphorylated *in vivo* in rats [242] and mice [243] and the mechanism also required PKA activity in primary cortical astrocytes. This data represents a novel mechanism that could suggest targets for therapeutic discovery in the treatment of cytotoxic brain oedema.

3.3 Results

3.3.1 AQP4-GFP undergoes a rapid and reversible sub-cellular relocalization in HEK293 cells in response to changes in the tonicity of the extracellular environment

HEK293 cells were used to investigate AQP4 sub-cellular relocalization as they are tractable for screening cellular inhibitors and protein mutants, as previously demonstrated by the discovery of the mechanism of tonicity-induced relocalization of human AQP1 using GFP-tagged proteins in our laboratory [169, 237]. The distribution of AQP4-GFP fusion proteins transfected into HEK293 cells was altered by changes in tonicity of the external environment, achieved by dilution of the culture media with dH₂O. Live-cell confocal microscopy (Figure 3-1 A-D) showed a rapid translocation of AQP4 to the cell surface in response to hypotonicity (following a 30s exposure from 340 mOsm/kg H₂O to 85 mOsm/kg H₂O). This effect was fully reversible. Surface expression of AQP4-GFP in fluorescence micrographs was quantified by calculating the relative membrane expression (RME) as described in section 2.4.1. Briefly, the difference between the average membrane fluorescence and the average intracellular fluorescence was calculated and this was normalized to the maximum fluorescence intensity (cells with protein evenly distributed between membrane and intracellular compartments have an RME of 0 and cells with 100% of the protein at the membrane have an RME of 100). Figure 3-1 shows that AQP4-GFP RME changed from 27.86 ± 3.52 to 67.11 ± 4.47 , $n=3$, $p=0.001$. The change in AQP4-GFP localization upon changing the extracellular tonicity from 340 mOsm/kg

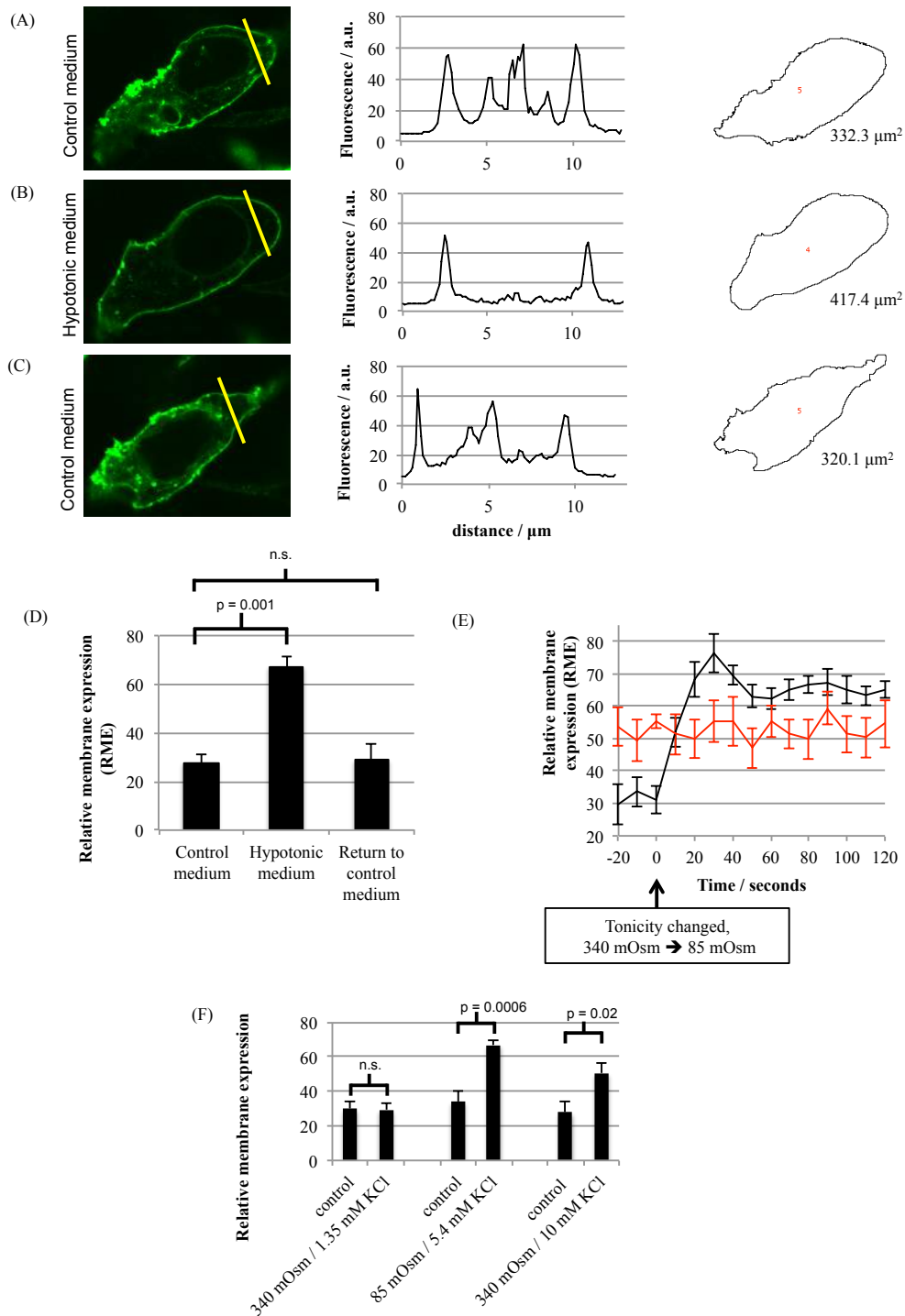


Figure 3-1 Representative fluorescence micrographs of AQP4-GFP in HEK293 cells following exposure to: (A) control medium (340 mOsm/kg H₂O); (B), 30-s exposure to hypotonic medium (85 mOsm); and (C) return to isotonic medium with fluorescence intensity profiles across the *yellow lines* and cross-sectional areas calculated using ImageJ. (D) RME in the three conditions. $n=3$. p values from paired t-tests with Bonferroni's correction following ANOVA. (E) RME timeseries of AQP4-GFP (black) and AQP3-GFP (red) in HEK293 cells. (F) $[\text{K}^+]_o$ reduction (*left pair* of bars) and hypotonicity (*central pair*) were applied independently and $[\text{K}^+]_o$ was increased to 10 mM in isotonic conditions (*right pair*). All data are presented as mean \pm S.E.

H₂O to 85 mOsm/kg H₂O happened on a timescale of 30 seconds. The change in RME was probably not due to a dilution effect or an artefact of the GFP tag as AQP3-GFP fusion proteins showed a similar distribution between membrane and cytoplasm, but no significant change in RME in response to reduced tonicity (Figure 3-1 E).

Increased [K⁺]_o has been reported to increase plasma membrane water permeability of cultured astrocytes, via phosphorylation of AQP4 at S111 [77]. It was not clear whether this effect was mediated by AQP4 translocation to the membrane or changes in single channel water permeability (or even an AQP4-independent effect). However, it does suggest that the translocation measured in our system could be a response to reduced [K⁺]_o, rather than a response to reduced extracellular osmolality *per se*. To investigate this, reduced osmolality and reduced [K⁺]_o were applied independently (Figure 3-1 F). The translocation response was not due to a reduction in extracellular potassium concentration as isotonic reduction of [K⁺]_o had no effect on RME, whereas hypotonicity in the presence of constant [K⁺]_o had the same effect as hypotonicity induced by dilution of all solutes (Figure 3-1 F). Cells swelled leading to a 45 ± 1% increase of cross-sectional area after 1 minute compared to a 5 ± 1% increase for non-transfected cells in the same images, visualized using the fluorescent membrane marker FM4-64 (Figure 3-2).

AQP4 translocation was observed following a reduction of the extracellular tonicity to 85 mOsm/kg H₂O (from 340). Reduction to 170 mOsm/kg H₂O had no effect (Figure 3-3). RME was 25.98 ± 5.32 in control medium, 33.07 ± 5.24 in 170 mOsm hypotonic medium (not significantly different from control) and

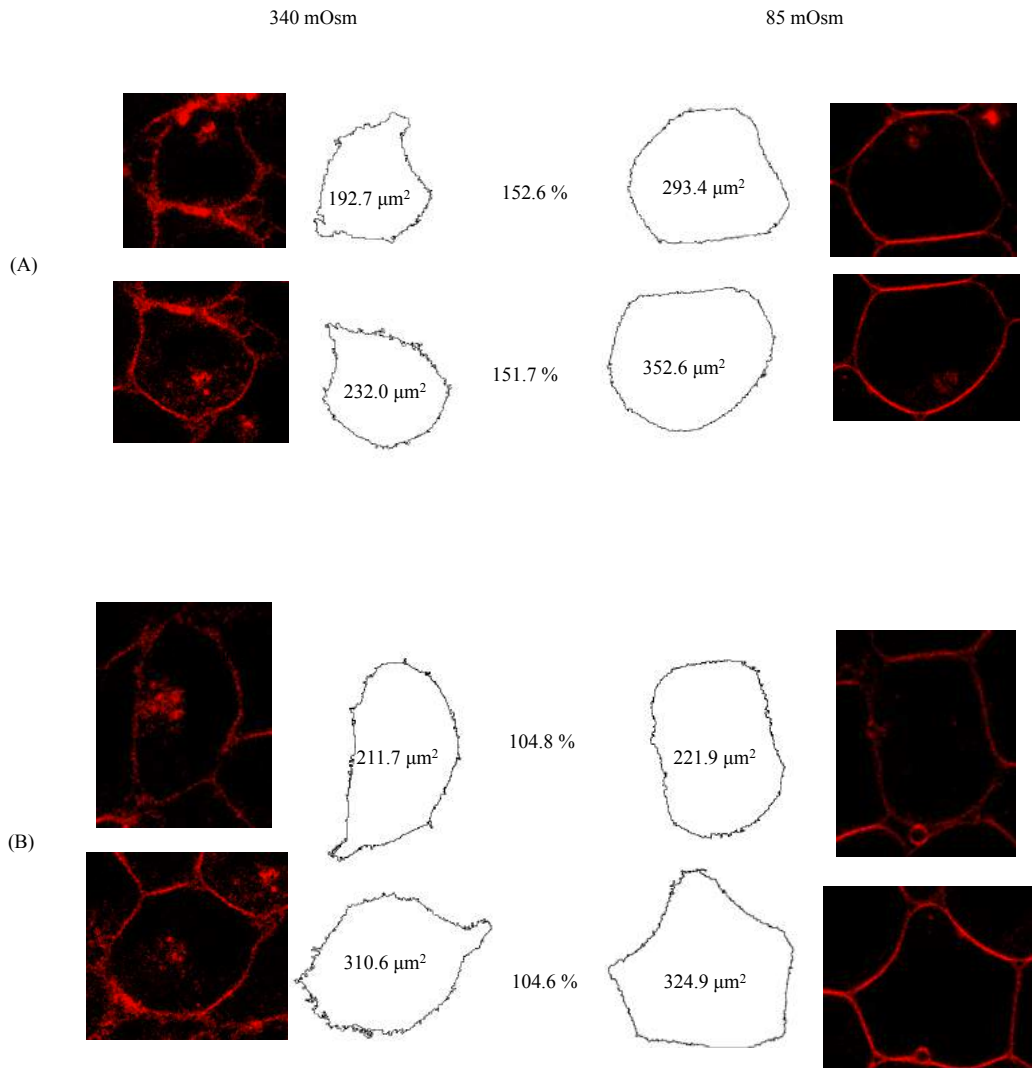


Figure 3-2 Representative cross-sectional areas of (A) AQP4-GFP transfected and (B) non-transfected HEK293 cells on the same plate before and after hypotonic challenge. Cells were visualized using the fluorescent membrane marker FM4-64 and AQP4 expression was determined by presence or absence of GFP signal. Areas were calculated using a particle detection algorithm built into ImageJ. The post-hypotonic challenge area as a percentage of the pre-challenge area is shown between each pair of images.

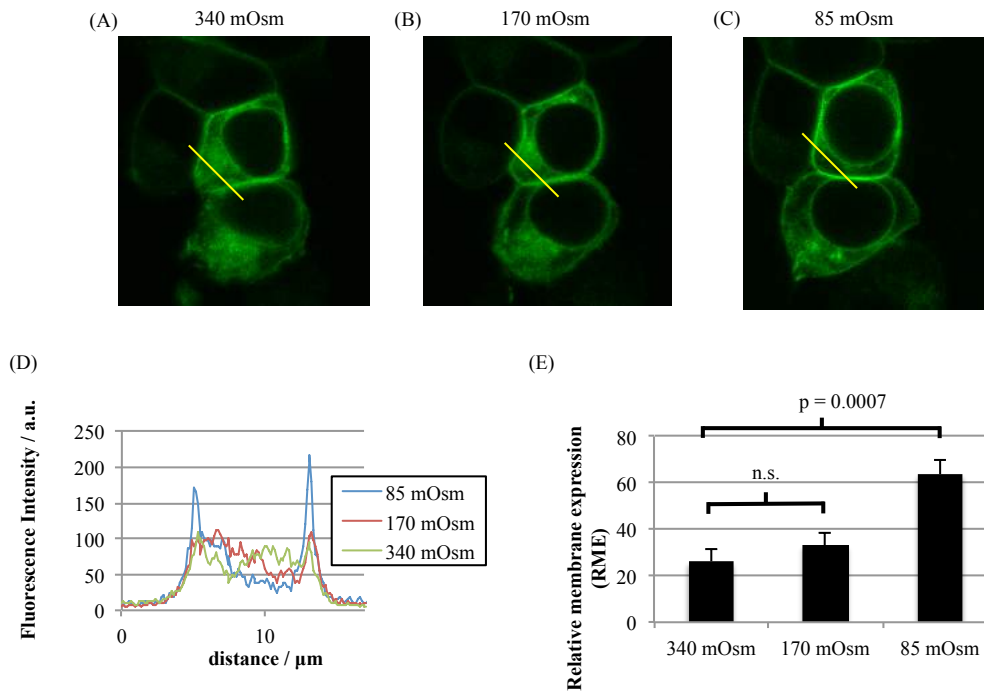
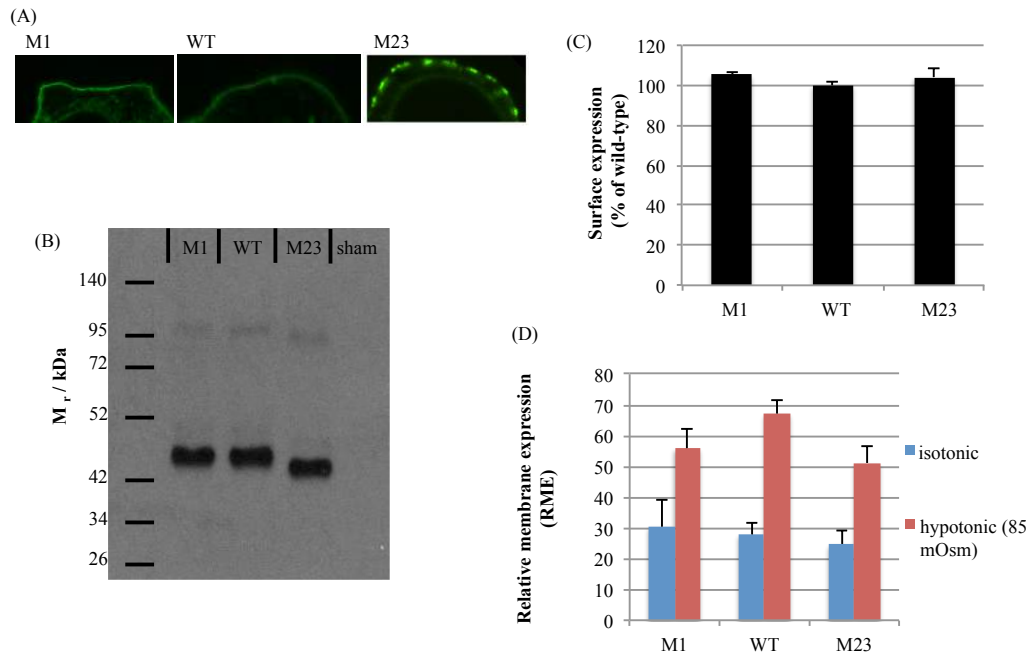


Figure 3-3 A–C, AQP4-GFP-transfected HEK293 cells were imaged by confocal microscopy in solutions of: (A) 340 mOsm/kg H₂O (B) 170 mOsm and (C) 85 mOsm. Capture of each image was started 30 s after the change in tonicity. For 170 mOsm, cells were allowed to equilibrate for 10 min to check for a slower translocation response. No difference was observed between 30 s and 10 min images. (D) Representative fluorescence profiles along the *yellow lines* in (A–C). (E) Mean RME for the three tonicities, averaged over at least three cells/experimental repeat, $n = 3$. p values are from paired t tests with Bonferroni's correction following ANOVA. All data are presented as mean \pm S.E. *n.s.*, not significant.

63.61 ± 6.16 in 85 mOsm hypotonic medium, $p=0.0007$ compared to 340 mOsm, after Bonferroni correction, $n=3$.

3.3.2 Both AQP4 isoforms relocated equally in HEK293 cells

Human AQP4 exists in two isoforms: a long M1 form and a shorter M23 form that lacks the initial 22 amino acids of M1 (and there is evidence of further isoforms in rat [244]). Both proteins can be translated from the same full-length transcript by a 'leaky scanning' mechanism and different cell types express different M1/M23 ratios [245] via an unknown regulatory mechanism. To determine whether both or a single isoform was expressed from the wild-type AQP4 gene in our HEK293 system, we created constructs lacking either the M1 or M23 translation initiation sites and compared the molecular weights of the resulting proteins with that translated from the wild-type gene, using SDS-PAGE. Figure 3-4 shows that only the M1 isoform was present in HEK293 cells transfected with the wild-type AQP4 gene. M1 and M23 constructs had basal surface expression (i.e. at 340 mOsm) equivalent to the wild-type, measured using cell surface biotinylation. The confocal microscopy experiments described in section 3.3.1 were repeated using the M1 and M23 constructs. M23 formed the punctate orthogonal arrays of particles (OAPs) that have been previously described for this isoform [246]. RME for M23 changed from 24.58±4.85 at 340 mOsm/kg H₂O to 51.15±5.25 at 85 mOsm/kg H₂O, $n=3$ $p=0.004$. The difference in hypotonic RME between M23, M1 and wild-type AQP4 were not significantly different ($p=0.33$). This suggested that both isoforms are equally translocated to the surface in response to hypotonic stimulus.



3.3.3 CaM, calcium and PKA regulate AQP4 relocalization

AQP surface expression is known to be regulated by numerous cellular mechanisms. These include protein kinases, calcium channels and cytoskeletal reorganization [236]. AQP4 relocalization following hypotonic challenge was compared in the presence of a number of inhibitory compounds. These are described in Table 3-1. Inhibition of PKA by (in increasing order of specificity) hypericin, H-89 and myristoylated PKA substrate peptide (myrPKI) prevented AQP4 translocation, as did removal of calcium from the extracellular medium, and two inhibitors of CaM (a calcium-binding protein that mediates many of the downstream effects of calcium influx or release from intracellular stores). These data suggest that a combination of PKA kinase activity and calcium signalling mechanisms are required for AQP4 translocation. Prevention of the translocation response by inhibitors correlated with a reduction in cell swelling, suggesting a functional increase in membrane water permeability.

3.3.4 Endogenous AQP4 in cultured primary rat astrocytes undergoes sub-cellular relocalization in response to hypotonicity

AQP4 is expressed in the astrocytes of the CNS. To investigate AQP4 relocalization in a more physiologically relevant system, surface expression of endogenous AQP4 in rat primary cortical astrocytes was measured using cell surface biotinylation followed by a neutravidin-based ELISA as described in section 0. Figure 3-5 shows that AQP4 surface localization increased 2.7-fold after 10 minutes of hypotonic challenge at 85 mOsm/kg H₂O (n=3, p=0.006) but

Inhibitor/Control Media	Isotonic RME (± SEM)	Hypotonic RME (± SEM)	Mean % area change (± SEM)	Translocation
Untreated control	28.77 (6.78)	78.84 (1.84)*	145.19 (1.11)*	Yes
Non-specific kinase inhibitor (hypericin)	21.85 (6.80)	38.22 (5.58)	103.50 (2.05)	No
PKC (myrPKCi)	27.27 (4.73)	55.28 (3.97)*	141.00 (2.05)*	Yes
PKA (H-89)	23.11 (6.91)	29.81 (4.93)	107.31 (4.17)	No
PKA (myrPKI)	25.62 (5.16)	33.66 (6.62)	102.97 (5.21)	No
Actin inhibition (cytochalasin D)	26.07 (6.10)	34.91 (5.48)	121.87 (4.81)	No
Microtubule inhibition (demecolcine)	26.14 (5.89)	27.17 (8.14)	107.68 (7.13)	No
Calcium-free media	26.69 (6.03)	32.16 (4.48)	111.60 (1.92)	No
CaM inhibitor (W7)	16.86 (8.43)	22.11 (8.14)	110.31 (14.21)	No
CaM inhibitor (trifluoperazine)	27.23 (7.11)	31.40 (5.91)	108.61 (5.47)	No

Table 3-1 Translocation of AQP4-GFP in HEK293 cells in the presence of various inhibitors, measured by confocal microscopy and subsequent image analysis. Cells were imaged before and after reduction of the extracellular osmolality to 85 mOsm/kg H₂O. Each RME value is an average over three independent experiments, with each experiment analyzing at least 3 cells/micrograph. $p < 0.05$ was considered statistically significant (*).

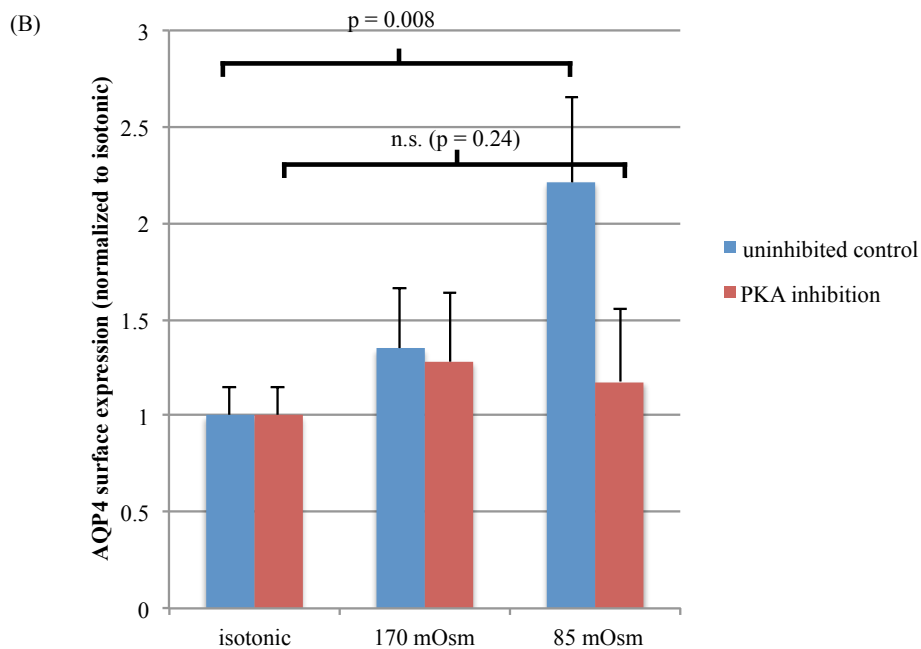
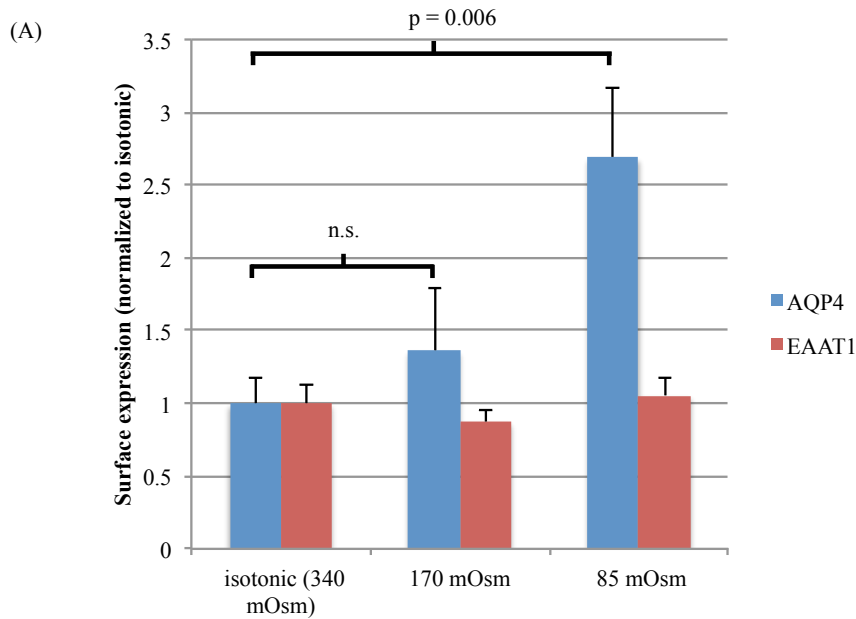


Figure 3-5 (A) Cell surface biotinylation of primary rat astrocytes subjected to hypotonicity and analysis of endogenous AQP4 surface expression. As a negative control for translocation, membrane expression of the glutamate transporter EAAT1 was measured under the same conditions, $n=3$. None of the variability in EAAT1 surface expression was statistically significant, $p=0.37$. (B) As above for AQP4 in the presence and absence of a PKA inhibitor (myrPKI). AQP4 surface expression increased 2.2-fold between 340 and 85 mOsm/kg H_2O , $n=3$, $p=0.008$. In the presence of the inhibitor, AQP4 surface expression did not change significantly between 340 and 85 mOsm/kg of H_2O , $n=3$, $p=0.24$. All data are presented as mean \pm S.E. *n.s.*, not significant.

did not change significantly after 10 minutes of hypotonic challenge at 140 mOsm/kg H₂O. It is important to confirm that this response is not due to a general effect of hypotonicity on vesicular membrane proteins or changes in protein availability for labelling due to membrane unfolding associated with cellular swelling. To discount these, we measured surface expression of the astrocytic excitatory amino acid transporter EAAT1. Surface expression of EAAT1 did not change significantly with either hypotonic treatment (n=3, $p=0.37$) and there was no significant effect on cell viability measured by trypan blue exclusion (data not shown).

3.3.5 PKA activity is required for endogenous AQP4 relocalization in primary astrocytes

HEK293 cells provide a tractable model for studying the cell signalling components required for AQP4 translocation. However, it is possible that, despite sharing the translocation response, HEK293 cells and primary astrocytes translocate AQP4 by different mechanisms. To validate the mechanistic information obtained in HEK293 cells, we repeated the primary astrocyte cell surface biotinylation experiments in the presence of a PKA inhibitor. Figure 3-5 shows that a 30 minute pre-incubation with myrPKI prevented the hypotonicity-induced relocalization of endogenous AQP4 in rat primary cortical astrocytes. This suggests that the mechanistic details elucidated using HEK293 cells are probably comparable to the translocation of endogenous AQP4 in primary astrocytes.

3.3.6 Hypotonicity induces intracellular cAMP production and PKA activity in primary rat astrocytes

Influx of extracellular calcium through several members of the TRP family of cation channels is a well-established cellular response to extracellular hypotonicity [247], although it is still unclear whether these channels open directly in response to swelling-associated changes in membrane tension or are activated downstream of some other mechanosensory or osmosensory system [248]. Previous work in our laboratory showed that this calcium response happens in HEK293 cells, is required for the hypotonicity-induced translocation of AQP1 and that the TRPC antagonist SKF96365 blocks the calcium response and the AQP1 relocalization [169]. In the case of AQP1, PKC was found to phosphorylate AQP1 to mediate the translocation. Some isoforms of PKC can be directly activated by calcium alone, suggesting a direct link between the TRP-mediated calcium influx and AQP1 phosphorylation.

Unlike AQP1, the relocalization of AQP4 required PKA (and not PKC) for the translocation response. To investigate how PKA might be activated by calcium influx, measurement of intracellular cAMP (the activator of PKA) accumulation in response to hypotonicity were made in the presence and absence of extracellular calcium and a CaM agonist and antagonist (Figure 3-6 A).

Hypotonicity (85 mOsm) increased intracellular cAMP by 11-fold ($n=3$, $p=0.01$), whereas hypotonicity in the absence of extracellular calcium or in the presence of the CaM antagonist W-7 did not change intracellular cAMP significantly (both $n=3$, $p=0.40$ and $p=0.22$ respectively). The CaM agonist CALP-3 was able to elicit the same cAMP response in isotonic conditions ($n=3$, $p=0.02$ vs. basal; $p=0.16$ vs. hypotonicity). PKA activity in response to the same

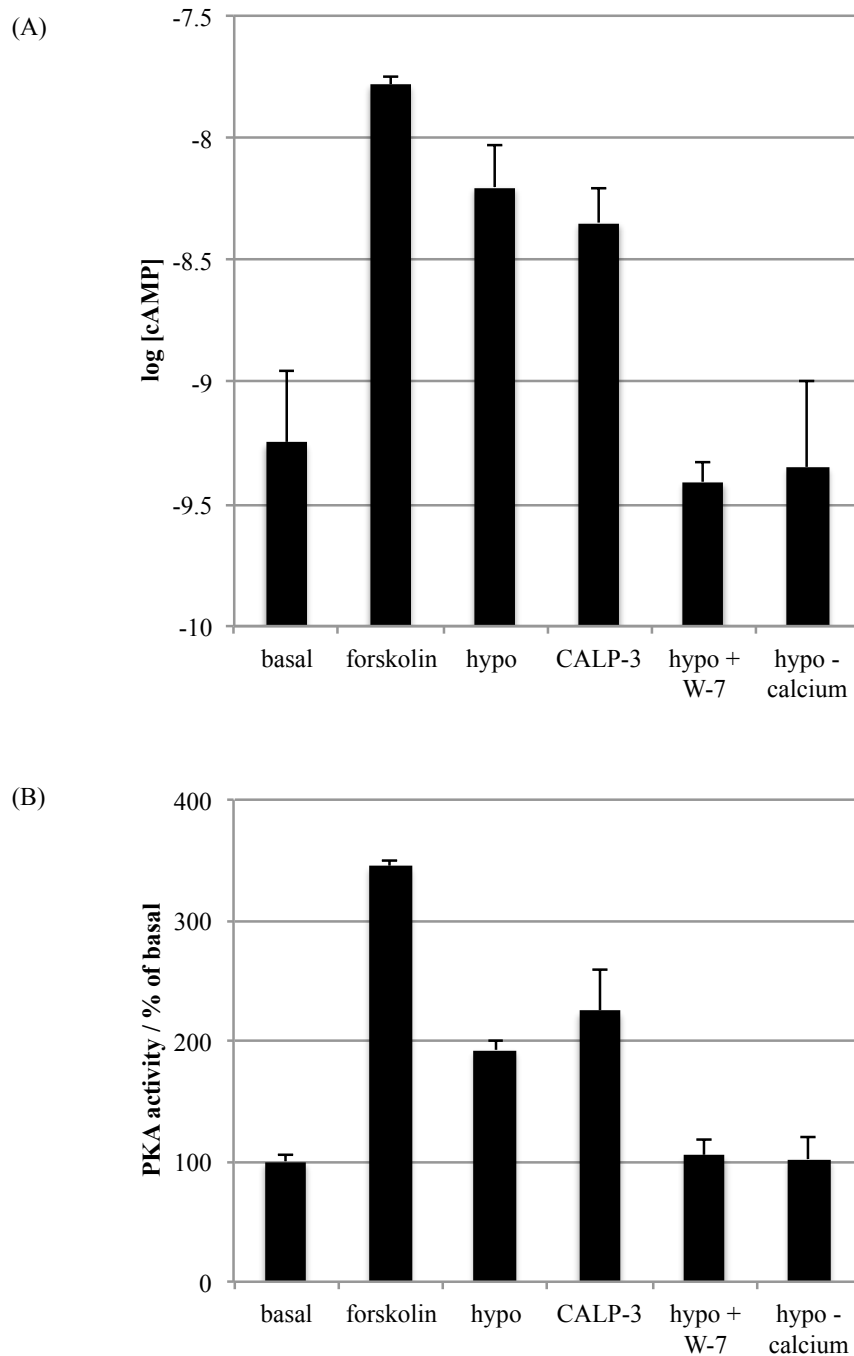


Figure 3-6 (A) Intracellular cAMP accumulation in rat primary cortical astrocytes in response to forskolin (adenylyl cyclase agonist, positive control), hypotonicity with and without extracellular calcium and CaM antagonist W-7, and the CaM agonist CALP-3. (B) PKA activity in lysates made from rat astrocytes subjected to the same treatments. Activity is normalized to the basal control. 100% on this scale is equivalent to 2.3 ± 0.1 ng active PKA / μ g of total cellular protein.

set of stimuli was also measured, and the PKA activity followed the same pattern as the cAMP accumulation (Figure 3-6 B).

3.3.7 S276 phosphorylation is required for relocalization

The data in Table 3-1 suggest a key role for PKA (but not PKC) in mediating AQP4 translocation. Using kinase site prediction software (NetPhosK 1.0 [249]), five serine residues were identified as PKA consensus sites. These were S52, S111, S180, S188 and S276. The locations of these residues in the AQP4 structure are shown in Figure 3-7.

The PKA consensus sites were individually mutated to alanine (to block phosphorylation) and aspartate (to act as a phosphomimetic). The effects of these mutations on the tonicity-induced relocalization of AQP4 are tabulated in Table 3-2. Only mutations to S276 had any effect on hypotonicity-induced translocation. Substitution of S276 with alanine (S276A) blocked hypotonicity-induced translocation while substitution with aspartate (S276D) had no effect, suggesting that PKA phosphorylation at S276 is necessary but not sufficient for translocation to occur or that S276D is a poor phosphomimetic. To determine whether this single phosphorylation event was the only mechanistic effect of PKA, translocation of the S276D mutant was measured in the presence of a PKA inhibitor (myrPKI). Unlike the wild-type protein, for which the translocation was inhibited by myrPKI, S276D still translocated to the membrane in the presence of the PKA inhibitor. This shows that S276D is a phosphomimetic and that PKA phosphorylation of AQP4 at S276 is a key step in the AQP4 translocation signalling pathway. Although the S52A mutant behaved like wild-type AQP4, S52D did not translocate, but also had greatly reduced basal surface expression in comparison to wild-type AQP4 and other phosphomimetic mutants. Low

Mutant	Isotonic RME (\pm SEM)	Hypotonic RME (\pm SEM)	Mean % CSA change (\pm SEM)	Translocation	Constitutive surface expression (% of wild-type)
S52A	34.18 (4.06)	59.34 (5.53)*	127.03 (5.99)*	Yes	98.1 (5.3)
S52D	N/A	N/A	N/A	No	17.0 (6.3)*
S111A	36.24 (9.95)	62.43 (5.42)*	130.69 (4.76)*	Yes	94.8 (6.4)
S111D	31.17 (4.22)	52.99 (5.41)*	120.62 (8.40)*	Yes	91.4 (4.6)
S180A	35.43 (7.78)	69.03 (6.94)*	142.65 (7.78)*	Yes	109.8 (4.5)
S180D	36.86 (6.07)	53.56 (4.96)*	148.16 (16.74)*	Yes	99.7 (5.0)
S188A	34.17 (7.21)	63.31 (7.00)*	137.01 (9.17)*	Yes	98.6 (3.2)
S188D	31.64 (9.11)	59.18 (5.60)*	135.53 (10.47)*	Yes	104.1 (4.2)
S276A	36.61 (4.64)	36.97 (5.53)	110.82 (3.85)	No	96.8 (3.2)
S276D	25.72 (5.42)	57.93 (11.01)*	134.18 (15.10)*	Yes	83.5 (5.7)*
S276D + PKA inhibitor	24.58 (4.85)	51.14 (5.25)*	127.12 (7.34)*	Yes	86.2 (5.1)*

Table 3-2 Translocation of phosphomimetic and phospho-blocking mutants of AQP4-GFP in HEK293 cells, measured by confocal microscopy and subsequent image analysis. Cells were imaged before and after reduction of the extracellular osmolality to 85 mOsm/kg H₂O. Each RME value is an average over three independent experiments, with each experiment analysing at least 3 cells/micrograph. Constitutive surface expression was measured by cell surface biotinylation and normalised to wild-type expression. $p < 0.05$ was considered statistically significant (*).

surface expression prevented calculation of the RME and measurement of cross-sectional area in confocal micrographs. S52D appeared to be localized throughout the cytoplasm (rather than degraded or held as inclusion bodies) suggesting that the protein is not simply grossly mis-folded. This may reflect a functional relevance, possibly interrupting processing through the Golgi apparatus or post-Golgi trafficking to the cell surface, which may be worthy of further study.

3.3.8 AQP5 surface localization is controlled by phosphorylation, PKA and hypotonicity

AQP5 is a water-selective channel expressed in the lacrimal and salivary glands and lungs, where it is thought to be important for generation of tears, saliva and pulmonary secretions [182, 192, 193]. Our data from this study on AQP4 combined with the publications on AQP1 suggest the possibility of a common relocalization machinery for these channels. There are two consensus PKA sites in AQP5: S156 in cytoplasmic loop D [27, 194] and T259 [195] in the C-terminus; the latter corresponds to S256 in AQP2. AQP5 can be directly phosphorylated by PKA at S156 and T259 [196]. Notably, S156 was phosphorylated preferentially in certain tumours suggesting that cell proliferation can be modulated by phosphorylation of this site although the constitutive membrane abundance of an S156A mutant was not distinguishable from wild-type AQP5 [197]. Based on the crystal structure of human AQP5 it was hypothesized that phosphorylation of S156 could cause structural changes in loop D that would break its interaction with the C-terminus, thereby flagging the protein for translocation to the plasma membrane [198]. In order to test this hypothesis on the role of S156 in the membrane translocation of AQP5, we used

real time translocation studies in living HEK293 cells as described earlier in this chapter (section 3.3.1).

The RME of AQP5-GFP was increased by the introduction of the S156E phosphomimetic mutation from 0.56 ± 0.02 to 0.67 ± 0.01 ($n=3$, $p=0.01$), whereas the RME of AQP5-S156A was not significantly different ($n=3$, $p=0.36$) to wild-type AQP5-GFP (Figure 3-8).

The RME of AQP5-GFP (wild-type and the S156A and S156E mutants) was measured after a 30 minute incubation with PKA inhibitor (myrPKI) or vehicle control. PKA inhibition increased the RME of all AQP5 constructs (Figure 3-9) compared to non-inhibited controls, suggesting a role for PKA signalling in the internalization of AQP5 as previously suggested [192]. PKA inhibition further increased the membrane abundance of the S156E mutant, indicating that the PKA inhibition effect is independent of the phosphorylation status of S156.

Reduction of the extracellular osmolality to 85 mOsm/kg H₂O caused rapid relocalization of AQP5 from intracellular compartments to the plasma membrane in a manner comparable to AQP1 [237] and AQP4 (Figure 3-10). The initial AQP5-GFP distribution profile was restored on returning to normal physiological osmolality. The RME of AQP5-GFP increased from 0.56 ± 0.03 in control medium to 0.72 ± 0.01 in hypotonic medium. Similarly, the RME increased from 0.55 ± 0.02 to 0.71 ± 0.02 for the S156A mutant and from 0.67 ± 0.02 to 0.81 ± 0.01 for the S156E mutant. Despite an increased level of constitutive surface expression, the change in RME for the S156E mutant ($\Delta RME = 0.14 \pm 0.01$) was similar to that for AQP5 or the S156A mutant ($\Delta RME = 0.15 \pm 0.03$ and 0.13 ± 0.02 respectively). Inhibition of PKA, despite increasing constitutive surface

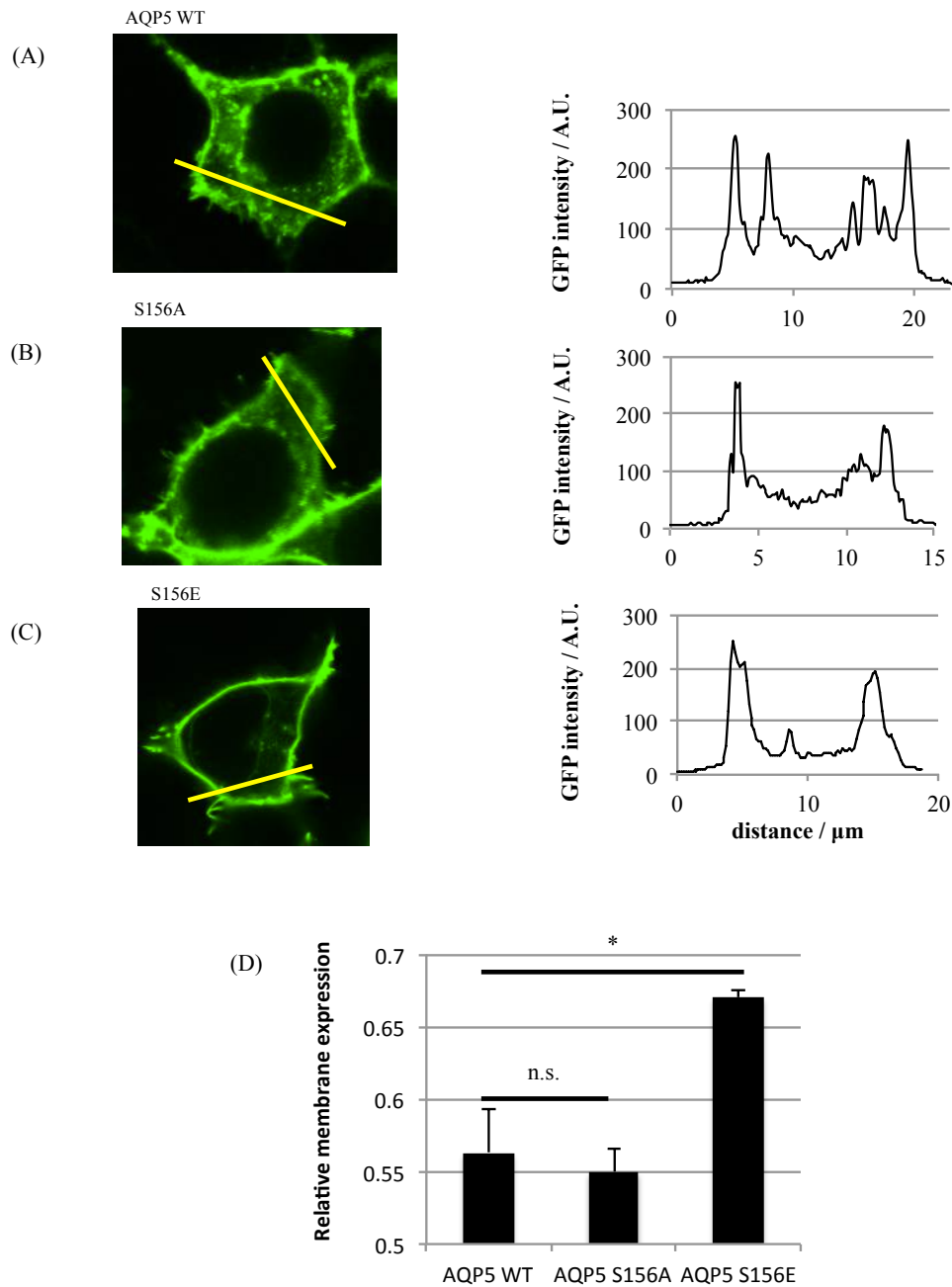


Figure 3-8 (A-C) Representative fluorescence micrographs of AQP5-GFP and S156 mutants in HEK293 cells in isotonic medium with fluorescence intensity profiles across the *yellow lines* (D) RME of the three constructs, $n=3$. * represents $p < 0.05$ and n.s. not significant ($p > 0.05$) from unpaired t-tests with Bonferroni's correction following ANOVA.

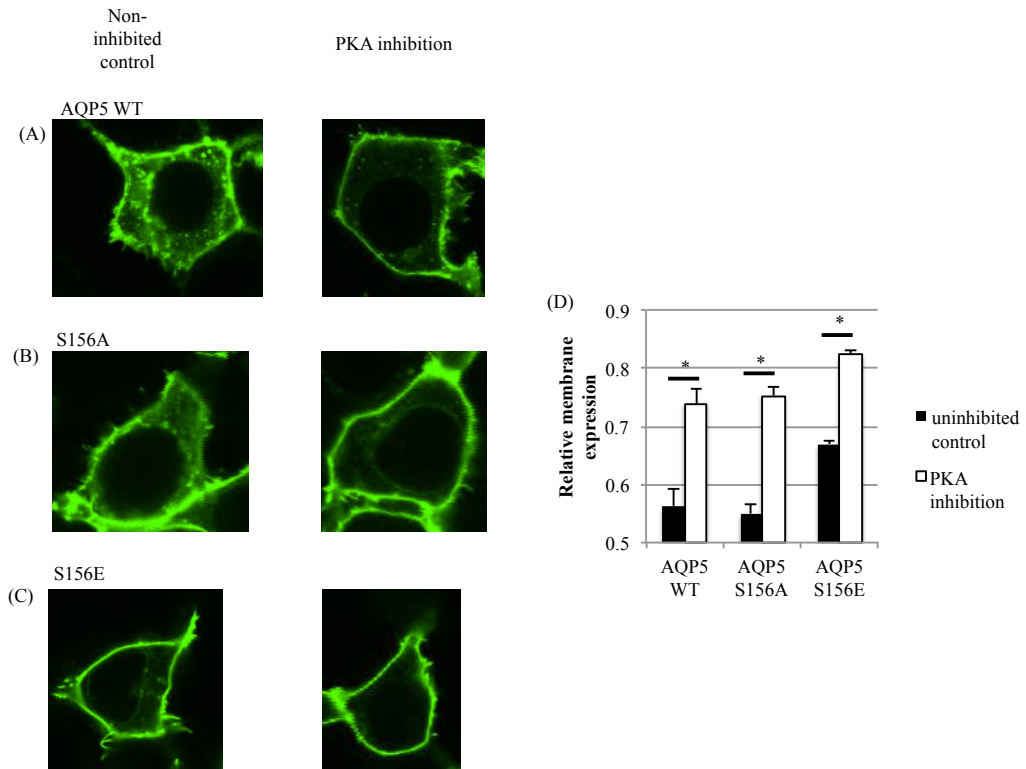


Figure 3-9 Representative fluorescence micrographs of AQP5-GFP and S156 mutants in HEK293 cells in isotonic medium, with and without 30 minute pre-incubation with the PKA inhibitor myrPKI (D) RME of the three constructs and two conditions, $n=3$. * represents $p<0.05$ from unpaired t-tests with Bonferroni's correction following ANOVA.

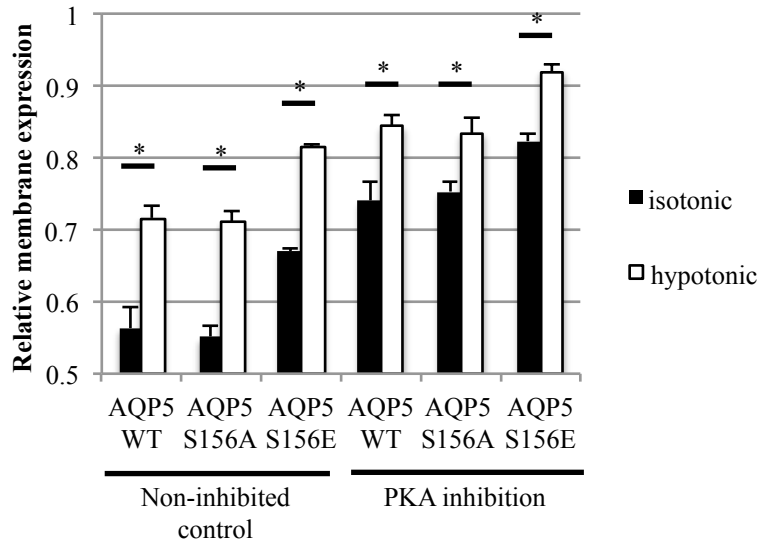


Figure 3-10) RME of the three AQP5 constructs in HEK293 cells subjected to a reduction of the extracellular osmolality from 340 mOsm/kg H₂O (isotonic, black bars) to 85 mOsm/kg H₂O (hypotonic, white bars), with and without inhibition of PKA by a 30 minute pre-treatment with myrPKI, *n*=3. * represents *p*<0.05 from paired t-tests with Bonferroni's correction following ANOVA.

expression of all constructs, did not inhibit the hypotonicity-induced relocalization of AQP5. Taken together, these results suggest that hypotonicity-induced relocalization of AQP5 is not mediated by either PKA activity or phosphorylation at S156.

3.4 Discussion

3.4.1 AQP4

AQP4-GFP fusion proteins in HEK293 cells and endogenous AQP4 in primary rat astrocytes rapidly relocalize to the plasma membrane in response to a reduction in local tonicity. The relocalization response takes about 30 seconds in HEK293 cells and is completely reversible upon return of the local tonicity to 340 mOsm/kg H₂O. The concomitant cell swelling following AQP4 relocalization (which was reduced by inhibitors that blocked the translocation response) suggests that there is an effective increase in cell membrane water permeability. The mechanisms involved in AQP4 relocalization require PKA activity and cytoskeletal elements. Extracellular calcium is required, presumably passing through TRP channels, which are known to mediate a calcium signalling response to osmotic cell swelling [250].

CaM inhibition using two different CaM inhibitors (W7 and trifluoperazine) also blocked AQP4 translocation in response to hypotonicity. CaM-mediated regulation of AQPs is well established. CaM has been shown to inhibit AQP0 water permeability by binding directly to the C-terminal tail [251, 252] and this binding can be inhibited by AQP0 phosphorylation [202]. In rat parotid cells, AQP5 was rapidly translocated to the apical membrane via acetylcholine signalling and inhibition of signalling elements downstream of CaM (CaM

kinase II, myosin light chain kinase and nitric oxide synthase) blocked this translocation response [253]. AVP-induced translocation of AQP2 in collecting duct cells can be attenuated by extracellular calcium in a CaM-dependent manner [254]. CaM has also been shown to bind directly to the N-terminal tail of AQP6 [255], although the functional relevance of this interaction is unknown. We showed previously that inhibition of CaM prevented hypotonicity-induced relocalization of AQP1 in HEK293 cells [169]. Our data showing Ca^{2+} /CaM dependent accumulation of cAMP and activation of PKA suggests the involvement of a Ca^{2+} /CaM dependent adenylyl cyclase. In mammals, two of these exist, AC1 and AC8 [256], both of which are expressed in the rat cerebral cortex [257] and are therefore both likely to be present in our cortical rat astrocytes. Microarray analysis of HEK293 cells suggested that they express AC1 but not AC8 [258]. Therefore, if the mechanism of AQP4 translocation is conserved between HEK293 cells and astrocytes, AC1 is the most likely target for CaM in this response. Interestingly, a CaM binding site prediction tool (CaM Target Database [259]) predicts that the most likely site for direct binding of CaM to AQP4 is the 20-residue peptide at positions 277–296, directly upstream of the S276 phosphorylation site we identified, suggesting that CaM could be performing a dual function, and that S276 phosphorylation could act as a switch for CaM binding or release.

Kinase-dependent translocation of AQPs to the plasma membrane from intracellular vesicles is an established regulatory mechanism that has been demonstrated for AQP2 in response to AVP signalling via PKA [260], AQP1 in response to hypotonicity via PKC [237], and AQP5 in response to acetylcholine via PKG[253]. Treatment with the broad-range kinase inhibitor, hypericin,

suggested a similar mechanism for AQP4 relocalization. Using specific inhibitors identified PKA activity as a requirement for tonicity-mediated translocation of AQP4. There is some evidence that PKA reduced surface availability of AQP4 in human gastric cells [239]. In our systems, PKA seems to be doing the opposite.

All potential PKA sites of AQP4 were mutated, suggesting a key requirement for S276 in the C-terminal tail of AQP4. Phosphorylation at this residue has been detected *in vivo* in murine AQP4 [243] and rat AQP4 [242]. It was recently reported that phosphomimetic (S276D) or phosphorylation-deficient (S276A) mutations at this residue have no effect on surface expression or water permeability leaving the mechanistic role of this phosphorylated residue unclear [261]. Our data provide evidence of a functional role for S276 phosphorylation. It has also been reported that phosphorylation at S276 can increase lysosomal targeting of AQP4 upon internalization [262]. This may explain the slight reduction in constitutive surface expression (to $83.5 \pm 5.7\%$) that we measured for the S276D mutant. PKC phosphorylation of S180 in response to AVP has been reported to cause AQP4 internalization in *Xenopus* oocytes [263]; we did not observe any change in constitutive surface expression or translocation response for the S180D phosphomimetic mutant in our system. This may reflect the lack of an element of this internalization pathway in HEK293 cells or a species-specific effect. Phosphorylation of AQP4 at S111 in response to elevated $[K^+]_o$ has been reported to increase membrane water permeability in an astrocytic cell line [77], although the mechanism was not established. Our data suggests that elevated $[K^+]_o$ caused translocation of AQP4 to the plasma membrane, which provides a mechanistic explanation for this observation. This is in line with MD

simulations and *Xenopus* oocyte swelling assays using S111A and S111D mutants that showed that phosphorylation at S111 does not change the single channel water permeability of AQP4 [264]. S111A and S111D mutations had no effect on tonicity-induced translocation or constitutive surface expression in our system.

The S276D phosphomimetic mutant translocated in the presence of a PKA inhibitor, suggesting that the only role of PKA in our system is to phosphorylate S276. Although it is probable that S276 is phosphorylated in our primary astrocyte experiments, we cannot rule out a difference in phosphorylation sites between different cells or a synergistic effect of several kinase sites in the primary cells as observed for the two threonine residues that are phosphorylated by PKC to facilitate translocation of AQP1 [169].

Interestingly, we found that transfected AQP4 (with and without GFP) did not relocalize in response to any tonicity change in the U373 glioblastoma cell line (Figure 3-11). There is some evidence that a dominant-negative splice variant of AQP4 lacking exon 4, which codes for the half-helix containing the second NPA motif, can inhibit surface expression of either the M1 or M23 isoforms of AQP4 when co-expressed [265]. This was reported in muscle cells, but it may be possible that dysregulation of this isoform inhibits surface expression in U373 cells. People with glioblastoma have a very poor prognosis. The cells are very invasive and oedema is a key problem (T. Belli, personal communication). This may be worthy of further investigation to determine whether this loss of the AQP4 translocation response is a peculiarity of the U373 cell line or representative of glioblastoma physiology.

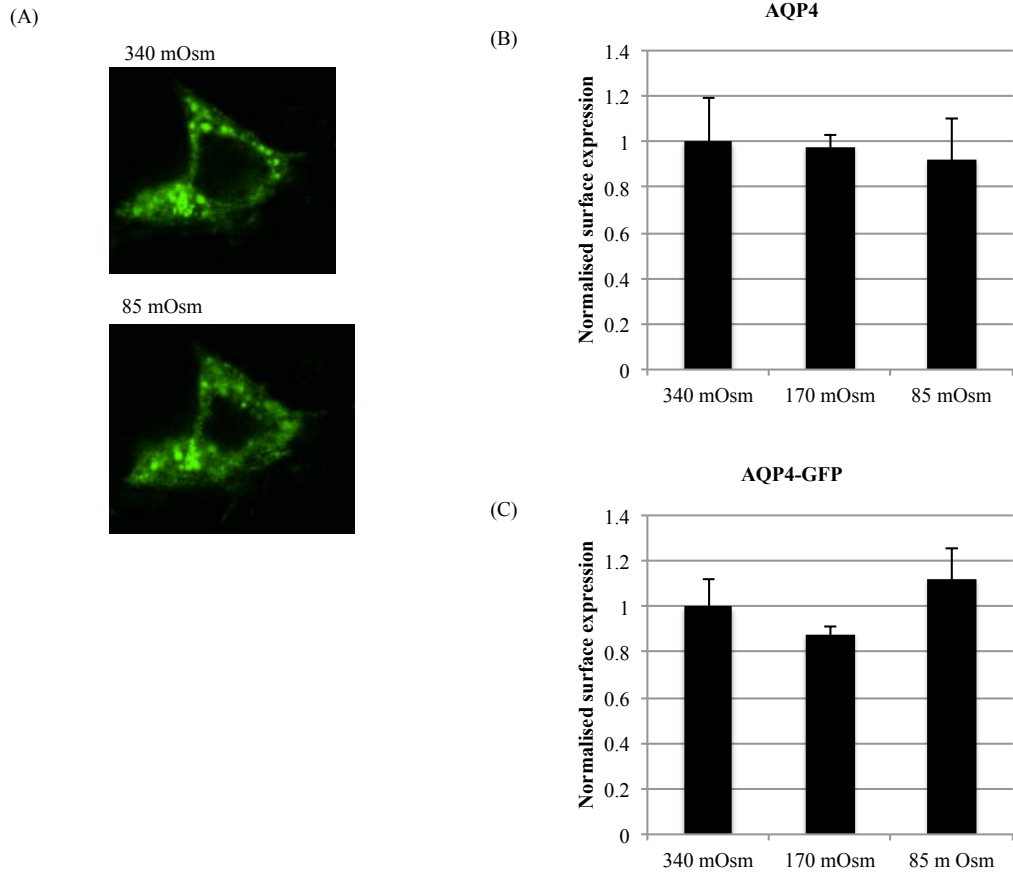


Figure 3-11 (A) Representative confocal micrographs of an AQP4-GFP-transfected U373 cell exposed to isotonic (340 mOsm/kg of H₂O) media and 5-min exposure to hypotonic (85 mOsm/kg of H₂O) media. (B) and (C) Cell surface biotinylation of U373 cells transfected with AQP4 (C) and AQP4-GFP (D). No statistically significant change was observed between any of the treatment groups (340, 170, and 85 mOsm/kg of H₂O), $n = 3$. Data are presented as mean \pm S.E.

Finally, based on the data reported here, we propose the signalling pathway represented in Figure 3-12 as the most likely mechanism for the hypotonicity-induced relocalization of AQP4.

To conclude, the data reported here identify and provide a mechanistic explanation of the physiological subcellular relocalization of AQP4 in response to changes in local tonicity. A change in local tonicity is the key driver of glial cell swelling in stroke and contributes to the effects of cytotoxic oedema following traumatic brain injury. Modulating the surface expression of AQP4 rather than trying to directly block its pore is a novel platform for developing therapies for these devastating conditions.

3.4.2 AQP5

Our data suggests that membrane expression of AQP5 in HEK293 cells is affected by phosphorylation of S156, either by increased membrane targeting or decreased internalization (or both). To our knowledge this is the first time that a specific phosphorylation site of AQP5 has been directly linked to a difference in membrane localization. The fact that the S156A mutant behaves like wild-type AQP5 indicates that phosphorylation of S156 may not occur under basal conditions. In this respect it is intriguing that S156 was preferentially phosphorylated in tumour cells [196]. It has been suggested that in tumours, PKA-dependent phosphorylation of S156 increased cell proliferation by activating the Ras pathway [266]. A number of studies have shown that upregulation of AQPs is common in a variety of cancers and that the AQP may promote cell proliferation and migration [11].

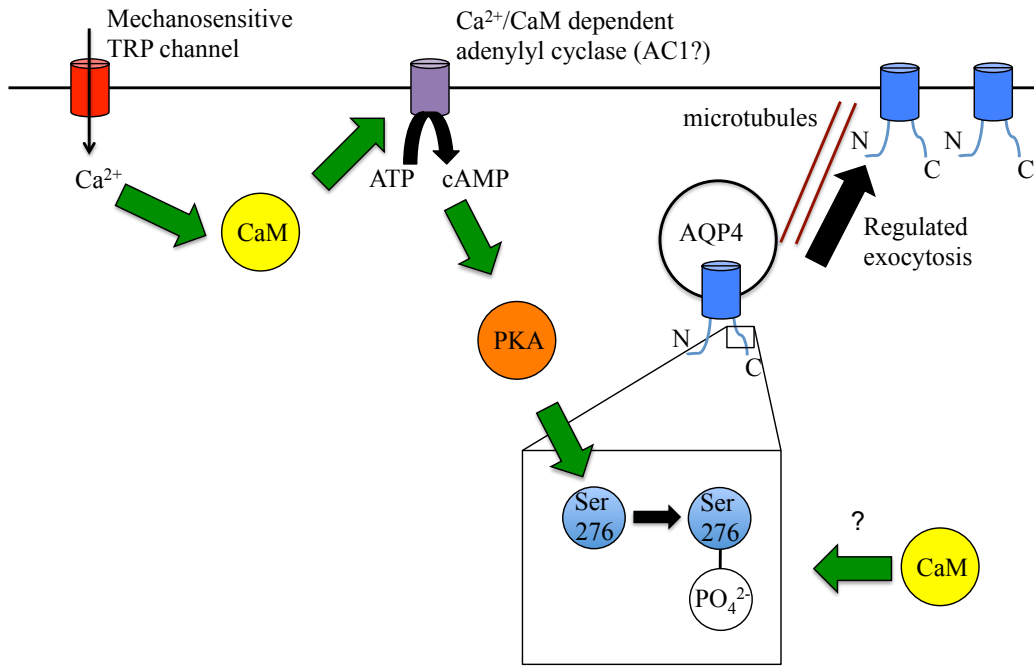


Figure 3-12 Schematic of the proposed signalling mechanisms involved in hypotonicity-induced relocation of AQP4 based on the data in this chapter. CaM – CaM; PKA – protein kinase A.

Our data hint at a mechanism whereby phosphorylation of S156 of AQP5 increases its membrane localization, thereby increasing the number of AQP5 molecules able to participate in events on the plasma membrane and enhancing cancer cell proliferation.

It was previously suggested that phosphorylation of S156 would break interactions between loop D and the C-terminus, thereby triggering a conformational change [198]. Significant conformational variability of the C-terminus was seen in the structure of human AQP2, where the C-terminal helix of each monomer adopted a unique conformation that had not been observed in any previous mammalian AQP structure [48]. As the C-terminal region is known to be important for membrane translocation of both AQP2 [190], AQP5 [195, 267], and AQP4 [268], such conformational changes may be recognized as a structural sorting signal by the cellular trafficking machinery. However, the structure of the AQP5 S156E mutant did not reveal any structural differences within loop D or the C-terminus (see Kitchen et al, PloS One, 2015, appendix 1). We therefore suggest that it is the presence of a phosphate group at S156 rather than a conformational change of the C-terminus that is recognized as a sorting signal, resulting in increased AQP5 membrane abundance.

Our data further show that, independent of S156, basal levels of PKA activity (i.e. in the absence of a cAMP-stimulating agonist) decrease the membrane abundance of AQP5. This fits well with the short-term effect of cAMP and PKA that has been seen previously and for which PKA has been suggested to be involved in AQP5 internalization [192]. As PKA inhibition further increased membrane expression of the S156E mutant, the phosphorylation of S156 is probably not responsible for this short-term effect. Instead, we suggest that S156

phosphorylation may be involved in the long-term cAMP and PKA-dependent effect whereby an increase in AQP5 membrane abundance is seen after several hours. This is in agreement with the observation that the long-term effect of cAMP and PKA involves direct phosphorylation of AQP5 while the short-term effect does not [192].

Finally, we show that AQP5-GFP is rapidly translocated to the plasma membrane of HEK293 cells in response to hypotonic conditions, but that this translocation is independent of S156 in loop D and also, unlike AQP4, independent of PKA activity. These three factors regulating AQP5 membrane localization are represented as a schematic in Figure 3-13.

The hypotonicity-induced membrane translocation of AQP5 described here is consistent with that of AQP1 where the phosphorylation of Thr157 and/or Thr239 by PKC results in rapid accumulation in the cell-surface membrane [169]. Whether direct phosphorylation of AQP5 by PKC or another kinase mediates hypotonicity-induced membrane translocation in a similar manner remains to be shown. AQP5 is found in tissues that are subject to rapid changes in osmolarity and has an important role in cell volume regulation [182, 192, 193]. Upon exposure to hypotonic conditions, cells undergo a rapid RVD to avoid rupture. This happens within a couple of minutes and involves the release of cellular water. RVD is often followed by RVI whereby the osmotically shrunken cell approaches its original volume [178]. The rapid response to

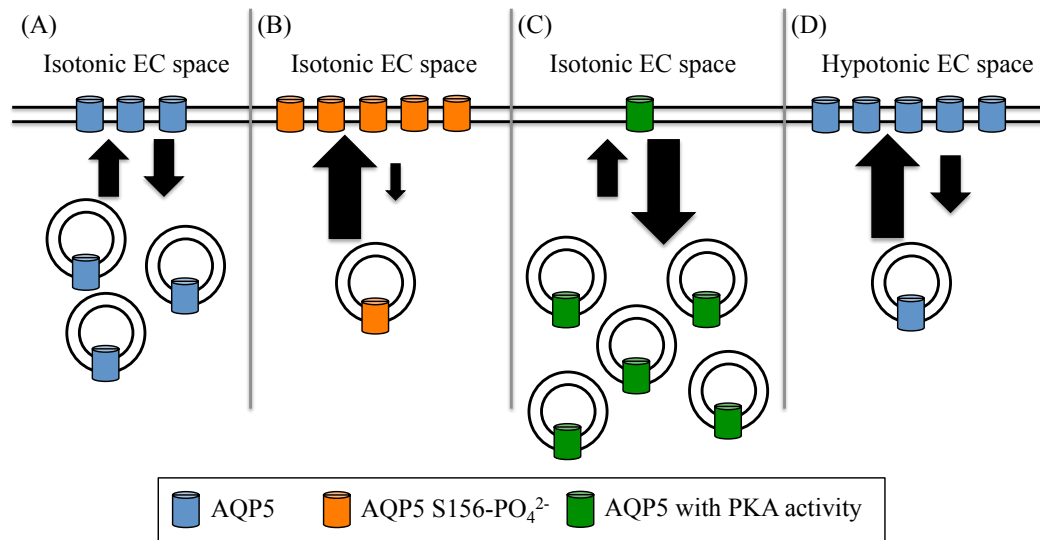


Figure 3-13 – A proposed model of the equilibrium between vesicular and surface-localized AQP5, regulated by three independent factors: phosphorylation of AQP5 at position S156 (panel B, shown by a phosphomimetic glutamate substitution (S156E) of AQP5); the effect of PKA (panel C) and the effect of decreasing the relative tonicity of the environment (panel D). Arrow sizes represent the relative rates of membrane trafficking and internalization. We speculate that these three pathways control the surface abundance of AQP5.

hypotonicity reported here supports the involvement of AQP5 in RVD as previously suggested [182]. On a longer time scale, hypotonic exposure has been shown to cause a decrease in AQP5 membrane abundance [193], most likely corresponding to the RVI response. Taken together, regulation of AQP5 membrane abundance seems to be important for both the RVD and RVI components of cell volume regulation. Data from our laboratory previously showed that hypotonicity-induced calcium influx through TRPC1 was vital for translocation of AQP1 [169] and others have shown that calcium influx through TRPV4 mediates the AQP5-dependent regulatory volume decrease in acinar cells [182]. We therefore speculate that the sensor of extracellular osmolality that leads to AQP5 translocation is a member of the TRP family of gated cation channels.

Due to its importance for fluid secretion in airway submucosal glands, AQP5 has been suggested to be a pharmacological target to treat the hyper-viscous and excessive gland secretions in cystic fibrosis and bronchitis/rhinitis respectively [269]. Our data provide the first link between a specific AQP5 phosphorylation site, S156, and changes in its subcellular localization. We further show that the S156-mediated change in localization does not require a substantial protein conformational change. We show that, independently of S156, PKA is further involved in basal recycling of AQP5 between the plasma membrane and intracellular compartments. Finally, we provide evidence of tonicity-induced changes in AQP5 localization that are not mediated by phosphorylation of S156 or PKA. This provides a platform for elucidating the detailed mechanism(s) by which post-translational modifications govern translocation of AQP5 from intracellular storage vesicles to the target membrane in response to protein kinase

activity and osmotic triggers, potentially providing key information for drug design targeting AQP5.

Finally, the data in this chapter showing tonicity-induced translocation of AQPs 4 and 5 along with the published observation of AQP1 translocation, suggests that tonicity-induced translocation of AQPs to the plasma membrane is a conserved mechanism by which cells may control their membrane water permeability.

4 Results – A comparative analysis of AQP solute exclusion and selectivity

4.1 Aims

The aims of the work presented in this chapter were:

1. To compare the neutral solute permeability of mutants of the AQP4 selectivity filter to those published for AQP1 to discuss a general model of solute exclusion in the AQP family.
2. To use homology modelling and mutagenesis of AQP3 to compare and contrast its solute permeability with AQP1/4 mutants.
3. To quantitatively compare the glycerol and urea permeabilities of the wild-type human GLPs.
4. To use water permeability measurements of AQP4 selectivity filter mutants to test a published prediction, based on MD simulations, about the role of this region in controlling water permeability.

4.2 Background

The AQPs can be split into two sub-families: the strictly water-selective AQPs and the aquaglyceroporins (GLPs), which facilitate the movement of small neutral polar solutes such as glycerol and urea in addition to water (to avoid confusion between the family as a whole and the water-selective sub-family, which are often interchangeably referred to as ‘AQPs’, in this chapter AQP will refer to the family as a whole and wAQP will be used to distinguish the strictly water-selective sub-family).

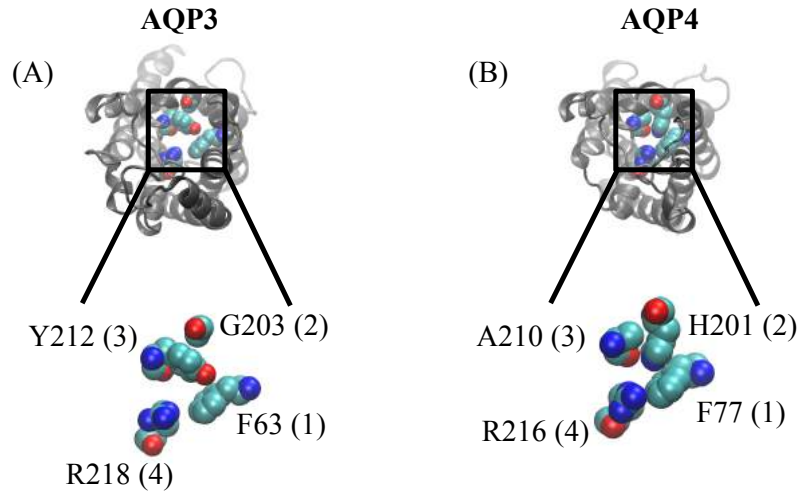
Two conserved structural features have been proposed to act as filters in the wAQPs to exclude the passage of neutral polar solutes and ions. The first of these is the constriction formed in the centre of the pore by two NPA motifs at the ends of two short alpha helices formed by the intracellular loop connecting the bottom (intracellular end) of TM2 to the bottom of TM3 and the extracellular loop connecting the top (extracellular end) of TM5 to the top of TM6. The asparagine residue is conserved in all known AQPs, whereas the proline and alanine residues, despite being highly conserved, can be substituted and still retain some AQP function (e.g. alanine to cysteine in AQP11 and proline to alanine in AQP7, both of which are functional water and glycerol channels). This structural feature is conserved across the whole AQP family and is not thought to contribute directly to the differences between the two sub-families, although subtle structural differences affecting this conserved motif could partially account for the differences in single channel water permeability between different members of the AQP family.

The second structural feature is the ar/R region, located between the extracellular channel mouth and the NPA constriction site. It is formed by four amino acid residues from different locations in the primary sequence; two from several turns below the tops of TMs 2 and 5, one directly adjacent to the second NPA motif (at the C-terminal side) and one from the loop connecting the top of TM5 to the second NPA motif. The exact residues that form the ar/R arginine motif are thought to form the structural basis for differences in permeability between strictly wAQPs and the neutral solute permeable GLPs. In the wAQPs, the ar/R region is comprised of a histidine residue at the top of TM5, a phenylalanine

residue in TM2, a small residue (e.g., cysteine in AQP1 or alanine in AQP4) before the NPA motif and an arginine residue after the NPA motif. The arginine is highly conserved across the whole AQP family although not absolutely; it is replaced by a leucine in AQPs 11 and 12. Substitution of the arginine with valine in AQP1 caused H⁺ permeability [58]. Although functional studies have yet to show H⁺ permeability of AQPs 11 and 12, it is possible that the loss of this arginine residue may represent roles in H⁺ homeostasis for these proteins.

The presence or absence of a histidine residue is the major difference at the ar/R region between wAQPs and GLPs. The histidine is conserved in the wAQPs and replaced by a smaller residue in the GLPs (glycine in AQPs 3,7 and 10, alanine in AQP9 and isoleucine in AQP8). Mutagenesis of AQP1 showed that replacement of the histidine with alanine, leucine or isoleucine (but not phenylalanine, glutamine, asparagine or methionine) converted AQP1 into an ammonia channel [270]. In the crystal structure of the bacterial GLP GlpF (the only GLP for which structural data has been reported), the glycine residue at the equivalent position to the histidine has a structural consequence, allowing a phenylalanine residue from the loop connecting the top of TM5 to the second NPA motif to pack in front of it. Based on sequence alignment (see Figure 4-1), in the mammalian GLPs, this member of the filter region is a tyrosine (AQPs 3 & 7), cysteine (AQP9) or isoleucine residue (AQP10).

The TM2 phenylalanine residue is also conserved in the wAQPs and is present in some of the GLPs (3, 7 and 9). Where this is not a phenylalanine residue it is usually replaced by another aromatic residue, such as a histidine residue in AQP8, a tyrosine residue in AQP11 or a tryptophan residue in GlpF.



(C)

	Position 1	2	3	4
AQP1	SLA F GLS	ALGH L LLA	YTG C GIN	NPA R SFG
AQP2	AMA F GLG	ALGH L LG	YTG C SMN	NPA R SLA
AQP3	NLA F GFA	LVI G TSM	NSG Y AVN	NP A RDFG
AQP4	SLC F GLS	AIGH L FA	YTG A SMN	NPA R SFG
AQP5	ALA F GLA	TLGH L VG	FTG C SMN	NPA R SFG
AQP6	AIT F NLV	ALGH L IG	FTG C SMN	NP A RDFG
AQP7	NLG F GFG	VII G VSL	NTG Y AIN	NP S RDLF
AQP8	ALA H GLA	TVD I LAG	VSG G CMN	NP A RAFG
AQP9	NVG F SMA	IVI A SSL	NSG C AMN	NP A RDLF
AQP10	FLA G SLA	LAL G LSM	NCG I PLN	NP A RDLF
AQP11	TLV Y FFS	TFL V YAG	LTG A VFN	NP A LALS
AQP12	TLL F LLF	TVT A YTA	FTS A FFN	NP A LAAS
AQP0	AMA F GLA	ALGH L FG	YTG A GMN	NP A RSFA
GlpF	SVI W GLG	AVI G ASM	LTG F AMN	NP A RDFG
AQPZ	ALA F GLT	TLI H LIS	VTN T SVN	NP A RSTA

Figure 4-1 Structure of the AQP ar/R region in a GLP and a water selective AQP, exemplified by (A) AQP3 (homology model to GlpF) and (B) AQP4 (crystal structure [222]). Numbers in brackets refer to the positions defined in the sequence alignment below. (C) Sequence alignment of human AQPs in the four regions contributing to the ar/R channel constriction. GLPs are highlighted in green. The conserved residues are highlighted in blue; deviations from this are highlighted in red.

Simultaneous replacement of the phenylalanine and histidine residues with alanine converted rat AQP1 into a urea and glycerol channel, with a higher permeability for urea than glycerol [58]. AQP10 is the only mammalian AQP to not have a bulky residue in this position; it is replaced by a glycine.

In silico experiments and an *in vitro* study of murine AQP, which created urea and glycerol permeable mutants [62][58] suggest that the ar/R region controls AQP solute selectivity and wAQP solute exclusion. However, a comparative study of GlpF and AQPZ failed to introduce glycerol permeability to AQPZ with GlpF-mimicking mutations to the selectivity filter [63]. Measurements of the electrostatic potential along the pore of two GLP and eight wAQP crystal structures suggested that a relatively flat potential profile is correlated with glycerol permeability [271], and solute hydrophobicity was also shown to be important for selectivity *in silico* [272].

Here we report a set of mutants of the ar/R region of the water-selective human AQP4 and compare and contrast their solute permeabilities to those of the analogous AQP1 mutants previously reported. We report several mutants of AQP3 that alter the relative specificity for glycerol compared to urea, and block solute permeation respectively. We also make (to our knowledge) the first direct and quantitative comparison of the relative glycerol and urea permeabilities of members of the mammalian GLP family in live mammalian cells. Our data suggest that AQPs 1 and 4 have different solute exclusion mechanisms and that a general model of solute exclusion and selectivity may not be directly applicable to the AQP family as a whole.

4.3 Results

4.3.1 AQP4 has a novel molecular mechanism for excluding glycerol and urea.

AQP4 selectivity filter region substitution mutants F77A, H201A, H201G, H201E, H201F, R216A, F77A/H201A, F77A/H201G, F77A/R216A and H201A/R216A were generated using site-directed mutagenesis as described in 2.1.2. These mutants were transiently transfected into HEK293 cells (chosen for their high transfection efficiency and low intrinsic glycerol/urea permeability) as described in 2.3.1 and cell swelling with iso-osmotic glycerol or urea solutions was measured using plate-reader based calcein fluorescence quenching as described in 0. Surface expression was measured using cell surface biotinylation as described in 0. Figure 4-2 shows that mutagenesis of the histidine at position 201 in AQP4 to different amino acid residues can selectively create channels permeable to either urea or glycerol but not both. Substitution to alanine (H201A) conferred glycerol permeability, whereas glycine substitution (H201G) created a urea channel, both with permeability around tenfold lower than that of AQP3 for glycerol. The R216A substitution conferred both urea and glycerol permeability to AQP4. In AQP1, alanine substitution of the equivalent histidine and arginine residues (H180A, R195A) did not confer either glycerol or urea permeability to human AQP1, in agreement with a previous study on rat AQP1 [58]. The H180G mutant of AQP1 was not urea permeable. The H201F mutant had reduced overall expression and minimal surface expression, possibly due to an interruption of protein folding by the introduction of steric clashes in the pore. Representative raw data is shown in Figure 4-3.

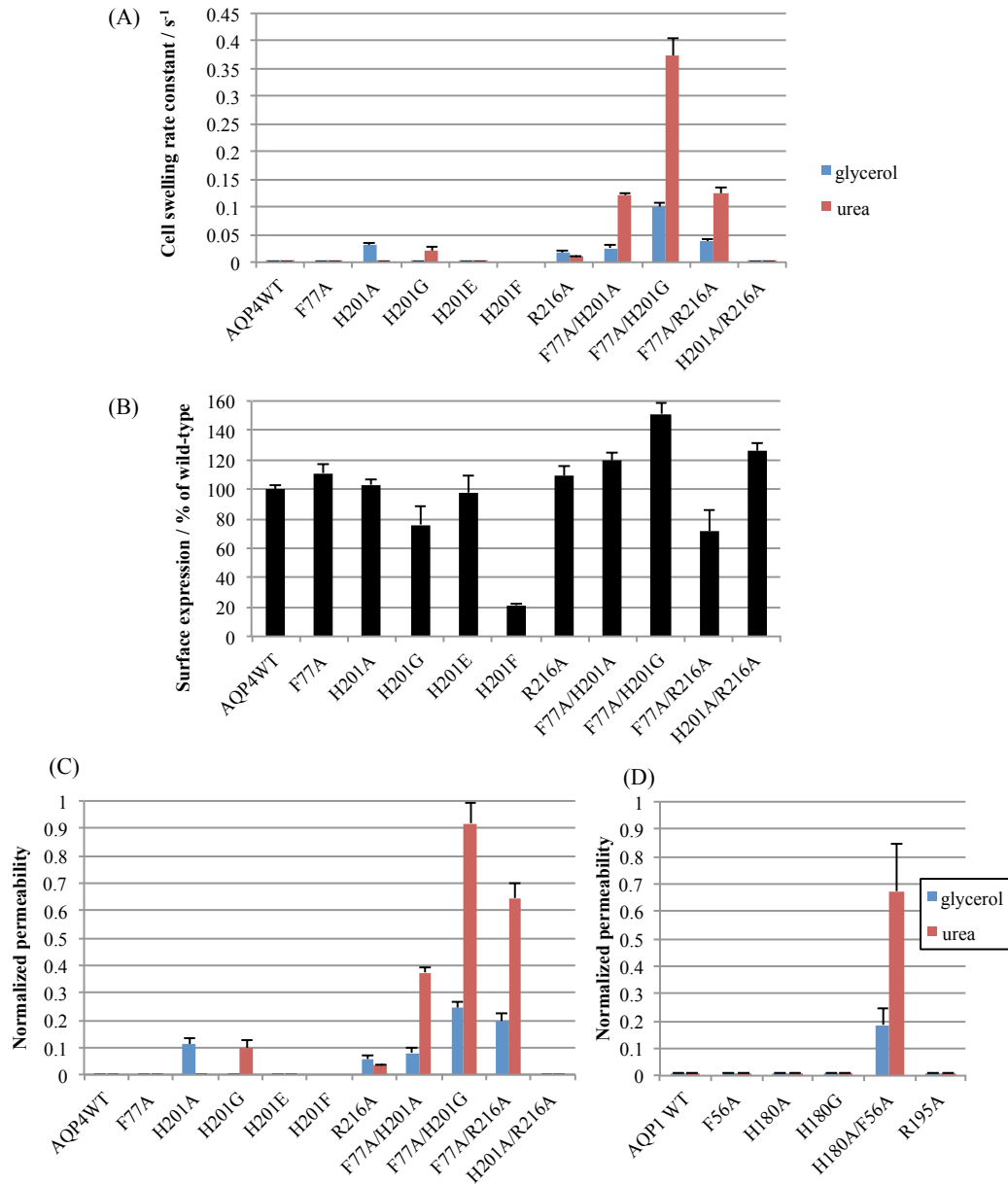


Figure 4-2 (A) Cell swelling rate constants of HEK293 cells transfected with AQP4 mutants, calculated from calcein fluorescence timeseries data. (B) Cell surface expression of AQP4 mutants in HEK293 cells measured by cell surface biotinylation and neutravidin ELISA. (C) Cell swelling rate constants normalized to surface expression and then normalized to AQP3 glycerol permeability. This gives a relative single channel permeability in units in which AQP3 glycerol permeability is 1. (D) Normalized permeabilities for the analogous mutants of AQP1 for comparison.

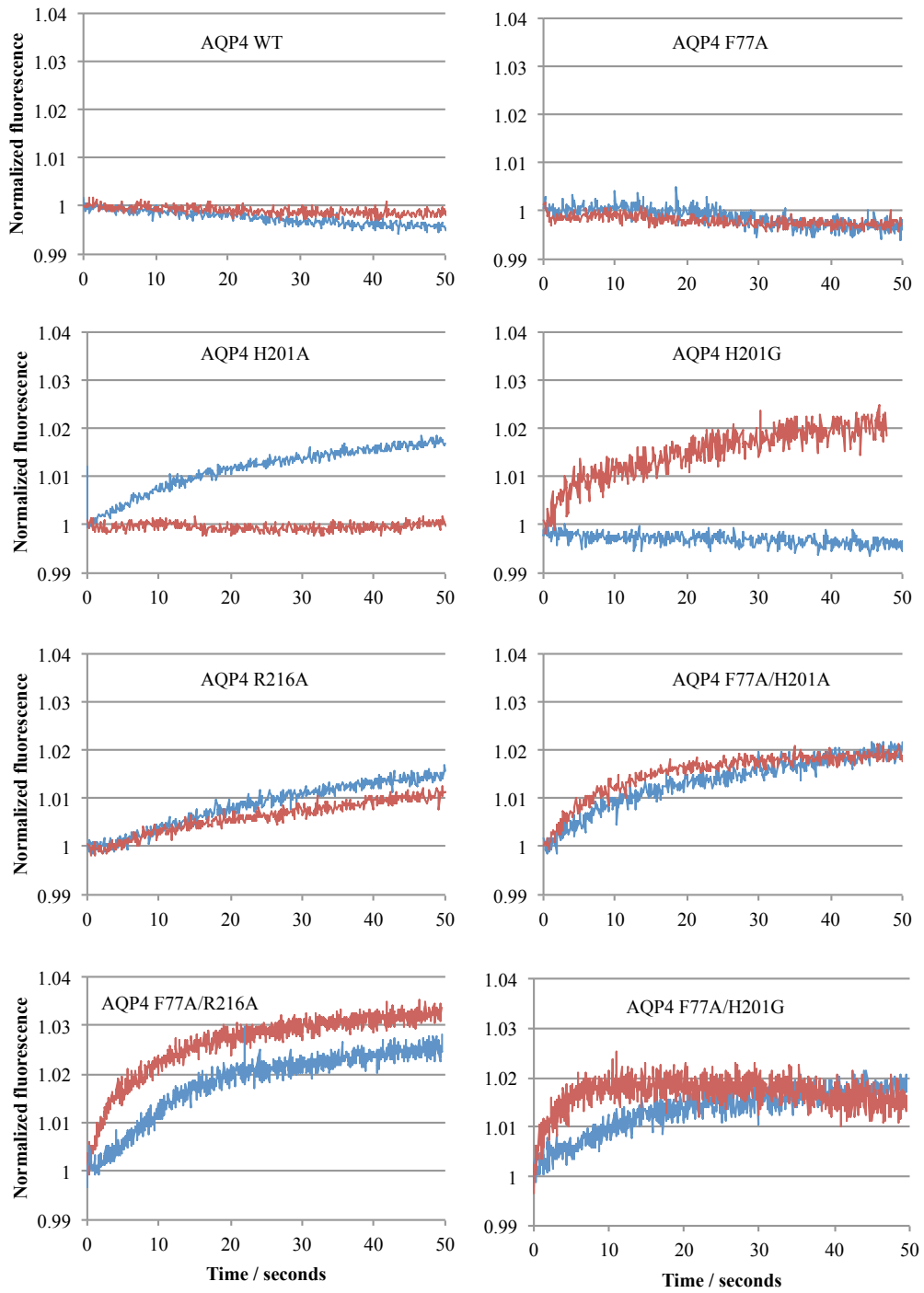


Figure 4-3 Representative calcein fluorescence timeseries for urea (red) and glycerol (blue) permeability of the AQP4 mutants described in **Figure 4-2**.

4.3.3 Water permeability of AQP4 mutants

AQP4 and all selectivity filter mutants were stably transfected into MDCK cells (chosen for their low intrinsic water permeability and their previous use in the literature for quantifying transfected AQP water permeability) as described in 2.3.2 to measure water permeability using a plate-reader based calcein fluorescence quenching method as described in 2.8.1. Cell swelling rates were background-subtracted (using an untransfected MDCK control) and normalised to surface expression (measured using a cell surface biotinylation-based ELISA) to give relative single channel water permeability. None of the substitution mutants except H201E and R216A had significantly different water channel activity to wild-type AQP4. Figure 4-4 shows that the water permeability of H201E was reduced to $63\pm 8\%$ of wild-type ($n=4$, $p=0.002$) and the water permeability of R216A was increased to $147\pm 3\%$ of wild-type ($n=4$, $p=0.005$). Representative raw data is shown in Figure 4-5.

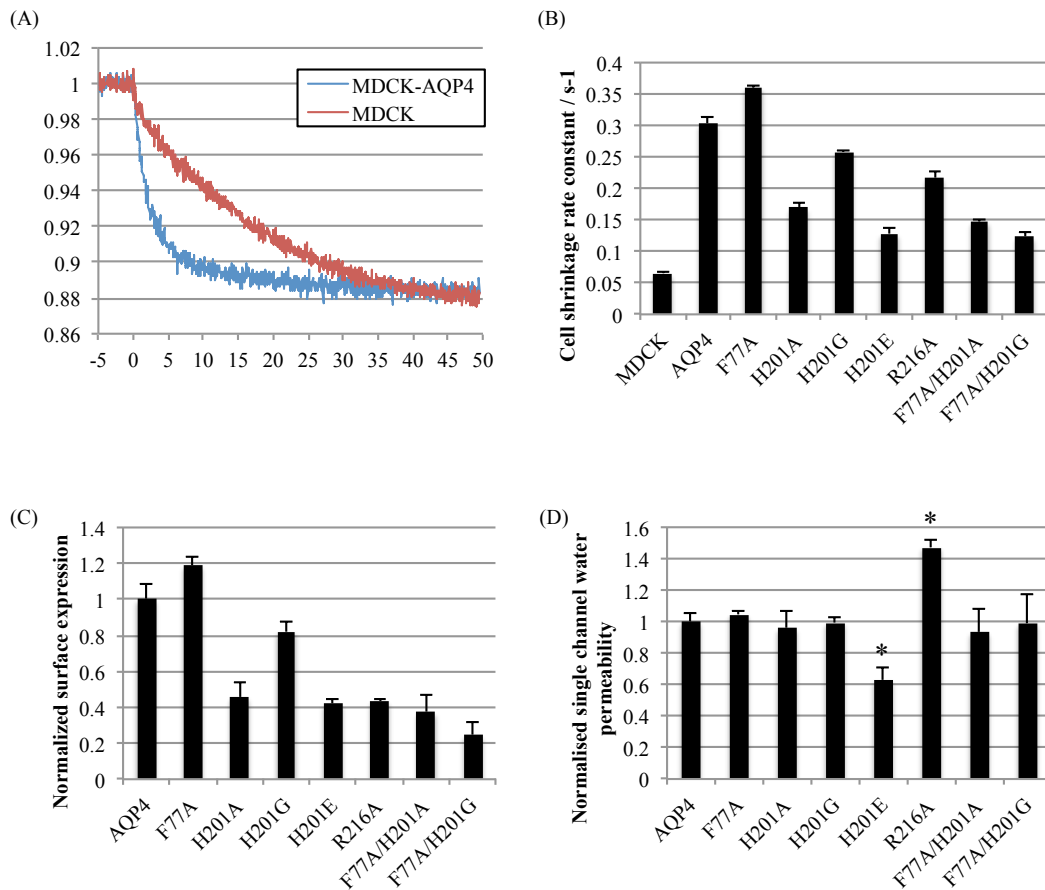


Figure 4-4 (A) Representative calcein fluorescence quenching curves of control MDCK cells and our stable MDCK-AQP4 cell line upon addition of 300 mM mannitol. (B) Cell shrinkage rates of MDCK cells stably transfected with AQP4 mutants. Relative fluorescence data were converted to relative volume, and exponential decay functions were fitted. (C) Surface expression of AQP4 mutants in stable MDCK clones, normalized to wild-type AQP4. (D) Normalized single-channel permeability calculated by subtracting the untransfected MDCK background and normalizing to surface expression. * represents $p < 0.01$ in unpaired t-tests after ANOVA, with the p values subjected to Bonferroni's correction.

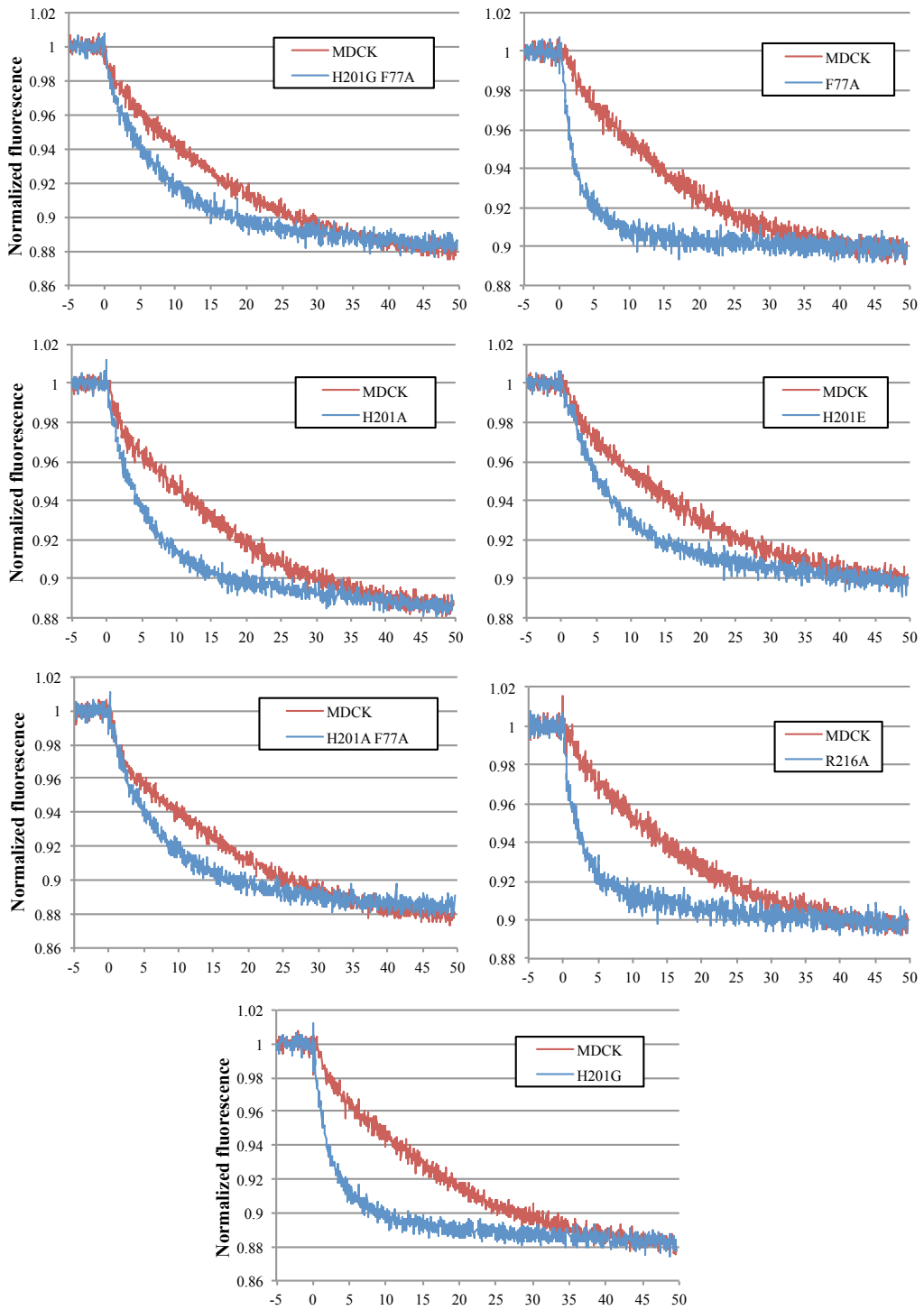


Figure 4-5 Representative calcein fluorescence timeseries for water permeability of the AQP4 mutants described in **Figure 4-4**.

4.3.4 GLP-mimetic mutants of AQP4 are not solute permeable

The pore layout of the GLPs is different to that of the water-selective AQPs. The aromatic histidine is replaced by a small residue e.g. glycine or alanine. There is also a further aromatic residue (usually tyrosine or phenylalanine), the sidechain of which packs in front of this glycine residue (based on the GlpF crystal structure). Creating this structural landscape in AQP4 (H201G/A210Y, H201G/A210F, H201A/A210Y, H201A/A210F) did not create a solute-permeable channel, despite robust surface expression determined by cell surface biotinylation, and despite the solute permeabilities of the H201A/G single mutants (Figure 4-6).

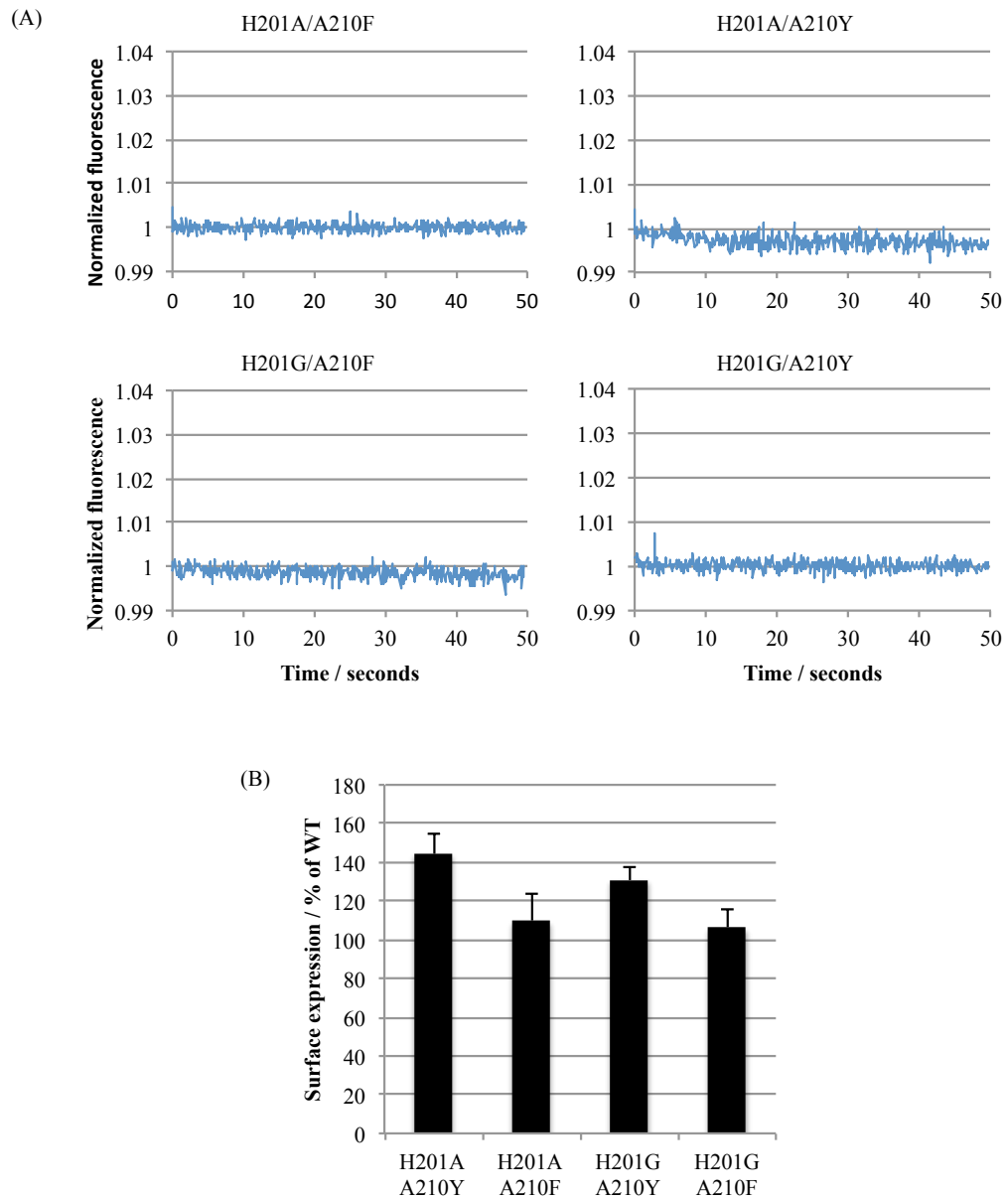


Figure 4-6 (A) Representative calcein fluorescence quenching curves for glycerol permeability of AQP4 GLP-mimetic double mutants. (B) Surface expression of AQP4 GLP-mimetic mutants measured by cell surface biotinylation.

4.3.5 AQP3 urea and glycerol permeability can be altered independently of each other

Based on sequence alignment, the conserved histidine of the selectivity filter is replaced by a glycine in AQP3, but there is a tyrosine residue in position 3 (see Figure 4-1) that may pack in front of the glycine, and this is what we observed when we built a homology model of AQP3 based on a GlpF crystal structure [46] using MODELLER [273] (Figure 4-7 A). Substitution of this tyrosine residue in AQP3 with alanine (Y212A) conferred measurable urea permeability to AQP3 (whereas the wild-type was not measurably permeable) whilst concomitantly reducing glycerol permeability to $47\pm 6\%$ of the wild-type. This swapping of selectivity suggests that the preference of AQP3 for glycerol over urea is not governed solely by the dimensions of the pore. Combining the Y212A mutation with G203H, to mimic the histidine residue present in wAQPs, produced a channel impermeable to both urea and glycerol (Figure 4-7).

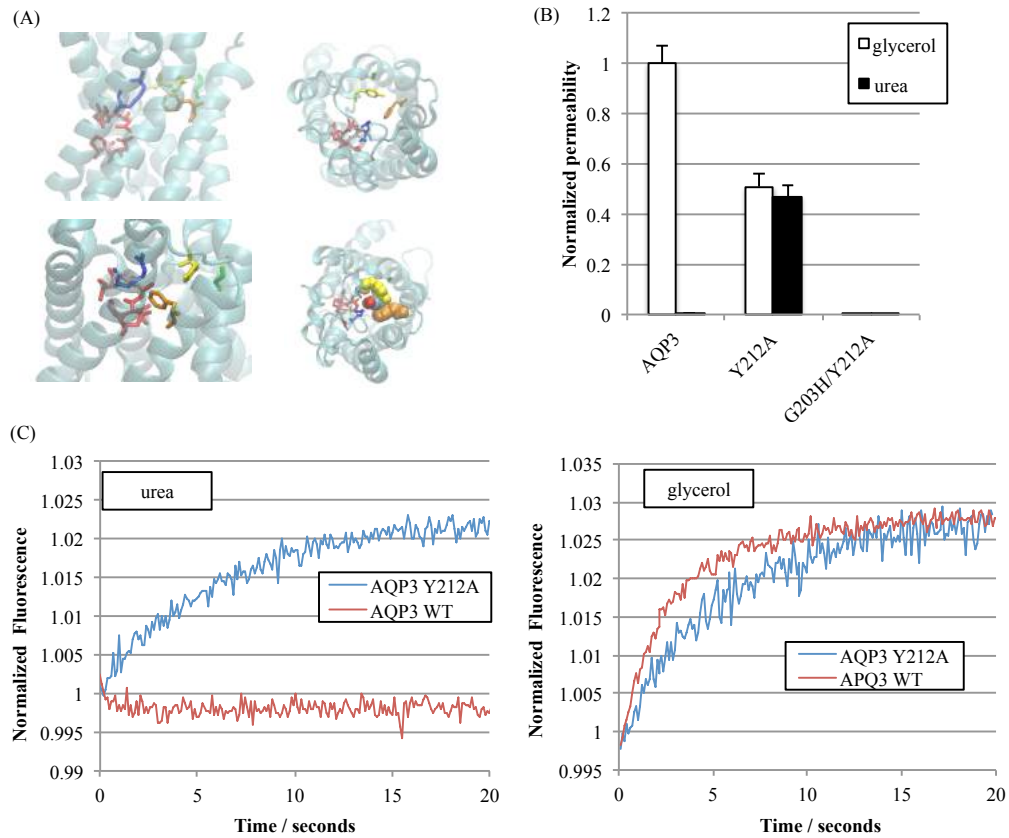


Figure 4-7 (A) homology model of AQP3 to GlpF. Selectivity filter residues are coloured: F63 yellow, G203 green, Y212 orange, R218 blue. NPA motifs are coloured red. Y212, F63 and a glycerol molecule are shown in space-filling representation in the lower right panel, showing the packing of the glycerol backbone into a 'hydrophobic corner'. (B) Solute permeabilities of wild-type AQP3 and the selectivity filter mutants Y212A and Y212A/G203H normalized to surface expression and then to AQP3 glycerol permeability. (C) Representative calcein fluorescence quenching curves of wild-type AQP3 and the Y212A mutant.

4.3.6 AQPs 3, 9 and 10 have different relative permeability for glycerol and urea

In our experiments, the GLPs AQP3, 9 and 10 had different, biased selectivity for urea and glycerol. AQP10 had glycerol permeability of 0.94 ± 0.11 when normalised to AQP3 permeability, whereas the permeability of AQP9 to glycerol was almost two-fold higher at 1.81 ± 0.12 . AQPs 9 and 10 had opposite biases towards glycerol and urea permeability, with P_u/P_g ratios of 0.84 ± 0.08 and 1.29 ± 0.09 respectively. These were both significantly different from 1 by one-sample t-tests followed by Bonferroni correction for multiple comparison ($p = 0.02$ and $p=0.01$ respectively). In our experimental setup, human AQP3 expressed in HEK293 cells was a glycerol channel but was not measurably urea permeable, Figure 4-8.

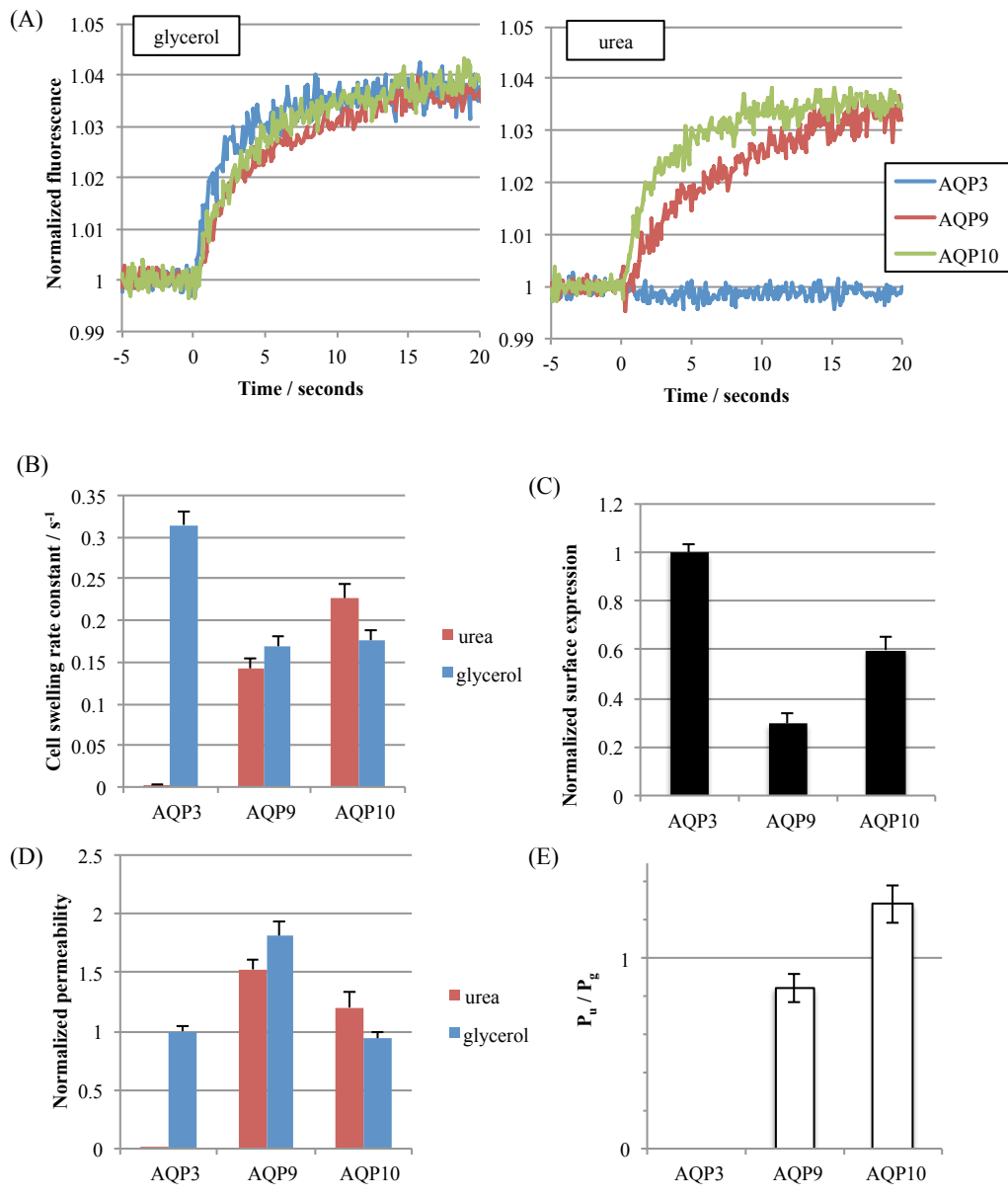


Figure 4-8 (A) Representative calcein fluorescence quenching curves for human AQPs 3,9 and 10 for glycerol and urea permeability. (B) Average cell swelling rate constants from fits to calcein fluorescence timeseries data. (C) Surface expression of GFP-tagged AQPs 3,9 and 10 in HEK293 cells measured by cell surface biotinylation followed by ELISA with an anti-GFP antibody. (D) Relative single channel solute permeabilities of AQPs 3, 9 and 10 calculated by normalizing the cell swelling rate constant to surface expression and then to AQP3 glycerol permeability. (E) Ratio of urea permeability to glycerol permeability for AQPs 3, 9 and 10.

4.3.7 Molecular dynamics and *in silico* mutagenesis

4.3.7.1 The role of R216 in AQP4 water permeability

Hub et al. previously reported that, in MD simulations, fluctuations of the AQP4 R216 sidechain between an ‘up’ state in which the sidechain packs against the pore wall and a ‘down’ state in which the sidechain points out into the pore (see Figure 4-9 A and B) could switch the channel between an open and a closed state, with an open probability of ~ 0.45 , measured using the OPLS force field [60] (with open defined as a distance of >0.57 nm between the arginine C $_{\zeta}$ atom and the closest histidine heavy atom). We performed molecular dynamics simulations of an AQP4 tetramer embedded in a POPC bilayer using the GROMOS 53A6 force field, based on the AQP4 crystal structure [222], to attempt to qualitatively validate this result and to address the possibility of quantitative differences in the open probability between different protein force fields. We found that the arginine sidechain reoriented on the nanosecond timescale (Figure 4-9 D), which was characterized using the C $_{\beta}$ -C $_{\gamma}$ -C $_{\delta}$ -N dihedral angle, following Wang et al [62]. We also found that a two-state model is appropriate for describing the simulation data, with the average R216 C $_{\zeta}$ -H201 distances of the open and closed states being 6.5 and 4.3 Å, respectively. Using the same definition of open, an open probability of 0.52 ± 0.12 was found (with the uncertainty estimated as the standard error over the four monomers). This is consistent with the work of Hub et al., suggesting that this probability is reasonably robust when measured using different force fields. Assuming this simple two-state model, our *in vitro* results allow us to estimate the open probability of the wild-type AQP4 channel, based on the idea that the R216A mutation forces the channel to permanently occupy the open state.

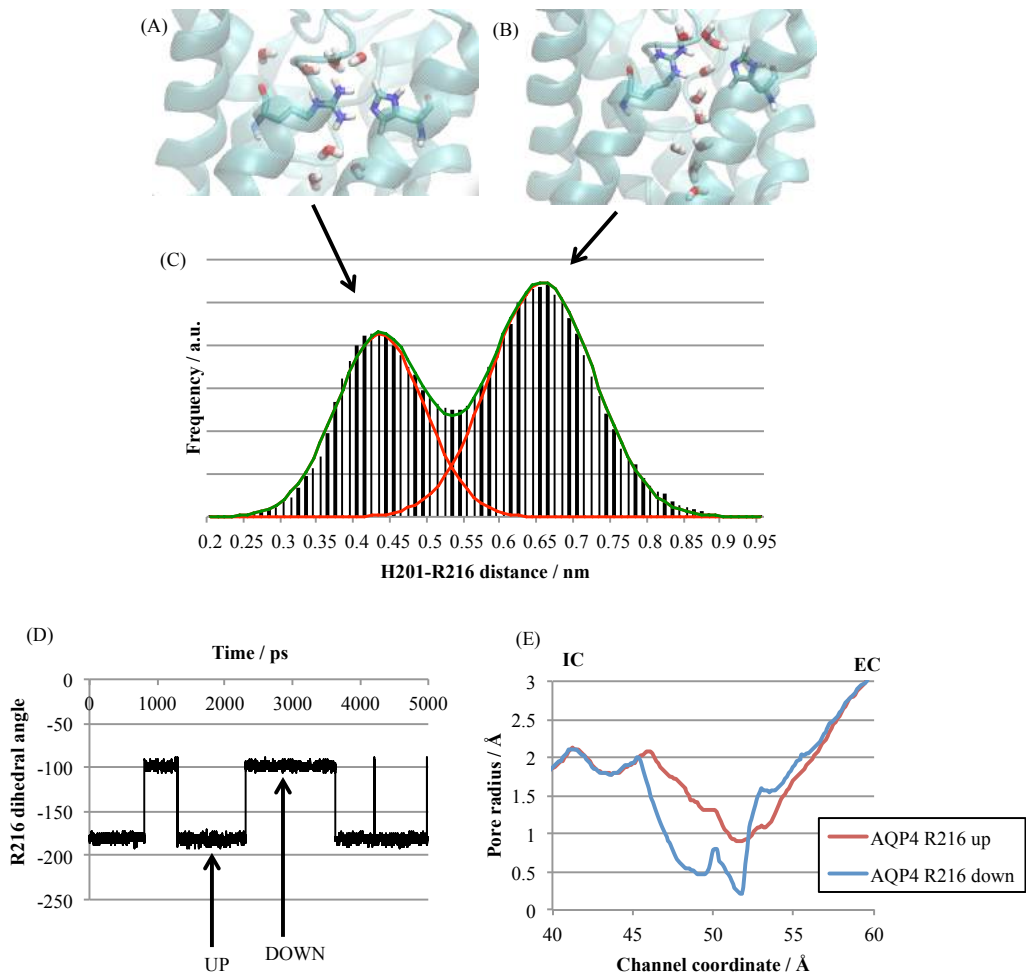


Figure 4-9 (A and B) Representative simulation snapshots of AQP4 showing the closed and open states of the channel with interrupted and continuous files of water molecules. R216 and H201 are shown in stick representation. (C) Histogram of the R216–H201 distance distribution in simulations, showing two clearly distinct states. Fitted Gaussians (red, sum in green) are centred at 0.43 and 0.65 nm. (D) Fluctuation of the R216 sidechain dihedral angle between two states. (E) Channel radii in representative snapshots in which R216 was in the up or the down state, calculated using HOLE2 [274].

Previous molecular dynamics simulations suggested an approximately 40-fold difference in permeability between the open and closed states of AQP4 [60].

Using the following equation:

$$\frac{P_{R216A}}{P_{WT}} = \frac{(P_o p_{o,R216A} + P_c(1 - p_{o,R216A}))}{(P_o p_{o,WT} + P_c(1 - p_{o,WT}))}$$

where P_{R216A} and P_{WT} are the permeabilities measured in experiments, P_o and P_c are the permeabilities of the open and closed states, respectively, and p_o is the channel open probability. Setting $p_{o,R216A}$ equal to 1 and P_o equal to $40P_c$ gives a wild-type open probability of 0.67 ± 0.02 (which is slightly higher than the value of 0.52 ± 0.12 that we estimated from simulations, but in reasonable agreement).

4.3.7.2 *In silico* mutagenesis of selectivity filter mutants

We generated models of all of our AQP4 and AQP3 mutants by *in silico* mutagenesis of the AQP4 crystal structure and the AQP3 homology model using Swiss PDBviewer [275] and compared the channel cross-sectional radii (Figure 4-10) and areas (Figure 4-11) using the program HOLE. As a way of roughly quantifying the channel *shape* at the selectivity filter, we also fit ellipses to the protein surface at the selectivity filter and calculated the ellipticity (which can be thought of as a measure of the deviation from circularity: a circle has ellipticity $e = 0$, and e tends to one as the ratio of semi-minor to semi-major axes tends to zero). We looked for correlation between these physical parameters of the channel and the solute permeability. Aside from the H201A/R216A mutant, above a cross-sectional area of $\sim 14 \text{ \AA}^2$, the area was reasonably well correlated with urea permeability for the AQP4 mutants ($R^2 = 0.83$). We made a linear fit to the data in this region (excluding H201A/R216A; black line in Figure 4-12, panel A). We then used this fit to predict urea permeabilities of AQPs 3, 9, 10 and the

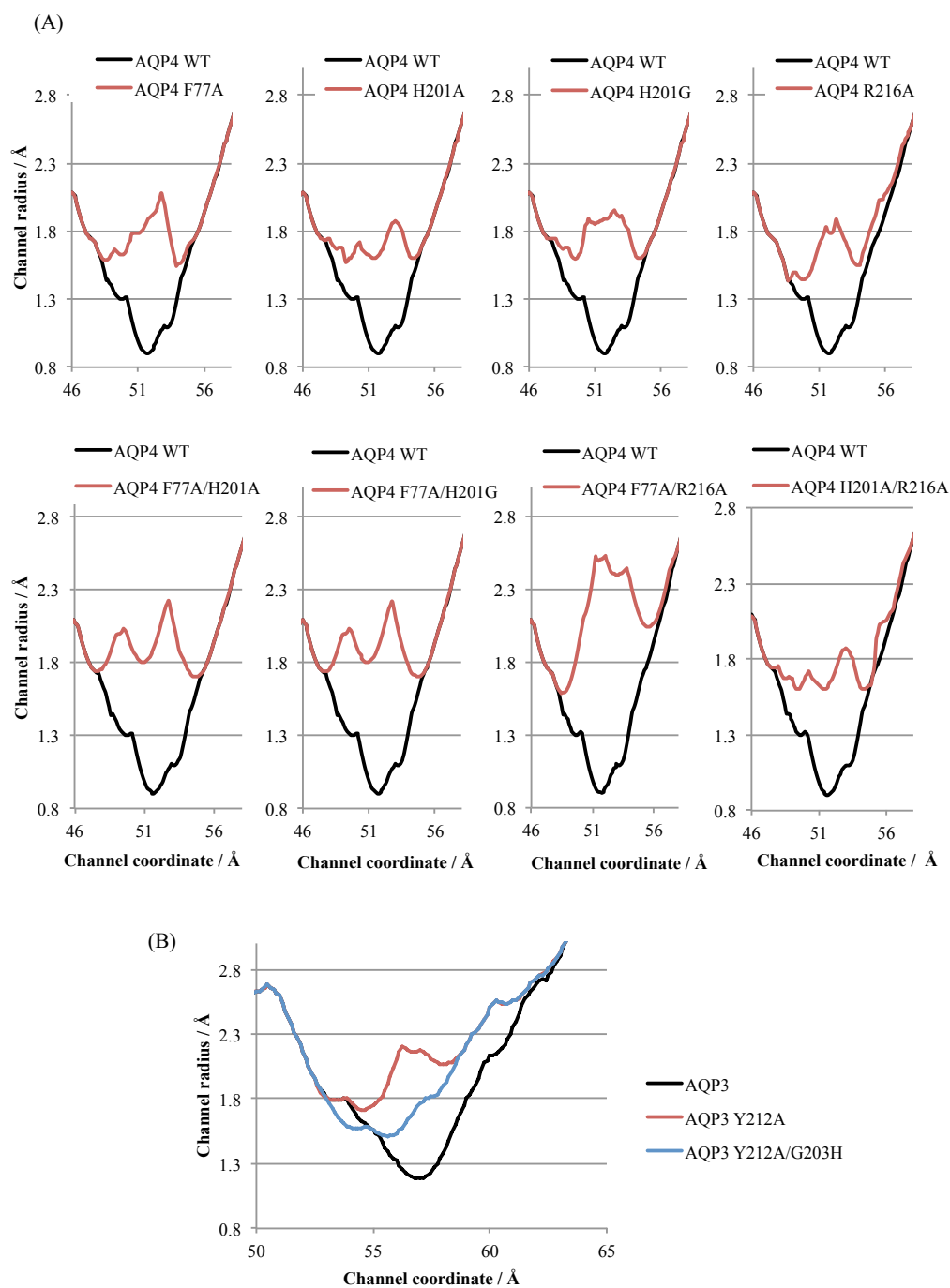


Figure 4-10 Channel radius profiles at the selectivity filter of (A) AQP4 mutants and (B) AQP3 mutants, calculated using HOLE.

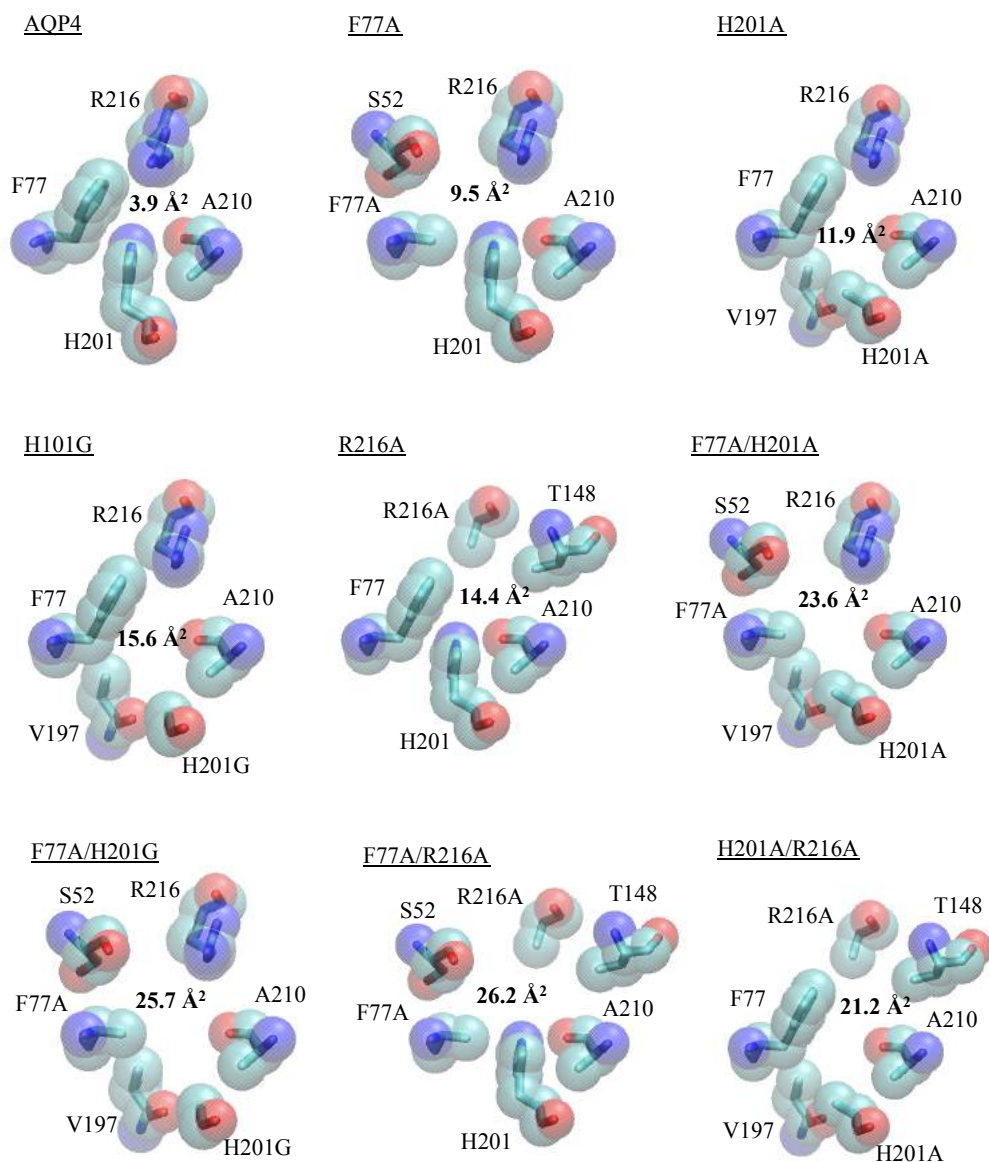


Figure 4-11 Pore-lining residues of AQP4 mutants at the selectivity filter and cross-sectional areas (**bold**) calculated using HOLE.

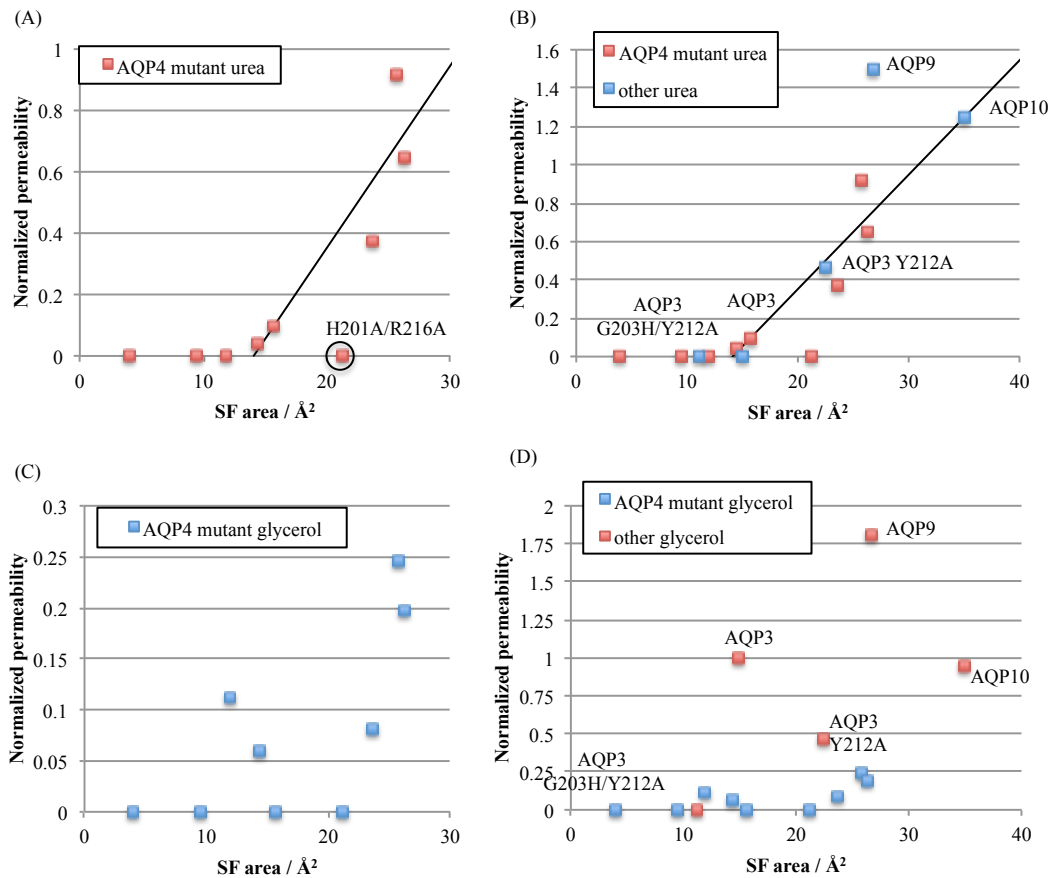


Figure 4-12 Correlation between selectivity filter (SF) cross-sectional area and: (A) urea permeability of AQP4 mutants, (B) urea permeability of AQP4 mutants and GLPs. The black line in (A) and (B) is a linear fit to all AQP4 mutants with non-zero urea permeability. (C) glycerol permeability of AQP4 mutants, (D) glycerol permeability of AQP4 mutants and GLPs.

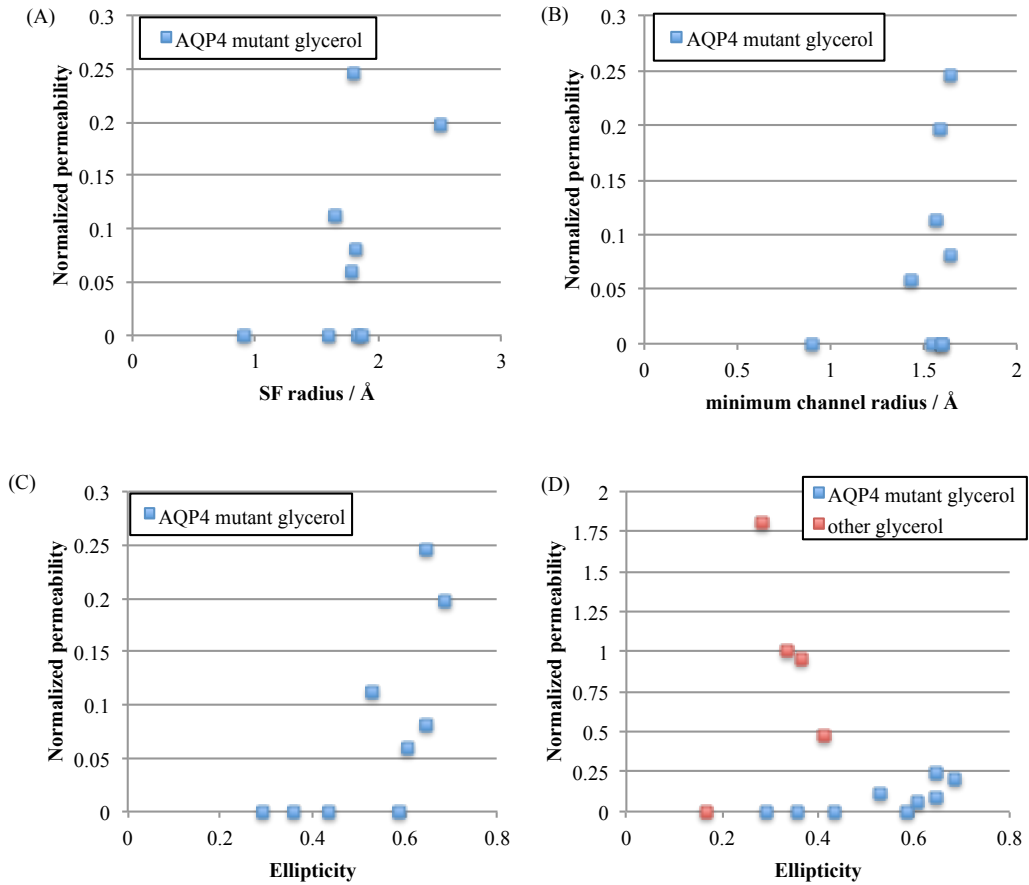


Figure 4-13 (A,B,C) Correlation between selectivity filter (SF) geometric properties and glycerol permeability of AQP4 mutants. (D) Correlation between ellipticity and glycerol permeability of AQP4 mutants and GLPs.

AQP3 mutants (**Figure 4-12** panel B). In contrast, glycerol permeability could not be explained by any of the geometric properties (**Figure 4-13**).

4.3.7.3 Molecular dynamics of AQP4 H201A and H201G mutants

In the *in vitro* experiments comparing urea/glycerol permeability of AQP4 mutants, we obtained the curious result that the mutation H201A created a glycerol channel, whilst the mutation H201G created a urea channel. We hypothesized that the ‘hydrophobic corner’ formed by F77 and H201A (see **Figure 4-11**), analogous to the one proposed in GlpF, may be disrupted by the H201G mutation and that the loss of the alanine sidechain may make the V187 sidechain carbonyl group solvent accessible and therefore be available for hydrogen bonding with water or solute molecules in the pore. We used 50 ns MD trajectories of the H201A, H201G and wild-type AQP4 tetramers to test this hypothesis. In wild-type AQP4 and the H201A mutant, no hydrogen bonds were observed between the V187 backbone and water molecules in the pore, using the Hbonds plugin for VMD with a 3 Å and 20° hydrogen bond cut-off. In contrast, in the H201G mutant, we found hydrogen bonds between V187 and water molecules in all four monomers, with occupancy of 24.7 ± 5.4 % (using the same 3 Å and 20° cut-off), with the error estimated as the standard deviation over the four monomers (**Figure 4-14 B**). For comparison, we measured the hydrogen bond occupancy of water molecules with the two asparagine residues forming the NPA motifs. These were 55.7 ± 7.0 % for N97 and 58.2 ± 10.2 % for N213. A representative simulation snapshot in which this bond is occupied is shown in **Figure 4-14 A**.

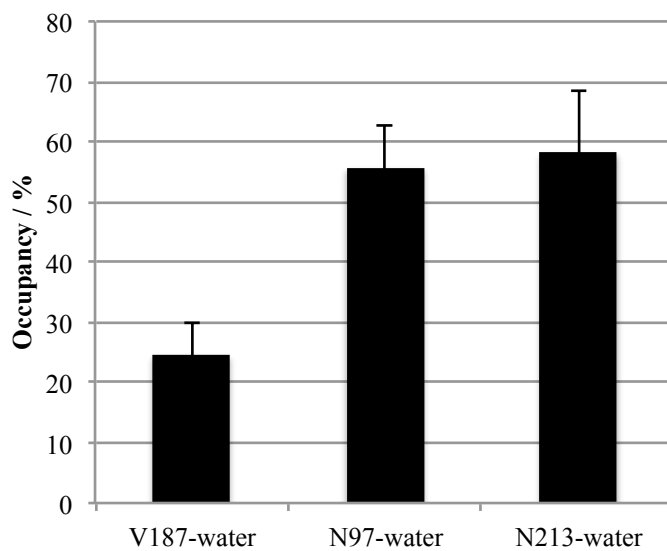
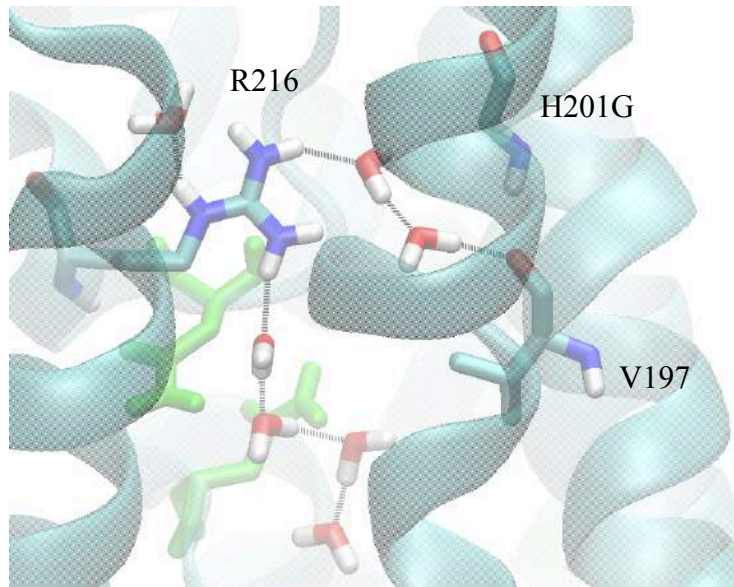


Figure 4-14 (A) Representative simulation snapshot of the AQP4 H201G mutant, showing the exposure of the V187 backbone to pore water molecules. Black lines represent hydrogen bonds. (B) Occupancy of the V187-water hydrogen bond, in comparison to the occupancy of the asparagine residues at the NPA motifs.

4.4 Discussion

Our data show that in human AQP4, both the histidine and arginine residues of the ar/R region are crucial for neutral solute exclusion. The AQP4 substitution mutant H201A formed a glycerol permeable channel, AQP4 H201G was a urea permeable channel and AQP4 R216A was permeable to both glycerol and urea. This contrasts with AQP1, in which it has previously been reported that neither the H180A nor R195V substitution mutants of rat AQP1 were glycerol or urea permeable [58]. In addition, our data show that in human AQP1 R195A was also not permeable to glycerol or urea. The AQP4 double mutant F77A/H201A was permeable to both urea and glycerol, with a preference for urea and a P_u/P_g ratio of 4.6 ± 1.1 . This is qualitatively similar to the equivalent human AQP1 mutant (F56A/H180A), which in our hands had a P_u/P_g ratio of 3.6 ± 1.4 ; this is somewhat higher than the 1.7 ± 0.6 previously reported for rat AQP1 [58], although these values are just compatible with one another within the experimental uncertainties. For the F77A/H201G double mutant, although the absolute glycerol and urea permeabilities were threefold higher than F77A/H201A, the P_u/P_g ratio stayed similar at 3.7 ± 0.4 ; similarly the P_u/P_g ratio for F77A/R216A was 3.3 ± 0.6 .

The H201A/R216A double mutant did not have measurable permeability for either glycerol or urea despite being highly expressed at the plasma membrane ($125 \pm 5\%$ of wild-type) and despite the glycerol permeability conferred by the individual H201A and R216A mutations. It is not clear whether this is due to the physicochemical properties of the H201A/R216A pore layout, or whether the mutation has a larger knock-on structural effect. Water permeability data for this mutant would help with interpretation of this result.

In the case of both AQP4 and AQP1, alanine substitution of the ar/R phenylalanine (F77A and F56A respectively) alone had no effect on either glycerol or urea permeation. Taken together, our data on the solute permeability of AQP4 mutants and the published literature on the permeability of AQP1 mutants, suggest that there are differences in the molecular details of how different wAQPs exclude neutral solutes and that care must be taken to compare several family members when developing a generalized model of how wAQPs exclude molecules other than water.

Of particular interest is the surprising result that mutating AQP4 H201 to alanine or glycine formed neutral solute channels with opposite glycerol and urea permeability behaviour: H201A was glycerol permeable but urea impermeable, H201G was urea permeable but glycerol impermeable. In the crystal structure of the bacterial glycerol facilitator GlpF, a co-crystallised glycerol molecule had its carbon backbone packed into a corner created by two hydrophobic residues (W48 and F200). It has been suggested that this hydrophobic corner facilitates preference of GlpF for glycerol over urea because glycerol has a hydrophobic face that can pack into the corner, whereas urea does not [46]. The H201A mutant, in combination with F77, could mimic this hydrophobic effect, whereas the glycine mutant, being less hydrophobic, does not. In addition, MD simulations suggested that this hydrophobic corner is further disrupted by the exposure of the V187 sidechain carbonyl group to the pore. This extra hydrogen-bonding site may provide an extra free energy penalty disfavouring the packing of the glycerol backbone (which cannot satisfy the bond) into this region of the selectivity filter.

Alternatively it is possible that knock-on structural effects of the mutations, leading to two proteins with considerably different channel size and/or shape to the *in silico* mutants, cause the difference. To settle this conclusively would require structural analysis of the mutant proteins *in vitro* (e.g. x-ray crystallography). In either case, the difference in solute preference of the two mutants (for glycerol and urea) cannot be explained by pore size alone.

Water permeability experiments showed a $47\pm 3\%$ increase in permeability for the AQP4 R216A mutant. Crystallographic analysis [276] and simulations [61] of AQPZ have suggested that the selectivity filter arginine residue may undergo fluctuations between ‘up’ and ‘down’ conformations, with the down conformation associated with a closed state of the channel and reduced channel permeability. Similar results were reported for fluctuations of the selectivity filter histidine residue in human AQP5 [277]. We found that R216 of AQP4 underwent the same fluctuations in molecular dynamics simulations. In situations such as these, the permeability measured in experiments would be an average of the permeabilities of the two states, weighted by their relative probabilities. *In silico* mutation of the AQPZ arginine to serine (R189S) increased the average water permeability by 26% [61], which agrees qualitatively with our *in vitro* result for AQP4 R216A. This suggests that R216 conformational fluctuations may switch AQP4 between high and low permeability states and that the alanine substitution forces the channel to permanently occupy the high permeability state. Water permeability of the H201E mutant was reduced to $63\pm 8\%$ of wild-type AQP4. Replacement of the histidine residue with a negatively charged glutamate residue may favour the closed state of the channel by interaction with the positively charged R216 sidechain. Taken together, these results suggest that

the dynamics of R216 are important for AQP4 water permeability. Control of the open/closed probabilities by e.g. protein post-translational modification or protein-protein interactions may represent an unexplored mechanism by which AQP4 water permeability could be regulated by physiological stimuli.

In our homology model of AQP3, a tyrosine residue, Y212, occupied a similar position to a phenylalanine (F200) in GlpF, producing a similar hydrophobic corner to that in the GlpF crystal structure. As this corner was previously suggested to facilitate glycerol selectivity in GlpF [46], we mutated the AQP3 tyrosine residue to alanine. This mutation reduced the glycerol permeability of AQP3 to 51 ± 5 % of the wild-type permeability. In contrast, the urea permeability of the channel was increased from zero (or at least undetectably low) to 47 ± 7 % of the wild-type glycerol permeability, giving a P_u/P_g ratio of 0.93 ± 0.16 . The GlpF F200 equivalent in AQP9 is a cysteine residue (C213). This is similar in size to alanine and AQP9 had a similar P_u/P_g ratio of 0.84 ± 0.08 , although the individual urea and glycerol permeabilities of AQP9 were about threefold higher.

Further mutations to AQP4 were made to mimic the pore layouts of GLPs. We replaced the histidine (H201) with both glycine and alanine in combination with replacement of the alanine (A210, analogous to AQP3 Y212) to either tyrosine or phenylalanine to give the following set of double mutations: H201G/A210F, H201G/A210Y, H201A/A210F and H201A/A210Y. None of these mutants were glycerol or urea permeable despite having surface expression that was comparable to wild-type AQP4 and despite the solute permeabilities of the single

H201A/G mutants. This suggests that the exact residues of the ar/R region are not the only molecular determinant of solute permeability, but that the structural context is also important. This is in agreement with a study in which mutation of the AQPZ selectivity filter residues to those of GlpF, alone and in combination, failed to introduce glycerol permeability to AQPZ. Crystallographic analyses of the AQPZ mutants and GlpF that suggested that the positioning of selectivity filter residues by the extracellular loop C and the unstructured loop connecting the top of TM5 to the second NPA half-helix may contribute to AQP solute permeability/exclusion [63].

We compared the glycerol and urea permeabilities of human AQPs 3, 9 and 10. To our knowledge, this is the first time this kind of comparison has been made in the same experimental system whilst controlling for relative surface expression. There are conflicting reports in the literature on whether AQP3 functions as a urea channel [126, 278] and it is not clear under what circumstances, if any, urea may permeate AQP3 (a detailed discussion of this is presented in Kitchen et al, *Biochimica et biophysica acta*, 2015, appendix 1). In our hands, human AQP3 was glycerol permeable, but was not measurably urea permeable when transiently expressed in HEK293 cells, either with or without a C-terminal GFP tag. AQP10 had similar glycerol permeability to AQP3, whereas the permeability of AQP9 to glycerol was almost two-fold higher. AQPs 9 and 10 had opposite biases towards glycerol and urea permeability with both having a P_u/P_g ratio significantly different to 1. It may be that these differences in the P_u/P_g ratio represent a physiological mechanism by which the different solute permeabilities of a membrane can be fine-tuned by altering the relative expression of different

GLPs. Regardless of the physiological implications, this data suggests that channel cross-sectional size is not the only molecular feature governing solute permeation and that there is a still-to-be-discovered molecular mechanism governing polar solute selectivity (rather than simply lack of exclusion). For our AQP4 mutants, we found that, above $\sim 14 \text{ \AA}^2$, channel cross-sectional area was reasonably correlated with urea permeability ($R^2 = 0.83$). We made a linear fit of this data and found that this model predicted AQP3, AQP3 Y212A, AQP3 G203H/Y212A and AQP10 urea permeability. In contrast, the geometric properties of the selectivity filter that we measured did not appear to correlate with glycerol permeability.

As a whole, our data show that the details of solute permeability of mammalian GLPs and solute exclusion by wAQPs depend on a complex interplay between the exact residues that form the ar/R region and the structural context in which they are situated. We also show that the residues of the ar/R region can have a direct effect on channel water permeability (for AQP4 at least), probably by dynamic transitions between high and low permeability states of the channel, providing the first *in vitro* evidence for an effect observed in molecular dynamics simulations. Finally, our data imply that care must be taken when attempting to generalize results of mutagenic experiments on just one or two representative members of the AQP family; in order to develop a detailed understanding of AQP solute and water permeation, data on as many members of the family as possible should be compared and contrasted.

5 Results – Molecular determinants and functional consequences of AQP4 tetramerization

5.1 Aims

1. To use the published crystal structure of AQP4 as a guide for directed mutagenesis aimed at disrupting the tetrameric quaternary structure of AQP4.
2. To use non-tetrameric mutants of AQP4 to investigate which aspects of AQP4 function require tetramerization.
3. To investigate whether the region identified as important for AQP4 tetramerization in aim 1 is important for other members of the AQP family.

5.2 Background

There is a wide variety in permeability properties, subcellular localization and trafficking responses between different members of the AQP family. Despite this, a wealth of medium to high resolution structural data for various members of the family (48 structures of 13 different AQPs deposited in the protein databank) all suggest that the AQP homotetrameric quaternary structure is highly conserved. Early biochemical work, using carboxyl-amine fusion dimers (consisting of one wild-type unit and one unit lacking the cysteine residue required for mercurial inhibition), showed that monomers are the functional AQP units [49]; numerous molecular dynamics simulation studies support this [50]. Recent work has suggested that isolated AQP monomers are equally capable of facilitating water transport as those incorporated into a tetramer [44]. Therefore it

is not clear why AQPs retain this tetrameric structure. Regulation of AQP function by the formation of heterotetramers with other AQPs has been suggested for some plant AQPs [51]. The fifth, central pore formed at the fourfold axis of the tetramer has also been suggested to transport carbon dioxide [52] and cations [53], at least in mammalian AQP1. Trigger-induced relocalization of AQP-containing vesicles to the plasma membrane is a well-established regulatory mechanism for AQPs; the best-studied example of this is relocalization of AQP2 to the apical membrane of the collecting duct in the mammalian kidney in response to AVP, but there is also evidence for similar mechanisms for various other AQPs including AQP5 [279], AQP7 [97] and AQP1 [169]. Given the ubiquity of these regulatory responses across the AQP family and the conservation of the tetrameric quaternary structure, it may be that these trigger-induced relocalization responses involve interaction with proteins that only recognize the tetrameric form of AQPs. A naturally occurring AQP2 mutant (R187C) has been reported which is unable to relocalize in response to AVP and is also unable to form tetramers [280], although it is not clear whether there is a direct link between these two observations.

In this chapter, evidence is presented that suggests that intracellular loop D of AQP4 forms homomeric interactions between AQP subunits that stabilize the tetrameric quaternary structure. We also show that loss of tetramerization does not affect single channel water permeability. Our data suggest that tetramerization is not required for AQP4 to be trafficked through the ER and Golgi to the plasma membrane, but that unlike wild-type AQP4, the non-tetrameric mutants are unable to relocalize to the plasma membrane in response

to changes in local osmolality as described in chapter 3. Finally, based on loss and gain of oligomerization mutants of AQP1 and AQP3, we suggest that loop D-mediated inter-monomer interactions may be a conserved mechanism by which AQPs control their quaternary structure.

5.3 Results

5.3.1 Compound mutations of loop D of AQP4 reduce tetrameric assembly

Using the crystal structure of AQP4 [222], residues likely to form the tetrameric interface were identified, based on the physical distance between residues on adjacent monomers. Any residue within 3 angstroms of an adjacent AQP4 molecule in the tetrameric structure was taken as a potential site of interaction, shown in orange and green in Figure 5-1 A and B. Alanine substitution mutagenesis was used to investigate the contribution of these residues to oligomeric assembly. The identified residues were clustered into two regions: The first cluster comprises a patch of hydrophobic residues at the interfaces of TM1 and TM2 of one monomer with TM4 and TM5 of the adjacent monomer (Figure 5-1 A); the second cluster comprises twelve predominantly polar and charged residues forming the intracellular loop D and the bottom of TM2 (Figure 5-1 B). 24 single point alanine-substitution mutants were made and six compound mutants were used to investigate the possibility of synergistic effects of several residues (Table 5-1). There are two protein kinase A/C consensus sites in loop D (S180 and S188) so we also made phosphomimetic mutations (S180D and S188D) of these residues. All mutants are listed in the left-hand column of Table 5-1. BN-PAGE followed by Western blotting (described in sections

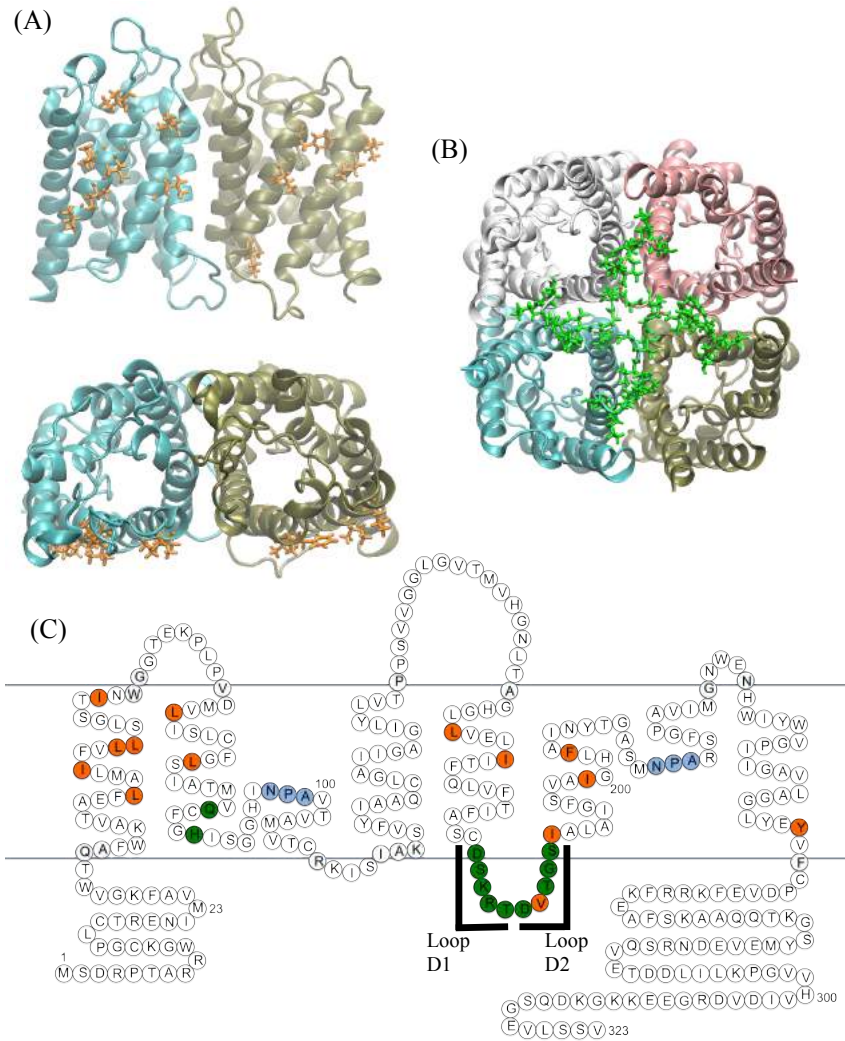


Figure 5-1 Residues at the AQP4 tetrameric interface. (A) We identified hydrophobic residues (orange) in TMs 1, 2, 4 and 5 that formed inter-monomer contacts in the crystal structure and (B) polar residues (green) at the bottom of TM2 and in the intracellular loop D. (C) Ball diagram showing the position of the identified residues in the primary sequences and secondary structural motifs of AQP4. Two regions of loop D were selected for compound mutation, which we denote loop D1 (179-DSKRT-183) and loop D2 (184-DVTGS-188). Blue lines represent approximate position of membrane lipid headgroups. All residues are listed in **Table 5-1**.

<u>Mutant</u>	<u>Oligomerization state</u>	<u>Surface expression (% of WT)</u>
<u>I43A</u>	<u>T</u>	<u>113.9±5.1</u>
<u>I47A</u>	<u>T</u>	<u>95.8±3.2</u>
<u>L50A</u>	<u>T</u>	<u>102.5±4.1</u>
<u>L51A</u>	<u>T</u>	<u>96.1±13.0</u>
<u>I57A</u>	<u>T</u>	<u>104.1±4.1</u>
<u>TM1</u> (<u>I43A/I47A/L50A/L51A/I57A</u>)	<u>T</u>	<u>86.9±3.1</u>
<u>L72A</u>	<u>T</u>	<u>121.1±25.6</u>
<u>L79A</u>	<u>T</u>	<u>88.9±13.3</u>
<u>TM2</u> (<u>L72A/L79A</u>)	<u>T</u>	<u>97.7±5.6</u>
<u>L161A</u>	<u>T</u>	<u>91.9±18.4</u>
<u>I165A</u>	<u>T</u>	<u>87.9±3.6</u>
<u>TM4</u> (<u>L161A/I165A</u>)	<u>T</u>	<u>85.4±11.2</u>
<u>I189A</u>	<u>T</u>	<u>97.7±5.9</u>
<u>I199A</u>	<u>T</u>	<u>96.2±8.5</u>
<u>F203A</u>	<u>T</u>	<u>112.4±13.3</u>
<u>TM5</u> (<u>I189A/I199A/F203A</u>)	<u>T</u>	<u>93.3±9.0</u>
<u>Q86A</u>	<u>T</u>	<u>118±4.4</u>
<u>H90A</u>	<u>T</u>	<u>113.5±4.1</u>
<u>D179A</u>	<u>T (95±2%)</u> <u>D (5±2%)</u>	<u>87.6±19.4</u>
<u>S180A</u>	<u>T</u>	<u>109.8±4.5</u>
<u>S180D</u>	<u>T</u>	<u>99.7±4.9</u>
<u>K181A</u>	<u>T</u>	<u>103.2±4.5</u>
<u>R182A</u>	<u>T</u>	<u>96.1±22.1</u>
<u>T183</u>	<u>T</u>	<u>105.6±3.6</u>
<u>Loop D1</u> (<u>D179A/S180A/K181A/R182A/T183A</u>)	<u>T (19±4%)</u> <u>D (27±5%)</u> <u>M (53±4%)</u>	<u>88.5±6.1</u>
<u>D184A</u>	<u>T</u>	<u>97.7±8.8</u>
<u>V185A</u>	<u>T</u>	<u>102.2±5.4</u>
<u>T186A</u>	<u>T</u>	<u>95.1±7.5</u>
<u>G187A</u>	<u>T</u>	<u>106.7±5.1</u>
<u>S188A</u>	<u>T</u>	<u>98.6±3.2</u>
<u>S188D</u>	<u>T</u>	<u>104.1±4.2</u>
<u>Loop D2</u> (<u>D184A/V185A/T186A/G187A/S188A</u>)	<u>T (33±7%)</u> <u>D (67±7%)</u>	<u>83.1±11.0</u>

Table 5-1 Oligomerization state and surface expression of AQP4 mutants. A solidus, e.g. L72A/L79A, represents compound mutations. T = tetramer, D = dimer, M = monomer. All data are reported as mean±S.E., n=3.

2.10 and 2.11) was used to assess the oligomeric state of all mutants expressed in HEK293 cells. Representative BN blots are shown in Figure 5-2 and the effect of all mutations on oligomeric assembly and surface expression is summarised in Table 5-1 and Figure 5-2.

None of the hydrophobic residues in the hydrophobic patches had any effect on tetramer formation, either in isolation or as compound mutants. TM compound mutants consisted of simultaneous mutations of all residues identified within that transmembrane segment (e.g. TM1 denotes the simultaneous mutations I43A/I47A/L50A/L51A/I57A).

Of the loop D single alanine mutants, only D179A had an effect on oligomeric assembly in isolation, and this effect was only slight, with $95\pm 2\%$ of the protein still assembled into tetramers. Unlike the hydrophobic cluster, the compound mutants of loop D had a clear effect on the ability of AQP4 to tetramerize. The two compound mutants loop D1 (D179A/S180A/K181A/R182A/T183A) and loop D2 (D184A/V185A/T186A/G187A/S188A) caused reductions in oligomeric assembly with only $19\pm 4\%$ of the loop D1 protein assembled into tetramers with both dimers ($27\pm 5\%$) and monomers ($53\pm 4\%$) present, whereas the loop D2 protein predominantly formed dimers ($67\pm 7\%$) with $33\pm 7\%$ assembled into tetramers.

5.3.2 Surface expression of non-tetrameric mutants

There was no significant difference in the surface expression of the loop D mutants compared with wild-type AQP4. Surface expression was assessed qualitatively by live cell confocal microscopy using GFP-tagged AQP4 mutant constructs and quantitatively by cell surface biotinylation. Figure 5-3 shows

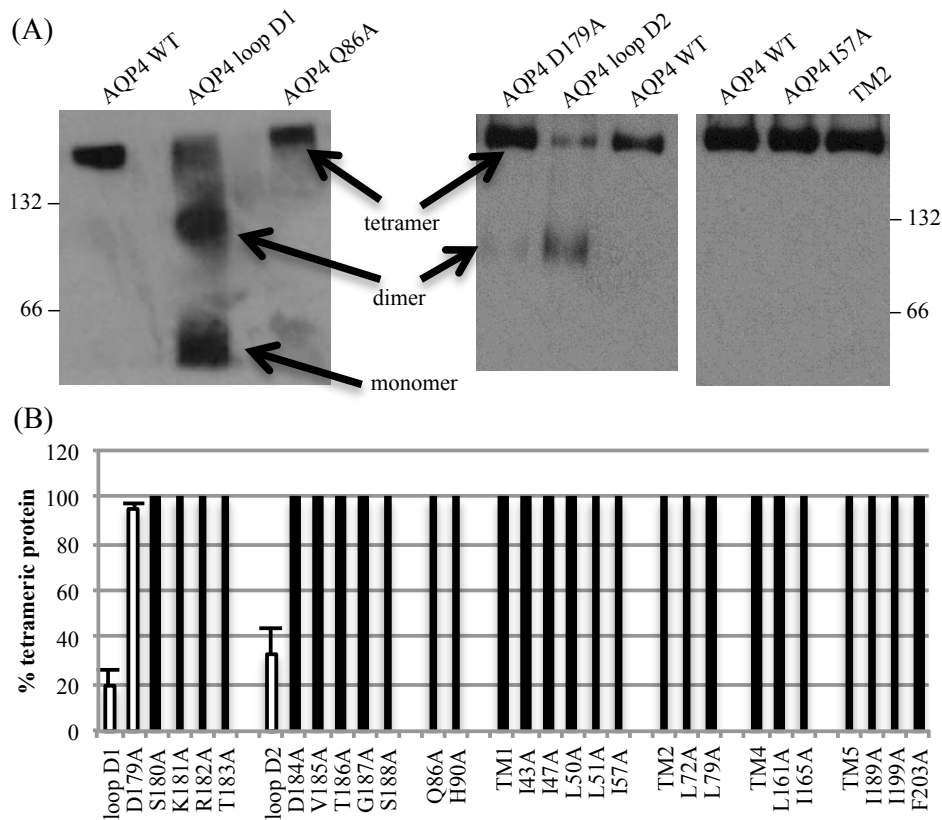


Figure 5-2 BN-PAGE and Western blotting of AQP4 mutants. (A) Representative Western blots following BN-PAGE of Triton X-100 solubilized AQP4 mutants, showing the effect of the loop D1 and loop D2 compound mutations, and a lack of effect of mutations to the transmembrane hydrophobic patch. 66 and 132 denote the positions of BSA molecular weight marker bands. The AQP4-GFP construct, has a predicted molecular weight of 63.1 kDa. (B) Percentage of protein assembled into tetramers calculated using densitometry following BN-PAGE and Western blotting. Effective mutations are highlighted with white bars. Data is presented as mean \pm S.E., n=3.

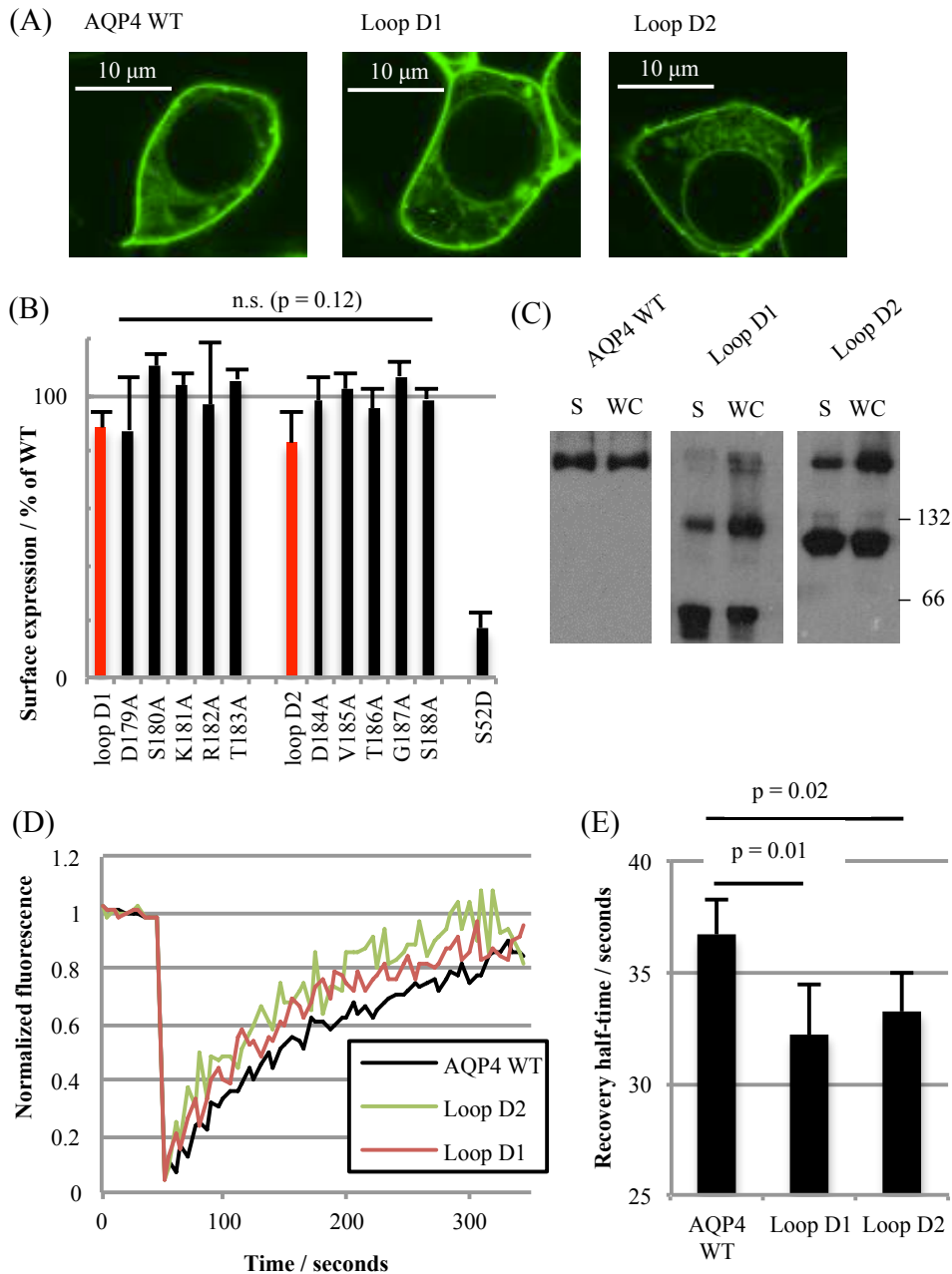


Figure 5-3 Plasma membrane localization of non-tetrameric mutants. (A) Representative fluorescence micrographs of HEK293 cells transfected with AQP4-GFP and loop D mutants. (B) Surface expression of AQP4 mutants in HEK 293 cells measured by cell surface biotinylation followed by neutravidin-based ELISA. Loop D compound mutants are highlighted in red. The S52D mutant identified in chapter 3 was used as a negative control for surface expression. n.s., not significant. (C) Representative blots of AQP4 mutants subjected to BN-PAGE. WC = whole cell lysate; S = surface protein only, isolated by cell surface biotinylation. (D) Representative FRAP curves from photobleaching AQP4-GFP fusion proteins in HEK 293 cells. (E) Average half-times of fluorescence recovery averaged over fits to 5 curves per experiment and 6 experimental repeats. All data is presented as mean \pm S.E.

representative confocal micrographs of HEK293 cells transfected with GFP fusion proteins of AQP4 wild-type, and the loop D1 and loop D2 mutants. Surface expression in transiently transfected HEK293 cells measured by cell surface biotinylation was not significantly different ($p=0.53$, one-way ANOVA) for either of the loop D compound mutants or the single alanine mutants. This suggests that the post-Golgi trafficking machinery is able to interact with non-tetrameric AQPs. The cell surface biotinylation data is summarized for all mutants in the third column of Table 5-1.

5.3.3 Mutants in the plasma membrane have reduced oligomeric state

It was important to confirm the reduced oligomeric state of AQP4 molecules that had been trafficked to the cell surface, rule out intracellular retention of dimeric/monomeric species, and to rule out changes in detergent sensitivity caused by loop D substitutions. Several complementary biophysical techniques were used to do this.

5.3.3.1 Fluorescence recovery after photobleaching (FRAP)

Recovery curves were collected from five different AQP-transfected HEK293 cells per experimental repeat ($n = 6$), as described in section 2.4.2.

Representative fluorescence recovery curves are shown in Figure 5-3, along with the average recovery half-times. From these, diffusion coefficients were calculated: $5.2 \pm 0.3 \times 10^{-3} \mu\text{m}^2\text{s}^{-1}$ (AQP4 WT), $5.9 \pm 0.3 \times 10^{-3} \mu\text{m}^2\text{s}^{-1}$ (Loop D1) and $5.8 \pm 0.2 \times 10^{-3} \mu\text{m}^2\text{s}^{-1}$ (Loop D2). Both Loop D mutant diffusion coefficients were significantly different from the wild-type (Loop D1 $p=0.01$ and loop D2 $p=0.02$ by Student's t-test following ANOVA, with p values subjected to

Bonferroni correction). The FRAP data suggests a reduced oligomeric state for the surface-localized loop D mutants, although the increased diffusion coefficient could also be explained by the inability of these mutants to form a complex with a third party protein.

5.3.3.2 BN-PAGE of biotinylated cell surface protein

To complement the FRAP experiments, biotinylated cell surface proteins were isolated using neutravidin-coated plates, eluted by reducing the S-S bond incorporated into the biotinylation reagent using 1% β -mercaptoethanol in BN lysis buffer and subjected to BN-PAGE (representative blots are shown in Figure 5-3). Surface-localized mutant AQP4 molecules subjected to BN-PAGE had the same loss of tetramerization seen in whole cell lysates.

5.3.3.3 Forster resonant energy transfer (FRET)

Finally, to complement the above analyses, AQP4 constructs tagged with Venus (a YFP derivative) and mTurquoise2 (a CFP derivative) were generated and co-transfected into HEK293 cells to form a FRET biosensor for homo-oligomerization in living cells as described in section 2.4.3. The wild-type AQP4 constructs gave a robust FRET signal with an average apparent efficiency of $44.2 \pm 3.6\%$ (Figure 5-4). We were unable to measure any FRET in cells co-transfected with AQP1-Venus and AQP4-Turquoise, suggesting that the FRET interactions occur primarily within the AQP4 tetramers and not between tetramers that are transiently close together in the plane of the membrane. The probability for a particular donor molecule to take part in FRET is dependent on the number of acceptors within the Forster radius and vice versa.

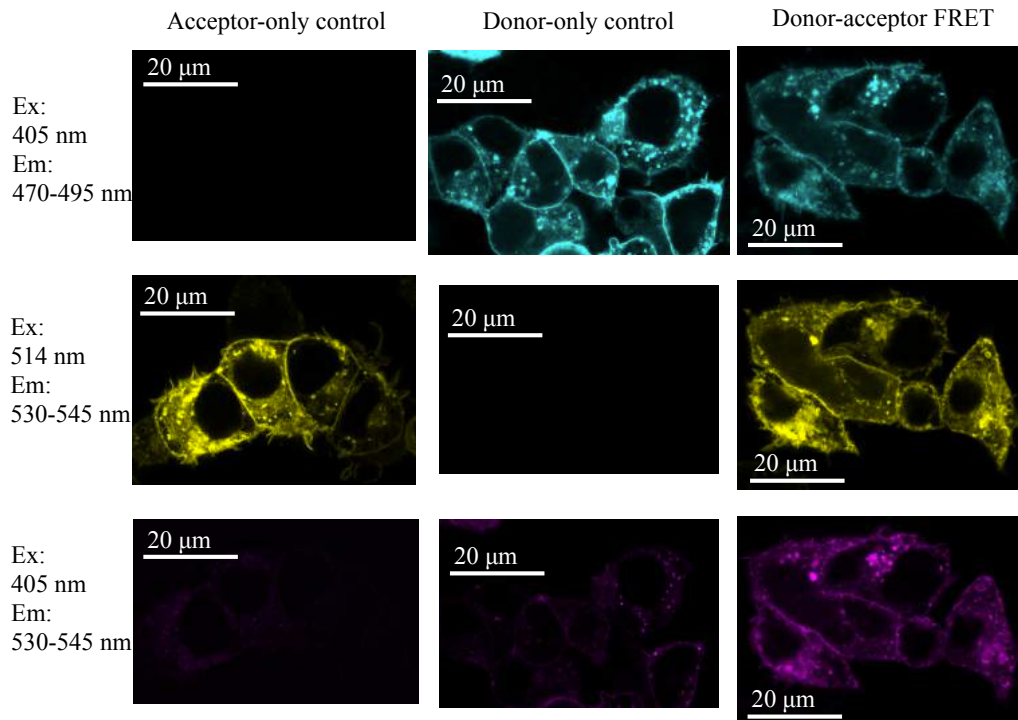


Figure 5-4 . A FRET biosensor for AQP4 oligomerization. Fluorescence confocal microscopy of live HEK293 cells transiently transfected with AQP4-Venus alone, AQP4-mTurquoise2 alone and the two co-transfected. Excitation at 405 nm is for Turquoise and 514 is for Venus.

For CFP-YFP, the Forster radius is ~5 nm [281]. Based on the AQP4 crystal structure, the monomer-monomer centre of mass separations are 2.8 nm (adjacent monomers) and 3.9 nm (diagonal monomers), so both would be expected to contribute to the FRET signal (assuming that the average separation of the C-terminal tails is similar). The average number of FRET pairings in a sample of co-transfected cells is therefore dependent on the level of AQP4 oligomerization. Both loop D1 and D2 compound mutants had a slightly larger than twofold reduction in FRET efficiency (to $17\pm 6\%$ and $20\pm 4\%$ respectively) compared to the wild-type (Figure 5-5), suggesting that these constructs have a reduced propensity to oligomerize in live cells, further confirming that the changes seen in the BN-PAGE were not mediated by changes in detergent sensitivity. Furthermore, for the mutants, there was no difference in FRET efficiency between plasma membrane and intracellular membranes (Figure 5-5), suggesting that the oligomerization state of these mutants is the same in intracellular membranes as in the plasma membrane. Taken together, these data suggest a reduced oligomeric state for the AQP4 loop D mutants in the plasma membrane of living cells.

5.3.4 Loop D mutants have wild-type water permeability

Both loop D compound mutants and wild-type AQP4 were stably transfected into MDCK cells (described in section 2.3.2) to measure water channel function. Membrane water permeability of MDCK cells, measured by calcein fluorescence quenching, as described in sections 2.8 and 2.8.1, (Figure 5-6), was increased sevenfold by stable expression of AQP4. Water permeability due to the transfected AQP was calculated by subtracting the permeability of untransfected cells and the resulting permeability was normalized to the surface expression

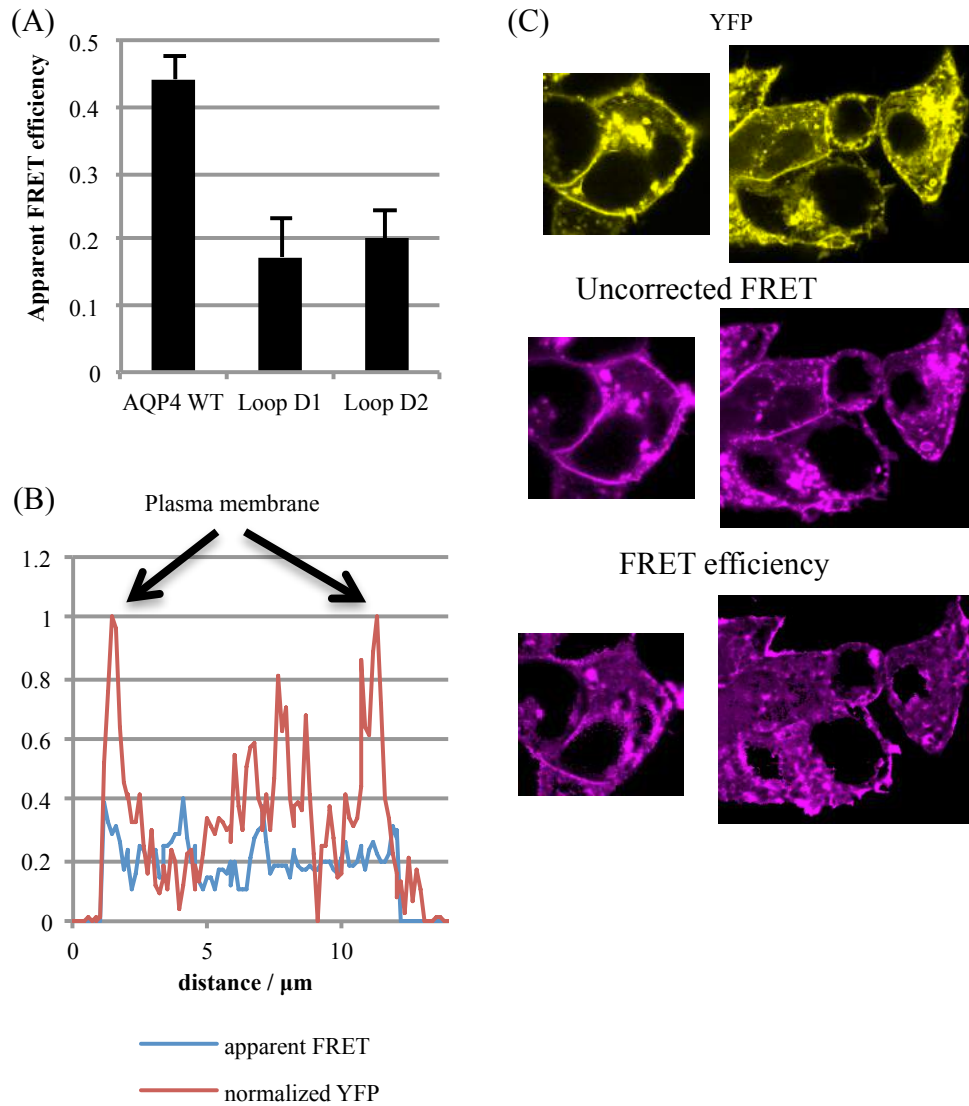


Figure 5-5 Reduced FRET from AQP4 mutants (A) Average apparent FRET efficiencies for AQP4 wild-type and the loop D1 and D2 mutants, calculated by normalizing the corrected FRET intensity to YFP intensity for each pixel. Five different areas on each plate were imaged per experimental repeat, $n=4$. (B) Representative line scan across a cell, passing through membrane and cytoplasm and avoiding the nucleus. Whereas the YFP signal (red) shows clear peaks at the plasma membrane, the FRET efficiency (blue) does not. (C) Representative processed FRET efficiency images compared to unprocessed FRET and YFP. Whereas both YFP and the raw FRET show clear membrane signals, the FRET efficiency does not.

measured by cell surface biotinylation to allow for differences in cellular expression due to differences in the position of chromosomal integration of the stably transfected gene. After normalization to surface expression, no significant difference in permeability was observed between the loop D mutants and wild-type AQP4, suggesting that tetramerization of AQP4 was not required for full water channel activity.

5.3.5 Loop D mutants do not relocalize in response to hypotonicity

We recently reported that AQP4 rapidly relocalizes to the plasma membrane from intracellular membranes in response to reduced extracellular tonicity [268] and this phenomenon is true for other mammalian AQPs [169]. Despite wild-type water permeability and constitutive surface expression of the loop D mutants, this response to hypotonicity was blocked by both of the loop D compound mutations. Relative membrane expression of wild-type AQP4-GFP imaged in live HEK 293 cells increased from 27.9 ± 3.5 to 67.1 ± 4.5 ($p=0.003$) upon reduction of the extracellular tonicity to 85 mOsm, whereas the distribution of both the loop D1 and loop D2 mutants did not change significantly ($p=0.29$ and $p=0.34$ respectively; Figure 5-7).

5.3.6 Molecular dynamics simulations suggest a dynamic network of loop D interactions

To investigate the contribution of loop D to AQP4 oligomerization we did five independent 100 ns molecular dynamics simulations of a hydrated AQP4 tetramer embedded in a POPC bilayer. We found a dynamic network of hydrogen bonds between loop D residues on adjacent monomers and also

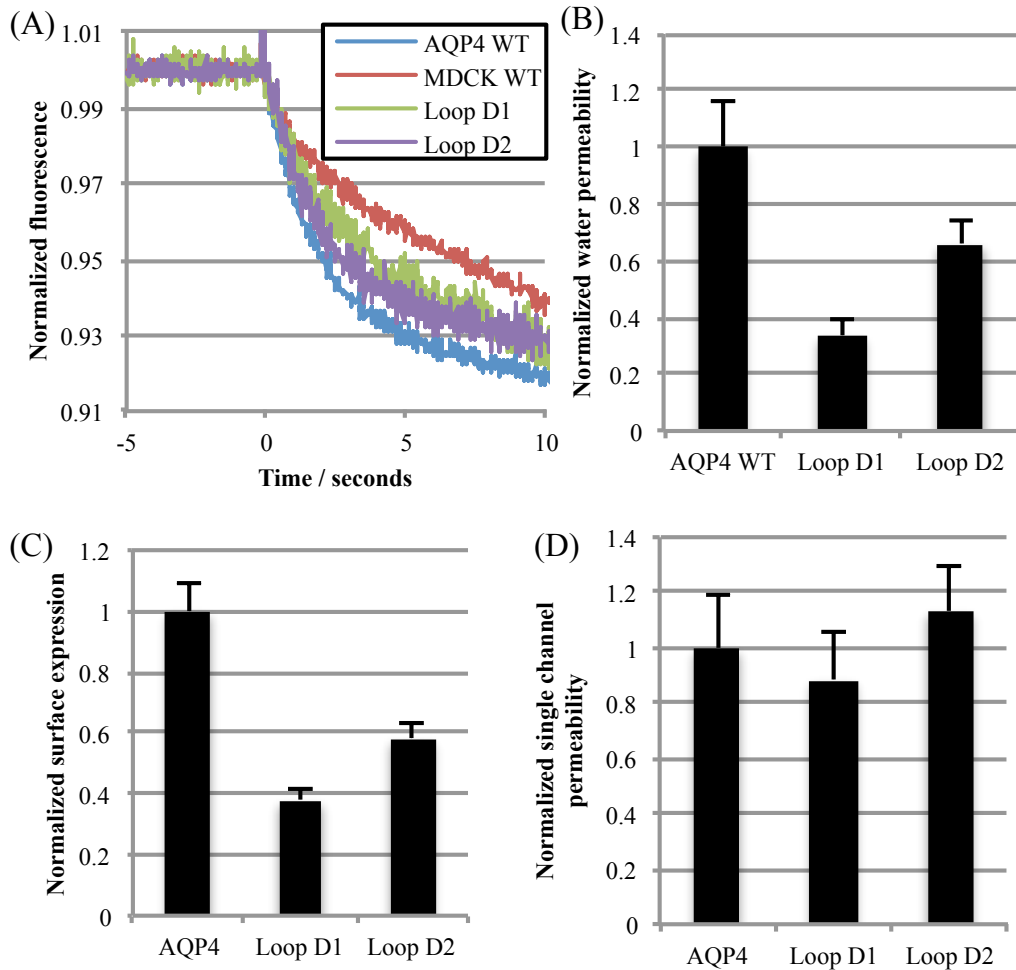


Figure 5-6 Water permeability of non-tetrameric mutants. (A) Representative calcein fluorescence quenching curves from stably transfected MDCK cells subjected to a 300 mOsm mannitol osmotic gradient. (B) Water permeability of MDCK cells normalized to AQP4 WT-transfected MDCK cells. (C) Normalized surface expression of AQP4 constructs in the stably expressing MDCK clones used for water permeability measurements, measured by cell surface biotinylation. (D) MDCK membrane water permeability normalized to surface expression, to give normalized single channel permeability. All data is presented as mean \pm SEM, n=4.

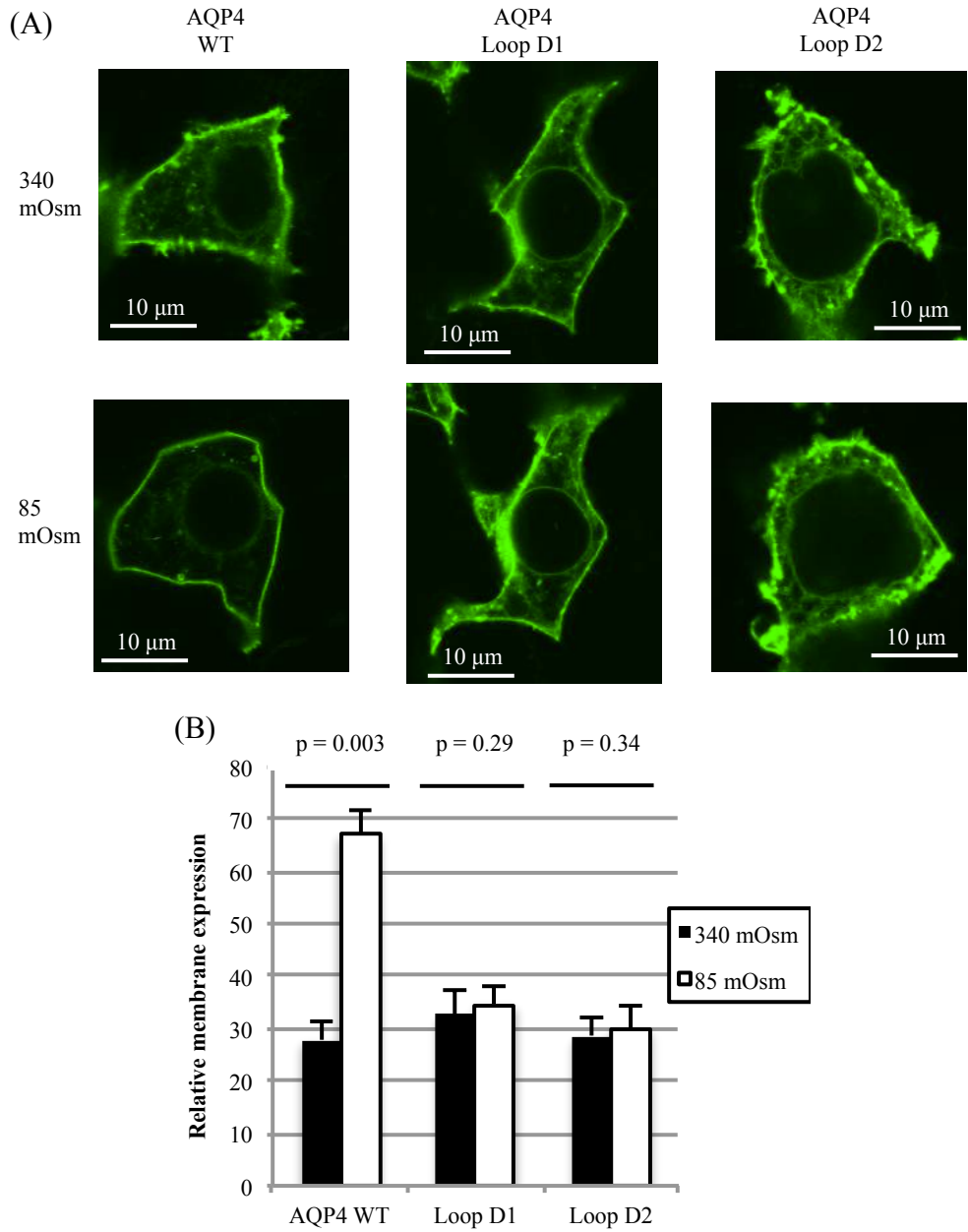


Figure 5-7 Tonicity-induced translocation of non-tetrameric mutants (A) Representative fluorescence micrographs of HEK 293 cells transfected with AQP4-GFP fusion proteins, before and after 30 seconds of exposure to hypotonic (85 mOsm) medium. (B) Relative membrane expression of AQP4-GFP fusion proteins before and after exposure to hypotonic medium. At least four cells per image were analyzed for each experimental repeat. $n = 3$. Data are presented as mean \pm S.E.M. p values are from paired t-tests, following ANOVA, with Bonferroni's correction.

between loop D residues and a glutamine (Q86) and histidine (H90) residue at the bottom of TM2. On average, each monomer was involved in 3.8 ± 1.4 (mean \pm standard deviation) loop D hydrogen bonds with its two neighbouring molecules at any given time, which is equivalent to 7.6 ± 2.8 loop D hydrogen bonds per tetramer. Every loop D residue apart from S180 was able to act as a hydrogen bond donor or acceptor with another loop D residue on one of the two adjacent monomers and seven residues (R182, T183, D184, V185, T186, G187 and S188) were found to have at least three different possible hydrogen bonding interactions. This network of interactions is represented as a heat map in Figure 5-8A. Interactions involving V185 and G187 were backbone hydrogen bonds. Both of these residues were able to act as hydrogen bond donors from the backbone amine group (V185 to an adjacent V185, and G187 to D184, V185 and T186) and acceptors at the backbone carbonyl group (V185 from an adjacent V185 as well as T183, T186, G187 and S188, and G187 from T186, S188 and Q86). Loop D (as well as loop A) showed relatively large structural fluctuations (Figure 5-8) despite maintaining an average of 3.8 ± 1.4 inter-monomer hydrogen bonding interactions. Representative snapshots showing the most highly occupied hydrogen bonds, H90-D179, S188-G187, S188-S188, Q86-D184, Q86-S188 and T183-D184 are shown in Figure 5-9. Loop D could potentially stabilize the AQP4 tetramer in one of two ways: by preventing monomers from drifting apart during rapid association/dissociation of the inter-monomer TM interfaces, or by providing inter-monomer interactions that stabilize the tetramer in a more permanent way, preventing dissociation in the first place. In simulations we found that the average monomer-monomer centre of mass separation was stable

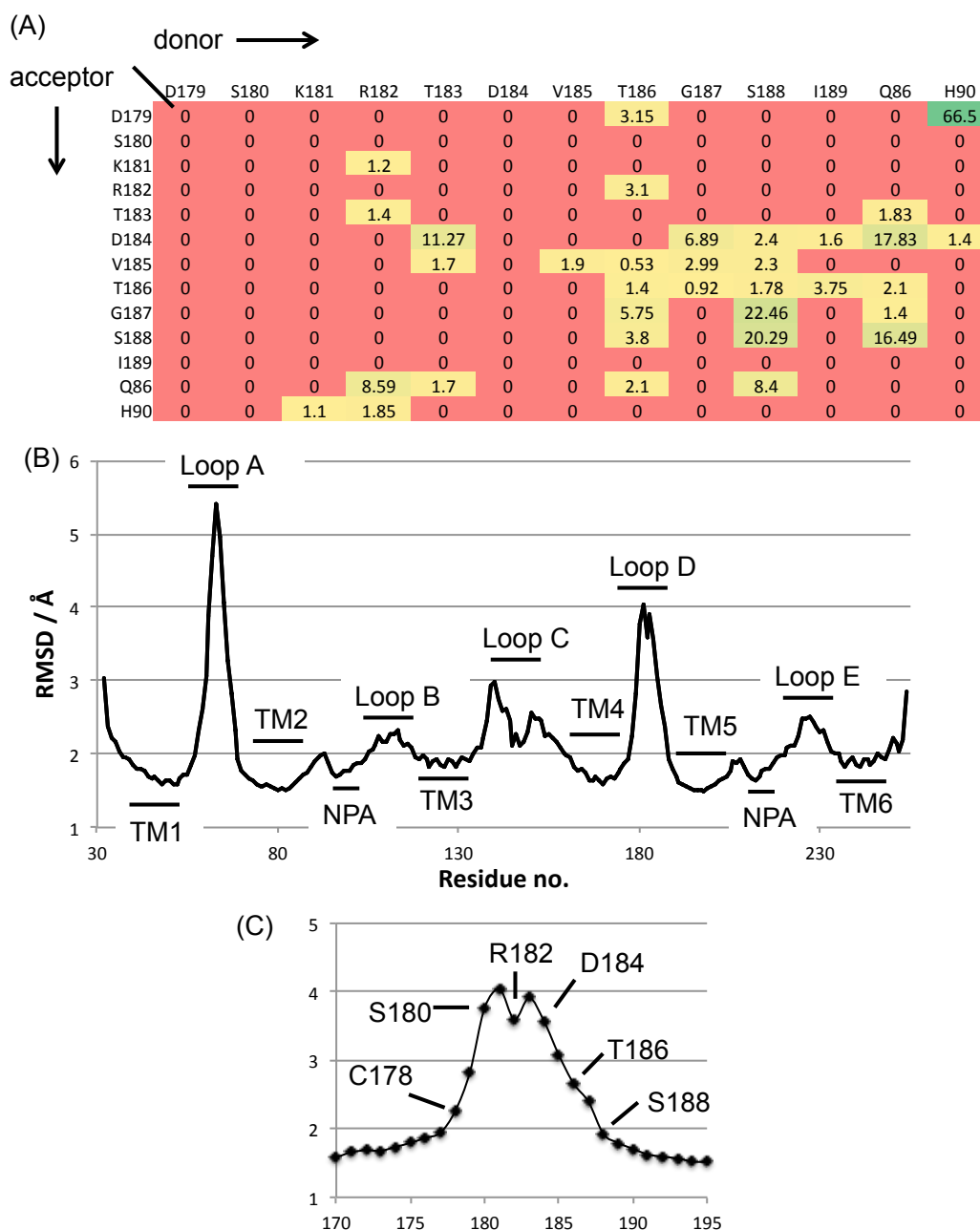


Figure 5-8 A dynamic network of loop D hydrogen bonds in simulations of AQP4. (A) Heat map showing percentage occupancy of loop D hydrogen bonds averaged over 4 monomers comprising a tetramer and over 5 independent 100 ns simulations. (B) Backbone heavy atom root mean-squared deviation (RMSD) of AQP4 residues, demonstrating the structural flexibility of loops A and D. RMSDs were calculated independently for each trajectory and averaged. (C) Zoomed view of loop D RMSD.

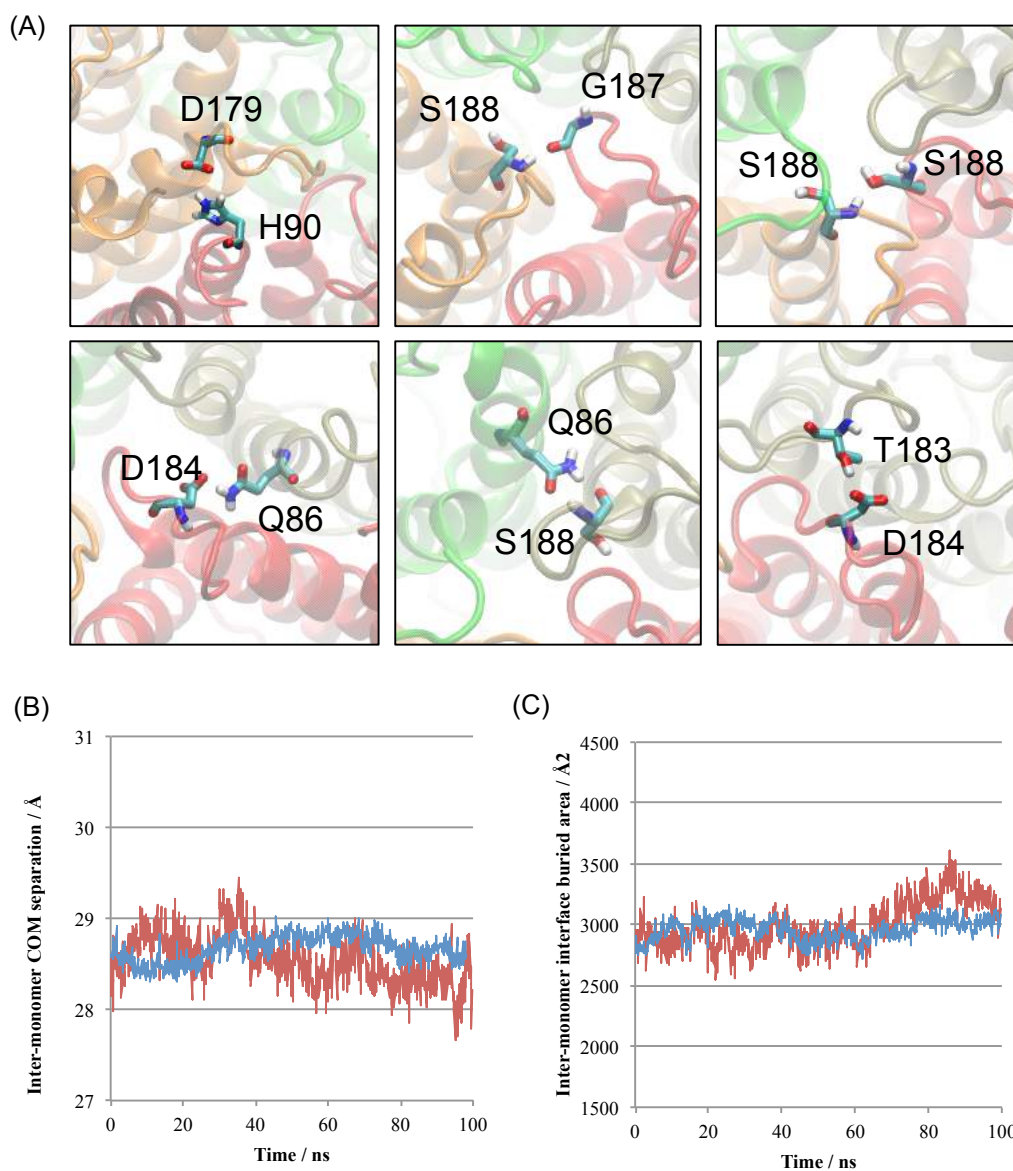


Figure 5-9 (A) Snapshots of molecular dynamics trajectories in which the six most highly occupied inter-monomer hydrogen bonds involving loop D residues are occupied. (B) Representative inter-monomer centre of mass distance for a single interface (red) and averaged over the four interfaces of a tetramer (blue). (E) Representative inter-monomer buried area for a single interface (red) and averaged over the four interfaces of a tetramer (blue).

with a root mean square fluctuation (RMSF) of only 0.53 Å (c.f. typical carbon-carbon bond length of ~1.5 Å) about a mean of 28.67 Å, and the inter-monomer buried (solvent-inaccessible) area was also stable, with a RMSF of 230 Å² about a mean of 2960 Å². Representative timeseries data are shown in Figure 5-9. This suggests that there is no spontaneous dissociation/reassociation of the inter-monomer interfaces, at least on the timescale of these simulations (100 ns).

5.3.7 Loop D may represent a common motif for oligomeric assembly across the AQP family

To investigate whether our AQP4 data could be more widely applicable to other members of the AQP family, we performed a sequence alignment of the loop in all human AQPs, as well as the *E. coli* AQPs as comparison (Figure 5-10) using the Clustal Omega software [282]. AQP1 contains a similar acidic-x-basic-basic motif to AQP4 in the first half of the loop (DRRRR vs. DSKRT), so we made the loop D1 mutant in AQP1 (D158A/K159A/K160A/K161A/K162A). This motif is lacking in AQP3, therefore we introduced it via 2 different mutations, P181S/Y182K/N183R and P181E/Y182K/N183R (to give DSKRN and DEKRN vs. the wild-type DPYNN). The loop D1 compound mutation to AQP1 caused a similar loss of oligomerization to that observed for AQP4, and both AQP3 mutations caused the protein to migrate primarily as a band with a molecular weight consistent with a dimeric species, whereas wild-type AQP3 appeared to migrate primarily as a monomer (Figure 5-10). Both AQP1 and AQP3 migrated as diffuse bands, consistent with glycosylation. PNGase F treatment was used to attempt deglycosylation. This appeared to be incompatible with the BN-PAGE experiments, as 1 hour treatments with PNGase F at 37 °C caused AQP1 and AQP3 wild-type and mutants to form aggregates that did not migrate beyond the

interface between stacking and separating gels (data not shown). This may be due to increased temperature sensitivity of Triton X-100 solubilized AQPs. Finally, to investigate whether loss of AQP oligomerization is a general feature of the GLP subfamily, we transfected HEK293 cells with AQPs 9 and 10 and subjected Triton X-100 extracted protein to BN-PAGE. Unlike AQP3, we found that AQPs 9 and 10 migrated exclusively as tetramers (Figure 5-10).

5.4 Discussion

Our data show that the plasma membrane abundance of AQP4 in HEK293 cells is unaffected by loss of tetrameric assembly. This strongly suggests that tetrameric assembly is not required for AQP4 to be correctly trafficked through the ER and Golgi to the plasma membrane. It is possible that our mutants are trafficked as tetramers and then dissociate once inserted into the plasma membrane; the FRET data suggest that this is unlikely to be the case, although we cannot differentiate between particular intracellular compartments on the basis of this data, leaving open the possibility of differences in oligomerization state between different intracellular compartments. Our diffusion coefficients calculated from the FRAP data are comparable with other reports of diffusion of AQP-GFP constructs in mammalian cells (e.g. $5.7 \times 10^{-3} \mu\text{m}^2\text{s}^{-1}$ for AQP2 [283], $3.1 \times 10^{-3} \mu\text{m}^2\text{s}^{-1}$ for AQP1 [284]). We found a small, but statistically significant increase in diffusion coefficient for the mutants that were non-tetrameric in BN-PAGE. Although we have not estimated hydrodynamic radii for our constructs, the relationship $D \propto \ln(1/R)$ derived by Saffman and Delbruck [285] suggests a hydrodynamic radius of 1.2 ± 1.0 nm for our non-tetrameric constructs (assuming $R = 4$ nm for a freely-diffusing AQP4 tetramer), which is at least consistent with a loss of tetrameric assembly. We found no difference in the mobile fraction

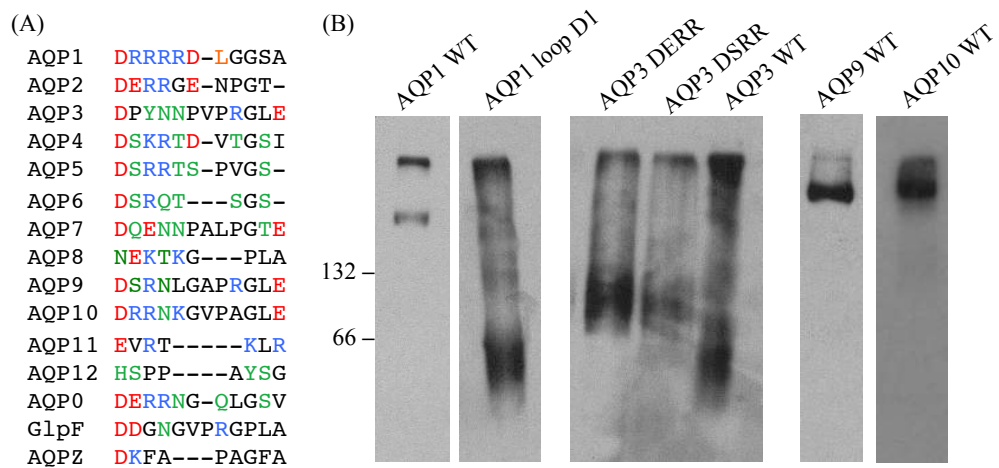


Figure 5-10 Comparison of loop D between different human AQPs. (A) All 13 human AQPs as well as AQPZ and GlpF (both from *E. coli*) were aligned using Clustal Omega (EMBL-EBI). Acidic residues are coloured red, basic blue, and neutral residues able to form sidechain hydrogen bonds green. (B) BN-PAGE and Western blotting of wild-type and mutant AQPs 1 and 3 and wild-type AQPs 9 and 10. 66 and 132 represent BSA molecular weight markers.

between the wild-type, D1 or D2 mutants ($90\pm 6\%$, $89\pm 4\%$ and $92\pm 7\%$ respectively, n.s. $p=0.28$), suggesting that there is no difference in the proportion of the protein involved in membrane-anchoring interactions. Although we cannot rule out loss of an AQP4 binding partner as an alternative explanation of these data with absolute certainty, in combination with the cell surface BN-PAGE and FRET data it is highly suggestive of non-tetrameric mutant AQP4 molecules in the plasma membrane. Human AQP3 was reported to exist in all four possible oligomeric states (monomer, dimer, trimer and tetramer) in the plasma membrane of erythrocytes [55]. It may be that some or all members of the AQP family can be trafficked to the plasma membrane independently of their oligomerization state.

Our MD simulations suggest a dynamic network of transient hydrogen bonds between the residues of loop D of adjacent monomers and also with two residues at the bottom of TM2. The fact that almost every residue involved in this network has several hydrogen bonding options may explain why none of the single alanine substitution mutations had an effect on tetrameric assembly. For example, the most highly occupied hydrogen bond that we found was H90-D179, which had 66.5% occupancy averaged over the four monomers and five trajectories. When this bond was not occupied, the D184 sidechain was able to act as a hydrogen bond acceptor from the histidine imidazole NH group, and the T186 sidechain hydroxyl group was able to act as a hydrogen bond donor to D179. These alternative interactions may be able to partially compensate for the loss of the D179-H90 interaction in the D179A and H90A single alanine substitutions. D179 had only one alternative interaction, whereas H90 had three.

This may explain why the D179A mutation had a slight effect on oligomerization, whereas the H90A mutant did not.

S-nitrosylation of AQP11 at a cysteine residue in the extracellular loop E (C227) has been suggested to be required for AQP11 oligomeric assembly, with the C227S mutant showing reduced oligomeric assembly in mouse kidney [286]. This supports the idea of a role for post-translational modification in AQP oligomerization. Loop D of AQP4 contains two sites predicted to be targets for post-translational modification. These are protein kinase sites at S180 and S188. Phosphorylation at S180 was suggested to reduce AQP4 water permeability via a gating effect in LLC-PK1 cells [287], but this was not supported by MD simulations of AQP4-pS180 [288], and structural studies showed no difference between wild-type AQP4 and a phosphomimetic S180D mutant [289, 290]. We used phosphomimetic (S180D, S188D) and phospho-blocking (S180A, S188A) mutations to investigate a potential role for post-translational modification in AQP4 oligomeric assembly. We found that all four phosphorylation mutants were able to assemble into tetramers, suggesting that phosphorylation of loop D is not involved in tetrameric assembly of AQP4.

We recently reported that AQP4 in primary rat astrocytes and HEK293 cells rapidly relocalized to the plasma membrane upon reduction of extracellular tonicity [268], and this may involve changes in interactions between AQP4-containing vesicles and cytoskeletal elements as described by others [291, 292]. Interestingly, neither of the mutants with reduced ability to tetramerize were able to relocalize in response to a hypotonic extracellular stimulus. It is possible that a

binding partner of AQP4 involved in the translocation response recognizes an epitope formed by the interface of several AQP molecules within a tetramer, and that disrupting tetrameric assembly disrupts this epitope. Although the C-terminal PKA phosphorylation site (S276) that controls this response is ~100 residues away in the primary sequence, it may be that phosphorylation of this residue causes a conformational change in the large (~70 residue) C-terminal tail of AQP4, which allows an AQP4-binding protein to bind to the intracellular face of AQP4 including loop D. Structural data for AQPs are routinely collected after cleaving the C-terminus at the bottom of TM6 to aid crystallization and high-resolution structure determination [47]. This is true for AQP4 and in the structure that we used to identify mutagenic targets and as input for our simulations, the protein was truncated at the bottom of TM6, at residue 254 of 323 [222]. This makes it difficult for us to make any concrete predictions about interactions of the AQP4 C-terminus, especially given its large size.

Based on a sequence alignment of loop D, we made mutants of human AQPs 1 and 3. Wild-type AQP1 was tetrameric when extracted from HEK293 membranes using Triton X-100, whereas AQP3 was primarily as a monomeric, both of which are in agreement with previous reports [55, 293]. Mutating the first five residues of AQP1 loop D to alanine (which rendered AQP4 primarily monomeric) caused the protein to migrate primarily as a monomer in BN-PAGE. Introducing the conserved acid-x-base-base motif (present in loop D of both AQPs 1 and 4) into AQP3 caused it to migrate primarily as a dimer. It has been suggested that lack of oligomerization may have a role in controlling substrate selectivity of the GLP subfamily [294], which consists of AQPs 3, 7, 9 and 10 in

humans. However we find that, unlike AQP3, both AQPs 9 and 10 both exist exclusively as tetramers when extracted from HEK293 membranes using Triton X-100. This suggests that solute permeability of AQPs is not correlated with oligomeric state.

Previous mutational analysis of AQP1 found an extracellular motif consisting of an aspartate residue (D185) at the top of TM5 that can interact with a lysine residue (K51) at the top of TM2 to increase tetramer stability in detergent [295]. Whether this had an effect on native protein in live cells was not clear. The S205D mutant of the insect aquaporin AQP_{cic} was shown to exist in a primarily monomeric state when extracted from yeast and *Xenopus* oocyte membranes, whereas the wild type was tetrameric [296, 297]. This mutant had a complete loss of water channel function, and it not clear whether this was due to subtle changes in structure leading to a gating effect, gross misfolding, loss of surface expression or a direct result of the loss of oligomerization through loss of monomer-monomer interactions that stabilize the open state of the pore. This makes interpretation of this result very difficult.

In summary, we show that loop D of AQP4 forms a hub for a dynamic network of interactions that stabilize the AQP4 tetramer, both when solubilized using nonionic detergent and in living mammalian cells. Tetrameric assembly was not required for either ER-to-Golgi-to-plasma membrane trafficking or water channel activity. Non-tetrameric mutants were unable to relocate in response to tonicity changes, which may reflect a requirement for tetramerization in the regulation of AQP relocation or key protein-protein interactions mediated by

loop D of AQP4. We conclude that loop D interactions may represent a conserved mechanism for controlling oligomerization across the AQP family.

6 Conclusions

6.1 General discussion and future directions

6.1.1 Hypotonicity-induced translocation of AQP4

The data reported in chapter 3 identify and partially elucidate the molecular mechanism of the subcellular relocalization of AQP4 in response to changes in local tonicity. A change in local tonicity is the key driver of glial cell swelling in stroke and contributes to the effects of cytotoxic oedema following traumatic brain injury. Modulating the surface expression of AQP4 rather than trying to directly block its pore is a novel platform for developing therapies for these devastating conditions. One of the compounds that we identified as an inhibitor of the AQP4 translocation response, trifluoperazine, is already licensed for use in humans as an anti-psychotic medication, primarily used as a treatment for schizophrenia. Our data raises the possibility of repurposing this drug for use in slowing or limiting the development of cytotoxic edema.

Intervention using trifluoperazine (and the other compounds identified) in a rodent model of stroke (such as middle cerebral artery occlusion) or head trauma could be used to investigate this possibility.

CaM appeared to be responsible for the activation of PKA via AC1 to facilitate AQP4 translocation. However, a CaM binding site prediction algorithm suggested that there could be a site for direct binding of CaM to AQP4 directly adjacent to the phosphorylation site (S276) controlling the translocation response. This raises the possibility of a dual role for CaM. Co-

immunoprecipitation (CoIP) could be used to investigate this, and the S276A/D mutants could be used to investigate whether S276 phosphorylation has any effect on a putative CaM interaction.

6.1.2 Regulation of AQP5 localization

Due to its importance for fluid secretion in airway submucosal glands, AQP5 has been suggested to be a pharmacological target to treat the hyper-viscous and excessive gland secretions in cystic fibrosis and bronchitis/rhinitis respectively. Our data provide the first link between a specific AQP5 phosphorylation site (S156) and changes in its subcellular localization. We further show that the S156-mediated change in localization does not require a substantial protein conformational change. We show that, independently of S156, PKA is further involved in basal recycling of AQP5 between the plasma membrane and intracellular compartments. Finally, we provide evidence for tonicity-induced changes in AQP5 localization that are not mediated by phosphorylation of S156 or PKA. The protein kinase responsible for the tonicity-dependent translocation of AQP5 was not identified in this work, although PKA was ruled out. PKC phosphorylation of AQP1 led to tonicity-induced relocalization so this would be the obvious next kinase to test. There is also a PKG phosphorylation site in the C-terminal tail of AQP5, corresponding to S276 of AQP4 and S256 of AQP2. Given the roles of these two sites in AQP4 and AQP2 translocation respectively, this would be another obvious target.

Furthermore, the physiological relevance of the AQP5 localization mechanisms need to be validated in more physiologically relevant cells, e.g. acinar cells or airway epithelial cells. This could be done using a similar methodology to that

used in chapter 3 to investigate endogenous AQP4 relocalization in primary astrocytes.

6.1.3 AQP solute permeability

The data presented in chapter 4 suggest that the details of solute permeability of mammalian GLPs and solute exclusion by water selective AQPs depend on a complex interplay between the exact residues that form the ar/R region and the structural context in which they are situated. The data imply that care must be taken when attempting to generalize results of mutagenic experiments on just one or two representative members of the AQP family; in order to develop a detailed understanding of AQP solute and water permeation, data on as many members of the family as possible should be compared and contrasted. An obvious extension of this work would be to make alanine substitution mutants to all of the water-selective AQPs and to make protein hybrids (e.g. swapping TM segments) to try to account for differences that are not explained by residues at the selectivity filter e.g. the fact that the AQP1 H180A substitution mutant is not glycerol permeable, but the analogous AQP4 H201A substitution mutant is.

Furthermore, we presented the first *in vitro* evidence that fluctuations of the selectivity filter arginine residue are important for the rate of water permeation through AQP4. It would be interesting to investigate whether or not this holds true for all members of the family and whether the size of the effect is conserved between different AQPs.

6.1.4 AQP4 tetramerization

The data reported in chapter 5 showed that loop D of AQP4 forms a hub for a dynamic network of interactions that stabilize the AQP4 tetramer, both when

solubilized using non-ionic detergent and in living HEK293 cells. Tetrameric assembly was not required for either ER-to-Golgi-to-plasma membrane trafficking or water channel activity. Non-tetrameric mutants were unable to relocate in response to tonicity changes, which may reflect a requirement for tetramerization in the regulation of AQP relocation or key protein-protein interactions mediated by loop D of AQP4. CoIP of wild-type, loop D1 and D2 mutants, followed by identification of binding partners by mass spectrometry could be used to investigate this. The lack of relocation of non-tetrameric mutants could also be used as the basis for a novel treatment approach similar to that described in chapter 3. For example, a cell-permeant AQP4 loop D peptide could be investigated as a potential competitive inhibitor of AQP4 oligomerization, and therefore as an inhibitor of tonicity-induced AQP4 relocation. Finally, we concluded that loop D interactions may represent a conserved mechanism for controlling oligomerization across the AQP family, but we only obtained data confirming this for AQP1, AQP3 and AQP4. The loop D alanine substitution mutagenic approach should therefore be extended to other members of the AQP family to assess the hypothesis that loop D is important for oligomerization of all members of the family.

References

1. M. L. Kortenoeven and R. A. Fenton, **Renal aquaporins and water balance disorders**, *Biochimica et biophysica acta*, 2014, **1840**, 1533-1549.
2. E. A. Nagelhus and O. P. Ottersen, **Physiological roles of aquaporin-4 in brain**, *Physiological reviews*, 2013, **93**, 1543-1562.
3. J. Lebeck, **Metabolic impact of the glycerol channels AQP7 and AQP9 in adipose tissue and liver**, *Journal of molecular endocrinology*, 2014, **52**, R165-178.
4. S. S. Kumari, S. Eswaramoorthy, R. T. Mathias and K. Varadaraj, **Unique and analogous functions of aquaporin 0 for fiber cell architecture and ocular lens transparency**, *Biochimica et biophysica acta*, 2011, **1812**, 1089-1097.
5. J. Badaut, A. M. Fukuda, A. Jullienne and K. G. Petry, **Aquaporin and brain diseases**, *Biochimica et biophysica acta*, 2014, **1840**, 1554-1565.
6. L. S. King, M. Yasui and P. Agre, **Aquaporins in health and disease**, *Molecular medicine today*, 2000, **6**, 60-65.
7. D. Bockenhauer and D. G. Bichet, **Pathophysiology, diagnosis and management of nephrogenic diabetes insipidus**, *Nature reviews. Nephrology*, 2015.
8. A. B. Chepelinsky, **Structural function of MIP/aquaporin 0 in the eye lens; genetic defects lead to congenital inherited cataracts**, *Handbook of experimental pharmacology*, 2009, 265-297.
9. A. Madeira, T. F. Moura and G. Soveral, **Aquaglyceroporins: implications in adipose biology and obesity**, *Cellular and molecular life sciences : CMLS*, 2015, **72**, 759-771.
10. J. Wang, L. Feng, Z. Zhu, M. Zheng, D. Wang, Z. Chen and H. Sun, **Aquaporins as diagnostic and therapeutic targets in cancer: how far we are?**, *Journal of translational medicine*, 2015, **13**, 96.
11. D. Ribatti, G. Ranieri, T. Annese and B. Nico, **Aquaporins in cancer**, *Biochimica et biophysica acta*, 2014, **1840**, 1550-1553.
12. A. S. Verkman, **Aquaporins at a glance**, *Journal of cell science*, 2011, **124**, 2107-2112.
13. D. M. Engelman, **Lipid bilayer structure in the membrane of Mycoplasma laidlawii**, *Journal of molecular biology*, 1971, **58**, 153-165.
14. S. J. Singer and G. L. Nicolson, **The fluid mosaic model of the structure of cell membranes**, *Science*, 1972, **175**, 720-731.
15. R. E. Day, P. Kitchen, D. S. Owen, C. Bland, L. Marshall, A. C. Conner, R. M. Bill and M. T. Conner, **Human aquaporins: regulators of transcellular water flow**, *Biochimica et biophysica acta*, 2014, **1840**, 1492-1506.
16. W. D. Stein and J. F. Danielli, **Structure and Function in Red Cell Permeability**, *Discuss Faraday Soc*, 1956, 238-251.
17. G. Benga, O. Popescu, V. Borza, V. I. Pop, A. Muresan, I. Mocsy, A. Brain and J. M. Wrigglesworth, **Water permeability in human erythrocytes: identification of membrane proteins involved in water transport**, *European journal of cell biology*, 1986, **41**, 252-262.

18. G. M. Preston, T. P. Carroll, W. B. Guggino and P. Agre, **Appearance of water channels in *Xenopus* oocytes expressing red cell CHIP28 protein**, *Science*, 1992, **256**, 385-387.
19. B. Yang and A. S. Verkman, **Water and glycerol permeabilities of aquaporins 1-5 and MIP determined quantitatively by expression of epitope-tagged constructs in *Xenopus* oocytes**, *The Journal of biological chemistry*, 1997, **272**, 16140-16146.
20. K. L. Nemeth-Cahalan, K. Kalman and J. E. Hall, **Molecular basis of pH and Ca²⁺ regulation of aquaporin water permeability**, *J Gen Physiol*, 2004, **123**, 573-580.
21. A. K. Meinild, D. A. Klaerke and T. Zeuthen, **Bidirectional water fluxes and specificity for small hydrophilic molecules in aquaporins 0-5**, *The Journal of biological chemistry*, 1998, **273**, 32446-32451.
22. R. R. Geyer, R. Musa-Aziz, X. Qin and W. F. Boron, **Relative CO₂/NH₃ selectivities of mammalian aquaporins 0-9**, *Am J Physiol-Cell Ph*, 2013, **304**, C985-C994.
23. L. M. Holm, T. P. Jahn, A. L. Moller, J. K. Schjoerring, D. Ferri, D. A. Klaerke and T. Zeuthen, **NH₃ and NH₄⁺ permeability in aquaporin-expressing *Xenopus* oocytes**, *Pflugers Archiv : European journal of physiology*, 2005, **450**, 415-428.
24. M. Echevarria, E. E. Windhager, S. S. Tate and G. Frindt, **Cloning and expression of AQP3, a water channel from the medullary collecting duct of rat kidney**, *Proceedings of the National Academy of Sciences of the United States of America*, 1994, **91**, 10997-11001.
25. A. Herraiz, F. Chauvigne, J. Cerda, X. Belles and M. D. Piulachs, **Identification and functional characterization of an ovarian aquaporin from the cockroach *Blattella germanica* L. (Dictyoptera, Blattellidae)**, *The Journal of experimental biology*, 2011, **214**, 3630-3638.
26. J. S. Jung, R. V. Bhat, G. M. Preston, W. B. Guggino, J. M. Baraban and P. Agre, **Molecular characterization of an aquaporin cDNA from brain: candidate osmoreceptor and regulator of water balance**, *Proceedings of the National Academy of Sciences of the United States of America*, 1994, **91**, 13052-13056.
27. S. Raina, G. M. Preston, W. B. Guggino and P. Agre, **Molecular cloning and characterization of an aquaporin cDNA from salivary, lacrimal, and respiratory tissues**, *The Journal of biological chemistry*, 1995, **270**, 1908-1912.
28. M. Yasui, A. Hazama, T. H. Kwon, S. Nielsen, W. B. Guggino and P. Agre, **Rapid gating and anion permeability of an intracellular aquaporin**, *Nature*, 1999, **402**, 184-187.
29. H. Nagase, J. Agren, A. Saito, K. Liu, P. Agre, A. Hazama and M. Yasui, **Molecular cloning and characterization of mouse aquaporin 6**, *Biochemical and biophysical research communications*, 2007, **352**, 12-16.
30. A. Hazama, D. Kozono, W. B. Guggino, P. Agre and M. Yasui, **Ion permeation of AQP6 water channel protein. Single channel recordings after Hg²⁺ activation**, *The Journal of biological chemistry*, 2002, **277**, 29224-29230.

31. K. Liu, D. Kozono, Y. Kato, P. Agre, A. Hazama and M. Yasui, **Conversion of aquaporin 6 from an anion channel to a water-selective channel by a single amino acid substitution**, *Proceedings of the National Academy of Sciences of the United States of America*, 2005, **102**, 2192-2197.
32. L. M. Holm, D. A. Klaerke and T. Zeuthen, **Aquaporin 6 is permeable to glycerol and urea**, *Pflugers Archiv : European journal of physiology*, 2004, **448**, 181-186.
33. K. Ishibashi, M. Kuwahara, Y. Gu, Y. Kageyama, A. Tohsaka, F. Suzuki, F. Marumo and S. Sasaki, **Cloning and functional expression of a new water channel abundantly expressed in the testis permeable to water, glycerol, and urea**, *The Journal of biological chemistry*, 1997, **272**, 20782-20786.
34. K. Liu, H. Nagase, C. G. Huang, G. Calamita and P. Agre, **Purification and functional characterization of aquaporin-8**, *Biology of the cell / under the auspices of the European Cell Biology Organization*, 2006, **98**, 153-161.
35. Y. Koyama, T. Yamamoto, D. Kondo, H. Funaki, E. Yaoita, K. Kawasaki, N. Sato, K. Hatakeyama and I. Kihara, **Molecular cloning of a new aquaporin from rat pancreas and liver**, *The Journal of biological chemistry*, 1997, **272**, 30329-30333.
36. T. Ma, B. Yang and A. S. Verkman, **Cloning of a novel water and urea-permeable aquaporin from mouse expressed strongly in colon, placenta, liver, and heart**, *Biochemical and biophysical research communications*, 1997, **240**, 324-328.
37. T. P. Jahn, A. L. B. Moller, T. Zeuthen, L. M. Holm, D. A. Klaerke, B. Mohsin, W. Kuhlbrandt and J. K. Schjoerring, **Aquaporin homologues in plants and mammals transport ammonia**, *FEBS letters*, 2004, **574**, 31-36.
38. J. M. Carbrey, D. A. Gorelick-Feldman, D. Kozono, J. Praetorius, S. Nielsen and P. Agre, **Aquaglyceroporin AQP9: solute permeation and metabolic control of expression in liver**, *Proceedings of the National Academy of Sciences of the United States of America*, 2003, **100**, 2945-2950.
39. K. Ishibashi, T. Morinaga, M. Kuwahara, S. Sasaki and M. Imai, **Cloning and identification of a new member of water channel (AQP10) as an aquaglyceroporin**, *Biochimica et biophysica acta*, 2002, **1576**, 335-340.
40. M. Ikeda, A. Andoo, M. Shimono, N. Takamatsu, A. Taki, K. Muta, W. Matsushita, T. Uechi, T. Matsuzaki, N. Kenmochi, K. Takata, S. Sasaki, K. Ito and K. Ishibashi, **The NPC Motif of Aquaporin-11, Unlike the NPA Motif of Known Aquaporins, Is Essential for Full Expression of Molecular Function**, *Journal of Biological Chemistry*, 2011, **286**, 3342-3350.
41. K. Yakata, K. Tani and Y. Fujiyoshi, **Water permeability and characterization of aquaporin-11**, *Journal of Structural Biology*, 2011, **174**, 315-320.
42. A. Madeira, S. Fernandez-Veledo, M. Camps, A. Zorzano, T. F. Moura, V. Ceperuelo-Mallafre, J. Vendrell and G. Soveral, **Human aquaporin-11 is a water and glycerol channel and localizes in the vicinity of lipid droplets in human adipocytes**, *Obesity*, 2014, **22**, 2010-2017.

43. U. Kosinska Eriksson, G. Fischer, R. Friemann, G. Enkavi, E. Tajkhorshid and R. Neutze, **Subangstrom resolution X-ray structure details aquaporin-water interactions**, *Science*, 2013, **340**, 1346-1349.
44. A. Horner, F. Zocher, J. Preiner, N. Ollinger, C. Siligan, S. A. Akimov and P. Pohl, **The mobility of single-file water molecules is governed by the number of H-bonds they may form with channel-lining residues**, *Science advances*, 2015, **1**, e1400083.
45. E. Tajkhorshid, P. Nollert, M. O. Jensen, L. J. Miercke, J. O'Connell, R. M. Stroud and K. Schulten, **Control of the selectivity of the aquaporin water channel family by global orientational tuning**, *Science*, 2002, **296**, 525-530.
46. D. Fu, A. Libson, L. J. Miercke, C. Weitzman, P. Nollert, J. Krucinski and R. M. Stroud, **Structure of a glycerol-conducting channel and the basis for its selectivity**, *Science*, 2000, **290**, 481-486.
47. J. Sjöhamn and K. Hedfalk, **Unraveling aquaporin interaction partners**, *Biochimica et biophysica acta*, 2014, **1840**, 1614-1623.
48. A. Frick, U. K. Eriksson, F. de Mattia, F. Oberg, K. Hedfalk, R. Neutze, W. J. de Grip, P. M. Deen and S. Tornroth-Horsefield, **X-ray structure of human aquaporin 2 and its implications for nephrogenic diabetes insipidus and trafficking**, *Proceedings of the National Academy of Sciences of the United States of America*, 2014, **111**, 6305-6310.
49. J. S. Jung, G. M. Preston, B. L. Smith, W. B. Guggino and P. Agre, **Molecular structure of the water channel through aquaporin CHIP. The hourglass model**, *The Journal of biological chemistry*, 1994, **269**, 14648-14654.
50. J. S. Hub, H. Grubmüller and B. L. de Groot, **Dynamics and energetics of permeation through aquaporins. What do we learn from molecular dynamics simulations?**, *Handbook of experimental pharmacology*, 2009, 57-76.
51. A. S. Chevalier and F. Chaumont, **Trafficking of plant plasma membrane aquaporins: multiple regulation levels and complex sorting signals**, *Plant & cell physiology*, 2015, **56**, 819-829.
52. R. Kaldenhoff, L. Kai and N. Uehlein, **Aquaporins and membrane diffusion of CO₂ in living organisms**, *Biochimica et biophysica acta*, 2014, **1840**, 1592-1595.
53. J. Yu, A. J. Yool, K. Schulten and E. Tajkhorshid, **Mechanism of gating and ion conductivity of a possible tetrameric pore in aquaporin-1**, *Structure*, 2006, **14**, 1411-1423.
54. M. J. Borgnia and P. Agre, **Reconstitution and functional comparison of purified GlpF and AqpZ, the glycerol and water channels from Escherichia coli**, *Proceedings of the National Academy of Sciences of the United States of America*, 2001, **98**, 2888-2893.
55. N. Roudier, P. Bailly, P. Gane, N. Lucien, R. Gobin, J. P. Cartron and P. Ripoche, **Erythroid expression and oligomeric state of the AQP3 protein**, *The Journal of biological chemistry*, 2002, **277**, 7664-7669.
56. T. Itoh, T. Rai, M. Kuwahara, S. B. Ko, S. Uchida, S. Sasaki and K. Ishibashi, **Identification of a novel aquaporin, AQP12, expressed in pancreatic acinar cells**, *Biochemical and biophysical research communications*, 2005, **330**, 832-838.

57. D. A. Gorelick, J. Praetorius, T. Tsunenari, S. Nielsen and P. Agre, **Aquaporin-11: a channel protein lacking apparent transport function expressed in brain**, *BMC biochemistry*, 2006, **7**, 14.
58. E. Beitz, B. Wu, L. M. Holm, J. E. Schultz and T. Zeuthen, **Point mutations in the aromatic/arginine region in aquaporin 1 allow passage of urea, glycerol, ammonia, and protons**, *Proceedings of the National Academy of Sciences of the United States of America*, 2006, **103**, 269-274.
59. E. Yamamoto, T. Akimoto, Y. Hirano, M. Yasui and K. Yasuoka, **1/ f Fluctuations of amino acids regulate water transportation in aquaporin 1**, *Physical review. E, Statistical, nonlinear, and soft matter physics*, 2014, **89**, 022718.
60. J. S. Hub, C. Aponte-Santamaria, H. Grubmuller and B. L. de Groot, **Voltage-regulated water flux through aquaporin channels in silico**, *Biophys J*, 2010, **99**, L97-99.
61. L. Xin, H. Su, C. H. Nielsen, C. Tang, J. Torres and Y. Mu, **Water permeation dynamics of AqpZ: a tale of two states**, *Biochimica et biophysica acta*, 2011, **1808**, 1581-1586.
62. Y. Wang, K. Schulten and E. Tajkhorshid, **What makes an aquaporin a glycerol channel? A comparative study of AqpZ and GlpF**, *Structure*, 2005, **13**, 1107-1118.
63. D. F. Savage, J. D. O'Connell, 3rd, L. J. Miercke, J. Finer-Moore and R. M. Stroud, **Structural context shapes the aquaporin selectivity filter**, *Proceedings of the National Academy of Sciences of the United States of America*, 2010, **107**, 17164-17169.
64. S. Nielsen, E. A. Nagelhus, M. Amiry-Moghaddam, C. Bourque, P. Agre and O. P. Ottersen, **Specialized membrane domains for water transport in glial cells: high-resolution immunogold cytochemistry of aquaporin-4 in rat brain**, *The Journal of neuroscience : the official journal of the Society for Neuroscience*, 1997, **17**, 171-180.
65. K. Oshio, H. Watanabe, Y. Song, A. S. Verkman and G. T. Manley, **Reduced cerebrospinal fluid production and intracranial pressure in mice lacking choroid plexus water channel Aquaporin-1**, *Faseb J*, 2005, **19**, 76-78.
66. J. Badaut, J. M. Petit, J. F. Brunet, P. J. Magistretti, C. Charriaud-Marlangue and L. Regli, **Distribution of Aquaporin 9 in the adult rat brain: preferential expression in catecholaminergic neurons and in glial cells**, *Neuroscience*, 2004, **128**, 27-38.
67. J. D. Neely, M. Amiry-Moghaddam, O. P. Ottersen, S. C. Froehner, P. Agre and M. E. Adams, **Syntrophin-dependent expression and localization of Aquaporin-4 water channel protein**, *Proceedings of the National Academy of Sciences of the United States of America*, 2001, **98**, 14108-14113.
68. X. Yao, S. Hrabetova, C. Nicholson and G. T. Manley, **Aquaporin-4-deficient mice have increased extracellular space without tortuosity change**, *The Journal of neuroscience : the official journal of the Society for Neuroscience*, 2008, **28**, 5460-5464.
69. O. Bloch, K. I. Auguste, G. T. Manley and A. S. Verkman, **Accelerated progression of kaolin-induced hydrocephalus in aquaporin-4-deficient mice**, *Journal of cerebral blood flow and metabolism : official*

- journal of the International Society of Cerebral Blood Flow and Metabolism*, 2006, **26**, 1527-1537.
70. N. N. Haj-Yasein, G. F. Vindedal, M. Eilert-Olsen, G. A. Gundersen, O. Skare, P. Laake, A. Klungland, A. E. Thoren, J. M. Burkhardt, O. P. Ottersen and E. A. Nagelhus, **Glial-conditional deletion of aquaporin-4 (Aqp4) reduces blood-brain water uptake and confers barrier function on perivascular astrocyte endfeet**, *Proceedings of the National Academy of Sciences of the United States of America*, 2011, **108**, 17815-17820.
 71. R. J. Fairclough, M. J. Wood and K. E. Davies, **Therapy for Duchenne muscular dystrophy: renewed optimism from genetic approaches**, *Nature reviews. Genetics*, 2013, **14**, 373-378.
 72. J. J. Iliff, M. Wang, Y. Liao, B. A. Plogg, W. Peng, G. A. Gundersen, H. Benveniste, G. E. Vates, R. Deane, S. A. Goldman, E. A. Nagelhus and M. Nedergaard, **A paravascular pathway facilitates CSF flow through the brain parenchyma and the clearance of interstitial solutes, including amyloid beta**, *Science translational medicine*, 2012, **4**, 147ra111.
 73. W. Walz, **Role of astrocytes in the clearance of excess extracellular potassium**, *Neurochemistry international*, 2000, **36**, 291-300.
 74. H. Kitaura, M. Tsujita, V. J. Huber, A. Kakita, K. Shibuki, K. Sakimura, I. L. Kwee and T. Nakada, **Activity-dependent glial swelling is impaired in aquaporin-4 knockout mice**, *Neuroscience research*, 2009, **64**, 208-212.
 75. S. Strohschein, K. Huttmann, S. Gabriel, D. K. Binder, U. Heinemann and C. Steinhäuser, **Impact of aquaporin-4 channels on K⁺ buffering and gap junction coupling in the hippocampus**, *Glia*, 2011, **59**, 973-980.
 76. B. J. Jin, H. Zhang, D. K. Binder and A. S. Verkman, **Aquaporin-4-dependent K⁽⁺⁾ and water transport modeled in brain extracellular space following neuroexcitation**, *J Gen Physiol*, 2013, **141**, 119-132.
 77. Y. Song and E. Gunnarson, **Potassium dependent regulation of astrocyte water permeability is mediated by cAMP signaling**, *PLoS one*, 2012, **7**, e34936.
 78. N. C. Connors and P. Kofuji, **Potassium channel Kir4.1 macromolecular complex in retinal glial cells**, *Glia*, 2006, **53**, 124-131.
 79. V. Crunelli, G. Carmignoto and C. Steinhäuser, **Novel astrocyte targets: new avenues for the therapeutic treatment of epilepsy**, *The Neuroscientist : a review journal bringing neurobiology, neurology and psychiatry*, 2015, **21**, 62-83.
 80. T. S. Lee, T. Eid, S. Mane, J. H. Kim, D. D. Spencer, O. P. Ottersen and N. C. de Lanerolle, **Aquaporin-4 is increased in the sclerotic hippocampus in human temporal lobe epilepsy**, *Acta neuropathologica*, 2004, **108**, 493-502.
 81. S. Alvestad, J. Hammer, E. H. Hoddevik, O. Skare, U. Sonnewald, M. Amiry-Moghaddam and O. P. Ottersen, **Mislocalization of AQP4 precedes chronic seizures in the kainate model of temporal lobe epilepsy**, *Epilepsy research*, 2013, **105**, 30-41.
 82. K. Heuser, E. A. Nagelhus, E. Tauboll, U. Indahl, P. R. Berg, S. Lien, S. Nakken, L. Gjerstad and O. P. Ottersen, **Variants of the genes encoding**

- AQP4 and Kir4.1 are associated with subgroups of patients with temporal lobe epilepsy**, *Epilepsy research*, 2010, **88**, 55-64.
83. G. T. Manley, M. Fujimura, T. Ma, N. Noshita, F. Filiz, A. W. Bollen, P. Chan and A. S. Verkman, **Aquaporin-4 deletion in mice reduces brain edema after acute water intoxication and ischemic stroke**, *Nature medicine*, 2000, **6**, 159-163.
84. C. Yang, Z. Liu, H. Li, F. Zhai, J. Liu and J. Bian, **Aquaporin-4 knockdown ameliorates hypoxic-ischemic cerebral edema in newborn piglets**, *IUBMB life*, 2015, **67**, 182-190.
85. T. Da and A. S. Verkman, **Aquaporin-4 gene disruption in mice protects against impaired retinal function and cell death after ischemia**, *Investigative ophthalmology & visual science*, 2004, **45**, 4477-4483.
86. M. Shenaq, H. Kassem, C. Peng, S. Schafer, J. Y. Ding, V. Fredrickson, M. Guthikonda, C. W. Kreipke, J. A. Rafols and Y. Ding, **Neuronal damage and functional deficits are ameliorated by inhibition of aquaporin and HIF1alpha after traumatic brain injury (TBI)**, *Journal of the neurological sciences*, 2012, **323**, 134-140.
87. T. Higashida, C. W. Kreipke, J. A. Rafols, C. Peng, S. Schafer, P. Schafer, J. Y. Ding, D. Dornbos, 3rd, X. Li, M. Guthikonda, N. F. Rossi and Y. Ding, **The role of hypoxia-inducible factor-1alpha, aquaporin-4, and matrix metalloproteinase-9 in blood-brain barrier disruption and brain edema after traumatic brain injury**, *Journal of neurosurgery*, 2011, **114**, 92-101.
88. B. Yang, Z. Zador and A. S. Verkman, **Glial cell aquaporin-4 overexpression in transgenic mice accelerates cytotoxic brain swelling**, *The Journal of biological chemistry*, 2008, **283**, 15280-15286.
89. Z. Vajda, M. Pedersen, E. M. Fuchtbauer, K. Wertz, H. Stodkilde-Jorgensen, E. Sulyok, T. Doczi, J. D. Neely, P. Agre, J. Frokiaer and S. Nielsen, **Delayed onset of brain edema and mislocalization of aquaporin-4 in dystrophin-null transgenic mice**, *Proceedings of the National Academy of Sciences of the United States of America*, 2002, **99**, 13131-13136.
90. M. Amiry-Moghaddam, R. Xue, F. M. Haug, J. D. Neely, A. Bhardwaj, P. Agre, M. E. Adams, S. C. Froehner, S. Mori and O. P. Ottersen, **Alpha-syntrophin deletion removes the perivascular but not endothelial pool of aquaporin-4 at the blood-brain barrier and delays the development of brain edema in an experimental model of acute hyponatremia**, *Faseb J*, 2004, **18**, 542-544.
91. L. Dmytrenko, M. Cicanic, M. Anderova, I. Vorisek, O. P. Ottersen, E. Sykova and L. Vargova, **The impact of alpha-syntrophin deletion on the changes in tissue structure and extracellular diffusion associated with cell swelling under physiological and pathological conditions**, *PloS one*, 2013, **8**, e68044.
92. J. A. Stokum, D. B. Kurland, V. Gerzanich and J. M. Simard, **Mechanisms of astrocyte-mediated cerebral edema**, *Neurochemical research*, 2015, **40**, 317-328.
93. C. E. Johanson, J. A. Duncan, 3rd, P. M. Klinge, T. Brinker, E. G. Stopa and G. D. Silverberg, **Multiplicity of cerebrospinal fluid functions:**

- New challenges in health and disease**, *Cerebrospinal fluid research*, 2008, **5**, 10.
94. H. Igarashi, M. Tsujita, I. L. Kwee and T. Nakada, **Water influx into cerebrospinal fluid is primarily controlled by aquaporin-4, not by aquaporin-1: 17O JVCPE MRI study in knockout mice**, *Neuroreport*, 2014, **25**, 39-43.
 95. S. K. Agarwal and A. Gupta, **Aquaporins: The renal water channels**, *Indian journal of nephrology*, 2008, **18**, 95-100.
 96. P. I. Nedvetsky, G. Tamma, S. Beulshausen, G. Valenti, W. Rosenthal and E. Klusmann, **Regulation of aquaporin-2 trafficking**, *Handbook of experimental pharmacology*, 2009, 133-157.
 97. K. Kishida, H. Kuriyama, T. Funahashi, I. Shimomura, S. Kihara, N. Ouchi, M. Nishida, H. Nishizawa, M. Matsuda, M. Takahashi, K. Hotta, T. Nakamura, S. Yamashita, Y. Tochino and Y. Matsuzawa, **Aquaporin adipose, a putative glycerol channel in adipocytes**, *The Journal of biological chemistry*, 2000, **275**, 20896-20902.
 98. M. T. Skowronski, J. Lebeck, A. Rojek, J. Praetorius, E. M. Fuchtbauer, J. Frokiaer and S. Nielsen, **AQP7 is localized in capillaries of adipose tissue, cardiac and striated muscle: implications in glycerol metabolism**, *American journal of physiology. Renal physiology*, 2007, **292**, F956-965.
 99. R. E. Duncan, M. Ahmadian, K. Jaworski, E. Sarkadi-Nagy and H. S. Sul, **Regulation of lipolysis in adipocytes**, *Annual review of nutrition*, 2007, **27**, 79-101.
 100. T. Miyauchi, H. Yamamoto, Y. Abe, G. J. Yoshida, A. Rojek, E. Sohara, S. Uchida, S. Nielsen and M. Yasui, **Dynamic subcellular localization of aquaporin-7 in white adipocytes**, *FEBS letters*, 2015, **589**, 608-614.
 101. M. Vaughan, **The production and release of glycerol by adipose tissue incubated in vitro**, *The Journal of biological chemistry*, 1962, **237**, 3354-3358.
 102. M. Hara-Chikuma, E. Sohara, T. Rai, M. Ikawa, M. Okabe, S. Sasaki, S. Uchida and A. S. Verkman, **Progressive adipocyte hypertrophy in aquaporin-7-deficient mice: adipocyte glycerol permeability as a novel regulator of fat accumulation**, *The Journal of biological chemistry*, 2005, **280**, 15493-15496.
 103. N. Maeda, T. Funahashi, T. Hibuse, A. Nagasawa, K. Kishida, H. Kuriyama, T. Nakamura, S. Kihara, I. Shimomura and Y. Matsuzawa, **Adaptation to fasting by glycerol transport through aquaporin 7 in adipose tissue**, *Proceedings of the National Academy of Sciences of the United States of America*, 2004, **101**, 17801-17806.
 104. H. Kondo, I. Shimomura, K. Kishida, H. Kuriyama, Y. Makino, H. Nishizawa, M. Matsuda, N. Maeda, H. Nagaretani, S. Kihara, Y. Kurachi, T. Nakamura, T. Funahashi and Y. Matsuzawa, **Human aquaporin adipose (AQPap) gene. Genomic structure, promoter analysis and functional mutation**, *European journal of biochemistry / FEBS*, 2002, **269**, 1814-1826.
 105. U. Laforenza, M. F. Scaffino and G. Gastaldi, **Aquaporin-10 represents an alternative pathway for glycerol efflux from human adipocytes**, *PloS one*, 2013, **8**, e54474.

106. T. Morinaga, M. Nakakoshi, A. Hirao, M. Imai and K. Ishibashi, **Mouse aquaporin 10 gene (AQP10) is a pseudogene**, *Biochemical and biophysical research communications*, 2002, **294**, 630-634.
107. C. F. Borchgrevink and R. J. Havel, **Transport of Glycerol in Human Blood**, *Proceedings of the Society for Experimental Biology and Medicine. Society for Experimental Biology and Medicine*, 1963, **113**, 946-949.
108. J. L. Nelson, M. E. Harmon and R. A. Robergs, **Identifying plasma glycerol concentration associated with urinary glycerol excretion in trained humans**, *Journal of analytical toxicology*, 2011, **35**, 617-623.
109. E. Sohara, T. Rai, J. Miyazaki, A. S. Verkman, S. Sasaki and S. Uchida, **Defective water and glycerol transport in the proximal tubules of AQP7 knockout mice**, *American journal of physiology. Renal physiology*, 2005, **289**, F1195-1200.
110. C. Goubau, J. Jaeken, E. N. Levchenko, C. Thys, M. Di Michele, G. A. Martens, E. Gerlo, R. De Vos, G. M. Buyse, N. Goemans, C. Van Geet and K. Freson, **Homozygosity for aquaporin 7 G264V in three unrelated children with hyperglyceroluria and a mild platelet secretion defect**, *Genet Med*, 2013, **15**, 55-63.
111. W. P. Russ and D. M. Engelman, **The GxxxG motif: a framework for transmembrane helix-helix association**, *Journal of molecular biology*, 2000, **296**, 911-919.
112. H. Tsukaguchi, C. Shayakul, U. V. Berger, B. Mackenzie, S. Devidas, W. B. Guggino, A. N. van Hoek and M. A. Hediger, **Molecular characterization of a broad selectivity neutral solute channel**, *The Journal of biological chemistry*, 1998, **273**, 24737-24743.
113. M. Elkjaer, Z. Vajda, L. N. Nejsum, T. Kwon, U. B. Jensen, M. Amiry-Moghaddam, J. Frokiaer and S. Nielsen, **Immunolocalization of AQP9 in liver, epididymis, testis, spleen, and brain**, *Biochemical and biophysical research communications*, 2000, **276**, 1118-1128.
114. S. J. Pilkis and D. K. Granner, **Molecular physiology of the regulation of hepatic gluconeogenesis and glycolysis**, *Annual review of physiology*, 1992, **54**, 885-909.
115. G. Calamita, P. Gena, D. Ferri, A. Rosito, A. Rojek, S. Nielsen, R. A. Marinelli, G. Fruhbeck and M. Svelto, **Biophysical assessment of aquaporin-9 as principal facilitative pathway in mouse liver import of glucogenetic glycerol**, *Biology of the cell / under the auspices of the European Cell Biology Organization*, 2012, **104**, 342-351.
116. A. M. Rojek, M. T. Skowronski, E. M. Fuchtbauer, A. C. Fuchtbauer, R. A. Fenton, P. Agre, J. Frokiaer and S. Nielsen, **Defective glycerol metabolism in aquaporin 9 (AQP9) knockout mice**, *Proceedings of the National Academy of Sciences of the United States of America*, 2007, **104**, 3609-3614.
117. G. Cui, M. M. Staron, S. M. Gray, P. C. Ho, R. A. Amezcua, J. Wu and S. M. Kaech, **IL-7-Induced Glycerol Transport and TAG Synthesis Promotes Memory CD8+ T Cell Longevity**, *Cell*, 2015, **161**, 750-761.
118. R. Sougrat, M. Morand, C. Gondran, P. Barre, R. Gobin, F. Bonte, M. Dumas and J. M. Verbavatz, **Functional expression of AQP3 in human skin epidermis and reconstructed epidermis**, *The Journal of investigative dermatology*, 2002, **118**, 678-685.

119. T. Ma, M. Hara, R. Sougrat, J. M. Verbavatz and A. S. Verkman, **Impaired stratum corneum hydration in mice lacking epidermal water channel aquaporin-3**, *The Journal of biological chemistry*, 2002, **277**, 17147-17153.
120. M. Hara, T. Ma and A. S. Verkman, **Selectively reduced glycerol in skin of aquaporin-3-deficient mice may account for impaired skin hydration, elasticity, and barrier recovery**, *The Journal of biological chemistry*, 2002, **277**, 46616-46621.
121. C. L. Froebe, F. A. Simion, H. Ohlmeyer, L. D. Rhein, J. Mattai, R. H. Cagan and S. E. Friberg, **Prevention of Stratum-Corneum Lipid Phase-Transitions In vitro by Glycerol - an Alternative Mechanism for Skin Moisturization**, *J Soc Cosmet Chem*, 1990, **41**, 51-65.
122. M. Hara and A. S. Verkman, **Glycerol replacement corrects defective skin hydration, elasticity, and barrier function in aquaporin-3-deficient mice**, *Proceedings of the National Academy of Sciences of the United States of America*, 2003, **100**, 7360-7365.
123. M. D. Norenberg, K. V. Rama Rao and A. R. Jayakumar, **Ammonia neurotoxicity and the mitochondrial permeability transition**, *Journal of bioenergetics and biomembranes*, 2004, **36**, 303-307.
124. F. Martini and J. L. Nath, *Anatomy & physiology*, 2nd edn., Benjamin Cummings, San Francisco, 2010.
125. K. Ishibashi, M. Kuwahara, Y. Gu, Y. Tanaka, F. Marumo and S. Sasaki, **Cloning and functional expression of a new aquaporin (AQP9) abundantly expressed in the peripheral leukocytes permeable to water and urea, but not to glycerol**, *Biochemical and biophysical research communications*, 1998, **244**, 268-274.
126. K. Ishibashi, S. Sasaki, K. Fushimi, S. Uchida, M. Kuwahara, H. Saito, T. Furukawa, K. Nakajima, Y. Yamaguchi, T. Gojobori and et al., **Molecular cloning and expression of a member of the aquaporin family with permeability to glycerol and urea in addition to water expressed at the basolateral membrane of kidney collecting duct cells**, *Proceedings of the National Academy of Sciences of the United States of America*, 1994, **91**, 6269-6273.
127. M. Echevarria, E. E. Windhager and G. Frindt, **Selectivity of the renal collecting duct water channel aquaporin-3**, *The Journal of biological chemistry*, 1996, **271**, 25079-25082.
128. S. Jelen, P. Gena, J. Lebeck, A. Rojek, J. Praetorius, J. Frokiaer, R. A. Fenton, S. Nielsen, G. Calamita and M. Rutzler, **Aquaporin-9 and urea transporter-A gene deletions affect urea transmembrane passage in murine hepatocytes**, *American journal of physiology. Gastrointestinal and liver physiology*, 2012, **303**, G1279-1287.
129. I. D. Weiner, W. E. Mitch and J. M. Sands, **Urea and Ammonia Metabolism and the Control of Renal Nitrogen Excretion**, *Clinical journal of the American Society of Nephrology : CJASN*, 2014.
130. S. M. Saparov, K. Liu, P. Agre and P. Pohl, **Fast and selective ammonia transport by aquaporin-8**, *The Journal of biological chemistry*, 2007, **282**, 5296-5301.
131. B. Yang, Y. Song, D. Zhao and A. S. Verkman, **Phenotype analysis of aquaporin-8 null mice**, *American journal of physiology. Cell physiology*, 2005, **288**, C1161-1170.

132. G. Calamita, D. Ferri, P. Gena, G. E. Liquori, A. Cavalier, D. Thomas and M. Svelto, **The inner mitochondrial membrane has aquaporin-8 water channels and is highly permeable to water**, *The Journal of biological chemistry*, 2005, **280**, 17149-17153.
133. B. Yang, D. Zhao, E. Solenov and A. S. Verkman, **Evidence from knockout mice against physiologically significant aquaporin 8-facilitated ammonia transport**, *American journal of physiology. Cell physiology*, 2006, **291**, C417-423.
134. A. M. Marini, G. Matassi, V. Raynal, B. Andre, J. P. Cartron and B. Cherif-Zahar, **The human Rhesus-associated RhAG protein and a kidney homologue promote ammonium transport in yeast**, *Nature genetics*, 2000, **26**, 341-344.
135. I. D. Weiner, R. T. Miller and J. W. Verlander, **Localization of the ammonium transporters, Rh B glycoprotein and Rh C glycoprotein, in the mouse liver**, *Gastroenterology*, 2003, **124**, 1432-1440.
136. I. D. Weiner and J. W. Verlander, **Role of NH₃ and NH₄⁺ transporters in renal acid-base transport**, *American journal of physiology. Renal physiology*, 2011, **300**, F11-23.
137. D. Goossens, M. M. Trinh-Trang-Tan, M. Debbia, P. Ripoché, C. Vilela-Lamego, F. Louache, W. Vainchenker, Y. Colin and J. P. Cartron, **Generation and characterisation of Rhd and Rhag null mice**, *British journal of haematology*, 2010, **148**, 161-172.
138. D. Goossens, V. Bony, P. Gane, Y. Colin and J. P. Cartron, **Generation of mice with inactivated Rh or Rhag genes**, *Transfusion clinique et biologique : journal de la Societe francaise de transfusion sanguine*, 2006, **13**, 164-166.
139. L. R. Soria, J. Marrone, G. Calamita and R. A. Marinelli, **Ammonia detoxification via ureagenesis in rat hepatocytes involves mitochondrial aquaporin-8 channels**, *Hepatology*, 2013, **57**, 2061-2071.
140. S. M. Molinas, L. Trumper and R. A. Marinelli, **Mitochondrial aquaporin-8 in renal proximal tubule cells: evidence for a role in the response to metabolic acidosis**, *American journal of physiology. Renal physiology*, 2012, **303**, F458-466.
141. S. M. Molinas, L. R. Soria, J. Marrone, M. Danielli, L. Trumper and R. A. Marinelli, **Acidosis-induced downregulation of hepatocyte mitochondrial aquaporin-8 and ureagenesis from ammonia**, *Biochemistry and cell biology = Biochimie et biologie cellulaire*, 2015, **93**, 417-420.
142. M. Esbjornsson, J. Bulow, B. Norman, L. Simonsen, J. Nowak, O. Rooyackers, L. Kaijser and E. Jansson, **Adipose tissue extracts plasma ammonia after sprint exercise in women and men**, *Journal of applied physiology*, 2006, **101**, 1576-1580.
143. V. Endeward, J. P. Cartron, P. Ripoché and G. Gros, **RhAG protein of the Rhesus complex is a CO₂ channel in the human red cell membrane**, *Faseb J*, 2008, **22**, 64-73.
144. M. E. Blank and H. Ehmke, **Aquaporin-1 and HCO₃⁻-Cl⁻ transporter-mediated transport of CO₂ across the human erythrocyte membrane**, *The Journal of physiology*, 2003, **550**, 419-429.

145. N. L. Nakhoul, B. A. Davis, M. F. Romero and W. F. Boron, **Effect of expressing the water channel aquaporin-1 on the CO₂ permeability of *Xenopus* oocytes**, *The American journal of physiology*, 1998, **274**, C543-548.
146. G. J. Cooper and W. F. Boron, **Effect of PCMBs on CO₂ permeability of *Xenopus* oocytes expressing aquaporin 1 or its C189S mutant**, *The American journal of physiology*, 1998, **275**, C1481-1486.
147. V. Endeward, R. Musa-Aziz, G. J. Cooper, L. M. Chen, M. F. Pelletier, L. V. Virkki, C. T. Supuran, L. S. King, W. F. Boron and G. Gros, **Evidence that aquaporin 1 is a major pathway for CO₂ transport across the human erythrocyte membrane**, *Faseb J*, 2006, **20**, 1974-1981.
148. B. Yang, N. Fukuda, A. van Hoek, M. A. Matthay, T. Ma and A. S. Verkman, **Carbon dioxide permeability of aquaporin-1 measured in erythrocytes and lung of aquaporin-1 null mice and in reconstituted proteoliposomes**, *The Journal of biological chemistry*, 2000, **275**, 2686-2692.
149. G. V. Prasad, L. A. Coury, F. Finn and M. L. Zeidel, **Reconstituted aquaporin 1 water channels transport CO₂ across membranes**, *The Journal of biological chemistry*, 1998, **273**, 33123-33126.
150. Y. Sheng, I. A. Abreu, D. E. Cabelli, M. J. Maroney, A. F. Miller, M. Teixeira and J. S. Valentine, **Superoxide dismutases and superoxide reductases**, *Chemical reviews*, 2014, **114**, 3854-3918.
151. L. A. Sena and N. S. Chandel, **Physiological roles of mitochondrial reactive oxygen species**, *Molecular cell*, 2012, **48**, 158-167.
152. G. P. Bienert, J. K. Schjoerring and T. P. Jahn, **Membrane transport of hydrogen peroxide**, *Biochimica et biophysica acta*, 2006, **1758**, 994-1003.
153. M. Reth, **Hydrogen peroxide as second messenger in lymphocyte activation**, *Nature immunology*, 2002, **3**, 1129-1134.
154. A. Almasalmeh, D. Krenc, B. Wu and E. Beitz, **Structural determinants of the hydrogen peroxide permeability of aquaporins**, *The FEBS journal*, 2014, **281**, 647-656.
155. E. W. Miller, B. C. Dickinson and C. J. Chang, **Aquaporin-3 mediates hydrogen peroxide uptake to regulate downstream intracellular signaling**, *Proceedings of the National Academy of Sciences of the United States of America*, 2010, **107**, 15681-15686.
156. M. Hara-Chikuma, S. Chikuma, Y. Sugiyama, K. Kabashima, A. S. Verkman, S. Inoue and Y. Miyachi, **Chemokine-dependent T cell migration requires aquaporin-3-mediated hydrogen peroxide uptake**, *The Journal of experimental medicine*, 2012, **209**, 1743-1752.
157. F. Vieceli Dalla Sega, L. Zambonin, D. Fiorentini, B. Rizzo, C. Caliceti, L. Landi, S. Hrelia and C. Prata, **Specific aquaporins facilitate Nox-produced hydrogen peroxide transport through plasma membrane in leukaemia cells**, *Biochimica et biophysica acta*, 2014, **1843**, 806-814.
158. M. J. Marchissio, D. E. Frances, C. E. Carnovale and R. A. Marinelli, **Mitochondrial aquaporin-8 knockdown in human hepatoma HepG2 cells causes ROS-induced mitochondrial depolarization and loss of viability**, *Toxicology and applied pharmacology*, 2012, **264**, 246-254.

159. E. E. Tchekneva, Z. Khuchua, L. S. Davis, V. Kadkina, S. R. Dunn, S. Bachman, K. Ishibashi, E. M. Rinchik, R. C. Harris, M. M. Dikov and M. D. Breyer, **Single amino acid substitution in aquaporin 11 causes renal failure**, *Journal of the American Society of Nephrology : JASN*, 2008, **19**, 1955-1964.
160. E. N. Atochina-Vasserman, A. Biktasova, E. Abramova, D. S. Cheng, V. V. Polosukhin, H. Tanjore, S. Takahashi, H. Sonoda, L. Foye, C. Venkov, S. V. Ryzhov, S. Novitskiy, N. Shlonimskaya, M. Ikeda, T. S. Blackwell, W. E. Lawson, A. J. Gow, R. C. Harris, M. M. Dikov and E. E. Tchekneva, **Aquaporin 11 insufficiency modulates kidney susceptibility to oxidative stress**, *American journal of physiology. Renal physiology*, 2013, **304**, F1295-1307.
161. A. J. Yool and E. M. Campbell, **Structure, function and translational relevance of aquaporin dual water and ion channels**, *Molecular aspects of medicine*, 2012, **33**, 553-561.
162. M. Ikeda, E. Beitz, D. Kozono, W. B. Guggino, P. Agre and M. Yasui, **Characterization of aquaporin-6 as a nitrate channel in mammalian cells. Requirement of pore-lining residue threonine 63**, *The Journal of biological chemistry*, 2002, **277**, 39873-39879.
163. X. Qin and W. F. Boron, **Mutation of a single amino acid converts the human water channel aquaporin 5 into an anion channel**, *American journal of physiology. Cell physiology*, 2013, **305**, C663-672.
164. J. W. Lee, Y. Zhang, C. D. Weaver, N. H. Shomer, C. F. Louis and D. M. Roberts, **Phosphorylation of nodulin 26 on serine 262 affects its voltage-sensitive channel activity in planar lipid bilayers**, *The Journal of biological chemistry*, 1995, **270**, 27051-27057.
165. C. D. Weaver, N. H. Shomer, C. F. Louis and D. M. Roberts, **Nodulin 26, a nodule-specific symbiosome membrane protein from soybean, is an ion channel**, *The Journal of biological chemistry*, 1994, **269**, 17858-17862.
166. A. J. Yool, W. D. Stamer and J. W. Regan, **Forskolin stimulation of water and cation permeability in aquaporin 1 water channels**, *Science*, 1996, **273**, 1216-1218.
167. T. L. Anthony, H. L. Brooks, D. Boassa, S. Leonov, G. M. Yanocho, J. W. Regan and A. J. Yool, **Cloned human aquaporin-1 is a cyclic GMP-gated ion channel**, *Molecular pharmacology*, 2000, **57**, 576-588.
168. W. Zhang, E. Zitron, M. Homme, L. Kihm, C. Morath, D. Scherer, S. Hegge, D. Thomas, C. P. Schmitt, M. Zeier, H. Katus, C. Karle and V. Schwenger, **Aquaporin-1 channel function is positively regulated by protein kinase C**, *The Journal of biological chemistry*, 2007, **282**, 20933-20940.
169. M. T. Conner, A. C. Conner, C. E. Bland, L. H. Taylor, J. E. Brown, H. R. Parri and R. M. Bill, **Rapid aquaporin translocation regulates cellular water flow: mechanism of hypotonicity-induced subcellular localization of aquaporin 1 water channel**, *The Journal of biological chemistry*, 2012, **287**, 11516-11525.
170. E. M. Campbell, D. N. Birdsell and A. J. Yool, **The activity of human aquaporin 1 as a cGMP-gated cation channel is regulated by tyrosine phosphorylation in the carboxyl-terminal domain**, *Molecular pharmacology*, 2012, **81**, 97-105.

171. S. M. Saparov, D. Kozono, U. Rothe, P. Agre and P. Pohl, **Water and ion permeation of aquaporin-1 in planar lipid bilayers. Major differences in structural determinants and stoichiometry**, *The Journal of biological chemistry*, 2001, **276**, 31515-31520.
172. S. P. Tsunoda, B. Wiesner, D. Lorenz, W. Rosenthal and P. Pohl, **Aquaporin-1, nothing but a water channel**, *The Journal of biological chemistry*, 2004, **279**, 11364-11367.
173. P. Agre, M. D. Lee, S. Devidas and W. B. Guggino, **Aquaporins and ion conductance**, *Science*, 1997, **275**, 1490; author reply 1492.
174. D. Boassa, W. D. Stamer and A. J. Yool, **Ion channel function of aquaporin-1 natively expressed in choroid plexus**, *The Journal of neuroscience : the official journal of the Society for Neuroscience*, 2006, **26**, 7811-7819.
175. N. W. Baetz, W. D. Stamer and A. J. Yool, **Stimulation of aquaporin-mediated fluid transport by cyclic GMP in human retinal pigment epithelium in vitro**, *Investigative ophthalmology & visual science*, 2012, **53**, 2127-2132.
176. S. Saadoun, M. C. Papadopoulos, M. Hara-Chikuma and A. S. Verkman, **Impairment of angiogenesis and cell migration by targeted aquaporin-1 gene disruption**, *Nature*, 2005, **434**, 786-792.
177. D. K. Binder, E. A. Nagelhus and O. P. Ottersen, **Aquaporin-4 and epilepsy**, *Glia*, 2012, **60**, 1203-1214.
178. E. K. Hoffmann, I. H. Lambert and S. F. Pedersen, **Physiology of cell volume regulation in vertebrates**, *Physiological reviews*, 2009, **89**, 193-277.
179. B. Nilius, J. Vriens, J. Prenen, G. Droogmans and T. Voets, **TRPV4 calcium entry channel: a paradigm for gating diversity**, *American journal of physiology. Cell physiology*, 2004, **286**, C195-205.
180. W. Liedtke, **Transient receptor potential vanilloid channels functioning in transduction of osmotic stimuli**, *The Journal of endocrinology*, 2006, **191**, 515-523.
181. W. Liedtke and C. Kim, **Functionality of the TRPV subfamily of TRP ion channels: add mechano-TRP and osmo-TRP to the lexicon!**, *Cellular and molecular life sciences : CMLS*, 2005, **62**, 2985-3001.
182. X. Liu, B. C. Bandyopadhyay, T. Nakamoto, B. Singh, W. Liedtke, J. E. Melvin and I. Ambudkar, **A role for AQP5 in activation of TRPV4 by hypotonicity: concerted involvement of AQP5 and TRPV4 in regulation of cell volume recovery**, *The Journal of biological chemistry*, 2006, **281**, 15485-15495.
183. Q. Chen and E. K. Duan, **Aquaporins in sperm osmoadaptation: an emerging role for volume regulation**, *Acta pharmacologica Sinica*, 2011, **32**, 721-724.
184. Q. Chen, H. Peng, L. Lei, Y. Zhang, H. Kuang, Y. Cao, Q. X. Shi, T. Ma and E. Duan, **Aquaporin3 is a sperm water channel essential for postcopulatory sperm osmoadaptation and migration**, *Cell research*, 2011, **21**, 922-933.
185. L. Galizia, A. Pizzoni, J. Fernandez, V. Rivarola, C. Capurro and P. Ford, **Functional interaction between AQP2 and TRPV4 in renal cells**, *Journal of cellular biochemistry*, 2012, **113**, 580-589.

186. A. E. Hill and Y. Shachar-Hill, **Are Aquaporins the Missing Transmembrane Osmosensors?**, *The Journal of membrane biology*, 2015, **248**, 753-765.
187. S. Hozawa, E. J. Holtzman and D. A. Ausiello, **cAMP motifs regulating transcription in the aquaporin 2 gene**, *The American journal of physiology*, 1996, **270**, C1695-1702.
188. S. Higuchi, M. Kubota, K. Iguchi, S. Usui, T. Kiho and K. Hirano, **Transcriptional regulation of aquaporin 3 by insulin**, *Journal of cellular biochemistry*, 2007, **102**, 1051-1058.
189. I. Abreu-Rodriguez, R. Sanchez Silva, A. P. Martins, G. Soveral, J. J. Toledo-Aral, J. Lopez-Barneo and M. Echevarria, **Functional and transcriptional induction of aquaporin-1 gene by hypoxia; analysis of promoter and role of Hif-1alpha**, *PLoS one*, 2011, **6**, e28385.
190. B. W. van Balkom, P. J. Savelkoul, D. Markovich, E. Hofman, S. Nielsen, P. van der Sluijs and P. M. Deen, **The role of putative phosphorylation sites in the targeting and shuttling of the aquaporin-2 water channel**, *The Journal of biological chemistry*, 2002, **277**, 41473-41479.
191. P. M. Deen, B. W. van Balkom and E. J. Kamsteeg, **Routing of the aquaporin-2 water channel in health and disease**, *European journal of cell biology*, 2000, **79**, 523-530.
192. V. Sidhaye, J. D. Hoffert and L. S. King, **cAMP has distinct acute and chronic effects on aquaporin-5 in lung epithelial cells**, *J Biol Chem*, 2005, **280**, 3590-3596.
193. V. K. Sidhaye, A. D. Guler, K. S. Schweitzer, F. D'Alessio, M. J. Caterina and L. S. King, **Transient receptor potential vanilloid 4 regulates aquaporin-5 abundance under hypotonic conditions**, *Proceedings of the National Academy of Sciences of the United States of America*, 2006, **103**, 4747-4752.
194. Y. K. Chae, J. Woo, M. J. Kim, S. K. Kang, M. S. Kim, J. Lee, S. K. Lee, G. Gong, Y. H. Kim, J. C. Soria, S. J. Jang, D. Sidransky and C. Moon, **Expression of aquaporin 5 (AQP5) promotes tumor invasion in human non small cell lung cancer**, *PLoS One*, 2008, **3**, e2162.
195. C. Kosugi-Tanaka, X. Li, C. Yao, T. Akamatsu, N. Kanamori and K. Hosoi, **Protein kinase A-regulated membrane trafficking of a green fluorescent protein-aquaporin 5 chimera in MDCK cells**, *Biochim Biophys Acta*, 2006, **1763**, 337-344.
196. J. Woo, J. Lee, Y. K. Chae, M. S. Kim, J. H. Baek, J. C. Park, M. J. Park, I. M. Smith, B. Trink, E. Ratovitski, T. Lee, B. Park, S. J. Jang, J. C. Soria, J. A. Califano, D. Sidransky and C. Moon, **Overexpression of AQP5, a putative oncogene, promotes cell growth and transformation**, *Cancer letters*, 2008, **264**, 54-62.
197. J. Woo, Y. K. Chae, S. J. Jang, M. S. Kim, J. H. Baek, J. C. Park, B. Trink, E. Ratovitski, T. Lee, B. Park, M. Park, J. H. Kang, J. C. Soria, J. Lee, J. Califano, D. Sidransky and C. Moon, **Membrane trafficking of AQP5 and cAMP dependent phosphorylation in bronchial epithelium**, *Biochem Biophys Res Commun*, 2008, **366**, 321-327.
198. R. Horsefield, K. Norden, M. Fellert, A. Backmark, S. Tornroth-Horsefield, A. C. Terwisscha van Scheltinga, J. Kvassman, P. Kjellbom, U. Johanson and R. Neutze, **High-resolution x-ray structure of human**

- aquaporin 5**, *Proceedings of the National Academy of Sciences of the United States of America*, 2008, **105**, 13327-13332.
199. R. Horsefield, V. Yankovskaya, G. Sexton, W. Whittingham, K. Shiomi, S. Omura, B. Byrne, G. Cecchini and S. Iwata, **Structural and computational analysis of the quinone-binding site of complex II (succinate-ubiquinone oxidoreductase): a mechanism of electron transfer and proton conduction during ubiquinone reduction**, *The Journal of biological chemistry*, 2006, **281**, 7309-7316.
200. A. B. Sorensen, M. T. Sondergaard and M. T. Overgaard, **Calmodulin in a heartbeat**, *The FEBS journal*, 2013, **280**, 5511-5532.
201. S. L. Reichow, D. M. Clemens, J. A. Freitas, K. L. Nemeth-Cahalan, M. Heyden, D. J. Tobias, J. E. Hall and T. Gonen, **Allosteric mechanism of water-channel gating by Ca²⁺-calmodulin**, *Nature structural & molecular biology*, 2013, **20**, 1085-1092.
202. K. Kalman, K. L. Nemeth-Cahalan, A. Froger and J. E. Hall, **Phosphorylation determines the calmodulin-mediated Ca²⁺ response and water permeability of AQP0**, *The Journal of biological chemistry*, 2008, **283**, 21278-21283.
203. D. F. Savage and R. M. Stroud, **Structural basis of aquaporin inhibition by mercury**, *Journal of molecular biology*, 2007, **368**, 607-617.
204. E. Beitz, A. Golldack, M. Rothert and J. von Bulow, **Challenges and achievements in the therapeutic modulation of aquaporin functionality**, *Pharmacology & therapeutics*, 2015.
205. V. J. Huber, M. Tsujita, M. Yamazaki, K. Sakimura and T. Nakada, **Identification of arylsulfonamides as Aquaporin 4 inhibitors**, *Bioorganic & medicinal chemistry letters*, 2007, **17**, 1270-1273.
206. B. Yang, H. Zhang and A. S. Verkman, **Lack of aquaporin-4 water transport inhibition by antiepileptics and arylsulfonamides**, *Bioorganic & medicinal chemistry*, 2008, **16**, 7489-7493.
207. A. S. Verkman, M. O. Anderson and M. C. Papadopoulos, **Aquaporins: important but elusive drug targets**, *Nature reviews. Drug discovery*, 2014, **13**, 259-277.
208. M. Kang, C. A. Day, A. K. Kenworthy and E. DiBenedetto, **Simplified equation to extract diffusion coefficients from confocal FRAP data**, *Traffic*, 2012, **13**, 1589-1600.
209. J. Goedhart, D. von Stetten, M. Noirclerc-Savoye, M. Lelimosin, L. Joosen, M. A. Hink, L. van Weeren, T. W. Gadella, Jr. and A. Royant, **Structure-guided evolution of cyan fluorescent proteins towards a quantum yield of 93%**, *Nature communications*, 2012, **3**, 751.
210. T. Nagai, K. Ibata, E. S. Park, M. Kubota, K. Mikoshiba and A. Miyawaki, **A variant of yellow fluorescent protein with fast and efficient maturation for cell-biological applications**, *Nature biotechnology*, 2002, **20**, 87-90.
211. J. van Rheenen, M. Langeslag and K. Jalink, **Correcting confocal acquisition to optimize imaging of fluorescence resonance energy transfer by sensitized emission**, *Biophys J*, 2004, **86**, 2517-2529.
212. E. Solenov, H. Watanabe, G. T. Manley and A. S. Verkman, **Sevenfold-reduced osmotic water permeability in primary astrocyte cultures from AQP-4-deficient mice, measured by a fluorescence quenching**

- method**, *American journal of physiology. Cell physiology*, 2004, **286**, C426-432.
213. R. A. Fenton, H. B. Moeller, S. Nielsen, B. L. de Groot and M. Rutzler, **A plate reader-based method for cell water permeability measurement**, *American journal of physiology. Renal physiology*, 2010, **298**, F224-230.
214. M. G. Mola, G. P. Nicchia, M. Svelto, D. C. Spray and A. Frigeri, **Automated cell-based assay for screening of aquaporin inhibitors**, *Analytical chemistry*, 2009, **81**, 8219-8229.
215. S. Jelen, S. Wacker, C. Aponte-Santamaria, M. Skott, A. Rojek, U. Johanson, P. Kjellbom, S. Nielsen, B. L. de Groot and M. Rutzler, **Aquaporin-9 protein is the primary route of hepatocyte glycerol uptake for glycerol gluconeogenesis in mice**, *The Journal of biological chemistry*, 2011, **286**, 44319-44325.
216. H. Prinz, **Hill coefficients, dose-response curves and allosteric mechanisms**, *Journal of chemical biology*, 2010, **3**, 37-44.
217. G. J. Fiala, W. W. Schamel and B. Blumenthal, **Blue native polyacrylamide gel electrophoresis (BN-PAGE) for analysis of multiprotein complexes from cellular lysates**, *Journal of visualized experiments : JoVE*, 2011.
218. S. Pronk, S. Pall, R. Schulz, P. Larsson, P. Bjelkmar, R. Apostolov, M. R. Shirts, J. C. Smith, P. M. Kasson, D. van der Spoel, B. Hess and E. Lindahl, **GROMACS 4.5: a high-throughput and highly parallel open source molecular simulation toolkit**, *Bioinformatics*, 2013, **29**, 845-854.
219. C. Oostenbrink, T. A. Soares, N. F. van der Vegt and W. F. van Gunsteren, **Validation of the 53A6 GROMOS force field**, *European biophysics journal : EBJ*, 2005, **34**, 273-284.
220. C. Oostenbrink, A. Villa, A. E. Mark and W. F. van Gunsteren, **A biomolecular force field based on the free enthalpy of hydration and solvation: the GROMOS force-field parameter sets 53A5 and 53A6**, *Journal of computational chemistry*, 2004, **25**, 1656-1676.
221. O. Berger, O. Edholm and F. Jahnig, **Molecular dynamics simulations of a fluid bilayer of dipalmitoylphosphatidylcholine at full hydration, constant pressure, and constant temperature**, *Biophys J*, 1997, **72**, 2002-2013.
222. J. D. Ho, R. Yeh, A. Sandstrom, I. Chorny, W. E. Harries, R. A. Robbins, L. J. Miercke and R. M. Stroud, **Crystal structure of human aquaporin 4 at 1.8 Å and its mechanism of conductance**, *Proceedings of the National Academy of Sciences of the United States of America*, 2009, **106**, 7437-7442.
223. T. H. Schmidt and C. Kandt, **LAMBADA and InflateGRO2: efficient membrane alignment and insertion of membrane proteins for molecular dynamics simulations**, *Journal of chemical information and modeling*, 2012, **52**, 2657-2669.
224. W. G. Hoover, **Canonical dynamics: Equilibrium phase-space distributions**, *Physical review. A*, 1985, **31**, 1695-1697.
225. M. Parrinello and A. Rahman, **Polymorphic transitions in single crystals: A new molecular dynamics method**, *Journal of Applied Physics*, 1981, **52**, 7182-7190.

226. U. Essmann, L. Perera, M. L. Berkowitz, T. Darden, H. Lee and L. G. Pedersen, **A smooth particle mesh Ewald method**, *The Journal of Chemical Physics*, 1995, **103**, 8577-8593.
227. W. Humphrey, A. Dalke and K. Schulten, **VMD: visual molecular dynamics**, *Journal of molecular graphics*, 1996, **14**, 33-38, 27-38.
228. M. C. Papadopoulos and A. S. Verkman, **Aquaporin water channels in the nervous system**, *Nature reviews. Neuroscience*, 2013, **14**, 265-277.
229. Z. Zador, S. Stiver, V. Wang and G. T. Manley, **Role of aquaporin-4 in cerebral edema and stroke**, *Handbook of experimental pharmacology*, 2009, 159-170.
230. V. J. Huber, M. Tsujita and T. Nakada, **Identification of aquaporin 4 inhibitors using in vitro and in silico methods**, *Bioorganic & medicinal chemistry*, 2009, **17**, 411-417.
231. Y. Tanimura, Y. Hiroaki and Y. Fujiyoshi, **Acetazolamide reversibly inhibits water conduction by aquaporin-4**, *J Struct Biol*, 2009, **166**, 16-21.
232. J. Kato, M. K. Hayashi, S. Aizu, Y. Yukutake, J. Takeda and M. Yasui, **A general anaesthetic propofol inhibits aquaporin-4 in the presence of Zn(2)(+)**, *The Biochemical journal*, 2013, **454**, 275-282.
233. D. Marples, M. A. Knepper, E. I. Christensen and S. Nielsen, **Redistribution of aquaporin-2 water channels induced by vasopressin in rat kidney inner medullary collecting duct**, *The American journal of physiology*, 1995, **269**, C655-664.
234. L. N. Nejsum, M. Zelenina, A. Aperia, J. Frokiaer and S. Nielsen, **Bidirectional regulation of AQP2 trafficking and recycling: involvement of AQP2-S256 phosphorylation**, *American journal of physiology. Renal physiology*, 2005, **288**, F930-938.
235. S. Gouraud, A. Laera, G. Calamita, M. Carmosino, G. Procino, O. Rossetto, R. Mannucci, W. Rosenthal, M. Svelto and G. Valenti, **Functional involvement of VAMP/synaptobrevin-2 in cAMP-stimulated aquaporin 2 translocation in renal collecting duct cells**, *Journal of cell science*, 2002, **115**, 3667-3674.
236. A. C. Conner, R. M. Bill and M. T. Conner, **An emerging consensus on aquaporin translocation as a regulatory mechanism**, *Molecular membrane biology*, 2013, **30**, 1-12.
237. M. T. Conner, A. C. Conner, J. E. Brown and R. M. Bill, **Membrane trafficking of aquaporin 1 is mediated by protein kinase C via microtubules and regulated by tonicity**, *Biochemistry*, 2010, **49**, 821-823.
238. M. Assentoft, B. R. Larsen and N. MacAulay, **Regulation and Function of AQP4 in the Central Nervous System**, *Neurochemical research*, 2015.
239. M. Carmosino, G. Procino, G. Tamma, R. Mannucci, M. Svelto and G. Valenti, **Trafficking and phosphorylation dynamics of AQP4 in histamine-treated human gastric cells**, *Biology of the cell / under the auspices of the European Cell Biology Organization*, 2007, **99**, 25-36.
240. E. Gunnarson, M. Zelenina, G. Axehult, Y. Song, A. Bondar, P. Krieger, H. Brismar, S. Zelenin and A. Aperia, **Identification of a molecular target for glutamate regulation of astrocyte water permeability**, *Glia*, 2008, **56**, 587-596.

241. G. P. Nicchia, A. Rossi, M. G. Mola, G. Procino, A. Frigeri and M. Svelto, **Actin cytoskeleton remodeling governs aquaporin-4 localization in astrocytes**, *Glia*, 2008, **56**, 1755-1766.
242. J. D. Hoffert, G. Wang, T. Pisitkun, R. F. Shen and M. A. Knepper, **An automated platform for analysis of phosphoproteomic datasets: application to kidney collecting duct phosphoproteins**, *Journal of proteome research*, 2007, **6**, 3501-3508.
243. J. R. Wisniewski, N. Nagaraj, A. Zougman, F. Gnad and M. Mann, **Brain phosphoproteome obtained by a FASP-based method reveals plasma membrane protein topology**, *Journal of proteome research*, 2010, **9**, 3280-3289.
244. S. E. Moe, J. G. Sorbo, R. Sogaard, T. Zeuthen, O. Petter Ottersen and T. Holen, **New isoforms of rat Aquaporin-4**, *Genomics*, 2008, **91**, 367-377.
245. A. Rossi, F. Pisani, G. P. Nicchia, M. Svelto and A. Frigeri, **Evidences for a leaky scanning mechanism for the synthesis of the shorter M23 protein isoform of aquaporin-4: implication in orthogonal array formation and neuromyelitis optica antibody interaction**, *The Journal of biological chemistry*, 2010, **285**, 4562-4569.
246. J. E. Rash, K. G. Davidson, T. Yasumura and C. S. Furman, **Freeze-fracture and immunogold analysis of aquaporin-4 (AQP4) square arrays, with models of AQP4 lattice assembly**, *Neuroscience*, 2004, **129**, 915-934.
247. W. J. Zou, G. F. Huang and L. J. Kang, **[Molecular mechanisms of TRP channels in mechano-sensory transduction]**, *Zhejiang da xue xue bao. Yi xue ban = Journal of Zhejiang University. Medical sciences*, 2012, **41**, 222-228.
248. M. Jin, J. Berrout and R. G. O'Neil, in *TRP Channels*, ed. M. X. Zhu, Boca Raton (FL), Editon edn., 2011.
249. N. Blom, T. Sicheritz-Ponten, R. Gupta, S. Gammeltoft and S. Brunak, **Prediction of post-translational glycosylation and phosphorylation of proteins from the amino acid sequence**, *Proteomics*, 2004, **4**, 1633-1649.
250. J. Vriens, H. Watanabe, A. Janssens, G. Droogmans, T. Voets and B. Nilius, **Cell swelling, heat, and chemical agonists use distinct pathways for the activation of the cation channel TRPV4**, *Proceedings of the National Academy of Sciences of the United States of America*, 2004, **101**, 396-401.
251. K. Varadaraj, S. Kumari, A. Shiels and R. T. Mathias, **Regulation of aquaporin water permeability in the lens**, *Investigative ophthalmology & visual science*, 2005, **46**, 1393-1402.
252. S. L. Reichow and T. Gonen, **Noncanonical binding of calmodulin to aquaporin-0: implications for channel regulation**, *Structure*, 2008, **16**, 1389-1398.
253. Y. Ishikawa, H. Iida and H. Ishida, **The muscarinic acetylcholine receptor-stimulated increase in aquaporin-5 levels in the apical plasma membrane in rat parotid acinar cells is coupled with activation of nitric oxide/cGMP signal transduction**, *Molecular pharmacology*, 2002, **61**, 1423-1434.

254. M. Bustamante, U. Hasler, V. Leroy, S. de Seigneux, M. Dimitrov, D. Mordasini, M. Rousselot, P. Y. Martin and E. Feraille, **Calcium-sensing receptor attenuates AVP-induced aquaporin-2 expression via a calmodulin-dependent mechanism**, *Journal of the American Society of Nephrology : JASN*, 2008, **19**, 109-116.
255. N. E. Rabaud, L. Song, Y. Wang, P. Agre, M. Yasui and J. M. Carbrejy, **Aquaporin 6 binds calmodulin in a calcium-dependent manner**, *Biochemical and biophysical research communications*, 2009, **383**, 54-57.
256. D. Willoughby and D. M. Cooper, **Organization and Ca²⁺ regulation of adenylyl cyclases in cAMP microdomains**, *Physiological reviews*, 2007, **87**, 965-1010.
257. C. Sanabra and G. Mengod, **Neuroanatomical distribution and neurochemical characterization of cells expressing adenylyl cyclase isoforms in mouse and rat brain**, *Journal of chemical neuroanatomy*, 2011, **41**, 43-54.
258. B. K. Atwood, J. Lopez, J. Wager-Miller, K. Mackie and A. Straiker, **Expression of G protein-coupled receptors and related proteins in HEK293, AtT20, BV2, and N18 cell lines as revealed by microarray analysis**, *BMC genomics*, 2011, **12**, 14.
259. K. L. Yap, J. Kim, K. Truong, M. Sherman, T. Yuan and M. Ikura, **Calmodulin target database**, *Journal of structural and functional genomics*, 2000, **1**, 8-14.
260. T. Katsura, C. E. Gustafson, D. A. Ausiello and D. Brown, **Protein kinase A phosphorylation is involved in regulated exocytosis of aquaporin-2 in transfected LLC-PK1 cells**, *The American journal of physiology*, 1997, **272**, F817-822.
261. M. Assentoft, B. R. Larsen, E. T. Olesen, R. A. Fenton and N. MacAulay, **AQP4 plasma membrane trafficking or channel gating is not significantly modulated by phosphorylation at C-terminal serine residues**, *American journal of physiology. Cell physiology*, 2014.
262. R. Madrid, S. Le Maout, M. B. Barrault, K. Janvier, S. Benichou and J. Merot, **Polarized trafficking and surface expression of the AQP4 water channel are coordinated by serial and regulated interactions with different clathrin-adaptor complexes**, *The EMBO journal*, 2001, **20**, 7008-7021.
263. H. B. Moeller, R. A. Fenton, T. Zeuthen and N. Macaulay, **Vasopressin-dependent short-term regulation of aquaporin 4 expressed in Xenopus oocytes**, *Neuroscience*, 2009, **164**, 1674-1684.
264. M. Assentoft, S. Kaptan, R. A. Fenton, S. Z. Hua, B. L. de Groot and N. MacAulay, **Phosphorylation of rat aquaporin-4 at Ser(111) is not required for channel gating**, *Glia*, 2013, **61**, 1101-1112.
265. M. De Bellis, F. Pisani, M. G. Mola, D. Basco, F. Catalano, G. P. Nicchia, M. Svelto and A. Frigeri, **A novel human aquaporin-4 splice variant exhibits a dominant-negative activity: a new mechanism to regulate water permeability**, *Molecular biology of the cell*, 2014, **25**, 470-480.
266. J. Woo, J. Lee, M. S. Kim, S. J. Jang, D. Sidransky and C. Moon, **The effect of aquaporin 5 overexpression on the Ras signaling pathway**, *Biochem Biophys Res Commun*, 2008, **367**, 291-298.

267. R. B. Wellner, S. Hong, A. P. Cotrim, W. D. Swaim and B. J. Baum, **Modifying the NH₂ and COOH termini of aquaporin-5: effects on localization in polarized epithelial cells**, *Tissue Eng*, 2005, **11**, 1449-1458.
268. P. Kitchen, R. E. Day, L. H. Taylor, M. M. Salman, R. M. Bill, M. T. Conner and A. C. Conner, **Identification and Molecular Mechanisms of the Rapid Tonicity-induced Relocalization of the Aquaporin 4 Channel**, *The Journal of biological chemistry*, 2015, **290**, 16873-16881.
269. Y. Song and A. S. Verkman, **Aquaporin-5 dependent fluid secretion in airway submucosal glands**, *The Journal of biological chemistry*, 2001, **276**, 41288-41292.
270. D. Krenc, J. Song, A. Almasalmeh, B. Wu and E. Beitz, **The arginine-facing amino acid residue of the rat aquaporin 1 constriction determines solute selectivity according to its size and lipophilicity**, *Molecular membrane biology*, 2014, **31**, 228-238.
271. R. Oliva, G. Calamita, J. M. Thornton and M. Pellegrini-Calace, **Electrostatics of aquaporin and aquaglyceroporin channels correlates with their transport selectivity**, *Proceedings of the National Academy of Sciences of the United States of America*, 2010, **107**, 4135-4140.
272. J. S. Hub and B. L. de Groot, **Mechanism of selectivity in aquaporins and aquaglyceroporins**, *Proceedings of the National Academy of Sciences of the United States of America*, 2008, **105**, 1198-1203.
273. A. Fiser and A. Sali, **Modeller: generation and refinement of homology-based protein structure models**, *Methods in enzymology*, 2003, **374**, 461-491.
274. O. S. Smart, J. G. Neduvilil, X. Wang, B. A. Wallace and M. S. Sansom, **HOLE: a program for the analysis of the pore dimensions of ion channel structural models**, *Journal of molecular graphics*, 1996, **14**, 354-360, 376.
275. N. Guex and M. C. Peitsch, **SWISS-MODEL and the Swiss-PdbViewer: an environment for comparative protein modeling**, *Electrophoresis*, 1997, **18**, 2714-2723.
276. J. Jiang, B. V. Daniels and D. Fu, **Crystal structure of AqpZ tetramer reveals two distinct Arg-189 conformations associated with water permeation through the narrowest constriction of the water-conducting channel**, *The Journal of biological chemistry*, 2006, **281**, 454-460.
277. L. Janosi and M. Ceccarelli, **The gating mechanism of the human aquaporin 5 revealed by molecular dynamics simulations**, *PloS one*, 2013, **8**, e59897.
278. T. Ma, A. Frigeri, H. Hasegawa and A. S. Verkman, **Cloning of a water channel homolog expressed in brain meningeal cells and kidney collecting duct that functions as a stilbene-sensitive glycerol transporter**, *The Journal of biological chemistry*, 1994, **269**, 21845-21849.
279. G. Cho, A. M. Bragiel, D. Wang, T. D. Pieczonka, M. T. Skowronski, M. Shono, S. Nielsen and Y. Ishikawa, **Activation of muscarinic receptors in rat parotid acinar cells induces AQP5 trafficking to nuclei and**

- apical plasma membrane**, *Biochimica et biophysica acta*, 2015, **1850**, 784-793.
280. E. J. Kamsteeg, T. A. Wormhoudt, J. P. Rijss, C. H. van Os and P. M. Deen, **An impaired routing of wild-type aquaporin-2 after tetramerization with an aquaporin-2 mutant explains dominant nephrogenic diabetes insipidus**, *The EMBO journal*, 1999, **18**, 2394-2400.
281. L. M. Felber, S. M. Cloutier, C. Kundig, T. Kishi, V. Brossard, P. Jichlinski, H. J. Leisinger and D. Deperthes, **Evaluation of the CFP-substrate-YFP system for protease studies: advantages and limitations**, *BioTechniques*, 2004, **36**, 878-885.
282. F. Sievers, A. Wilm, D. Dineen, T. J. Gibson, K. Karplus, W. Li, R. Lopez, H. McWilliam, M. Remmert, J. Soding, J. D. Thompson and D. G. Higgins, **Fast, scalable generation of high-quality protein multiple sequence alignments using Clustal Omega**, *Molecular systems biology*, 2011, **7**, 539.
283. F. Umenishi, J. M. Verbavatz and A. S. Verkman, **cAMP regulated membrane diffusion of a green fluorescent protein-aquaporin 2 chimera**, *Biophys J*, 2000, **78**, 1024-1035.
284. M. R. Cho, D. W. Knowles, B. L. Smith, J. J. Moulds, P. Agre, N. Mohandas and D. E. Golan, **Membrane dynamics of the water transport protein aquaporin-1 in intact human red cells**, *Biophys J*, 1999, **76**, 1136-1144.
285. P. G. Saffman and M. Delbruck, **Brownian motion in biological membranes**, *Proceedings of the National Academy of Sciences of the United States of America*, 1975, **72**, 3111-3113.
286. E. N. Atochina-Vasserman, **S-nitrosylation of surfactant protein D as a modulator of pulmonary inflammation**, *Biochimica et biophysica acta*, 2012, **1820**, 763-769.
287. M. Zelenina, S. Zelenin, A. A. Bondar, H. Brismar and A. Aperia, **Water permeability of aquaporin-4 is decreased by protein kinase C and dopamine**, *American journal of physiology. Renal physiology*, 2002, **283**, F309-318.
288. R. Sachdeva and B. Singh, **Phosphorylation of Ser-180 of rat aquaporin-4 shows marginal affect on regulation of water permeability: molecular dynamics study**, *Journal of biomolecular structure & dynamics*, 2014, **32**, 555-566.
289. T. Mitsuma, K. Tani, Y. Hiroaki, A. Kamegawa, H. Suzuki, H. Hibino, Y. Kurachi and Y. Fujiyoshi, **Influence of the cytoplasmic domains of aquaporin-4 on water conduction and array formation**, *Journal of molecular biology*, 2010, **402**, 669-681.
290. K. Tani, T. Mitsuma, Y. Hiroaki, A. Kamegawa, K. Nishikawa, Y. Tanimura and Y. Fujiyoshi, **Mechanism of aquaporin-4's fast and highly selective water conduction and proton exclusion**, *Journal of molecular biology*, 2009, **389**, 694-706.
291. M. Potokar, M. Stenovec, J. Jorgacevski, T. Holen, M. Kreft, O. P. Ottersen and R. Zorec, **Regulation of AQP4 surface expression via vesicle mobility in astrocytes**, *Glia*, 2013, **61**, 917-928.

292. J. Mazzaferri, S. Costantino and S. Lefrancois, **Analysis of AQP4 trafficking vesicle dynamics using a high-content approach**, *Biophys J*, 2013, **105**, 328-337.
293. J. C. Mathai and P. Agre, **Hourglass pore-forming domains restrict aquaporin-1 tetramer assembly**, *Biochemistry*, 1999, **38**, 923-928.
294. L. Duchesne, S. Deschamps, I. Pellerin, V. Lagree, A. Froger, D. Thomas, P. Bron, C. Delamarche and J. F. Hubert, **Oligomerization of water and solute channels of the major intrinsic protein (MIP) family**, *Kidney international*, 2001, **60**, 422-426.
295. T. M. Buck, J. Wagner, S. Grund and W. R. Skach, **A novel tripartite motif involved in aquaporin topogenesis, monomer folding and tetramerization**, *Nature structural & molecular biology*, 2007, **14**, 762-769.
296. V. Lagree, A. Froger, S. Deschamps, I. Pellerin, C. Delamarche, G. Bonnac, J. Gouranton, D. Thomas and J. F. Hubert, **Oligomerization state of water channels and glycerol facilitators. Involvement of loop E**, *The Journal of biological chemistry*, 1998, **273**, 33949-33953.
297. L. Duchesne, I. Pellerin, C. Delamarche, S. Deschamps, V. Lagree, A. Froger, G. Bonnac, D. Thomas and J. F. Hubert, **Role of C-terminal domain and transmembrane helices 5 and 6 in function and quaternary structure of major intrinsic proteins: analysis of aquaporin/glycerol facilitator chimeric proteins**, *The Journal of biological chemistry*, 2002, **277**, 20598-20604.

Appendix: Publications arising from the data presented in this thesis

The discussion presented in the introduction (chapter 1) has been adapted for two review articles. These are appended on the following pages, followed by four original research articles, presented in the order in which the data appear in the thesis.



Review

Beyond water homeostasis: Diverse functional roles of mammalian aquaporins



Philip Kitchen ^a, Rebecca E. Day ^b, Mootaz M. Salman ^b, Matthew T. Conner ^b, Roslyn M. Bill ^c, Alex C. Conner ^{d,*}

^a Molecular Organisation and Assembly in Cells Doctoral Training Centre, University of Warwick, Coventry CV4 7AL, UK

^b Biomedical Research Centre, Sheffield Hallam University, Howard Street, Sheffield S1 1WB, UK

^c School of Life & Health Sciences and Aston Research Centre for Healthy Ageing, Aston University, Aston Triangle, Birmingham B4 7ET, UK

^d Institute of Clinical Sciences, University of Birmingham, Edgbaston, Birmingham B15 2TT, UK

ARTICLE INFO

Article history:

Received 17 June 2015

Received in revised form 25 August 2015

Accepted 30 August 2015

Available online 10 September 2015

Keywords:

Aquaporin

Solute transport

Ion transport

Membrane trafficking

Cell volume regulation

ABSTRACT

Background: Aquaporin (AQP) water channels are best known as passive transporters of water that are vital for water homeostasis.

Scope of review: AQP knockout studies in whole animals and cultured cells, along with naturally occurring human mutations suggest that the transport of neutral solutes through AQPs has important physiological roles. Emerging biophysical evidence suggests that AQPs may also facilitate gas (CO₂) and cation transport. AQPs may be involved in cell signalling for volume regulation and controlling the subcellular localization of other proteins by forming macromolecular complexes. This review examines the evidence for these diverse functions of AQPs as well their physiological relevance.

Major conclusions: As well as being crucial for water homeostasis, AQPs are involved in physiologically important transport of molecules other than water, regulation of surface expression of other membrane proteins, cell adhesion, and signalling in cell volume regulation.

General significance: Elucidating the full range of functional roles of AQPs beyond the passive conduction of water will improve our understanding of mammalian physiology in health and disease. The functional variety of AQPs makes them an exciting drug target and could provide routes to a range of novel therapies.

© 2015 Elsevier B.V. All rights reserved.

1. Introduction

The aquaporin (AQP) protein family is comprised of many small integral membrane proteins found in all phylogenetic kingdoms. There are up to 13 mammalian AQPs, which are found in most tissues with functions ranging from the regulation of renal water balance [1], brain-fluid homeostasis [2], triglyceride cycling between adipocytes and the liver [3] and structural integrity of the eye lens [4]. Because of this, understanding AQP function is crucial for the study of healthy ageing as well as the onset of many disease states such as brain swelling following stroke or head injury [5], nephrogenic diabetes insipidus [6,7], cataracts [8], obesity [9], cancer cell proliferation and migration [10] and tumour angiogenesis [11]. Many of these functions and diseases involve either permeability of molecules other than water, or a function of the AQP other than facilitating membrane permeability.

Abbreviations: GLP, glyceroporin; MD, molecular dynamics; SC, stratum corneum; ANP, atrial natriuretic peptide; NSCC, non-selective cation channel; RVD/RVI, regulatory volume decrease/increase; TM, transmembrane; ROS, reactive oxygen species.

* Corresponding author at: School of Clinical and Experimental Medicine, University of Birmingham, Edgbaston, Birmingham B15 2TT, UK.

E-mail address: a.c.conner@bham.ac.uk (A.C. Conner).

Thirteen human AQPs have been discovered to date; they range in size (before post-translational modification) from 27 kDa (AQP8) to 37 kDa (AQP7) and, for those proteins for which single channel permeability has been quantified, have a 100-fold range in water permeability. A sub-set of these AQPs also function as channels for glycerol (and other solutes) and are referred to as (aqua)glyceroporins (GLPs). In humans, these are AQP3, -7, -9 and -10. AQP6 has also (controversially, see Section 4) been shown to be permeable to glycerol, although phylogenetically it is a member of the water-selective AQP subfamily [12]. It also is notable for its unusual permeability properties (activation by low pH and anion permeability) and intracellular localization. The permeability properties of the mammalian AQPs are summarized in Table 1.

This review discusses how AQPs select and regulate the passage of solutes such as glycerol, urea and ammonia across cell membranes and the physiological relevance of this solute flow as well as putative functions of AQPs beyond facilitation of membrane permeability.

2. The structural biology of the AQP family is established

There is a large amount of medium-to-high-resolution structural data available for the AQP family (43 structures deposited in the Protein Data Bank for 11 different AQPs). These structures suggest that the AQPs

Table 1

Water, glycerol, urea and ammonia (NH₃) permeabilities of known human AQPs. Quantitative water permeability is per AQP channel i.e. after subtraction of the basal permeability of the expression membrane and normalized to the number of AQP molecules. Expression systems: X – *Xenopus* oocytes, PL – proteoliposomes, M – mammalian cells, V – vesicles derived from membrane fragmentation of AQP-expressing mammalian cells, Y – ammonia transport deficient yeast.

AQP	Single channel water permeability ($\times 10^{-14} \text{ cm}^3 \text{ s}^{-1}$)	Glycerol permeability	Urea permeability	Ammonia permeability
AQP0	0.25 [13]; gated by calmodulin [14]; X, PL	No [13]; X	No [15]; X	No [16]; X
AQP1	6.0 [13]; X	No [13]; X	No [17]; X	No [17]; X
AQP2	3.3 [13]; X	No [13]; X	No [15]; X	No [16]; X
AQP3	2.1 [13]; X	Yes [13]; X	Controversial [15,17–19]; X	Yes [16,17]; X
AQP4	24 [13]; X	No [13]; X	No [20]; X	No [16]; X
AQP5	5.0 [13]; X	No [13]; X	No [21]; X	No [16]; X
AQP6	Low pH and Hg ²⁺ induce water permeability [22,23]. Basal permeability either is very low [23,24] or zero [25,26]; X	Yes ^b [26]; X	Yes ^b [26]; X	Yes [16]; X
AQP7	Permeable [27]; no quantitative data; X	Yes [27]; X	Yes [27]; X	Yes [16]; X
AQP8	Permeable [28,29]; no quantitative data; X, PL	No [28,29]; X, PL	Controversial [28–30]; X, PL	Yes [17,31]; X, Y
AQP9	Permeable [32]; no quantitative data; PL	Yes [17,32]; X, PL	Yes [17,32]; X, PL	Yes [17]; X
AQP10	Permeable [33]; no quantitative data; X	Yes [33]; X	Yes [33]; X	Unknown
AQP11	Permeable [34]; ~2 [35] ^a ; M, V	Yes ^b [36]; M	Unknown	Unknown
AQP12	Unknown	Unknown	Unknown	Unknown

^a Estimated from membrane fragment vesicle water permeability relative to AQP1-containing vesicles and relative expression level.

^b These data have not been independently replicated.

share many common structural features. The AQP monomer is composed of six tilted transmembrane (TM) helices that surround a central cavity containing two helix-forming loops that enter and exit from the same side of the membrane (see Fig. 1A). This central cavity is the pathway for water and solute transport. The two helical loops contain highly conserved asparagine–proline–alanine (NPA) motifs. Crystallography and molecular dynamics (MD) simulations suggest that the asparagine residues act, in concert with surrounding backbone carbonyl groups, to enable water transport by providing hydrogen bonds to water molecules [37], thereby lowering the free energy penalty (caused by breaking of water–water hydrogen bonds) of removing a water molecule from bulk solution. Recent biophysical experiments comparing AQPs with gramicidin and the potassium channel KcsA [38] suggest that the number of pore-lining hydrogen-bonding sites for water determines the channel water permeability. In addition to providing hydrogen-bonding sites, the asparagine residues help to orient the water molecules such that the hydrogen atoms point ‘outwards’ from the pore, creating a barrier to proton transport [39]. A recent sub-angstrom crystal

structure of the *Pichia pastoris* AQY1 found overlapping water densities in the pore that, supported by MD simulations, suggested a correlated pairwise movement of water molecules through the extracellular end of the pore. This correlated motion may help to minimise water–water hydrogen bonds in this region, providing a further barrier to proton permeation, without compromising water transport [37].

Crystallographic analysis of the *Escherichia coli*, GlpF (a GLP), suggests that the same asparagine residues also form hydrogen bonds with glycerol [40]. This is likely to be also true of other polar solutes that permeate GLPs.

AQPs have intracellular amino (N-) and carboxyl (C-) termini of varying lengths; AQP8 has a short C-terminus of 10–15 residues, whereas AQP4 has a large C-terminus consisting of ~70 residues. AQP11 has a large N-terminal tail of ~40 residues, whereas AQPs 1, 2 and 5 have short N-termini of <10 residues. In contrast to the structural conservation of the TM region of AQPs, much less is known about the structure of the termini. This is because the majority of AQP crystal structures are obtained using constructs in which the N- and C-terminal tails of

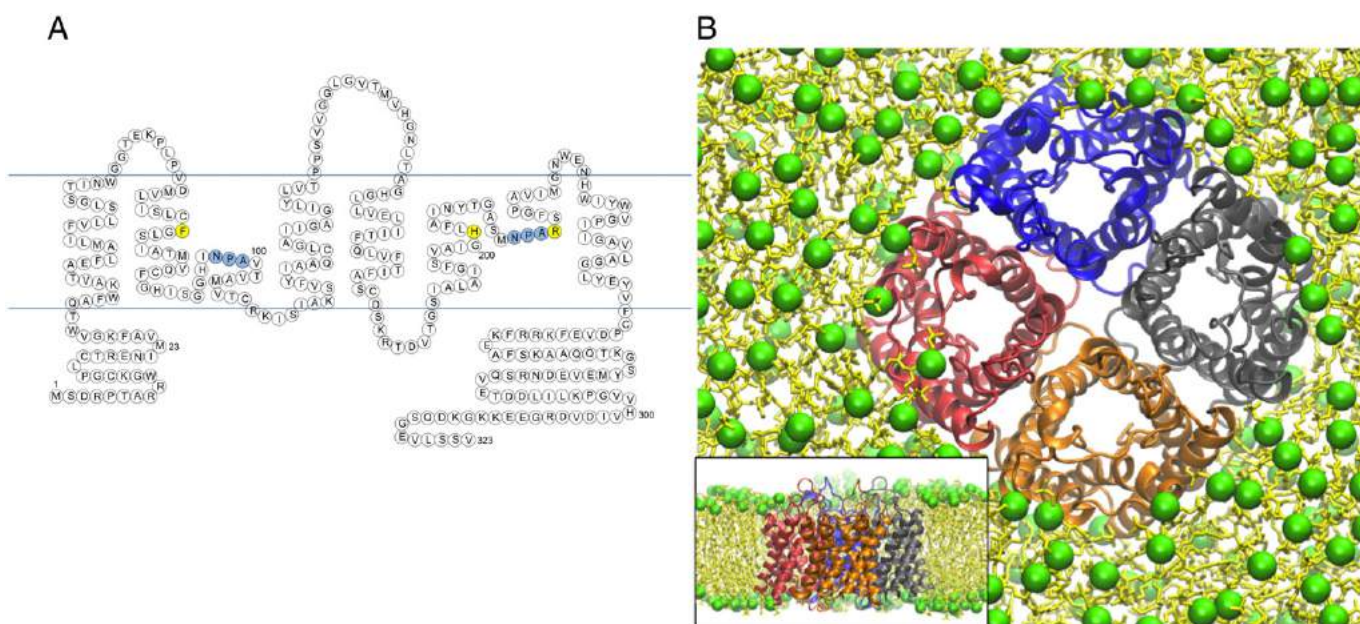


Fig. 1. Structure of AQPs exemplified by human AQP4. (A) AQPs have six bilayer-spanning helices and two helix-forming loops. These loops contain the conserved NPA motifs (coloured blue). The residues forming the arginine/aromatic region thought to be important for solute selectivity are coloured yellow. (B) Simulation snapshot of AQP4 embedded in a POPC bilayer. Phosphorus atoms in the lipid headgroups are coloured green and the fatty acid tails are yellow. Visualized using VMD [189].

the protein have been truncated due to the difficulty of obtaining well-diffracting crystals using full-length AQP molecules [41]. This suggests an inherent structural flexibility in these regions of AQP molecules and indeed a recent X-ray structure of AQP2, which included ~20 residues of the (truncated) C-terminal tail, found this fragment of the C-terminus in four strikingly different conformations in each of the four AQP2 monomers within the tetrameric unit cell [42].

AQPs are generally agreed to form tetramers [43–45] assembled around a central axis perpendicular to the plane of the membrane (see Fig. 1B). A fifth, hydrophobic pore appears to form around this central axis with each of the monomers contributing one of the four 'walls' of the pore. The function, if any, of this fifth pore is not yet known, although postulated functions will be discussed in later sections. Some biochemical studies have suggested that tetramers formed by GLPs have reduced stability compared to tetramers formed by AQPs with strict water selectivity [46,47].

3. The principles of solute selectivity by AQPs remain to be established

All AQPs (except AQP12, which has yet to be characterized) transport water (Table 1), while some also transport glycerol. The glycerol permeable GLPs (e.g. human AQPs 7, 9 and 10) are also permeable to urea. The urea permeability of AQP3 is controversial, with some studies reporting urea transport and others no transport [15,17–19]. This may be due to methodological differences, and is discussed in detail in Section 4.2.1.

Of the mammalian GLPs AQP3, -7, and -9 are also permeable to ammonia. AQP8 is the only glycerol impermeable mammalian AQP that is permeable to ammonia (excluding 11 and 12, whose glycerol and/or ammonia permeabilities are currently unknown). The ammonia permeability of the most recently discovered member of the GLP group, AQP10, is still unknown.

AQP11 and -12 are the most recently discovered members of the AQP family [48,49]; due to this and their localisation to intracellular membranes, non-water permeability experiments and functional studies have yet to be reported for AQP11 and AQP12 respectively. There is one report that AQP11 increased the glycerol permeability of an adipocyte cell line [36], but this permeability of AQP11 has yet to be replicated.

The 'size exclusion' model of AQP selectivity posits a correlation between the size of channel entrance and the permeability of the channel to different polar molecules. Notably, this model is based on *in silico* and crystallographic experiments, but minimal *in vitro* experiments; it is therefore unclear whether this model is broadly applicable to the AQP family as a whole. A conserved arginine residue (in the second helical loop directly after the NPA motif) forms part of a channel constriction known as the aromatic/arginine (ar/R) selectivity filter (see Fig. 1A). In water-selective AQPs, the other components of this filter are a phenylalanine in the top half of the pore-facing side of transmembrane helix 2 (TM2) and a histidine in a similar position in TM5. In glycerol and urea permeable AQPs, this histidine is replaced by a small amino acid residue such as glycine (AQP3, -7, -10) or alanine (AQP9), although if the histidine is mutated to alanine in AQP1 it does not become a glycerol channel. If both aromatic members of the filter (H and F) are mutated to alanine, AQP1 functions as a urea channel and to a lesser extent as a glycerol channel [50]. Based on this observation and molecular simulations of AQP1 and the *E. coli* GLP, GlpF [50,51], it has been suggested that the cross-sectional area of the pore at the ar/R region determines AQP selectivity for neutral polar solutes. Additionally, based on crystallographic analysis of GlpF and the bacterial water-selective AQP, AQPZ, it has been suggested that the positioning of the ar/R residues by the surrounding unstructured loops has a role in determining the channel size [52]. In AQP8, the only glycerol-impermeable, ammonia-permeable mammalian AQP, the third member of the filter is likely an isoleucine residue (based on sequence alignment), which is slightly

larger than alanine or glycine. Overall, current thinking on solute selectivity suggests that the aromatic residues of the ar/R filter are important for solute exclusion in the water selective AQPs, but further molecular factors may be involved in mediating solute selectivity.

4. Physiological solute transport by AQPs

4.1. Glycerol transport

The movement of glycerol around the body is predominantly thought to include glycerol release from fat tissue through AQP7, entry into the liver through AQP9 and movement in the skin and kidneys through AQP3.

4.1.1. AQP7

AQP7 is expressed in adipose tissue in adipocytes [53] and capillary endothelia [54]. Upon hypoglycaemia, triglycerides are broken down within adipocytes to glycerol and free fatty acids [55]. Adrenaline, the plasma level of which is elevated upon hypoglycaemia, caused translocation of AQP7 from intracellular membranes to the plasma membrane [53]. Adrenaline signals through the β_3 -adrenergic receptor to initiate adipocytic lipolysis [56] making this the most likely link between adrenaline and AQP7 translocation although this has yet to be verified. Recent work has also suggested that AQP7 can be relocalised to lipid droplets by noradrenaline, possibly in a PKA dependent manner [57], raising the possibility of differential effects of lipolysis-inducing hormones on AQP7 localization.

The glycerol liberated from triglyceride storage is released from adipocytes [58] and plasma glycerol becomes elevated. In AQP7 $-/-$ mice, adipocyte plasma membrane glycerol permeability was reduced three-fold [59]. Plasma glycerol levels in the fasting state and in response to β_3 -adrenergic agonist were reduced and adrenaline-induced glycerol secretion by cultured mouse adipocytes (differentiated 3T3-L1 cells) was reduced approximately two-fold [60]. These results suggest that the major pathway for glycerol efflux from adipocytes after lipolysis is AQP7.

AQP7 $-/-$ mice develop adipocyte hypertrophy and subsequent obesity in adulthood [59]. A loss of function mutation in the human AQP7 gene has been discovered (G264→V) although this genotype was not correlated with obesity in humans [61]. This may be due to the presence of AQP10 in human adipocyte membranes, which was found to contribute ~50% of the water and glycerol permeability of healthy human adipocyte plasma membrane vesicles [62]. Mouse AQP10 is a pseudogene [63] and therefore this secondary route for glycerol efflux does not exist in mice.

The serum concentration of glycerol in humans under normal physiological conditions is typically between 0.05 and 0.1 mM [64] and increases several-fold upon fasting (due to glycerol and free fatty acid liberation from adipose triglyceride storage) [65]. Glycerol is almost completely reabsorbed by the kidneys [66] (unless it is raised above ~0.3 mM [67]), suggesting the existence of a glycerol reabsorption pathway. AQP7 is expressed in the proximal tubule of the kidney. AQP7 $-/-$ mice showed marked glyceroluria in comparison to wild type (~400-fold increase in urine glycerol) [68]. Human children homozygous for the AQP7 G264V mutant were found to have hyperglyceroluria, with a ~1000-fold increase in urine glycerol when compared to heterozygous familial controls [69]. The G264V mutant has been shown to have no activity as a glycerol or water channel in *Xenopus* oocytes [61], although plasma membrane expression was not verified in this study so that it could not differentiate between a non-functional channel and an incorrectly localised channel. The mutation disrupts a conserved GxxxG motif. These are important motifs for transmembrane helix–helix interactions because they allow close contact between the backbone atoms of the two helices of an interacting pair [70]. It may be that the protein is incorrectly trafficked and localised in intracellular membranes due to an inability to form tetramers or an interaction required for membrane

trafficking. Regardless of the loss of function mechanism, these data strongly suggest that AQP7 is the TM glycerol reabsorption pathway in the renal proximal tubule.

4.1.2. AQP9

AQP9 is expressed in the liver [71], primarily in the hepatocytes with the strongest expression at the sinusoidal surface [72] (the liver sinusoids are continuous with the hepatic artery and portal vein). Upon fasting, glycerol released into the plasma from adipocytes is taken up by hepatocytes and used as a substrate for gluconeogenesis [73].

In rats, AQP9 protein expression is increased up to 20-fold after 24–96 hour fasting [32]. In mice, AQP9 expression measured in purified hepatocyte plasma membrane vesicles increased 10-fold after 18 hour fasting. This 10-fold increase was accompanied by a two-fold increase in hepatocyte plasma membrane glycerol permeability, which was reversed by addition of phloretin (an apple polyphenol that inhibits AQP9, AQP3 and several non-AQP membrane channel proteins including the SGLT1&2 glucose transporters and UT-A urea channels [74]). The increase was abolished in AQP9 $-/-$ mice [75]. Fasted AQP9 $-/-$ mice have elevated plasma glycerol compared to wild-type [75,76]. In addition, plasma glucose concentration was decreased [76], indicating a gluconeogenic deficiency. This data supports a physiological role for AQP9-mediated glycerol uptake by hepatocytes during fasting-induced hypoglycaemia.

Although the AQP9-mediated diffusion of glycerol into hepatocytes forms a sizeable proportion of the glycerol uptake in the fasting state (~50% in fasting mice), the fact that the membrane permeability to glycerol only doubles upon such a large increase in AQP9 expression suggests that there is also an AQP9-independent route for glycerol uptake. Whether this is directly across the lipid bilayer or through a phloretin insensitive glycerol channel is not clear.

CD8⁺ (cytotoxic) T cells are white blood cells that facilitate the destruction of infected or otherwise damaged cells. During infection, antigen-specific CD8⁺ cells proliferate and differentiate into effector cells, which are involved in combatting infection. After pathogen clearance, most of the effector cells die and a small population remains as memory T cells, which can survive for decades [77]. In mouse memory cells, AQP9 expression was upregulated post-infection via IL-7 signalling, allowing cells to import glycerol for triglyceride synthesis. AQP9 $-/-$ T cells had reduced long-term survival compared to $+/+$ cells and the long-term survival of the $+/+$ cells could be inhibited by phloretin [78]. This suggests that AQP9 expression can act as a metabolic switch, enabling long-term survival of memory T cells by enabling triglyceride synthesis to build up an energetic reserve, allowing cell survival in nutrient poor conditions.

Similarly to that seen in hepatocytes, intracellular glycerol in CD8⁺ T cells was reduced by ~50% in the AQP9 $-/-$ cells, again suggesting a secondary route for glycerol uptake.

4.1.3. AQP3

AQP3 is expressed in the skin in keratinocytes below the stratum corneum (SC). It is most strongly expressed at the plasma membrane in these cells with some intracellular labelling reported in cells of the basal layer [79]. The ability of the epidermis to maintain hydration is impaired in AQP3 $-/-$ mice. In dry conditions, AQP3 $-/-$ mice showed comparable (reduced) levels of SC hydration to wild-type mice, whereas at normal humidity, SC hydration was lower in the AQP3 $-/-$ mice [80]. Elevated humidity (which prevents water loss via evaporation) did not correct the deficiency, which suggests that the primary role of AQP3 in skin hydration is not to provide water to replace that lost by evaporation.

SC glycerol concentration in AQP3 $-/-$ mice is reduced to ~40% of that of wild-type, with no significant difference in the levels of other osmolytes (ions, glucose, urea, lactate and free amino acids) [81]. Glycerol acts as a humectant (a 'water-retaining' osmolyte), which may be the mechanism by which it maintains skin hydration. It has also been

suggested that glycerol may prevent SC water loss by inhibiting the phase transition of intercellular lipids from the liquid crystalline to the solid phase [82] due to the fact that breaks in a solid crystal lattice increase the water permeability in in vitro models of the SC intercellular lipid barrier [83]. The rate of transport of glycerol from blood to the SC was reduced in AQP3 $-/-$ mice resulting in reduced lipid biosynthesis [84]. This suggests a further role for glycerol in maintaining skin hydration by allowing the maintenance of the SC lipid barrier.

Further evidence for the role of AQP3-mediated glycerol transport is provided by the fact that topical or systemic administration of glycerol was found to correct the skin deficiencies in AQP3 $-/-$ mice [84].

4.2. Urea transport

Urea is produced in the liver (as a non-toxic carrier of waste nitrogen) from ammonia, which is a neurotoxic product of protein degradation. Ammonia causes cell death of astrocytes by stimulating the mitochondrial permeability transition [85] (opening of promiscuous mitochondrial membrane channels that leads to apoptosis or necrosis, depending on cellular ATP availability [86]), although the mechanism by which this happens is not clear. An adult human excretes about 25 g/day of urea in the urine, and urea transport in the kidney is vital for the urinary concentrating mechanism [87]. The physiological roles of urea transport by AQPs are less clear than those of water and glycerol transport.

4.2.1. Which mammalian AQPs are urea channels?

AQPs 7 [27], 9 [88] and 10 [33] have been shown to be urea permeable and there is a consensus in the literature on the urea permeability of these AQPs. For example, AQP9 is a urea channel in the liver expressed in hepatocytes at the sinusoidal surface. Urea permeability measurements performed on mouse hepatocyte plasma membrane vesicles of AQP9 $-/-$ and urea transporter type A1/3 (UT-A1/3) $-/-$ mice showed that AQP9 contributes ~30% to mouse hepatocyte membrane permeability and a member(s) of the UT-A family contributes ~40% [91]. However, AQP9 $-/-$ mice did not demonstrate any deficiency in urea clearance from hepatocytes in a state that promotes elevated hepatic urea production (high protein diet), suggesting that AQP9 and UT-A provide redundant pathways for urea transport from hepatocytes to the blood.

However, there is conflicting evidence in the literature on whether AQPs 3 and 8 are urea channels. Early work on AQP3 suggested that rat AQP3 was urea permeable, with expression of AQP3 in *Xenopus* oocytes increasing urea uptake twofold after 30 minute incubations of oocytes with radiolabelled urea [89] or threefold in oocyte swelling assays [18]. Further studies on rat AQP3 found no urea transport using similar oocyte volumetric techniques [15,17]. These studies differed in that the former used 165 mM urea whereas the latter two used 20 mM urea. It may be that AQP3 urea transport is so slow that at 20 mM it does not induce large enough volume changes to be measured on the timescale of an oocyte swelling experiment (~1 min), or that the transport is non-linear, although this seems unlikely given the linear nature of water and glycerol transport by AQP3 [90].

In one study, human AQP3 was used a positive control for AQP urea permeability. 1 mM of urea was added to AQP3-expressing oocytes and after a 10 minute incubation, the oocytes had an intracellular urea concentration of ~75 μ M (assuming an oocyte volume of 1 μ L) [19]. This is ~10% of the expected equilibrium value, and the fact that it is still so far from equilibrium even after 10 min suggests that urea transport through AQP3, whilst non-zero, is very slow. This may explain the different results between short (typically ~1 min) volumetric experiments and the longer timescale radiolabelled solute uptake experiments.

Early work on mouse AQP8 suggested that it was urea permeable [30], whereas rat AQP8 was not [29], both using radiolabelled solute uptake measurements in *Xenopus* oocytes. Work on purified rat, mouse and human AQP8 in proteoliposomes suggested that neither rat nor

human AQP8 were urea permeable [28]. This study did not report mouse urea permeability due to liposome swelling discrepancies, probably caused by the ionic detergent required to solubilize mouse AQP8.

There is considerable interspecies amino acid sequence variability for AQP8 (e.g. 74% identity between human and mouse AQP8, c.f. 94% for AQP1 and 93% for AQP4). Interestingly, one difference between human and mouse AQP8 is a residue that is predicted to be pore-lining (based on a homology model to bovine AQP0 [28]) and situated at the ar/R filter, G207 (in human; A205 in mouse). The idea of species-specific differences in permeability of AQP8 is intriguing, but studies performed in parallel in the same experimental system are required to validate this.

4.3. Ammonia transport

Ammonia is produced as a by-product of protein breakdown and quickly converted to urea via the hepatic urea cycle to prevent ammonia neurotoxicity. It is important for control of acid–base balance in the kidney, where ammonia synthesis and excretion are tightly regulated and change in response to acid- or alkalosis [92].

Members of the GLP subfamily, AQPs 3 [17], 7 [16] and 9 [17], have been reported to be permeable to ammonia, as has AQP8 [17,93]. There is also evidence of ammonia permeability of AQPs 1, 6 and 7 using microelectrode measurements of oocyte surface pH [16]. The physiological relevance of ammonia permeability of AQPs is unclear.

AQP8 $-/-$ mice have only the very mild phenotypic abnormality of slight hypertriglyceridaemia after three weeks on a high (50%) fat diet [94]. AQP8 is expressed in the inner mitochondrial membrane of hepatocytes [95] and increased the transport of an ammonia analogue into AQP8-expressing *Saccharomyces cerevisiae* and rat hepatocyte mitochondria by three-fold. However, AQP8 $-/-$ mice do not show any impairment in ammonia clearance under physiological conditions or when chronically or acutely loaded with ammonia [96]. This suggests a secondary (non-AQP) pathway for ammonia, which either provides the majority of ammonia permeability in these tissues, or is up-regulated in ammonia-permeable AQP knockouts. The proteins associated with the Rhesus (Rh) blood group system have been shown to function as ammonia channels [97]. Several of these are expressed in the liver [98] (RhB and RhC) and the kidneys (again RhB and RhC), where ammonia has an important role in acid–base balance [99]. Rh $-/-$ mice have been generated, however these studies have focused on the erythrocytic Rh proteins [100,101]. Phenotype analysis of RhB and RhC $-/-$ organisms and double AQP/Rh knockouts could provide an answer. Knockdown of AQP8 in primary rat hepatocytes by ~80% reduced ammonium chloride-induced ureagenesis by 30% and abolished glucagon-stimulated increases in ureagenesis [102]. AQP8 knockdown in a human proximal tubule cell line decreased the rate of ammonia excretion by 31% at pH 7.4 and by 90% at pH 6.9 [103], suggesting that AQP8 ammonia permeability might be required for renal ammonia excretion and be involved in the renal adaptive response to acidosis. Furthermore, acid-induced downregulation of AQP8 by 30% in primary rat hepatocytes was correlated with a 31% reduction in hepatocyte ureagenesis, and AQP8 downregulation was correlated with reduced liver urea content in rats subjected to seven days of acidosis [104]. These data support the idea of a physiological role for AQP8 in either plasma membrane diffusion of ammonia, mitochondrial ammonia transport, or both in support of renal and hepatic ammonia handling.

AQP3 $-/-$ mice have several physiological abnormalities including reduced skin elasticity [80] and polyuria [105], but these can all be explained in terms of reduced glycerol and water permeability, so it is unclear whether AQP3 ammonia permeability has any physiological function.

AQP7 is present in adipocytes. It has been shown in humans that during intense exercise, adipose tissue removes ammonia from the plasma and increases its glutamine/glutamate ratio [106], suggesting

incorporation of ammonia into glutamine through glutamine synthase as a secondary detoxification pathway in support of the hepatic urea cycle at times of elevated plasma ammonia. Whether AQP7 contributes to this ammonia uptake is yet to be investigated.

4.4. Carbon dioxide transport

The majority of carbon dioxide (CO_2) produced by cellular metabolism (~70%) is transported to the lungs for expulsion from the body via the bicarbonate (HCO_3^-) system. Briefly, carbon dioxide diffuses out of the cells in which it is produced and into the plasma. It moves down its concentration gradient into erythrocytes (red blood cells), where carbonic anhydrase catalyses conversion into carbonic acid. Upon dissociation ($\text{H}_2\text{CO}_3 \rightarrow \text{H}^+ + \text{HCO}_3^-$), the HCO_3^- ion is exchanged across the erythrocyte membrane for a chloride ion and the proton binds to haemoglobin [87].

There has been speculation that CO_2 transport across the plasma membrane of erythrocytes might be aided by channel proteins [107, 108]. There is conflicting data on whether an AQP contributes to this potential CO_2 pathway. AQP1 is expressed at the plasma membrane of erythrocytes [109]. Human AQP1 has been reported to increase the CO_2 permeability of *Xenopus* oocytes four-fold in the presence of carbonic anhydrase suggesting that AQP1 functions as a CO_2 channel [110]. Further work ruled out the possibility of AQP1 increasing the oocyte membrane permeability by altering local lipid composition or structure, interaction between AQP1 and carbonic anhydrase or up-regulating a native CO_2 channel by use of a mercurial AQP1 inhibitor (pCMBS) and the AQP1 C189S mutant, which is insensitive to mercury [111].

AQP1 $-/-$ human erythrocytes (Colton-null cells) retain HCO_3^- permeability, but have a 60% reduction in CO_2 permeability when compared to human erythrocytes expressing AQP1 (i.e. not Colton-null) [112]. However, the CO_2 permeability of AQP1 $-/-$ mouse erythrocytes from AQP1 knockout mice was not different to wild-type [113].

Stopped flow experiments with AQP1 reconstituted into liposomes have also given conflicting results. AQP1 from human blood increased the CO_2 permeability of liposomes four-fold [114], whereas mouse AQP1 showed no increase [113]. This agrees qualitatively with the results from measurements on intact erythrocytes in that human AQP1 appears to increase CO_2 permeability of the membrane, whereas mouse AQP1 does not. This may be due to methodological differences, but it also raises the intriguing possibility that human AQP1 is CO_2 permeable whereas mouse AQP1 is not.

It is possible that if CO_2 permeates AQP1, it does so through the central tetrameric pore rather than the monomeric water pore. Molecular dynamics simulations using a variety of enhanced sampling methods and unbiased simulation consistently suggest that the free energy barrier to permeation of the central, hydrophobic pore of AQP1 is considerably smaller than the barrier to permeation of the water pores [115–117], probably due to the water–protein hydrogen bonds at the selectivity filter and NPA sites that need to be disrupted in order for a CO_2 molecule to traverse the water pore. Simulation of model bilayers suggest that the free energy barrier for passage of CO_2 directly across the membrane is much smaller than for permeation through AQP1, and in this kind of system, AQP expression would probably serve to decrease the CO_2 permeability by reducing the surface area available for diffusion directly across the membrane [115,116]. However, it is not clear how good of a model a single species phospholipid bilayer is for a cellular membrane. It is possible that a simulated bilayer containing a mixture of lipid species along with sterols would display different resistance to CO_2 passage, and biophysical measurements of CO_2 diffusion into artificial lipid vesicles showed that addition of cholesterol could reduce membrane CO_2 permeability by up to 100-fold [118]. This agrees qualitatively with MD simulations that include cholesterol [119]. In addition to CO_2 , MD simulations have also suggested that the central pore could be permeable to molecular oxygen [115] and there is some

evidence that AQP1 overexpression could accelerate cellular hypoxia [120], although whether this was a direct or indirect effect was not clear.

It seems apparent that AQP1 can conduct CO₂ (possibly along with AQP0, 5, 6 and 9 and the M23 isoform of AQP4 [16]), however the physiological relevance (if any) of AQP CO₂ permeability is yet to be demonstrated. There is also a similar debate in the plant AQP field on whether AQPs might contribute to regulating CO₂ levels for photosynthesis [121]. A recent review dedicated to AQPs and CO₂ permeability of biological membranes [122] concluded that “the debate about the mechanism of membrane CO₂ diffusion continues and it is difficult to draw general conclusions”. This is still very much an open question.

4.5. Hydrogen peroxide transport

Superoxide (O₂⁻) molecules are produced in the mitochondria as a by-product of ATP synthesis (particularly by complexes I and III in the electron transport chain) and by the NADPH oxidase (NOX) family of enzyme complexes, which couple intracellular oxidation of NADPH to extracellular production of superoxide (O₂⁻) molecules. High levels of reactive oxygen species (ROS) derived from these pathways are well known to cause cellular damage and even death and mitochondrial ROS were long considered to be purely harmful by-products of an imperfect metabolic system. However, work in the last decade has shown that they are crucial for a variety of physiological processes including adaptation to hypoxia, immune function and regulation of autophagy (probably mediated by redox modification of cysteine residues) [123], so clearly there is a need for tight regulation of ROS levels. Superoxide undergoes disproportionation to molecular oxygen and hydrogen peroxide (H₂O₂), which can be catalysed by the enzyme superoxide dismutase [124], and the highly reactive H₂O₂ can then go on to form a variety of further ROS.

H₂O₂ and H₂O have similar molecular sizes, dipole moments and hydrogen bonding capacities [125], therefore it would not be surprising to find that some AQPs could transport H₂O₂. The half-life for H₂O₂ in cells is very short (e.g. ~1 ms in lymphocytes [126]), making biophysical experiments of the kind used for e.g. glycerol or urea permeation very difficult. Growth assays using H₂O₂ transport-deficient yeast are typically used, and reduced growth after expression of an AQP is interpreted as an AQP-mediated increase in membrane H₂O₂ permeability causing cellular damage and/or metabolic disruption. Using this technique, human AQP8, rat (but not human) AQP1 and several mutants thereof were shown to be H₂O₂ permeable [127]. Based on this data, the authors suggested that all AQPs function as H₂O₂ channels. It is not clear whether this is a valid generalization, but clearly some mammalian AQPs are H₂O₂ channels.

Imaging studies using a novel H₂O₂ sensitive fluorescent dye in transiently transfected HEK293 cells demonstrated H₂O₂ permeability for human AQP8 and AQP3 (but not AQP1). Furthermore, AQP3 overexpression in HeLa cells allowed the cells to respond to serum starvation via ROS mediated activation of the AKT (protein kinase B) signalling pathway, whereas cells not expressing AQP3 could not. Knockdown of AQP3 in a colon cancer cell line inhibited the AKT response to epidermal growth factor (EGF) [128], which can initiate ROS signalling via activation of NOX complexes. This suggests that AQP3 is required for uptake of NOX-generated H₂O₂ in EGF signalling.

T cell migration along chemokine gradients is vital for correct immune responses. T cells from AQP3^{-/-} mice had 40–60% reductions in migration distance in response to a variety of chemokines and had a ~50% reduction in chemokine-induced transendothelial migration. Activation of Cdc42, a small GTPase involved in cytoskeletal reorganization associated with chemotaxis, was completely inhibited in the AQP3^{-/-} cells. Treatment with extracellular catalase, which catalyses H₂O₂ breakdown to H₂O and O₂, prevented the Cdc42 response in AQP3^{+/+} cells and treatment with high concentration (100 μM) of exogenous H₂O₂ recovered both the Cdc42 response and the T cell migration in AQP3^{-/-} cells [129]. Together, these data suggest that AQP3 is

required for uptake of extracellular H₂O₂ (probably NOX-generated) in the T cell chemotactic response.

Intracellular ROS levels can be elevated in leukaemia cells and NOX-derived ROS can activate leukaemia cell survival pathways. In a leukaemia cell line, shRNA-mediated knockdown of AQP8 reduced and overexpression increased intracellular H₂O₂ content as well as H₂O₂ uptake after 10 min in 100 μM H₂O₂. Furthermore, cellular glucose uptake and proliferation were correlated with intracellular H₂O₂ and AQP8 expression [130], suggesting that AQP8 can facilitate increased metabolism and proliferation in leukaemia.

AQP8 is also expressed in inner mitochondrial membranes (IMM) in hepatocytes. Knockdown of AQP8 by 60% using siRNA in a hepatocyte cell line caused a twofold increase in mitochondrial ROS concentration and a 45% decrease in H₂O₂ output in isolated mitochondria. This was correlated with an 80% depolarization of the mitochondrial membrane, which was reversible by cyclosporin A (an inhibitor of the mitochondrial permeability transition) or a mitochondrial antioxidant, and a ~30% reduction in cell viability [131]. This suggests that AQP8-mediated H₂O₂ release from hepatic mitochondria acts as a mechanism to minimise mitochondrial oxidative stress.

AQP11 is localised to the ER in the renal proximal tubule. The C227S mutation of AQP11 caused proximal tubule injury and eventual renal failure in mice [132]. Mice heterozygous for the AQP11 C227S mutant were predisposed to glucose-induced accumulation of ROS in the proximal tubule and reduction of kidney function. Inhibition of glucose uptake by the non-specific inhibitor phlorizin or antioxidant (sulforaphane) treatment was able to protect kidney function. This effect was reproduced in a proximal tubule cell line, in which siRNA-mediated knockdown of AQP11 increased intracellular ROS concentration twofold in the absence of glucose and fourfold in the presence of glucose [133]. It is not clear whether AQP11 was controlling intracellular ROS accumulation by acting as an ER H₂O₂ channel, or whether this was an indirect effect.

Taken together, these examples provide clear evidence for AQP-mediated H₂O₂ membrane permeability and suggest physiological roles in redox signalling via uptake of NOX-derived H₂O₂ and in cellular mechanisms for minimizing oxidative stress.

A recent review of H₂O₂ permeability of AQPs suggested that rat AQP1 may be permeable to H₂O₂ whereas human AQP1 is not [134]. The authors of the cited study [127] suggest that the difference is due to differences in plasma membrane localization, although surface expression was not measured directly. This difference is particularly interesting given the speculation that we made regarding differences in CO₂ permeability between human and mouse AQP1 and the possible differences in AQP8 urea permeability between species and raises the important point that despite high levels of conservation between AQPs from different mammals, they are not exactly the same proteins (e.g. rAQP1 and hAQP1 differ by 18 residues), and direct comparison between AQPs from different mammals in different experimental systems may not always be appropriate.

5. The physiological role of AQP6: an unusual AQP

AQP6 is expressed primarily in kidney epithelia, where it is expressed only in intracellular membranes. Immunostaining was observed in podocyte intracellular vesicles, sub-apical vesicles in straight proximal tubule cells, and in both sub-apical and sub-basolateral domains within type A (acid-secreting) intercalated cells in the collecting duct [135].

AQP6 has low intrinsic water permeability: The membrane water permeability of *Xenopus* oocytes expressing AQP6 was increased less than threefold [22,136], and in some experiments, not at all [25,26]. In contrast to other members of the AQP family, mercury increases rather than inhibits AQP6 water permeability, which is reversibly increased approximately tenfold upon HgCl₂ application. Low pH activated a reversible anion permeability of AQP6 [22] which was also shown to be

~tenfold more permeable to nitrate than chloride [137]. In rat collecting duct, intercalated cells, AQP6 co-localises with H⁺-ATPase in intracellular vesicles [22], and in the intercalated cells of alkali-loaded rats, AQP6 mRNA and protein levels increased after a week [138]. These results, along with the pH-activation of AQP6 water and anion permeability suggest involvement of AQP6 in acid–base balance in the renal collecting duct. However the lack of *in vivo* experiments with AQP6 knockouts or naturally occurring mutations precludes any meaningful conclusions about the physiological roles of AQP6.

6. Ion permeability of AQPs: an unresolved controversy

AQPs support bulk movements of fluid by giving high water permeability to membranes that secrete osmolytes. These osmolytes are often ions (e.g. Na⁺, K⁺ and Cl⁻) and this is reflected in the fact that several AQPs form macromolecular complexes with ion channels and transporters [41]. Perhaps a more efficient way for nature to achieve this dual permeability would be to have both ions and water pass through the same channel. Indeed it has been observed that several ion channels can transport water [38], but it has also been suggested that some AQPs may function as ion channels.

The pH-sensitive ion permeability of AQP6 is well established, and it is likely that the monomeric pore is the ion pathway given that a point mutation to a pore-lining residue of AQP6 abolished ion permeability [137] and AQP6-mimicking mutations of a pore-lining amino acid residue of AQP5 conferred anion permeability [139]. There is also some evidence that the plant AQP nodulin-26 from soybean can act as a voltage-gated, anion-biased ion channel [140,141].

More controversial is the idea that the fifth pore formed at the four-fold axis of the tetramer of AQP1 may function as a cation channel. In *Xenopus* oocytes, heterologous expression of human AQP1 led to a PKA-activated cation permeability probably mediated by phosphorylation of AQP1 [142] and a cGMP-activated cation permeability via direct binding of cGMP to the C-terminus of AQP1 [143]. PKC activity was shown to increase the cation permeability of AQP1 in *Xenopus* oocytes via direct phosphorylation of AQP1 at residues T157 and T239 [144]. We recently showed that phosphorylation at these sites by PKC is required for trigger-induced translocation of AQP1 to the plasma membrane [145], so this may represent more AQP1 molecules in the membrane rather than an increase in the cation permeability or open probability of a single channel. Phosphorylation of a tyrosine residue (Y253) in the C-terminal tail of AQP1 was recently shown to be required for activation by cGMP [146]. The cGMP-activated cation current was verified for purified AQP1 in planar artificial membranes and the AQP1 water permeability inhibitor pCMBS did not inhibit ion permeation, suggesting that the water and ion pathways through AQP1 are not the same [147]. Furthermore, point mutations to residues lining the tetrameric pore altered conductance properties [146]. The open probability was found to be very small (<10⁻⁶) in the planar bilayer system [147], which raises doubts over the physiological relevance of this cation conductance. This study suggested that this very low probability could reflect a misfolding or protein degradation artefact rather than a “real” function of AQP1. Furthermore, human AQP1 expressed in HEK293 cells did not induce an above-background cation conductance when cells were loaded with either cGMP or analogues thereof [148]. Additionally, after the initial report of AQP1 cation permeability by Yool et al., several laboratories reported being unable to replicate this result in the same experimental system (and in some cases, with exactly the same AQP1 construct) [149]. High variability in oocyte response to forskolin was also reported. It was suggested that the discrepancy could be due the protocol for choosing ‘healthy’ oocytes on which to perform experiments. A cut-off for oocyte membrane potential is routinely used for this. Yool et al. choose oocytes with a potential <- 20 mV, whereas others used a - 35 mV cut-off. If AQP1 does indeed act as a cation channel it is plausible that it could cause a slight

depolarization, leading to oocytes in which AQP1 is acting as an ion channel to be falsely excluded as unhealthy.

Rat choroid plexus cells, which strongly express AQP1, were found to have a cGMP-activated cation conductance that was abolished by treatment with AQP1 siRNA. Activation of the current by atrial natriuretic peptide (ANP), which signals through guanylate cyclase, inhibited basal-to-apical fluid transport. The contribution of AQP1 to this inhibition was not confirmed directly, although Cd²⁺, which was shown to inhibit cGMP-induced cation conduction of AQP1, reversed the inhibition of fluid transport [150]. ANP and a cGMP analogue were also shown to upregulate apical-to-basal fluid transport in cultured retinal pigment epithelial cells, but this was reversed by an inhibitor of AQP1 water permeability [151].

It is clear that, under the right set of circumstances, AQP1 can act as a cation channel, with the ion pathway probably residing in the central pore formed by tetrameric assembly. Whether or not this ion conductance has physiological relevance remains an open question. However, coupled water and ion movement are vital for several pathophysiological processes including tumour angiogenesis and cell migration [152] and epilepsy [153], so it remains an intriguing possibility that AQPs are performing a dual function.

7. Cell volume regulation by AQPs

Many cells have the ability to modulate their physical size. This is achieved by the import or export of osmolytes in order to move water into or out of the cell by osmosis. Regulatory cell volume decrease (RVD) is mediated by potassium chloride and taurine efflux and regulatory cell volume increase (RVI) by sodium influx [154]. AQPs play a role in mediating the osmotic water movement in cell volume regulation [155], but there is some evidence that their role may go beyond acting as a passive water pore.

The stretch-activated transient receptor potential vanilloid type 4 (TRPV4) channel is a Ca²⁺-biased non-selective cation channel (NSCC) that is activated by cell swelling [156] and has been implicated in cellular responses to osmotic stimuli [157]. In some cell types TRPV4 has been shown to provide a Ca²⁺ signal that is correlated with activation of the K⁺ and Cl⁻ channels responsible for the decrease in cellular osmolality associated with RVD [157,158]. In human and murine salivary gland cells, TRPV4 has a functional interaction with AQP5; in AQP5 knockout cells, the hypotonicity-induced calcium influx through TRPV4 was attenuated and subsequent RVD was abolished. Hypotonicity also increased cell surface expression of both TRPV4 and AQP5 and increased their co-localisation [159]. This suggests a role for AQP5 in the regulation of TRPV4 surface expression or hypotonicity-induced activity.

In another example, the RVD of sperm of AQP3^{-/-} mice was inhibited compared to wild-type mice and the mice displayed reduced fertility [160] [161]. Upon entry into the female reproductive tract, sperm normally encounter a decrease in extracellular osmolality, which is thought to be the signal that activates sperm motility [160]. However, this hypotonic stress also causes cell swelling which, if left uncorrected by RVD, leads to impaired fertilisation, likely due to excessive bending of the sperm tail inside the uterus [161]. If AQP3 was simply acting passively as a water channel, RVD would not be abolished in AQP3^{-/-} sperm but rather the timescale on which the cell reaches osmotic equilibrium would be increased. A possible explanation for reduced fertility and altered RVD in AQP3^{-/-} mice is therefore that AQP3, either alone or as part of a macromolecular complex which is disrupted by AQP3 knockout, is involved in the signalling pathway that activates RVD in sperm.

In a further example, when exposed to a hypotonic extracellular solution, cultured renal cortical collecting duct (CCD) cells, which do not endogenously express AQP2, swelled in proportion to the change in extracellular osmolality but did not exhibit RVD. However, when transfected with AQP2, these cells showed an RVD of approximately

40%. Shrinkage was mediated by Ca^{2+} influx through TRPV4, which activated Ca^{2+} -dependent K^+ and Cl^- channels and Ca^{2+} -dependent Ca^{2+} release from intracellular stores. In renal CCD cells expressing AQP2, hypotonic stress caused translocation of TRPV4 to the plasma membrane. This response did not occur in AQP2-negative cells. When TRPV4 was pre-translocated to the cell surface prior to hypotonic exposure, RVD was recovered in AQP2-null cells, showing that it is not simply the high water permeability of AQP2 that allows RVD. However, there did not appear to be any co-localisation between endogenous TRPV4 and overexpressed AQP2 in this system, either before or after hypotonic shock, indicating a functional rather than physical interaction [162]. These observations suggest that AQP2 forms part of a sensory and signalling pathway that results in TRPV4 translocation, possibly via sensing of extracellular osmolality.

In a nasopharyngeal cancer cell line, swelling-induced chloride currents could be inhibited by siRNA-mediated knockdown of AQP3, extracellular application of CuCl_2 (a non-specific AQP3 inhibitor) or injection of AQP3 antibodies via recording pipettes. AQP3 also co-immunoprecipitated with the CIC3 chloride channel in this system [163]. The effect of the current-inhibiting treatments on AQP3-CIC3 interaction or CIC3 subcellular localization was not investigated, but this data suggests a role for AQP3 in RVD chloride efflux in these cells, possibly mediated via activation or localization of the CIC3 chloride channel.

It has been suggested that AQPs could act as direct sensors of osmotic gradients by coupling conformational changes of the protein to a pressure gradient within the pore [164]. This argument relies on the idea of the hydrostatic pressure within the pore and it is not clear that the application of classical fluid mechanics is applicable to a system typically consisting of < 10 water molecules. Nonetheless it is an intriguing idea, and taken together, these examples clearly support the idea of a signalling or sensory role for AQPs in cell volume regulation beyond a passive water conduction mechanism.

8. Regulation of membrane protein localization by AQPs

There is some evidence that the expression of one AQP can regulate the expression, localization or membrane trafficking of other AQPs and of other membrane proteins.

AQP3 $-/-$ mice have polyuria and a urinary concentrating defect. In the cortical collecting ducts of knockout mice, apical AQP2 expression was reduced compared to controls and basolateral AQP4 localization was completely absent. In contrast, medullary collecting duct levels of both AQP2 and AQP4 was not different between wild-type and AQP3 $-/-$ mice [105]. This may reflect a requirement of AQP3 for expression or trafficking of AQPs 2 and 4 in certain cell types, although these observations could also be due to regulation of AQPs 2 and 4 in response to the polyuria phenotype.

AQP11 $-/-$ mice develop polycystic kidney disease (PKD). In AQP11 $-/-$ mice, polycystin 1 (PC1), a protein to which loss of function mutations are associated with autosomal dominant PKD, was upregulated twofold. However, the plasma membrane localization of PC1 was almost completely abolished and PC1 was differentially glycosylated in the AQP11 $-/-$ mice compared to AQP11 $+/+$ [165]. Glycosylation of some membrane proteins is a crucial step in protein folding and passage through the ER quality control system [166]. Other membrane proteins (AQP1 and PC2) were correctly glycosylated, suggesting that this was a PC1 specific effect. This data suggests that AQP11 can regulate the surface expression of PC1, possibly by mediating an interaction with a glycosyltransferase or part of the ER quality control system.

The interactions between the stretch-activated cation channel TRPV4 and both AQP2 and AQP5 has been discussed in Section 6. Briefly, expression of these AQPs was required for the hypotonicity-induced translocation of TRPV4 to the plasma membrane associated with RVD [159,162]. It may be that in these systems, AQPs and TRPV4 are present in the same vesicles, but the trafficking machinery interacts only with

the AQP. We have recently described hypotonicity-induced translocation of AQP1 in HEK293 cells [145] and AQP4 in primary rat astrocytes [167], so this may reflect a general regulatory mechanism by which AQPs can mediate the subcellular localization of other membrane proteins.

The histone methyltransferase Dot1a was shown to inhibit the expression of AQP5 in murine renal cells. Knocking out Dot1a led to AQP5 expression in these cells. The total level of AQP2 expression was unchanged in the presence of AQP5, but AQP2 membrane trafficking was impaired. In addition to this, co-transfection of AQP5 and AQP2 into IMCD3 cells reduced AQP2 surface expression compared to transfection of AQP2 alone, suggesting that AQP5 can regulate AQP2 localization. Furthermore, AQP2 and AQP5 co-immunoprecipitated with one another, suggesting a direct physical interaction [168]. The stoichiometry of the AQP2/AQP5 complexes was not investigated, so it is not clear whether the interaction was between AQP2 and AQP5 homotetramers, or through the formation of AQP2/AQP5 heterotetramers (which is an established regulatory mechanism employed by some plant AQPs [169]).

9. AQPs and cell–cell adhesion

Adhesion of cells to one another is a vital process that paved the way for evolution of multicellular organisms, and allows for the formation of the varied and complex structures that make up the anatomy of modern animals and plants.

There is evidence that some AQPs can perform a cell–cell adhesion function by forming a direct interaction with a membrane component on an adjacent cell (possibly another AQP molecule). This is well established for AQP0 and there is controversial evidence that AQP4 may also be able to perform this function.

9.1. AQP0

AQP0 (also called MIP, for lens Membrane Intrinsic Protein) is expressed primarily in lens fibre cells, which are cells of the eye specialized to form a tightly-packed transparent layer that scatters a minimal amount of incident light to support the function of the eye [8]. It is the most highly expressed membrane protein in these cells (45% by molarity of all lens fibre membrane protein in mice [170]). AQP0 tetramers assemble into large arrays in junctional microdomains [171], which dynamically associate and dissociate at the array edges, with only an estimated 1% existing as free tetramers at a given time, measured by high-speed atomic force microscopy of isolated sheep lens fibre membranes [172].

Knockout studies and a variety of naturally-occurring AQP0 mutations in humans and mice [8] consistently show that loss of AQP0 function in the lens fibre cells causes cataracts, likely via loss of the tight packing of the cells required to minimise light scattering. It has also been suggested, based on analysis of lenses of AQP0 $-/-$ and $-/+$ mice, that AQP0 is vital for creating the lens refractive index gradient required to minimise spherical aberration, via an unknown mechanism [173].

A qualitative analysis of lens fibre cell–cell adhesion in AQP0 $-/-$ mice showed that transgenic expression of AQP1 in the AQP0 $-/-$ model could not rescue fibre adhesion [4], nor correct lens transparency defects [174], supporting the idea that the role of AQP0 in lens physiology is not related to membrane water permeability. Furthermore, expression of AQP0 in several in vitro model systems consistently shows that it is able to mediate cell–cell adhesion [175].

Early biophysical work on AQP0 proteoliposomes showed that AQP0 is able to mediate interactions with membranes containing negatively charged lipids [176]. It was suggested that this is due to the presence of several positively charged (and no negatively charged) residues in the extracellular loops A, C and E of AQP0. In human AQP0 this positively charged surface is made up of two arginine residues (R33 and R113) and three histidine residues (H40, H122 and H201).

A naturally occurring AQP0 mutation, R33C, showed a reduction in cell–cell adhesion of 18, 27 or 34% (depending on methodology) for the mutant when compared to wild-type AQP0, despite no effect on membrane localization [177]. This suggests that removal of the conserved positive charge in loop A has a deleterious effect on AQP0-mediated cell adhesion, supporting the idea of a positively charged face of AQP0 that forms electrostatic interactions with negatively charged molecules on an adjacent membrane. It is also possible that addition of the cysteine sulfhydryl group facilitates a novel post-translational modification that inhibits adhesive interactions.

Crystallographic analyses of AQP0 suggest a different model of AQP0 mediated cell–cell adhesion in which AQP0 molecules on adjacent cells interact with one another directly. An electron crystal structure of double-layered 2D AQP0 crystals suggested that two AQP0 molecules on adjacent membranes might be able to form an interaction via their extracellular loops, primarily mediated by proline residues [178]. Follow-up work showed that the way in which the AQP0 extracellular domains (ECDs) interact in these crystals is strongly dependent on the headgroup of co-crystallized lipids [179]. It has been suggested, based on comparison of the electron structure with a 3D X-ray structure of full-length AQP0 [180], that a conformational change in loop A induced by proteolytic truncation of the C-terminus (which is observed in vivo [8]) could facilitate direct binding of AQP0 molecules to one another [181]. However biochemical analysis showed that truncation of either the N- or C-terminus has no effect on the adhesion properties of AQP0 [182].

Experiments with a fusion protein consisting of the sequences of the three extracellular loops of AQP0 fused directly adjacent to one another showed that this protein was able to competitively inhibit AQP0 mediated cell–cell adhesion [183]. Given the relative location of the three loops in the AQP0 fold and the lack of transmembrane anchoring in the fusion protein, it is very unlikely that this protein is structurally similar to the ECD of intact AQP0. The fact that, despite this, it functions as an inhibitor of AQP0 mediated cell–cell adhesion does not support the idea of the adhesion being mediated by direct AQP0–AQP0 binding, which would depend on the structure of the ECD. It does, however, support the idea of mediation via an (structure independent) electrostatic interaction between the positively charged AQP0 ECD and a negatively charged membrane component on an adjacent cell.

9.2. AQP4

AQP4 is a water-selective AQP primarily expressed in glial cells (astrocytes and retinal Müller cells) of the central nervous system and the basolateral membranes of kidney collecting duct cells [155]. AQP4 exists in two major isoforms (although there is emerging evidence of further isoforms [184]). These are the long (323 amino acids) M1 isoform and the shorter (301 amino acids) M23 isoform, named for the position of the N-terminal methionine. Similarly to AQP0, the M23 isoform of AQP4 is able to form large supramolecular arrays (termed OAPs for Orthogonal Array of Particles).

Electron crystallography of double-layered 2D AQP4-M23 crystals suggested that AQP4 molecules on adjacent cells could interact via their ECDs in a similar way to that suggested for AQP0, again mediated by interaction between proline residues [185]. In the same study, AQP4-M23 was shown to facilitate cell–cell interactions between adhesion-deficient mouse fibroblasts. This result was corroborated in a similar experimental system, and it was shown that the adhesion generated by AQP4-M23 was considerably weaker than that by AQP0. Furthermore, AQP4-M1 was shown not to facilitate adhesion [175]. Another study in the same experimental system failed to reproduce these results and furthermore failed to find AQP4-mediated adhesion in primary mouse glia or AQP4-transfected CHO cell membrane vesicles [186].

Transfection of AQP4-M23 into a glioblastoma cell line (D54, which lacks endogenous AQP4 expression) increased adhesion of the cells to collagen, fibronectin, laminin, and vitronectin substrates [187]. Clearly

this is not due to any potential cell–cell adhesion properties of AQP4 and the lack of substrate specificity makes this a difficult result to interpret. However, AQP4-M23 was shown to preferentially localise to membrane–substrate adhesion sites [188], so it is possible that AQP4-M23 could facilitate aggregation or localization of adhesion molecules, thereby having an indirect effect on cellular adhesion, both to other cells and to basement membrane components.

10. Conclusion

Mammalian AQPs are primarily known as facilitators of physiological processes through bi-directional, passive water transport. We have reviewed evidence demonstrating that this is far from all they do. AQPs facilitate physiological processes by mediating the diffusion of small, neutral solutes. This is best understood for AQP-mediated glycerol transport that facilitates glycerol metabolism, triglyceride cycling and skin hydration. AQPs also have a role in cell volume regulation and it is becoming increasingly clear that this role can extend beyond simply acting as a passive water pore and may involve AQP-mediated signal transduction, although the mechanisms that may be involved in this are not well understood. Many cell types express several different members of the AQP family and there is emerging evidence that the different members can interact with one another either physically or functionally. The involvement of AQPs in human physiology and cellular homeostasis goes far beyond their acting as simple water pores with implications for a range of physiological processes and pathophysiological conditions.

Transparency Document

The [Transparency document](#) associated with this article can be found, in online version.

Acknowledgements

This work was supported by the Engineering and Physical Sciences Research Council via a Molecular Organisation and Assembly in Cells Doctoral Training Centre studentship to PK (grant no: EP/F500378/1). RMB acknowledges funding from the Biotechnology and Biological Sciences Research Council (BBSRC; via grants BB/I019960/1, BB/K013319/1 and BB/L502194/1) and the Innovative Medicines Joint Undertaking under Grant Agreement no. 115583 to the ND4BB ENABLE Consortium.

References

- [1] M.L. Kortenoeven, R.A. Fenton, Renal aquaporins and water balance disorders, *Biochim. Biophys. Acta* 1840 (2014) 1533–1549.
- [2] E.A. Nagelhus, O.P. Ottersen, Physiological roles of aquaporin-4 in brain, *Physiol. Rev.* 93 (2013) 1543–1562.
- [3] J. Lebeck, Metabolic impact of the glycerol channels AQP7 and AQP9 in adipose tissue and liver, *J. Mol. Endocrinol.* 52 (2014) R165–R178.
- [4] S.S. Kumari, S. Eswaramoorthy, R.T. Mathias, K. Varadaraj, Unique and analogous functions of aquaporin 0 for fiber cell architecture and ocular lens transparency, *Biochim. Biophys. Acta* 1812 (2011) 1089–1097.
- [5] J. Badaut, A.M. Fukuda, A. Jullienne, K.G. Petry, Aquaporin and brain diseases, *Biochim. Biophys. Acta* 1840 (2014) 1554–1565.
- [6] L.S. King, M. Yasui, P. Agre, Aquaporins in health and disease, *Mol. Med. Today* 6 (2000) 60–65.
- [7] D. Bockenhauer, D.G. Bichet, Pathophysiology, diagnosis and management of nephrogenic diabetes insipidus, *Nat. Rev. Nephrol.* (2015).
- [8] A.B. Chepelinsky, Structural function of MIP/aquaporin 0 in the eye lens; genetic defects lead to congenital inherited cataracts, *Handb. Exp. Pharmacol.* (2009) 265–297.
- [9] A. Madeira, T.F. Moura, G. Soveral, Aquegliceroporins: implications in adipose biology and obesity, *Cell. Mol. Life Sci.* 72 (2015) 759–771.
- [10] J. Wang, L. Feng, Z. Zhu, M. Zheng, D. Wang, Z. Chen, H. Sun, Aquaporins as diagnostic and therapeutic targets in cancer: how far we are? *J. Transl. Med.* 13 (2015) 96.
- [11] D. Ribatti, G. Ranieri, T. Annese, B. Nico, Aquaporins in cancer, *Biochim. Biophys. Acta* 1840 (2014) 1550–1553.
- [12] F. Abascal, I. Irisarri, R. Zardoya, Diversity and evolution of membrane intrinsic proteins, *Biochim. Biophys. Acta* 1840 (2014) 1468–1481.

- [13] B. Yang, A.S. Verkman, Water and glycerol permeabilities of aquaporins 1–5 and MIP determined quantitatively by expression of epitope-tagged constructs in *Xenopus* oocytes, *J. Biol. Chem.* 272 (1997) 16140–16146.
- [14] K.L. Nemeth-Cahalan, K. Kalman, J.E. Hall, Molecular basis of pH and Ca^{2+} regulation of aquaporin water permeability, *J. Gen. Physiol.* 123 (2004) 573–580.
- [15] A.K. Meinild, D.A. Klaerke, T. Zeuthen, Bidirectional water fluxes and specificity for small hydrophilic molecules in aquaporins 0–5, *J. Biol. Chem.* 273 (1998) 32446–32451.
- [16] R.R. Geyer, R. Musa-Aziz, X. Qin, W.F. Boron, Relative CO_2/NH_3 selectivities of mammalian aquaporins 0–9, *Am. J. Physiol. Cell Physiol.* 304 (2013) C985–C994.
- [17] L.M. Holm, T.P. Jahn, A.L. Moller, J.K. Schjoerring, D. Ferri, D.A. Klaerke, T. Zeuthen, NH_3 and NH_4^+ permeability in aquaporin-expressing *Xenopus* oocytes, *Pflügers Arch. - Eur. J. Physiol.* 450 (2005) 415–428.
- [18] M. Echevarria, E.E. Windhager, S.S. Tate, G. Frindt, Cloning and expression of AQP3, a water channel from the medullary collecting duct of rat kidney, *Proc. Natl. Acad. Sci. U. S. A.* 91 (1994) 10997–11001.
- [19] A. Herraiz, F. Chauvigne, J. Cerda, X. Belles, M.D. Piulachs, Identification and functional characterization of an ovarian aquaporin from the cockroach *Blattella germanica* L. (Dictyoptera, Blattellidae), *J. Exp. Biol.* 214 (2011) 3630–3638.
- [20] J.S. Jung, R.V. Bhat, G.M. Preston, W.B. Guggino, J.M. Baraban, P. Agre, Molecular characterization of an aquaporin cDNA from brain: candidate osmoreceptor and regulator of water balance, *Proc. Natl. Acad. Sci. U. S. A.* 91 (1994) 13052–13056.
- [21] S. Raina, G.M. Preston, W.B. Guggino, P. Agre, Molecular cloning and characterization of an aquaporin cDNA from salivary, lacrimal, and respiratory tissues, *J. Biol. Chem.* 270 (1995) 1908–1912.
- [22] M. Yasui, A. Hazama, T.H. Kwon, S. Nielsen, W.B. Guggino, P. Agre, Rapid gating and anion permeability of an intracellular aquaporin, *Nature* 402 (1999) 184–187.
- [23] H. Nagase, J. Agren, A. Saito, K. Liu, P. Agre, A. Hazama, M. Yasui, Molecular cloning and characterization of mouse aquaporin 6, *Biochem. Biophys. Res. Commun.* 352 (2007) 12–16.
- [24] A. Hazama, D. Kozono, W.B. Guggino, P. Agre, M. Yasui, Ion permeation of AQP6 water channel protein. Single channel recordings after Hg^{2+} activation, *J. Biol. Chem.* 277 (2002) 29224–29230.
- [25] K. Liu, D. Kozono, Y. Kato, P. Agre, A. Hazama, M. Yasui, Conversion of aquaporin 6 from an anion channel to a water-selective channel by a single amino acid substitution, *Proc. Natl. Acad. Sci. U. S. A.* 102 (2005) 2192–2197.
- [26] L.M. Holm, D.A. Klaerke, T. Zeuthen, Aquaporin 6 is permeable to glycerol and urea, *Pflügers Arch. - Eur. J. Physiol.* 448 (2004) 181–186.
- [27] K. Ishibashi, M. Kuwahara, Y. Gu, Y. Kageyama, A. Tohsaka, F. Suzuki, F. Marumo, S. Sasaki, Cloning and functional expression of a new water channel abundantly expressed in the testis permeable to water, glycerol, and urea, *J. Biol. Chem.* 272 (1997) 20782–20786.
- [28] K. Liu, H. Nagase, C.G. Huang, G. Calamita, P. Agre, Purification and functional characterization of aquaporin-8, *Biol. Cell* 98 (2006) 153–161.
- [29] Y. Koyama, T. Yamamoto, D. Kondo, H. Funaki, E. Yaoita, K. Kawasaki, N. Sato, K. Hatakeyama, I. Kihara, Molecular cloning of a new aquaporin from rat pancreas and liver, *J. Biol. Chem.* 272 (1997) 30329–30333.
- [30] T. Ma, B. Yang, A.S. Verkman, Cloning of a novel water and urea-permeable aquaporin from mouse expressed strongly in colon, placenta, liver, and heart, *Biochem. Biophys. Res. Commun.* 240 (1997) 324–328.
- [31] T.P. Jahn, A.L.B. Moller, T. Zeuthen, L.M. Holm, D.A. Klaerke, B. Mohsin, W. Kuhlbrandt, J.K. Schjoerring, Aquaporin homologues in plants and mammals transport ammonia, *FEBS Lett.* 574 (2004) 31–36.
- [32] J.M. Carbrey, D.A. Gorelick-Feldman, D. Kozono, J. Praetorius, S. Nielsen, P. Agre, Aquaglyceroporin AQP9: solute permeation and metabolic control of expression in liver, *Proc. Natl. Acad. Sci. U. S. A.* 100 (2003) 2945–2950.
- [33] K. Ishibashi, T. Morinaga, M. Kuwahara, S. Sasaki, M. Imai, Cloning and identification of a new member of water channel (AQP10) as an aquaglyceroporin, *Biochim. Biophys. Acta* 1576 (2002) 335–340.
- [34] M. Ikeda, A. Andoo, M. Shimono, N. Takamatsu, A. Taki, K. Muta, W. Matsushita, T. Uechi, T. Matsuzaki, N. Kenmochi, K. Takata, S. Sasaki, K. Ito, K. Ishibashi, The NPC motif of aquaporin-11, unlike the NPA motif of known aquaporins, is essential for full expression of molecular function, *J. Biol. Chem.* 286 (2011) 3342–3350.
- [35] K. Yakata, K. Tani, Y. Fujiyoshi, Water permeability and characterization of aquaporin-11, *J. Struct. Biol.* 174 (2011) 315–320.
- [36] A. Madeira, S. Fernandez-Veledo, M. Camps, A. Zorzano, T.F. Moura, V. Ceperuelo-Mallafre, J. Vendrell, G. Soveral, Human aquaporin-11 is a water and glycerol channel and localizes in the vicinity of lipid droplets in human adipocytes, *Obesity* 22 (2014) 2010–2017.
- [37] U. Kosinska Eriksson, G. Fischer, R. Friemann, G. Enkavi, E. Tajkhorshid, R. Neutze, Subangstrom resolution X-ray structure details aquaporin–water interactions, *Science* 340 (2013) 1346–1349.
- [38] A. Horner, F. Zocher, J. Preiner, N. Ollinger, C. Siligan, S.A. Akimov, P. Pohl, The mobility of single-file water molecules is governed by the number of H-bonds they may form with channel-lining residues, *Sci. Adv.* 1 (2015), e1400083.
- [39] E. Tajkhorshid, P. Nollert, M.O. Jensen, L.J. Miercke, J. O'Connell, R.M. Stroud, K. Schulten, Control of the selectivity of the aquaporin water channel family by global orientational tuning, *Science* 296 (2002) 525–530.
- [40] D. Fu, A. Libson, L.J. Miercke, C. Weitzman, P. Nollert, J. Krucinski, R.M. Stroud, Structure of a glycerol-conducting channel and the basis for its selectivity, *Science* 290 (2000) 481–486.
- [41] J. Sjöhamn, K. Hedfalk, Unraveling aquaporin interaction partners, *Biochim. Biophys. Acta* 1840 (2014) 1614–1623.
- [42] A. Frick, U.K. Eriksson, F. de Mattia, F. Oberg, K. Hedfalk, R. Neutze, W.J. de Grip, P.M. Deen, S. Tornroth-Horsefield, X-ray structure of human aquaporin 2 and its implications for nephrogenic diabetes insipidus and trafficking, *Proc. Natl. Acad. Sci. U. S. A.* 111 (2014) 6305–6310.
- [43] J.D. Ho, R. Yeh, A. Sandstrom, I. Chorny, W.E. Harries, R.A. Robbins, L.J. Miercke, R.M. Stroud, Crystal structure of human aquaporin 4 at 1.8 Å and its mechanism of conductance, *Proc. Natl. Acad. Sci. U. S. A.* 106 (2009) 7437–7442.
- [44] J. Jiang, B.V. Daniels, D. Fu, Crystal structure of AqpZ tetramer reveals two distinct Arg-189 conformations associated with water permeation through the narrowest constriction of the water-conducting channel, *J. Biol. Chem.* 281 (2006) 454–460.
- [45] T. Watz, T. Hirai, K. Murata, J.B. Heymann, K. Mitsuoka, Y. Fujiyoshi, B.L. Smith, P. Agre, A. Engel, The three-dimensional structure of aquaporin-1, *Nature* 387 (1997) 624–627.
- [46] M.J. Borgnia, P. Agre, Reconstitution and functional comparison of purified GlpF and AqpZ, the glycerol and water channels from *Escherichia coli*, *Proc. Natl. Acad. Sci. U. S. A.* 98 (2001) 2888–2893.
- [47] N. Roudier, P. Bailly, P. Gane, N. Lucien, R. Gobin, J.P. Cartron, P. Ripoche, Erythroid expression and oligomeric state of the AQP3 protein, *J. Biol. Chem.* 277 (2002) 7664–7669.
- [48] T. Itoh, T. Rai, M. Kuwahara, S.B. Ko, S. Uchida, S. Sasaki, K. Ishibashi, Identification of a novel aquaporin, AQP12, expressed in pancreatic acinar cells, *Biochem. Biophys. Res. Commun.* 330 (2005) 832–838.
- [49] D.A. Gorelick, J. Praetorius, T. Tsunenari, S. Nielsen, P. Agre, Aquaporin-11: a channel protein lacking apparent transport function expressed in brain, *BMC Biochem.* 7 (2006) 14.
- [50] E. Beitz, B. Wu, L.M. Holm, J.E. Schultz, T. Zeuthen, Point mutations in the aromatic/arginine region in aquaporin 1 allow passage of urea, glycerol, ammonia, and protons, *Proc. Natl. Acad. Sci. U. S. A.* 103 (2006) 269–274.
- [51] Y. Wang, K. Schulten, E. Tajkhorshid, What makes an aquaporin a glycerol channel? A comparative study of AqpZ and GlpF, *Structure* 13 (2005) 1107–1118.
- [52] D.F. Savage, J.D. O'Connell 3rd, L.J. Miercke, J. Finer-Moore, R.M. Stroud, Structural context shapes the aquaporin selectivity filter, *Proc. Natl. Acad. Sci. U. S. A.* 107 (2010) 17164–17169.
- [53] K. Kishida, H. Kuriyama, T. Funahashi, I. Shimomura, S. Kihara, N. Ouchi, M. Nishida, H. Nishizawa, M. Matsuda, M. Takahashi, K. Hotta, T. Nakamura, S. Yamashita, Y. Tochino, Y. Matsuzawa, Aquaporin adipose, a putative glycerol channel in adipocytes, *J. Biol. Chem.* 275 (2000) 20896–20902.
- [54] M.T. Skowronski, J. Lebeck, A. Rojek, J. Praetorius, E.M. Fuchtbauer, J. Frokier, S. Nielsen, AQP7 is localized in capillaries of adipose tissue, cardiac and striated muscle: implications in glycerol metabolism, *Am. J. Physiol. Renal Physiol.* 292 (2007) F956–F965.
- [55] R.E. Duncan, M. Ahmadian, K. Jaworski, E. Sarkadi-Nagy, H.S. Sul, Regulation of lipolysis in adipocytes, *Annu. Rev. Nutr.* 27 (2007) 79–101.
- [56] B.J. Lipworth, Clinical pharmacology of beta 3-adrenoceptors, *Br. J. Clin. Pharmacol.* 42 (1996) 291–300.
- [57] T. Miyachi, H. Yamamoto, Y. Abe, G.J. Yoshida, A. Rojek, E. Sahara, S. Uchida, S. Nielsen, M. Yasui, Dynamic subcellular localization of aquaporin-7 in white adipocytes, *FEBS Lett.* 589 (2015) 608–614.
- [58] M. Vaughan, The production and release of glycerol by adipose tissue incubated in vitro, *J. Biol. Chem.* 237 (1962) 3354–3358.
- [59] M. Hara-Chikuma, E. Sahara, T. Rai, M. Ikawa, M. Okabe, S. Sasaki, S. Uchida, A.S. Verkman, Progressive adipocyte hypertrophy in aquaporin-7-deficient mice: adipocyte glycerol permeability as a novel regulator of fat accumulation, *J. Biol. Chem.* 280 (2005) 15493–15496.
- [60] N. Maeda, T. Funahashi, T. Hibuse, A. Nagasawa, K. Kishida, H. Kuriyama, T. Nakamura, S. Kihara, I. Shimomura, Y. Matsuzawa, Adaptation to fasting by glycerol transport through aquaporin 7 in adipose tissue, *Proc. Natl. Acad. Sci. U. S. A.* 101 (2004) 17801–17806.
- [61] H. Kondo, I. Shimomura, K. Kishida, H. Kuriyama, Y. Makino, H. Nishizawa, M. Matsuda, N. Maeda, H. Nagaretani, S. Kihara, Y. Kurachi, T. Nakamura, T. Funahashi, Y. Matsuzawa, Human aquaporin adipose (AQPap) gene. Genomic structure, promoter analysis and functional mutation, *Eur. J. Biochem.* 269 (2002) 1814–1826.
- [62] U. Laforenza, M.F. Scaffino, G. Gastaldi, Aquaporin-10 represents an alternative pathway for glycerol efflux from human adipocytes, *PLoS One* 8 (2013), e54474.
- [63] T. Morinaga, M. Nakakoshi, A. Hirao, M. Imai, K. Ishibashi, Mouse aquaporin 10 gene (AQP10) is a pseudogene, *Biochem. Biophys. Res. Commun.* 294 (2002) 630–634.
- [64] E.C. Lin, Glycerol utilization and its regulation in mammals, *Annu. Rev. Biochem.* 46 (1977) 765–795.
- [65] W.M. Bortz, P. Paul, A.C. Haff, W.L. Holmes, Glycerol turnover and oxidation in man, *J. Clin. Invest.* 51 (1972) 1537–1546.
- [66] C.F. Borchgrevink, R.J. Havel, Transport of glycerol in human blood, *Proc. Soc. Exp. Biol. Med.* 113 (1963) 946–949.
- [67] J.L. Nelson, M.E. Harmon, R.A. Robergs, Identifying plasma glycerol concentration associated with urinary glycerol excretion in trained humans, *J. Anal. Toxicol.* 35 (2011) 617–623.
- [68] E. Sahara, T. Rai, J. Miyazaki, A.S. Verkman, S. Sasaki, S. Uchida, Defective water and glycerol transport in the proximal tubules of AQP7 knockout mice, *Am. J. Physiol. Renal Physiol.* 289 (2005) F1195–F1200.
- [69] C. Goubau, J. Jaeken, E.N. Levchenko, C. Thys, M. Di Michele, G.A. Martens, E. Gerlo, R. De Vos, G.M. Buyse, N. Goemans, C. Van Geet, K. Freson, Homozygosity for aquaporin 7 G264V in three unrelated children with hyperglyceroluria and a mild platelet secretion defect, *Genet. Med.* 15 (2013) 55–63.
- [70] W.P. Russ, D.M. Engelman, The GxxxG motif: a framework for transmembrane helix–helix association, *J. Mol. Biol.* 296 (2000) 911–919.

- [71] H. Tsukaguchi, C. Shayakul, U.V. Berger, B. Mackenzie, S. Devidas, W.B. Guggino, A.N. van Hoek, M.A. Hediger, Molecular characterization of a broad selectivity neutral solute channel, *J. Biol. Chem.* 273 (1998) 24737–24743.
- [72] M. Elkjaer, Z. Vajda, L.N. Nejsum, T. Kwon, U.B. Jensen, M. Amiry-Moghaddam, J. Frokiaer, S. Nielsen, Immunolocalization of AQP9 in liver, epididymis, testis, spleen, and brain, *Biochem. Biophys. Res. Commun.* 276 (2000) 1118–1128.
- [73] S.J. Pilkis, D.K. Granner, Molecular physiology of the regulation of hepatic gluconeogenesis and glycolysis, *Annu. Rev. Physiol.* 54 (1992) 885–909.
- [74] R.A. Fenton, C.L. Chou, G.S. Stewart, C.P. Smith, M.A. Knepper, Urinary concentrating defect in mice with selective deletion of phloretin-sensitive urea transporters in the renal collecting duct, *Proc. Natl. Acad. Sci. U. S. A.* 101 (2004) 7469–7474.
- [75] G. Calamita, P. Gena, D. Ferri, A. Rosito, A. Rojek, S. Nielsen, R.A. Marinelli, G. Fruhbeck, M. Svelto, Biophysical assessment of aquaporin-9 as principal facilitative pathway in mouse liver import of glucogenic glycerol, *Biol. Cell.* 104 (2012) 342–351.
- [76] A.M. Rojek, M.T. Skowronski, E.M. Fuchtbauer, A.C. Fuchtbauer, R.A. Fenton, P. Agre, J. Frokiaer, S. Nielsen, Defective glycerol metabolism in aquaporin 9 (AQP9) knockout mice, *Proc. Natl. Acad. Sci. U. S. A.* 104 (2007) 3609–3614.
- [77] N. Zhang, M.J. Bevan, CD8(+) T cells: foot soldiers of the immune system, *Immunity* 35 (2011) 161–168.
- [78] G. Cui, M.M. Staron, S.M. Gray, P.C. Ho, R.A. Amezquita, J. Wu, S.M. Kaech, IL-7-induced glycerol transport and TAG synthesis promotes memory CD8+ T cell longevity, *Cell* 161 (2015) 750–761.
- [79] R. Sougrat, M. Morand, C. Gondran, P. Barre, R. Gobin, F. Bonte, M. Dumas, J.M. Verbavatz, Functional expression of AQP3 in human skin epidermis and reconstructed epidermis, *J. Invest. Dermatol.* 118 (2002) 678–685.
- [80] T. Ma, M. Hara, R. Sougrat, J.M. Verbavatz, A.S. Verkman, Impaired stratum corneum hydration in mice lacking epidermal water channel aquaporin-3, *J. Biol. Chem.* 277 (2002) 17147–17153.
- [81] M. Hara, T. Ma, A.S. Verkman, Selectively reduced glycerol in skin of aquaporin-3-deficient mice may account for impaired skin hydration, elasticity, and barrier recovery, *J. Biol. Chem.* 277 (2002) 46616–46621.
- [82] C.L. Froebe, F.A. Simion, H. Ohlmeyer, L.D. Rhein, J. Mattai, R.H. Cagan, S.E. Friberg, Prevention of stratum-corneum lipid phase-transitions *in vitro* by glycerol – an alternative mechanism for skin moisturization, *J. Soc. Cosmet. Chem.* 41 (1990) 51–65.
- [83] S.E. Friberg, I. Kayali, L. Rhein, Direct role of linoleic-acid in barrier function – effect of linoleic-acid on the crystalline-structure of oleic-acid oleate model stratum-corneum lipid, *J. Dispers. Sci. Technol.* 11 (1990) 31–47.
- [84] M. Hara, A.S. Verkman, Glycerol replacement corrects defective skin hydration, elasticity, and barrier function in aquaporin-3-deficient mice, *Proc. Natl. Acad. Sci. U. S. A.* 100 (2003) 7360–7365.
- [85] M.D. Norenberg, K.V. Rama Rao, A.R. Jayakumar, Ammonia neurotoxicity and the mitochondrial permeability transition, *J. Bioenerg. Biomembr.* 36 (2004) 303–307.
- [86] J.S. Kim, L. He, J.J. Lemasters, Mitochondrial permeability transition: a common pathway to necrosis and apoptosis, *Biochem. Biophys. Res. Commun.* 304 (2003) 463–470.
- [87] F. Martini, J.L. Nath, *Anatomy & Physiology*, 2nd ed. Benjamin Cummings, San Francisco, 2010.
- [88] K. Ishibashi, M. Kuwahara, Y. Gu, Y. Tanaka, F. Marumo, S. Sasaki, Cloning and functional expression of a new aquaporin (AQP9) abundantly expressed in the peripheral leukocytes permeable to water and urea, but not to glycerol, *Biochem. Biophys. Res. Commun.* 244 (1998) 268–274.
- [89] K. Ishibashi, S. Sasaki, K. Fushimi, S. Uchida, M. Kuwahara, H. Saito, T. Furukawa, K. Nakajima, Y. Yamaguchi, T. Gojibori, et al., Molecular cloning and expression of a member of the aquaporin family with permeability to glycerol and urea in addition to water expressed at the basolateral membrane of kidney collecting duct cells, *Proc. Natl. Acad. Sci. U. S. A.* 91 (1994) 6269–6273.
- [90] M. Echevarria, E.E. Windhager, G. Frindt, Selectivity of the renal collecting duct water channel aquaporin-3, *J. Biol. Chem.* 271 (1996) 25079–25082.
- [91] S. Jelen, P. Gena, J. Lebeck, A. Rojek, J. Praetorius, J. Frokiaer, R.A. Fenton, S. Nielsen, G. Calamita, M. Rutzler, Aquaporin-9 and urea transporter-A gene deletions affect urea transmembrane passage in murine hepatocytes, *Am. J. Physiol. Gastrointest. Liver Physiol.* 303 (2012) G1279–G1287.
- [92] I.D. Weiner, W.E. Mitch, J.M. Sands, Urea and ammonia metabolism and the control of renal nitrogen excretion, *Clin. J. Am. Soc. Nephrol.* (2014).
- [93] S.M. Saparov, K. Liu, P. Agre, P. Pohl, Fast and selective ammonia transport by aquaporin-8, *J. Biol. Chem.* 282 (2007) 5296–5301.
- [94] B. Yang, Y. Song, D. Zhao, A.S. Verkman, Phenotypic analysis of aquaporin-8 null mice, *Am. J. Physiol. Cell Physiol.* 288 (2005) C1161–C1170.
- [95] G. Calamita, D. Ferri, P. Gena, G.E. Liguori, A. Cavalier, D. Thomas, M. Svelto, The inner mitochondrial membrane has aquaporin-8 water channels and is highly permeable to water, *J. Biol. Chem.* 280 (2005) 17149–17153.
- [96] B. Yang, D. Zhao, E. Solenov, A.S. Verkman, Evidence from knockout mice against physiologically significant aquaporin 8-facilitated ammonia transport, *Am. J. Physiol. Cell Physiol.* 291 (2006) C417–C423.
- [97] A.M. Marini, G. Matassi, V. Raynal, B. Andre, J.P. Cartron, B. Cherif-Zahar, The human Rhesus-associated RhAG protein and a kidney homologue promote ammonium transport in yeast, *Nat. Genet.* 26 (2000) 341–344.
- [98] I.D. Weiner, R.T. Miller, J.W. Verlander, Localization of the ammonium transporters, Rh B glycoprotein and Rh C glycoprotein, in the mouse liver, *Gastroenterology* 124 (2003) 1432–1440.
- [99] I.D. Weiner, J.W. Verlander, Role of NH₃ and NH₄⁺ transporters in renal acid-base transport, *Am. J. Physiol. Renal Physiol.* 300 (2011) F11–F23.
- [100] D. Goossens, M.M. Trinh-Trang-Tan, M. Debbia, P. Ripoché, C. Vilela-Lamego, F. Louache, W. Vainchenker, Y. Colin, J.P. Cartron, Generation and characterisation of Rhd and Rhag null mice, *Br. J. Haematol.* 148 (2010) 161–172.
- [101] D. Goossens, V. Bony, P. Gane, Y. Colin, J.P. Cartron, Generation of mice with inactivated Rh or Rhag genes, *Transfus. Clin. Biol.* 13 (2006) 164–166.
- [102] L.R. Soria, J. Marrone, G. Calamita, R.A. Marinelli, Ammonia detoxification via ureagenesis in rat hepatocytes involves mitochondrial aquaporin-8 channels, *Hepatology* 57 (2013) 2061–2071.
- [103] S.M. Molinas, L. Trumper, R.A. Marinelli, Mitochondrial aquaporin-8 in renal proximal tubule cells: evidence for a role in the response to metabolic acidosis, *Am. J. Physiol. Renal Physiol.* 303 (2012) F458–F466.
- [104] S.M. Molinas, L.R. Soria, J. Marrone, M. Danielli, L. Trumper, R.A. Marinelli, Acidosis-induced downregulation of hepatocyte mitochondrial aquaporin-8 and ureagenesis from ammonia, *Biochem. Cell Biol.* 93 (2015) 417–420.
- [105] T. Ma, Y. Song, B. Yang, A. Gillespie, E.J. Carlson, C.J. Epstein, A.S. Verkman, Nephrogenic diabetes insipidus in mice lacking aquaporin-3 water channels, *Proc. Natl. Acad. Sci. U. S. A.* 97 (2000) 4386–4391.
- [106] M. Esbjornsson, J. Bulow, B. Norman, L. Simonsen, J. Nowak, O. Rooyackers, L. Kaijser, E. Jansson, Adipose tissue extracts plasma ammonia after sprint exercise in women and men, *J. Appl. Physiol.* 101 (2006) 1576–1580.
- [107] V. Endeward, J.P. Cartron, P. Ripoché, G. Gros, RhAG protein of the Rhesus complex is a CO₂ channel in the human red cell membrane, *FASEB J.* 22 (2008) 64–73.
- [108] M.E. Blank, H. Ehmke, Aquaporin-1 and HCO₃⁻-Cl⁻ transporter-mediated transport of CO₂ across the human erythrocyte membrane, *J. Physiol.* 550 (2003) 419–429.
- [109] G.M. Preston, T.P. Carroll, W.B. Guggino, P. Agre, Appearance of water channels in *Xenopus* oocytes expressing red cell CHIP28 protein, *Science* 256 (1992) 385–387.
- [110] N.L. Nakhoul, B.A. Davis, M.F. Romero, W.F. Boron, Effect of expressing the water channel aquaporin-1 on the CO₂ permeability of *Xenopus* oocytes, *Am. J. Physiol.* 274 (1998) C543–C548.
- [111] G.J. Cooper, W.F. Boron, Effect of PCMBs on CO₂ permeability of *Xenopus* oocytes expressing aquaporin 1 or its C189S mutant, *Am. J. Physiol.* 275 (1998) C1481–C1486.
- [112] V. Endeward, R. Musa-Aziz, G.J. Cooper, L.M. Chen, M.F. Pelletier, L.V. Virkki, C.T. Supuran, L.S. King, W.F. Boron, G. Gros, Evidence that aquaporin 1 is a major pathway for CO₂ transport across the human erythrocyte membrane, *FASEB J.* 20 (2006) 1974–1981.
- [113] B. Yang, N. Fukuda, A. van Hoek, M.A. Matthay, T. Ma, A.S. Verkman, Carbon dioxide permeability of aquaporin-1 measured in erythrocytes and lung of aquaporin-1 null mice and in reconstituted proteoliposomes, *J. Biol. Chem.* 275 (2000) 2686–2692.
- [114] G.V. Prasad, L.A. Coury, F. Finn, M.L. Zeidel, Reconstituted aquaporin 1 water channels transport CO₂ across membranes, *J. Biol. Chem.* 273 (1998) 33123–33126.
- [115] Y. Wang, J. Cohen, W.F. Boron, K. Schulten, E. Tajkhorshid, Exploring gas permeability of cellular membranes and membrane channels with molecular dynamics, *J. Struct. Biol.* 157 (2007) 534–544.
- [116] J.S. Hub, B.L. de Groot, Does CO₂ permeate through aquaporin-1? *Biophys. J.* 91 (2006) 842–848.
- [117] Y. Wang, S.A. Shaikh, E. Tajkhorshid, Exploring transmembrane diffusion pathways with molecular dynamics, *Physiology* 25 (2010) 142–154.
- [118] F. Itel, S. Al-Samir, F. Oberg, M. Chami, M. Kumar, C.T. Supuran, P.M. Deen, W. Meier, K. Hedfalk, G. Gros, V. Endeward, CO₂ permeability of cell membranes is regulated by membrane cholesterol and protein gas channels, *FASEB J.* 26 (2012) 5182–5191.
- [119] J.S. Hub, F.K. Winkler, M. Merrick, B.L. de Groot, Potentials of mean force and permeabilities for carbon dioxide, ammonia, and water flux across a Rhesus protein channel and lipid membranes, *J. Am. Chem. Soc.* 132 (2010) 13251–13263.
- [120] M. Echevarria, A.M. Munoz-Cabello, R. Sanchez-Silva, J.J. Toledo-Aral, J. Lopez-Barneo, Development of cytosolic hypoxia and hypoxia-inducible factor stabilization are facilitated by aquaporin-1 expression, *J. Biol. Chem.* 282 (2007) 30207–30215.
- [121] G. Li, V. Santoni, C. Maurel, Plant aquaporins: roles in plant physiology, *Biochim. Biophys. Acta* 1840 (2014) 1574–1582.
- [122] R. Kaldenhoff, L. Kai, N. Uehlein, Aquaporins and membrane diffusion of CO₂ in living organisms, *Biochim. Biophys. Acta* 1840 (2014) 1592–1595.
- [123] L.A. Sena, N.S. Chandel, Physiological roles of mitochondrial reactive oxygen species, *Mol. Cell* 48 (2012) 158–167.
- [124] Y. Sheng, I.A. Abreu, D.E. Cabelli, M.J. Maroney, A.F. Miller, M. Teixeira, J.S. Valentine, Superoxide dismutases and superoxide reductases, *Chem. Rev.* 114 (2014) 3854–3918.
- [125] G.P. Bienert, J.K. Schjoerring, T.P. Jahn, Membrane transport of hydrogen peroxide, *Biochim. Biophys. Acta* 1758 (2006) 994–1003.
- [126] M. Reth, Hydrogen peroxide as second messenger in lymphocyte activation, *Nat. Immunol.* 3 (2002) 1129–1134.
- [127] A. Almasalmeh, D. Krenc, B. Wu, E. Beitz, Structural determinants of the hydrogen peroxide permeability of aquaporins, *FEBS J.* 281 (2014) 647–656.
- [128] E.W. Miller, B.C. Dickinson, C.J. Chang, Aquaporin-3 mediates hydrogen peroxide uptake to regulate downstream intracellular signaling, *Proc. Natl. Acad. Sci. U. S. A.* 107 (2010) 15681–15686.
- [129] M. Hara-Chikuma, S. Chikuma, Y. Sugiyama, K. Kabashima, A.S. Verkman, S. Inoue, Y. Miyachi, Chemokine-dependent T cell migration requires aquaporin-3-mediated hydrogen peroxide uptake, *J. Exp. Med.* 209 (2012) 1743–1752.
- [130] F. Viecelli Dalla Sega, L. Zamboni, D. Fiorentini, B. Rizzo, C. Caliceti, L. Landi, S. Hrelia, C. Prata, Specific aquaporins facilitate Nox-produced hydrogen peroxide transport through plasma membrane in leukaemia cells, *Biochim. Biophys. Acta* 1843 (2014) 806–814.
- [131] M.J. Marchisio, D.E. Frances, C.E. Carnovale, R.A. Marinelli, Mitochondrial aquaporin-8 knockdown in human hepatoma HepG2 cells causes ROS-induced mitochondrial depolarization and loss of viability, *Toxicol. Appl. Pharmacol.* 264 (2012) 246–254.

- [132] E.E. Tchekneva, Z. Khuchua, L.S. Davis, V. Kadkina, S.R. Dunn, S. Bachman, K. Ishibashi, E.M. Rinchik, R.C. Harris, M.M. Dikov, M.D. Breyer, Single amino acid substitution in aquaporin 11 causes renal failure, *J. Am. Soc. Nephrol.* 19 (2008) 1955–1964.
- [133] E.N. Atochina-Vasserman, A. Biktasova, E. Abramova, D.S. Cheng, V.V. Polosukhin, H. Tanjore, S. Takahashi, H. Sonoda, L. Foye, C. Venkov, S.V. Ryzhov, S. Novitskiy, N. Shlonimskaya, M. Ikeda, T.S. Blackwell, W.E. Lawson, A.J. Gow, R.C. Harris, M.M. Dikov, E.E. Tchekneva, Aquaporin 11 insufficiency modulates kidney susceptibility to oxidative stress, *Am. J. Physiol. Renal Physiol.* 304 (2013) F1295–F1307.
- [134] G.P. Bienert, F. Chaumont, Aquaporin-facilitated transmembrane diffusion of hydrogen peroxide, *Biochim. Biophys. Acta* 1840 (2014) 1596–1604.
- [135] M. Yasui, T.H. Kwon, M.A. Knepper, S. Nielsen, P. Agre, Aquaporin-6: an intracellular vesicle water channel protein in renal epithelia, *Proc. Natl. Acad. Sci. U. S. A.* 96 (1999) 5808–5813.
- [136] T. Ma, B. Yang, W.L. Kuo, A.S. Verkman, cDNA cloning and gene structure of a novel water channel expressed exclusively in human kidney: evidence for a gene cluster of aquaporins at chromosome locus 12q13, *Genomics* 35 (1996) 543–550.
- [137] M. Ikeda, E. Beitz, D. Kozono, W.B. Guggino, P. Agre, M. Yasui, Characterization of aquaporin-6 as a nitrate channel in mammalian cells. Requirement of pore-lining residue threonine 63, *J. Biol. Chem.* 277 (2002) 39873–39879.
- [138] D. Promeneur, T.H. Kwon, M. Yasui, G.H. Kim, J. Frokiaer, M.A. Knepper, P. Agre, S. Nielsen, Regulation of AQP6 mRNA and protein expression in rats in response to altered acid–base or water balance, *Am. J. Physiol. Renal Physiol.* 279 (2000) F1014–F1026.
- [139] X. Qin, W.F. Boron, Mutation of a single amino acid converts the human water channel aquaporin 5 into an anion channel, *Am. J. Physiol. Cell Physiol.* 305 (2013) C663–C672.
- [140] J.W. Lee, Y. Zhang, C.D. Weaver, N.H. Shomer, C.F. Louis, D.M. Roberts, Phosphorylation of nodulin 26 on serine 262 affects its voltage-sensitive channel activity in planar lipid bilayers, *J. Biol. Chem.* 270 (1995) 27051–27057.
- [141] C.D. Weaver, N.H. Shomer, C.F. Louis, D.M. Roberts, Nodulin 26, a nodule-specific symbiosome membrane protein from soybean, is an ion channel, *J. Biol. Chem.* 269 (1994) 17858–17862.
- [142] A.J. Yool, W.D. Stamer, J.W. Regan, Forskolin stimulation of water and cation permeability in aquaporin 1 water channels, *Science* 273 (1996) 1216–1218.
- [143] T.L. Anthony, H.L. Brooks, D. Boassa, S. Leonov, G.M. Yanochko, J.W. Regan, A.J. Yool, Cloned human aquaporin-1 is a cyclic GMP-gated ion channel, *Mol. Pharmacol.* 57 (2000) 576–588.
- [144] W. Zhang, E. Zitron, M. Homme, L. Kihm, C. Morath, D. Scherer, S. Hegge, D. Thomas, C.P. Schmitt, M. Zeier, H. Katus, C. Karle, V. Schwenger, Aquaporin-1 channel function is positively regulated by protein kinase C, *J. Biol. Chem.* 282 (2007) 20933–20940.
- [145] M.T. Conner, A.C. Conner, C.E. Bland, L.H. Taylor, J.E. Brown, H.R. Parri, R.M. Bill, Rapid aquaporin translocation regulates cellular water flow: mechanism of hypotonicity-induced subcellular localization of aquaporin 1 water channel, *J. Biol. Chem.* 287 (2012) 11516–11525.
- [146] E.M. Campbell, D.N. Birdsell, A.J. Yool, The activity of human aquaporin 1 as a cGMP-gated cation channel is regulated by tyrosine phosphorylation in the carboxyl-terminal domain, *Mol. Pharmacol.* 81 (2012) 97–105.
- [147] S.M. Saparov, D. Kozono, U. Rothe, P. Agre, P. Pohl, Water and ion permeation of aquaporin-1 in planar lipid bilayers. Major differences in structural determinants and stoichiometry, *J. Biol. Chem.* 276 (2001) 31515–31520.
- [148] S.P. Tsunoda, B. Wiesner, D. Lorenz, W. Rosenthal, P. Pohl, Aquaporin-1, nothing but a water channel, *J. Biol. Chem.* 279 (2004) 11364–11367.
- [149] P. Agre, M.D. Lee, S. Devidas, W.B. Guggino, Aquaporins and ion conductance, *Science* 275 (1997) 1490 author reply 1492.
- [150] D. Boassa, W.D. Stamer, A.J. Yool, Ion channel function of aquaporin-1 natively expressed in choroid plexus, *J. Neurosci.* 26 (2006) 7811–7819.
- [151] N.W. Baetz, W.D. Stamer, A.J. Yool, Stimulation of aquaporin-mediated fluid transport by cyclic GMP in human retinal pigment epithelium *in vitro*, *Invest. Ophthalmol. Vis. Sci.* 53 (2012) 2127–2132.
- [152] S. Saadoun, M.C. Papadopoulos, M. Hara-Chikuma, A.S. Verkman, Impairment of angiogenesis and cell migration by targeted aquaporin-1 gene disruption, *Nature* 434 (2005) 786–792.
- [153] D.K. Binder, E.A. Nagelhus, O.P. Ottersen, Aquaporin-4 and epilepsy, *Glia* 60 (2012) 1203–1214.
- [154] E.K. Hoffmann, I.H. Lambert, S.F. Pedersen, Physiology of cell volume regulation in vertebrates, *Physiol. Rev.* 89 (2009) 193–277.
- [155] R.E. Day, P. Kitchen, D.S. Owen, C. Bland, L. Marshall, A.C. Conner, R.M. Bill, M.T. Conner, Human aquaporins: regulators of transcellular water flow, *Biochim. Biophys. Acta* 1840 (2014) 1492–1506.
- [156] B. Nilius, J. Vriens, J. Prenen, G. Droogmans, T. Voets, TRPV4 calcium entry channel: a paradigm for gating diversity, *Am. J. Physiol. Cell Physiol.* 286 (2004) C195–C205.
- [157] W. Liedtke, Transient receptor potential vanilloid channels functioning in transduction of osmotic stimuli, *J. Endocrinol.* 191 (2006) 515–523.
- [158] W. Liedtke, C. Kim, Functionality of the TRPV subfamily of TRP ion channels: add mechano-TRP and osmo-TRP to the lexicon! *Cell. Mol. Life Sci.* 62 (2005) 2985–3001.
- [159] X. Liu, B.C. Bandyopadhyay, T. Nakamoto, B. Singh, W. Liedtke, J.E. Melvin, I. Ambudkar, A role for AQP5 in activation of TRPV4 by hypotonicity: concerted involvement of AQP5 and TRPV4 in regulation of cell volume recovery, *J. Biol. Chem.* 281 (2006) 15485–15495.
- [160] Q. Chen, E.K. Duan, Aquaporins in sperm osmoadaptation: an emerging role for volume regulation, *Acta Pharmacol. Sin.* 32 (2011) 721–724.
- [161] Q. Chen, H. Peng, L. Lei, Y. Zhang, H. Kuang, Y. Cao, Q.X. Shi, T. Ma, E. Duan, Aquaporin3 is a sperm water channel essential for postcopulatory sperm osmoadaptation and migration, *Cell Res.* 21 (2011) 922–933.
- [162] L. Galizia, A. Pizzoni, J. Fernandez, V. Rivarola, C. Capurro, P. Ford, Functional interaction between AQP2 and TRPV4 in renal cells, *J. Cell. Biochem.* 113 (2012) 580–589.
- [163] H. Zhang, H. Li, E. Liu, Y. Guang, L. Yang, J. Mao, L. Zhu, L. Chen, L. Wang, The AQP-3 water channel and the ClC-3 chloride channel coordinate the hypotonicity-induced swelling volume in nasopharyngeal carcinoma cells, *Int. J. Biochem. Cell Biol.* 57 (2014) 96–107.
- [164] A.E. Hill, Y. Shachar-Hill, Are aquaporins the missing transmembrane osmosensors? *J. Membr. Biol.* 248 (2015) 753–765.
- [165] Y. Inoue, E. Sohara, K. Kobayashi, M. Chiga, T. Rai, K. Ishibashi, S. Horie, X. Su, J. Zhou, S. Sasaki, S. Uchida, Aberrant glycosylation and localization of polycystin-1 cause polycystic kidney in an AQP11 knockout model, *J. Am. Soc. Nephrol.* 25 (2014) 2789–2799.
- [166] S.P. Ferris, V.K. Kodali, R.J. Kaufman, Glycoprotein folding and quality-control mechanisms in protein-folding diseases, *Dis. Model. Mech.* 7 (2014) 331–341.
- [167] P. Kitchen, R.E. Day, L.H. Taylor, M.M. Salman, R.M. Bill, M.T. Conner, A.C. Conner, Identification and molecular mechanisms of the rapid tonicity-induced relocalization of aquaporin 4, *J. Biol. Chem.* (2015).
- [168] H. Wu, L. Chen, X. Zhang, Q. Zhou, J.M. Li, S. Berger, Z. Borok, B. Zhou, Z. Xiao, H. Yin, M. Liu, Y. Wang, J. Jin, M.R. Blackburn, Y. Xia, W. Zhang, Aqp5 is a new transcriptional target of Dot1a and a regulator of Aqp2, *PLoS One* 8 (2013), e53342.
- [169] C. Hachez, A. Besserer, A.S. Chevalier, F. Chaumont, Insights into plant plasma membrane aquaporin trafficking, *Trends Plant Sci.* 18 (2013) 344–352.
- [170] S. Bassnett, P.A. Wilmarth, L.L. David, The membrane proteome of the mouse lens fiber cell, *Mol. Vis.* 15 (2009) 2448–2463.
- [171] S. Scheuring, N. Buzhynskyy, S. Jaroslowski, R.P. Goncalves, R.K. Hite, T. Walz, Structural models of the supramolecular organization of AQP0 and connexons in junctional microdomains, *J. Struct. Biol.* 160 (2007) 385–394.
- [172] A. Colom, I. Casuso, T. Boudier, S. Scheuring, High-speed atomic force microscopy: cooperative adhesion and dynamic equilibrium of junctional microdomain membrane proteins, *J. Mol. Biol.* 423 (2012) 249–256.
- [173] S.S. Kumari, K. Varadaraj, Aquaporin 0 plays a pivotal role in refractive index gradient development in mammalian eye lens to prevent spherical aberration, *Biochem. Biophys. Res. Commun.* 452 (2014) 986–991.
- [174] K. Varadaraj, S.S. Kumari, R.T. Mathias, Transgenic expression of AQP1 in the fiber cells of AQP0 knockout mouse: effects on lens transparency, *Exp. Eye Res.* 91 (2010) 393–404.
- [175] S.S. Kumari, K. Varadaraj, Intact AQP0 performs cell-to-cell adhesion, *Biochem. Biophys. Res. Commun.* 390 (2009) 1034–1039.
- [176] L.F. Michea, M. de la Fuente, N. Lagos, Lens major intrinsic protein (MIP) promotes adhesion when reconstituted into large unilamellar liposomes, *Biochemistry* 33 (1994) 7663–7669.
- [177] S.S. Kumari, J. Gandhi, M.H. Mustehsan, S. Eren, K. Varadaraj, Functional characterization of an AQP0 missense mutation, R33C, that causes dominant congenital lens cataract, reveals impaired cell-to-cell adhesion, *Exp. Eye Res.* 116 (2013) 371–385.
- [178] T. Gonen, P. Sliz, J. Kistler, Y. Cheng, T. Walz, Aquaporin-0 membrane junctions reveal the structure of a closed water pore, *Nature* 429 (2004) 193–197.
- [179] R.K. Hite, P.L. Chiu, J.M. Schuller, T. Walz, Effect of lipid head groups on double-layered two-dimensional crystals formed by aquaporin-0, *PLoS One* 10 (2015), e0117371.
- [180] W.E. Harries, D. Akhavan, L.J. Miercke, S. Khademi, R.M. Stroud, The channel architecture of aquaporin 0 at a 2.2-Å resolution, *Proc. Natl. Acad. Sci. U. S. A.* 101 (2004) 14045–14050.
- [181] A. Engel, Y. Fujiyoshi, T. Gonen, T. Walz, Junction-forming aquaporins, *Curr. Opin. Struct. Biol.* 18 (2008) 229–235.
- [182] S. Sindhu Kumari, K. Varadaraj, Intact and N- or C-terminal end truncated AQP0 function as open water channels and cell-to-cell adhesion proteins: end truncation could be a prelude for adjusting the refractive index of the lens to prevent spherical aberration, *Biochim. Biophys. Acta* 1840 (2014) 2862–2877.
- [183] J. Liu, J. Xu, S. Gu, B.J. Nicholson, J.X. Jiang, Aquaporin 0 enhances gap junction coupling via its cell adhesion function and interaction with connexin 50, *J. Cell Sci.* 124 (2011) 198–206.
- [184] M. De Bellis, F. Pisani, M.G. Mola, D. Basco, F. Catalano, G.P. Nicchia, M. Svelto, A. Frigeri, A novel human aquaporin-4 splice variant exhibits a dominant-negative activity: a new mechanism to regulate water permeability, *Mol. Biol. Cell* 25 (2014) 470–480.
- [185] Y. Hiroaki, K. Tani, A. Kamegawa, N. Gyobu, K. Nishikawa, H. Suzuki, T. Walz, S. Sasaki, K. Mitsuoka, K. Kimura, A. Mizoguchi, Y. Fujiyoshi, Implications of the aquaporin-4 structure on array formation and cell adhesion, *J. Mol. Biol.* 355 (2006) 628–639.
- [186] H. Zhang, A.S. Verkman, Evidence against involvement of aquaporin-4 in cell–cell adhesion, *J. Mol. Biol.* 382 (2008) 1136–1143.
- [187] E. McCoy, H. Sontheimer, Expression and function of water channels (aquaporins) in migrating malignant astrocytes, *Glia* 55 (2007) 1034–1043.
- [188] A.J. Smith, B.J. Jin, J. Ratelade, A.S. Verkman, Aggregation state determines the localization and function of M1- and M23-aquaporin-4 in astrocytes, *J. Cell Biol.* 204 (2014) 559–573.
- [189] W. Humphrey, A. Dalke, K. Schulten, VMD: visual molecular dynamics, *J. Mol. Graph.* 14 (1996) 33–38 27–38.



Review

Human aquaporins: Regulators of transcellular water flow☆☆



Rebecca E. Day^a, Philip Kitchen^b, David S. Owen^a, Charlotte Bland^d, Lindsay Marshall^d, Alex C. Conner^{c,*}, Roslyn M. Bill^{d,*}, Matthew T. Conner^{a,*}

^a Biomedical Research Centre, Sheffield Hallam University, Howard Street, Sheffield S1 1WB, UK

^b Molecular Organisation and Assembly in Cells Doctoral Training Centre, University of Warwick, Coventry CV4 7AL, UK

^c School of Clinical and Experimental Medicine, University of Birmingham, Edgbaston, Birmingham B15 2TT, UK

^d School of Life and Health Sciences, Aston University, Aston Triangle, Birmingham B4 7ET, UK

ARTICLE INFO

Article history:

Received 5 July 2013

Received in revised form 19 September 2013

Accepted 23 September 2013

Available online 30 September 2013

Keywords:

Aquaporin regulation

Transcellular water flow

Homeostasis

Cell volume regulation

Regulatory volume increase

Regulatory volume decrease

ABSTRACT

Background: Emerging evidence supports the view that (AQP) aquaporin water channels are regulators of transcellular water flow. Consistent with their expression in most tissues, AQPs are associated with diverse physiological and pathophysiological processes.

Scope of review: AQP knockout studies suggest that the regulatory role of AQPs, rather than their action as passive channels, is their critical function. Transport through all AQPs occurs by a common passive mechanism, but their regulation and cellular distribution varies significantly depending on cell and tissue type; the role of AQPs in cell volume regulation (CVR) is particularly notable. This review examines the regulatory role of AQPs in transcellular water flow, especially in CVR. We focus on key systems of the human body, encompassing processes as diverse as urine concentration in the kidney to clearance of brain oedema.

Major conclusions: AQPs are crucial for the regulation of water homeostasis, providing selective pores for the rapid movement of water across diverse cell membranes and playing regulatory roles in CVR. Gating mechanisms have been proposed for human AQPs, but have only been reported for plant and microbial AQPs. Consequently, it is likely that the distribution and abundance of AQPs in a particular membrane is the determinant of membrane water permeability and a regulator of transcellular water flow.

General significance: Elucidating the mechanisms that regulate transcellular water flow will improve our understanding of the human body in health and disease. The central role of specific AQPs in regulating water homeostasis will provide routes to a range of novel therapies. This article is part of a Special Issue entitled Aquaporins.

© 2013 The Authors. Published by Elsevier B.V. Open access under [CC BY license](http://creativecommons.org/licenses/by/3.0/).

1. Introduction: Transcellular water flow: a regulatory role for human

1.1. Aquaporins

A striking property of most human tissues is their capacity for extremely rapid fluid transport. This is exemplified by urine concentration in the kidney [1], the rapid formation of a fluid-filled cavity adjacent to the oocyte during ovarian folliculogenesis [2] and secretion of saliva from salivary glands [3]. These processes are essential to human health and rely on the highly-regulated transport of water through tissues [4,5]. Such trans-tissue water flow is possible by two routes: transcellular water flow across both basal and apical membranes, which occurs in response to the osmotic stimuli [4] created by salt transport [6]; or

paracellular flow across cell–cell junctions into intercellular spaces, driven by salt or solute gradients [6]. Paracellular water flow plays an important role in leaky epithelia such as the corneal endothelium [7]. In this review, we focus on the regulatory role of aquaporin (AQP) water channels in mediating transcellular water flow across cell membranes in the major systems of the human body (Fig. 1). The study of the mechanisms of human AQP regulation that mediate transcellular water flow is still in its infancy and therefore this review will also discuss mammalian AQPs as potential models for the regulation of human AQPs (Table 1).

Transcellular water flow is dependent on the permeability of the plasma membrane to water molecules. Water movement by osmosis may be through the lipid bilayer, by passive co-transport with other ions and solutes [8] or through AQP water channels [9]. Many AQP channels are thought to have an exquisite specificity for water and are capable of rapidly transporting it in response to changes in tonicity; evidence suggests that they make a critical contribution to the regulation of transcellular water flow [10].

Since the first AQP was identified by Peter Agre in 1988 [11], thirteen human AQPs have been discovered. Structural results for several family members [12–14] have established that AQP channels share a common

☆☆ This article is part of a Special Issue entitled Aquaporins.

* Corresponding authors.

E-mail addresses: a.c.conner@bham.ac.uk (A.C. Conner), r.m.bill@aston.ac.uk (R.M. Bill), M.Conner@shu.ac.uk (M.T. Conner).

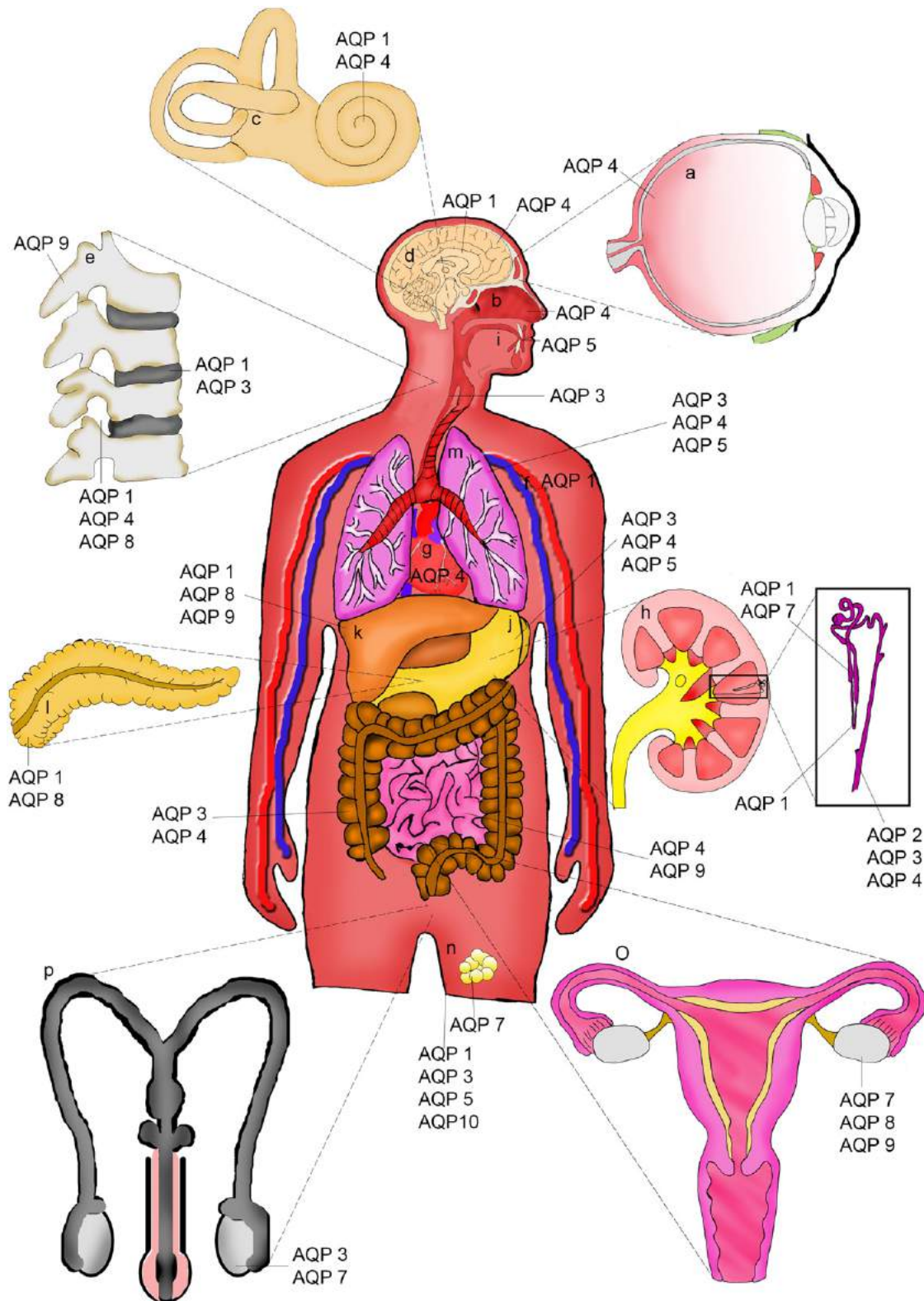


Fig. 1. Aquaporin expression in humans. The figure shows the wide distribution of AQP water channels throughout the human body. Organs are highlighted, starting at top right; within each organ, the major AQPs involved in transcellular water flow are denoted; a) Retina – AQP4, b) Olfactory epithelium – AQP4, c) The inner ear – AQP4 and AQP1, d) Brain – AQP4 in astrocytes and AQP1 in choroid plexus, e) Spinal cord – AQP1, AQP4 and AQP8; Nucleus pulposus cells of the intervertebral disc – AQP1 and AQP3; Osteoclasts – AQP9, f) Blood vessels – AQP1 in endothelial cells, g) Heart – AQP4, h) Kidney (showing the nephron in detail) – AQP1, AQP2, AQP3, AQP4 and AQP7, i) Salivary glands – AQP5, j) Gastrointestinal tract – AQP3, AQP4, AQP5 and AQP9, k) Liver – AQP1, AQP8 and AQP9, l) Pancreas – AQP1 and AQP8, m) Lungs – AQP3, AQP4, AQP5, n) Fat (adipocytes) – AQP7; Skin – AQP1, AQP3, AQP5 and AQP10, o) Female reproductive tract – AQP7, AQP8 and AQP9 in ovaries, and p) Male reproductive system – AQP3 and AQP7 in sperm cells.

Table 1

Tissue distribution and roles of AQPs in transcellular water flow. AQPs discussed in this review are presented in terms of their localisation and regulatory roles in transcellular water flow within organ tissues.

System	AQP protein localisation	Role of aquaporins in transcellular water flow	References
Nervous	Retina – AQP4	Suggested role in Muller cell water balance.	[64]
	Olfactory epithelium – AQP4	Membrane permeability - link to olfaction.	[65]
	Inner ear – AQP4 (hensons, claudius and Inner Succus cells), AQP1 (fibrocytes)	AQP4 mediated transcellular water flow in to Henson cells exiting via AQP4 on basal membrane of Claudius cells	[66]
	Brain – AQP4 astrocytes, AQP1 (choroid plexus)	AQP4 at astrocyte end feet for BBB water permeability. AQP1 secretion of CSF, AQP4 absorption of CSF	[62,47]
	Spinal cord – AQP1, AQP4, AQP8	Localisation of AQPs suggests transcellular water flow from perivascular space to interstitium, into central canal	[54]
Renal (kidney)	Proximal tubule – AQP1 (apical and basolateral), AQP7 (apical of convoluted and straight)	Water reabsorption, importance of AQP7 unknown	[9,69]
	Renal collecting duct cells – AQP2 (apical, sub apical vesicles), AQP3 and AQP4 (basolateral)	Urine concentration by AQP2 AVP mediated water absorption - AQP3 and 4 exit pathways into blood	[63,68]
	Descending thin limb of henle – AQP1	Water reabsorption	[9]
	Descending vasa recta – AQP1	Water reabsorption	[9]
	Connecting tubule – AQP3	Water homeostasis	[9]
Integumentary	Skin – AQP1 (endothelia of dermis), AQP3 + 10 (keratinocytes of epidermis), AQP5 (sweat glands)	Homeostasis, glycerol or water transport for skin hydration, sweat excretion	[96–98]
	Fat – AQP7 (adipocytes)	Glycerol transport	[102]
Cardiovascular	Blood vessels – AQP1 strongly expressed in endothelia outside of brain	i.e. Airspace-Capillary osmotic water permeability and heart vasculature	[112]
	Cardiomyocytes – AQP4	Absorption of excess water from interstitial space into to capillaries	[113]
Respiratory	Lung alveolar epithelium – AQP5 (apical membrane)	Transcellular water flow route for water absorption and secretion in airway, Role in airway hydration	[117]
	Airway epithelial lining – AQP3 and AQP4	Possibly provide route for water into capillaries of airway	[87]
	Airway sub-mucosal glands – AQP5 (apical membrane)	Fluid secretions into lumen of submusosal glands for mucous production and hydration	[119]
Reproductive	Ovarian granulosa cells – AQP7, AQP8, AQP9	Transcellular water flow in folliculogenesis	[2]
	Epididymis	Transepithelial water transport and sperm concentration	[129,135,137,138]
	Sperm – AQP3, AQP7	CVR to prevent swelling and to aid mobility	[41]
Digestive	Salivary Glands – AQP5 (acinar cells, intercalated duct cells), AQP8 (myoepithelial cells)	Transcellular water transfer in process of primary saliva secretion	[87,147]
	Oesophagus – AQP3 (stratified epithelia)	Intracellular osmolarity and CVR to water deprived cells	[143]
	Stomach – AQP3 (stratified epithelia), AQP4 (BLM parietal cells), AQP5 (pyloric gland)	Provide water to cells facing harsh conditions, AQP4 - gastric acid secretion, AQP5 transcellular water secretion for mucous production	[141,143,144]
	Small intestine – AQP4, AQP9 (goblet cells)	Transcellular colonic fluid transport, AQP9 aids in mucous secretion	[149]
	Colon – AQP3 (simple + stratified epithelia of distal colon), AQP4 (surface epithelia)	Water absorption from intestine and colonic fluid transport	[144,149]
	Liver – AQP1 (cholangiocytes), AQP8 (hepatocytes), AQP9 (sinusoidol membrane of hepatocyte)	AQP8 – osmotic driven water transfer and homeostasis, AQP9 – glycerol uptake from blood released by AQP7	[82,152]
	Pancreas – AQP1 (inter/intralobular ducts), AQP8 (acinar cells)	AQP1 – Transcellular water transfer and pancreatic juice secretion, AQP8 – Pancreatic juice secretion	[146]
	Muscle fibres – AQP4	Contraction-induced muscle swelling	
	Articular cartilage – AQP1, AQP3	Involved in cell swelling during mechanistic load	[160]
	Intervertebral disc – AQP1, AQP3 (nucleus pulposus cells)	AQP1 and 3 involved in NP cell swelling during mechanistic load	[159]
Osteoclasts – AQP9	AQP9 osteoclast differentiation and cell fusion – increase in cell volume	[154,156]	

structural architecture. Together with biochemical studies, these structural data [15] have revealed that the functional AQP unit is a homotetramer [15] and that each AQP monomer is composed of six transmembrane (TM) α -helices connected by alternating intracellular (ICL) and extracellular (ECL) loops. The TM domains form a right-handed bundle around the central pore of each AQP monomer through which water transport occurs [16]. The specificity of the pore for water is a result of direct hydrogen bonding, in a pairwise manner, between a single file of water molecules and the AQP family's signature Asn-Pro-Ala motif at the narrowest part of the pore [16]. Water selectivity is further aided by interactions with the aromatic/arginine constriction site, which physically restricts the pore [16]. While the structural biology of the AQP family is therefore widely accepted, the mechanisms that regulate the physiological function of AQPs are less well established [17].

AQPs are expressed in a wide range of tissues (Fig. 1), often spatially located within a certain region of the cell. This enables them to play a central role in the flow of water through those tissues, which typically triggers cell volume regulation (CVR) mechanisms. Whilst transport through all AQPs utilises a common passive mechanism, their regulation and cellular distribution varies significantly between systems, specifically in constituent tissues and cells [17]. This review examines the regulation of transcellular water flow in the human body by AQP channels with a particular focus on CVR.

2. Transcellular water flow and cell volume regulation

CVR is a necessary mechanistic component of AQP-mediated transcellular water flow (Fig. 2). It comprises regulatory volume decrease (RVD), usually in response to hypotonicity-induced cell swelling, and regulatory volume increase (RVI), usually in response to hypertonicity-induced cell shrinkage. The molecular mechanisms underlying these responses are not yet fully understood, but it is unlikely that there is a

single common mechanism [18]. The signalling pathways associated with CVR appear to be cell-type dependent [18]. Nonetheless, the end results of these varied pathways are similar: RVD relies on osmolyte (potassium chloride and taurine [19]) and water efflux from the cell to reduce cell volume whereas RVI is achieved by osmolyte and associated water influx via import of sodium to the cell. Although the rapid RVI process following cell shrinkage involves inorganic ions, after hours of prolonged hypertonic exposure, animal cells often replace the ions with non-perturbing organic osmolytes. The mechanisms for this include external transport into the cell, down-regulation of organic degradation and up-regulation of organic synthesis [20]. These mechanisms facilitate the homeostasis of osmolality within the cell.

2.1. Regulatory volume decrease

In RVD (Fig. 2), the activation of K^+ channels allows efflux of K^+ from the cell and subsequent water loss by osmosis either through AQPs or directly through the lipid bilayer; biophysical data show that AQP expression can increase membrane water permeability by up to ~50 fold [21,22]. This K^+ efflux can be either dependent on intracellular calcium concentration [Ca^{2+}] (e.g. in human cervical cancer cells [23]) or [Ca^{2+}]_i independent (e.g. in Ehrlich ascites tumour cells [24]). In most cell types an intact actin cytoskeleton is necessary for hypotonicity-induced K^+ efflux. However, in trigeminal ganglion neurons, cytochalasin D (an actin polymerisation inhibitor) treatment stimulated swelling activation of a K^+ current [25] demonstrating that in these cells an intact actin network not only is unnecessary for RVD, but also appears to be inhibitory. In some cells, protein kinase C (PKC) activation has also been shown to induce an outward K^+ current via the same channels that are activated in RVD [26]. Movement of K^+ out of the cell is favoured by the concentration gradient but to maintain the electrostatic membrane potential, volume-regulated anion channel(s) (VRAC) simultaneously move anions (mainly Cl^- during RVD)

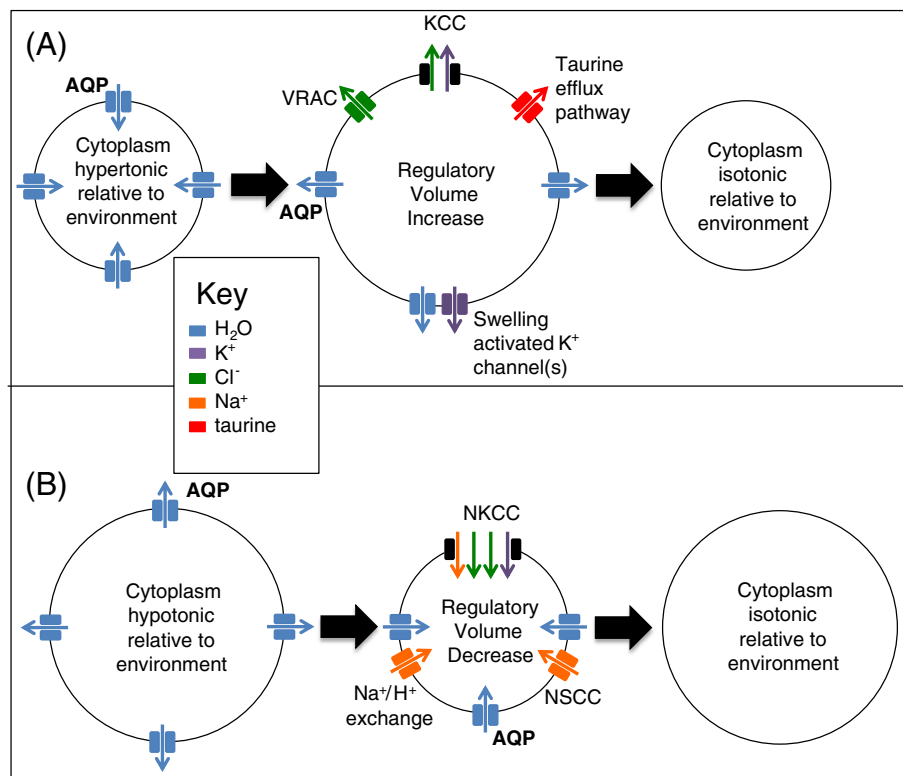


Fig. 2. Solute transport pathways mediating CVR (A) regulatory volume decrease and (B) regulatory volume increase. Water movement by osmosis may be through AQPs or directly through the cell membrane depending on the cellular AQP isoforms and expression levels. KCC: potassium chloride co-transporter; NKCC: sodium potassium chloride co-transporter; VRAC: volume regulated anion channel; NSCC: non-selective cation channel.

out of the cell, probably activated by tyrosine kinases [27,28]. It is also thought that four K^+-Cl^- co-transporters (KCCs), known to be activated by cell swelling, may be involved [29,30].

2.2. Regulatory volume increase

In RVI (Fig. 2), the activation of Na^+-H^+ exchangers and $Na^+-K^+-2Cl^-$ co-transporters (NKCCs) causes cellular influx of Na^+ and subsequent volume increase by osmotic movement of water [18]. The Na^+-H^+ exchange pump, NHE1, is known to be activated by cell shrinkage [31], which may be mediated by binding of calmodulin to its carboxy-terminus [32]. The co-transporter, NKCC1, is known to be activated by cell shrinkage, potentially through lysine-deficient protein kinase 1 (WNK1) and proline/alanine-rich protein kinase (SPAK) signalling [33]. Amiloride-sensitive non-selective cation channels (NSCCs) may also play a role [34].

2.3. The regulatory role of aquaporins

The water permeability of cell membranes may not be the rate-limiting factor in CVR [35], but any rapid change in cell volume is likely to involve AQP. For example, the stretch-activated transient receptor potential vanilloid type 4 (TRPV4) channel is a Ca^{2+} -biased NSCC that is activated by cell swelling [36] and has been implicated in osmosensing [37]. In some cell types TRPV4 has been shown to provide a Ca^{2+} signal that is correlated with activation of the K^+ and Cl^- channels responsible for the decrease in cellular osmolality associated with RVD [38,39]. In human and murine salivary gland cells, TRPV4 has a functional interaction with AQP5: in AQP5 knockout cells, the hypotonicity-induced calcium influx through TRPV4 was attenuated and subsequent RVD was abolished. Hypotonicity also increased cell surface expression of both TRPV4 and AQP5 and increased their co-localisation [40].

In another example, the sperm of AQP3 $-/-$ mice did not undergo their normal RVD process and the mice displayed reduced fertility [41,42]. Upon entry into the female reproductive tract, sperms normally encounter a decrease in extracellular osmolality, which is thought to be the signal that activates sperm motility [41]. However, this hypotonic stress also causes cell swelling which, if left uncorrected by RVD, leads to impaired fertilisation caused by excessive bending of the sperm tail inside the uterus [42]. If AQP3 was simply acting passively as a water channel, RVD would not be abolished in AQP3 $-/-$ mice but rather the timescale on which the cell reaches osmotic equilibrium would be increased. One explanation for reduced fertility and altered RVD in AQP3 $-/-$ mice is therefore that AQP3, either alone or as part of a macromolecular complex, is involved in the signalling pathway that activates RVD in sperm.

When exposed to a hypotonic extracellular solution, cultured renal cortical collecting duct (renal CCD) cells, which do not endogenously express AQP2, swell in proportion to the change in extracellular osmolality but do not exhibit RVD. However, when they are transfected with AQP2, these cells show an RVD of approximately 40%. Shrinkage is mediated by Ca^{2+} influx through TRPV4, which activates Ca^{2+} -dependent K^+ and Cl^- channels and Ca^{2+} -dependent Ca^{2+} release from intracellular stores. In renal CCD cells expressing AQP2, hypotonic stress causes translocation of TRPV4 to the plasma membrane, which is absent in AQP2-negative cells. When TRPV4 was translocated to the cell surface prior to hypotonic exposure using 4 α -phorbol 12,13-didecanoate, RVD was recovered in AQP2-null cells, showing that it is not simply the high water permeability of AQP2 that allows RVD. However, there does not appear to be any co-localisation between endogenous TRPV4 and overexpressed AQP2 in this system, either before or after hypotonic shock, indicating a functional rather than physical interaction [43]. These observations suggest that AQP2 (and therefore possibly other members of the AQP family) forms part of a sensory and signalling pathway that results in TRPV4 translocation, possibly via sensing of extracellular osmolality.

Taken together, these examples support the idea of a signalling or sensory role for AQP in RVD mechanisms. We have been unable to find any evidence of AQP playing similar roles in RVI. However, given that a variety of AQP could be involved in the RVD mechanism and that RVI and RVD share a common basic mechanism involving the movement of osmolytes to elicit a volume change, it would not be surprising to discover a link between RVI and AQP that goes beyond a passive water conduction mechanism.

3. Regulation of transcellular water flow in the human body

3.1. The brain and nervous system

3.1.1. Localisation of AQP

AQP are widely expressed in the central nervous system (CNS); indeed, more studies have been conducted on AQP in the CNS than on AQP in the peripheral and enteric nervous systems (for a detailed review on AQP in the nervous system see Papadopoulos et al. [44]). The major AQP found in the CNS are (i) AQP4 in the glia [45] and neurons [46], (ii) AQP1 in the epithelia of the choroid plexus (which forms the cerebrospinal fluid (CSF)-brain barrier) [47], dorsal root ganglia [48] and oesophageal neurons [49] and (iii) AQP9 in the substantia nigra [50]. Glial cells are not nerve cells but are essential for regulation and homeostasis of the CNS and comprise approximately 90% of cells in the brain [51]. Astrocytes are the most abundant glial cells within the brain [51] and high levels of AQP4 are expressed in their plasma membranes. The distribution of AQP4 is highly polarised to the astrocytic end feet, which contact the blood vessels associated with the blood-brain and brain-fluid interfaces [81]. The astrocytic end feet therefore function as part of the blood-brain-barrier (BBB) water exchange mechanism; this has been established to be AQP4 dependent since deletion of AQP4 in mice resulted in a 31% decrease in brain water uptake measured using the wet/dry mass method to determine brain water content [52].

3.1.2. Regulatory role of AQP

As the main AQP of the CNS, AQP4 is expected to play a major role in the regulation of water flow in the brain, spinal cord [53,54] and interstitial fluid surrounding neurons, thereby maintaining the K^+ concentrations required for neuroexcitation [46,55]. In support of this, when AQP4 was silenced in astrocytes by RNA interference, the apparent diffusion coefficient (which is a measure of water movement within tissues, determined by magnetic resonance imaging) was decreased by 50% in rat brain [56]. It is in this context that low AQP4 expression levels have been associated with epileptic seizures [55].

There is evidence that AQP translocation occurs in astrocytes, which may be responsible for the regulation of AQP abundance in the plasma membrane [57]. Although AQP4 is primarily expressed at the plasma membrane, its surface abundance is increased by AQP4-carrying vesicles in response to hypotonic stimuli in cultured rat cortical astrocytes: a positive correlation between vesicle mobility and AQP4 density at the plasma membrane was observed [58]. As well as AQP4, the stretch-activated TRPV4 channel is also strongly expressed in astrocytic end feet [59]. It has been suggested that AQP4 and TRPV4 are co-expressed and form a molecular complex, interacting at the plasma membrane to control CVR in astrocytes. When mouse primary astrocytes were put under hypotonic stress, an increase in intracellular Ca^{2+} was followed by an RVD response; this mechanism failed in cells deficient in AQP4 and in cells where RNA interference was used to silence TRPV4, even if they were transfected with AQP1 [59,60]. This suggests that RVD in astrocytes may be AQP4/TRPV4 specific, although the swelling of AQP1-expressing cells in this study was not as marked as for AQP4-expressing cells. Therefore, if total cell volume is the biophysical quantity being detected during the RVD response, it is possible that the loss of RVD simply reflects the fact that a volume threshold has not been met. If

there is an AQP4/TRPV4 interaction, it may be similar to the interaction between AQP2 and TRPV4 in renal cells [43], discussed above.

AQP4 has been largely associated with the pathophysiology of brain oedema [61] of which there are two major types: vasogenic oedema is the accumulation of water in the extracellular space, usually due to impaired function of the BBB; cytotoxic oedema is the swelling of astrocytes whilst maintaining their cellular integrity [44]. Movement of water from the blood across endothelia into astrocytes is mediated by AQP4 channels; reduced cytotoxic oedema was seen in AQP4 $-/-$ mice [62]. AQP4 is also thought to mediate the reabsorption of excess fluid in vasogenic brain oedema by transcellular movement of fluid from the extracellular space at the astrocytic end feet to the vascular and ventricular regions of the brain through the endothelial and epithelial barriers. In support of this, AQP4 null mice show an increase in brain water accumulation due to the reduction of transcellular water transfer to blood or CSF [61].

AQP1 expression is restricted to the choroid plexus region of the brain under normal conditions [47], but it is expressed in microvascular endothelia and reactive astrocytes of brain tumours where it is thought to play a role in the development of vasogenic oedema [63]. Osmotically-induced water transport was reduced 5-fold in AQP1 null mice along with a decrease in intracranial pressure and a 25% decrease in CSF production [47]. The same group also investigated the expression and localisation of AQPs in mouse spinal cord, an area that has not been the focus of many studies. Expression of AQP4 was detected in the astrocytic end feet of the grey matter in contact with capillaries and the fibrous glial processes of the white matter, again surrounding the blood vessels. The distribution of several other AQPs throughout the spinal cord suggests a role in maintenance of water balance via transcellular water flow; fluid moves rapidly from the spinal subarachnoid space into the perivascular space and across the interstitium into the central canal. This rapid water movement may be mediated by AQP4 and AQP9 in the glia limitans and AQP8 across the ependymal layer into the central canal [54].

In addition to its localisation in astrocytes, AQP4 is also expressed in the retina [64], the olfactory epithelium [65] and within Claudius' and Henson's cells of the inner ear [66]. Large K^+ fluxes trigger an AQP4-mediated transcellular water influx that exits via AQP4 channels localised on the basal membrane of Claudius' cells [66]; AQP4 involvement in CVR may be an important mechanistic component of acoustic signal transduction since AQP4 null mice are completely deaf but have no alterations to the morphology of the inner ear [66].

3.1.3. Conclusions

Transcellular water flow within the brain is largely associated with the formation and clearance of oedema; the highly-polarised distribution of AQP4 at the end feet of astrocytes is key in the absorption of excess vasogenic fluid for clearance by the capillaries into the bloodstream. However, AQP4 may have an additive effect on water accumulation in cytotoxic oedema as summarised in Fig. 3. The positioning of AQP1 along the epithelial barrier of the CSF-containing choroid plexus indicates a role in supplying water for CSF via a transcellular route. It is also evident that AQPs play an important role in signalling throughout the nervous system's peripheral and sensory organs by their contribution to CVR mechanisms and K^+ concentration maintenance. Understanding these mechanisms will be essential in developing treatments for brain oedema following stroke, trauma and meningitis.

3.2. The renal system

3.2.1. Localisation of AQPs

The role of AQPs in the kidney is one of the most extensively studied areas in AQP research [67]. The kidney is the major site of arginine vasopressin – (AVP; also called anti-diuretic hormone or ADH) mediated body water homeostasis; in response to osmotic stimuli, water reabsorption occurs through AQP channels enabling urine concentration.

AQPs in the kidney exhibit a highly-polarised and specific localisation pattern (Fig. 1): AQP1 is expressed in proximal tubule (PT) cells; AQP2 is very prominent in the renal collecting duct (renal CD) principal cells and is found at the apical plasma membrane [68] and in sub-apical vesicles [1]; AQP3 and AQP4 are expressed in renal CD cells at the basolateral membrane [69,70]. AQP1 is responsible for most water reabsorption in the kidney [71] while AQP2 fine tunes water reabsorption; it is translocated within the sub-apical vesicles to the apical membrane after AVP activation, increasing membrane water permeability [1]. Once water has entered a renal CD cell, AQP3 and AQP4 provide exit routes to the blood [72].

3.2.2. Regulatory role of AQPs

AQP2/AVP-activated translocation is induced by a well-studied protein kinase A (PKA)-dependent pathway [73]. Upon recognition of an osmotic stimulus, AVP is released and subsequently binds the G protein-coupled receptor (GPCR), vasopressin V_2 receptor (V2R), on the basolateral membrane of renal CD principal cells. This results in G protein activation of PKA and subsequent phosphorylation of AQP2 at Ser266 within intracellular vesicles; this facilitates vesicle translocation along the microtubule networks to the apical membrane [74] (Fig. 3A, B). The critical role of this mechanism in the fine control of water reabsorption is exemplified by its dysfunction in nephrogenic diabetes insipidus; in this disease, mutations in the vasopressin 2 receptor or in AQP2 itself lead to a decreased ability to concentrate urine [75].

An intracellular Ca^{2+} influx is needed to generate the necessary RVD response following hypotonic exposure; in the distal kidney, this only occurs in the presence of AQP2 [76]. A functional interaction between the Ca^{2+} -permeable TRPV4 ion channel and AQP2 has been demonstrated to occur under hypotonic conditions in renal CD cells and is involved in RVD. Notably, the TRPV4 channel is only activated in cells that express AQP2. When TRPV4 is blocked by ruthenium red, Ca^{2+} entry is abolished along with RVD. This confirms AQP2 and TRPV4 as essential components of the hypotonicity-induced RVD cellular response [43]. It has also been shown that AQP2 can regulate CVR by interacting with tropomyosin 5b (TM5b) and altering the dynamics of the cytoskeleton. Ser256 phosphorylation induces an AQP2-TM5b interaction leading to depolymerisation of actin filaments; this mechanism is reversible [77].

AQP2 is also regulated independently of AVP in response to hypertonic conditions. Hypertonic exposure (600 mOsm/kg) was shown to significantly increase activity of the AQP2 promoter, independent of AVP, in MDCK cells expressing murine AQP2. The responsive element was suggested to reside between -6.1 and -4.3 kb 5' flanking region of the AQP2 gene [78]. Acute hypotonicity has also been shown to induce translocation of AQP2 to the plasma membrane in the absence of AVP: rapid plasma membrane and trans-Golgi network accumulation of AQP2 in rat renal CD cells were shown to be dependent on MAPK, P38 and ERK1/2 activity [79].

Early reports suggested that AQP1 was constitutively expressed in PT cell membranes in the kidney [80], however recent studies have shown that AQP1 is expressed in both the cytoplasm and in the membrane of cultured cells and can be induced to undergo rapid and reversible translocation to the plasma membrane upon hypotonic stimulation mediated by TRP channels, calcium, PKC and microtubules [57,81]. AQP1 has also been shown to undergo translocation to the plasma membrane of cholangiocytes in response to secretin activation of specific G protein-coupled receptors [82]. Further studies have demonstrated that the diuretic effect of acetazolamide involves triggered AQP1 translocation by promoting AQP1 and myosin heavy chain interactions causing AQP1 localisation to proximal tubule cell membranes followed by ubiquitin-mediated AQP1 degradation through the proteasome [83]. AQP2 ubiquitination has also been shown to be involved in AQP2 expression and localisation [84]. Phosphorylation of AQP1 has been shown to be involved in translocation of AQP1 to the plasma membrane in oocytes [85].

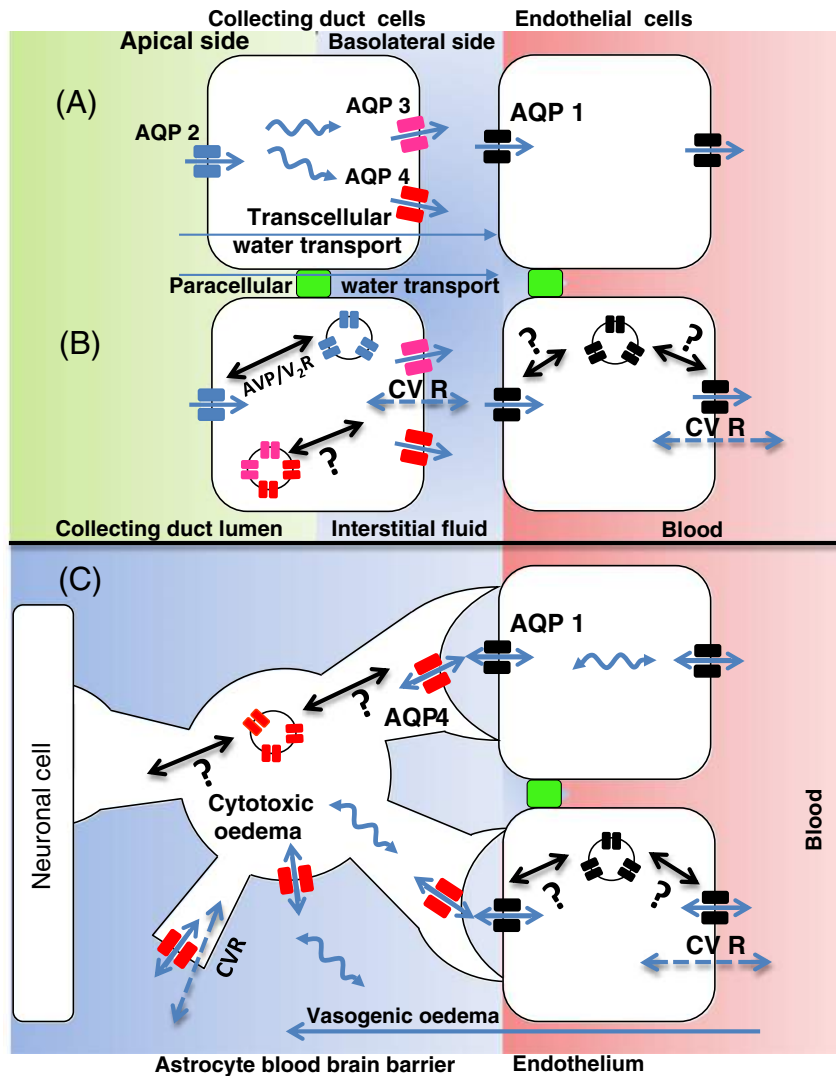


Fig. 3. Human AQPs are regulators of transcellular water flow. (A) Paracellular water flow and AQP-mediated transcellular water flow in the kidney collecting duct. (B) Mechanisms of AQP regulation in kidney collecting duct via triggered translocation. (C) Involvement of AQPs in transcellular water flow in brain oedema. Blue arrows, H₂O movement; black arrows, AQP translocation; green box, tight junction; AVP/V₂R, arginine vasopressin/vasopressin 2 receptor-stimulated AQP2 translocation; ?, Unknown translocation mechanism, and blue dashed arrow: regulatory role of AQPs in CVR (for details see Fig. 2).

3.2.3. Conclusions

Kidney AQPs form a highly-organised network that facilitates the maintenance of water homeostasis. The specific localisation of AQPs within renal CD cells provides a transcellular pathway for water to be reabsorbed from the urine through AQP2 channels into renal CD cells and back into the blood via AQP3 and AQP4 on basolateral membranes. The regulation of AQP1 expression and translocation mediates transcellular water flow in PT cells [83].

3.3. Specialised secretory tissues

3.3.1. Localisation and regulatory roles of AQPs

Specialised secretory tissues rely on AQP-dependent transcellular water flow to facilitate their fluid homeostasis. In the salivary gland, AQP5 facilitates transcellular water flow in both acinar and parotid salivary cells [86]; the salivary cells isolated from AQP5 ^{-/-} mice had dramatically reduced membrane water permeability following exposure to hypertonic or hypotonic conditions [3]. The localisation of AQP5 on the luminal membrane is consistent with the membrane's high water permeability and its role in osmotic water transport from the acinar cells to the lumen of the gland used in the production of saliva [87,88].

Immunohistochemistry of human salivary glands (HSG) has demonstrated that AQP3 is present on the basolateral membranes of mucous and serous acinar cells [89], indicating a possible role for AQP3 as well as AQP5 in transcellular water flow during saliva formation [89].

In HSG, AQP5 translocation was shown to occur in a microtubule-dependent manner; elevation of [Ca²⁺]_i by stimulation with thapsigargin (a Ca²⁺-ATPase inhibitor) and a Ca²⁺ ionophore resulted in AQP5 localisation at the plasma membrane, which was inhibited by pre-treatment with the microtubule inhibitors, colchicine and vinblastine [90]. GFP-tagged human AQP5 has been shown to translocate to the plasma membrane of HSG cells upon stimulation with carbachol (a muscarinic type 3 receptor (M₃R) agonist) [91], but little is known about the molecular mechanisms involved.

AQP5 translocation to the apical membrane of rat parotid gland cells has been shown to occur following stimulation of M₃R with acetylcholine (ACh) and subsequent [Ca²⁺]_i elevation. Furthermore, following incubation with a Ca²⁺ ionophore translocation was activated without ACh stimulation [92]. Increased levels of AQP5 mRNA and protein were observed when rat submandibular acinar cell lines were exposed to hypotonic conditions causing rapid cell swelling and more efficient RVD. EGTA chelation of intracellular and extracellular Ca²⁺ did not

affect CVR in a rat acinar cell line; in fact CVR was found to be K^+ - and Cl^- -dependent, with mitogen-activated ERK-activating kinase (MEK) and the β -amino acid, taurine, playing important roles [93].

Increasing $[Ca^{2+}]_i$ has been shown to trigger AQP5 translocation from cytosolic compartments to the plasma membrane while the removal of extracellular Ca^{2+} has been shown to inhibit translocation of AQP1 in HEK293 cells [57]. Acinar cells from mice lacking the TRPV4 channel or AQP5 display reduced hypotonicity-induced Ca^{2+} influx and a suppressed RVD response suggesting an important role for TRPV4 and AQP5 interactions in generating the Ca^{2+} response required for effective RVD after hypotonic cell stress [40]. There is little knowledge on the regulation of AQP5 in sweat glands. Eccrine sweat glands have a high water permeability to support their role in fluid secretion; primary sweat is deposited into the lumen of the eccrine gland before water movements allow sweat to be secreted through the ductal region [94]. Recently, AQP5 has been shown to be expressed in apical membranes, intracellular canaliculi of secretory coils and in basolateral membranes of human eccrine sweat glands. Rapid apical translocation of human AQP5 occurs in stably-transfected MDCK cells after treatment with the Ca^{2+} ionophore, A23187, suggesting the involvement of $[Ca^{2+}]_i$ in AQP5 translocation. Rapid translocation of AQP5 to the apical plasma membrane of cells has also been shown in mouse sweat glands during sweating [95]. In humans, ACh activation of muscarinic receptors raises $[Ca^{2+}]_i$ and induces sweating [94]. It is thought that AQP5 regulation by $[Ca^{2+}]_i$ contributes to sweat release by increasing apical membrane permeability, and that AQP5 may co-localise with the Ca^{2+} channel, ANO1, at the plasma membrane [95]. However, the mechanisms behind AQP5 translocation within the sweat gland, including the role of phosphorylation, still require further elucidation.

3.3.2. Conclusions

AQP5 is involved in regulating transcellular water flow in the luminal regions of glands. This facilitates the formation of secretions at the necessary concentrations and viscosities required to maintain water homeostasis.

3.4. The integumentary system

3.4.1. Localisation and regulatory roles of AQPs

The integumentary system comprises the skin, hair and nails, but nerves, certain glands and fat are often also classified as parts of the integument. The skin plays an integral part in water homeostasis and provides a barrier function against excessive water loss. Its water and glycerol content is essential for normal function; this is largely under the control of AQP3, which is expressed mainly in the plasma membranes of the stratum basale of the epidermis, with decreasing expression towards the stratum granulosum and none in the stratum corneum [96]. Sugiyama and colleagues [97] first reported expression of AQPs 3 and 9 in human cultured keratinocytes, although AQP9 was only observed in differentiating cells. AQP3-null mice display impaired barrier function and reduced stratum corneum hydration, which was not corrected by skin occlusion or exposure to high humidity. However, topical or oral administration of glycerol has shown to correct many defective skin functions in AQP3-null mice [98].

AQP1 has been detected in skin biopsies in a study of atopic eczema, although its expression was no different in diseased or control skin, whereas up-regulation of AQP3 was found [99]. Skin diseases that show reduced stratum corneum hydration display altered expression levels of AQP3, dependent upon the disease. In 2011, Voss and colleagues showed that in psoriatic skin, AQP3 was preferentially expressed in the cytoplasm rather than the plasma membrane suggesting that AQP3 may be important for transcellular water and glycerol transport. AQP5 is also thought to be expressed at the plasma membrane in the stratum granulosum and may play a role in transcellular water homeostasis in the skin [100].

AQP7 is the primary glycerol transporter in white (WAT) and brown (BAT) adipose tissues. AQP7 is abundantly expressed in the plasma membrane of adipocytes and fasting has been shown to up-regulate AQP7 mRNA in the adipocytes of rodents [101]. In the model mouse adipocyte cell line, 3T3-L1, increases in AQP7 mRNA expression and glycerol release were correlated during cell differentiation indicating that plasma membrane glycerol permeability may mediate the accumulation of fat in adipocytes [102]. AQP3 and 9 are also expressed in human adipose tissue, with AQP3 predominantly localised in the cytoplasm and AQP9 constitutively expressed in the plasma membrane; a positive correlation between the transcript levels of AQPs 3, 7 and 9 and body weight (BMI) has been suggested [103]. AQP7 gene expression is down-regulated in the WAT of obese human subjects compared with normal controls [104,105], but unchanged in type 2 diabetes [104]. However, the link between human AQPs and obesity is contradictory; a review by Maeda et al. [106] describes some of these studies. More recently AQP10 has been proposed to be an alternative pathway for glycerol efflux in human adipocytes [107].

3.4.2. Conclusions

AQP3, 7, 9 and 10 are aquaglyceroporins. It is therefore likely that the roles of these AQPs in the integumentary system primarily involve transport of glycerol, although they may also be involved in the regulation of transcellular water flow; this remains to be determined.

3.5. The cardiovascular system

3.5.1. Localisation and regulatory roles of AQPs

Cardiac AQPs have not been investigated to the same extent as AQPs in the brain and kidney. In the heart, water moves from the interstitial space, across endothelia and into blood vessels. This process is typically attributed to paracellular water transport through the endothelium of the heart since it is considered to be 'leaky' compared to the endothelium of other organs [108]. Myocardial stunning is the reduced output of the heart, often seen following cardiac surgery such as heart bypass, and has been associated with cell swelling and oedema. The expression of members of the AQP family in the myocardium has been poorly characterised and their role, if any, in the pathology and resolution of cardiomyocyte swelling, oedema and general function within the heart has not been investigated (for a detailed review on AQPs and myocardial water management see Egan [109]).

AQP1 has been detected in the human, rat and mouse heart tissue [110], while AQP4 has only been detected in the mouse heart [110]. Immunofluorescence images revealed that the abundantly-expressed AQP1 is distributed in human and murine cardiac microvasculature at high levels only because of the dense vascularity of the heart muscle [110]. Immunofluorescence also showed that AQP4 was localised in the plasma membranes of the cardiomyocytes of the mouse heart tissue. Functional studies on cardiac membrane vesicles from AQP1 and AQP4 knockout mice found that only AQP1 had a role in water permeability in the heart; vesicles from AQP1-null mice had reduced permeability but deletion of AQP4 produced no reduction in water permeability [110]. A study using rabbit ventricular cardiomyocytes suggested that water movement in the heart is mediated by paracellular water flow and does not occur via AQPs [111]. On the rare occasion that an osmotic gradient is present in the heart (e.g. during cell swelling after cardiac surgery), endothelial AQP1 might mediate the flow of water from the expanded interstitial space into the capillaries [112]; indeed AQP1 is the major AQP expressed in vascular endothelial cells [113].

There is controversy over the details of AQP4 expression in the human heart; some studies have reported mRNA expression but no or very little protein [110]. However, a recent study [114] demonstrated the presence of AQP4 protein in the human heart using Western blotting; it was localised to the plasma membrane with a very weak signal in the cytosol. Immunoblot analyses of cultured mouse cardiomyocytes also showed that AQP4 was present while immuno-gold

electron microscopy images showed AQP4 protein on the plasma membrane of the cardiomyocytes. Cardiac oedema arises when tissue with a reduced blood supply (ischemic) becomes hypertonic, causing water to flow from the capillaries (possibly via AQP1) into cardiomyocytes; this causes cell swelling and reduced cardiac output. Ischemic mice had a decrease in AQP4 mRNA, as measured by RT-PCR. AQP4 knockout mice presented with lower cardiac ischemic injury, measured as infarction, suggesting that AQP4 may be a possible target for treatment of myocardial infarction.

3.5.2. Conclusions

The major AQP of the cardiovascular system is AQP1 (Fig. 1), which probably regulates water permeability of the heart's capillary networks by mediating the flow of water through the endothelial layer into the blood. AQP1 may aid the absorption of excess water from the interstitial space into the capillaries, however this is controversial. Further research is therefore required on the role of AQPs in the heart; this might provide evidence for AQP1 and/or AQP4 as drug targets for the treatment of myocardial stunning oedema within the interstitium. AQP4 has only recently been detected at the protein level within human cardiomyocytes, which could lead to research into AQPs as transcellular water transporters for clearance and formation of interstitial oedema and cardiomyocyte swelling.

3.6. The airway

3.6.1. Localisation of AQPs

Airway hydration, sub-mucosal secretions and alveolar fluid transport all require water permeability of the epithelial and endothelial membranes of the airway [115]. AQPs are consequently expressed in bronchopulmonary tissues (Fig. 1) and are regulated in a way that facilitates transcellular water transport [116,117]. AQP1 is expressed predominantly in the microvascular endothelia throughout the lung and upper airways [117], while AQP3 and AQP4 are present in the basolateral membranes of the airways' epithelial lining [88]. AQP5 is expressed in the apical membrane of type I alveolar epithelial cells of the distal lung and acinar sub-epithelial glandular cells, which provides the major route (along with AQP1) for the osmotically driven flow of water within the entire airway system [118]. AQP5 is also expressed superficial epithelium of the bronchus and, as such, is ideally placed to regulate the hydration of the airway surfaces [119]. Indeed, studies with knockout mice have shown that AQP5 enhances fluid secretion [120]. In addition, AQP5 expression is reduced in inflammatory airway conditions, such as chronic obstructive pulmonary disease (COPD), that associate with mucus hypersecretion [119]. Modulation of AQP5 expression could therefore serve as therapy for inflammatory airway conditions, alleviating symptoms such as the increase in desiccated mucus which potentiates the chronic airways infections typical of cystic fibrosis [121].

3.6.2. Regulatory role of AQPs

When AQP expression within the airway was first discovered, several murine AQP knockout studies were published that investigated the hypothesis that water can be transported from the alveolar airspace across the interstitial and capillary compartments via osmotically-driven AQP transport. Initially, osmotic water permeability (P_f) of the lungs was measured in AQP1 and AQP4 knockout mice; P_f was reduced by 10-fold in the endothelia of AQP1 null mice suggesting a transcellular route. However, it was concluded that AQP1 does not provide the route for alveolar fluid absorption and little effect was observed on P_f in the AQP4 knockout studies [122]. A year later, the same group conducted a very similar study, this time using AQP5 knockout mice; the airspace-capillary P_f was reduced by 10-fold in the AQP5 knockout and a further 2–3-fold when a double knockout of AQP1/AQP5 was used. The authors concluded that AQP5 and AQP1 are the main routes for transcellular water flow in the airway with the primary role of

AQP5 being water transport across the apical plasma membrane of type I alveolar epithelial cells [123].

TRPV4 was subsequently shown to regulate AQP5 abundance under hypotonic conditions in mouse lung epithelial (MLE) cells [124]. After 2 h in hypotonic medium, a decrease in AQP5 abundance in MLE cells was observed; this result was observable after 30 min but not before 10 min exposure. This decline in AQP5 was blocked in the presence of ruthenium red, which is a TRPV4 inhibitor, and also when the cells were cultured in Ca^{2+} -free medium, even when the osmolality was reduced to 127 mOsm (which is hypotonic); these data support a role for extracellular Ca^{2+} in the regulation of AQP5 abundance. RT-PCR results showed that mRNA levels were not affected when protein levels decreased. When a lysosomal inhibitor was added, a reduction in AQP5 mRNA levels was not seen suggesting that AQP5 protein is probably undergoing degradation. The same results were observed in TRPV4-expressing and control HEK-293 cells transfected with AQP5; an AQP5 reduction in response to hypotonicity was only seen in cells expressing TRPV4, which was also blocked by ruthenium red. The regulation of membrane permeability by AQP5 abundance was concluded to be tightly controlled by osmolality and mediated by TRPV4 [124].

Further evidence that osmolality regulates AQP5 expression was provided by Hoffert and colleagues [125], who showed that hypertonic stress induces AQP5 expression in MLE cells cultured in hypertonic medium (500 mOsm). AQP5 protein levels increased after 8 h and peaked 24 h post-exposure, returning to baseline after 6 h in isotonic medium. Only relatively impermeable solutes affected AQP5 expression, suggesting that an osmotic gradient between a cell and its environment is involved in the regulation of AQP5 expression. This expression mechanism was demonstrated to require the activation of the extracellular signal-regulated kinase (ERK) pathway since several ERK inhibitors blocked AQP5 expression; however without a hypertonic stimulus, AQP5 expression was inhibited and ERK activators failed to induce expression. In the same study, rats that had been given daily intraperitoneal injections of hypertonic saline had a 2-fold increase in AQP5 expression in the lung compared with control rats, suggesting the physiological relevance of AQP5 regulation mechanisms in vivo [125].

AQP5 expression has also been shown to be regulated by a cyclic AMP/protein kinase A (cAMP/PKA)-dependent pathway. In MLE cells, addition of the cell-permeable cAMP analogue, cpt-cAMP, caused a 4-fold increase in AQP5 mRNA and protein levels in a dose-dependent manner; increased protein synthesis was ablated by the addition of the PKA inhibitor, H89. Immunofluorescence studies using confocal microscopy on MLE cells after a 24 h cpt-cAMP treatment revealed that AQP5 was translocated to the apical plasma membrane. Increasing endogenous cAMP levels by treatment with forskolin and the β -adrenergic agonist, isoproterenol, also induced AQP5 protein expression. The forskolin effect was also seen to work ex vivo in murine lung tissue suggesting that this cAMP-dependent molecular mechanism may occur in vivo [126].

Sidhaye and colleagues [127] looked at the effects of cAMP on the regulation of AQP5 distribution and abundance. Using AQP5-expressing mouse lung epithelial cells, the distribution of AQP5 was observed by immunofluorescence and surface biotinylation. After short-term treatment of cells with cAMP, AQP5 was internalised and there was a reduced abundance of AQP5 at the membrane; long term exposure to cAMP (approximately 8 h) resulted in higher-than-baseline AQP5 abundance at the apical membrane indicating an up-regulation of AQP5 membrane expression. Following short-term exposure, AQP5 abundance was also temporarily decreased followed by a marked increase after an 8 h exposure. When cells were treated with the β -adrenergic agonist, tetrabutaline, which is known to increase intracellular levels of cAMP, identical results to those observed after cAMP addition were seen in terms of distribution and protein abundance. The same effects were observed in vivo using mice injected subcutaneously with the agonist. When the PKA inhibitor, H89, was

added, all cAMP-dependent effects were inhibited, additionally purified AQP5 was phosphorylated by PKA but not PKC or casein, indicating that PKA activation is required for AQP5 regulation in the airways.

Contrasting results were obtained from a study in which human bronchial epithelial cells were stably transfected with wild type (WT) AQP5 and two AQP5 mutants [128]. The first mutant was an alanine substitution of Ser156, the PKA substrate site for phosphorylation of both AQP2 and AQP5, which is involved in AQP2 apical membrane translocation. The second mutation was within the second Asn-Pro-Ala motif, which forms the AQP pore. These experiments were designed to examine the importance of pore formation and PKA phosphorylation on the membrane expression of AQP5. WT-AQP5 was shown to be expressed at the apical plasma membrane and in sub-apical vesicles, while the Ser156Ala mutant also showed membrane expression. This indicated that blocking the PKA binding site did not affect AQP5 translocation as in the case of AQP2. Expression of an Asn185Asp mutant was localised throughout the cytoplasm suggesting that like AQP1, AQP5 requires the Asn-Pro-Ala motif for correct channel formation and that it may have a role in either protein folding or oligomerisation. When the PKA inhibitor, H89, was used, no difference in membrane expression compared to the basal level was seen after 30 min, which was also the case after a 30 min cAMP treatment in all three stable cell types. AQP2 translocation to the apical membrane was induced by the addition of cAMP and this was blocked by pre-treatment with H89. Also when the AQP2 Ser156 was mutated, AQP2 was expressed within the cytoplasm and unable to translocate to the membrane. In WT-AQP5 and Asn185Asp mutant cells, phosphorylation was seen before the addition of cAMP. However, in the Ser156Ala mutant cells, AQP5 was never phosphorylated indicating that Ser156 is the PKA substrate in AQP5, that membrane localisation of the protein is not regulated by PKA and that cAMP stimulation may be a separate event in contrast to the AQP2 mechanism and the previous studies conducted by other groups [128].

3.6.3. Conclusions

Direct evidence has been published for the involvement of AQPs in transcellular water flow across the alveolar epithelium via an apical AQP5 route and through AQP1 in the endothelia [118]. This movement of water between the alveolar airspace and capillary compartments is essential for airway hydration, effective airways defences and reabsorption of excess alveolar fluid.

3.7. The reproductive system

The permeability of cell membranes to water and hormones in both the male and female reproductive systems is essential for folliculogenesis [2], spermatogenesis [129] and sperm osmoadaptation [41]. There are few studies on the regulation of AQPs in the reproductive system, but expression profiles have been outlined and up-to-date reviews are available [41,129,130]. Emerging evidence suggests physiological roles for AQPs within human reproductive systems and that water shifts are often transcellular and AQP mediated [2]; AQPs have recently been associated with the pathogenesis of some reproductive disorders such as polycystic ovary syndrome (PCOS) [131] and ovarian cancer, where AQP5 and AQP9 up-regulation were observed within the tissue of malignant ovarian tumours [130].

3.7.1. The female reproductive system

The role of AQPs in the ovary, specifically the ovarian follicle, has been well studied. During folliculogenesis, the antrum is expanded by a large, rapid influx of water through the granulosa cell (GC) lining; it is unknown whether this water transport is mediated by paracellular mechanisms or by transcellular flow through AQP channels. McConnell and colleagues [2] demonstrated that water movement into the antrum of isolated rat follicles was 3.5-fold greater than that of C-inulin (a complex sugar that moves through tissues via paracellular transfer),

indicating that the influx of water into the antral cavity has a transcellular component. When follicles were pre-treated with HgCl₂ (an AQP inhibitor), the movement of water was reduced to that of inulin. This suggested a role for AQPs in mediating water movement during folliculogenesis, especially in light of the detection of AQP7, AQP8 and AQP9 in GCs by flow cytometry [2]. AQP7 and AQP9 are aquaglyceroporins; their presence within the ovarian follicle suggests that the ability of small neutral solutes to be transported rapidly across the plasma membrane may be a requirement of folliculogenesis.

In a recent study in women with PCOS, immunofluorescence was used to confirm the presence of AQP9 in the nucleus, cytoplasm and plasma membrane of human GCs. In a study of 14 PCOS sufferers and 31 control subjects who were infertile from tubal blockage, GCs and follicular fluid were collected from the participants. Total testosterone (TT) and luteinising hormone (LH) levels were elevated in follicular fluid from PCOS compared with samples from control women; sex hormone binding globulin (SHBG) levels were lower in PCOS patients. RT-PCR results indicated that AQP9 mRNA levels were decreased in PCOS sufferers and that there was a significant correlation between AQP9 mRNA and TT, LH and SHBG levels in PCOS samples, but no correlations in control samples. In vitro studies showed that the treatment of GCs with dihydrotestosterone (DHT) had an inhibitory effect on AQP9 mRNA expression and that the addition of LY294002, a phosphatidylinositol 3-kinase (PIK3) inhibitor, attenuated this down-regulation such that AQP9 mRNA levels were raised compared with those treated with DHT alone. The addition of H89 and forskolin did not rectify the DHT-initiated AQP9 mRNA decrease suggesting that PKA and cAMP pathways are not involved in this mechanism. This suggests that hyperandrogenism (excess of androgenic hormones) of the follicular fluid occurs in PCOS and this suppresses AQP9 expression in GCs through a PIK3 pathway affecting follicular development [131]. Further work into the mechanisms behind AQP9 regulation in healthy and pathogenic ovaries may provide insight into possible treatments for diseases where hyperandrogenism is an issue.

The data discussed above suggest that transcellular water flow into the antrum of the ovarian follicle is a key aspect of folliculogenesis and that the movement of water for expansion of the antrum is likely to be AQP mediated.

3.7.2. The male reproductive system

There is increasing evidence that AQPs play an important role in sperm cell RVD; this ensures maintenance of the structure and function of sperm and thus male fertility. AQP7 cDNA was first isolated from rat testis and was shown to be expressed abundantly throughout the testis and in the plasma membrane of late stage spermatoids [132]. Aquaglyceroporins, AQP3 and AQP7, have been identified within human sperm [40,41,42,131,132,133] and their roles investigated. AQP3 has been described as the regulator of sperm osmoadaptation during male to female transition, during which sperm are exposed to a hypo-osmotic environment with the potential to harm the sperm by excess swelling and reduced motility [41]. AQP3 is located at the plasma membrane of the sperm flagellum; AQP3 mutant cells show decreased motility, increased swelling and tail bending after entering the hypotonic environment of the uterus therefore hindering the sperm's chances of reaching the oviduct and mediating a fertilisation event. These defects are probably due to ineffective RVD mechanisms and consequent swelling after hypotonic stress [42]. A more recent study has outlined a relationship between AQP7 localisation and sperm characteristics; transmission electron microscopy images showed expression of AQP7 within the pericentriolar region of the neck, equatorial region of the acrosome and a diffuse staining along the tail. Abnormal sperm samples, characterised by malformations of the head, midpiece, or tail, displayed lower intensity and diffuse staining in the cytoplasmic residual bodies, head and tail. A specific correlation between normal sperm AQP7 labelling and sperm

motility and morphology suggested that AQP7 also has a role in regulation of sperm cells and male fertility [134].

Several members of the AQP family are expressed within the epididymis of the male reproductive tract [129]. They are localised to the epithelial layer and are thought to play an important role in trans-epithelial water transport and sperm concentration [129]. AQP9 was the first AQP identified in the epididymis [135] and has been labelled the major apical AQP of the epithelium principal cells; it allows transepithelial flow of solutes such as glycerol, urea, mannitol and sorbitol and is modulated by androgens in male adult rats [136]. AQP3 is localised exclusively to the basal cell membranes of the epididymis and although AQP1 is absent from the epididymis epithelial cells it is expressed within the smooth muscle and endothelium of the vascular channels throughout the epididymis [137], together with AQP10 [138].

AQPs are important in facilitating an RVD response in sperm cells especially upon the introduction to the hypotonic environment of the female reproductive tract, which in AQP3-deficient sperm can cause detrimental swelling and reduced mobility. If the regulation of sperm cells is dependent upon RVD mechanisms, future work into this field should concentrate on elucidating these mechanisms. RVD mechanisms in other tissues often involve complexes with AQPs, such as the AQP4/TRPV4 complex in astrocytes [60] and the AQP2/TM5b interaction in the kidney [77]. It is therefore feasible that AQP3 and/or AQP7 in human sperm might form molecular complexes with ion channels such as the volume sensitive chloride channel CLC-3, which has been identified in mammalian sperm and implicated in RVD [139,140].

3.8. The digestive system

3.8.1. Localisation and regulatory roles of AQPs

Secretion and absorption, two of the main functions of the digestive system, both require the transfer of fluid across cellular membranes. Daily secretions in the form of saliva, gastric juices, intestinal mucous, bile and pancreatic juice comprise a total volume of approximately 7.5 L of fluid in the human digestive system; approximately 9 L of fluid is absorbed daily [141]. Several members of the AQP family are expressed throughout the digestive system including AQP1 in the apical and basolateral membranes and the cytoplasm of cholangiocytes, the pancreas and throughout the endothelial cells of capillaries responsible for transendothelial water transfer [142]; the epithelial lining of the gastrointestinal tract contains AQP3 [143] and AQP4 [144,145]. Pancreatic duct cells express AQP8 in the apical plasma membrane [146] and AQP8 [147] and AQP9 [148] are found in the hepatocytes of the liver; in-depth reviews on the expression and localisation of AQPs in the digestive system are available elsewhere [141,149].

In the upper digestive tract, AQP3 is expressed abundantly in stratified epithelia of the oral cavity to the fore-stomach. AQP3 is localised in the basal and intermediate cell membrane becoming less abundant towards the epithelial surface and is thought to provide a supply of water from the sub-epithelial side of these cells which face harsh conditions, such as the low pH of the stomach, to prevent them from dehydration [143]. Immunocytochemistry has shown strong AQP4 expression at the basolateral membrane of the gastric parietal cells in mice and was hypothesised to play a role in gastric acid secretion. Wang and colleagues [144] used several secretory agonists to increase gastric acid output in AQP4 null and control mice; no significant differences were seen in secretion levels suggesting that the deletion of AQP4 did not affect the stomach's ability to secrete gastric acid [144].

In the distal colon and rectum, AQP3 is localised on the basolateral membrane of the epithelial cells lining the lumen [143]. Inhibition of AQP3 by HgCl₂ in rats induced severe diarrhoea, suggesting a role for AQP3 in regulating faecal water content [150], although it should be noted that mercury is a toxic, non-specific inhibitor of AQP3 [151]. AQP3 may mediate the reabsorption of water from faeces by transporting it from the lumen, across the endothelial layer into the blood vessels via AQP1 [113]. The mechanism by which this is

controlled is unknown but further understanding could lead to treatments for over- or under-active bowel problems. For example, the temporary inhibition of AQP3 could have a laxative effect.

AQP8 may have a role in bile secretion in hepatocytes, which are responsible for the formation of bile before it is secreted into the bile duct and modified by cholangiocytes. AQP8 was detected in the cytoplasm and intracellular vesicles of rat hepatocytes by confocal microscopy. Short-term treatment with cAMP induced re-distribution of AQP8 to the plasma membrane and an increase in water permeability within 10 min. The microtubule inhibitor, colchicine, blocked the effects of the cAMP treatment indicating that AQP8 translocation is stimulated by cAMP and is microtubule dependent [152].

3.8.2. Conclusions

The digestive system is a major site of fluid movement and has a wide AQP expression profile within its organ network. A polarised AQP expression pattern suggests that an organised transcellular route for water is an essential role of AQPs in facilitating high secretion and absorption rates.

3.9. The musculoskeletal system

3.9.1. Localisation and regulatory roles of AQPs

Articular cartilage and intervertebral disc (IVD) tissue are specialised biomechanical structures that are under constant compressive loads [153,154]. The cells within these avascular tissues are exposed to constantly harsh conditions as the IVD is ~80% water [155] and articular cartilage tissue is around ~70% water [156]. The IVD is composed of three distinct regions: the gelatinous nucleus pulposus (NP), which is encapsulated by the annulus fibrosus and the cartilaginous end plates [153]. The native cells of the NP and cartilage tissue both secrete proteoglycans and type II collagen; the collagen meshwork traps negatively-charged proteoglycans (such as aggrecan) which attract cations (mainly K⁺, Na⁺ and Ca⁺) resulting in the influx of water; this process is responsible for the high osmotic potential of these tissues [157,158] enabling them to resist static and dynamic biomechanical loads [154]. Both the NP cells and the chondrocytes must regulate their volume and water content in these rapidly changing osmotic environments; however little is known about the mechanisms which they employ to do this. Recently, studies have taken place to identify which AQPs are expressed in these tissues; AQP1 and low levels of AQP3 have also been identified within the NP cells of the human IVD [159] while AQP1 and AQP3 have been shown to be expressed and co-localised at the membrane of equine articular cartilage chondrocyte cells [154] and chondrocytes of the human knee [156].

AQP1 and AQP4 are expressed in skeletal muscle and a study has shown that cell volume changes that occur during muscle contraction rely on rapid water influx [160]. AQP1 was found in the endothelial cells of capillaries within the muscle tissue and AQP4 on the plasma membrane of muscle fibre cells [160]. The localisation of AQP1 and AQP4 within the muscle tissue suggests a pathway for transcellular water flow through the endothelial cell membrane and the sarcolemma; these AQPs may function together as transporters for water between the blood and myofibrils during mechanical muscle activity.

3.9.2. Conclusions

It is not surprising that the native cells of the NP and articular cartilage express AQPs and it is highly likely that AQPs are responsible for CVR in these highly osmotic environments. More work is required to elucidate the functional roles of aquaporins in these tissues; a number of published studies have suggested roles for AQPs as components of the vital cellular apparatus for maintenance of physiological homeostasis of the musculoskeletal system.

4. Conclusions

The constitutive distribution of AQPs is achieved by AQP gene expression and/or AQP protein degradation on a timescale from hours to days [161]. Further rapid spatial and temporal distribution of AQPs is regulated by stimulated or triggered translocation of AQP-containing vesicles to and from a particular membrane. This is particularly well studied for V2R-mediated AQP2 translocation in kidney collecting duct cells [74] (Fig. 3B). Similar mechanisms of triggered translocation have been demonstrated for other AQPs [57]. We propose that the resulting spatial and temporal distribution of AQPs is crucial for the regulation of transcellular water flow in the major systems of the human body.

For example, reabsorption of water from the lumen of the kidney collecting duct involves transcellular water flow mediated by AQP2 at the apical membrane and AQP3 and AQP4 at the basolateral membrane. Transcellular water flow through endothelial cells of the capillary into the blood is then mediated by AQP1 (Fig. 3A). In another example, AQP4 knockout mice show near normal levels of intracranial pressure and water content but reduced accumulation of water in the brain following cytotoxic oedema caused by ischemic stroke, cerebral injury and meningitis [162,163]. In vasogenic oedema mouse models, AQP4 null mice show greater water accumulation in the brain [61]. These studies suggest that water homeostasis in a non-pathological state may be independent of AQP4-mediated transcellular water flow but that AQP4 regulates transcellular water flow in cerebral oedema (Fig. 3C). In vasogenic oedema, water is eliminated from the extracellular space through AQP4 into the intact astrocytes that make up the BBB. Water then exits the astrocyte through AQP4 in the membrane of astrocytic foot processes that surround the capillary. Transcellular water flow through endothelial capillary cells into the blood is mediated by AQP1. However, in cytotoxic oedema, transcellular water flow from the blood into astrocytes is mediated by AQP4.

In conclusion, it appears that AQPs are crucial for the regulation of water homeostasis, providing selective pores for the rapid movement of water, and other uncharged solutes, across diverse cell membranes and playing regulatory roles in CVR. Gating mechanisms, which allow conformationally distinct open and closed states, have been proposed for human AQPs through molecular dynamic simulations [164], but have only been specifically reported for plant and microbial AQPs [165]. Consequently, it is likely that the distribution and abundance of AQPs in a particular membrane are the determinants of membrane water permeability and a regulator of transcellular water flow.

Acknowledgements

We thank Ashton Moran for generating Fig. 1. This work was supported by the Biomedical Research Centre at Sheffield Hallam University and grants from BBSRC to RMB.

References

- [1] D. Marples, M.A. Knepper, E.I. Christensen, S. Nielsen, Redistribution of aquaporin-2 water channels induced by vasopressin in rat kidney inner medullary collecting duct, *Am. J. Physiol.* 269 (1995) C655–C664.
- [2] N.A. McConnell, R.S. Yunus, S.A. Gross, K.L. Bost, M.G. Clemens, F.M. Hughes Jr., Water permeability of an ovarian antral follicle is predominantly transcellular and mediated by aquaporins, *Endocrinology* 143 (2002) 2905–2912.
- [3] C.M. Krane, J.E. Melvin, H.V. Nguyen, L. Richardson, J.E. Towne, T. Doetschman, A.G. Menon, Salivary acinar cells from aquaporin 5-deficient mice have decreased membrane water permeability and altered cell volume regulation, *J. Biol. Chem.* 276 (2001) 23413–23420.
- [4] T. Zeuthen, General models for water transport across leaky epithelia, *Int. Rev. Cytol.* 215 (2002) 285–317.
- [5] S. Tripathi, E.L. Boulpaep, Mechanisms of water transport by epithelial cells, *Q. J. Exp. Physiol.* 74 (1989) 385–417.
- [6] M.J. O'Donnell, S.H. Maddrell, Paracellular and transcellular routes for water and solute movements across insect epithelia, *J. Exp. Biol.* 106 (1983) 231–253.
- [7] J. Fischberg, Fluid transport across leaky epithelia: central role of the tight junction and supporting role of aquaporins, *Physiol. Rev.* 90 (2010) 1271–1290.
- [8] D.D. Loo, T. Zeuthen, G. Chandry, E.M. Wright, Cotransport of water by the Na⁺/glucose cotransporter, *Proc. Natl. Acad. Sci. U. S. A.* 93 (1996) 13367–13370.
- [9] S. Nielsen, B.L. Smith, E.I. Christensen, M.A. Knepper, P. Agre, CHIP28 water channels are localized in constitutively water-permeable segments of the nephron, *J. Cell Biol.* 120 (1993) 371–383.
- [10] O. Carlsson, S. Nielsen, E. Zakaria, B. Rippe, In vivo inhibition of transcellular water channels (aquaporin-1) during acute peritoneal dialysis in rats, *Am. J. Physiol.* 271 (1996) H2254–H2262.
- [11] B.M. Denker, B.L. Smith, F.P. Kuhajda, P. Agre, Identification, purification, and partial characterization of a novel Mr 28,000 integral membrane protein from erythrocytes and renal tubules, *J. Biol. Chem.* 263 (1988) 15634–15642.
- [12] W.E. Harries, D. Akhavan, L.J. Miercke, S. Khademi, R.M. Stroud, The channel architecture of aquaporin 0 at a 2.2-Å resolution, *Proc. Natl. Acad. Sci. U. S. A.* 101 (2004) 14045–14050.
- [13] R. Horsefield, K. Norden, M. Fellert, A. Backmark, S. Tomroth-Horsefield, A.C. Terwisscha van Scheltinga, J. Kvassman, P. Kjellbom, U. Johanson, R. Neutze, High-resolution x-ray structure of human aquaporin 5, *Proc. Natl. Acad. Sci. U. S. A.* 105 (2008) 13327–13332.
- [14] K. Murata, K. Mitsuoka, T. Hirai, T. Walz, P. Agre, J.B. Heymann, A. Engel, Y. Fujiyoshi, Structural determinants of water permeation through aquaporin-1, *Nature* 407 (2000) 599–605.
- [15] S. Tomroth-Horsefield, K. Hedfalk, G. Fischer, K. Lindkvist-Petersson, R. Neutze, Structural insights into eukaryotic aquaporin regulation, *FEBS Lett.* 584 (2010) 2580–2588.
- [16] U. Kosinska Eriksson, G. Fischer, R. Friemann, G. Enkavi, E. Tajkhorshid, R. Neutze, Subangstrom resolution X-ray structure details aquaporin-water interactions, *Science* 340 (2013) 1346–1349.
- [17] A.C. Conner, R.M. Bill, M.T. Conner, An emerging consensus on aquaporin translocation as a regulatory mechanism, *Mol. Membr. Biol.* 30 (2013) 1–12.
- [18] E.K. Hoffmann, I.H. Lambert, S.F. Pedersen, Physiology of cell volume regulation in vertebrates, *Physiol. Rev.* 89 (2009) 193–277.
- [19] R.J. Huxtable, Physiological actions of taurine, *Physiol. Rev.* 72 (1992) 101–163.
- [20] D.H. Evans, *Osmotic and Ionic Regulation: Cells and Animals*, CRC Press, Boca Raton, 2009.
- [21] B. Yang, A.S. Verkman, Water and glycerol permeabilities of aquaporins 1–5 and MIP determined quantitatively by expression of epitope-tagged constructs in *Xenopus* oocytes, *J. Biol. Chem.* 272 (1997) 16140–16146.
- [22] A.N. van Hoek, A.S. Verkman, Functional reconstitution of the isolated erythrocyte water channel CHIP28, *J. Biol. Chem.* 267 (1992) 18267–18269.
- [23] M.R. Shen, C.Y. Chou, J.A. Browning, R.J. Wilkins, J.C. Ellory, Human cervical cancer cells use Ca²⁺ signalling, protein tyrosine phosphorylation and MAP kinase in regulatory volume decrease, *J. Physiol.* 537 (2001) 347–362.
- [24] N.K. Jorgensen, S. Christensen, H. Harbak, A.M. Brown, I.H. Lambert, E.K. Hoffmann, L.O. Simonsen, On the role of calcium in the regulatory volume decrease (RVD) response in Ehrlich mouse ascites tumor cells, *J. Membr. Biol.* 157 (1997) 281–299.
- [25] L. Piao, H. Lee, C.K. Park, I.H. Cho, Z.G. Piao, S.J. Jung, S.Y. Choi, S.J. Lee, K. Park, J.S. Kim, S.B. Oh, Mechanosensitivity of voltage-gated K⁺ currents in rat trigeminal ganglion neurons, *J. Neurosci. Res.* 83 (2006) 1373–1380.
- [26] W.Z. Lan, P.Y. Wang, C.E. Hill, Modulation of hepatocellular swelling-activated K⁺ currents by phosphoinositide pathway-dependent protein kinase C, *Am. J. Physiol. Cell Physiol.* 291 (2006) C93–C103.
- [27] A. Lepple-Wienhues, I. Szabo, T. Laun, N.K. Kaba, E. Gulbins, F. Lang, The tyrosine kinase p56lck mediates activation of swelling-induced chloride channels in lymphocytes, *J. Cell Biol.* 141 (1998) 281–286.
- [28] B.C. Tilly, N. van den Berghe, L.G. Teertoolen, M.J. Edixhoven, H.R. de Jonge, Protein tyrosine phosphorylation is involved in osmoregulation of ionic conductances, *J. Biol. Chem.* 268 (1993) 19919–19922.
- [29] H. Guizouarn, R. Motais, Swelling activation of transport pathways in erythrocytes: effects of Cl⁻, ionic strength, and volume changes, *Am. J. Physiol.* 276 (1999) C210–C220.
- [30] G. Gamba, Molecular physiology and pathophysiology of electroneutral cation-chloride cotransporters, *Physiol. Rev.* 85 (2005) 423–493.
- [31] A. Kapus, S. Grinstein, S. Wasan, R. Kandasamy, J. Orłowski, Functional characterization of three isoforms of the Na⁺/H⁺ exchanger stably expressed in Chinese hamster ovary cells. ATP dependence, osmotic sensitivity, and role in cell proliferation, *J. Biol. Chem.* 269 (1994) 23544–23552.
- [32] S. Wakabayashi, B. Bertrand, T. Ikeda, J. Pouyssegur, M. Shigekawa, Mutation of calmodulin-binding site renders the Na⁺/H⁺ exchanger (NHE1) highly H⁺-sensitive and Ca²⁺ regulation-defective, *J. Biol. Chem.* 269 (1994) 13710–13715.
- [33] K.B. Gagnon, R. England, E. Delpire, Volume sensitivity of cation-Cl⁻ cotransporters is modulated by the interaction of two kinases: Ste20-related proline-alanine-rich kinase and WNK4, *Am. J. Physiol. Cell Physiol.* 290 (2006) C134–C142.
- [34] S.B. Ross, C.M. Fuller, J.K. Bubián, D.J. Benos, Amiloride-sensitive Na⁺ channels contribute to regulatory volume increases in human glioma cells, *Am. J. Physiol. Cell Physiol.* 293 (2007) C1181–C1185.
- [35] A.S. Verkman, More than just water channels: unexpected cellular roles of aquaporins, *J. Cell Sci.* 118 (2005) 3225–3232.
- [36] B. Nilius, J. Vriens, J. Prenen, G. Droogmans, T. Voets, TRPV4 calcium entry channel: a paradigm for gating diversity, *Am. J. Physiol. Cell Physiol.* 286 (2004) C195–C205.
- [37] W. Liedtke, Transient receptor potential vanilloid channels functioning in transduction of osmotic stimuli, *J. Endocrinol.* 191 (2006) 515–523.
- [38] R.G. O'Neil, S. Heller, The mechanosensitive nature of TRPV channels, *Pflugers Arch.* 451 (2005) 193–203.
- [39] W. Liedtke, C. Kim, Functionality of the TRPV subfamily of TRP ion channels: add mechano-TRP and osmo-TRP to the lexicon! *Cell. Mol. Life Sci.* 62 (2005) 2985–3001.
- [40] X. Liu, B.C. Bandayopadhyay, T. Nakamoto, B. Singh, W. Liedtke, J.E. Melvin, I. Ambudkar, A role for AQP5 in activation of TRPV4 by hypotonicity: concerted involvement of AQP5 and TRPV4 in regulation of cell volume recovery, *J. Biol. Chem.* 281 (2006) 15485–15495.

- [41] Q. Chen, E.K. Duan, Aquaporins in sperm osmoadaptation: an emerging role for volume regulation, *Acta Pharmacol. Sin.* 32 (2011) 721–724.
- [42] Q. Chen, H. Peng, L. Lei, Y. Zhang, H. Kuang, Y. Cao, Q.X. Shi, T. Ma, E. Duan, Aquaporin3 is a sperm water channel essential for postcopulatory sperm osmoadaptation and migration, *Cell Res.* 21 (2011) 922–933.
- [43] L. Galizia, A. Pizzoni, J. Fernandez, V. Rivarola, C. Capurro, P. Ford, Functional interaction between AQP2 and TRPV4 in renal cells, *J. Cell. Biochem.* 113 (2012) 580–589.
- [44] M.C. Papadopoulos, A.S. Verkman, Aquaporin water channels in the nervous system, *Nat. Rev. Neurosci.* 14 (2013) 265–277.
- [45] S. Nielsen, E.A. Nagelhus, M. Amiry-Moghaddam, C. Bourque, P. Agre, O.P. Ottersen, Specialized membrane domains for water transport in glial cells: high-resolution immunogold cytochemistry of aquaporin-4 in rat brain, *J. Neurosci.* 17 (1997) 171–180.
- [46] D.K. Binder, X. Yao, Z. Zador, T.J. Sick, A.S. Verkman, G.T. Manley, Increased seizure duration and slowed potassium kinetics in mice lacking aquaporin-4 water channels, *Glia* 53 (2006) 631–636.
- [47] K. Oshio, H. Watanabe, Y. Song, A.S. Verkman, G.T. Manley, Reduced cerebrospinal fluid production and intracranial pressure in mice lacking choroid plexus water channel Aquaporin-1, *FASEB J.* 19 (2005) 76–78.
- [48] S.D. Shields, J. Mazario, K. Skinner, A.I. Basbaum, Anatomical and functional analysis of aquaporin 1, a water channel in primary afferent neurons, *Pain* 131 (2007) 8–20.
- [49] H. Gao, C. He, X. Fang, X. Hou, X. Feng, H. Yang, X. Zhao, T. Ma, Localization of aquaporin-1 water channel in glial cells of the human peripheral nervous system, *Glia* 53 (2006) 783–787.
- [50] J. Badaut, J.M. Petit, J.F. Brunet, P.J. Magistretti, C. Charriat-Marlangue, L. Regli, Distribution of Aquaporin 9 in the adult rat brain: preferential expression in catecholaminergic neurons and in glial cells, *Neuroscience* 128 (2004) 27–38.
- [51] F. He, Y.E. Sun, Glial cells more than support cells? *Int. J. Biochem. Cell Biol.* 39 (2007) 661–665.
- [52] N.N. Haj-Yasein, G.F. Vindedal, M. Eilert-Olsen, G.A. Gundersen, O. Skare, P. Laake, A. Klungland, A.E. Thoren, J.M. Burkhardt, O.P. Ottersen, E.A. Nagelhus, Glial-conditional deletion of aquaporin-4 (Aqp4) reduces blood–brain water uptake and confers barrier function on perivascular astrocyte endfeet, *Proc. Natl. Acad. Sci. U. S. A.* 108 (2011) 17815–17820.
- [53] J.E. Rash, T. Yasumura, C.S. Hudson, P. Agre, S. Nielsen, Direct immunogold labeling of aquaporin-4 in square arrays of astrocyte and ependymocyte plasma membranes in rat brain and spinal cord, *Proc. Natl. Acad. Sci. U. S. A.* 95 (1998) 11981–11986.
- [54] K. Oshio, D.K. Binder, B. Yang, S. Schecter, A.S. Verkman, G.T. Manley, Expression of aquaporin water channels in mouse spinal cord, *Neuroscience* 127 (2004) 685–693.
- [55] V. Medici, C. Frassoni, L. Tassi, R. Spreafico, R. Garbelli, Aquaporin 4 expression in control and epileptic human cerebral cortex, *Brain Res.* 1367 (2011) 330–339.
- [56] J. Badaut, S. Ashwal, A. Adami, B. Tone, R. Recker, D. Spagnoli, B. Teron, A. Obenaus, Brain water mobility decreases after astrocytic aquaporin-4 inhibition using RNA interference, *J. Cereb. Blood Flow Metab.* 31 (2011) 819–831.
- [57] M.T. Conner, A.C. Conner, C.E. Bland, L.H. Taylor, J.E. Brown, H.R. Parri, R.M. Bill, Rapid aquaporin translocation regulates cellular water flow: mechanism of hypotonicity-induced subcellular localization of aquaporin 1 water channel, *J. Biol. Chem.* 287 (2012) 11516–11525.
- [58] M. Potokar, M. Stenovec, J. Jorgačevski, T. Holen, M. Kreft, O.P. Ottersen, R. Zorec, Regulation of AQP4 surface expression via vesicle mobility in astrocytes, *Glia* 61 (2013) 917–928.
- [59] V. Benfenati, M. Amiry-Moghaddam, M. Caprini, M.N. Mylonakou, C. Rapisarda, O.P. Ottersen, S. Ferroni, Expression and functional characterization of transient receptor potential vanilloid-related channel 4 (TRPV4) in rat cortical astrocytes, *Neuroscience* 148 (2007) 876–892.
- [60] V. Benfenati, M. Caprini, M. Dovizio, M.N. Mylonakou, S. Ferroni, O.P. Ottersen, M. Amiry-Moghaddam, An aquaporin-4/transient receptor potential vanilloid 4 (AQP4/TRPV4) complex is essential for cell-volume control in astrocytes, *Proc. Natl. Acad. Sci. U. S. A.* 108 (2011) 2563–2568.
- [61] M.C. Papadopoulos, G.T. Manley, S. Krishna, A.S. Verkman, Aquaporin-4 facilitates reabsorption of excess fluid in vasogenic brain edema, *FASEB J.* 18 (2004) 1291–1293.
- [62] S. Saadoun, B.A. Bell, A.S. Verkman, M.C. Papadopoulos, Greatly improved neurological outcome after spinal cord compression injury in AQP4-deficient mice, *Brain* 131 (2008) 1087–1098.
- [63] S. Saadoun, M.C. Papadopoulos, D.C. Davies, B.A. Bell, S. Krishna, Increased aquaporin-1 water channel expression in human brain tumours, *Br. J. Cancer* 87 (2002) 621–623.
- [64] J. Li, R.V. Patil, A.S. Verkman, Mildly abnormal retinal function in transgenic mice without Muller cell aquaporin-4 water channels, *Invest. Ophthalmol. Vis. Sci.* 43 (2002) 573–579.
- [65] D.C. Lu, H. Zhang, Z. Zador, A.S. Verkman, Impaired olfaction in mice lacking aquaporin-4 water channels, *FASEB J.* 22 (2008) 3216–3223.
- [66] J. Li, A.S. Verkman, Impaired hearing in mice lacking aquaporin-4 water channels, *J. Biol. Chem.* 276 (2001) 31233–31237.
- [67] L.N. Nejsum, The renal plumbing system: aquaporin water channels, *Cell. Mol. Life Sci.* 62 (2005) 1692–1706.
- [68] K. Fushimi, S. Uchida, Y. Hara, Y. Hirata, F. Marumo, S. Sasaki, Cloning and expression of apical membrane water channel of rat kidney collecting tubule, *Nature* 361 (1993) 549–552.
- [69] K. Ishibashi, S. Sasaki, K. Fushimi, S. Uchida, M. Kuwahara, H. Saito, T. Furukawa, K. Nakajima, Y. Yamaguchi, T. Gojohori, Molecular cloning and expression of a member of the aquaporin family with permeability to glycerol and urea in addition to water expressed at the basolateral membrane of kidney collecting duct cells, *Proc. Natl. Acad. Sci. U. S. A.* 91 (1994) 6269–6273.
- [70] J. Terris, C.A. Ecelbarger, D. Marples, M.A. Knepper, S. Nielsen, Distribution of aquaporin-4 water channel expression within rat kidney, *Am. J. Physiol.* 269 (1995) F775–F785.
- [71] F. Magni, C. Sarto, D. Ticozzi, M. Soldi, N. Bosso, P. Mocarelli, M.G. Kienle, Proteomic knowledge of human aquaporins, *Proteomics* 6 (2006) 5637–5649.
- [72] T. Ma, Y. Song, B. Yang, A. Gillespie, E.J. Carlson, C.J. Epstein, A.S. Verkman, Nephrogenic diabetes insipidus in mice lacking aquaporin-3 water channels, *Proc. Natl. Acad. Sci. U. S. A.* 97 (2000) 4386–4391.
- [73] Y. Noda, S. Sasaki, Trafficking mechanism of water channel aquaporin-2, *Biol. Cell.* 97 (2005) 885–892.
- [74] P.I. Nedvetsky, G. Tamma, S. Beulshausen, G. Valenti, W. Rosenthal, E. Klusmann, Regulation of aquaporin-2 trafficking, *Handb. Exp. Pharmacol.* (190) (2009) 133–157(133–157).
- [75] S. Sasaki, Aquaporin 2: from its discovery to molecular structure and medical implications, *Mol. Aspects Med.* 33 (2012) 535–546.
- [76] L. Galizia, M.P. Flamenco, V. Rivarola, C. Capurro, P. Ford, Role of AQP2 in activation of calcium entry by hypotonicity: implications in cell volume regulation, *Am. J. Physiol. Renal Physiol.* 294 (2008) F582–F590.
- [77] Y.H. Li, K. Eto, S. Horikawa, S. Uchida, S. Sasaki, X.J. Li, Y. Noda, Aquaporin-2 regulates cell volume recovery via tropomyosin, *Int. J. Biochem. Cell Biol.* 41 (2009) 2466–2476.
- [78] K. Kasono, T. Saito, T. Saito, H. Tamemoto, C. Yanagida, S. Uchida, M. Kawakami, S. Sasaki, S.E. Ishikawa, Hypertonicity regulates the aquaporin-2 promoter independently of arginine vasopressin, *Nephrol. Dial. Transplant.* 20 (2005) 509–515.
- [79] U. Hasler, P. Nunes, R. Bouley, H.A. Lu, T. Matsuzaki, D. Brown, Acute hypertonicity alters aquaporin-2 trafficking and induces a MAPK-dependent accumulation at the plasma membrane of renal epithelial cells, *J. Biol. Chem.* 283 (2008) 26643–26661.
- [80] M.A. Knepper, J.B. Wade, J. Terris, C.A. Ecelbarger, D. Marples, B. Mandon, C.L. Chou, B.K. Kishore, S. Nielsen, Renal aquaporins, *Kidney Int.* 49 (1996) 1712–1717.
- [81] M.T. Conner, A.C. Conner, J.E. Brown, R.M. Bill, Membrane trafficking of aquaporin 1 is mediated by protein kinase C via microtubules and regulated by tonicity, *Biochemistry* 49 (2010) 821–823.
- [82] R.A. Marinelli, N.F. LaRusso, Aquaporin water channels in liver: their significance in bile formation, *Hepatology* 26 (1997) 1081–1084.
- [83] J. Zhang, Y. An, J. Gao, J. Han, X. Pan, Y. Pan, L. Tie, X. Li, Aquaporin-1 translocation and degradation mediates the water transportation mechanism of acetazolamide, *PLoS One* 7 (2012) e45976.
- [84] E.J. Kamsteeg, P.J. Savelkoul, G. Hendriks, I.B. Konings, N.M. Nivillac, A.K. Lagendijk, P. van der Sluijs, P.M. Deen, Misrouting of the Aquaporin-2 mutant E258K to multivesicular bodies/lysosomes in dominant NDI is associated with its monoubiquitination and increased phosphorylation by PKC but is due to the loss of E258, *Pflügers Arch.* 455 (2008) 1041–1054.
- [85] Z. Han, R.V. Patil, Protein kinase A-dependent phosphorylation of aquaporin-1, *Biochem. Biophys. Res. Commun.* 273 (2000) 328–332.
- [86] S. Raina, G.M. Preston, W.B. Guggino, P. Agre, Molecular cloning and characterization of an aquaporin cDNA from salivary, lacrimal, and respiratory tissues, *J. Biol. Chem.* 270 (1995) 1908–1912.
- [87] X. He, C.M. Tse, M. Donowitz, S.L. Alper, S.E. Gabriel, B.J. Baum, Polarized distribution of key membrane transport proteins in the rat submandibular gland, *Pflügers Arch.* 433 (1997) 260–268.
- [88] S. Nielsen, L.S. King, B.M. Christensen, P. Agre, Aquaporins in complex tissues. II. Subcellular distribution in respiratory and glandular tissues of rat, *Am. J. Physiol.* 273 (1997) C1549–C1561.
- [89] V. Gresz, T.H. Kwon, P.T. Hurley, G. Varga, T. Zelles, S. Nielsen, R.M. Case, M.C. Steward, Identification and localization of aquaporin water channels in human salivary glands, *Am. J. Physiol. Gastrointest. Liver Physiol.* 281 (2001) G247–G254.
- [90] J. Tada, T. Sawa, N. Yamanaka, M. Shono, T. Akamatsu, K. Tsumura, M.N. Parvin, N. Kanamori, K. Hosoi, Involvement of vesicle-cytoskeleton interaction in AQP5 trafficking in AQP5-gene-transfected HSG cells, *Biochem. Biophys. Res. Commun.* 266 (1999) 443–447.
- [91] B.H. Lee, A.E. Gauna, G. Perez, Y.J. Park, K.M. Pauley, T. Kawai, S. Cha, Autoantibodies against muscarinic type 3 receptor in Sjogren's syndrome inhibit aquaporin 5 trafficking, *PLoS One* 8 (2013) e53113.
- [92] Y. Ishikawa, T. Eguchi, M.T. Skowronski, H. Ishida, Acetylcholine acts on M3 muscarinic receptors and induces the translocation of aquaporin5 water channel via cytosolic Ca²⁺ elevation in rat parotid glands, *Biochem. Biophys. Res. Commun.* 245 (1998) 835–840.
- [93] A.K. Hansen, H.K. Galtung, Aquaporin expression and cell volume regulation in the SV40 immortalized rat submandibular acinar cell line, *Pflügers Arch.* 453 (2007) 787–796.
- [94] K. Sato, The physiology, pharmacology, and biochemistry of the eccrine sweat gland, *Rev. Physiol. Biochem. Pharmacol.* 79 (1977) 51–131.
- [95] R. Inoue, E. Sohara, T. Rai, T. Satoh, H. Yokozeki, S. Sasaki, S. Uchida, Immunolocalization and translocation of aquaporin-5 water channel in sweat glands, *J. Dermatol. Sci.* 70 (2013) 26–33.
- [96] R. Sougrat, M. Morand, C. Gondran, P. Barre, R. Gobin, F. Bonte, M. Dumas, J.M. Verbavatz, Functional expression of AQP3 in human skin epidermis and reconstructed epidermis, *J. Invest. Dermatol.* 118 (2002) 678–685.
- [97] Y. Sugiyama, Y. Ota, M. Hara, S. Inoue, Osmotic stress up-regulates aquaporin-3 gene expression in cultured human keratinocytes, *Biochim. Biophys. Acta* 1522 (2001) 82–88.
- [98] M. Hara, A.S. Verkman, Glycerol replacement corrects defective skin hydration, elasticity, and barrier function in aquaporin-3-deficient mice, *Proc. Natl. Acad. Sci. U. S. A.* 100 (2003) 7360–7365.

- [99] M. Olsson, A. Broberg, M. Jernas, L. Carlsson, M. Rudemo, M. Suurkula, P.A. Svensson, M. Benson, Increased expression of aquaporin 3 in atopic eczema, *Allergy* 61 (2006) 1132–1137.
- [100] D. Blaydon, L. Lind, V. Plagnol, K. Linton, F.D. Smith, N. Wilson, W.H. McLean, C. Munro, A. South, I. Leigh, E. O'Toole, A. Lundström, D. Kelsell, Mutations in AQP5, encoding a water-channel protein, cause autosomal-dominant diffuse nonepidermolytic palmoplantar keratoderma, *Am. J. Hum. Genet.* 93 (2013) 330–335.
- [101] K. Kishida, I. Shimomura, H. Nishizawa, N. Maeda, H. Kuriyama, H. Kondo, M. Matsuda, H. Nagaretani, N. Ouchi, K. Hotta, S. Kihara, T. Kadowaki, T. Funahashi, Y. Matsuzawa, Enhancement of the aquaporin adipose gene expression by a peroxisome proliferator-activated receptor gamma, *J. Biol. Chem.* 276 (2001) 48572–48579.
- [102] K. Kishida, H. Kuriyama, T. Funahashi, I. Shimomura, S. Kihara, N. Ouchi, M. Nishida, H. Nishizawa, M. Matsuda, M. Takahashi, K. Hotta, T. Nakamura, S. Yamashita, Y. Tochino, Y. Matsuzawa, Aquaporin adipose, a putative glycerol channel in adipocytes, *J. Biol. Chem.* 275 (2000) 20896–20902.
- [103] A. Rodriguez, V. Catalan, J. Gomez-Ambrosi, S. Garcia-Navarro, F. Rotellar, V. Valenti, C. Silva, M.J. Gil, J. Salvador, M.A. Burrell, G. Calamita, M.M. Malagon, G. Fruhbeck, Insulin- and leptin-mediated control of aquaglyceroporins in human adipocytes and hepatocytes is mediated via the PI3K/Akt/mTOR signaling cascade, *J. Clin. Endocrinol. Metab.* 96 (2011) E586–E597.
- [104] V. Ceperuelo-Mallafre, M. Miranda, M.R. Chacon, N. Vilarrasa, A. Megia, C. Gutierrez, J.M. Fernandez-Real, J.M. Gomez, E. Caubet, G. Fruhbeck, J. Vendrell, Adipose tissue expression of the glycerol channel aquaporin-7 gene is altered in severe obesity but not in type 2 diabetes, *J. Clin. Endocrinol. Metab.* 92 (2007) 3640–3645.
- [105] M.P. Marrades, F.I. Milagro, J.A. Martinez, M.J. Moreno-Aliaga, Differential expression of aquaporin 7 in adipose tissue of lean and obese high fat consumers, *Biochem. Biophys. Res. Commun.* 339 (2006) 785–789.
- [106] N. Maeda, Implications of aquaglyceroporins 7 and 9 in glycerol metabolism and metabolic syndrome, *Mol. Aspects Med.* 33 (2012) 665–675.
- [107] U. Laforenza, M.F. Scaffino, G. Gastaldi, Aquaporin-10 represents an alternative pathway for glycerol efflux from human adipocytes, *PLoS One* 8 (2013) e54474.
- [108] U. Mehlhorn, H.J. Geissler, G.A. Laine, S.J. Allen, Myocardial fluid balance, *Eur. J. Cardiothorac. Surg.* 20 (2001) 1220–1230.
- [109] J.R. Egan, T.L. Butler, C.G. Au, Y.M. Tan, K.N. North, D.S. Winlaw, Myocardial water handling and the role of aquaporins, *Biochim. Biophys. Acta Biomembr.* 1758 (2006) 1043–1052.
- [110] T.L. Butler, C.G. Au, B. Yang, J.R. Egan, Y.M. Tan, E.C. Hardeman, K.N. North, A.S. Verkman, D.S. Winlaw, Cardiac aquaporin expression in humans, rats, and mice, *Am. J. Physiol. Heart Circ. Physiol.* 291 (2006) H705–H713.
- [111] M.A. Suleymanian, C.M. Baumgarten, Osmotic gradient-induced water permeation across the sarcolemma of rabbit ventricular myocytes, *J. Gen. Physiol.* 107 (1996) 503–514.
- [112] M.R. Kellen, J.B. Bassingthwaite, Transient transcappillary exchange of water driven by osmotic forces in the heart, *Am. J. Physiol. Heart Circ. Physiol.* 285 (2003) H1317–H1331.
- [113] A.S. Verkman, Aquaporin water channels and endothelial cell function*, *J. Anat.* 200 (2002) 617–627.
- [114] A. Rutkovskiy, K.O. Stenslokken, L.H. Mariero, B. Skrbic, M. Amiry-Moghaddam, V. Hillestad, G. Valen, M.C. Perreault, O.P. Ottersen, L. Gullestad, C.P. Dahl, J. Vaage, Aquaporin-4 in the heart: reexpression, regulation and functional role in ischemia, *Basic Res. Cardiol.* 107 (2012) 280(012-0280-6. Epub 2012 Jul 10).
- [115] M.A. Matthay, H.G. Folkesson, A.S. Verkman, Salt and water transport across alveolar and distal airway epithelia in the adult lung, *Am. J. Physiol.* 270 (1996) L487–L503.
- [116] A.S. Verkman, M.A. Matthay, Y. Song, Aquaporin water channels and lung physiology, *Am. J. Physiol. Lung Cell. Mol. Physiol.* 278 (2000) L867–L879.
- [117] H.G. Folkesson, M.A. Matthay, H. Hasegawa, F. Kheradmand, A.S. Verkman, Transcellular water transport in lung alveolar epithelium through mercury-sensitive water channels, *Proc. Natl. Acad. Sci. U. S. A.* 91 (1994) 4970–4974.
- [118] Z. Borok, A.S. Verkman, Lung edema clearance: 20 years of progress: invited review: role of aquaporin water channels in fluid transport in lung and airways, *J. Appl. Physiol.* 93 (2002) 2199–2206.
- [119] K. Wang, Y.L. Feng, F.Q. Wen, X.R. Chen, X.M. Ou, D. Xu, J. Yang, Z.P. Deng, Decreased expression of human aquaporin-5 correlated with mucus overproduction in airways of chronic obstructive pulmonary disease, *Acta Pharmacol. Sin.* 28 (2007) 1166–1174.
- [120] Y. Song, A.S. Verkman, Aquaporin-5 dependent fluid secretion in airway submucosal glands, *J. Biol. Chem.* 276 (2001) 41288–41292.
- [121] G. Doring, P. Flume, H. Heijerman, J.S. Elborn, Consensus Study Group, Treatment of lung infection in patients with cystic fibrosis: current and future strategies, *J. Cyst. Fibros.* 11 (2012) 461–479.
- [122] C. Bai, N. Fukuda, Y. Song, T. Ma, M.A. Matthay, A.S. Verkman, Lung fluid transport in aquaporin-1 and aquaporin-4 knockout mice, *J. Clin. Invest.* 103 (1999) 555–561.
- [123] T. Ma, N. Fukuda, Y. Song, M.A. Matthay, A.S. Verkman, Lung fluid transport in aquaporin-5 knockout mice, *J. Clin. Invest.* 105 (2000) 93–100.
- [124] V.K. Sidhaye, A.D. Guler, K.S. Schweitzer, F. D'Alessio, M.J. Caterina, L.S. King, Transient receptor potential vanilloid 4 regulates aquaporin-5 abundance under hypotonic conditions, *Proc. Natl. Acad. Sci. U. S. A.* 103 (2006) 4747–4752.
- [125] J.D. Hoffert, V. Leitch, P. Agre, L.S. King, Hypertonic induction of aquaporin-5 expression through an ERK-dependent pathway, *J. Biol. Chem.* 275 (2000) 9070–9077.
- [126] F. Yang, J.D. Kawedia, A.G. Menon, Cyclic AMP regulates aquaporin 5 expression at both transcriptional and post-transcriptional levels through a protein kinase A pathway, *J. Biol. Chem.* 278 (2003) 32173–32180.
- [127] V. Sidhaye, J.D. Hoffert, L.S. King, cAMP has distinct acute and chronic effects on aquaporin-5 in lung epithelial cells, *J. Biol. Chem.* 280 (2005) 3590–3596.
- [128] J. Woo, Y.K. Chae, S.J. Jang, M.S. Kim, J.H. Baek, J.C. Park, B. Trink, E. Ratovitski, T. Lee, B. Park, M. Park, J.H. Kang, J.C. Sorim, J. Lee, J. Califano, D. Sidransky, C. Moon, Membrane trafficking of AQP5 and cAMP dependent phosphorylation in bronchial epithelium, *Biochem. Biophys. Res. Commun.* 366 (2008) 321–327.
- [129] H.F. Huang, R.H. He, C.C. Sun, Y. Zhang, Q.X. Meng, Y.Y. Ma, Function of aquaporins in female and male reproductive systems, *Hum. Reprod. Update* 12 (2006) 785–795.
- [130] J. Frede, S.P. Fraser, G. Oskay-Ozcelik, Y. Hong, E. Ioana Braicu, J. Sehoul, H. Gabra, M.B. Djamgoz, Ovarian cancer: ion channel and aquaporin expression as novel targets of clinical potential, *Eur. J. Cancer* 49 (2013) 2331–2344.
- [131] F. Qu, F.F. Wang, X.E. Lu, M.Y. Dong, J.Z. Sheng, P.P. Lv, G.L. Ding, B.W. Shi, D. Zhang, H.F. Huang, Altered aquaporin expression in women with polycystic ovary syndrome: hyperandrogenism in follicular fluid inhibits aquaporin-9 in granulosa cells through the phosphatidylinositol 3-kinase pathway, *Hum. Reprod.* 25 (2010) 1441–1450.
- [132] K. Ishibashi, M. Kuwahara, Y. Gu, Y. Kageyama, A. Tohsaka, F. Suzuki, F. Marumo, S. Sasaki, Cloning and functional expression of a new water channel abundantly expressed in the testis permeable to water, glycerol, and urea, *J. Biol. Chem.* 272 (1997) 20782–20786.
- [133] C.H. Yeung, Aquaporins in spermatozoa and testicular germ cells: identification and potential role, *Asian J. Androl.* 12 (2010) 490–499.
- [134] E. Moretti, G. Terzuoli, L. Mazzi, F. Iacoponi, G. Collodel, Immunolocalization of aquaporin 7 in human sperm and its relationship with semen parameters, *Syst. Biol. Reprod. Med.* 58 (2012) 129–135.
- [135] H. Tsukaguchi, C. Shayakul, U.V. Berger, B. Mackenzie, S. Devidas, W.B. Guggino, A.N. van Hoek, M.A. Hediger, Molecular characterization of a broad selectivity neutral solute channel, *J. Biol. Chem.* 273 (1998) 24737–24743.
- [136] N. Pastor-Soler, C. Isnard-Bagnis, C. Herak-Kramberger, I. Sabolic, A. Van Hoek, D. Brown, S. Bretien, Expression of aquaporin 9 in the adult rat epididymal epithelium is modulated by androgens, *Biol. Reprod.* 66 (2002) 1716–1722.
- [137] H.H. Badran, L.S. Hermo, Expression and regulation of aquaporins 1, 8, and 9 in the testis, efferent ducts, and epididymis of adult rats and during postnatal development, *J. Androl.* 23 (2002) 358–373.
- [138] L. Hermo, D. Krzczunowicz, R. Ruz, Cell specificity of aquaporins 0, 3, and 10 expressed in the testis, efferent ducts, and epididymis of adult rats, *J. Androl.* 25 (2004) 494–505.
- [139] D. Duan, C. Winter, S. Cowley, J.R. Hume, B. Horowitz, Molecular identification of a volume-regulated chloride channel, *Nature* 390 (1997) 417–421.
- [140] C.H. Yeung, J.P. Barfield, T.G. Cooper, Chloride channels in physiological volume regulation of human spermatozoa, *Biol. Reprod.* 73 (2005) 1057–1063.
- [141] T. Matsuzaki, Y. Tajika, A. Ablimit, T. Aoki, H. Hagiwara, K. Takata, Aquaporins in the digestive system, *Med. Electron. Microsc.* 37 (2004) 71–80.
- [142] T. Ma, S. Jayaraman, K.S. Wang, Y. Song, B. Yang, J. Li, J.A. Bastidas, A.S. Verkman, Defective dietary fat processing in transgenic mice lacking aquaporin-1 water channels, *Am. J. Physiol. Cell Physiol.* 280 (2001) C126–C134.
- [143] T. Matsuzaki, T. Suzuki, H. Koyama, S. Tanaka, K. Takata, Water channel protein AQP3 is present in epithelia exposed to the environment of possible water loss, *J. Histochem. Cytochem.* 47 (1999) 1275–1286.
- [144] K.S. Wang, A.R. Komar, T. Ma, F. Filiz, J. McLeroy, K. Hoda, A.S. Verkman, J.A. Bastidas, Gastric acid secretion in aquaporin-4 knockout mice, *Am. J. Physiol. Gastrointest. Liver Physiol.* 279 (2000) G448–G453.
- [145] K.S. Wang, T. Ma, F. Filiz, A.S. Verkman, J.A. Bastidas, Colon water transport in transgenic mice lacking aquaporin-4 water channels, *Am. J. Physiol. Gastrointest. Liver Physiol.* 279 (2000) G463–G470.
- [146] P.T. Hurley, C.J. Ferguson, T.H. Kwon, M.L. Andersen, A.G. Norman, M.C. Steward, S. Nielsen, R.M. Case, Expression and immunolocalization of aquaporin water channels in rat exocrine pancreas, *Am. J. Physiol. Gastrointest. Liver Physiol.* 280 (2001) G701–G709.
- [147] M.L. Elkjaer, L.N. Nejsum, V. Gresz, T.H. Kwon, U.B. Jensen, J. Frokiaer, S. Nielsen, Immunolocalization of aquaporin-8 in rat kidney, gastrointestinal tract, testis, and airways, *Am. J. Physiol. Renal Physiol.* 281 (2001) F1047–F1057.
- [148] K. Nihei, Y. Koyama, T. Tani, E. Yaoita, K. Ohshiro, L.P. Adhikary, I. Kurosaki, Y. Shirai, K. Hatakeyama, T. Yamamoto, Immunolocalization of aquaporin-9 in rat hepatocytes and Leydig cells, *Arch. Histol. Cytol.* 64 (2001) 81–88.
- [149] Y. Koyama, T. Yamamoto, T. Tani, K. Nihei, D. Kondo, H. Funaki, E. Yaoita, K. Kawasaki, N. Sato, K. Hatakeyama, I. Kihara, Expression and localization of aquaporins in rat gastrointestinal tract, *Am. J. Physiol.* 276 (1999) C621–C627.
- [150] N. Ikarashi, R. Kon, T. Iizasa, N. Suzuki, R. Hiruma, K. Suenaga, T. Toda, M. Ishii, M. Hoshino, W. Ochiai, K. Sugiyama, Inhibition of aquaporin-3 water channel in the colon induces diarrhea, *Biol. Pharm. Bull.* 35 (2012) 957–962.
- [151] M. Kuwahara, Y. Gu, K. Ishibashi, F. Marumo, S. Sasaki, Mercury-sensitive residues and pore site in AQP3 water channel, *Biochemistry* 36 (1997) 13973–13978.
- [152] F. Garcia, A. Kierbel, M.C. Larooca, S.A. Gradihone, P. Splinter, N.F. LaRusso, R.A. Marinelli, The water channel aquaporin-8 is mainly intracellular in rat hepatocytes, and its plasma membrane insertion is stimulated by cyclic AMP, *J. Biol. Chem.* 276 (2001) 12147–12152.
- [153] M.D. Humzah, R.W. Soames, Human intervertebral disc: structure and function, *Anat. Rec.* 220 (1988) 337–356.
- [154] A. Mobasher, E. Trujillo, S. Bell, S.D. Carter, P.D. Clegg, P. Martin-Vasallo, D. Marples, Aquaporin water channels AQP1 and AQP3, are expressed in equine articular chondrocytes, *Vet. J.* 168 (2004) 143–150.
- [155] J. Kraemer, D. Kolditz, R. Gowin, Water and electrolyte content of human intervertebral discs under variable load, *Spine* 10 (1985) 69–71 (Phila Pa.1976).

- [156] K. Hagiwara, T. Shinozaki, T. Matsuzaki, K. Takata, K. Takagishi, Immunolocalization of water channel aquaporins in human knee articular cartilage with intact and early degenerative regions, *Med. Mol. Morphol.* 46 (2013) 104–108.
- [157] J.C. Iatridis, J.J. MacLean, M. O'Brien, I.A. Stokes, Measurements of proteoglycan and water content distribution in human lumbar intervertebral discs, *Spine* 32 (2007) 1493–1497 (Phila Pa.1976).
- [158] A. Maroudas, H. Muir, J. Wingham, The correlation of fixed negative charge with glycosaminoglycan content of human articular cartilage, *Biochim. Biophys. Acta* 177 (1969) 492–500.
- [159] S.M. Richardson, R. Knowles, D. Marples, J.A. Hoyland, A. Mobasheri, Aquaporin expression in the human intervertebral disc, *J. Mol. Histol.* 39 (2008) 303–309.
- [160] A. Frigeri, G.P. Nicchia, R. Balena, B. Nico, M. Svelto, Aquaporins in skeletal muscle: reassessment of the functional role of aquaporin-4, *FASEB J.* 18 (2004) 905–907.
- [161] E. Gunnarson, M. Zelenina, A. Aperia, Regulation of brain aquaporins, *Neuroscience* 129 (2004) 947–955.
- [162] G.T. Manley, M. Fujimura, T. Ma, N. Noshita, F. Filiz, A.W. Bollen, P. Chan, A.S. Verkman, Aquaporin-4 deletion in mice reduces brain edema after acute water intoxication and ischemic stroke, *Nat. Med.* 6 (2000) 159–163.
- [163] M.C. Papadopoulos, A.S. Verkman, Aquaporin-4 gene disruption in mice reduces brain swelling and mortality in pneumococcal meningitis, *J. Biol. Chem.* 280 (2005) 13906–13912.
- [164] L. Janosi, M. Ceccarelli, The gating mechanism of the human aquaporin 5 revealed by molecular dynamics simulations, *PLoS One* 8 (2013) e59897.
- [165] S. Tornroth-Horsefield, Y. Wang, K. Hedfalk, U. Johanson, M. Karlsson, E. Tajkhorshid, R. Neutze, P. Kjellbom, Structural mechanism of plant aquaporin gating, *Nature* 439 (2006) 688–694.

Identification and Molecular Mechanisms of the Rapid Tonicity-induced Relocalization of the Aquaporin 4 Channel*

Received for publication, February 16, 2015, and in revised form, May 21, 2015. Published, JBC Papers in Press, May 26, 2015, DOI 10.1074/jbc.M115.646034

Philip Kitchen[‡], Rebecca E. Day[§], Luke H. J. Taylor[‡], Mootaz M. Salman[§], Roslyn M. Bill^{¶1}, Matthew T. Conner^{§2}, and Alex C. Conner^{||3}

From the [‡]Molecular Organisation and Assembly in Cells Doctoral Training Centre, University of Warwick, Coventry CV4 7AL, the [§]Biomedical Research Centre, Sheffield Hallam University, Howard Street, Sheffield S1 1WB, the [¶]School of Life & Health Sciences and Aston Research Centre for Healthy Ageing, Aston University, Aston Triangle, Birmingham B4 7ET, and the ^{||}School of Clinical and Experimental Medicine, University of Birmingham, Edgbaston, Birmingham B15 2TT, United Kingdom

Background: The water channel protein aquaporin 4 (AQP4) controls water permeability of the blood-brain barrier.

Results: Hypotonicity induces rapid relocalization of AQP4 in a calcium-, calmodulin-, and kinase-dependent manner.

Conclusion: AQP4 can be relocalized between the cell membrane and intracellular compartments.

Significance: Pharmacological modulation of AQP4 membrane localization could provide a new approach to treating brain edema.

The aquaporin family of integral membrane proteins is composed of channels that mediate cellular water flow. Aquaporin 4 (AQP4) is highly expressed in the glial cells of the central nervous system and facilitates the osmotically driven pathological brain swelling associated with stroke and traumatic brain injury. Here we show that AQP4 cell surface expression can be rapidly and reversibly regulated in response to changes of tonicity in primary cortical rat astrocytes and in transfected HEK293 cells. The translocation mechanism involves PKA activation, influx of extracellular calcium, and activation of calmodulin. We identify five putative PKA phosphorylation sites and use site-directed mutagenesis to show that only phosphorylation at one of these sites, serine 276, is necessary for the translocation response. We discuss our findings in the context of the identification of new therapeutic approaches to treating brain edema.

AQP4 has been shown to be important for brain edema formation following traumatic brain injury, stroke, and meningitis (3). AQP4 knock-out mice were protected from the formation of cytotoxic edema in a stroke model (4), providing an explicit target for managing this condition. Despite extensive research that has built on the well understood structural biology of the AQP family, there are no drugs available to restrict water movement through AQP4, and in general, known AQP inhibitors are either cytotoxic (mercurial compounds) or nonspecific, leading to off-target effects (5–7). Understanding the regulation of AQP4 now provides a novel therapeutic approach for the prevention of cytotoxic edema.

The most well studied system in which cellular water flow is regulated is the translocation of AQP2 in response to vasopressin (Arg-8 vasopressin (AVP); anti-diuretic hormone (ADH)) in the cells of the collecting duct of the mammalian kidney (8). AQP2 is shuttled between the apical cell surface and intracellular vesicles to regulate water reabsorption. The mechanism involves AVP-mediated production of cAMP resulting in the activation of PKA and direct phosphorylation of the AQP2 C-terminal tail at serine 256 (9). Specific SNARE proteins that facilitate the exocytosis of AQP2-containing vesicles have been identified (10). Other AQPs have been shown to be translocated in response to environmental stimuli; we recently reviewed an emerging consensus on subcellular relocalization as a regulatory mechanism for the AQP family (11) following our discovery of the PKC-mediated translocation of threonine-phosphorylated AQP1 in response to changes of tonicity (12, 13).

There is a requirement for rapid, physiological regulation of AQP4, which could be achieved at the transcriptional level or by short-term subcellular relocalization. Despite this, there is no description of a mechanism of AQP4 translocation, and the effect of stimuli on AQP4 localization is contradictory. AQP4 localization is thought to be affected by numerous intracellular mechanisms including PKA (14), PKC (15), and actin reorganization (16). It is not clear whether there are common mechanisms either within the AQP family or even for AQP4 in differ-

The aquaporins (AQPs)⁴ form a family of small integral membrane proteins found in all phylogenetic kingdoms. They act as channels for the osmotic passage of water through biological membranes and they mediate cellular water flow.

Human AQP4 is a relatively recently discovered member of the 13-strong family of mammalian AQPs (1). AQP4 is found in a number of tissues including the kidney and gastrointestinal tract but is notable for its high levels in astrocytes and its role in brain water homeostasis (2).

* This work was supported by the Engineering and Physical Sciences Research Council through the Molecular Organisation and Assembly in Cells Doctoral Training Centre, University of Warwick, Grant EP/F500378/1 (to P. K. and L. H. J. T.). The authors declare that they have no conflicts of interest with the contents of this article.

⌘ Author's Choice—Final version free via Creative Commons CC-BY license.

¹ To whom correspondence may be addressed. E-mail: r.m.bill@aston.ac.uk.

² To whom correspondence may be addressed. E-mail: m.conner@shu.ac.uk.

³ To whom correspondence may be addressed. E-mail: a.c.conner@bham.ac.uk.

⁴ The abbreviations used are: AQP, aquaporin; Myr, myristoylated; PKI, protein kinase inhibitor; RME, relative membrane expression; AVP, Arg-8 vasopressin; ER, endoplasmic reticulum.

Tonicity-induced Relocalization of Aquaporin 4

ent cell types; this indicates a general lack of mechanistic awareness of AQP regulation.

We have identified a novel regulatory pathway of endogenous AQP4 translocation in primary cortical astrocytes. This study describes this mechanism in a model HEK293 cell line and shows how tonicity-dependent changes in the environment lead to a calcium-dependent, calmodulin-dependent, and PKA-specific, reversible translocation of AQP4 to the cell surface. We also identify a known kinase site and putative PKA target site, serine 276, in the C-terminal tail of AQP4 that is necessary for the translocation response. This site has been shown to be phosphorylated *in vivo*, and we show that the mechanism requires PKA activity in primary cortical astrocytes. Our data represent a novel mechanism that could be a new avenue for therapeutic discovery in the treatment of cytotoxic brain edema.

Experimental Procedures

Materials—Cell-permeable inhibitors were purchased as follows: trifluoperazine and W7 calmodulin antagonists from Sigma (Poole, UK); the myristoylated PKA inhibitor Myr-PKI 14-22 amide from Merck Chemicals (Nottingham, UK); and Myr-PKC 19-27 and hypericin from Fisher Scientific (Loughborough, UK). FluoroDish™ dishes were from World Precision Instruments Ltd. (Stevenage, UK). Monoclonal rabbit anti-AQP4 antibody was from Abcam (Cambridge, UK, product code ab128906), and secondary goat anti-rabbit IgG-HRP was from Santa Cruz Biotechnology. Gateway vectors and enzymes were from Invitrogen (Paisley, UK). Unless otherwise specified, all other chemicals were from Sigma or Fisher Scientific. Cell culture reagents, including calcium-free DMEM, were from Sigma. In each experiment, all inhibitors were analyzed using uninhibited cells transfected with wild-type AQP4-GFP as a positive control.

Cell Culture and Transfection—HEK293 cells were cultured routinely in DMEM supplemented with 10% (v/v) fetal bovine serum in humidified 5% (v/v) CO₂ in air at 37 °C. Cells were seeded into 35-mm FluoroDish™ dishes (World Precision Instruments) and transfected after 24 h using PEI. 2 μg of DNA was added to 100 μl of pre-warmed serum-free DMEM followed by 12 μl of 1 mg/ml PEI (pH 7.4). The mixture was incubated at room temperature for 10 min. 600 μl of pre-warmed growth media was added, and cell culture media were replaced with the transfection mix. 2 ml of growth media was added after 2 h. The transfection mix was replaced by 2 ml of culture medium after a further 22 h. Transfected cells were imaged 24–36 h after transfection. Rat primary cortical astrocytes were isolated and cultured as described previously (12). All cells tested negative for mycoplasma using the EZ-PCR mycoplasma test kit (Biological Industries).

Expression Constructs and Mutagenesis—Human AQP4 cDNA was a kind gift of Dr. Kristina Hedfalk (University of Gothenburg). This was fused with C-terminal GFP in the pDEST47 expression vector using the Gateway cloning system (Invitrogen) as described previously (12). Site-directed mutagenesis was performed using the QuikChange procedure (Stratagene).

Confocal Microscopy—AQP4-GFP constructs were imaged in live cells using a Zeiss LSM780 confocal microscope with a 63 × 1.3 NA water immersion objective and an incubated stage held at 37 °C. GFP was excited using the 488-nm line of an argon laser. FM4-64 was excited using the 514-nm line of an argon laser. ER-Tracker Blue-White was excited using a 405-nm diode laser. Hypotonic challenges were achieved by dilution of medium with distilled H₂O on the microscope stage.

Image Analysis—Line profiles across the cell membrane and cytoplasm were extracted using ImageJ as described previously (13) in a semi-automated fashion using an in-house ImageJ macro. Line scan positions were chosen to avoid the nucleus and perinuclear region. Relative membrane expression (RME) was calculated from profiles using an in-house MATLAB code. ER-localized AQP4 affected the calculated RME by <10%. This was confirmed by recalculating the RME after subtracting the GFP signal that co-localized with ER-Tracker Blue-White. Cell cross-sectional areas were calculated in ImageJ using the particle detection tool. Transfected and non-transfected cell swelling was compared using the FM4-64 membrane dye (see Fig. 3).

SDS-PAGE and Western Blotting—HEK293 cells were lysed in radioimmunoprecipitation assay buffer (pH 8.0). 2 μg of total cellular protein was electrophoresed on 8% polyacrylamide gels. Blocking buffer was 20% w/v nonfat powdered milk in PBS-Tween (0.1%). Anti-AQP4 primary antibody (Abcam, ab128906) was diluted 1:10,000 in 0.1% PBS-Tween. Donkey anti-rabbit IgG-HRP (Santa Cruz Biotechnology, sc2313) was diluted 1:20,000 in 0.1% PBS-Tween.

Biotinylation—Primary astrocytes were plated in 6-well plates 2 days before the experiments. Cell surface amines were biotinylated using a cell-impermeable amine-reactive biotinylation reagent (EZ-Link Sulfo-NHS-SS-Biotin, Thermo Scientific). Cells were exposed to reductions in extracellular tonicity by diluting culture medium with distilled H₂O. Cell culture media were washed out with PBS (with Ca²⁺/Mg²⁺) while avoiding completely drying the cells. Cells were incubated in 600 μl of 0.5 mg/ml biotinylation reagent in PBS diluted to the tonicity matching the cell treatment on ice for 30 min. For basal surface expression experiments, cells were washed twice in ice-cold PBS instead of hypotonic treatment. Unreacted reagent was quenched in 25 mM glycine in PBS three times for 5 min. Cells were lysed in Tris-Triton (1%) lysis buffer (pH 7.4). The lysate was centrifuged at 21,000 × *g* at 4 °C for 10 min to remove insoluble material. Biotinylated proteins were pulled out by incubation in NeutrAvidin-coated 96-well plates (Pierce) for 2 h at 4 °C. Each lysate was loaded in triplicate with the same amount of total cellular protein (measured by BCA assay) per lysate. Plates were blocked with 3% w/v BSA in PBS for 1 h at room temperature. Plates were incubated overnight at 4 °C with an AQP4 antibody (Abcam, ab128906) diluted 1:2,000 in 0.05% PBS-Tween. Plates were washed with 0.1% PBS-Tween and incubated at room temperature for 1 h with HRP-conjugated secondary antibody (Santa Cruz Biotechnology, sc-2313). Plates were washed with 0.1% PBS-Tween and incubated with *o*-phenylenediamine dihydrochloride (Sigma-Aldrich) for 30 min, wrapped in foil. Absorbance was measured at 450 nm using a BioTek Synergy HT plate reader.

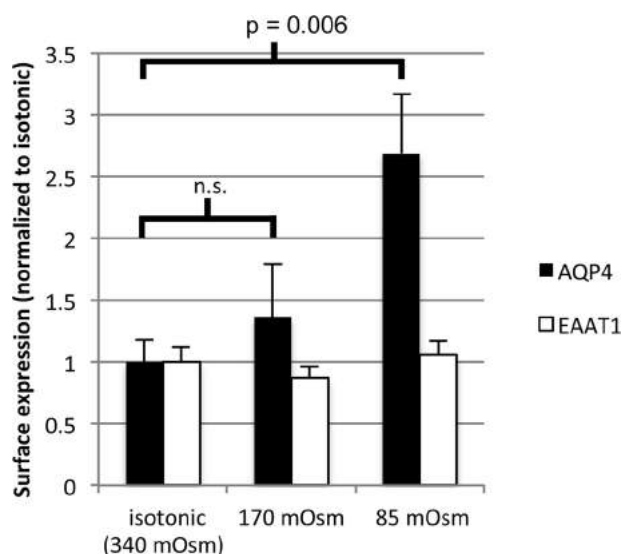


FIGURE 1. Endogenous AQP4 relocalization in primary cortical astrocytes. Cell surface biotinylation of primary rat astrocytes subjected to hypotonic stress and analysis of endogenous AQP4 surface expression is shown, $n = 3$. As a negative control for translocation, membrane expression of the glutamate transporter EAAT1 was measured under the same hypotonic conditions, $n = 3$. All data are presented as mean \pm S.E. p values and significance on the graph refer to AQP4. None of the variability in EAAT1 surface expression was statistically significant, $p = 0.37$. *n.s.*, not significant.

Osmolality—Osmolalities of all treatment solutions were measured using an Osmomat 3000 freezing point depression osmometer (Gonotec).

Statistics—For microscopy experiments in which the same cells were imaged before and after tonicity changes, paired t tests were used. For multiple treatments of the same cells, analysis of variance was used followed by paired t tests, with p values subjected to Bonferroni's correction. For biotinylation experiments in which different cells were subject to different treatments, unpaired t tests were used following analysis of variance and p values subjected to Bonferroni's correction. All p values referred to in the text and figures are the post-correction values, rounded up to 1 significant figure. $p < 0.05$ was considered statistically significant (*).

Results

AQP4 Undergoes a Rapid and Reversible Subcellular Relocalization in Primary Cortical Astrocytes in Response to Changes in the Tonicity of the Extracellular Environment—Surface expression of endogenous AQP4 in rat primary cortical astrocytes was measured using cell surface biotinylation followed by a NeutrAvidin-based ELISA. Fig. 1 shows that AQP4 surface localization increased 2.7-fold after 10 min of hypotonic challenge at 85 mosM/kg of H₂O ($n = 3$, $p = 0.006$) but did not change significantly after 10 min of hypotonic challenge at 140 mosM/kg of H₂O. It is important to confirm that this response is not due to a general effect of hypotonicity on vesicular membrane proteins or changes in protein availability due to membrane unfolding associated with cellular swelling. To discount these, we measured surface expression of the astrocytic excitatory amino acid transporter EAAT1. Surface expression of EAAT1 did not change significantly with either hypotonic treatment ($n = 3$, $p = 0.37$), and there was no significant effect on cell viability measured by trypan blue exclusion (data not shown).

Primary astrocytes suffer from poor transfection efficiencies and slow growth. HEK293 cells were therefore used to further investigate AQP4 subcellular relocalization because they are much more tractable for screening cellular inhibitors and protein mutants, as demonstrated previously by our discovery of the mechanism of tonicity-induced relocalization of human AQP1 using GFP-tagged proteins (12, 13). The distribution of AQP4-GFP fusion proteins transfected into HEK293 cells was altered by changes in tonicity of the external environment. Live-cell confocal microscopy (Fig. 2) showed a rapid translocation of AQP4 to the cell surface in response to hypotonicity (following a 30-s exposure from 340 mosM/kg of H₂O to 85 mosM/kg of H₂O). This effect was fully reversible. Surface expression of AQP4-GFP in fluorescence micrographs was quantified by calculating the RME as described previously (13). Briefly, the difference between the average membrane fluorescence and the average intracellular fluorescence was calculated, and this was normalized to the maximum fluorescence intensity (cells with protein evenly distributed between membrane and intracellular compartments have an RME of 0, and cells with 100% of the protein at the membrane have an RME of 100). Fig. 2 shows that relative membrane expression changed from 27.86 ± 3.52 to 67.11 ± 4.47 , $n = 3$, $p = 0.001$. The change in AQP4-GFP localization upon changing the extracellular tonicity from 340 mosM/kg of H₂O to 85 mosM/kg of H₂O happened on a timescale of 30 s. The change in RME was not due to a dilution effect or an artifact of the GFP tag as AQP3-GFP fusion proteins showed a similar distribution between membrane and cytoplasm, but no significant change in RME in response to reduced tonicity. The translocation response was not due to a reduction in extracellular potassium concentration as isotonic reduction of $[K^+]_o$ had no effect on RME (Fig. 2*F*, left), whereas hypotonicity in the presence of constant $[K^+]_o$ had the same effect as hypotonicity induced by dilution of all solutes (Fig. 2*F*, center). Furthermore, elevation of $[K^+]_o$ to 10 mM in isotonic conditions increased AQP4 RME from 27.8 ± 6.3 to 50.6 ± 6.1 in agreement with published data (17) (Fig. 2*F*, right). AQP4-GFP-transfected cells swelled, leading to a $45 \pm 1\%$ increase of cross-sectional area after 1 min as compared with a $5 \pm 1\%$ increase for non-transfected cells in the same images (Fig. 3).

There Is a Threshold Tonicity for the Translocation Response—AQP4 translocation in primary astrocytes was observed following a reduction of the extracellular tonicity to 85 mosM/kg of H₂O (from 340). Reduction to 170 mosM/kg of H₂O had no effect (Fig. 1). Fig. 4 shows that this phenomenon was reproduced in HEK293 cells. RME was 25.98 ± 5.32 in control medium, 33.07 ± 5.24 in 170 mosM hypotonic medium (not significantly different from control), and 63.61 ± 6.16 in 85 mosM hypotonic medium, $p = 0.0007$ as compared with 340 mosM, after Bonferroni's correction, $n = 3$.

Both AQP4 Isoforms Are Relocalized Equally—AQP4 exists in two isoforms: a long M1 form and a shorter M23 form that lacks the initial 22 amino acids of M1. Both proteins can be translated from the same full-length transcript by a "leaky scanning" mechanism, and different cell types express different M1/M23 ratios (18) via an unknown regulatory mechanism. To determine whether both isoforms or a single isoform was expressed

Tonicity-induced Relocalization of Aquaporin 4

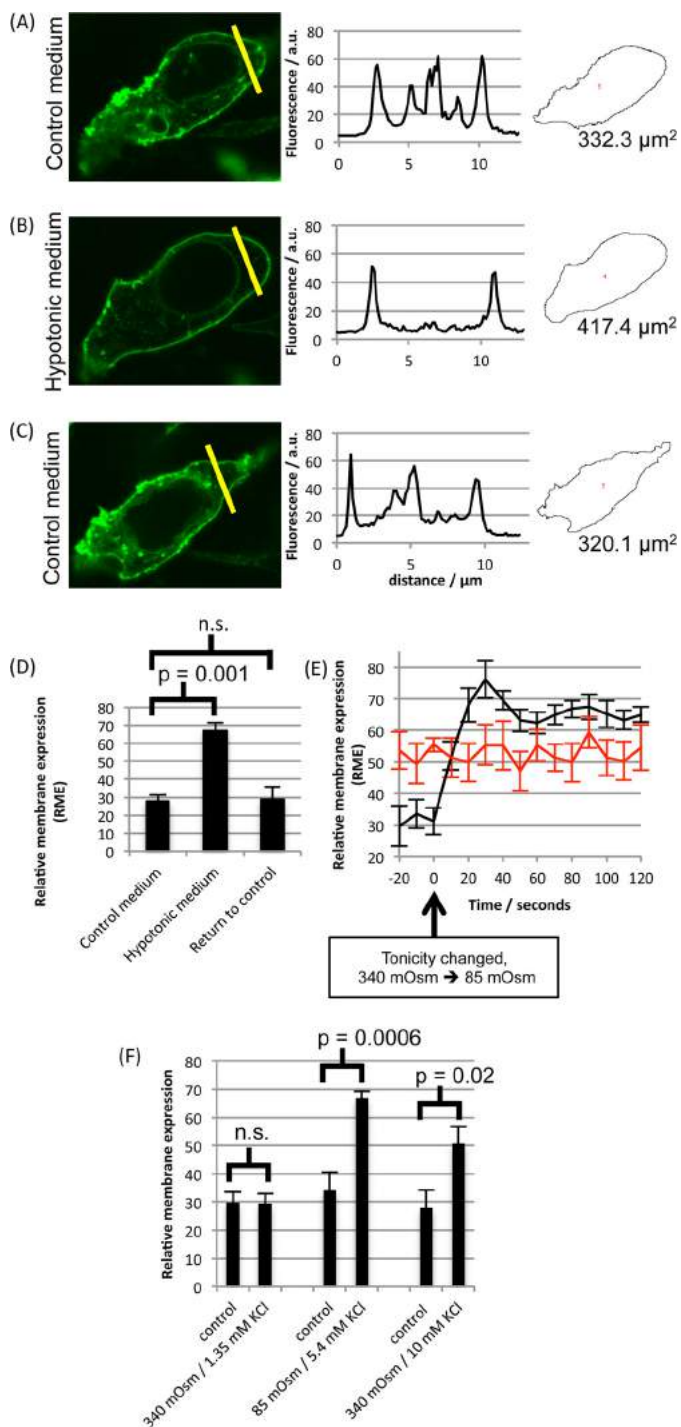


FIGURE 2. AQP4-GFP relocalization in HEK293 cells. A–C, representative fluorescence micrographs of AQP4-GFP fusion proteins in HEK293 cells following exposure to isotonic medium (340 mosm/kg of H_2O) (A), a 30-s exposure to hypotonic medium (85 mosm/kg of H_2O) (B), and return to isotonic extracellular environments (C), with fluorescence intensity profiles across the yellow lines and cross-sectional areas calculated using ImageJ. *a. u.*, arbitrary units. **D**, mean RME in the three conditions. Three line profiles for each experimental repeat. $n = 3$. *p* values are from paired *t* tests with Bonferroni's correction following analysis of variance. *n.s.*, not significant. **E**, RME of AQP4-GFP fusion proteins in HEK293 cells (black curve, $n = 3$), measured by confocal fluorescence microscopy at a frame rate of 0.1 s^{-1} , changed on a timescale of $\sim 30 \text{ s}$ in response to reduction of extracellular tonicity from 340 mosm/kg of H_2O to 85 mosm/kg of H_2O , whereas membrane expression of AQP3-GFP fusion proteins did not change (red curve, $n = 3$). **F**, translocation is not due to a reduction in extracellular potassium. Extracellular potassium reduction (left pair of

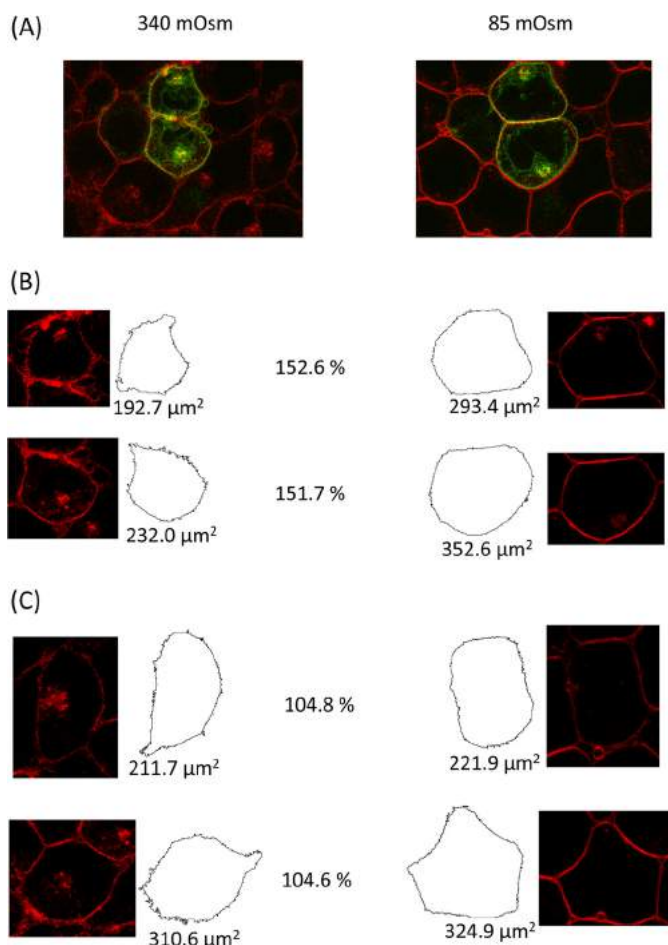


FIGURE 3. Cell swelling of AQP4-transfected cells. AQP4-GFP-transfected HEK293 cells were imaged using the GFP tag and FM4-64, a fluorescent membrane marker. **A**, two-color fluorescence micrograph of AQP4-GFP-transfected cells (green) loaded with FM4-64 (red), before and after reduction of extracellular osmolality from 340 mosm/kg of H_2O to 85 mosm/kg of H_2O . **B**, representative cross-sectional areas of transfected cells before and after hypotonic challenge, calculated using a particle detection algorithm. The post-hypotonic challenge area as a percentage of the pre-challenge area is shown between each pair of images. **C**, representative cross-sectional areas of non-transfected cells from the same image.

from the wild-type AQP4 mRNA in our HEK293 system, we created constructs lacking either the M1 or the M23 translation initiation sites and compared the molecular weights of the resulting proteins with that translated from the wild-type mRNA, using SDS-PAGE. Fig. 5 shows that only the M1 isoform was present in HEK293 cells transfected with the wild-type AQP4 mRNA. M1 and M23 constructs had basal surface expression (*i.e.* at 340 mosm) equivalent to the wild type, measured using cell surface biotinylation. The confocal microscopy experiments described previously were repeated using the M1 and M23 constructs. M23 formed the punctate orthogonal arrays of particles that have been described previously for this isoform (19). RME for M23 changed from 24.58 ± 4.85 at 340 mosm/kg of H_2O to 51.15 ± 5.25 at 85 mosm/kg of H_2O , $n = 3$

data points) and hypotonicity (central pair of data points) were applied independently by diluting media 4-fold with either isotonic NaCl (170 mM = 340 mosm) or 5.4 mM KCl in distilled H_2O . Extracellular potassium was also increased to 10 mM in isotonic conditions (right pair of data points). All data are presented as mean \pm S.E.

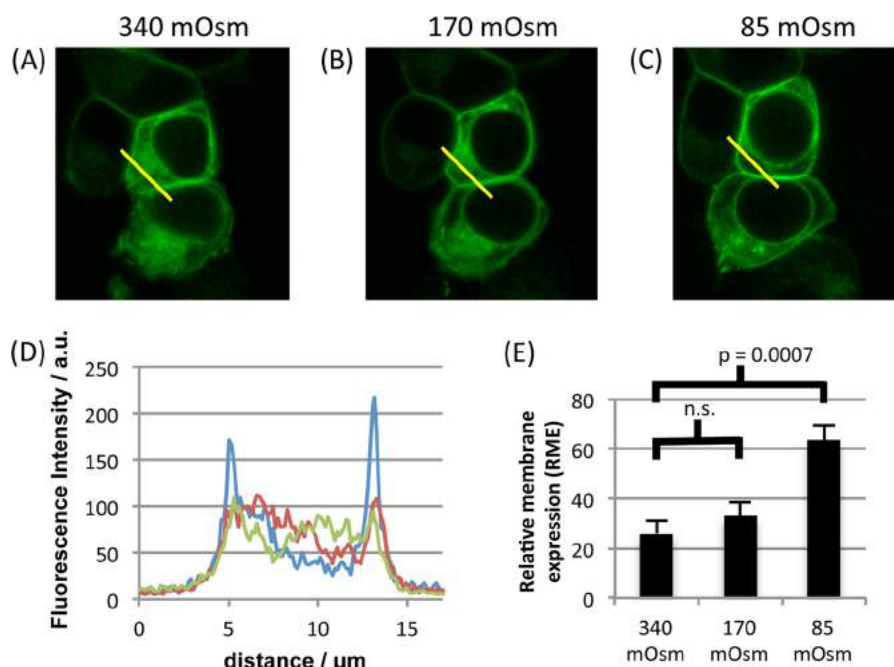


FIGURE 4. **Tonicity dependence of AQP4 relocalization.** A–C, AQP4-GFP-transfected HEK293 cells were imaged by confocal microscopy in a solution of 340 mosm/kg of H₂O (A), 170 mosm/kg of H₂O (B), and 85 mosm/kg of H₂O (C). Capture of each image was started 30 s after the change in tonicity. For 170 mosm, cells were allowed to equilibrate for 10 min to check for a slower translocation response. No difference was observed between 30 s and 10 min images. D, representative fluorescence profiles along the yellow lines in A, B, and C. *a. u.*, arbitrary units. E, mean RME for the three tonicities, averaged over three profiles/cell and at least three cells/experimental repeat, $n = 3$. *p* values are from paired *t* tests with Bonferroni's correction following analysis of variance. All data are presented as mean \pm S.E. *n.s.*, not significant.

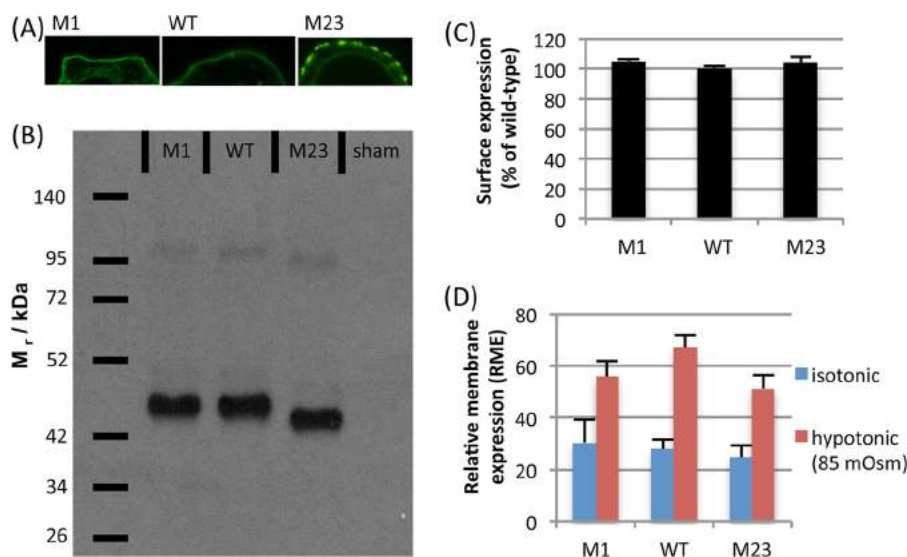


FIGURE 5. **Both AQP4 isoforms are relocalized.** Both the M1 and the M23 isoforms of AQP4 are translocated to the cell surface upon hypotonic stimulus. A, membrane organization of AQP4-GFP transfected into HEK293 cells. The M1 isoform has a homogeneous membrane distribution, whereas M23 clusters into orthogonal arrays of particles. B, SDS-PAGE of protein transcribed in HEK293 cells from the AQP4 wild-type mRNA, AQP4 M1 construct, and AQP4 M23 construct. No M23 protein was detected in the wild-type sample. C, there was no significant difference in constitutive surface expression between the three constructs. D, both isoforms of AQP4 are relocalized in response to reduction of the extracellular osmolality to 85 mosm/kg of H₂O (M1: $p = 0.002$, $n = 3$. M23: $p = 0.004$, $n = 3$. WT: $p = 0.001$, $n = 3$). All data are presented as mean \pm S.E.

$p = 0.004$. Although the hypotonic RME is lower than for the wild type, it is not significantly so ($p = 0.33$). This suggested that both isoforms are equally translocated to the surface in response to hypotonic stimulus.

Calmodulin, Calcium, and Protein Kinase A Regulate AQP4 Relocalization—AQP surface expression is known to be regulated by numerous cell signaling mechanisms. These include kinases, calcium channels, and cytoskeletal reorganization (11).

AQP4 relocalization following hypotonic challenge was compared in the presence of a number of inhibitory compounds. These are described in Table 1. These data suggest that a combination of PKA kinase activity and calcium signaling mechanisms is required for AQP4 translocation. Prevention of the translocation response by inhibitors correlated with a reduction in cell swelling, suggesting a functional increase in membrane water permeability.

Tonicity-induced Relocalization of Aquaporin 4

TABLE 1

Relative membrane expression of AQP4-GFP in response to hypotonic stimulus in the presence of inhibitors

Translocation of AQP4-GFP in HEK293 cells in the presence of various inhibitors, measured by confocal microscopy and subsequent image analysis, is shown. Cells were imaged before and after reduction of the extracellular osmolality to 85 mosM/kg of H₂O. Each RME value is an average over three independent experiments, with each experiment analyzing at least 3 cells/micrograph and 3 line profiles/cell. $p < 0.05$ was considered statistically significant (*). Abbreviations: PKCi, PKC inhibitor; PKAi, PKA inhibitor.

Inhibitor/control media	Isotonic RME (± S.E.)	Hypotonic RME (± S.E.)	Mean % of area change (± S.E.)	Translocation
Untreated control	28.77 (6.78)	78.84 (1.84)*	145.19 (1.11)*	Yes
Non-specific kinase inhibitor (hypericin)	21.85 (6.80)	38.22 (5.58)	103.50 (2.05)	No
PKC (Myr-PKCi)	27.27 (4.73)	55.28 (3.97)*	141.00 (2.05)*	Yes
PKA (Myr-PKAi)	25.62 (5.16)	33.66 (6.62)	102.97 (5.21)	No
Calcium-free media	26.69 (6.03)	32.16 (4.48)	111.60 (1.92)	No
Calmodulin inhibitor (trifluoperazine)	27.23 (7.11)	31.40 (5.91)	108.61 (5.47)	No
Calmodulin inhibitor (W7)	16.86 (8.43)	22.11 (8.14)	110.31 (14.21)	No

Ser-276 Phosphorylation Is Required for Relocalization—The data in Table 1 suggest a key role for PKA (but not PKC) in mediating AQP4 translocation. Using kinase site prediction software (NetPhosK 1.0 (20)), five serine residues were identified as PKA consensus sites. These were Ser-52, Ser-111, Ser-180, Ser-188, and Ser-276. The locations of these residues in the AQP4 structure are shown in Fig. 6.

The PKA consensus sites were individually mutated to alanine (to block phosphorylation) and aspartate (to act as a phosphomimetic). The effects of these mutations on the tonicity-induced relocalization of AQP4 are tabulated in Table 2. Only mutations to Ser-276 had any effect on hypotonicity-induced translocation. Substitution of Ser-276 with alanine (S276A) blocked hypotonicity-induced translocation, whereas substitution with aspartate (S276D) had no effect, suggesting that PKA phosphorylation at Ser-276 is necessary but not sufficient for translocation to occur or that S276D is a poor phosphomimetic. To determine whether this single phosphorylation event was the only mechanistic effect of PKA, translocation of the S276D mutant was measured in the presence of a myristoylated PKA inhibitory peptide (Myr-PKI). Unlike the wild-type protein, for which the translocation was inhibited by Myr-PKI, S276D still translocated to the membrane in the presence of the PKA inhibitor. This shows that S276D is a phosphomimetic and that PKA phosphorylation of AQP4 at Ser-276 is a key step in the AQP4 translocation signaling pathway. Although the S52A mutant behaved like wild-type AQP4, S52D did not translocate, but also had greatly reduced basal surface expression in comparison with wild-type AQP4 and other phosphomimetic mutants. Low surface expression prevented calculation of the RME and measurement of cross-sectional area in confocal micrographs. S52D appeared to be localized throughout the cytoplasm (rather than degraded or held as inclusion bodies), suggesting that the protein is not simply grossly misfolded. This may reflect a functional relevance, possibly interrupting processing through the Golgi apparatus or post-Golgi trafficking to the cell surface, which may be worthy of further study.

PKA Activity Is Required for Endogenous AQP4 Relocalization in Primary Astrocytes—HEK293 cells provide a tractable model for studying the cell signaling components required for AQP4 translocation. However, it is possible that, despite sharing the translocation response, HEK293 cells and primary astrocytes translocate AQP4 by different mechanisms. To validate the mechanistic information obtained in HEK293 cells, we repeated the primary astrocyte cell surface biotinylation

experiments in the presence of a PKA inhibitor. Fig. 7 shows that a 30-min pre-incubation with Myr-PKI prevented the hypotonicity-induced relocalization of endogenous AQP4 in rat primary cortical astrocytes. This suggests that the mechanistic details elucidated using HEK293 cells are physiologically relevant to the translocation of endogenous AQP4 in primary astrocytes.

Discussion

AQP4-GFP fusion proteins in HEK293 cells and endogenous AQP4 in primary rat astrocytes rapidly relocalize to the plasma membrane in response to a reduction in local tonicity. The relocalization response takes about 30 s in HEK293 cells and is completely reversible upon return of the local tonicity to 340 mosM/kg of H₂O. The concomitant cell swelling following AQP4 relocalization (which was reduced by inhibitors that blocked the translocation response) suggests that there is an effective increase in cell membrane water permeability. The mechanisms involved in AQP4 relocalization require PKA activity and cytoskeletal elements. Extracellular calcium is required, presumably passing through transient receptor potential (TRP) channels, which are known to mediate a calcium signaling response to osmotic cell swelling (21).

Calmodulin inhibition using two different calmodulin inhibitors (W7 and trifluoperazine) also blocked AQP4 translocation in response to hypotonicity. Calmodulin-mediated regulation of AQPs is well established. Calmodulin has been shown to inhibit AQP0 water permeability by binding directly to the C-terminal tail (22, 23), and this binding can be inhibited by AQP0 phosphorylation (24). In rat parotid cells, AQP5 was rapidly translocated to the apical membrane via acetylcholine signaling and inhibition of signaling elements downstream of calmodulin (calmodulin kinase II, myosin light chain kinase, and nitric-oxide synthase) blocked this translocation response (25). Vasopressin-induced translocation of AQP2 in collecting duct cells can be attenuated by extracellular calcium in a calmodulin-dependent manner (26). Calmodulin has also been shown to bind directly to the N-terminal tail of AQP6 (27), although the functional relevance of this interaction is unknown. We showed previously that inhibition of calmodulin prevented hypotonicity-induced relocalization of AQP1 in HEK293 cells (12). It is not clear from our data whether calmodulin binds directly to AQP4 or activates a third party protein to mediate AQP4 translocation, although a calmodulin binding site prediction tool (Calmodulin Target Database (28)) does predict that the most likely

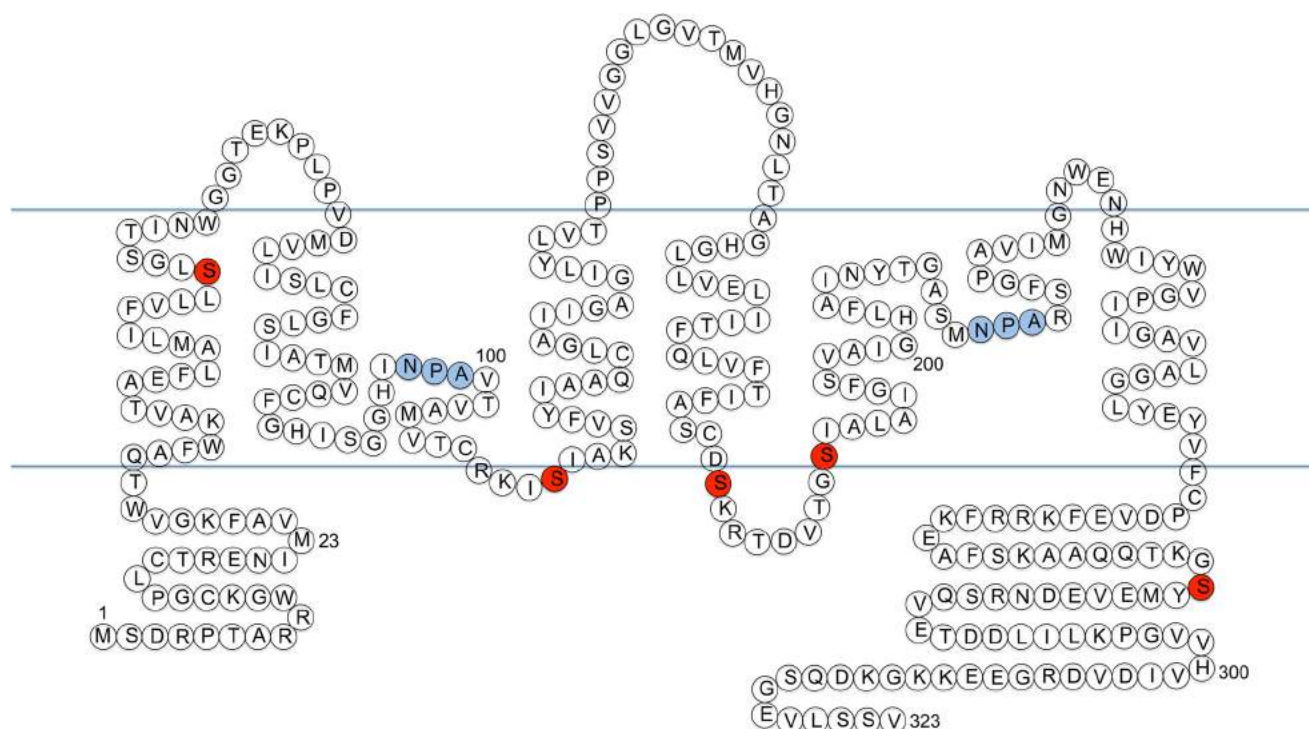


FIGURE 6. **Phosphomimetic mutagenesis of AQP4.** Locations within the AQP4 structure of identified putative PKA sites that were mutated (red) and the AQP family conserved NPA motifs (blue) are shown.

TABLE 2

Relative membrane expression of AQP4 phosphorylation mutants in response to hypotonic stimulus

Translocation of phosphomimetic and phospho-blocking mutants of AQP4-GFP in HEK293 cells, measured by confocal microscopy and subsequent image analysis, is shown. Cells were imaged before and after reduction of the extracellular osmolality to 85 mosm/kg of H₂O. Each RME value is an average over three independent experiments, with each experiment analyzing at least 3 cells/micrograph and 3 line profiles/cell. Constitutive surface expression was measured by cell surface biotinylation and normalized to wild-type expression. $p < 0.05$ was considered statistically significant (*). Abbreviation: NA, not applicable.

Mutant	Isotonic RME (± S.E.)	Hypotonic RME (± S.E.)	Mean % of area change (± S.E.)	Translocation	Constitutive surface expression (% of wild-type)
S52A	34.18 (4.06)	59.34 (5.53)*	127.03 (5.99)*	Yes	98.1 (5.3)
S52D	NA	NA	NA	No	17.0 (6.3)*
S111A	36.24 (9.95)	62.43 (5.42)*	130.69 (4.76)*	Yes	94.8 (6.4)
S111D	31.17 (4.22)	52.99 (5.41)*	120.62 (8.40)*	Yes	91.4 (4.6)
S180A	35.43 (7.78)	69.03 (6.94)*	142.65 (7.78)*	Yes	109.8 (4.5)
S180D	36.86 (6.07)	53.56 (4.96)*	148.16 (16.74)*	Yes	99.7 (5.0)
S188A	34.17 (7.21)	63.31 (7.00)*	137.01 (9.17)*	Yes	98.6 (3.2)
S188D	31.64 (9.11)	59.18 (5.60)*	135.53 (10.47)*	Yes	104.1 (4.2)
S276A	36.61 (4.64)	36.97 (5.53)	110.82 (3.85)	No	96.8 (3.2)
S276D	25.72 (5.42)	57.93 (11.01)*	134.18 (15.10)*	Yes	83.5 (5.7)*
S276D + PKA inhibitor	24.58 (4.85)	51.14 (5.25)*	127.12 (7.34)*	Yes	86.2 (5.1)*

site for direct binding of calmodulin to AQP4 is the 20-residue peptide at positions 277–296, directly upstream of the Ser-276 phosphorylation site we identified.

Kinase-dependent translocation of AQPs to the plasma membrane from intracellular vesicles is an established regulatory mechanism that has been demonstrated for AQP2 in response to vasopressin signaling via PKA (29), AQP1 in response to hypotonicity via PKC (13), and AQP5 in response to acetylcholine via PKG (25). Treatment with the broad-range kinase inhibitor, hypericin, suggested a similar mechanism for AQP4 relocalization. Using specific inhibitors identified PKA activity as a requirement for tonicity-mediated translocation of AQP4. There is some evidence that PKA reduced surface availability of AQP4 in human gastric cells (14). In our systems, PKA seems to be doing the opposite.

All potential PKA sites of AQP4 were mutated, suggesting a key requirement for serine at position 276 (Ser-276) in the

C-terminal tail of AQP4. Phosphorylation at this residue has been detected *in vivo* in murine AQP4 (30) and rat AQP4 (31). It was recently reported that phosphomimetic (S276D) or phospho-blocking (S276A) mutations at this residue have no effect on surface expression or water permeability, leaving the purpose of this phosphorylated residue unclear (32). Our data provide evidence of a functional role for Ser-276 phosphorylation. It has also been reported that phosphorylation at Ser-276 can increase lysosomal targeting of AQP4 upon internalization (33). This may explain the slight reduction in constitutive surface expression (to $83.5 \pm 5.7\%$) that we measured for the S276D mutant. PKC phosphorylation of Ser-180 in response to AVP has been reported to cause AQP4 internalization (34); we did not observe any change in constitutive surface expression or translocation response for the S180D phosphomimetic mutant in our system. This may reflect the lack of an element of this internalization pathway in HEK293 cells or a species-specific

Tonicity-induced Relocalization of Aquaporin 4

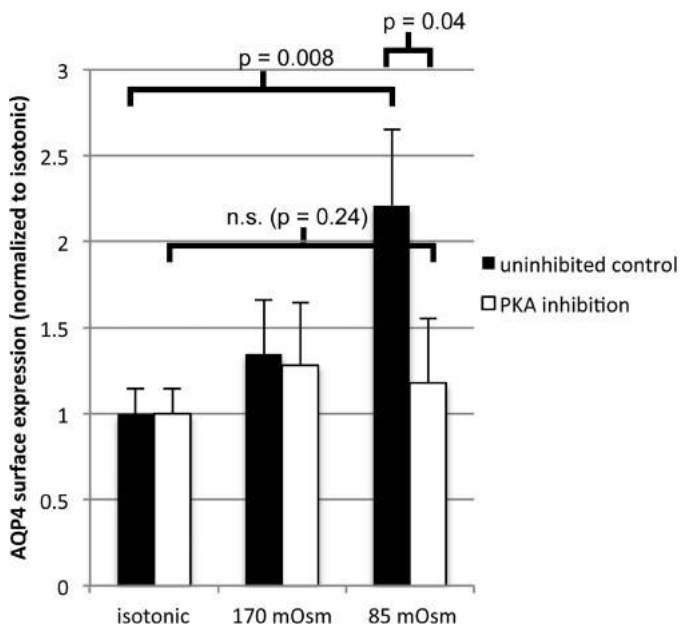


FIGURE 7. Validation of the PKA-dependent mechanism in primary astrocytes. Cell surface biotinylation of primary rat astrocytes exposed to hypotonic stimulus in the presence and absence of PKA inhibition and analysis of endogenous AQP4 surface expression is shown. In the absence of the inhibitor, AQP4 surface expression increased 2.2-fold between 340 and 85 mosm/kg of H₂O, $n = 3$, $p = 0.008$. In the presence of the inhibitor, AQP4 surface expression did not change significantly between 340 and 85 mosm/kg of H₂O, $n = 3$, $p = 0.24$. All data are presented as mean \pm S.E. *n.s.*, not significant.

effect (these experiments were done in *Xenopus* oocytes). Phosphorylation of AQP4 at Ser-111 in response to elevated extracellular potassium has been reported to increase membrane water permeability in an astrocytic cell line (17). S111A and S111D mutations had no effect in our system, and furthermore S276D translocated in the presence of a PKA inhibitor, suggesting that the only role of PKA in our system is to phosphorylate Ser-276. Although an isotonic increase in extracellular potassium induced AQP4 translocation in our system, which agrees with a previous study (17), the hypotonicity-induced translocation of AQP4 was independent of any reduction in extracellular potassium associated with the hypotonic challenge. Although it is probable that Ser-276 is phosphorylated in our primary astrocyte experiments, we cannot rule out a difference in phosphorylation sites between different cells or a synergistic effect of several kinase sites in the primary cells.

Interestingly, we found that both endogenous and transfected AQP4 (with and without GFP) did not relocalize in response to any tonicity change in the U373 glioblastoma cell line (Fig. 8). There is some evidence that a dominant-negative splice variant of AQP4 lacking exon 4, which codes for the half-helix containing the second NPA motif, can inhibit surface expression of either the M1 or the M23 isoforms of AQP4 when co-expressed (35). This was reported in muscle cells, but it may be possible that dysregulation of this isoform inhibits surface expression in U373 cells. People with glioblastoma have a very poor prognosis. The cells are very invasive, and edema is a key problem. This may be worthy of further investigation to determine whether this is a peculiarity of the U373 cell line or representative of glioblastoma physiology.

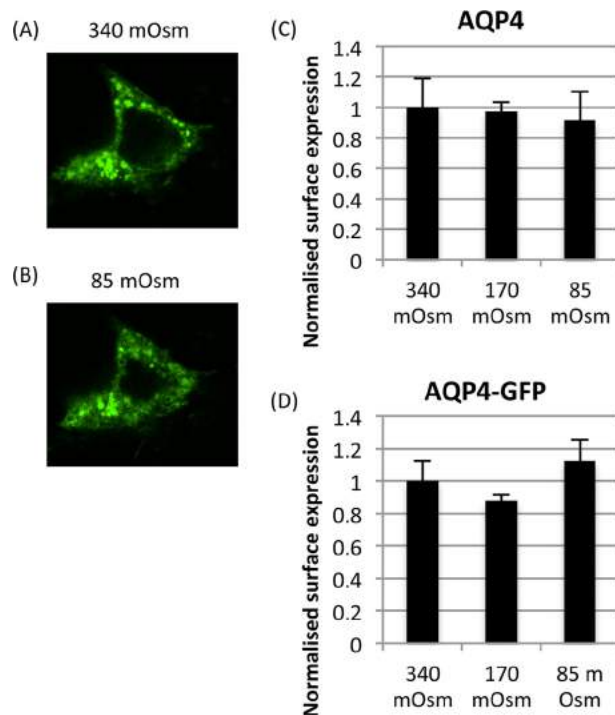


FIGURE 8. Lack of AQP4 translocation response in the U373 glioblastoma cell-line. *A* and *B*, representative confocal micrographs of an AQP4-GFP-transfected U373 cell exposed to isotonic (340 mosm/kg of H₂O) media (*A*) and 5-min exposure to hypotonic (85 mosm/kg of H₂O) media (*B*). *C* and *D*, cell surface biotinylation of U373 cells transfected with AQP4 (*C*) and AQP4-GFP (*D*). No statistically significant change was observed between any of the treatment groups (340, 170, and 85 mosm/kg of H₂O), $n = 3$. Data are presented as mean \pm S.E.

To conclude, the data reported here provide a mechanistic explanation for our discovery of the physiological relocalization of AQP4 in response to changes in local tonicity. A change in local tonicity is the key driver of cell swelling in stroke and contributes to the effects of cytotoxic edema following traumatic brain injury. Modulating the surface expression of AQP4 rather than trying to directly block its pore is a novel platform for developing therapies for these devastating conditions.

Author Contributions—PK, RED, MTC, RMB, and ACC designed all experiments. PK performed and analyzed experiments shown in Figs. 1, 2, 3, 4, 5, and 8 and prepared Fig. 6. PK and LHJT performed and analyzed experiments shown in Tables 1 and 2. RED and MMS performed and analyzed experiments shown in Figs. 1 and 7. PK and ACC drafted the manuscript. RMB, MMS, RED and MTC critically revised the manuscript. All authors approved the final version of the manuscript.

References

- Jung, J. S., Bhat, R. V., Preston, G. M., Guggino, W. B., Baraban, J. M., and Agre, P. (1994) Molecular characterization of an aquaporin cDNA from brain: candidate osmoreceptor and regulator of water balance. *Proc. Natl. Acad. Sci. U.S.A.* **91**, 13052–13056
- Papadopoulos, M. C., and Verkman, A. S. (2013) Aquaporin water channels in the nervous system. *Nat. Rev. Neurosci.* **14**, 265–277
- Zador, Z., Stiver, S., Wang, V., and Manley, G. T. (2009) Role of aquaporin-4 in cerebral edema and stroke. *Handb. Exp. Pharmacol.* 159–170, 10.1007/978-3-540-79885-9_7
- Manley, G. T., Fujimura, M., Ma, T., Noshita, N., Filiz, F., Bollen, A. W.,

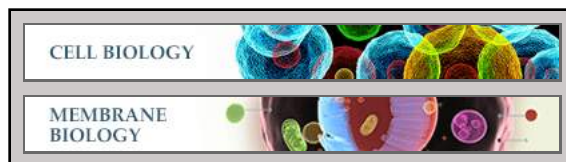
- Chan, P., and Verkman, A. S. (2000) Aquaporin-4 deletion in mice reduces brain edema after acute water intoxication and ischemic stroke. *Nat. Med.* **6**, 159–163
5. Huber, V. J., Tsujita, M., and Nakada, T. (2009) Identification of aquaporin 4 inhibitors using in vitro and in silico methods. *Bioorg. Med. Chem.* **17**, 411–417
 6. Tanimura, Y., Hiroaki, Y., and Fujiyoshi, Y. (2009) Acetazolamide reversibly inhibits water conduction by aquaporin-4. *J. Struct. Biol.* **166**, 16–21
 7. Kato, J., Hayashi, M. K., Aizu, S., Yukutake, Y., Takeda, J., and Yasui, M. (2013) A general anaesthetic propofol inhibits aquaporin-4 in the presence of Zn²⁺. *Biochem. J.* **454**, 275–282
 8. Marples, D., Knepper, M. A., Christensen, E. I., and Nielsen, S. (1995) Redistribution of aquaporin-2 water channels induced by vasopressin in rat kidney inner medullary collecting duct. *Am. J. Physiol.* **269**, C655–C664
 9. Nejsum, L. N., Zelenina, M., Aperia, A., Frøkiaer, J., and Nielsen, S. (2005) Bidirectional regulation of AQP2 trafficking and recycling: involvement of AQP2-S256 phosphorylation. *Am. J. Physiol. Renal Physiol.* **288**, F930–F938
 10. Gouraud, S., Laera, A., Calamita, G., Carmosino, M., Procino, G., Rossetto, O., Mannucci, R., Rosenthal, W., Svelto, M., and Valenti, G. (2002) Functional involvement of VAMP/synaptobrevin-2 in cAMP-stimulated aquaporin 2 translocation in renal collecting duct cells. *J. Cell Sci.* **115**, 3667–3674
 11. Conner, A. C., Bill, R. M., and Conner, M. T. (2013) An emerging consensus on aquaporin translocation as a regulatory mechanism. *Mol. Membr. Biol.* **30**, 1–12, 10.3109/09687688.2012.743194
 12. Conner, M. T., Conner, A. C., Bland, C. E., Taylor, L. H., Brown, J. E., Parri, H. R., and Bill, R. M. (2012) Rapid aquaporin translocation regulates cellular water flow: mechanism of hypotonicity-induced subcellular localization of aquaporin 1 water channel. *J. Biol. Chem.* **287**, 11516–11525
 13. Conner, M. T., Conner, A. C., Brown, J. E., and Bill, R. M. (2010) Membrane trafficking of aquaporin 1 is mediated by protein kinase C via microtubules and regulated by tonicity. *Biochemistry* **49**, 821–823
 14. Carmosino, M., Procino, G., Tamma, G., Mannucci, R., Svelto, M., and Valenti, G. (2007) Trafficking and phosphorylation dynamics of AQP4 in histamine-treated human gastric cells. *Biol. Cell* **99**, 25–36
 15. Gunnarson, E., Zelenina, M., Axehult, G., Song, Y., Bondar, A., Krieger, P., Brismar, H., Zelenin, S., and Aperia, A. (2008) Identification of a molecular target for glutamate regulation of astrocyte water permeability. *Glia* **56**, 587–596
 16. Nicchia, G. P., Rossi, A., Mola, M. G., Procino, G., Frigeri, A., and Svelto, M. (2008) Actin cytoskeleton remodeling governs aquaporin-4 localization in astrocytes. *Glia* **56**, 1755–1766
 17. Song, Y., and Gunnarson, E. (2012) Potassium dependent regulation of astrocyte water permeability is mediated by cAMP signaling. *PLoS One* **7**, e34936
 18. Rossi, A., Pisani, F., Nicchia, G. P., Svelto, M., and Frigeri, A. (2010) Evidences for a leaky scanning mechanism for the synthesis of the shorter M23 protein isoform of aquaporin-4: implication in orthogonal array formation and neuromyelitis optica antibody interaction. *J. Biol. Chem.* **285**, 4562–4569
 19. Rash, J. E., Davidson, K. G., Yasumura, T., and Furman, C. S. (2004) Freeze-fracture and immunogold analysis of aquaporin-4 (AQP4) square arrays, with models of AQP4 lattice assembly. *Neuroscience* **129**, 915–934
 20. Blom, N., Sicheritz-Pontén, T., Gupta, R., Gammeltoft, S., and Brunak, S. (2004) Prediction of post-translational glycosylation and phosphorylation of proteins from the amino acid sequence. *Proteomics* **4**, 1633–1649
 21. Vriens, J., Watanabe, H., Janssens, A., Droogmans, G., Voets, T., and Nilius, B. (2004) Cell swelling, heat, and chemical agonists use distinct pathways for the activation of the cation channel TRPV4. *Proc. Natl. Acad. Sci. U.S.A.* **101**, 396–401
 22. Varadaraj, K., Kumari, S., Shiels, A., and Mathias, R. T. (2005) Regulation of aquaporin water permeability in the lens. *Invest. Ophthalmol. Vis. Sci.* **46**, 1393–1402
 23. Reichow, S. L., and Gonen, T. (2008) Noncanonical binding of calmodulin to aquaporin-0: implications for channel regulation. *Structure* **16**, 1389–1398
 24. Kalman, K., Németh-Cahalan, K. L., Froger, A., and Hall, J. E. (2008) Phosphorylation determines the calmodulin-mediated Ca²⁺ response and water permeability of AQP0. *J. Biol. Chem.* **283**, 21278–21283
 25. Ishikawa, Y., Iida, H., and Ishida, H. (2002) The muscarinic acetylcholine receptor-stimulated increase in aquaporin-5 levels in the apical plasma membrane in rat parotid acinar cells is coupled with activation of nitric oxide/cGMP signal transduction. *Mol. Pharmacol.* **61**, 1423–1434
 26. Bustamante, M., Hasler, U., Leroy, V., de Seigneux, S., Dimitrov, M., Moradasini, D., Rousselot, M., Martin, P. Y., and Féraille, E. (2008) Calcium-sensing receptor attenuates AVP-induced aquaporin-2 expression via a calmodulin-dependent mechanism. *J. Am. Soc. Nephrol.* **19**, 109–116
 27. Rabaud, N. E., Song, L., Wang, Y., Agre, P., Yasui, M., and Carbrey, J. M. (2009) Aquaporin 6 binds calmodulin in a calcium-dependent manner. *Biochem. Biophys. Res. Commun.* **383**, 54–57
 28. Yap, K. L., Kim, J., Truong, K., Sherman, M., Yuan, T., and Ikura, M. (2000) Calmodulin target database. *J. Struct. Funct. Genomics* **1**, 8–14
 29. Katsura, T., Gustafson, C. E., Ausiello, D. A., and Brown, D. (1997) Protein kinase A phosphorylation is involved in regulated exocytosis of aquaporin-2 in transfected LLC-PK1 cells. *Am. J. Physiol.* **272**, F817–F822
 30. Wiśniewski, J. R., Nagaraj, N., Zougman, A., Gnäd, F., and Mann, M. (2010) Brain phosphoproteome obtained by a FASP-based method reveals plasma membrane protein topology. *J. Proteome Res.* **9**, 3280–3289
 31. Hoffert, J. D., Wang, G., Pisitkun, T., Shen, R. F., and Knepper, M. A. (2007) An automated platform for analysis of phosphoproteomic datasets: application to kidney collecting duct phosphoproteins. *J. Proteome Res.* **6**, 3501–3508
 32. Assentoft, M., Larsen, B. R., Olesen, E. T., Fenton, R. A., and MacAulay, N. (2014) AQP4 plasma membrane trafficking or channel gating is not significantly modulated by phosphorylation at COOH-terminal serine residues. *Am. J. Physiol. Cell Physiol.* **307**, C957–C965
 33. Madrid, R., Le Maout, S., Barrault, M. B., Janvier, K., Benichou, S., and Mérot, J. (2001) Polarized trafficking and surface expression of the AQP4 water channel are coordinated by serial and regulated interactions with different clathrin-adaptor complexes. *EMBO J.* **20**, 7008–7021
 34. Moeller, H. B., Fenton, R. A., Zeuthen, T., and Macaulay, N. (2009) Vasopressin-dependent short-term regulation of aquaporin 4 expressed in *Xenopus* oocytes. *Neuroscience* **164**, 1674–1684
 35. De Bellis, M., Pisani, F., Mola, M. G., Basco, D., Catalano, F., Nicchia, G. P., Svelto, M., and Frigeri, A. (2014) A novel human aquaporin-4 splice variant exhibits a dominant-negative activity: a new mechanism to regulate water permeability. *Mol. Biol. Cell* **25**, 470–480

Cell Biology:

**Identification and Molecular Mechanisms
of the Rapid Tonicity-induced
Relocalization of the Aquaporin 4 Channel**

Philip Kitchen, Rebecca E. Day, Luke H. J.
Taylor, Mootaz M. Salman, Roslyn M. Bill,
Matthew T. Conner and Alex C. Conner
J. Biol. Chem. 2015, 290:16873-16881.

doi: 10.1074/jbc.M115.646034 originally published online May 26, 2015



Access the most updated version of this article at doi: [10.1074/jbc.M115.646034](https://doi.org/10.1074/jbc.M115.646034)

Find articles, minireviews, Reflections and Classics on similar topics on the [JBC Affinity Sites](https://www.jbc.org/).

Alerts:

- [When this article is cited](#)
- [When a correction for this article is posted](#)

[Click here](#) to choose from all of JBC's e-mail alerts

This article cites 35 references, 14 of which can be accessed free at
<http://www.jbc.org/content/290/27/16873.full.html#ref-list-1>

RESEARCH ARTICLE

Plasma Membrane Abundance of Human Aquaporin 5 Is Dynamically Regulated by Multiple Pathways

Philip Kitchen¹, Fredrik Öberg², Jennie Sjöhamn², Kristina Hedfalk², Roslyn M. Bill³, Alex C. Conner^{4*}, Matthew T. Conner^{5*}, Susanna Törnroth-Horsefield^{6*}

1 Molecular Organization and Assembly in Cells Doctoral Training Centre, University of Warwick, Coventry, United Kingdom, **2** Department of Chemistry, University of Gothenburg, Gothenburg, Sweden, **3** School of Life and Health Sciences, Aston University, Birmingham, United Kingdom, **4** Clinical and Experimental Medicine, The Medical School, University of Birmingham, Birmingham, United Kingdom, **5** Biomedical Research Centre, Sheffield Hallam University, Sheffield, United Kingdom, **6** Department of Biochemistry and Structural Biology, Centre for Molecular Protein Science, Lund University, Lund, Sweden

* susanna.horsefield@biochemistry.lu.se (STH); m.t.conner@shu.ac.uk (MTC); a.c.conner@bham.ac.uk (ACC)



OPEN ACCESS

Citation: Kitchen P, Öberg F, Sjöhamn J, Hedfalk K, Bill RM, Conner AC, et al. (2015) Plasma Membrane Abundance of Human Aquaporin 5 Is Dynamically Regulated by Multiple Pathways. *PLoS ONE* 10(11): e0143027. doi:10.1371/journal.pone.0143027

Editor: Giovanna Valenti, University of Bari Aldo Moro, ITALY

Received: July 1, 2015

Accepted: October 29, 2015

Published: November 16, 2015

Copyright: © 2015 Kitchen et al. This is an open access article distributed under the terms of the [Creative Commons Attribution License](http://creativecommons.org/licenses/by/4.0/), which permits unrestricted use, distribution, and reproduction in any medium, provided the original author and source are credited.

Data Availability Statement: Coordinates and structure factors are available from the Protein Data Bank, accession codes 5DYE and 5C5X. All other relevant data are within the paper.

Funding: This work was supported by the Swedish Research Council (www.vr.se) grants 2009-360 and 2010-5208 (to STH), European Commission Framework Programme 7 (http://ec.europa.eu/research/fp7/index_en.cfm) Grant 201924 EDICT (to RMB) and by the Engineering and Physical Sciences Research Council (<https://www.epsrc.ac.uk>) through the Molecular Organisation and Assembly in Cells Doctoral Training Centre, University of Warwick, grant

Abstract

Aquaporin membrane protein channels mediate cellular water flow. Human aquaporin 5 (AQP5) is highly expressed in the respiratory system and secretory glands where it facilitates the osmotically-driven generation of pulmonary secretions, saliva, sweat and tears. Dysfunctional trafficking of AQP5 has been implicated in several human disease states, including Sjögren's syndrome, bronchitis and cystic fibrosis. In order to investigate how the plasma membrane expression levels of AQP5 are regulated, we studied real-time translocation of GFP-tagged AQP5 in HEK293 cells. We show that AQP5 plasma membrane abundance in transfected HEK293 cells is rapidly and reversibly regulated by at least three independent mechanisms involving phosphorylation at Ser156, protein kinase A activity and extracellular tonicity. The crystal structure of a Ser156 phosphomimetic mutant indicates that its involvement in regulating AQP5 membrane abundance is not mediated by a conformational change of the carboxy-terminus. We suggest that together these pathways regulate cellular water flow.

Introduction

The flux of water across biological membranes is facilitated by transmembrane protein channels called aquaporins (AQPs). AQPs passively transport water in response to osmotic gradients, while excluding the movement of ions and protons [1] and thus are important for cell volume regulation [2]. In humans, thirteen members of the AQP family (AQP0-12), with subtle functional differences, are expressed with different tissue-specific and time-dependent profiles [3].

number EP/F500378/1 (PK). The funders had no role in study design, data collection and analysis, decision to publish, or preparation of the manuscript.

Competing Interests: The authors have declared that no competing interests exist.

Eukaryotes have evolved to fine-tune water transport through AQPs by three main regulatory mechanisms: (i) at the transcriptional/translational level; (ii) by conformational change or “gating” and (iii) by translocation to the membrane in response to a trigger. Regulation by AQP gene expression and/or AQP protein degradation can be achieved over a timescale from hours to days. However, this does not account for the dynamic control of AQPs that may be necessary to rapidly alter membrane water permeability in response to environmental or cellular signals. Instead, this can be achieved by gating; a conformational change of the AQP protein that alters the permeability of the pore. In addition, translocation can regulate the number of AQP molecules present in the target membrane, altering membrane water permeability by changing the number of pores present.

Structures of gated AQPs have revealed the molecular details of AQP gating by phosphorylation, pH and Ca^{2+} for the spinach aquaporin SoPIP2;1 [4] and mechanosensitivity for the yeast aquaporin AQY1 [5]. Furthermore, mammalian AQP0 is suggested to be gated in a pH and Ca^{2+} -dependent manner, the latter being mediated by an interaction with calmodulin, as described by a recent structural model [6]. While gating of other mammalian AQPs remains to be conclusively shown, translocation is a common regulatory mechanism. The best-characterised example of this type of regulation is that of human AQP2 in the kidney: AQP2 abundance in the apical membrane is dependent on vasopressin-activated phosphorylation of a carboxy-terminal serine residue (Ser 256) by cAMP-dependent protein kinase A (PKA) [7]. Phosphorylation in response to a hormonal trigger has also been shown to mediate membrane translocation of AQP1 [8], AQP5 [9–11] and AQP8 [12], on a timescale of minutes to hours. Translocation in response to an osmotic stimulus has been demonstrated to regulate AQP1 activity on a timescale of seconds; exposure to hypotonic conditions resulted in rapid recruitment to the cell surface via a mechanism dependent on transient receptor potential channels, extracellular calcium influx, calmodulin, and the phosphorylation of two threonine residues (Thr 157 and Thr 239) of AQP1 [13].

AQP5 is found in tissues such as the lungs, airways and secretory glands and consequently plays a major role in the generation of saliva, tears and pulmonary secretions [14–16]. AQP5 dysregulation has been implicated in several disease states, including bronchitis, cystic fibrosis [17] and Sjögren’s syndrome [18]. AQP5 translocation has been shown to be affected by cAMP in a PKA-dependent manner, with exposure to elevated intracellular cAMP levels causing a short-term (minutes) decrease in AQP5 membrane abundance whereas long-term (8 hours) exposure increased total AQP5 protein [15]. There are two consensus PKA sites in AQP5: Ser 156 in cytoplasmic loop D [19, 20] and Thr 259 [10] in the carboxy-terminus; the latter corresponds to Ser 256 in AQP2. AQP5 can be directly phosphorylated by PKA at Ser 156 and Thr 259 [21]. Notably, Ser 156 was phosphorylated preferentially in certain tumors suggesting that cell proliferation can be modulated by phosphorylation of this site although the constitutive membrane abundance of an S156A mutant was not distinguishable from wild-type AQP5 [22]. Based on the crystal structure of human AQP5 it was hypothesized that phosphorylation of Ser 156 could cause structural changes in loop D that would break its interaction with the carboxy-terminus, thereby flagging the protein for translocation to the plasma membrane [23].

In order to investigate the role of Ser 156 in the membrane translocation of AQP5, we used real time translocation studies in living HEK293 cells; GFP-tagged full-length AQP5 mutants were designed to either abolish or mimic phosphorylation of Ser 156. Our data show that the phosphomimetic mutation of Ser 156 to glutamate (S156E) increased constitutive membrane expression of AQP5. Inhibition of PKA increased constitutive membrane expression of wild-type, S156E and S156A, suggesting that the effect of PKA on AQP5 translocation is not solely dependent Ser 156. We further show rapid membrane translocation upon a hypotonic stimulus independently of both Ser 156 phosphorylation and PKA activity. Finally, we have used x-ray

crystallography to show that the phosphomimetic S156E mutation does not cause any significant structural changes to the protein as previously suggested. We propose that three independent mechanisms regulate the membrane abundance of AQP5, one of which involves phosphorylation of Ser 156.

Materials and Methods

Cloning of AQP5-GFP fusion constructs for analysis in HEK293 cells

Human full-length AQP5 was fused with carboxy-terminal GFP using the Invitrogen Gateway™ cloning system according to the instructions provided by the supplier. For directional cloning of blunt-ended PCR products into an entry vector using the Gateway™ system, four bases (GGGG) were added to the 5′-end of the forward primer followed by the 25bp *attB1* attachment sequence (underlined, below). This was followed by five bases (bold) to introduce a Kozak sequence upstream and to keep the sequence in frame with the AQP coding sequence. Finally 18–25bp of the AQP5 sequence were added to create the amino-terminal forward primers, 5′-GGGG ACA AGT TTG TAC AAA AAA GCA GGC TCC ACC ATG–AQP5(18–25bp)-3′. For the reverse primer, four bases (GGGG) were added to the 5′-end followed by the 25bp *attB2* attachment sequence (underlined) and then one base (bold) was added to keep the sequence in frame with the AQP5 coding sequence. Finally 18–25bp of the AQP sequence without the stop codon were added to create the carboxy-terminal forward primers 5′-GGG GAC CAC TTT GTA CAA GAA AGC TGG GTC–AQP5(18–25bp)-3′. KOD polymerase was used in PCR amplification of the AQP cDNA. Samples were heated to 94°C for 2 min, followed by 30 cycles of 94°C for 30 s, 55°C for 30 s and 68°C for 3 min and then 68°C for 7 min. Purified PCR products were sub-cloned into the pDONR221™ entry vector (Invitrogen) using the *attB1* and *attB2* sites in a reaction with Gateway™ BP Clonase™ enzyme mix (Invitrogen). pDONR221™ vectors containing the required sequences were recombined with the pcDNA-D-EST47 Gateway™ vector using the *attL* and *attR* reaction with Gateway™ LR Clonase™ enzyme mix (Invitrogen). This created expression vectors with the cycle 3 mutant of the GFP gene at the carboxy-terminus of the AQP gene of interest, which were subsequently expressed as fusion proteins. The mutant constructs S156E and S156A were amplified using the well-established, modified QuikChange procedure (Stratagene), as previously described [13] and according to their manual. All plasmids were handled and purified using standard molecular biological procedures.

Cell culture and transfection

HEK 293 cells were routinely cultured in Dulbecco's modified Eagle's medium (DMEM) supplemented with 10% (v/v) fetal bovine serum in humidified 5% (v/v) CO₂ in air at 37°C. Cells were seeded into 30 mm Fluorodish™ dishes and transfected after 24 h at 50% confluence using the Transfast (Promega) transfection protocol with 2 µg of DNA/dish. PKA inhibition was achieved by incubation with 3.6 µM myristoylated PKI 14–22 amide (Enzo Life Sciences, Exeter UK) for 30 minutes.

Confocal microscopy

AQP5-GFP fusion proteins were visualized in live cells enclosed in a full environmental chamber by confocal laser scanning microscopy. Confocal images were acquired 24 h post-transfection with a Leica SP5 or Zeiss 780 laser scanning microscope using a 63× (1.2 NA) water immersion objective. Images were acquired using an argon laser (excitation 488 nm; emission band pass 505–530 nm) for GFP, UV excitation and a He-Ne laser (excitation 543nm; emission

filter long pass (LP) 650 nm). Cells were visualized in control medium (DMEM) that had an inorganic salt concentration of 120 mM, a glucose concentration of 25 mM and an osmolality in the range 322–374 mosM/kg H₂O. Hypotonic medium has an osmolality in the range 107–125 mosM/kg H₂O through dilution of DMEM by a factor of 3 with water.

Determination of sub-cellular localization

Protein localization was measured using a line profile (pixel density) traced on each transfected cell. Localization data are representative of three to five cells from at least three independent experiments. Line expression profiles were generated and analyzed with the program ImageJ (<http://rsb.info.nih.gov/ij/>) and are indicated in yellow and displayed beside each confocal image. A minimum of five line profiles were measured, distributed at regular intervals covering the plasma membrane and the cytosol, but avoiding the nucleus of a minimum of three cells from at least three independent experiments. The fluorescence intensity over this distance was also measured and the difference between the peak and the plateau of fluorescence was divided by the maximum fluorescence along the line scan to calculate the percentage of fluorescence at the membrane. This was termed the relative membrane expression (RME) [24, 25]. The overlay of the GFP image with the bright-field image indicated integration of GFP-tagged AQP5 at the plasma membrane as well as in the cytoplasm of HEK293 cells. In addition, correct membrane insertion of AQP5-GFP and both S156 mutants was suggested by colocalization with the fluorescent plasma membrane marker FM 4–64 as previously described for AQP4-GFP.

RME values were compared by one way ANOVA followed by either paired (for images of the same cell before and after treatment) or unpaired (for images of different cells under different conditions) post-hoc t-tests. The p values from the post-hoc tests were multiplied by the number of pairwise comparisons (Bonferroni correction); $p < 0.05$ after correction was considered statistically significant.

Cloning of hAQP5 S156E for structural analysis

A single mutation of Ser 156 to glutamate was introduced into a vector encoding wild-type human AQP5 using the QuikChange[®] Site-Directed Mutagenesis Kit (Stratagene) according to their protocol. In addition, a construct was made in which the carboxy-terminus was truncated by introducing a stop codon after Pro 245. All mutations were confirmed by sequencing and the construct was subsequently used to transform *Pichia pastoris* X-33 cells. High yielding transformants were selected based on growth on high Zeocin concentrations as described previously [25].

Protein production and purification

Clones were grown in 3L fermentors with glycerol and methanol feed phases. Harvested cells were resuspended in breaking buffer (50 mM phosphate buffer pH7.5, 5% glycerol) and broken by three passages through an X-press cell (Biox AB). Cell debris was pelleted by centrifugation at 10,000 × g for 30 minutes. This centrifugation step was repeated to ensure that all debris had been removed. Membranes were collected at 200,000 × g for 90 minutes, washed in urea buffer (4M urea, 5 mM Tris, 2 mM EDTA 2 mM EGTA) and NaOH (20 mM) and finally resuspended in 7 ml resuspension buffer (20 mM Hepes pH7.8, 50 mM NaCl, 10% glycerol, 2 mM β-MeOH) per gram of membrane.

Membranes were solubilized in resuspension buffer with 6% n-nonyl-β-D-glucoside for 1h at room temperature. Unsolubilized material was removed by centrifugation at 186,000g for 30min. The supernatant was diluted with dilution buffer (20 mM MES pH6.0, 10% glycerol, 0.4% NG and 2 mM β-MeOH) and purified using a Resource S column (GE Healthcare, 20

mM MES pH6.0, 0.4% NG and 15 mM-1M NaCl) followed by gel filtration on Superdex 200 column (GE Healthcare, 20 mM Tris-HCl pH7.5, 100 mM NaCl, 0.4% NG). Fractions containing hAQP5 S156E was concentrated in a 10,000 MWCO concentrator (Vivaspin) to a final concentration of 7–13 mg/ml.

Crystallization

Crystallization experiments were set up at 8°C using the hanging drop vapor diffusion technique. 7.2 μ l reservoir solution (100 mM Tris-HCl pH7.8 or 7.9, 100 mM NaCl, 21% PEG400) was mixed with 1.8 μ l each of 1,6-hexanediol (30%, v/v) and 1,3-propanediol (40%, v/v) and mixed with the protein in a 1:1 ratio. Crystals were obtained within 5–7 days and were fished and flash frozen in liquid nitrogen without any addition of cryoprotectant.

Data collection and structure determination of AQP5 S156E

Complete X-ray diffraction data were collected on frozen crystals at cryo temperature (100 K) at the European Synchrotron Radiation Facility (ESRF) beamline ID23-2. Crystals of full-length AQP5 S156E diffracted to 3.5 Å and belonged to space group $P3_12$ with one tetramer in the asymmetric unit. Cell dimensions were $a = b = 174.3$, $c = 100.9$ Å, $A = B = 90^\circ$, $\gamma = 120^\circ$. Crystals of truncated AQP5 S156E crystals diffracted to 2.6 Å and belonged to the space group $P6_3$ with two tetramers in the asymmetric unit. Cell dimensions were $a = b = 171$ Å, $c = 171, 190$ Å, $A = B = \gamma = 90^\circ$. Images were processed and scaled using iMosflm and Scala from the CCP4 suite [26]. The structures were solved using molecular replacement using Phaser [27] with the wild-type hAQP5 structure (PDB code 3D9S [23]) as a model. Further refinement of full-length and truncated AQP5 S156E was done in Refmac5 [28] and Phenix [29] respectively, with iterative manual rebuilding in Coot [30]. The quality of the structure was checked using MolProbity included in Phenix. The current model of full length AQP5 S156S contains 4 chains (A-D) with the following amino acids: A 2–245, B 5–247, C 4–245 and D 2–254. A-D as well as one phosphatidylserine. The current model of truncated hAQP5-S156E contains 8 chains A-H with amino acids 2–245, one phosphatidyl serine and 690 waters. The two structures refined to an R_{work} and R_{free} of 28.0 and 31.1% for full length AQP5 S156E and 18.7% and 23.0% for truncated AQP5 S156E. For crystallographic statistics, see Table 1.

Results

A phosphomimetic mutation at Ser 156 increases constitutive AQP5 surface abundance

An expression vector was made in which GFP was fused to the carboxy-terminus of full-length human AQP5 (AQP5-GFP). This expression vector was used to transfect live HEK293 cells. Real-time localization and translocation of the corresponding fusion protein was measured using confocal microscopy; the relative membrane expression (RME) was determined using line intensity profiles generated from confocal images of individual live cells. An RME of 0 corresponds to an equal distribution of GFP signal between membrane and intracellular compartments and an RME of 1 corresponds to 100% of the GFP signal at the membrane. The RME of AQP5-GFP was increased by the introduction of the S156E mutation from 0.56 ± 0.02 to 0.67 ± 0.01 ($p = 0.01$), whereas the RME of AQP5-S156A was not significantly different ($p = 0.36$) to wild-type AQP5-GFP (Fig 1).

Table 1. Crystallographic data and refinement statistics for full-length and truncated hAQP5 S156E structures.

	Full length	Truncated
<i>Data collection</i>		
Beamline	ESRF ID23-2	ESRF ID23-2
Wavelength (Å)	0.8726	0.8726
Detector distance (mm)	413	306.6
Oscillation/collection range (°)	1/100	0.4 (92)
Resolution ^a (Å)	101.02–3.5 (3.69–3.5)	50.81–2.60 (2.74–2.60)
Total observations ^a	142,487 (20,652)	375,143 (54,612)
Unique reflections ^a	21,914 (3,193)	94,885 (13,925)
Completeness ^a	98.9 (99.8)	98.8 (99.4)
Redundancy ^a	6.5 (6.5)	4.0 (3.9)
I/σ ^a	13 (1.9)	7.0 (2.1)
R _{sym} ^{a,b} (%)	0.095 (0.799)	0.180 (0.778)
<i>Refinement</i>		
Resolution ^a (Å)	100–3.5	48.2–2.60
Space group (α, β, γ)	P3 ₁ 2 (90, 90, 120)	P6 ₃ (90, 90, 120)
Cell dimensions (a, b, c)	174, 174, 101	171, 171, 190
Molecules in the asymmetric unit	4	8
R _{work} ^c /R _{free} ^d (%)	28.0/31.1	18.7/23.0
Average B values, entire model (Å ²)	161.6	31.4
Average B values, protein/waters (Å ²)	163.4/-	31.1/35.6
<i>Root-mean-square deviations from ideal values</i>		
Bond lengths (Å)	0.007	0.008
Bond angles (°)	1.084	1.058
PDB accession code	5DYE	5C5X

^a Values in brackets are for the highest resolution shell

^b $R_{sym} = \sum_h \sum_i |I_i(h) - \langle I(h) \rangle| / \sum_h \sum_i I_i(h)$, where $I_i(h)$ is the i th measurement.

^c $R_{work} = \sum_h ||F(h)_{obs}| - |F(h)_{calc}|| / \sum_h |F(h)_{obs}|$

^d R_{free} was calculated for 5% of reflections randomly excluded from the refinement

doi:10.1371/journal.pone.0143027.t001

PKA inhibition increases constitutive AQP5 surface abundance

The RME of AQP5-GFP (wild-type and the two S156 mutants) was measured after a 30 minute incubation with a cell-permeable PKA inhibitory peptide (myrPKI) or vehicle control. PKA inhibition increased the RME of all AQP5 constructs (Fig 2) compared to non-inhibited controls, suggesting a role for PKA signalling in the internalization of AQP5 as previously suggested [15]. PKA inhibition further increased the membrane abundance of the S156E mutant, indicating that this effect is independent of the phosphorylation status of Ser 156.

Hypotonicity-induced AQP5 translocation is independent of PKA activity and phosphorylation at S156

Reduction of the extracellular osmolality to 85 mOsm/kg H₂O caused rapid relocalization of AQP5 from intracellular compartments to the plasma membrane (Fig 3). The initial AQP5-GFP distribution profile was restored on returning to normal physiological osmolality. The RME of AQP5-GFP increased from 0.56 ± 0.03 in control medium to 0.72 ± 0.01 in hypotonic medium. This result was similar to that seen for AQP1, which translocated to and from

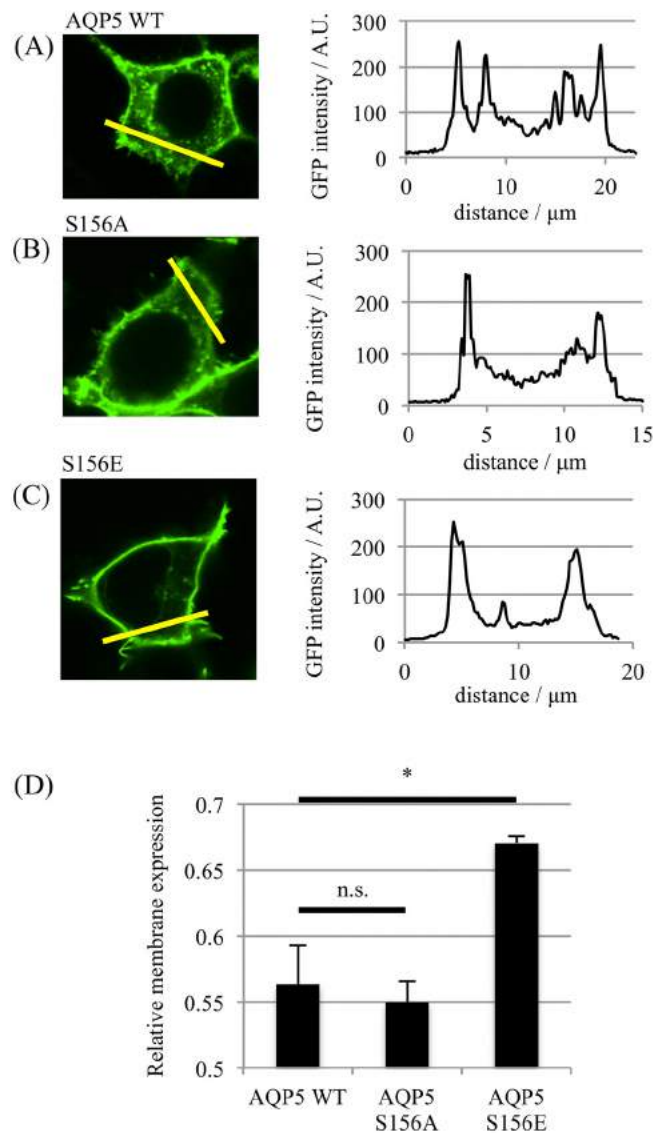


Fig 1. Surface expression of AQP5 S156 mutants. Representative fluorescence confocal micrographs of HEK293 cells transfected with GFP-tagged (A) AQP5 wild-type, (B) AQP5-S156A and (C) AQP5-S156E; the fluorescence intensity profiles along each yellow line are shown. (D) Relative membrane expression calculated from fluorescence intensity profiles: 5 profiles were taken per cell and at least 3 cells per micrograph, repeated in 3 independent experiments. Asterisks denote $p < 0.05$ using Student's t-test followed by Bonferroni correction for multiple comparisons.

doi:10.1371/journal.pone.0143027.g001

the membrane in response to altered tonicity in the surrounding media [24]. Similarly, the RME increased from 0.55 ± 0.02 to 0.71 ± 0.02 for the S156A mutant and from 0.67 ± 0.02 to 0.81 ± 0.01 for the S156E mutant. Despite an increased level of constitutive surface expression, the change in RME for the S156E mutant ($\Delta RME = 0.14 \pm 0.01$) was similar to that for AQP5 or the S156A mutant ($\Delta RME = 0.15 \pm 0.03$ and 0.13 ± 0.02 respectively). Inhibition of PKA, despite increasing constitutive surface expression of all constructs, did not inhibit the hypotonicity-induced relocalization of AQP5. Taken together, these results suggest that hypotonicity-

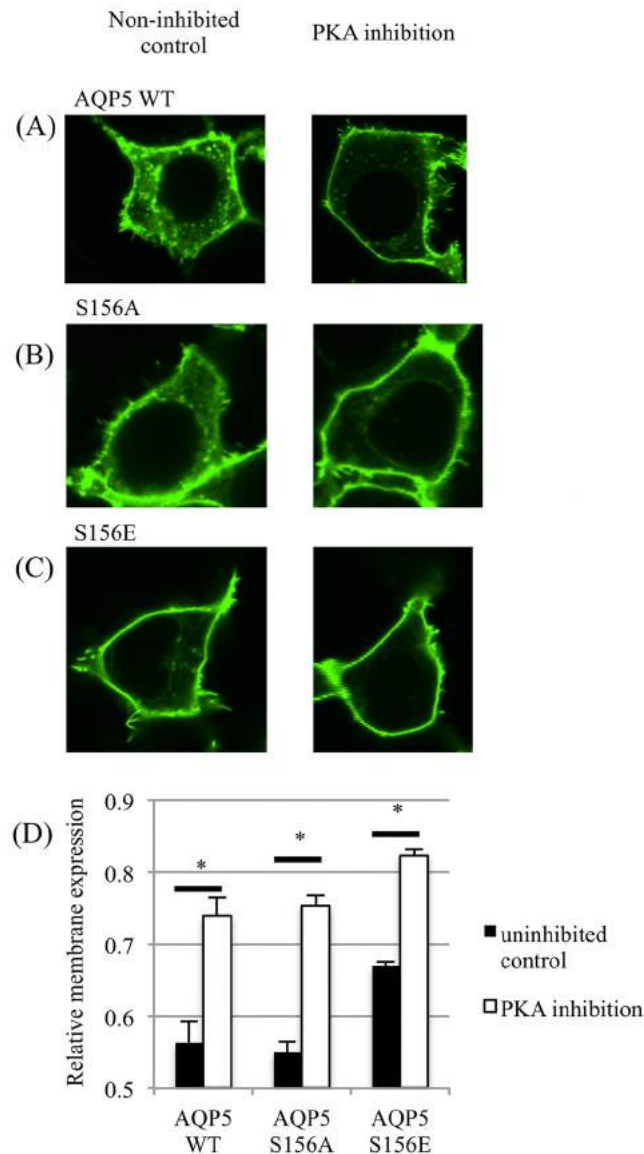


Fig 2. Effect of PKA inhibition on surface expression of AQP5. Representative fluorescence confocal micrographs of HEK293 cells transfected with GFP-tagged (A) AQP5 wild-type, (B) AQP5-S156A and (C) AQP5-S156E that were treated with a PKA inhibitory peptide for 30 minutes. (D) Relative membrane expression of the 3 AQP5 constructs with and without PKA inhibition. Asterisks denote $p < 0.05$ using Student's t-test followed by Bonferroni correction for multiple comparisons.

doi:10.1371/journal.pone.0143027.g002

induced relocalization of AQP5 is not mediated by either PKA activity or phosphorylation at Ser 156.

The crystal structure of AQP5 S156E suggests phosphorylation is not accompanied by a conformational change

We previously solved the structure of wild-type human AQP5 expressed in *P. pastoris* to 2.0 Å resolution [23]. To determine whether phosphorylation of Ser 156 confers any structural changes that could be important for membrane translocation, we crystallized and solved the

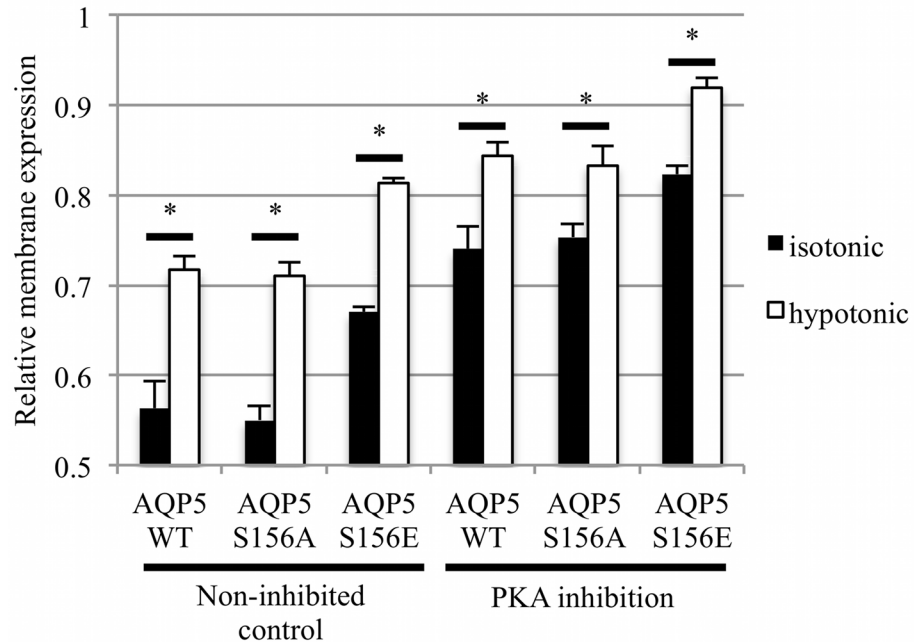


Fig 3. Hypotonicity-induced translocation of AQP5. Relative membrane expression of AQP5 and mutants was measured in the same cells before and 1 minute after reduction of the extracellular osmolality to 85 mOsm/kg H₂O by fourfold dilution of the culture medium with dH₂O. PKA inhibition was achieved by a 30 minute incubation with a PKA inhibitory peptide. Asterisks denote $p < 0.05$ by paired t-tests followed by Bonferroni correction for multiple comparisons.

doi:10.1371/journal.pone.0143027.g003

structure of a single phosphomimetic mutant (S156E) of full-length AQP5 at 3.5 Å resolution (PDB code 5DYE). Since at this resolution, information about side-chain positions and interactions is limited, we truncated AQP5 S156E at Pro 245, the last visible residue in the high-resolution wild-type structure AQP5. The truncated AQP5 S156E construct crystallized in a different space group and diffracted to significantly higher resolution, allowing us to solve the structure at 2.6 Å resolution (PDB code 5CX6). Both full-length and truncated AQP5 S156E crystallized in space groups lacking the four-fold symmetry otherwise commonly associated with AQP crystals (P₃12 with one tetramer in the asymmetric unit for full-length AQP5 S156E and P6₃ with two tetramers in the asymmetric unit for truncated AQP5 S156E), thereby allowing for structural differences between monomers in the tetramer to be examined. Crystallographic data and refinement statistics are summarized in Table 1.

Both structures of AQP5 S156E are very similar to that of wild-type AQP5; overlaying with a root-mean-square deviation of 0.51 Å for 970 C_α-atoms for full-length AQP5 S156E and of 0.37 Å for 975 C_α-atoms for truncated AQP5 S156E (Fig 4A & 4B). For full-length AQP5 S156E, additional electron density could be seen beyond Pro 245 in one of the monomers (monomer D), allowing us to build nine more residues (Fig 4C). However, this region does not interact with any other residues within the tetramer. Instead, it forms crystal contacts with symmetry-related AQP5 molecules in the crystal packing, explaining why this region is ordered in this particular monomer of the full-length structure.

In the truncated AQP5 S156E structure, seven water molecules were observed in the water-conducting channel of all monomers with one exception, monomer F, which contained six water molecules. For full-length AQP5 S156E, the limited resolution prevented the identification of water molecules in the channel. In both structures, a lipid molecule could be observed

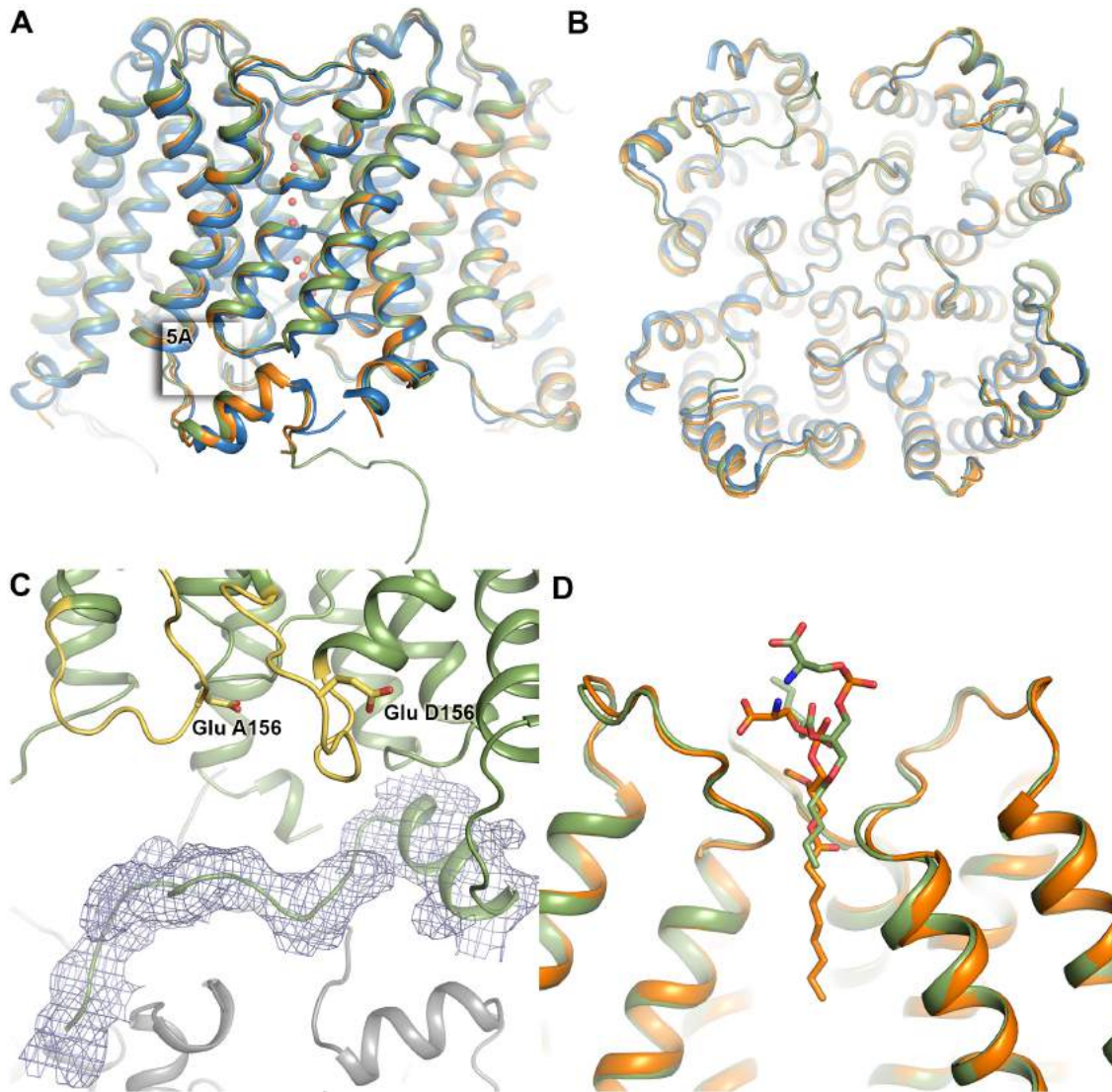


Fig 4. Overall structure of AQP5 S156E. (A) The structure of full length (green, PDB code 4DYE) and truncated S156E AQP5 (orange, PDB code 5CX6) overlaid on the wild-type structure of AQP5 in blue (PDB code 3D9S). Water molecules in the water-conducting channel of truncated S156E AQP5 are shown as red spheres. (B) Same as in (A), viewed from the cytoplasmic side. (C) Structure of the carboxy-terminus of full-length S156E monomer D, showing its interactions with a symmetry-related molecule (grey). $2F_{obs}-F_{calc}$ electron density is displayed at 1.0σ . Loop D and Glu 156 in monomers A and D are highlighted in yellow. (D) Lipid molecule in the tetrameric channel of full-length and truncated AQP5 S156E.

doi:10.1371/journal.pone.0143027.g004

in the central channel formed between monomers in the tetramer, albeit at slightly different positions. Similarly to wild-type AQP5, this lipid was modelled as phosphatidyl serine (Fig 4D).

Loop D and the carboxy-terminus retain their native conformations in AQP5 S156E

In the wild-type AQP5 structure, an interaction between loop D and the carboxy-terminal region was observed [23]. This interaction anchored at the carboxy-terminal helix in a manner that was well conserved in other mammalian AQP structures and involved hydrogen bonds between the sidechain of Arg 153 and the backbone atoms of Pro 226 and Phe 227 (Fig 5A). It

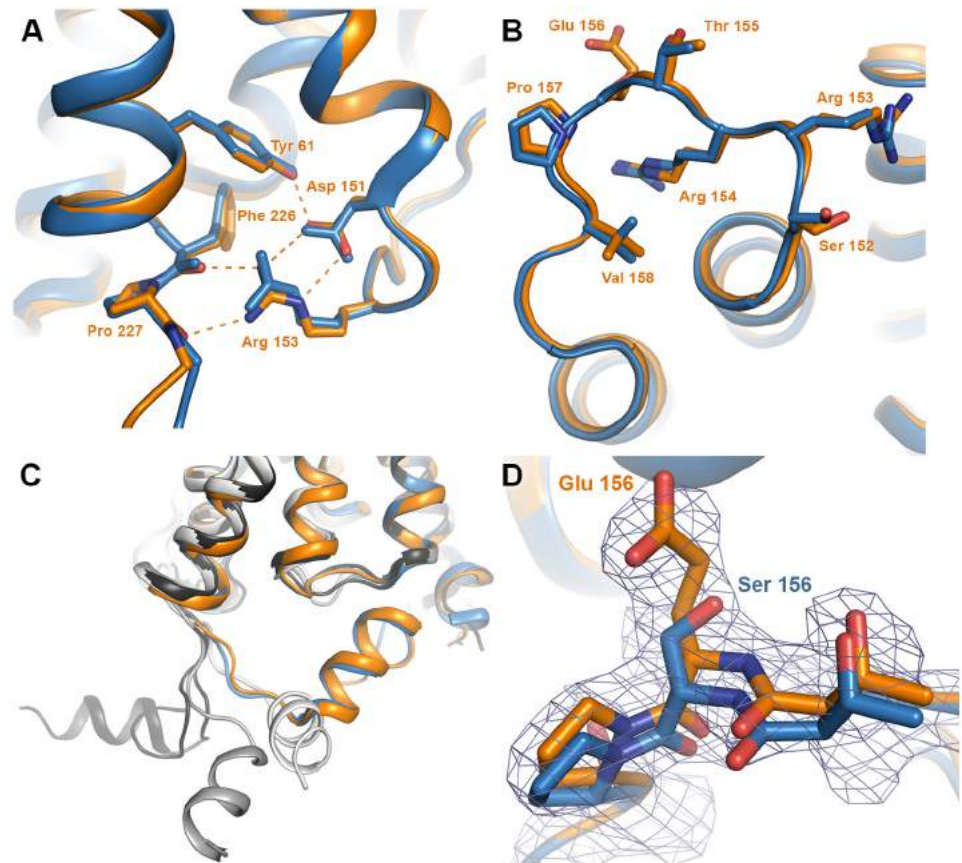


Fig 5. Structure of loop D and its interaction with the carboxy-terminus. Wild-type AQP5 and AQP5 S156E are coloured blue and orange respectively. (A) Zoomed in view of the boxed area in Fig 4A showing that the interactions between loop D and the carboxy-terminus are maintained in the S156E mutant structure. Hydrogen bonds are shown as dashed lines. Structural comparison of (B) loop D and (C) the carboxy-terminus shows that there are no structural differences between wild-type AQP5 and AQP5 S156E. In (D), the four monomers from the crystal structure of human AQP2 are overlaid, showing a significant conformational variability of the carboxy-terminal helix within the tetramer. The four AQP2 monomers are colored in different shades of grey. (D) Structure of the S156E mutation site showing $2F_{\text{obs}} - F_{\text{calc}}$ electron density contoured at 1.0σ . The structure of wild-type AQP5 is shown in blue for comparison.

doi:10.1371/journal.pone.0143027.g005

was hypothesized that phosphorylation of Ser 156 may cause structural changes within loop D that breaks these interactions, allowing for a conformational change of the carboxy-terminus.

Since there were no significant differences between the structures of full-length and truncated AQP5 S156E, we used the higher-resolution truncated AQP5 S156E structure to examine the finer structural details (from hereon denoted as AQP5 S156E). No structural change of loop D was observed in any of the eight monomers when compared to wild-type hAQP5 (Fig 5B) and the interactions between loop D and the carboxy-terminus were conserved (Fig 5A). The carboxy-terminus retained the same conformation as in the wild-type AQP5 structure (Fig 5C). In two of the monomers in each tetramer, there was a 1–2 Å shift in the position of the small carboxy-terminal helix when compared to wild-type AQP5. Comparison between the 8 monomers of AQP5 S156E shows that the carboxy-terminal helices overlap perfectly, suggesting that the shift in position arises from minor structural differences between monomers in wild-type AQP5. As is apparent from the electron density map in Fig 5D, serine was successfully replaced by glutamate at position 156.

Discussion

The regulation of protein abundance in a particular membrane requires a delicate balance between two opposing processes: Translocation to and internalization from the membrane. This is achieved through multiple sorting signals, often consisting of post-translational modifications in the cytoplasmic regions of the protein. One of the best-characterized examples is AQP2, for which phosphorylation of multiple sites in the carboxy-terminus governs its translocation to the apical membrane [31]. Internalization of AQP2 is triggered by ubiquitination of the carboxy-terminus [32] and the internalization rate is also influenced by the phosphorylation status of AQP2 in the membrane [33].

Emerging evidence suggests that the regulation of AQP5 cell surface abundance is equally complex. It is known that AQP5 translocation between intracellular storage vesicles and the apical membrane can occur upon agonist stimulation of the muscarinic (M3) receptor [34] or α -1 adrenergic receptor [35]. Furthermore, intracellular cAMP levels have been shown to regulate AQP5 abundance at the transcriptional level as well as affect the long-term (≥ 24 hours) sub-cellular distribution of the protein in a PKA-dependent manner [11]. Interestingly, increased cAMP levels have been shown to have a biphasic effect on the sub-cellular distribution of AQP5 with decreased expression in the apical membrane in the short term due to increased internalization, followed by an increase in membrane abundance in the long-term [15]. While inhibition of PKA had an effect on both components of this biphasic response, an increase in levels of phosphorylated AQP5 could only be seen for the long-term effect, suggesting that the target for PKA-phosphorylation in the short-term response is not AQP5 itself. This dual response to increased levels of cAMP on the trafficking of AQP5 could help explain why increased as well decreased expression in the apical membrane have been reported [14, 16].

AQP5 contains two consensus PKA-sites but unlike AQP2, their roles in AQP5 translocation have not been determined. PKA-mediated phosphorylation of AQP5 has been demonstrated at both Ser 156 [21] and Thr 259 [36]. However, removal of these phosphorylation sites by mutation to alanine resulted in constructs with the same membrane abundance as wild-type AQP5. Additional phosphorylation sites are predicted to be present in AQP5, for example a PKC site at Ser 152 that overlaps with the PKA site at Ser 156. Furthermore, Thr 259 is also part of a PKG consensus site. These are additional components that may affect the overall translocation of AQP5 in a cell-dependent manner.

Our data suggest that membrane-localization of AQP5 is regulated by at least three independent pathways (Fig 6). We show that membrane expression of AQP5 is affected by phosphorylation of Ser 156, either by increased targeting or decreased internalization or both. To our knowledge this is the first time a phosphorylation site has been directly linked to a difference in membrane expression. The fact that the S156A mutant behaves like wild-type AQP5 indicates that phosphorylation of Ser 156 may not occur under basal conditions. In this respect it is intriguing that Ser 156 has been shown to be preferentially phosphorylated in tumour cells [21]. It has been suggested that in tumours, PKA-dependent phosphorylation of Ser 156 increases cell proliferation by activating the Ras-pathway [37]. A number of studies have shown that upregulation of AQPs promotes cell proliferation and migration [38] Our data hint at a mechanism whereby phosphorylation of Ser 156 in AQP5 increases its membrane localization, thereby enhancing cancer cell proliferation.

It was previously suggested that phosphorylation of Ser156 would break interactions between loop D and the carboxy-terminus, thereby triggering a conformational change [23]. Significant conformational variability of the carboxy-terminus was seen in the structure of human AQP2, where the carboxy-terminal helix of each monomer adopted a unique

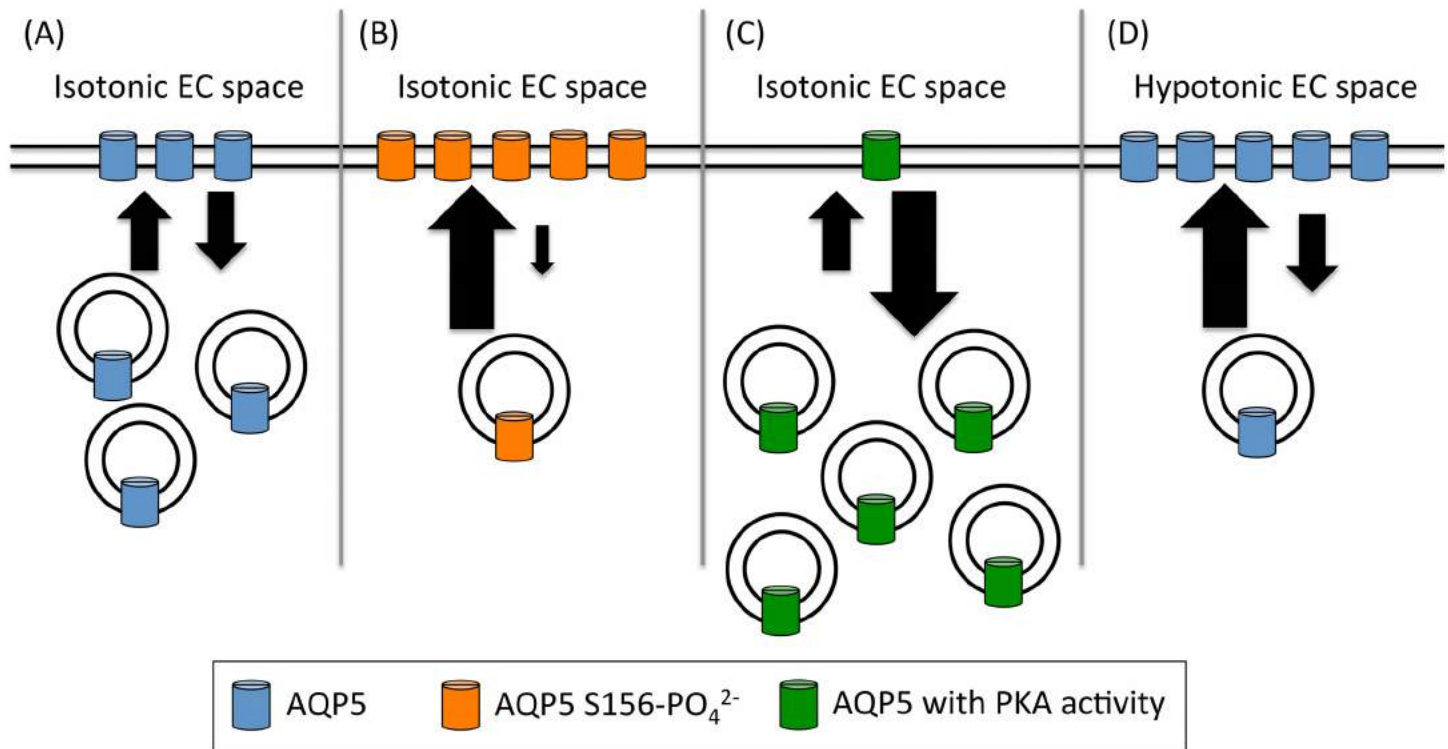


Fig 6. A proposed model of the equilibrium between vesicular and surface-localized AQP5. Panel A shows wild-type AQP5 under isotonic conditions. The large arrows represent an increase in AQP5 translocation (and the small arrows are a decrease). This is regulated by three independent factors: Phosphorylation of AQP5 at position S156 (orange cylinders in panel B; shown by a phosphomimetic glutamate substitution (S156E) of AQP5); the effect of PKA (green cylinders in panel C) and the effect of decreasing the relative tonicity of the environment (panel D). We speculate that these three pathways control the surface abundance of AQP5.

doi:10.1371/journal.pone.0143027.g006

conformation that had not been observed in any previous mammalian AQP structure (Fig 5C) [39]. As the carboxy-terminal region is known to be important for membrane translocation of both AQP2 [31] and AQP5 [10, 40], such conformational changes may be recognized as a structural sorting signal by the cellular trafficking machinery. However, our structure of the AQP5 S156E mutant did not reveal any structural differences within loop D or the carboxy-terminus (Fig 5B and 5C). We therefore suggest that it is the presence of a phosphate group at Ser 156 rather than a conformational change of the carboxy-terminus that is recognized as a sorting signal, resulting in increased AQP5 membrane abundance.

Our data further show that, independent of Ser 156, basal levels of PKA activity (i.e. in the absence of a cAMP-stimulating agonist) decrease the membrane abundance of AQP5 (Fig 2). This fits well with the short-term effect of cAMP and PKA that has been seen previously and for which PKA has been suggested to be involved in AQP5 internalization [15]. Since PKA-inhibition further increased membrane expression of the S156E mutant, this indicates that phosphorylation of Ser 156 is not responsible for this short-term effect. Instead, we suggest that Ser 156 phosphorylation may be involved in the long-term cAMP and PKA-dependent effect whereby an increase in AQP5 membrane abundance is seen after several hours. This is in agreement with the observation that the long-term effect of cAMP and PKA involves direct phosphorylation of AQP5 while the short-term effect does not [15].

Finally, we show that AQP5-GFP is rapidly translocated to the target membrane of HEK293 cells in response to hypotonic conditions, but that this translocation is independent of Ser 156 in loop D and also independent of PKA (Fig 3).

The hypotonicity-induced membrane translocation of AQP5 described here is consistent with that of AQP1 where the phosphorylation of Thr157 and/or Thr239 by PKC results in rapid accumulation in the cell-surface membrane [13]. Whether direct phosphorylation of AQP5 by PKC or another kinase mediates hypotonicity-induced membrane translocation in a similar manner remains to be shown. AQP5 is found in tissues that are subject to rapid changes in osmolarity and has been shown to play an important role in cell volume regulation [14–16]. Upon exposure to hypotonic conditions, cells undergo a rapid cellular volume decrease (RVD) to avoid rupture. This happens within a couple of minutes and involves the release of cellular water. RVD is often followed by a regulatory volume increase (RVI) whereby the osmotically shrunken cell approaches its original volume [2]. The rapid response to hypotonicity reported here supports the involvement of AQP5 in RVD as previously suggested [14]. On a longer time scale, hypotonic exposure has been shown to cause a decrease in AQP5 membrane abundance [16], most likely corresponding to the RVI response. Taken together, regulation of AQP5 membrane abundance seems to be important for both the RVD and RVI components of cell volume regulation.

We previously showed that hypotonicity-induced calcium influx through TRPC1 was vital for translocation of AQP1 [13] and others have shown that calcium influx through TRPV4 mediates the AQP5-dependent regulatory volume decrease in acinar cells [14]. We therefore speculate that the sensor of extracellular osmolality that leads to AQP5 translocation is a member of the TRP family of gated cation channels.

Conclusion

Due to its importance for fluid secretion in airways submucosal glands, AQP5 has been suggested to be a pharmacological target to treat the hyper-viscous and excessive gland secretions in cystic fibrosis and bronchitis/rhinitis, respectively. Our data provide the first link between a specific AQP5 phosphorylation site, Ser 156, and changes in its sub-cellular localization. We further show that the Ser 156-mediated change in localization does not require a substantial protein conformational change. We show that, independent of Ser 156, PKA is further involved in basal recycling of AQP5 between the plasma membrane and intracellular compartments. Finally, we provide evidence of tonicity-regulated changes in AQP5 localization that are not mediated by phosphorylation of Ser 156 or PKA. This will now enable us to elucidate the detailed mechanism by which these post-translational modifications govern translocation of the protein from intracellular storage vesicles to the target membrane in response to protein kinase activity and osmotic triggers, thus providing key information for drug design targeting AQP5.

Author Contributions

Conceived and designed the experiments: PK ACC MTC RMB KH STH. Performed the experiments: PK FÖ JS. Analyzed the data: PK FÖ ACC MTC RMB STH. Contributed reagents/materials/analysis tools: ACC KH STH. Wrote the paper: PK ACC MTC RMB STH.

References

1. Verkman AS, Mitra AK. Structure and function of aquaporin water channels. *American journal of physiology Renal physiology*. 2000; 278(1):F13–28. PMID: [10644652](#).
2. Hoffmann EK, Lambert IH, Pedersen SF. Physiology of cell volume regulation in vertebrates. *Physiological reviews*. 2009; 89(1):193–277. doi: [10.1152/physrev.00037.2007](#) PMID: [19126758](#).
3. Day RE, Kitchen P, Owen DS, Bland C, Marshall L, Conner AC, et al. Human aquaporins: regulators of transcellular water flow. *Biochim Biophys Acta*. 2014; 1840(5):1492–506. doi: [10.1016/j.bbagen.2013.09.033](#) PMID: [24090884](#).

4. Tornroth-Horsefield S, Wang Y, Hedfalk K, Johanson U, Karlsson M, Tajkhorshid E, et al. Structural mechanism of plant aquaporin gating. *Nature*. 2006; 439(7077):688–94. PMID: [16340961](#).
5. Fischer G, Kosinska-Eriksson U, Aponte-Santamaria C, Palmgren M, Geijer C, Hedfalk K, et al. Crystal structure of a yeast aquaporin at 1.15 angstrom reveals a novel gating mechanism. *PLoS Biol*. 2009; 7(6):e1000130. Epub 2009/06/17. doi: [10.1371/journal.pbio.1000130](#) PMID: [19529756](#).
6. Reichow SL, Clemens DM, Freites JA, Nemeth-Cahalan KL, Heyden M, Tobias DJ, et al. Allosteric mechanism of water-channel gating by Ca²⁺-calmodulin. *Nature structural & molecular biology*. 2013; 20(9):1085–92. doi: [10.1038/nsmb.2630](#) PMID: [23893133](#); PubMed Central PMCID: PMC3766450.
7. Fushimi K, Sasaki S, Marumo F. Phosphorylation of serine 256 is required for cAMP-dependent regulatory exocytosis of the aquaporin-2 water channel. *J Biol Chem*. 1997; 272(23):14800–4. Epub 1997/06/06. PMID: [9169447](#).
8. Han Z, Patil RV. Protein kinase A-dependent phosphorylation of aquaporin-1. *Biochem Biophys Res Commun*. 2000; 273(1):328–32. Epub 2000/06/30. doi: [10.1006/bbrc.2000.2944](#) S0006-291X(00)92944-9 [pii]. PMID: [10873606](#).
9. Ishikawa Y, Yuan Z, Inoue N, Skowronski MT, Nakae Y, Shono M, et al. Identification of AQP5 in lipid rafts and its translocation to apical membranes by activation of M3 mAChRs in interlobular ducts of rat parotid gland. *Am J Physiol Cell Physiol*. 2005; 289(5):C1303–11. Epub 2005/08/19. 00211.2005 [pii] doi: [10.1152/ajpcell.00211.2005](#) PMID: [16107506](#).
10. Kosugi-Tanaka C, Li X, Yao C, Akamatsu T, Kanamori N, Hosoi K. Protein kinase A-regulated membrane trafficking of a green fluorescent protein-aquaporin 5 chimera in MDCK cells. *Biochim Biophys Acta*. 2006; 1763(4):337–44. Epub 2006/04/11. doi: S0167-4889(06)00028-0 [pii] doi: [10.1016/j.bbamcr.2006.02.005](#) PMID: [16603260](#).
11. Yang F, Kawedia JD, Menon AG. Cyclic AMP regulates aquaporin 5 expression at both transcriptional and post-transcriptional levels through a protein kinase A pathway. *J Biol Chem*. 2003; 278(34):32173–80. Epub 2003/06/05. doi: [10.1074/jbc.M305149200](#) M305149200 [pii]. PMID: [12783871](#).
12. Garcia F, Kierbel A, Larocca MC, Gradilone SA, Splinter P, LaRusso NF, et al. The water channel aquaporin-8 is mainly intracellular in rat hepatocytes, and its plasma membrane insertion is stimulated by cyclic AMP. *J Biol Chem*. 2001; 276(15):12147–52. Epub 2001/03/30. doi: [10.1074/jbc.M009403200](#) M009403200 [pii]. PMID: [11278499](#).
13. Conner MT, Conner AC, Bland CE, Taylor LH, Brown JE, Parri HR, et al. Rapid aquaporin translocation regulates cellular water flow: mechanism of hypotonicity-induced subcellular localization of aquaporin 1 water channel. *J Biol Chem*. 2012; 287(14):11516–25. doi: [10.1074/jbc.M111.329219](#) PMID: [22334691](#); PubMed Central PMCID: PMC3322852.
14. Liu X, Bandyopadhyay BC, Nakamoto T, Singh B, Liedtke W, Melvin JE, et al. A role for AQP5 in activation of TRPV4 by hypotonicity: concerted involvement of AQP5 and TRPV4 in regulation of cell volume recovery. *J Biol Chem*. 2006; 281(22):15485–95. Epub 2006/03/31. doi: M600549200 [pii] doi: [10.1074/jbc.M600549200](#) PMID: [16571723](#).
15. Sidhaye V, Hoffert JD, King LS. cAMP has distinct acute and chronic effects on aquaporin-5 in lung epithelial cells. *J Biol Chem*. 2005; 280(5):3590–6. Epub 2004/11/13. doi: M411038200 [pii] doi: [10.1074/jbc.M411038200](#) PMID: [15536076](#).
16. Sidhaye VK, Guler AD, Schweitzer KS, D'Alessio F, Caterina MJ, King LS. Transient receptor potential vanilloid 4 regulates aquaporin-5 abundance under hypotonic conditions. *Proc Natl Acad Sci U S A*. 2006; 103(12):4747–52. Epub 2006/03/16. doi: 0511211103 [pii] doi: [10.1073/pnas.0511211103](#) PMID: [16537379](#).
17. Song Y, Verkman AS. Aquaporin-5 dependent fluid secretion in airway submucosal glands. *J Biol Chem*. 2001; 276(44):41288–92. Epub 2001/08/22. doi: [10.1074/jbc.M107257200](#) PMID: [11514581](#).
18. Tsubota K, Hirai S, King LS, Agre P, Ishida N. Defective cellular trafficking of lacrimal gland aquaporin-5 in Sjogren's syndrome. *Lancet*. 2001; 357(9257):688–9. Epub 2001/03/15. doi: S0140-6736(00)04140-4 [pii] doi: [10.1016/S0140-6736\(00\)04140-4](#) PMID: [11247557](#).
19. Raina S, Preston GM, Guggino WB, Agre P. Molecular cloning and characterization of an aquaporin cDNA from salivary, lacrimal, and respiratory tissues. *J Biol Chem*. 1995; 270(4):1908–12. Epub 1995/01/27. PMID: [7530250](#).
20. Chae YK, Woo J, Kim MJ, Kang SK, Kim MS, Lee J, et al. Expression of aquaporin 5 (AQP5) promotes tumor invasion in human non small cell lung cancer. *PLoS One*. 2008; 3(5):e2162. Epub 2008/05/15. doi: [10.1371/journal.pone.0002162](#) PMID: [18478076](#).
21. Woo J, Lee J, Chae YK, Kim MS, Baek JH, Park JC, et al. Overexpression of AQP5, a putative oncogene, promotes cell growth and transformation. *Cancer letters*. 2008; 264(1):54–62. doi: [10.1016/j.canlet.2008.01.029](#) PMID: [18423983](#); PubMed Central PMCID: PMC3074481.

22. Woo J, Chae YK, Jang SJ, Kim MS, Baek JH, Park JC, et al. Membrane trafficking of AQP5 and cAMP dependent phosphorylation in bronchial epithelium. *Biochem Biophys Res Commun*. 2008; 366(2):321–7. Epub 2007/11/29. doi: S0006-291X(07)02469-2 [pii] doi: [10.1016/j.bbrc.2007.11.078](https://doi.org/10.1016/j.bbrc.2007.11.078) PMID: [18042467](https://pubmed.ncbi.nlm.nih.gov/18042467/).
23. Horsefield R, Norden K, Fellert M, Backmark A, Tornroth-Horsefield S, Terwisscha van Scheltinga AC, et al. High-resolution x-ray structure of human aquaporin 5. *Proc Natl Acad Sci U S A*. 2008; 105(36):13327–32. Epub 2008/09/05. doi: 0801466105 [pii] doi: [10.1073/pnas.0801466105](https://doi.org/10.1073/pnas.0801466105) PMID: [18768791](https://pubmed.ncbi.nlm.nih.gov/18768791/).
24. Conner MT, Conner AC, Brown JE, Bill RM. Membrane trafficking of aquaporin 1 is mediated by protein kinase C via microtubules and regulated by tonicity. *Biochemistry*. 2010; 49(5):821–3. doi: [10.1021/bi902068b](https://doi.org/10.1021/bi902068b) PMID: [20063900](https://pubmed.ncbi.nlm.nih.gov/20063900/).
25. Oberg F, Sjöhamn J, Conner MT, Bill RM, Hedfalk K. Improving recombinant eukaryotic membrane protein yields in *Pichia pastoris*: the importance of codon optimization and clone selection. *Molecular membrane biology*. 2011; 28(6):398–411. Epub 2011/07/21. doi: [10.3109/09687688.2011.602219](https://doi.org/10.3109/09687688.2011.602219) PMID: [21770695](https://pubmed.ncbi.nlm.nih.gov/21770695/).
26. Winn MD, Ballard CC, Cowtan KD, Dodson EJ, Emsley P, Evans PR, et al. Overview of the CCP4 suite and current developments. *Acta crystallographica Section D, Biological crystallography*. 2011; 67(Pt 4):235–42. doi: [10.1107/S0907444910045749](https://doi.org/10.1107/S0907444910045749) PMID: [21460441](https://pubmed.ncbi.nlm.nih.gov/21460441/); PubMed Central PMCID: PMC3069738.
27. McCoy AJ, Grosse-Kunstleve RW, Adams PD, Winn MD, Storoni LC, Read RJ. Phaser crystallographic software. *Journal of applied crystallography*. 2007; 40(Pt 4):658–74. doi: [10.1107/S0021889807021206](https://doi.org/10.1107/S0021889807021206) PMID: [19461840](https://pubmed.ncbi.nlm.nih.gov/19461840/); PubMed Central PMCID: PMC2483472.
28. Murshudov GN, Skubak P, Lebedev AA, Pannu NS, Steiner RA, Nicholls RA, et al. REFMAC5 for the refinement of macromolecular crystal structures. *Acta crystallographica Section D, Biological crystallography*. 2011; 67(Pt 4):355–67. doi: [10.1107/S0907444911001314](https://doi.org/10.1107/S0907444911001314) PMID: [21460454](https://pubmed.ncbi.nlm.nih.gov/21460454/); PubMed Central PMCID: PMC3069751.
29. Adams PD, Afonine PV, Bunkoczi G, Chen VB, Davis IW, Echols N, et al. PHENIX: a comprehensive Python-based system for macromolecular structure solution. *Acta crystallographica Section D, Biological crystallography*. 2010; 66(Pt 2):213–21. doi: [10.1107/S0907444909052925](https://doi.org/10.1107/S0907444909052925) PMID: [20124702](https://pubmed.ncbi.nlm.nih.gov/20124702/); PubMed Central PMCID: PMC2815670.
30. Emsley P, Cowtan K. Coot: model-building tools for molecular graphics. *Acta crystallographica Section D, Biological crystallography*. 2004; 60(Pt 12 Pt 1):2126–32. doi: [10.1107/S0907444904019158](https://doi.org/10.1107/S0907444904019158) PMID: [15572765](https://pubmed.ncbi.nlm.nih.gov/15572765/).
31. van Balkom BW, Savelkoul PJ, Markovich D, Hofman E, Nielsen S, van der Sluijs P, et al. The role of putative phosphorylation sites in the targeting and shuttling of the aquaporin-2 water channel. *J Biol Chem*. 2002; 277(44):41473–9. doi: [10.1074/jbc.M207525200](https://doi.org/10.1074/jbc.M207525200) PMID: [12194985](https://pubmed.ncbi.nlm.nih.gov/12194985/).
32. Kamsteeg EJ, Hendriks G, Boone M, Konings IB, Oorschot V, van der Sluijs P, et al. Short-chain ubiquitination mediates the regulated endocytosis of the aquaporin-2 water channel. *Proc Natl Acad Sci U S A*. 2006; 103(48):18344–9. doi: [10.1073/pnas.0604073103](https://doi.org/10.1073/pnas.0604073103) PMID: [17101973](https://pubmed.ncbi.nlm.nih.gov/17101973/); PubMed Central PMCID: PMC1838753.
33. Moeller HB, Praetorius J, Rutzler MR, Fenton RA. Phosphorylation of aquaporin-2 regulates its endocytosis and protein-protein interactions. *Proc Natl Acad Sci U S A*. 2010; 107(1):424–9. doi: [10.1073/pnas.0910683107](https://doi.org/10.1073/pnas.0910683107) PMID: [19966308](https://pubmed.ncbi.nlm.nih.gov/19966308/); PubMed Central PMCID: PMC2806726.
34. Ishikawa Y, Eguchi T, Skowronski MT, Ishida H. Acetylcholine acts on M3 muscarinic receptors and induces the translocation of aquaporin5 water channel via cytosolic Ca²⁺ elevation in rat parotid glands. *Biochem Biophys Res Commun*. 1998; 245(3):835–40. Epub 1998/05/20. doi: S0006-291X(98)98395-4 [pii] doi: [10.1006/bbrc.1998.8395](https://doi.org/10.1006/bbrc.1998.8395) PMID: [9588201](https://pubmed.ncbi.nlm.nih.gov/9588201/).
35. Ishikawa Y, Skowronski MT, Inoue N, Ishida H. alpha(1)-adrenoceptor-induced trafficking of aquaporin-5 to the apical plasma membrane of rat parotid cells. *Biochem Biophys Res Commun*. 1999; 265(1):94–100. doi: [10.1006/bbrc.1999.1630](https://doi.org/10.1006/bbrc.1999.1630) PMID: [10548496](https://pubmed.ncbi.nlm.nih.gov/10548496/).
36. Hasegawa T, Azlina A, Javkhlan P, Yao C, Akamatsu T, Hosoi K. Novel phosphorylation of aquaporin-5 at its threonine 259 through cAMP signaling in salivary gland cells. *Am J Physiol Cell Physiol*. 2011; 301(3):C667–78. doi: [10.1152/ajpcell.00058.2011](https://doi.org/10.1152/ajpcell.00058.2011) PMID: [21633078](https://pubmed.ncbi.nlm.nih.gov/21633078/).
37. Woo J, Lee J, Kim MS, Jang SJ, Sidransky D, Moon C. The effect of aquaporin 5 overexpression on the Ras signaling pathway. *Biochem Biophys Res Commun*. 2008; 367(2):291–8. doi: [10.1016/j.bbrc.2007.12.073](https://doi.org/10.1016/j.bbrc.2007.12.073) PMID: [18155156](https://pubmed.ncbi.nlm.nih.gov/18155156/).
38. Ribatti D, Ranieri G, Annese T, Nico B. Aquaporins in cancer. *Biochim Biophys Acta*. 2014; 1840(5):1550–3. doi: [10.1016/j.bbagen.2013.09.025](https://doi.org/10.1016/j.bbagen.2013.09.025) PMID: [24064112](https://pubmed.ncbi.nlm.nih.gov/24064112/).
39. Frick A, Eriksson UK, de Mattia F, Oberg F, Hedfalk K, Neutze R, et al. X-ray structure of human aquaporin 2 and its implications for nephrogenic diabetes insipidus and trafficking. *Proc Natl Acad Sci U S A*.

2014; 111(17):6305–10. doi: [10.1073/pnas.1321406111](https://doi.org/10.1073/pnas.1321406111) PMID: [24733887](https://pubmed.ncbi.nlm.nih.gov/24733887/); PubMed Central PMCID: PMC4035913.

40. Wellner RB, Hong S, Cotrim AP, Swaim WD, Baum BJ. Modifying the NH₂ and COOH termini of aquaporin-5: effects on localization in polarized epithelial cells. *Tissue Eng.* 2005; 11(9–10):1449–58. Epub 2005/11/02. doi: [10.1089/ten.2005.11.1449](https://doi.org/10.1089/ten.2005.11.1449) PMID: [16259600](https://pubmed.ncbi.nlm.nih.gov/16259600/).

Control of the Aquaporin-4 Channel Water Permeability by Structural Dynamics of Aromatic/Arginine Selectivity Filter Residues

Philip Kitchen[†] and Alex C. Conner^{*,‡}

[†]Molecular Organisation and Assembly in Cells Doctoral Training Centre, University of Warwick, Coventry CV4 7AL, U.K.

[‡]Institute of Clinical Sciences, University of Birmingham, Edgbaston, Birmingham B15 2TT, U.K.

S Supporting Information

ABSTRACT: The aquaporins (AQPs) make up a family of integral membrane proteins that control cellular water flow. Gating of the water channel by conformational changes induced by phosphorylation or protein–protein interactions is an established regulatory mechanism for AQPs. Recent *in silico* and crystallographic analyses of the structural biology of AQPs suggest that the rate of water flow can also be controlled by small movements of single-amino acid side chains lining the water pore. Here we use measurements of the membrane water permeability of mammalian cells expressing AQP4 mutants to provide the first *in vitro* evidence in support of this hypothesis.

Rapid modulation of aquaporin (AQP)-mediated cell membrane water permeability in response to external stimuli is a vital regulatory mechanism that underlies a variety of physiological processes in mammals and plants.^{1,2} There are two ways in which this could be achieved: by changing the number of AQP molecules in the membrane via exo- or endocytosis or by directly blocking or activating AQP molecules via a conformational change that opens or closes the pore. There are examples of each of these approaches to AQP regulation being taken in nature, the best-studied examples of which are the arginine-8 vasopressin (AVP)-mediated trafficking of AQP2 to the apical membrane of kidney collecting duct cells³ and the phosphorylation-mediated gating of spinach AQP SoPIP2, involving a large scale motion of an intracellular loop that stabilizes a closed conformation of the aqueous pore.⁴

A conceptual model of AQP gating in which the channel is either open or closed and can be “switched off” by stimuli is probably overly simplistic, and indeed, researchers in the field of G protein-coupled receptor (GPCR) structural biology have long since abandoned conceptual models in which receptors are thought to be “on” or “off” in favor of models in which receptors are thought to be continually visiting various conformations, each with unique ligand affinities and signaling capacities. In this framework, rather than “switching on” a receptor, ligands are thought to stabilize (increasing the probability to visit) a particular conformation with a particular signaling capacity. *In silico* work on the bacterial AQPZ,⁵ human AQP5,⁶ AQP1,⁷ and human AQP1 and -4⁸ suggests that a similar model may be appropriate for AQPs and that particularly important local conformational changes may

involve the pore-lining residues within the aromatic/arginine (ar/R) selectivity filter region.

Here we show that specific site-directed mutations to the selectivity filter region of human AQP4 can quantitatively alter the permeability of the channel in a manner independent of surface expression. We made alanine substitution mutants of the three AQP4 residues whose side chains form the ar/R selectivity filter, F77A, H201A, and R216A. The histidine is typically replaced by a glycine in the GLP subfamily, so we also made a H201G mutant. After finding that the H201A and F77A mutations had no effect, we combined them into the H201A/F77A and H201G/F77A double mutants. Finally, we made the H201E mutant to try to form a salt bridge between the glutamate residue and R216. Mutants were generated by site-directed mutagenesis as previously described.⁹ The M1 isoform of AQP4 with a C-terminal GFP tag and all selectivity filter mutants of this construct were stably transfected into type I MDCK cells (ATCC CRL-2935) to measure water permeability using a plate reader-based calcein fluorescence quenching method adapted from ref 10. Expression of AQP4 mutants in stable clones was checked visually using the GFP tag and sodium dodecyl sulfate–polyacrylamide gel electrophoresis/Western blotting against AQP4. Endogenous AQP4 was not detected in MDCK cells in Western blots. After 5 s of reading at 50 ms intervals in isotonic culture medium, an equal volume of 600 mM mannitol in culture medium was injected to give a final mannitol concentration of 300 mM and an osmotic gradient of 300 mOsm/kg of H₂O, and fluorescence was measured for a further 50 s. Normalized fluorescence time series were converted to volume time series. Cell shrinkage rates were background-subtracted (using an untransfected MDCK control to correct for any basal water permeability of the cells) and normalized to surface expression (measured using a cell surface biotinylation-based enzyme-linked immunosorbent assay as previously described⁹) to give relative single-channel water permeability. For most mutants, the variations in the shrinkage rates of individual clones (Figure 1B) were consistent with the variation in surface expression (Figure 2A). After normalization, none of the mutants except H201E and R216A had water permeability significantly different from that of wild-type AQP4. The water permeability of H201E was reduced to 63 ± 8% of that of the wild type ($n = 4$; $p = 0.002$), and the water permeability of R216A was increased to 147 ±

Received: September 25, 2015

Revised: October 22, 2015

Published: October 29, 2015

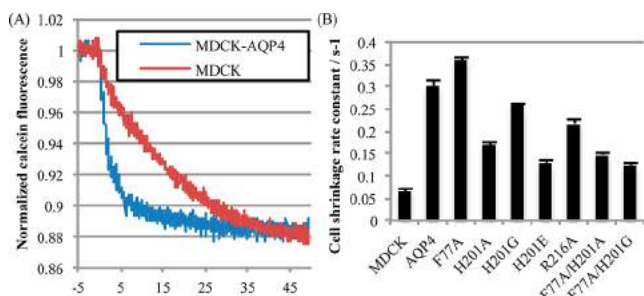


Figure 1. (A) Representative calcein fluorescence quenching curves of control MDCK cells and our stable MDCK-AQP4 cell line upon addition of 300 mM mannitol. (B) Cell shrinkage rates of MDCK cells stably transfected with AQP4 mutants. Relative fluorescence data were converted to relative volume, and exponential decay functions were fitted.

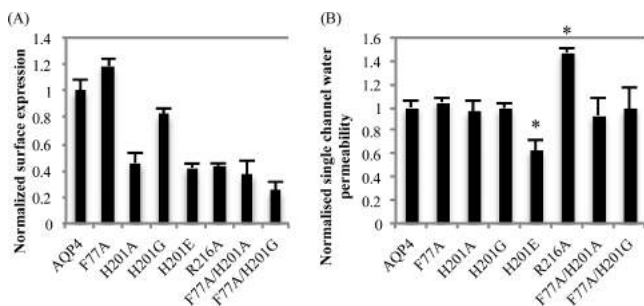


Figure 2. (A) Surface expression of AQP4 mutants in stable MDCK clones, normalized to wild-type AQP4. (B) Normalized single-channel permeability calculated by subtracting the untransfected MDCK background (see Figure 1B) and normalizing to surface expression. An asterisk represents $p < 0.01$.

3% of that of the wild type ($n = 4$; $p = 0.005$); this is shown in Figures 1 and 2.

Hub et al. previously reported that, in molecular dynamics simulations, fluctuations of R216 of AQP4 could switch the channel between an open and a closed state with an open probability of ~ 0.45 using the OPLS force field⁸ (with open defined as a distance of >0.57 nm between the arginine C_ζ atom and the closest histidine heavy atom). We performed molecular dynamics simulations of an AQP4 tetramer embedded in a POPC bilayer using the GROMOS 53A6 force field, based on the AQP4 crystal structure,¹¹ to attempt to qualitatively validate this result and to address the possibility of quantitative differences in the open probability between different protein force fields. We also found that a two-state model is appropriate for describing the simulation data, with the average R216–H201 distances of the open and closed states being 6.5 and 4.3 Å, respectively (Figure 3). Using the same definition of open, we find an open probability of 0.52 ± 0.12 (with the uncertainty estimated as the standard error over the four monomers). This is consistent with the work of Hub et al., suggesting that this probability is reasonably robust when measured using different force fields.

Assuming this simple two-state model, our *in vitro* results allow us to estimate the open probability of the wild-type AQP4 channel, based on the idea that the R216A mutation forces the channel to permanently occupy the open state. Previous molecular dynamics simulations suggested an approximately 40-fold difference in permeability between the open and closed states of AQP4.⁸ Using the following equation

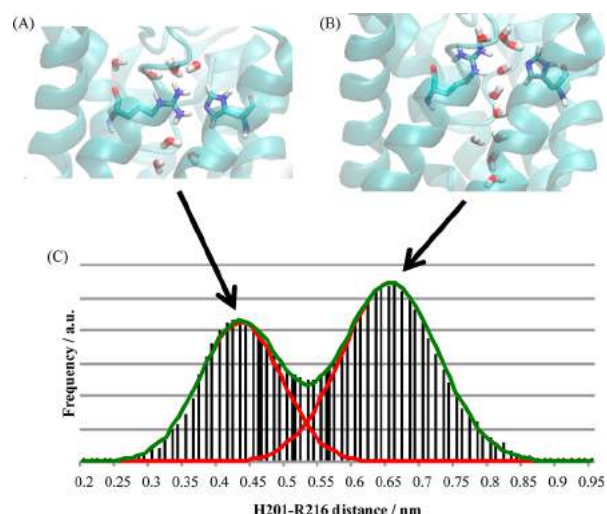


Figure 3. Representative molecular dynamics simulation snapshots of wild-type AQP4 with R216 and H201 and channel water molecules highlighted as sticks of (A) the open state of the selectivity filter and (B) the closed state of the selectivity filter. (C) Histogram of the R216–H201 distance distribution in simulations, showing two clearly distinct states. Fitted Gaussians (red, sum in green) are centered at 0.43 and 0.65 nm.

$$\frac{P_{R216A}}{P_{WT}} = \frac{P_o p_{o,R216A} + P_c(1 - p_{o,R216A})}{P_o p_{o,WT} + P_c(1 - p_{o,WT})}$$

where P_{R216A} and P_{WT} are the permeabilities measured in our experiments, P_o and P_c are the permeabilities of the open and closed states, respectively, and p_o is the channel open probability. Setting $p_{o,R216A}$ equal to 1 and P_o equal to $40P_c$ gives a wild-type open probability of 0.67 ± 0.02 (which is slightly higher than the value of 0.52 ± 0.12 that we estimated from simulations, but in reasonable agreement).

Crystallographic analysis¹² and simulations⁵ of AQPZ have also suggested that the selectivity filter arginine residue may undergo fluctuations between “up” and “down” conformations, with the down conformation associated with a closed state of the channel and reduced channel permeability. Similar results were reported for fluctuations of the selectivity filter histidine residue in human AQP5.⁶ *In silico* mutation of the AQPZ arginine to serine (R189S) increased the average water permeability by 26% in molecular dynamics simulations.⁵ Although this result was not validated *in vitro*, it is qualitatively similar to our *in vitro* result for AQP4 R216A.

To further test the idea of the R216 side chain dynamics controlling the average channel permeability, the selectivity filter histidine residue (H201), which is directly opposite R216 in the AQP4 ar/R selectivity filter region, was replaced with the similarly sized glutamate (H201E) to attempt to stabilize the closed conformation of the arginine residue by formation of a salt bridge between the arginine and glutamate residues. Initial mutation of this histidine to both alanine and glycine did not affect water permeability, showing that the histidine side chain is not a crucial factor for the permeability in AQP4. The water permeability of the H201E mutant was reduced to $63 \pm 8\%$ of that of wild-type AQP4; we hypothesize that this mutation reduces the average permeability by stabilizing the closed conformation of the arginine residue. Although we have interpreted our *in vitro* data in terms of changes in the ar/R selectivity filter open probability, it remains a possibility that

the H201E mutation decreases the open state permeability rather than the open probability and the R216A mutation increases the permeability of the open state rather than the open probability. We think it would be an unlikely coincidence if both of these mutations had exactly the effect that would be predicted on the basis of published *in silico* data, but mediated in a different way, but it cannot be excluded on the basis of our data alone. It is also possible that the effect of our mutations is to reposition the peptide backbone rather than a direct effect of the side chains per se. We think that the fact that our data agree with published predictions based on atomic-resolution molecular dynamics simulations makes this unlikely, but again this cannot be excluded.

Taken together, our results support predictions previously made in the literature, based on molecular dynamics simulations, that the dynamics of the ar/R selectivity filter arginine residue are important for determining the quantitative water permeability of AQP.

Interestingly, a study of the selectivity filter of AQP1 found that the R195A mutant (analogous to R216A in AQP4) did not have water permeability significantly different from that of wild-type AQP1 expressed in *Xenopus* oocytes.¹³ The volumetric data were not normalized to AQP1 surface expression, so it is possible that a subtle difference in membrane expression masked a difference in water permeability in this study. Simulations suggest that the balance of open and closed probabilities for AQP1 is very similar to that of AQP4,⁸ but it is also possible that the closed probability is close to zero in AQP1, making any measurement of the difference between the wild type and a constitutively open channel very difficult.

Control of the balance of open and closed probabilities by, e.g., protein post-translational modification or protein–protein interactions may represent an unexplored mechanism by which AQP water permeability could be regulated by physiological stimuli.

■ ASSOCIATED CONTENT

📄 Supporting Information

The Supporting Information is available free of charge on the ACS Publications website at DOI: 10.1021/acs.biochem.5b01053.

Detailed methods (PDF)

■ AUTHOR INFORMATION

Corresponding Author

*School of Clinical and Experimental Medicine, University of Birmingham, Edgbaston, Birmingham B15 2TT, U.K. Telephone: 0044 121 415 8809. E-mail: a.c.conner@bham.ac.uk.

Funding

P.K. thanks EPSRC for a Ph.D. studentship through MOAC Doctoral Training Centre Grant EP/F500378/1. A.C.C. has funding from the BHF (Grant PG/12/59/29795).

Notes

The authors declare no competing financial interest.

■ ABBREVIATIONS

AQP, aquaporin; MDCK, Madin-Darby canine kidney (cells); POPC, 1-palmitoyl-2-oleoyl-*sn*-glycero-3-phosphocholine.

■ REFERENCES

- (1) Day, R. E., Kitchen, P., Owen, D. S., Bland, C., Marshall, L., Conner, A. C., Bill, R. M., and Conner, M. T. (2014) Human aquaporins: regulators of transcellular water flow. *Biochim. Biophys. Acta, Gen. Subj.* 1840, 1492–1506.
- (2) Chaumont, F., and Tyerman, S. D. (2014) Aquaporins: highly regulated channels controlling plant water relations. *Plant Physiol.* 164, 1600–1618.
- (3) Nedvetsky, P. I., Tamma, G., Beulshausen, S., Valenti, G., Rosenthal, W., and Klussmann, E. (2009) Regulation of aquaporin-2 trafficking. *Handbook of experimental pharmacology* 190, 133–157.
- (4) Tornroth-Horsefield, S., Wang, Y., Hedfalk, K., Johanson, U., Karlsson, M., Tajkhorshid, E., Neutze, R., and Kjellbom, P. (2006) Structural mechanism of plant aquaporin gating. *Nature* 439, 688–694.
- (5) Xin, L., Su, H., Nielsen, C. H., Tang, C., Torres, J., and Mu, Y. (2011) Water permeation dynamics of AqpZ: a tale of two states. *Biochim. Biophys. Acta, Biomembr.* 1808, 1581–1586.
- (6) Janosi, L., and Ceccarelli, M. (2013) The gating mechanism of the human aquaporin 5 revealed by molecular dynamics simulations. *PLoS One* 8, e59897.
- (7) Yamamoto, E., Akimoto, T., Hirano, Y., Yasui, M., and Yasuoka, K. (2014) 1/ f Fluctuations of amino acids regulate water transportation in aquaporin 1. *Physical review. E, Statistical, nonlinear, and soft matter physics* 89, 022718.
- (8) Hub, J. S., Aponte-Santamaria, C., Grubmuller, H., and de Groot, B. L. (2010) Voltage-regulated water flux through aquaporin channels in silico. *Biophys. J.* 99, L97–99.
- (9) Kitchen, P., Day, R. E., Taylor, L. H., Salman, M. M., Bill, R. M., Conner, M. T., and Conner, A. C. (2015) Identification and Molecular Mechanisms of the Rapid Tonicity-induced Relocalization of the Aquaporin 4 Channel. *J. Biol. Chem.* 290, 16873–16881.
- (10) Fenton, R. A., Moeller, H. B., Nielsen, S., de Groot, B. L., and Rutzler, M. (2010) A plate reader-based method for cell water permeability measurement. *American journal of physiology. Renal physiology* 298, F224–230.
- (11) Jiang, J., Daniels, B. V., and Fu, D. (2006) Crystal structure of AqpZ tetramer reveals two distinct Arg-189 conformations associated with water permeation through the narrowest constriction of the water-conducting channel. *J. Biol. Chem.* 281, 454–460.
- (12) Ho, J. D., Yeh, R., Sandstrom, A., Chorny, I., Harries, W. E., Robbins, R. A., Miercke, L. J., and Stroud, R. M. (2009) Crystal structure of human aquaporin 4 at 1.8 Å and its mechanism of conductance. *Proc. Natl. Acad. Sci. U. S. A.* 106, 7437–7442.
- (13) Beitz, E., Wu, B., Holm, L. M., Schultz, J. E., and Zeuthen, T. (2006) Point mutations in the aromatic/arginine region in aquaporin 1 allow passage of urea, glycerol, ammonia, and protons. *Proc. Natl. Acad. Sci. U. S. A.* 103, 269–274.

Structural Determinants of Oligomerization of the Aquaporin-4 Channel*

Received for publication, October 2, 2015, and in revised form, January 15, 2016. Published, JBC Papers in Press, January 19, 2016, DOI 10.1074/jbc.M115.694729

Philip Kitchen^{‡§¶}, Matthew T. Conner^{||}, Roslyn M. Bill^{§¶}, and Alex C. Conner^{¶12}

From the [‡]Molecular Assembly and Organisation in Cells Doctoral Training Centre, University of Warwick, Coventry CV4 7AL, the ^{||}School of Biology, Chemistry and Forensic Science, Faculty of Science and Engineering, University of Wolverhampton, Wolverhampton WV1 1LY, the [§]School of Life & Health Sciences and Aston Research Centre for Healthy Ageing, Aston University, Aston Triangle, Birmingham, B4 7ET, and the [¶]Institute of Clinical Sciences, University of Birmingham, Edgbaston, Birmingham B15 2TT, United Kingdom

The aquaporin (AQP) family of integral membrane protein channels mediate cellular water and solute flow. Although qualitative and quantitative differences in channel permeability, selectivity, subcellular localization, and trafficking responses have been observed for different members of the AQP family, the signature homotetrameric quaternary structure is conserved. Using a variety of biophysical techniques, we show that mutations to an intracellular loop (loop D) of human AQP4 reduce oligomerization. Non-tetrameric AQP4 mutants are unable to relocalize to the plasma membrane in response to changes in extracellular tonicity, despite equivalent constitutive surface expression levels and water permeability to wild-type AQP4. A network of AQP4 loop D hydrogen bonding interactions, identified using molecular dynamics simulations and based on a comparative mutagenic analysis of AQPs 1, 3, and 4, suggest that loop D interactions may provide a general structural framework for tetrameric assembly within the AQP family.

The aquaporin (AQP)³ family of integral membrane proteins facilitate both osmosis and diffusion of small polar molecules through biological membranes. A wealth of medium-to-high resolution structural data for various family members (there are 48 AQP structures in the Protein Data Bank) all suggest that the AQP homotetrameric quaternary structure is highly conserved despite diversity in solute permeability, subcellular localization, and trafficking responses of individual AQPs. Early biochemical work, using carboxyl-amine fusion dimers (consisting of 1 wild-type unit and 1 unit lacking the cysteine residue required for mercurial inhibition), showed that monomers are the functional AQP units (1); numerous molecular dynamics simulation

studies support this (2). Recent work has suggested that isolated AQP monomers are equally capable of facilitating water transport as those incorporated into a tetramer (3). Therefore it is not clear why AQPs retain this tetrameric structure. Regulation of AQP function by the formation of heterotetramers has been suggested for some plant AQPs (4). The fifth, central pore formed at the 4-fold axis of the tetramer has also been suggested to transport carbon dioxide (5) and cations (6), at least in mammalian AQP1. Trigger-induced relocalization of AQP-containing vesicles to the plasma membrane is a well established regulatory mechanism for AQPs; the best studied example of this is relocalization of AQP2 to the apical membrane of the collecting duct in the mammalian kidney in response to arginine vasopressin (also called anti-diuretic hormone). There is also evidence for similar mechanisms for other AQPs including AQP1 (7), AQP5 (8), and AQP7 (9). A naturally occurring AQP2 mutant (R187C) has also been reported that is unable to relocalize in response to arginine vasopressin or to form tetramers (10). Given the ubiquity of these regulatory responses across the AQP family and the conservation of the tetrameric quaternary structure, it may be that these trigger-induced relocalization responses involve interaction with proteins that only recognize the tetrameric form of AQPs.

Here we demonstrate that intracellular loop D of AQP4 forms vital homomeric interactions between AQP subunits that stabilize the tetrameric quaternary structure. We also show that loss of tetramerization does not affect single channel water permeability. Our data suggest that tetramerization is not required for AQP4 to be trafficked through the endoplasmic reticulum and Golgi to the plasma membrane, but that unlike wild-type AQP4, the non-tetrameric mutants are unable to relocalize to the plasma membrane in response to changes in local osmolality. Finally, based on loss and gain of oligomerization mutants of AQP1 and AQP3, we suggest that loop D-mediated inter-monomer interactions may control formation of the signature quaternary structure of the family.

Experimental Procedures

Expression Constructs and Mutagenesis—Human AQP4 cDNA cloned into pDEST47 (Life Technologies) was used as previously described (11). An untagged AQP4 construct was created from this by mutagenesis of the first two codons of the GFP linker peptide to stop codons. These were used as templates for mutagenesis following the QuikChange protocol

* The authors report no conflicts of interest.

✂ Author's Choice—Final version free via Creative Commons CC-BY license.

¹ Supported by Biotechnology and Biological Sciences Research Council Grants BB/I019960/1, BB/K013319/1, and BB/L502194/1 and Innovative Medicines Joint Undertaking under Grant Agreement 115583 to the ND4BB ENABLE Consortium. To whom correspondence may be addressed. E-mail: r.m.bill@aston.ac.uk.

² To whom correspondence may be addressed. E-mail: a.c.conner@bham.ac.uk.

³ The abbreviations used are: AQP, aquaporin; FRET, Forster resonant energy transfer; FRAP, fluorescence recovery after photobleaching; TM, transmembrane domain; MDCK, Madin-Darby canine kidney cells; BN-PAGE, blue native-PAGE; bis-tris, 2-[bis(2-hydroxyethyl)amino]-2-(hydroxymethyl)propane-1,3-diol; Tricine, N-[2-hydroxy-1,1-bis(hydroxymethyl)ethyl]glycine; ANOVA, analysis of variance.

(Stratagene). Mutagenic primers were synthesized by Sigma. Mutant plasmids were amplified in TOP10 *Escherichia coli* with 100 ng/ml of ampicillin selection. Plasmid DNA was purified using a Wizard Maxiprep kit (Promega) and diluted to 1 mg/ml for transfection.

Cell Culture and Transfection—HEK293 cells were cultured routinely in DMEM with L-glutamine (Sigma) supplemented with 10% (v/v) fetal bovine serum (Sigma) and without antibiotics in humidified 5% (v/v) CO₂ in air at 37 °C. Cells were seeded into either tissue culture treated 6-well plates (Falcon) for Blue Native (BN)-PAGE and biotinylation or 35-mm FluoroDishes™ (World Precision Instruments) for confocal microscopy. Cells were transfected (at 50% confluence) using polyethyleneimine (branched, average M_r ~25,000, Sigma) as previously described (11). MDCK cells were cultured in the same conditions as HEK293 cells. Stable transfections were done using the neomycin resistance gene on the pDEST47 vector. Cells were transiently transfected as described above, then trypsinized and serially diluted into tissue culture plates after 24 h. Cells were treated with 700 μg/ml of G418 antibiotic for 2 weeks, with medium replaced every third day. GFP-expressing resistant colonies were picked using cloning cylinders (Sigma) and serially diluted. The lowest dilution that grew to confluence was used to generate a stable cell line. Cellular protein was subjected to SDS-PAGE and Western blotting as previously described (11), and the highest expressing clone was chosen for experiments. No endogenous AQP4 was detected in Western blots. Reduced G418 pressure (300 μg/ml) was used to maintain the stable cell lines after colony isolation. All cells were routinely tested for mycoplasma using the EZ-PCR test kit (Biological Industries), and all data reported are from cells that tested negative. HEK293 and MDCK cells both expressed only the M1 isoform of AQP4 from the wild-type AQP4 construct. This was confirmed by Western blotting comparing the wild-type construct to AQP4 constructs in which either the M1 or M23 translation initiation sites were removed, as previously described (11).

Confocal Microscopy—AQP4-GFP constructs were imaged in live HEK293 cells using a Zeiss LSM 780 confocal microscope with a ×63 1.4 NA oil immersion objective. GFP was excited using the 488-nm line of an argon laser, Venus using the 514-nm line and mTurquoise2 using a 405-nm diode laser. Hypotonic exposure was performed by adding 3 ml of ddH₂O to cells in 1 ml of growth medium (280 to 70 mosmol/kg of H₂O). Line profiles across the cell membrane and cytoplasm were extracted using ImageJ as previously described (7). Relative membrane expression was calculated from these profiles (3 profiles per cell and at least 3 cells per image) using in-house Matlab code. Fluorescence recovery after photobleaching (FRAP) was done using a circular bleaching 1-μm area of radius. Recovery curves were fitted to a single phase exponential recovery function and diffusion coefficients were calculated using the approach and equations of Kang *et al.* (12). Recovery curves were collected from 5 different cells on the same plate per experiment. FRET experiments were done using the sensitized emission methodology with the FRET signal corrected for donor emission in the acceptor channel and direct excitation of the acceptor, following van Rheenen *et al.* (13) and normalized

to the acceptor emission to give an apparent FRET efficiency. The contrast of some images in the figures was adjusted manually using ImageJ to aid the eye. All analysis was performed on raw, unadjusted images.

Cell Surface Biotinylation—Cell surface amines were biotinylated using an amine-reactive biotinylation reagent that is not cell permeable (Thermo number 21328, EZ-Link Sulfo-NHS-SS-Biotin), and surface AQPs were detected using a neutravidin-based ELISA as previously described (11).

BN-PAGE—Transfected cells were lysed in ice-cold BN lysis buffer (1% (v/v) Triton X-100, 10% (v/v) glycerol, 20 mM bis-tris, 500 mM aminohexanoic acid, 20 mM NaCl, 2 mM EDTA, pH 7.0, 250 μl/well). The lysate was centrifuged at 21,000 × *g* at 4 °C for 10 min to remove insoluble material. The supernatant was collected and diluted 10-fold in Triton lysis buffer. 8% bis-tris-buffered polyacrylamide gels (0.75 mm) at pH 7.0 containing 66 mM aminohexanoic acid were used. Wells were topped up with cathode buffer (50 mM Tricine, 15 mM bis-tris, 0.02% (w/v) Coomassie G-250, pH 7.0). 10 μg of BSA was used as a molecular mass marker, giving bands at 66 and 132 kDa. Gels were run on ice at 100 V until samples entered the gel, then at 180 V until the Coomassie dye front reached the end of the gel.

Immunoblotting—BN-PAGE gels were destained with 40% (v/v) methanol, 10% (v/v) glacial acetic acid for 30 min, refreshing the destaining solution every 10 min. Gels were soaked for 30 min in 1% SDS in Tris-buffered saline, pH 7.4, at room temperature. Proteins were blotted onto PVDF membrane by wet transfer at 100 V for 1 h. Coomassie-stained BSA marker bands were marked onto the membrane using a felt-tipped pen. Membranes were blocked in 20% (w/v) Marvel-skimmed milk powder in 0.1% PBS-Tween for 1 h. Membranes were incubated overnight at 4 °C on a roller in rabbit anti-AQP4 antibody (Abcam, ab128906) diluted 1:5,000 or rabbit anti-GFP (Abcam, ab6556) diluted 1:10,000, both in 5 ml of 0.1% PBS-Tween. Membranes were washed in 0.1% PBS-Tween and incubated with donkey anti-rabbit HRP (Santa Cruz, sc-2313) diluted 1:10,000 in 20 ml of 0.1% PBS-Tween at room temperature for 1 h. HRP was detected on x-ray film using ECL reagent (Amersham Biosciences).

Statistics—For multiple comparisons, one-way ANOVA was used, followed by post hoc *t*-tests with the *p* values subjected to Bonferroni correction for multiple comparisons. All data are presented as mean ± S.E.

Simulations—Simulations were done using the GROMOS 53A6 forcefield (14) extended to include lipid parameters (15) in Gromacs version 4.5.5 (16). An AQP4 tetramer was generated according to the biological assembly entry in the AQP4 Protein Data Bank file 3GD8 (17). N and C termini of the protein were truncated in the structure so proteins were simulated with neutral termini. The AQP4 tetramer was embedded into 5 pre-equilibrated 1-palmitoyl-2-oleoyl-*sn*-glycero-3-phosphocholine bilayers using inflateGRO (18) and hydrated using Gromacs. Na⁺ and Cl⁻ were added to a final concentration of 100 mM. Equilibration was achieved by steepest gradient energy minimization, 100-ps NPT simulation with 1,000 kJmol⁻¹ nm⁻¹ restraints on protein heavy atoms followed by three 1-ns NVT simulations with 1000, 100, and 10 kJmol⁻¹ nm⁻¹ restraints on protein heavy atoms followed by 30-ns unre-

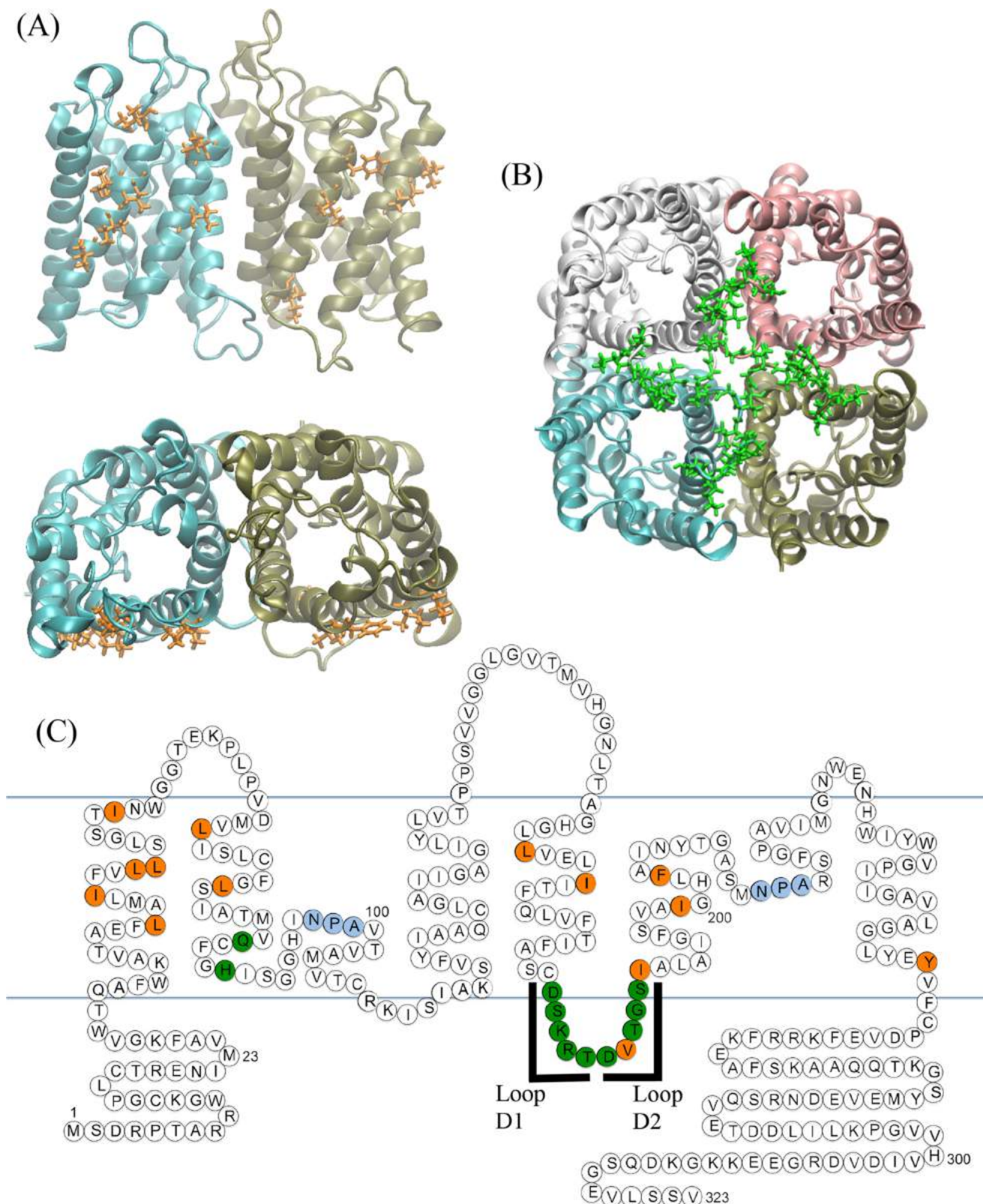


FIGURE 1. **Residues at the AQP4 tetrameric interface.** *A*, we identified hydrophobic residues (orange) in TMs 1, 2, 4, and 5 that formed inter-monomer contacts in the crystal structure and *B*, polar residues (green) at the bottom of TM2 and in the intracellular loop D. *C*, ball diagram showing the position of the identified residues in the primary sequences and secondary structural motifs of AQP4. Two regions of loop D were selected for compound mutation, which we denote loop D1 (¹⁷⁹DSKRT¹⁸³) and loop D2 (¹⁸⁴DVTGS¹⁸⁸). Blue lines represent the approximate position of membrane lipid headgroups. All residues are listed in Table 1.

TABLE 1

Oligomerization state and surface expression of AQP4 mutants

Oligomerization state of all AQP4 mutants analyzed. Compound mutations are represented by a solid slash between the relevant point mutations, e.g. L72A/L79A. T = tetramer, D = dimer, M = monomer. All data are reported as mean \pm S.E., $n = 3$.

Mutant	Oligomerization state	Surface expression
		% of WT
I43A	T	113.9 \pm 5.1
I47A	T	95.8 \pm 3.2
L50A	T	102.5 \pm 4.1
L51A	T	96.1 \pm 13.0
I57A	T	104.1 \pm 4.1
TM1 (I43A/I47A/L50A/L51A/I57A)	T	86.9 \pm 3.1
L72A	T	121.1 \pm 25.6
L79A	T	88.9 \pm 13.3
TM2 (L72A/L79A)	T	97.7 \pm 5.6
L161A	T	91.9 \pm 18.4
I165A	T	87.9 \pm 3.6
TM4 (L161A/I165A)	T	85.4 \pm 11.2
I189A	T	97.7 \pm 5.9
I199A	T	96.2 \pm 8.5
F203A	T	112.4 \pm 13.3
TM5 (I189A/I199A/F203A)	T	93.3 \pm 9.0
Q86A	T	118 \pm 4.4
H90A	T	113.5 \pm 4.1
D179A	T (95 \pm 2%) D (5 \pm 2%)	87.6 \pm 19.4
S180A	T	109.8 \pm 4.5
S180D	T	99.7 \pm 4.9
K181A	T	103.2 \pm 4.5
R182A	T	96.1 \pm 22.1
T183	T	105.6 \pm 3.6
Loop D1 (D179A/S180A/K181A/R182A/T183A)	T (19 \pm 4%) D (27 \pm 5%) M (53 \pm 4%)	88.5 \pm 6.1
D184A	T	97.7 \pm 8.8
V185A	T	102.2 \pm 5.4
T186A	T	95.1 \pm 7.5
G187A	T	106.7 \pm 5.1
S188A	T	98.6 \pm 3.2
S188D	T	104.1 \pm 4.2
Loop D2 (D184A/V185A/T186A/G187A/S188A)	T (33 \pm 7%) D (67 \pm 7%)	83.1 \pm 11.0

strained simulation. A Nosé-Hoover thermostat (0.5 ps, 310 K) was used to maintain constant temperature and 2 Parinello-Rahmann barostats (2 ps, 1 atm) were used to maintain constant pressure with zero surface tension. 1.4-nm cut-offs were applied for dispersion and short-range electrostatic interactions. Long-range electrostatics were treated using particle mesh Ewald. Hydrogen bonds were identified using the H-bonds plugin of visual molecular dynamics (19) using 3 Å and 20° cut-offs. Hydrogen bond occupancy was calculated according to these cut-offs at 100-ps intervals along the 100-ns trajectories and averaged over the 4 monomers and 5 trajectories.

Calcein Fluorescence Quenching—Plate reader-based calcein fluorescence quenching was done following Fenton *et al.* (20). MDCK cells were plated into black-walled, clear-bottomed tissue culture treated 96-well plates (Greiner) at 50% confluence 24 h before the experiment. Cells were loaded with 5 μ M calcein-AM in growth medium supplemented with 1 mM probenecid (to inhibit dye leakage) for 90 min. Cells were washed twice with HEPES-buffered growth medium supplemented with 1 mM probenecid, then covered with 75 μ l of probenecid-supplemented HEPES-buffered medium. Fluorescence was read on a BioTek synergy HT plate reader with injector system. Each well was read continuously ($dt = 50$ ms) for 5 s, followed

by injection of 75 μ l of HEPES-buffered medium containing 400 mM mannitol to give a final concentration of 200 mM and an osmotic gradient of 200 mosmol. Fluorescence was read for a further 50 s. Normalized fluorescence values were converted to normalized volumes using a Coulter counter generated standard curve. Single-phase exponential decay functions were fitted and rate constants were taken as proportional to the membrane water permeability.

Results

Mutation of Loop D of AQP4 Reduces Tetrameric Assembly

Using the crystal structure of AQP4 (17), residues likely to form the tetrameric interface were identified, based on the physical distance between residues on adjacent monomers. Alanine substitution mutagenesis was used to investigate the contribution of these residues to oligomeric assembly. The identified residues were clustered into two regions. The first cluster comprises a patch of hydrophobic residues at the interfaces of TM1 and TM2 of one monomer with TM4 and TM5 of the adjacent monomer (Fig. 1A); the second cluster comprises 12 predominantly polar and charged residues forming intracellular loop D and the bottom of TM2 (Fig. 1B). 24 single point alanine-substitution mutants were made and six compound mutants were used to investigate the possibility of synergistic effects of several residues. There are two protein kinase A/C consensus sites in loop D (Ser¹⁸⁰ and Ser¹⁸⁸) so phosphomimetic mutations were also made (S180D and S188D). All mutants are listed in the left-hand column of Table 1. BN-PAGE followed by immunoblotting was used to assess the oligomeric state of all mutants expressed in HEK293 cells. Representative BN blots are shown in Fig. 2A and the effect of all mutations on oligomeric assembly and surface expression summarized in Table 1 and Fig. 2B. None of the hydrophobic residues in the hydrophobic patches had any effect on tetramer formation, either in isolation or in compound mutants. TM compound mutants consisted of simultaneous mutations of all residues identified within that transmembrane segment (e.g. TM1 denotes the simultaneous mutations I43A/I47A/L50A/L51A/I57A). Of the loop D single alanine mutants, only D179A had an effect on oligomeric assembly in isolation, and this effect was only minimal, with 95 \pm 2% of the protein still assembled into tetramers. Unlike the hydrophobic cluster, the compound mutants of loop D had a clear effect on the ability of AQP4 to tetramerize. The two compound mutants, loop D1 (D179A/S180A/K181A/R182A/T183A) and loop D2 (D184A/V185A/T186A/G187A/S188A), caused reductions in oligomeric assembly: only 19 \pm 4% of the loop D1 protein assembled into tetramers with both dimers (27 \pm 5%) and monomers (53 \pm 4%) being present, whereas the loop D2 protein predominantly formed dimers (67 \pm 7%) with 33 \pm 7% assembled into tetramers ($n = 3$).

Surface Expression of Non-tetrameric Mutants

There was no significant difference in the surface expression of the loop D mutants compared with wild-type AQP4. Surface expression was assessed qualitatively by live cell confocal microscopy using GFP-tagged AQP4 mutant constructs and quantitatively by cell surface biotinylation. Fig.

Oligomerization of Aquaporin-4

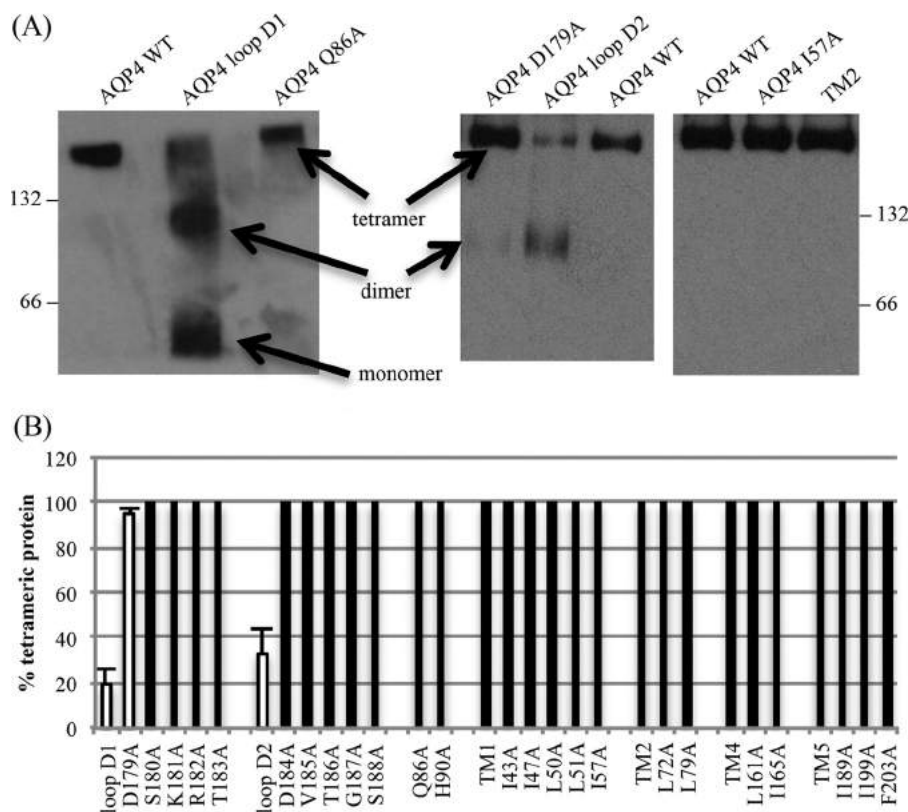


FIGURE 2. **BN-PAGE and Western blotting of AQP4 mutants.** A, representative Western blots following BN-PAGE of Triton X-100-solubilized AQP4 mutants, showing the effect of the loop D1 and loop D2 compound mutations, and a lack of effect of mutations on the transmembrane hydrophobic patch. 66 and 132 denote the positions of BSA molecular weight marker bands. The AQP4-GFP construct, including linker peptide, has a predicted molecular mass of 63.1 kDa. B, percentage of protein assembled into tetramers calculated using densitometry following BN-PAGE and Western blotting. Effective mutations are highlighted with white bars. Data are presented as mean \pm S.E. from 3 experimental repeats.

3A shows representative confocal micrographs of HEK293 cells transfected with GFP fusion proteins of AQP4 wild-type, and the loop D1 and loop D2 mutants. Surface expression in transiently transfected HEK293 cells measured by cell surface biotinylation was not significantly different ($p = 0.53$, one-way ANOVA, $n = 3$) for either of the loop D compound mutants (D1 and D2) or the single alanine mutants (Fig. 3B). This suggests that the trafficking machinery is able to interact with non-tetrameric aquaporins. The cell surface biotinylation data are summarized for all mutants in the third column of Table 1.

Mutants in the Plasma Membrane Exhibit Reduced Tetramerization

It was important to confirm the reduction in tetramerization of AQP4 molecules that had been constitutively trafficked to the cell surface and to rule out intracellular retention of dimeric/monomeric species or changes in detergent sensitivity caused by loop D substitutions. Several complementary biochemical techniques were used to address this.

Fluorescence Recovery after Photobleaching (FRAP)—Recovery curves were collected from 5 different cells per experimental repeat ($n = 6$). Representative fluorescence recovery curves are shown in Fig. 3D, along with the average recovery half-times. From these, diffusion coefficients were calculated: $5.2 \pm 0.3 \times 10^{-3} \mu\text{m}^2 \text{s}^{-1}$ (AQP4 WT), $5.9 \pm 0.3 \times 10^{-3} \mu\text{m}^2 \text{s}^{-1}$ (loop D1), and $5.8 \pm 0.2 \times 10^{-3} \mu\text{m}^2 \text{s}^{-1}$ (loop D2). Both loop D

mutant diffusion coefficients were significantly different from the wild-type (D1 $p = 0.01$ and D2 $p = 0.02$ by Student's t test following ANOVA, with p values subjected to Bonferroni correction). The FRAP data suggest reduced tetramerization for the surface-localized loop D mutants, although the increased diffusion coefficient could also be explained by the inability of these mutants to form a complex with a third party protein.

BN-PAGE of Biotinylated Cell Surface Protein—To complement these FRAP experiments, biotinylated cell surface proteins were isolated using neutravidin-coated plates, eluted by reducing the S-S bond incorporated into the biotinylation reagent (using 1% β -mercaptoethanol in BN lysis buffer) and subjected to BN-PAGE (representative blots are shown in Fig. 3C). Surface-localized mutant AQP4 molecules subjected to BN-PAGE had the same changes in tetramerization seen in whole cell lysates ($n = 3$).

Forster Resonant Energy Transfer (FRET)—To complement the above analyses, AQP4 constructs tagged with Venus (a yellow fluorescent protein (YFP) derivative) and mTurquoise2 (a cyan fluorescent protein (CFP) derivative) were generated and co-transfected into HEK293 cells to form a FRET biosensor for homo-oligomerization in living cells. The wild-type AQP4 constructs gave a robust FRET signal with an average apparent efficiency of $44.2 \pm 3.6\%$ (Fig. 4). We were unable to measure any FRET in cells co-transfected with AQP1-Venus and AQP4-

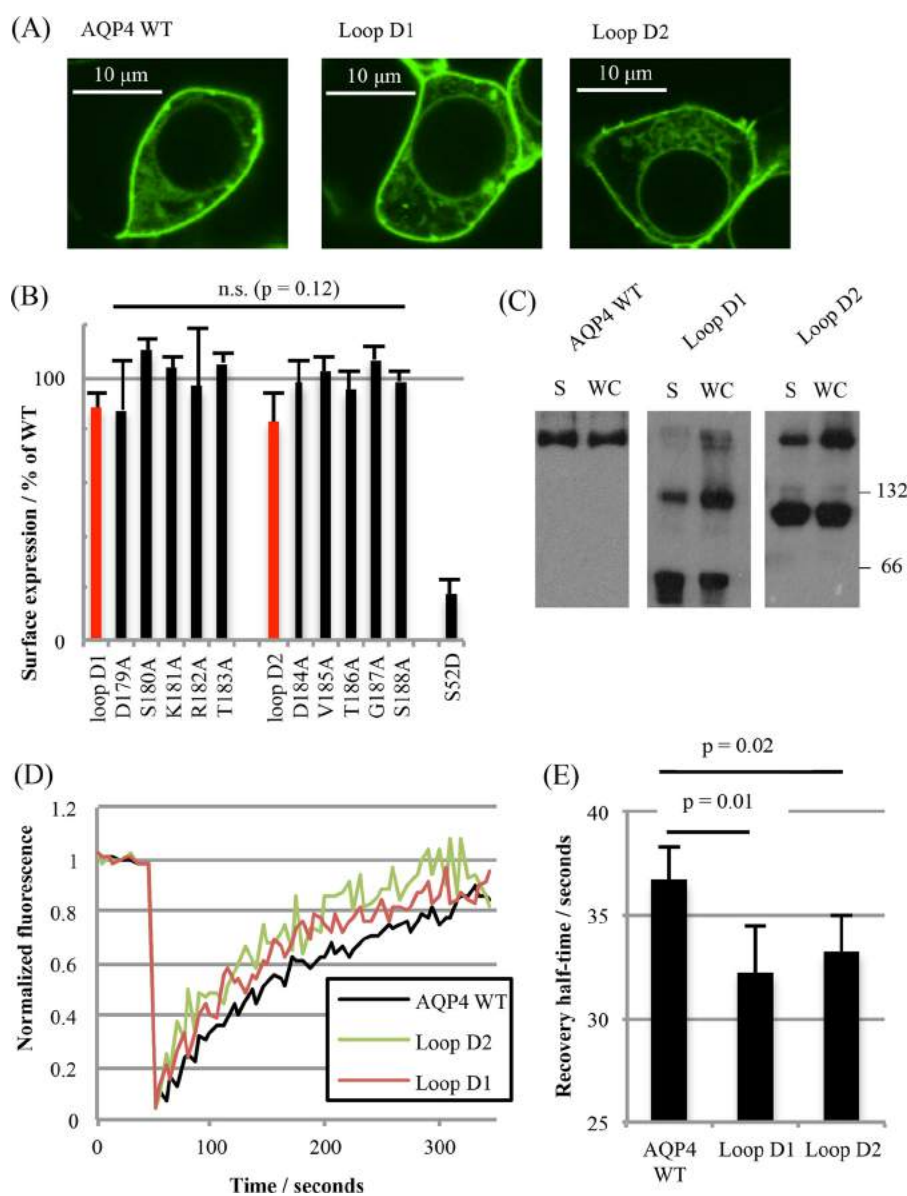


FIGURE 3. Plasma membrane localization of non-tetrameric mutants. *A*, representative fluorescence micrographs of HEK293 cells transfected with C-terminal GFP fusions of AQP4 WT and loop D mutants. *B*, surface expression of AQP4 mutants in HEK293 cells measured by cell surface biotinylation followed by a neutravidin-based ELISA. Loop D compound mutants are highlighted in red. The S52D mutant was used as a negative control for surface expression. *n.s.*, not significant. *C*, representative blots of AQP4 mutants subjected to BN-PAGE. WC, whole cell lysate; S, surface protein only, isolated by cell surface biotinylation. *D*, representative FRAP curves from photobleaching AQP4-GFP fusion proteins in HEK293 cells. *E*, average half-times of fluorescence recovery averaged over fits to 5 curves per experiment and 6 experimental repeats. All data are presented as mean \pm S.E.

Turquoise despite high co-localization (data not shown), suggesting that the FRET interactions occur primarily within the AQP4 tetramers and not between tetramers that are transiently close together in the plane of the membrane. The probability of a particular donor molecule taking part in FRET is dependent on the number of acceptors within the Forster radius and vice versa. For CFP-YFP, the Forster radius is ~ 5 nm (21). Based on the AQP4 crystal structure, the monomer-monomer center of mass separations are 2.8 (adjacent monomers) and 3.9 nm (diagonal monomers), respectively, so both would be expected to contribute to the FRET signal (assuming that the average separation of the C-terminal tails is similar). The average number of FRET pairings in a sample of co-transfected cells is therefore dependent on the level of AQP4 oligomerization. Both D1

and D2 compound mutants had a slightly larger than 2-fold reduction in FRET efficiency (to 17 ± 6 and $20 \pm 4\%$, respectively, $p = 0.003$ and $p = 0.005$, $n = 4$) compared with the wild-type (Fig. 5A), suggesting that these constructs have a reduced propensity to oligomerize in live cells, further confirming that the changes seen in the BN-PAGE were not mediated by changes in detergent sensitivity. Furthermore, for the mutants, there was no difference in FRET efficiency between plasma membrane and intracellular membranes (Figs. 5, B and C), suggesting that the oligomerization state of these mutants is the same in all membrane compartments (e.g. Golgi, vesicles, plasma membrane). Taken together, these data suggest reduced tetramerization for the AQP4 loop D mutants in the plasma membrane of living cells.

Oligomerization of Aquaporin-4

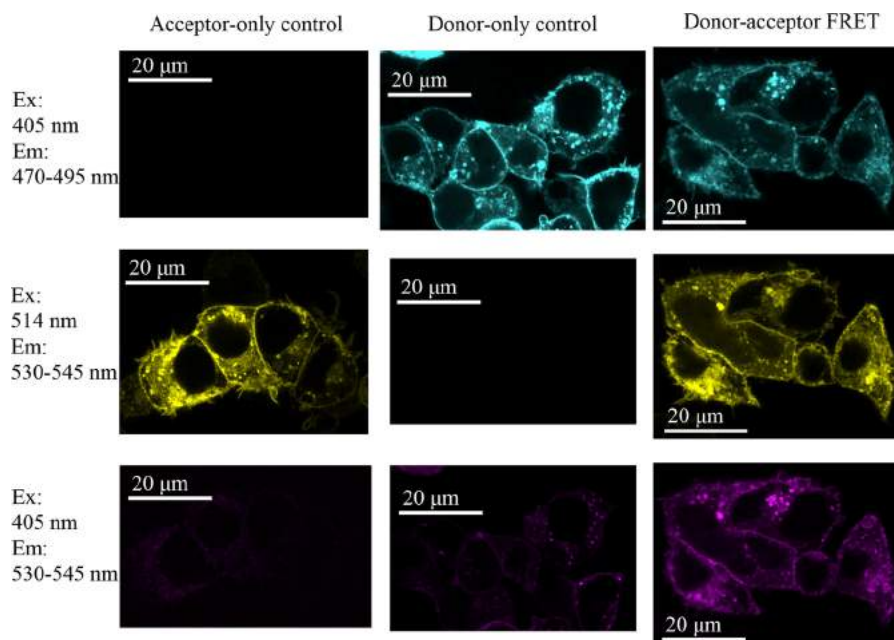


FIGURE 4. **A FRET biosensor for AQP4 oligomerization.** *A*, fluorescence confocal microscopy of live HEK293 cells transiently transfected with AQP4-Venus alone, AQP4-mTurquoise2 alone, and the two co-transfected. Excitation (*Ex*) at 405 nm is for Turquoise and 514 nm is for Venus. The contrast of these images has been manually optimized to aid the eye. All analysis was performed on raw, unadjusted images. *Em*, emission.

Loop D Mutants Have Wild-type Water Permeability—Both loop D compound mutants (D1 and D2) and wild-type AQP4 were stably transfected into MDCK cells to measure water channel function. Membrane water permeability of MDCK cells, measured by calcein fluorescence quenching (Fig. 6*A*), was increased 7-fold by stable expression of AQP4. Water permeability due to the transfected AQP was calculated by subtracting the permeability of untransfected cells (Fig. 6*B*); the resulting permeability was normalized to the surface expression measured by cell surface biotinylation to allow for differences in cellular expression due to differences in the position of chromosomal integration of the stably transfected gene (Fig. 6, *C* and *D*). After normalization to surface expression, no significant difference in permeability was observed between the loop D mutants and wild-type AQP4 (one-way ANOVA, $p = 0.17$, $n = 4$), suggesting that tetramerization of AQP4 is not required for full water channel activity.

Loop D Mutants Do Not Relocalize to the Plasma Membrane in Response to Hypotonicity—We recently reported that AQP4 rapidly relocalizes to the plasma membrane from intracellular membranes in response to reduced extracellular tonicity (11) and that this phenomenon is true for other mammalian AQPs (7, 22). Despite wild-type water permeability and constitutive surface expression of the loop D mutants, D1 and D2, this response to hypotonicity was not observed for either. Relative membrane expression of wild-type AQP4-GFP imaged in live HEK293 cells increased from 27.9 ± 3.5 to 67.1 ± 4.5 ($p = 0.003$, $n = 3$) upon reduction of the extracellular tonicity to 85 mosmol, whereas the distribution of both the D1 and D2 mutants did not change significantly ($p = 0.29$ and $p = 0.34$ respectively, $n = 3$; Fig. 7).

Molecular Dynamics Simulations Suggest a Dynamic Network of Loop D Interactions—To investigate the contribution of loop D to AQP4 oligomerization we did five independent

100-ns molecular dynamics simulations of a hydrated AQP4 tetramer embedded in a 1-palmitoyl-2-oleoyl-*sn*-glycero-3-phosphocholine bilayer. We found a dynamic network of hydrogen bonds between loop D residues on adjacent monomers and also between loop D residues and both a glutamine (Gln⁸⁶) and histidine (His⁹⁰) residue at the bottom of TM2. On average, each monomer was involved in 3.8 ± 1.4 (mean \pm S.D.) loop D hydrogen bonds with its two neighboring molecules at any given time, which is equivalent to 7.6 ± 2.8 loop D hydrogen bonds per tetramer. Every loop D residue apart from Ser¹⁸⁰ was able to act as a hydrogen bond donor or acceptor with another loop D residue on one of the two adjacent monomers; 7 residues (Arg¹⁸², Thr¹⁸³, Asp¹⁸⁴, Val¹⁸⁵, Thr¹⁸⁶, Gly¹⁸⁷, and Ser¹⁸⁸) were found to have at least 3 different possible hydrogen bonding interactions. This network of interactions is represented as a heat map in Fig. 8*A*. Interactions involving Val¹⁸⁵ and Gly¹⁸⁷ were backbone hydrogen bonds. Both of these residues were able to act as hydrogen bond donors from the backbone amine group (Val¹⁸⁵ to an adjacent Val¹⁸⁵, and Gly¹⁸⁷ to Asp¹⁸⁴, Val¹⁸⁵ and Thr¹⁸⁶) and acceptors at the backbone carbonyl group (Val¹⁸⁵ from an adjacent Val¹⁸⁵ as well as Thr¹⁸³, Thr¹⁸⁶, Gly¹⁸⁷, and Ser¹⁸⁸, and Gly¹⁸⁷ from Thr¹⁸⁶, Ser¹⁸⁸, and Gln⁸⁶). Loop D (as well as loop A) showed relatively large structural fluctuations (Fig. 8, *B* and *C*) despite maintaining an average of 3.8 ± 1.4 inter-monomer hydrogen bonding interactions. Representative snapshots showing the most highly occupied hydrogen bonds, His⁹⁰-Asp¹⁷⁹, Ser¹⁸⁸-Gly¹⁸⁷, Ser¹⁸⁸-Ser¹⁸⁸, Gln⁸⁶-Asp¹⁸⁴, Gln⁸⁶-Ser¹⁸⁸, and Thr¹⁸³-Asp¹⁸⁴ are shown in Fig. 8*F*. Loop D could potentially stabilize the AQP4 tetramer in one of two ways: by preventing monomers from drifting apart during rapid association/dissociation of the inter-monomeric TM interfaces, or by providing inter-monomer interactions that stabilize the tetramer in a more permanent way, preventing dissociation in the first place. In simulations we found that the

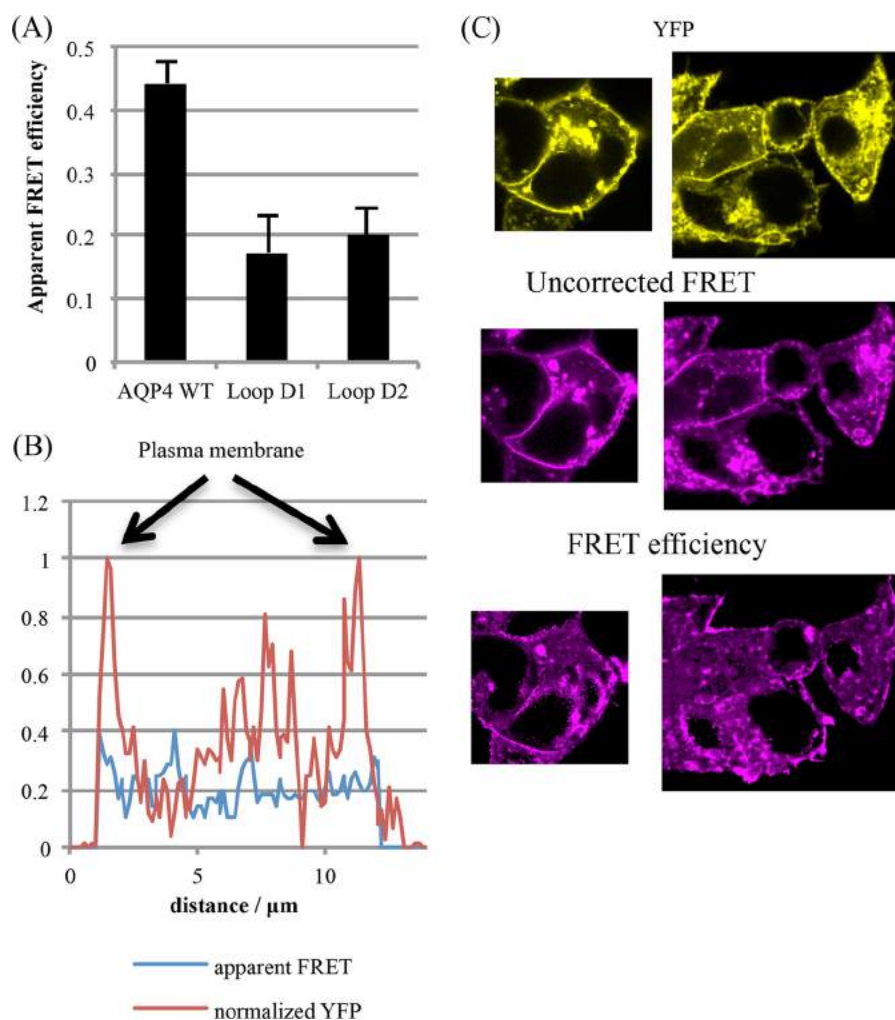


FIGURE 5. **Reduced FRET from AQP4 mutants.** *A*, average apparent FRET efficiencies for AQP4 wild-type and loop D1 and D2 mutants, calculated by normalizing the corrected FRET intensity to YFP intensity for each pixel. Five different areas on each plate were imaged per experimental repeat, $n = 4$. *B*, representative line scan across a cell, passing through membrane and cytoplasm and avoiding the nucleus. Whereas the YFP signal (*red*) shows clear peaks at the plasma membrane, the FRET efficiency (*blue*) does not. *C*, representative processed FRET efficiency images compared with unprocessed FRET and YFP. Whereas both YFP and the raw FRET show clear membrane signals, the FRET efficiency does not.

average monomer-monomer center of mass separation was stable with a root mean square fluctuation of only 0.53 \AA (*c.f.* typical carbon-carbon bond length of $\sim 1.5 \text{ \AA}$) about a mean of 28.67 \AA , and the inter-monomer buried (solvent-inaccessible) area was also stable, with a root mean square fluctuation of 230 \AA^2 about a mean of 2960 \AA^2 . Representative traces are shown in Fig. 8, *D* and *E*. This suggests that there is no spontaneous dissociation/reassociation of the inter-monomer interfaces, at least on the time scale of these simulations (100 ns).

Loop D May Represent a Common Motif for Oligomeric Assembly Across the AQP Family—To investigate whether our AQP4 data could be more widely applicable to other members of the AQP family, we performed a sequence alignment of the loop in all human AQPs, as well as the *E. coli* AQPs as comparison (Fig. 9*A*) using the Clustal Omega software (23). AQP1 contains a similar acidic-*X*-basic-basic motif to AQP4 in the first half of the loop (DRRRR *versus* DSKRT), so we made the D1 mutant in AQP1 (D158A/K159A/K160A/K161A/K162A). This motif is lacking in AQP3, therefore we introduced it via 2 different mutations, P181S/Y182K/N183R and P181E/Y182K/

N183R (to give DSKRN and DEKRN *versus* the wild-type DPYNN). The D1 compound mutation in AQP1 caused a similar loss of oligomerization to that observed for AQP4. Both AQP3 mutations caused the protein to migrate primarily as a band with a molecular weight consistent with a dimeric species, whereas wild-type AQP3 appeared to migrate primarily as a monomer (Fig. 9*B*), consistent with previous studies on the oligomerization state of this AQP. Both AQP1 and AQP3 migrated as diffuse bands, consistent with glycosylation. PNGase F treatment was used to attempt deglycosylation. This appeared to be incompatible with the BN-PAGE experiments, because 1-h treatments with PNGase F at 37°C caused AQP1 and -3 wild-type and mutants to form aggregates that did not migrate beyond the interface between the stacking and separating gels (data not shown). This may be due to increased temperature sensitivity of Triton X-100-solubilized AQPs. Finally, to investigate whether loss of AQP oligomerization is a general feature of the glyceroporin subfamily, we transfected HEK293 cells with AQPs 9 and 10 and subjected Triton X-100-extracted protein to BN-PAGE. Unlike AQP3, we found that AQPs 9 and 10 migrated exclusively as tetramers (Fig. 9*B*).

Oligomerization of Aquaporin-4

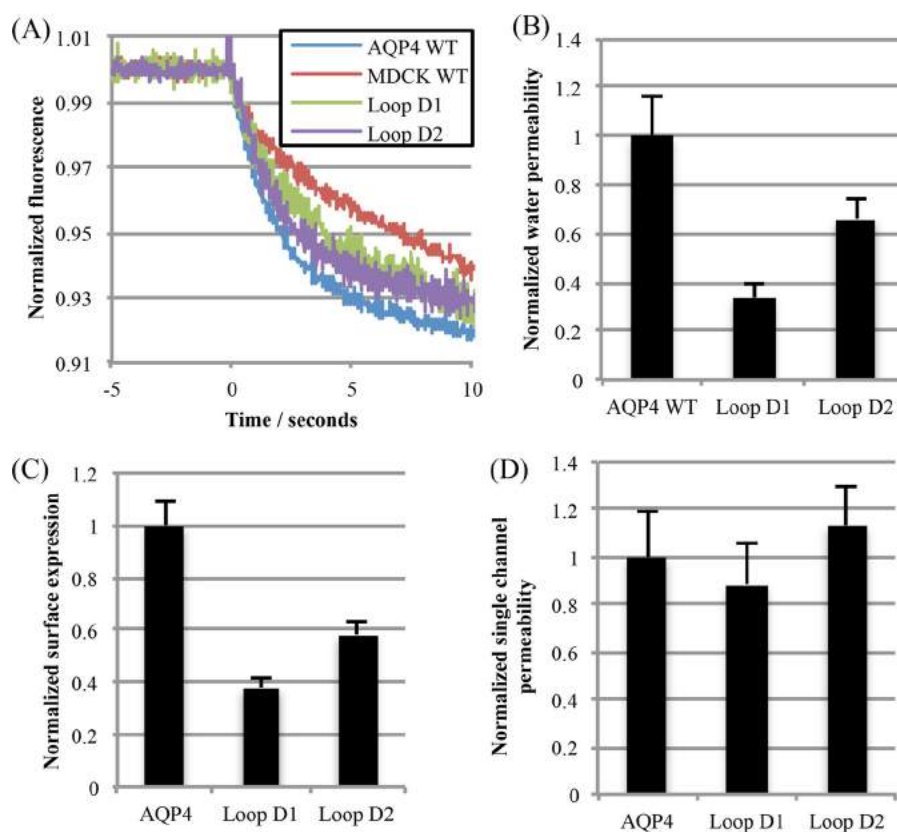


FIGURE 6. **Water permeability of non-tetrameric mutants.** *A*, representative calcein fluorescence quenching curves from stably transfected MDCK cells subjected to a 200 mosmol of mannitol osmotic gradient. *B*, water permeability of MDCK cells normalized to AQP4 WT-transfected MDCK cells. *C*, normalized surface expression of AQP4 constructs in the stably expressing MDCK clones used for water permeability measurements, measured by cell surface biotinylation. *D*, MDCK membrane water permeability normalized to surface expression, to give normalized single channel permeability. All data are presented as mean \pm S.E., $n = 4$.

Discussion

Our data show that the plasma membrane abundance of AQP4 in HEK293 cells is unaffected by the oligomeric state of the protein. This strongly suggests that tetrameric assembly is not required for AQP4 to be correctly trafficked through the endoplasmic reticulum and Golgi to the plasma membrane. It is possible that our mutants are trafficked as tetramers and then dissociate once inserted into the plasma membrane; the FRET data suggest that this is unlikely to be the case, although we cannot differentiate between particular intracellular compartments on the basis of this data, leaving open the possibility of differences in oligomerization state between different intracellular compartments. Our diffusion coefficients calculated from the FRAP data compare reasonably with other reports of diffusion of AQP-GFP constructs in mammalian cells (e.g. $5.7 \times 10^{-3} \mu\text{m}^2 \text{s}^{-1}$ for AQP2 (24), $3.1 \times 10^{-3} \mu\text{m}^2 \text{s}^{-1}$ for AQP1 (25)). We found a small, but statistically significant increase in diffusion coefficient for the mutants that were non-tetrameric in BN-PAGE. Although we have not estimated hydrodynamic radii for our constructs, the relationship $D \propto \ln(1/R)$ derived by Saffman and Delbruck (26) suggests a hydrodynamic radius of 1.2 ± 1.0 nm for our non-tetrameric constructs (assuming $r = 4$ nm for a freely diffusing AQP4 tetramer), which is at least consistent with a loss of tetrameric assembly. We found no difference in the mobile fraction between the wild-type and D1 or D2 mutants (90 ± 6 , 89 ± 4 , and $92 \pm 7\%$, respectively, n.s.

$p = 0.28$), suggesting that there is no difference in the proportion of the protein involved in membrane anchoring interactions. Although we cannot rule out loss of an AQP4 binding partner as an alternative explanation of these data with absolute certainty, in combination with the cell surface BN-PAGE and FRET data it is highly suggestive of non-tetrameric mutant AQP4 molecules in the plasma membrane. Human AQP3 was reported to exist in all four possible oligomeric states (monomer, dimer, trimer, and tetramer) in the plasma membrane of erythrocytes (27). It may be that some or all members of the AQP family can be trafficked to the plasma membrane independently of their oligomerization state.

Our molecular dynamics simulations suggest a dynamic network of transient hydrogen bonds between the residues of loop D of adjacent monomers and also with two residues at the bottom of TM2. The fact that almost every residue involved in this network has several hydrogen bonding options may explain why none of the single alanine substitution mutations had an effect on tetrameric assembly. For example, the most highly occupied hydrogen bond that we found was His⁹⁰-Asp¹⁷⁹, which had 66.5% occupancy averaged over the four monomers and five trajectories. When this bond was not occupied, the Asp¹⁸⁴ side chain was able to act as a hydrogen bond acceptor from the histidine imidazole NH group, and the Thr¹⁸⁶ side chain hydroxyl group was able to act as a hydrogen bond donor to Asp¹⁷⁹. These alternative interactions may be able to par-

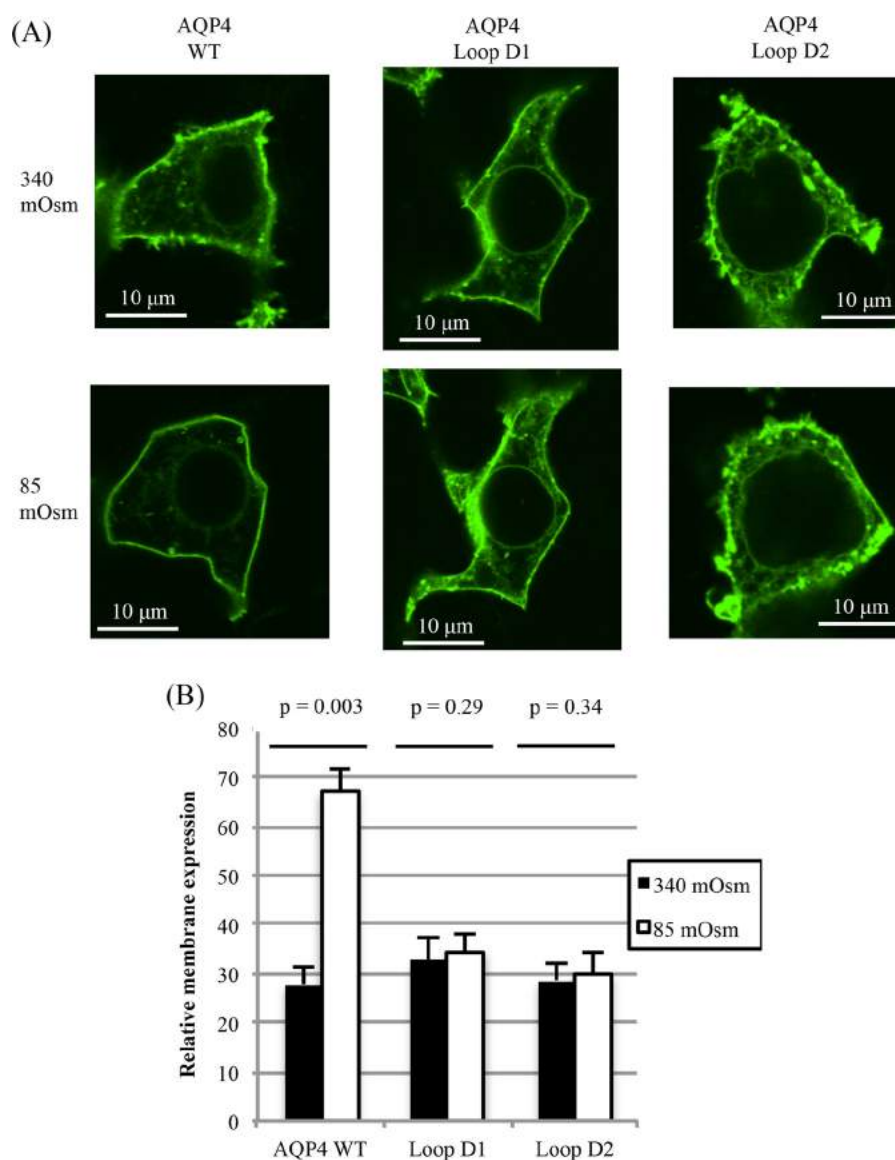
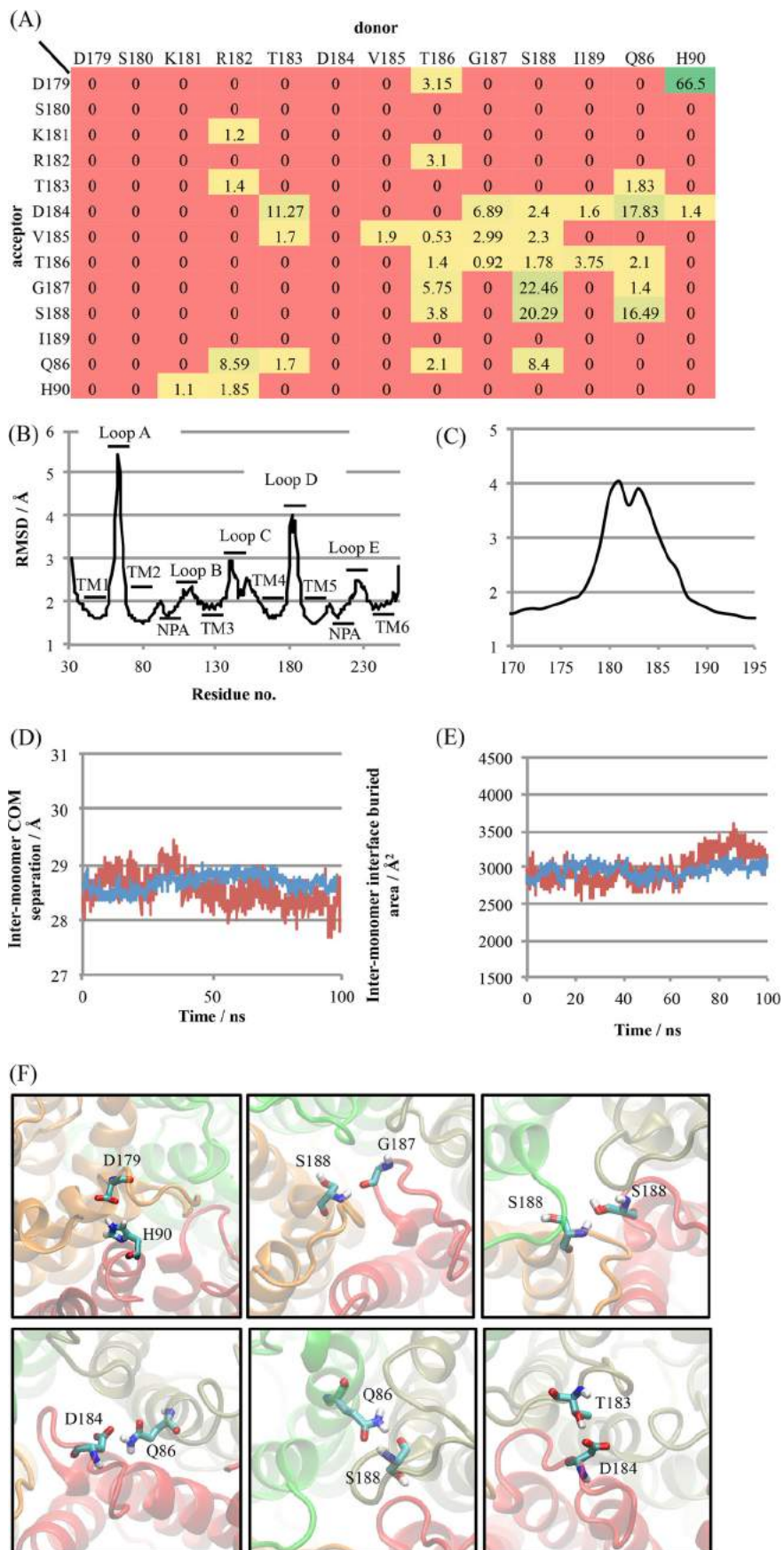


FIGURE 7. **Tonicity-induced translocation of non-tetrameric mutants.** *A*, representative fluorescence micrographs of HEK293 cells transfected with AQP4-GFP fusion proteins, before and after 30 s of exposure to hypotonic (85 mosmol) medium. *B*, relative membrane expression of AQP4-GFP fusion proteins before and after exposure to hypotonic medium. At least 4 cells per image were analyzed for each experimental repeat, $n = 3$. Data are presented as mean \pm S.E.

tially compensate for the loss of the Asp¹⁷⁹-His⁹⁰ interaction in the D179A and H90A single mutations. Asp¹⁷⁹ had only one alternative interaction, whereas His⁹⁰ had three. This may explain why the D179A mutation had a slight effect on oligomerization, whereas the H90A mutant did not. Interestingly, MD simulations have suggested that a histidine residue just beyond the bottom of TM2 in the intracellular loop B (H95) could modulate the channel open probability via spontaneous formation and dissociation of a hydrogen bond with a cysteine residue at the interface between TM4 and loop D (Cys¹⁷⁸) (28). In our simulations, we did not observe this hydrogen bond. A recent study combining *in silico* and *in vitro* evidence also did not observe this hydrogen bond in simulations and suggested that His⁹⁵ may indeed act as a channel gating residue, but by formation of a histidine protonation state-dependent salt bridge with a glutamate residue (Glu⁴¹), independent of Cys¹⁷⁸ (29).

S-Nitrosylation of AQP11 at a cysteine residue in the extracellular loop E (Cys²²⁷) has been suggested to be required for AQP11 oligomeric assembly, with the C227S mutant showing reduced oligomeric assembly in mouse kidney (30). This supports the idea of a role for post-translational modification in AQP oligomerization. Loop D of AQP4 contains two sites predicted to be targets for post-translational modification. These are protein kinase sites at Ser¹⁸⁰ and Ser¹⁸⁸. Phosphorylation at Ser¹⁸⁰ was suggested to reduce AQP4 water permeability via a gating effect in LLC-PK1 cells (31), but this was not supported by molecular dynamics simulations of AQP4-Ser(P)¹⁸⁰ (32), and structural studies showed no difference between wild-type AQP4 and a phosphomimetic S180D mutant (33, 34). We used phosphomimetic (S180D, S188D) and phospho-blocking (S180A, S188A) mutations to investigate a potential role for post-translational modification in the AQP4 oligomeric assembly. We found that all four phosphorylation mutants were able

Oligomerization of Aquaporin-4



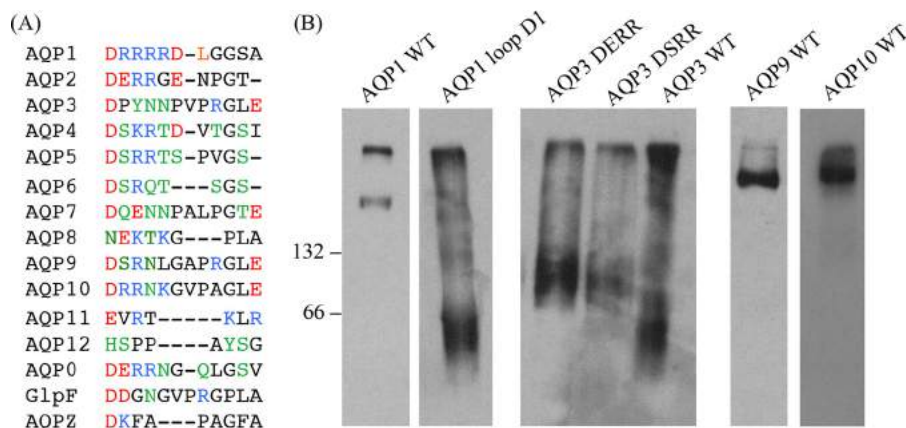


FIGURE 9. Comparison of loop D between different human AQPs. A, all 13 human AQPs as well as AQPZ and GlpF (both from *E. coli*) were aligned using Clustal Omega (EMBL-EBI). Acidic residues are colored red; basic, blue; and neutral residues able to form sidechain hydrogen bonds, green. B, BN-PAGE and Western blotting of wild-type and mutant AQPs 1 and 3 and wild-type AQPs 9 and 10. 66 and 132 represent BSA molecular weight markers.

to assemble into tetramers, suggesting that phosphorylation of loop D is not involved in tetrameric assembly of AQP4.

We recently reported that AQP4 in primary rat astrocytes and HEK293 cells rapidly relocalizes to the plasma membrane upon reduction of extracellular tonicity (11); this may involve changes in interactions between AQP4-containing vesicles and cytoskeletal elements as described by others (35, 36). Interestingly, neither of the mutants with reduced ability to tetramerize were able to relocalize in response to a hypotonic extracellular stimulus. It is possible that a binding partner of AQP4 involved in the translocation response recognizes an epitope formed by the interface of several AQP molecules within a tetramer, and that disrupting tetrameric assembly disrupts this epitope. Although the C-terminal PKA phosphorylation site (Ser²⁷⁶), which controls this response is ~100 residues away in the primary sequence, it may be that phosphorylation of this residue causes a conformational change in the large (~70 residue) C-terminal tail of AQP4, which allows an AQP4-binding protein to bind to the intracellular face of AQP4 including loop D. Structural data for AQPs are routinely collected after cleaving the C terminus at the bottom of TM6 to aid crystallization and high-resolution structure determination (37). This is true for AQP4 and in the structure that we used to identify mutagenic targets and as input for our simulations, the protein was truncated at the bottom of TM6, at residue 254 of 323 (17). This makes it difficult for us to make any concrete predictions about interactions of the AQP4 C terminus, especially given its large size.

Based on a sequence alignment of loop D, we made mutants of human AQPs 1 and 3. Wild-type AQP1 existed as a tetramer when extracted from HEK293 membranes using Triton X-100, whereas AQP3 existed primarily as a monomer, both of which are in agreement with previous reports (27, 38). Mutating the first five residues of AQP1 loop D to alanine (which rendered AQP4 primarily monomeric) caused the protein to migrate pri-

marily as a monomer in BN-PAGE. Introducing the conserved acid-X-base-base motif (present in loop D of both AQPs 1 and 4) into AQP3 caused it to migrate primarily as a dimer. It has been suggested that lack of oligomerization may have a role in controlling substrate selectivity of the glyceroporin subfamily (39), which consists of AQPs 3, 7, 9, and 10 in humans. However, we find that, unlike AQP3, both AQPs 9 and 10 both exist exclusively as tetramers when extracted from HEK293 membranes. This suggests that solute permeability of AQPs is not correlated with the oligomeric state.

Previous mutational analysis of AQP1 found an extracellular motif consisting of an aspartate residue (Asp¹⁸⁵) at the top of TM5 that can interact with a lysine residue (Lys⁵¹) at the top of TM2 to increase tetramer stability in detergent (40). Whether this had an effect on native protein in live cells was not clear. The S205D mutant of an insect AQP (AQP_{cic}) was shown to exist in a primarily monomeric state when extracted from yeast and *Xenopus* oocyte membranes, whereas the wild-type was tetrameric (41, 42). This mutant had a complete loss of water channel function, and it is not clear whether this was due to subtle changes in structure leading to a gating effect, gross misfolding, loss of surface expression, or a direct result of the loss of oligomerization through loss of monomer-monomer interactions that stabilize the open state of the pore. This makes interpretation of this result very difficult.

In summary, we show that loop D of AQP4 forms a hub for a dynamic network of interactions that stabilize the AQP4 tetramer, both when solubilized using non-ionic detergent and in living mammalian cells. Tetrameric assembly is not required for either endoplasmic reticulum-to-Golgi-to-plasma membrane trafficking or water channel activity. Mutants with reduced tetrameric assembly are unable to relocalize in response to tonicity changes, which may reflect a requirement for tetramerization in the regulation of AQP relocalization or key protein-protein interactions mediated by loop D of AQP4.

FIGURE 8. A dynamic network of loop D hydrogen bonds in simulations of AQP4. A, heat map showing percentage occupancy of loop D hydrogen bonds averaged over 4 monomers comprising a tetramer and over 5 independent 100-ns simulations. B, backbone heavy atom root mean square deviation (RMSD) of AQP4 residues, demonstrating the structural flexibility of loops A and D. RMSDs were calculated independently for each trajectory and averaged. C, close-up view of loop D RMSD. D, representative inter-monomer center of mass distance for a single interface (red) and averaged over the four interfaces of a tetramer (blue). E, representative inter-monomer buried area for a single interface (red) and averaged over the four interfaces of a tetramer (blue). F, snapshots of molecular dynamics trajectories in which the six most highly occupied inter-monomer hydrogen bonds involving loop D residues are occupied.

Oligomerization of Aquaporin-4

We conclude that loop D interactions may represent a conserved mechanism for controlling oligomerization across the AQP family.

Author Contributions—A. C. C., P. K., M. T. C., and R. M. B. designed all experiments. P. K. performed and analyzed all experiments and prepared figures. P. K. and A. C. C. drafted the manuscript. R. M. B. and M. T. C. critically revised the manuscript. All authors approved the final version of the manuscript.

Acknowledgment—The computing facilities were provided by the Centre for Scientific Computing of the University of Warwick with support from the Science Research Investment Fund.

References

- Jung, J. S., Preston, G. M., Smith, B. L., Guggino, W. B., and Agre, P. (1994) Molecular structure of the water channel through aquaporin CHIP: the hourglass model. *J. Biol. Chem.* **269**, 14648–14654
- Hub, J. S., Grubmuller, H., and de Groot, B. L. (2009) Dynamics and energetics of permeation through aquaporins: what do we learn from molecular dynamics simulations? *Handb. Exp. Pharmacol.* **2009**, 57–76
- Horner, A., Zocher, F., Preiner, J., Ollinger, N., Siligan, C., Akimov, S. A., and Pohl, P. (2015) The mobility of single-file water molecules is governed by the number of H-bonds they may form with channel-lining residues. *Sci. Adv.* **1**, e1400083
- Chevalier, A. S., and Chaumont, F. (2015) Trafficking of plant plasma membrane aquaporins: multiple regulation levels and complex sorting signals. *Plant Cell Physiol.* **56**, 819–829
- Kaldenhoff, R., Kai, L., and Uehlein, N. (2014) Aquaporins and membrane diffusion of CO₂ in living organisms. *Biochim. Biophys. Acta* **1840**, 1592–1595
- Yu, J., Yool, A. J., Schulten, K., and Tajkhorshid, E. (2006) Mechanism of gating and ion conductivity of a possible tetrameric pore in aquaporin-1. *Structure* **14**, 1411–1423
- Conner, M. T., Conner, A. C., Bland, C. E., Taylor, L. H., Brown, J. E., Parri, H. R., and Bill, R. M. (2012) Rapid aquaporin translocation regulates cellular water flow: mechanism of hypotonicity-induced subcellular localization of aquaporin 1 water channel. *J. Biol. Chem.* **287**, 11516–11525
- Cho, G., Bragiel, A. M., Wang, D., Pieczonka, T. D., Skowronski, M. T., Shono, M., Nielsen, S., and Ishikawa, Y. (2015) Activation of muscarinic receptors in rat parotid acinar cells induces AQP5 trafficking to nuclei and apical plasma membrane. *Biochim. Biophys. Acta* **1850**, 784–793
- Kishida, K., Kuriyama, H., Funahashi, T., Shimomura, I., Kihara, S., Ouchi, N., Nishida, M., Nishizawa, H., Matsuda, M., Takahashi, M., Hotta, K., Nakamura, T., Yamashita, S., Tochino, Y., and Matsuzawa, Y. (2000) Aquaporin adipose, a putative glycerol channel in adipocytes. *J. Biol. Chem.* **275**, 20896–20902
- Kamsteeg, E. J., Wormhoudt, T. A., Rijss, J. P., van Os, C. H., and Deen, P. M. (1999) An impaired routing of wild-type aquaporin-2 after tetramerization with an aquaporin-2 mutant explains dominant nephrogenic diabetes insipidus. *EMBO J.* **18**, 2394–2400
- Kitchen, P., Day, R. E., Taylor, L. H., Salman, M. M., Bill, R. M., Conner, M. T., and Conner, A. C. (2015) Identification and molecular mechanisms of the rapid tonicity-induced relocalization of the aquaporin 4 channel. *J. Biol. Chem.* **290**, 16873–16881
- Kang, M., Day, C. A., Kenworthy, A. K., and DiBenedetto, E. (2012) Simplified equation to extract diffusion coefficients from confocal FRAP data. *Traffic* **13**, 1589–1600
- van Rheenen, J., Langeslag, M., and Jalink, K. (2004) Correcting confocal acquisition to optimize imaging of fluorescence resonance energy transfer by sensitized emission. *Biophys. J.* **86**, 2517–2529
- Oostenbrink, C., Villa, A., Mark, A. E., and van Gunsteren, W. F. (2004) A biomolecular force field based on the free enthalpy of hydration and solvation: the GROMOS force-field parameter sets 53A5 and 53A6. *J. Comput. Chem.* **25**, 1656–1676
- Berger, O., Edholm, O., and Jähnig, F. (1997) Molecular dynamics simulations of a fluid bilayer of dipalmitoylphosphatidylcholine at full hydration, constant pressure, and constant temperature. *Biophys. J.* **72**, 2002–2013
- Pronk, S., Páll, S., Schulz, R., Larsson, P., Bjelkmar, P., Apostolov, R., Shirts, M. R., Smith, J. C., Kasson, P. M., van der Spoel, D., Hess, B., and Lindahl, E. (2013) GROMACS 4.5: a high-throughput and highly parallel open source molecular simulation toolkit. *Bioinformatics* **29**, 845–854
- Ho, J. D., Yeh, R., Sandstrom, A., Chorny, I., Harries, W. E., Robbins, R. A., Miercke, L. J., and Stroud, R. M. (2009) Crystal structure of human aquaporin 4 at 1.8 Å and its mechanism of conductance. *Proc. Natl. Acad. Sci. U.S.A.* **106**, 7437–7442
- Schmidt, T. H., and Kandt, C. (2012) LAMBADA and InflateGRO2: efficient membrane alignment and insertion of membrane proteins for molecular dynamics simulations. *J. Chem. Inf. Model.* **52**, 2657–2669
- Humphrey, W., Dalke, A., and Schulten, K. (1996) VMD: visual molecular dynamics. *J. Mol. Graph.* **14**, 33–38, 27–38
- Fenton, R. A., Moeller, H. B., Nielsen, S., de Groot, B. L., and Rützler, M. (2010) A plate reader-based method for cell water permeability measurement. *Am. J. Physiol. Renal Physiol.* **298**, F224–230
- Felber, L. M., Cloutier, S. M., Kündig, C., Kishi, T., Brossard, V., Jichlinski, P., Leisinger, H. J., and Deperthes, D. (2004) Evaluation of the CFP-substrate-YFP system for protease studies: advantages and limitations. *Bio-Techniques* **36**, 878–885
- Kitchen, P., Öberg, F., Sjöhamn, J., Hedfalk, K., Bill, R. M., Conner, A. C., Conner, M. T., and Törnroth-Horsefield, S. (2015) Plasma membrane abundance of human aquaporin 5 is dynamically regulated by multiple pathways. *PLoS One* **10**, e0143027
- Sievers, F., Wilm, A., Dineen, D., Gibson, T. J., Karplus, K., Li, W., Lopez, R., McWilliam, H., Remmert, M., Söding, J., Thompson, J. D., and Higgins, D. G. (2011) Fast, scalable generation of high-quality protein multiple sequence alignments using Clustal Omega. *Mol. Systems Biol.* **7**, 539
- Umenishi, F., Verbavatz, J. M., and Verkman, A. S. (2000) cAMP regulated membrane diffusion of a green fluorescent protein-aquaporin 2 chimera. *Biophys. J.* **78**, 1024–1035
- Cho, M. R., Knowles, D. W., Smith, B. L., Moulds, J. J., Agre, P., Mohandas, N., and Golan, D. E. (1999) Membrane dynamics of the water transport protein aquaporin-1 in intact human red cells. *Biophys. J.* **76**, 1136–1144
- Saffman, P. G., and Delbrück, M. (1975) Brownian motion in biological membranes. *Proc. Natl. Acad. Sci. U.S.A.* **72**, 3111–3113
- Roudier, N., Bailly, P., Gane, P., Lucien, N., Gobin, R., Cartron, J. P., and Ripoche, P. (2002) Erythroid expression and oligomeric state of the AQP3 protein. *J. Biol. Chem.* **277**, 7664–7669
- Alberga, D., Nicolotti, O., Lattanzi, G., Nicchia, G. P., Frigeri, A., Pisani, F., Benfenati, V., and Mangiardi, G. F. (2014) A new gating site in human aquaporin-4: insights from molecular dynamics simulations. *Biochim. Biophys. Acta* **1838**, 3052–3060
- Kaptan, S., Assentoft, M., Schneider, H. P., Fenton, R. A., Deitmer, J. W., MacAulay, N., and de Groot, B. L. (2015) H95 is a pH-dependent gate in aquaporin 4. *Structure* **23**, 2309–2318
- Atochina-Vasserman, E. N. (2012) S-Nitrosylation of surfactant protein D as a modulator of pulmonary inflammation. *Biochim. Biophys. Acta* **1820**, 763–769
- Zelenina, M., Zelenin, S., Bondar, A. A., Brismar, H., and Aperia, A. (2002) Water permeability of aquaporin-4 is decreased by protein kinase C and dopamine. *Am. J. Physiol. Renal Physiol.* **283**, F309–318
- Sachdeva, R., and Singh, B. (2014) Phosphorylation of Ser-180 of rat aquaporin-4 shows marginal affect on regulation of water permeability: molecular dynamics study. *J. Biomol. Struct. Dyn.* **32**, 555–566
- Mitsuma, T., Tani, K., Hiroaki, Y., Kamegawa, A., Suzuki, H., Hibino, H., Kurachi, Y., and Fujiyoshi, Y. (2010) Influence of the cytoplasmic domains of aquaporin-4 on water conduction and array formation. *J. Mol. Biol.* **402**, 669–681
- Tani, K., Mitsuma, T., Hiroaki, Y., Kamegawa, A., Nishikawa, K., Tanimura, Y., and Fujiyoshi, Y. (2009) Mechanism of aquaporin-4's fast and highly selective water conduction and proton exclusion. *J. Mol. Biol.* **389**, 694–706
- Potokar, M., Stenovec, M., Jorgačevski, J., Holen, T., Kreft, M., Ottersen, O. P., and Zorec, R. (2013) Regulation of AQP4 surface expression via

- vesicle mobility in astrocytes. *Glia* **61**, 917–928
36. Mazzaferri, J., Costantino, S., and Lefrancois, S. (2013) Analysis of AQP4 trafficking vesicle dynamics using a high-content approach. *Biophys. J.* **105**, 328–337
37. Sjöhamn, J., and Hedfalk, K. (2014) Unraveling aquaporin interaction partners. *Biochim. Biophys. Acta* **1840**, 1614–1623
38. Mathai, J. C., and Agre, P. (1999) Hourglass pore-forming domains restrict aquaporin-1 tetramer assembly. *Biochemistry* **38**, 923–928
39. Duchesne, L., Deschamps, S., Pellerin, I., Lagree, V., Froger, A., Thomas, D., Bron, P., Delamarche, C., and Hubert, J. F. (2001) Oligomerization of water and solute channels of the major intrinsic protein (MIP) family. *Kidney Int.* **60**, 422–426
40. Buck, T. M., Wagner, J., Grund, S., and Skach, W. R. (2007) A novel tripartite motif involved in aquaporin topogenesis, monomer folding and tetramerization. *Nat. Struct. Mol. Biol.* **14**, 762–769
41. Lagrée, V., Froger, A., Deschamps, S., Pellerin, I., Delamarche, C., Bonnac, G., Gouranton, J., Thomas, D., and Hubert, J. F. (1998) Oligomerization state of water channels and glycerol facilitators: involvement of loop E. *J. Biol. Chem.* **273**, 33949–33953
42. Duchesne, L., Pellerin, I., Delamarche, C., Deschamps, S., Lagree, V., Froger, A., Bonnac, G., Thomas, D., and Hubert, J. F. (2002) Role of C-terminal domain and transmembrane helices 5 and 6 in function and quaternary structure of major intrinsic proteins: analysis of aquaporin/glycerol facilitator chimeric proteins. *J. Biol. Chem.* **277**, 20598–20604

Structural Determinants of Oligomerization of the Aquaporin-4 Channel

Philip Kitchen, Matthew T. Conner, Roslyn M. Bill and Alex C. Conner

J. Biol. Chem. 2016, 291:6858-6871.

doi: 10.1074/jbc.M115.694729 originally published online January 19, 2016

Access the most updated version of this article at doi: [10.1074/jbc.M115.694729](https://doi.org/10.1074/jbc.M115.694729)

Alerts:

- [When this article is cited](#)
- [When a correction for this article is posted](#)

[Click here](#) to choose from all of JBC's e-mail alerts

This article cites 42 references, 15 of which can be accessed free at <http://www.jbc.org/content/291/13/6858.full.html#ref-list-1>